HAL
open science

Lumière dans les milieux atomiques désordonnés : théorie des matrices euclidiennes et lasers aléatoires

Arthur Goetschy

To cite this version:

Arthur Goetschy. Lumière dans les milieux atomiques désordonnés : théorie des matrices euclidiennes et lasers aléatoires. Autre. Université de Grenoble, 2011. Français. NNT : 2011GRENY083 . tel-00676988v2

HAL Id: tel-00676988

https://theses.hal.science/tel-00676988v2

Submitted on 12 Aug 2014

HAL is a multi-disciplinary open access archive for the deposit and dissemination of scientific research documents, whether they are published or not. The documents may come from teaching and research institutions in France or abroad, or from public or private research centers.

L'archive ouverte pluridisciplinaire **HAL**, est destinée au dépôt et à la diffusion de documents scientifiques de niveau recherche, publiés ou non, émanant des établissements d'enseignement et de recherche français ou étrangers, des laboratoires publics ou privés.

UNIVERSITÉ DE GRENOBLE

THÈSE

Pour obtenir le grade de

DOCTEUR DE L'UNIVERSITÉ DE GRENOBLE

Spécialité : **Physique**

Arrêté ministériel : 7 août 2006

Présentée par

Arthur GOETSCHY

Thèse dirigée par **Sergey E. SKIPETROV**

préparée au sein du **Laboratoire de Physique et de Modélisation des Milieux Condensés**

dans **l'École Doctorale de Physique**

Lumière dans les milieux atomiques désordonnés: théorie des matrices euclidiennes et lasers aléatoires

Thèse soutenue publiquement le **lundi 28 novembre 2011**,
devant le jury composé de :

Eric AKKERMANS
Professeur au Technion, Haïfa (Israël). Membre.
Jean DALIBARD
Professeur au Collège de France, Paris (France). Rapporteur.
Vladimir E. KRAVTSOV
Professeur à l'ICTP, Trieste (Italie). Rapporteur.
Giorgio PARISI
Professeur à l'Université La Sapienza, Rome (Italie). Rapporteur.
Patrick SEBBAH
Directeur de recherche à l'Institut Langevin, Paris (France). Membre.
Sergey E. SKIPETROV
Directeur de recherche au LPMMC, Grenoble (France). Membre.
Bart VAN TIGGELEN
Directeur de recherche au LPMMC, Grenoble (France). Président du Jury.

Remerciements

Avant d'accompagner le lecteur sur les chemins sinueux et néanmoins lumineux de la physique des milieux désordonnés, il est bon d'exprimer mes remerciements aux différentes personnes qui ont su donner corps et souffle au Laboratoire de Physique et Modélisation des Milieux Condensés (LPMMC) durant les trois années où j'ai pu y travailler. Qu'on me pardonne ici un brin de grandiloquence. Le LPMMC est un laboratoire de physique théorique, et à ce titre il est comme une hétérotopie dans le monde: un lieu où des individus, dans le silence ou le vacarme de leurs pensées, se confrontent à l'inconnu, s'aventurent en des territoires où règne bien souvent le froid de la solitude comme le grand vent des découvertes. Un laboratoire est un lieu bifrons, comme une boîte magique qui ouvrirait sur une part encore vierge et silencieuse du monde, un vaste océan dans lequel on serait tenté de se perdre. C'est donc toujours une surprise, au retour d'une de ces terribles expéditions, de retrouver, dans la chaleur d'un port, une humanité qui parle une langue qu'on avait presque oubliée. Le laboratoire est cette passe entre deux mondes, tout à la fois cet océan impétueux et ce port chaleureux. Je souhaite ici remercier les personnes que j'ai pu côtoyées au LPMMC pour avoir su faire vivre ces deux composantes qu'on ne saurait dissocier.

Pour son goût du grand jeu, son sérieux, son efficacité, et sa bonté, c'est avant tout Sergey Skipetrov que je souhaite saluer. Avec finesse, il a su tout à la fois laisser à ma curiosité l'ampleur de son déploiement, m'accompagner dans les étroits défilés de la pensée lorsque ceux-ci se faisaient trop sauvages, et me conseiller chaque fois que le doute me saisissait. Un grand merci, Sergey. Je remercie également chaleureusement Jean Dalibard, Vladimir Kravtsov, et Giorgio Parisi pour leurs évidentes qualités de rapporteurs de mon travail de thèse, ainsi qu' Eric Akkermans et Patrick Sebbah pour tous les commentaires et appréciations qu'ils ont pu formuler en tant que membres de mon jury de thèse. Je veux aussi exprimer ma gratitude à Bart van Tiggelen, Vincent Rossetto, Thierry Champel, Denis Basko, et Dominique Spehner, ainsi qu'aux autres chercheurs permanents du LPMMC, pour les nombreux et savoureux échanges que l'on a pu avoir, tant du point de vue scientifique qu'humain au cours de ces trois années passées en bon voisinage.

C'est avec un grand plaisir que je salue Françoise Berthoud, Jean-Daniel Dubois, Michèle Peretto, et Laurence Magnino, eux qui m'ont toujours épauler lorsque je jouais à l'apprenti-sorcier avec les clusters de calculs ou m'égarais dans les arcanes administratives qui assurent le bon fonctionnement d'un laboratoire et l'heureux déroulement d'une thèse; eux qui n'ont jamais été avares de sourires, et ont toujours fait la preuve de leur grande gentillesse, leur disponibilité, et leur appréciable gourmandise.

Enfin, je souhaite adresser un salut particulier à tous ceux qui ont traversé comme des étoiles le LPMMC, que ce soit le temps d' une thèse ou d'un postdoc. Je pense à Giulia Ferrini pour nos longues, nombreuses, et en un sens fort sérieuses discussions sur la liberté et le désir; à Sébastien Kawka avec qui je partage une certaine forme de pensée sauvage; à Nicolas Didier qui m'a toujours impressioné par son énergie et son appétit de vivre. Je pense à Vladimir Fedorov pour son punch slave et son amour du blues, à Vitalie Eremeev, ce grand bonhomme curieux et plein sourire, à Gianluca Rastelli et son goût des années 80, à James Babington pour son infinie délicatesse et sa passion incontrôlable et incontrôlée de la physique. Je pense enfin à Christoph Schenke toujours à la fois extrêmement attentif et incorrigiblement taquin, à Thomas Klauss, l'ami électro-chat, et à Manutea Candé, le camarade existentiel.

À Grenoble, novembre 2011

Arthur Goetschy

Abstract

This thesis is devoted to the study of the properties of light emitted by a collection of atomic scatterers distributed at random positions in Euclidean space. In this respect, an *ab initio* theory of random lasing is formulated in terms of the statistical properties of the so-called 'Green's matrix'. This matrix belongs to the family of Euclidean random matrices (ERMs), for which we develop an analytic theory giving access to their eigenvalue distribution.

First, we derive quantum microscopic equations for the electric field and atomic operators, and show how the non-Hermitian Green's matrix (a matrix with elements equal to the Green's function of the Hemholtz equation between pairs of atoms in the system) emerges in the quantum formalism. We provide expressions for the intensity and the spectrum of light in terms of the Green's matrix, characterize quantum Langevin forces, and reveal how the semiclassical random laser threshold is washed out by quantum fluctuations (chapters 2 and 3).

A mesoscopic and semiclassical description of light scattered by pumped atoms is the subject of chapter 4. We provide a microscopic derivation of the transport equation in the presence of gain, reveal a mapping to ERMs, and analyze the lasing threshold inferred from the transport equation.

In chapters 5 and 6, we develop an analytic theory for Hermitian and non-Hermitian ERMs in the limit of large matrix size. We obtain self-consistent equations for the resolvent and the eigenvector correlator of an arbitrary ERM and apply our results to three different ERMs relevant to wave propagation in random media: the random Green's matrix, its imaginary part, and its real part. We are able to describe analytically with reasonable precision the full probability distribution of decay rates of light emitted by a large number of atoms, as well as of the collective frequency shift induced by the light-matter interaction. The signatures of Anderson localization in the properties of the Green's matrix are also discussed.

Finally, we combine microscopic equations of motion of light-matter interaction with our results for non-Hermitian ERMs to tackle the problem of random lasing (chapter 7). The lasing threshold and the intensity of laser emission are calculated analytically in the semiclassical approximation, and the spectrum of light below threshold is computed by taking into account quantum effects. Our theory applies from low to high density of atoms.

Résumé

Cette thèse présente une étude des propriétés de la lumière émise par des diffuseurs atomiques distribués aléatoirement dans l'espace euclidien. Dans ce cadre, une théorie *ab initio* des lasers aléatoires est formulée en terme des propriétés statistiques de la 'matrice de Green'. Cette dernière appartient à la famille des matrices aléatoires euclidiennes (MAE) pour lesquelles nous développons une théorie analytique donnant notamment accès à la distribution de probabilité de leurs valeurs propres.

Dans un premier temps, nous établissons les équations quantiques microscopiques régissant la dynamique du champ électrique ainsi que celle des opérateurs atomiques, et explicitons comment la matrice de Green (dont les éléments sont égaux à la fonction de Green de l'équation de Helmholtz évaluée entre les différentes paires d'atomes constituant le milieu) émerge du formalisme quantique. Nous exprimons à la fois l'intensité et le spectre de la lumière en termes de la matrice de Green, caractérisons les forces de Langevin quantiques, et montrons de quelle manière le seuil semi-classique d'un laser aléatoire est affecté par la prise en considération des fluctuations quantiques (chapitres 2 et 3).

Une description mésoscopique et semi-classique de la lumière diffusée par des atomes soumis à une pompe externe est présentée dans le quatrième chapitre. Nous dérivons une équation de transport obéie par l'intensité moyenne en présence de gain, établissons un 'mapping' avec les MAE, et analysons la condition de seuil laser déduite de l'équation de transport.

Dans les chapitres 5 et 6, nous développons une théorie générale des MAE, hermitiennes et non hermitiennes, valide dans la limite de grande taille matricielle. Nous obtenons des équations couplées pour la résolvante et le corrélateur des vecteur propres d'une MAE arbitraire, puis testons la validité de nos résultats sur trois matrices jouant un rôle important dans l'étude de la propagation des ondes en milieux désordonnés: la matrice de Green, sa partie imaginaire, et sa partie réelle. Nous sommes ainsi capables de décrire analytiquement avec une bonne précision la distribution de probabilité des taux d'émission lumineux dus à un grand nombre d'atomes, ainsi que celle du déplacement lumineux collectif dû à l'interaction lumière-matière. Les signatures de la localisation d'Anderson dans les propriétés de la matrice de Green sont également discutées.

Finalement, nous combinons les équations microscopiques de l'interaction lumière-matière avec nos résultats relatifs aux MAE non-hermitiennes afin de caractériser dans le détail le comportement des lasers aléatoires (chapitre 7). Le seuil laser ainsi que l'intensité au delà du seuil sont calculés analytiquement dans l'approximation semi-classique, et le spectre de la lumière sous le seuil est évalué en prenant en compte les effets quantiques. Notre théorie s'applique aussi bien à basse densité qu'à haute densité de diffuseurs atomiques.

Contents

1 Introduction: Random lasing in a nutshell **1**
1.1 How can a laser be random? . . . 1
1.2 The first simple picture . . . 3
1.3 Overview of the thesis . . . 7

2 Light-matter interaction in a quantum framework **11**
2.1 General Hamiltonian . . . 11
2.2 Choice of a formalism . . . 14
2.3 Heisenberg equations of motion . . . 18
2.3.1 Electric field dynamics . . . 19
2.3.2 Dynamics of atomic variables . . . 21
2.4 Microscopic and mesoscopic pictures . . . 25
2.4.1 Microscopic excitations . . . 26
2.4.2 Toward mesoscopic transport . . . 29
2.5 The Green's matrix in the literature . . . 32
2.5.1 Cooperative emission of large atomic samples . . . 32
2.5.2 Anderson localization in an open medium . . . 33
2.5.3 Optical instabilities and random lasers . . . 34

3 How much quantum is the radiation process ? **37**
3.1 Intensity and spectrum of light emitted by a cloud of atoms . . . 37
3.2 Introduction of a pumping mechanism . . . 41
3.2.1 Coherent pump . . . 41
3.2.2 Incoherent pump . . . 42
3.2.3 One atom spectrum: coherent vs incoherent pump . . . 45
3.3 Properties of quantum Langevin forces . . . 46
3.4 Semiclassical treatment of two atoms . . . 48
3.5 Quantum treatment of two atoms . . . 52
3.6 Increasing the number of atoms . . . 58

4 Multiple-scattering of light in the presence of gain: a mesoscopic description **63**
4.1 Fictitious Hamiltonian and scattering building blocks . . . 63
4.1.1 Atomic polarizability . . . 63
4.1.2 Fictitious Hamiltonian . . . 65

4.1.3 Atomic t-operator . . . 66
4.1.4 Scattering cross-section and optical theorem . . . 67
4.2 A simple but universal semiclassical laser threshold . . . 68
4.2.1 Threshold condition . . . 68
4.2.2 Polarizability models . . . 69
4.3 Extinction mean free path in a gas of pumped atoms . . . 70
4.4 Mapping to the Green's matrix properties . . . 74
4.5 Transport equation in the presence of gain . . . 78
4.5.1 Definition of notation . . . 78
4.5.2 From Bethe-Salpeter equation to Boltzmann equation . . . 80
4.5.3 Diffusion equation . . . 82
4.6 Laser threshold from transport equation . . . 85

5 Hermitian Euclidean random matrix theory 89
5.1 Random matrix ensembles of interest . . . 90
5.1.1 Gaussian matrices . . . 90
5.1.2 Wishart matrices . . . 91
5.1.3 Euclidean random matrices . . . 92
5.2 Resolvent, Blue function, and $\mathcal{R}$-transform . . . 93
5.3 Mapping to the Dyson gas . . . 95
5.3.1 Dyson gas picture . . . 95
5.3.2 Brownian motion of eigenvalues . . . 96
5.3.3 Mean field approximation . . . 97
5.3.4 Examples of application . . . 99
5.4 Field representation . . . 100
5.5 Diagrammatic approach . . . 104
5.5.1 From Gaussian and Wishart ensembles to ERMs . . . 104
5.5.2 ERM: high density expansion . . . 106
5.5.3 ERM: self-consistent equations . . . 108
5.5.4 Solving Eq. (5.115) in practice . . . 112
5.6 Free probability theory . . . 113
5.6.1 Theoretical framework . . . 113
5.6.2 Application 1: Gaussian and Wishart ensembles revisited . . . 115
5.6.3 Application 2: ERMs . . . 116
5.7 ERM $\mathrm{Im}G(\omega_0)$ in three-dimensional space . . . 117
5.7.1 Approximate solution for the eigenvalue density . . . 118
5.7.2 Exact solution for the eigenvalue density . . . 121
5.8 ERM $\mathrm{Re}G(\omega_0)$ in three-dimensional space . . . 124
5.8.1 Approximate solution for the eigenvalue density . . . 124
5.8.2 Exact solution for the eigenvalue density . . . 128
5.9 Work in progress and perspectives . . . 132

6 Non-Hermitian Euclidean random matrix theory 135
6.1 Foundations of the non-Hermitian random matrix theory . . . 136
6.1.1 Eigenvalue density and Hermitization . . . 136
6.1.2 Quaternions and the eigenvector correlator . . . 137
6.1.3 Bi-orthogonal basis of left and right eigenvectors . . . 139
6.2 Diagrammatic approach for non-Hermitian ERMs . . . 139

6.2.1 Derivation of self-consistent equations 139
6.2.2 Analysis of self-consistent equations 142
6.3 Other approaches 144
6.3.1 Mapping to the Dyson gas 144
6.3.2 Field representation 146
6.3.3 Free probability 147
6.4 Independent Re$G(\omega_0)$ and Im$G(\omega_0)$ 149
6.4.1 Analytical solutions for the resolvent and the eigenvector correlator 150
6.4.2 Scattering matrix and effective Hamiltonian 151
6.5 Eigenvalue density of the random Green's matrix $G(\omega_0)$ 153
6.5.1 Borderline of the eigenvalue domain 154
6.5.2 Hyperbolic spiral branches and subradiant states 162
6.5.3 Dyadic random Green's matrix 166
6.5.4 $G(\omega_0)$: eigenvalue density profile and projections 168
6.6 Green's matrix and Anderson localization in a finite and open medium . . 171
6.6.1 Statistics of resonances of the random Green's matrix 173
6.6.2 Inverse participation ratio 176
6.6.3 Scaling theory and the Green's matrix 177

7 Euclidean matrix theory of random lasing 181
7.1 Threshold in a cloud of cold atoms 181
7.1.1 Threshold condition 181
7.1.2 Threshold due to the 'bulk' of eigenvalues 185
7.1.3 Threshold due to the 'subradiant branch' 187
7.2 Behavior below and above threshold 188
7.2.1 Spectrum below threshold 188
7.2.2 Non-linear dynamics of laser emission and rate equations 190
7.2.3 Stationary solutions 192
7.2.4 Statistical treatment 194
7.3 Threshold for passive scatterers embedded in an amplifying medium . . . 197
7.3.1 Threshold condition 197
7.3.2 Eigenvalue distribution of an amplifying Green's matrix 198
7.3.3 Prediction for the lasing threshold 200
7.4 Conclusion and perspectives 202

Bibliography 203

List of publications 217

Chapter 1

Introduction: Random lasing in a nutshell

1.1 How can a laser be random?

A conventional laser is a device constructed from two essential elements: an active medium that amplifies light by stimulated emission, and a cavity that provides feedback. If the gain is sufficient to exceed the losses (due to partial reflections on the mirrors of the cavity, or absorption), the system reaches a threshold beyond which the properties of the emitted light are radically different from what can be observed below threshold. Three main signatures of laser light may be identified: (1) its high degree of monochromaticity, (2) its directionality and brightness and (3) the Poisson statistics of the number of emitted photons [1, 2]. These key properties of laser light follow from the special way of generating it, and in particular from the fact that the gain medium is placed in a cavity with a high quality factor. Narrow resonances of the cavity give rise to well-defined lasing modes, ensuring small fluctuations of the emitted field (first-oder temporal coherence). If the wave-front is well defined, light has also a good spatial coherence that may give rise to high directionality, eventually limited by diffraction. In addition, small fluctuations of the intensity (second-order coherence) are due to saturation of gain induced by nonlinear effects beyond threshold.

Obviously, if we remove the cavity of a laser, feedback is suppressed and lasing stops. A way to restore feedback is to introduce disorder in the active medium. We call 'random' a laser in which the feedback is provided by multiple scattering of light on the random heterogeneities of the active medium and not by a well-defined cavity [3, 4]. A random laser has completely open boundaries with strong coupling to the environment, and light can escape from the medium via any point on the boundaries, see Fig. 1.1. It should not be confused with chaotic cavity lasers which have well-defined reflecting boundaries with a few openings, and are characterized by chaotic ray dynamics [5].

Since the pioneering work of Letokhov and co-workers in the 1960's [6–8], lasing in disordered media has been the subject of various theoretical and experimental studies, with a resurgence of interest in the mid 1990's because of a possible relation to the phenomenon of Anderson localization [9]. The term 'random lasing' was actually introduced in 1995 [10]. In the course of the last decade, random lasing has been observed in different kinds of optically thick disordered materials: powders [11], polymer films [12], clusters [13], ceramics [14], porous materials [15], or colloidal solutions of nanoparticles [16, 17], and hence it can be regarded as a universal property of disordered structures

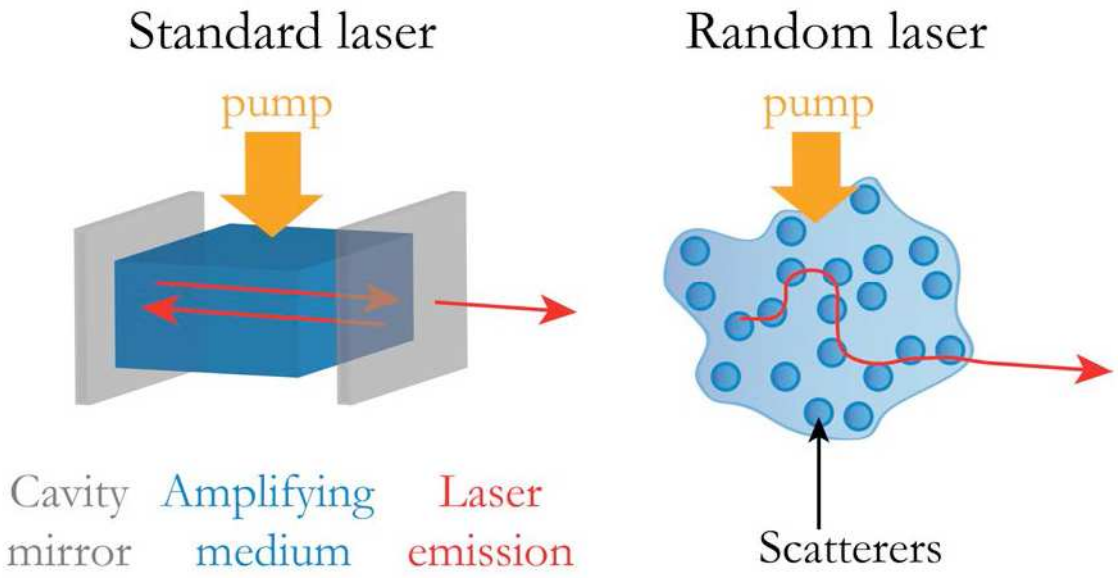

Figure 1.1: In a random laser, feeedback is provided by multiple scattering of light on the random heterogeneities (scatterers) of the amplifying medium.

(for a review see [3, 4]).

With the renewed experimental interest in random lasers, numerous attempts to generalize laser theory to such systems have been undertaken. In particular, two observations, that seemed at first sight contradictory, stimulated the elaboration of new theoretical models. On the one hand, the vast majority of experiments on random lasers were performed in the weak scattering regime (diffusive or quasi-ballistic regime), meaning that the modes (or resonances) of the passive disordered system strongly overlap, in contrast with a high-Q cavity laser. And on the other hand, sharp laser peaks were observed in the spectrum of light emitted by a random laser, that emerged one by one when increasing the pump above threshold. The situation was confusing because the common belief is that interference effects can be to some extent neglected in the diffusive regime[1], while the structure of sharp laser lines can be understood only if interferences in the multiple scattering are considered [3]. Various exotic scenarios were therefore originally proposed to explain the existence of sharp peaks. Most of them were based on 'rare events' that break away from the diffusive picture. It was suggested that the feedback is provided by closed trajectories formed by multiply scattered light [11]. Then, this picture was developed and the probability of having ring-shaped resonators with index of refraction higher than average (corresponding therefore to 'prelocalized states') was calculated; it was shown to be substantially increased by disorder correlation due to finite-size scatterers [18]. More recently, mechanisms involving breakdown of diffusion [19], or spontaneously emitted 'lucky photons' that travel much longer distances than the average ones [20] were put forward. As a result of the multiplication of the various possible scenarios, a simple comprehensive picture of random lasing was lacking.

In order to clarify the situation, it may be useful to make the following comments:

- Saying that a disordered system is in a diffusive regime does not mean that the

[1] If we disregard effects due to weak-localization corrections, such as, *e.g.*, coherent backscattering, the dynamics of light is well described by a diffusion equation for the average intensity (see chapter 4).

underlying modes of the system are inaccessible or irrelevant.

- Among all the resonances of an open system, modes supported by rare events are not *a priori* better candidates than modes giving rise to diffusion to explain both the laser threshold and the existence of sharp peaks above threshold.

- Although all the scenarios mentioned above may effectively arise in a random laser, identifying for each specific system the special configuration responsible for lasing is not really satisfactory: we would prefer a unified picture that tells us when the diffusion prediction is reliable and when and to which extent rare events need to be considered. Such a picture is briefly introduced in the next section.

At the present time, it seems accepted that a random laser is potentially a multimode system that has therefore to be treated within the framework of a complete multimode lasing theory [21, 22].

From a broader perspective, random lasers are usually considered to be difficult to describe analytically because several features must be treated with care: (1) saturation of the gain medium and nonlinearities of the coupled matter-field equations, (2) openness of the medium coupled to its environment, (3) interference effects that may play a role in all regimes of disorder, (4) quantum nature of the light-matter interaction. The goal of this thesis is to provide foundations of an *ab initio* analytic theory that correctly describes these different aspects. In the standard laser theory [23], the situation is simplified for two reasons: disorder is absent, and there is a well-defined cavity. Existence of the cavity has deep consequences, inasmuch as it allows to decouple the treatment of features (1), (2), and (4). Indeed, once a high-Q cavity is assumed, we already know almost everything about the nature of the modes that will support laser action. Therefore, there is no need for a refined description of the light-matter interaction, in the sense that both the openness of the cavity and quantum fluctuations are well captured by the introduction of a phenomenological bath for the laser modes (see [23] and section 2.2). This is in sharp contrast with random lasers, for which a modal theory (semiclassical or quantum) is still under construction [21, 22]. The result of our experience facing the problem of constructing an analytic random laser theory is that features (1)-(4) must not be considered as independent building blocks that we should properly adjust together. On the contrary, all these features should be seen as manifestations of a single well-defined problem: the light-matter interaction at a microscopic level. In this thesis, we shall see that starting from the very bottom of light matter-interaction naturally leads to a proper description of the openness of the system (and the non-Hermiticity that follows), as well as of quantum fluctuations.[2]

1.2 The first simple picture

There are two alternative ways to deal with the problem of light interacting with an arbitrary medium: either we pay attention to the light dynamics, and in that case we

[2]Complications may occur when trying to consider the problem the other way around. For example, if we wish to define an appropriate basis of modes to quantize the field in an open medium, using the Feshbach projection technique [24], we have to identify an interface between the open system and its environment, which is in general difficult (think of atoms distributed in free space with an arbitrary density), leading eventually to expressions for the modes that require a fair amount of computation to be constructed explicitly [21, 24–27].

attempt to work with a dynamical equation for the field or the intensity; or we focus on collective excitations of the 'light-matter' system (see section 2.4). We believe that keeping in mind these two faces of the light-matter coin — and confronting them as often as possible — is very fruitful. Let us consider both of them to get a first insight in the physics of random lasers, namely to study the laser transition.

In a standard laser, disorder is absent from the amplifying medium. Formally, this means that the transport mean free path $l_{\rm tr}$ is larger than the sample size R (see chapter 4). In that case, light propagation is described by the Helmholtz equation for the electric field. Interaction with matter (the gain medium) can be described by a source term in this equation that features polarization of the medium. Lasing starts when the gain (contained in the polarization term) exceeds losses due to absorption (also contained in the polarization) and to partial reflections on the mirrors of the cavity. Boundary conditions used to find the solutions of the propagation equation determine the latter source of loss. In this sense, the mode of the cavity that minimizes the loss is the first lasing mode. When we remove the mirrors surrounding the gain medium and add impurities (disorder), description of light propagation needs to be reconsidered because beyond $l_{\rm tr}$ the propagation direction of an emitted photon is lost and its phase is scrambled (see sections 4.3 and 4.5). If disorder is 'weak' and $R \gg l_{\rm tr}$, transport is well described by a diffusion equation for the average intensity. Again, a source term appears in this equation that features the gain provided by the amplifying matrix where the impurities are embedded. But contrary to the Helmholtz equation (which is time-reversal invariant), losses are now directly encompassed in the structure of the diffusion equation, since attenuation of the radiation occurs due to diffusion spreading. As realized by Lethokov a long time ago [7], there exists a threshold at which the radiation losses are compensated by the gain. If now we increase the strength of disorder, $l_{\rm tr}$ eventually becomes of the order of the wavelength of the propagating wave and the diffusive description breaks down. In oder to find the lasing threshold in this new situation, we could repeat the previous procedure: first establish a propagation-like equation, then look for its instability point. Rather than following this line, we would like to mention an inherent drawback of the preceding approaches used to determine the lasing threshold. The diffusion equation or any other dynamic equation for the average intensity is based on some assumptions about disorder, and for this reason may miss certain features of light propagation, such as, *e.g.*, the existence of rare events. In addition, even if the diffusion equation may predict the laser threshold properly in a certain regime of disorder, it cannot capture the mode structure of a random laser. In this situation, we may wonder whether a description of lasing valid for *any* realization of disorder exists. Such a description is precisely given by the 'collective excitation' picture (or 'modal' picture), that we now briefly discuss.

To be concrete, let us assume that the disordered medium is made of N scatterers of negligibly small size, such as atoms, distributed at fixed positions $\mathbf{r}_i$ in the gain medium. A possible way to characterize collective excitations of this system below threshold is to consider its scattering matrix. In a semiclassical description, we will show that the latter is given by

$$\mathcal{S}(\omega_L) \sim \frac{1}{\mathcal{A}(\omega_L)^{-1} - G(\omega_L)}, \tag{1.1}$$

where ω_L is the frequency of light, and the $N \times N$ non-Hermitian matrices $\mathcal{A}(\omega_L)$ and $G(\omega_L)$ are the 'polarizability matrix' and the 'Green's matrix'. The former is diagonal: the element $\mathcal{A}_{ii}(\omega_L) = \tilde{\alpha}_i(\omega_L)$ is proportional to the polarizability of the scatterer i featuring the linear response to the field. And the element ij of $G(\omega_L)$, $G_{ij}(\omega_L)$, is

proportional to the Green's function of the Hemholtz equation describing propagation of light between atoms i and j.[3] The general expression (1.1) applies for any number and configuration of atoms, any dimensionality of space, any polarizability, and any form of the Green's matrix that, in particular, can account for an external cavity and amplification or absorption of light in the space between the atoms. Very generally, the linear description breaks down and lasing starts when the scattering matrix 'diverges', *i.e.* when at least one eigenvalue of the matrix $G(\omega_L)\mathcal{A}(\omega_L)$ is equal to one.[4] In the absence of external cavity, the Green's function has no resonance in the frequency domain where atoms scatter strongly, that is in the vicinity of their atomic frequency ω_0 (we assume two-level atoms for simplicity). Hence, we can approximate $G(\omega_L)$ by $G(\omega_0)$.[5] Two different cases may be considered.

- First, let us assume that the scatterers (atoms) are passive, meaning that the gain is provided by their surrounding medium only. Then, Eq. (1.1) can be rewritten as
$$\mathcal{S}(\omega_L) \sim \frac{1}{\omega_L - H^e(\omega_0)}, \tag{1.2}$$
where H^e is the effective Hamiltonian of the system under study, simply related to the Green's matrix by $H_e = (\omega_0 - \mathrm{i}\Gamma_0/2)I_N - \Gamma_0 G(\omega_0)/2$ (Γ_0 is the natural linewidth of the atomic transition, and I_N is the identity matrix). In the absence of pump, the eigenvectors of H_e [and therefore of $G(\omega_0)$] are the modes (or quasi-modes, or quasi-bound sates) of the open system, and the corresponding complex eigenvalues are its 'resonances'. By virtue of causality, these resonances — that are identical to the poles $\omega_L \in \mathbb{C}$ of the $\mathcal{S}$-matrix (1.2) — are located in the lower half of the complex plane. When gain is progressively added to the amplifying medium, the form of the Green's matrix is modified, and the eigenvalues of the effective Hamiltonian H_e continuously shift in the complex plane. Lasing occurs when one of these eigenvalues reaches the real axis. In this picture, it is reasonable to think that the first lasing mode originates from the resonance that was the closest to the real axis in the absence of pump. This corresponds to the eigenvalue of $G(\omega_0)$ that had the smallest imaginary part. Intuitively, the larger is the distance from the real axis, the more it is necessary to pump in order to reach the threshold, and the more the spatial structure of the lasing mode at threshold will differ from what it was in the absence of pump [22]. The difficult task is therefore to understand, from a statistical point of view, how the poles of the $\mathcal{S}$-matrix (1.2), *i.e.* the eigenvalues of $G(\omega_0)$, are distributed in the complex plane. The analytic determination of this distribution is one of the topics treated in this manuscript.

- A second interesting case is the situation where scattering and gain are not independent, but due to the same atoms. For simplicity, let us assume that these atoms are distributed in free space. Formally, this means that the gain is not implemented in the Green's matrix $G(\omega_0)$ appearing in Eq. (1.1), but in the polarizability matrix

[3] We use here, for simplicity, a scalar approximation for the electromagnetic field. If the vector nature of the field is taken into account, $\mathcal{A}(\omega_L)$ and $G(\omega_L)$ are $3N \times 3N$ matrices, see section 4.2.

[4] For a more rigorous statement, see section 4.2.

[5] Note that in the following chapters, $G(\omega_0)$ will refer to the Green's matrix without gain medium between scatterers [the scalar Green's matrix in three-dimensional space is then given by Eq. (6.101)], while the Green's matrix for atoms embedded in a gain medium will be denoted $G_a(\omega_0)$ [Eq. (7.67)]. In this introduction, we do not distinguish between $G(\omega_0)$ and $G_a(\omega_0)$.

$\mathcal{A}(\omega_L)$, in contrast with the previous situation. If the pump providing the gain is spatially uniform [$\mathcal{A}_{ii}(\omega_L) = \tilde{\alpha}(\omega_L)$ for $i = 1, \ldots, N$], Eq. (1.1) reduces to

$$\mathcal{S}(\omega_L) \sim \frac{1}{1/\tilde{\alpha}(\omega_L) - G(\omega_0)}, \tag{1.3}$$

showing that lasing starts when one of the eigenvalue Λ_n of the free-space Green's matrix $G(\omega_0)$ satisfies $\Lambda_n = 1/\tilde{\alpha}(\omega_L)$. Now the gain [described by the polarizability $\tilde{\alpha}(\omega_L)$] is decoupled from geometry-dependent collective effects [quantified by the eigenvalues of $G(\omega_0)$]. As a result, different types of modes can trigger the lasing transition, depending on the specific model of polarizability. Quite strikingly, for the polarizability models considered in this thesis, we shall see that lasing modes are the eigenvectors of $G(\omega_0)$ that have the largest imaginary part, *i.e.* those that have, *in the absence of pump*, the largest decay rates. This situation is opposite to what we predicted above for passive scatterers embedded in an amplifying medium. Note also that the lasing modes [the eigenvectors of $\mathcal{A}(\omega_L)^{-1} - G(\omega_0)$ at threshold] are identical to the modes of the passive system [the eigenvectors of $G(\omega_0)$] only if the pump is spatially uniform. Statistical properties of the free-space Green's matrix $G(\omega_0)$ are studied in great details in chapter 6.

The modal picture presented above is perfectly adapted to describe the lasing threshold from the semiclassical point of view. It is able to predict the spatial structure of the modes, as well as their frequencies, whatever the density of atoms.[6] On the other hand, in order to characterize the nonlinear dynamics beyond threshold, as well as the quantum aspects of the light-matter interaction, a microscopic model is required.

Among the recent theoretical studies of random lasing, we can distinguish three different and complementary approaches. Vanneste, Sebbah, Cao and coworkers [22, 28, 29], as well as Jiang and Soukoulis [30], or Conti and Fratalocchi [31] investigated the nature of lasing modes and nonlinear effects beyond threshold by solving numerically Maxwell's equations coupled to rate equations of a four-level atomic system. This method is limited by the available computational resources and therefore mainly restricted to one- or two-dimensional geometries. An alternative approach, promoted under the name of 'ab initio self-consistent laser theory', was proposed by Türecci, Stone, Ge and coworkers [32–35]. It is based on the idea that lasing modes can be significantly different from the modes of the system in the absence of pump (the 'cold cavity') and must be determined self-consistently. The modes are found using an expansion on the so-called 'constant-flux' states that obey physical non-Hermitian boundary conditions. Neglecting population pulsation of the active medium allows one to take into account nonlinear interactions in all orders in the field intensity (see [22] for a recent review). The theory developed in [32–35] applies for a given realization of disorder, and as such it does not make any prediction about the statistical properties of random lasers. Statistical properties of random lasers with strong radiative losses were first studied by Hackenbroich [36], and then by Zaytsev, Deych and Shuvayev [37, 38] using a combination of *ad hoc* random matrix models with the Feshbach projection technique developed by Hackenbroich and coworkers [24–27, 36]. To some extent, these works were initially inspired by the study of

[6] Note that the spectral width of a mode above threshold is determined by the strength of the fluctuations acting on this mode. Ultimately, these fluctuations are of quantum nature. Therefore, the semiclassical picture without 'noise' predicts the spectral width which is zero, whatever the nature of the mode.

mode statistics in chaotic resonators [39]. For one-dimensional systems, modes following from the Feshbach projection technique can be calculated with a reasonable effort; their statistics was studied numerically in [40] (for a recent review see [21]).

All preceding approaches lack a proper statistical description of laser modes, their frequencies, and decay rates. They do not provide any well justified analytic theory for the statistical properties of a random laser. One goal of this thesis is to fill this gap. In particular, the analytic theory developed in chapter 6 for arbitrary non-Hermitian Euclidean random matrices, and illustrated with the problem of random lasing in chapter 7, is *a priori* applicable for any geometry or dimensionality of the problem.

1.3 Overview of the thesis

The physical system studied in this thesis is an ensemble of N atoms at random positions interacting with the electromagnetic field. A microscopic quantum description of this system is the subject of chapter 2, where coupled equations of motion for the electric field operator and atomic operators are derived. A particular effort is made to distinguish effects that are of purely quantum nature from those that may also arise in a simpler semiclassical formalism. In this respect, we decided to work in the Heisenberg picture rather than in the Schrödinger picture (section 2.2). We show, in particular, how the Green's function of the classical Helmholtz equation emerges in the quantum formalism. The Green's matrix, that couples different atoms and describes propagation of light between atoms is introduced (section 2.4.1), and the recent works where this matrix has already been encountered are reviewed (section 2.5).

The pump providing the gain necessary for lasing is introduced in chapter 3. Two simple but well justified pumping mechanisms are considered (section 3.2). They allow us to study in some details the intensity and the spectrum of light emitted by a cloud of atoms. In the case of two incoherently pumped atoms at rest in free space, we derive exact analytic solutions for both the intensity and the spectrum. While the semiclassical treatment predicts the existence of a sharp laser threshold (section 3.4), the full quantum treatment reveals that the semiclassical threshold is completely washed out (section 3.5). At the same time, we identify signatures of the Green's matrix in the spectrum of light. Using the formal approach developed in section 3.1, and taking into account quantum effects, we introduce a simple perturbative procedure to express the spectrum emitted below the lasing threshold by an arbitrary number of atoms in terms of the eigenvalues and eigenvectors of the Green's matrix (section 3.6). Properties of the quantum Langevin forces that naturally emerge in the equations of motion for the atomic operators are also discussed in section 3.3.

Chapter 4 is devoted to the semiclassical description of the properties of light emitted by an arbitrarily large number of pumped atoms randomly distributed in free space. After deriving a universal lasing threshold condition valid for any configuration of atoms (section 4.2), we present the statistical treatment of disorder. In particular, we provide a microscopic derivation of transport equation in the presence of gain, a situation that is not sufficiently well covered by the existing literature (section 4.5). Following the original idea of Letokhov, we discuss the lasing threshold inferred from the transport equation (section 4.6). Chapter 4 is the occasion to define and discuss familiar notions of the mesoscopic transport theory (scattering cross-section, extinction, scattering, and transport mean free paths, optical theorem, *etc.*). On the other hand, a mapping to the

properties of Euclidean random matrices is presented, allowing to make a link between diagrammatic techniques used in mesoscopic transport, and those developed in chapters 5 and 6 in the framework of random matrix theory (sections 4.4 and 4.6).

Facing the problem of characterizing analytically the statistical properties of the Green's matrix that belongs to the family of Euclidean random matrices (ERMs), we develop in chapters 5 and 6 a theory for arbitrary Hermitian and non-Hermitian ERMs in the limit of large matrix size. Since the eigenvalues of Hermitian matrices are constrained to the real axis, in contrast with non-Hermitian matrices, the two cases are considered separately. Self-consistent equations for the eigenvalue distribution of Hermitian ERMs are derived using two different methods (sections 5.5 and 5.6), and are applied to Hermitian ERMs that appear in the problem of wave propagation in three-dimensional random media (sections 5.7 and 5.8). These results are then generalized to the non-Hermitian case. We obtain self-consistent equations for the resolvent and the eigenvector correlator of non-Hermitian ERMs (section 6.2), and illustrate our approach by applying it to the three-dimensional free-space random Green's matrix (sections 6.5 and 6.6). From the physical point of view, we are able to describe analytically with a fair precision the full probability distribution of decay rates of light emitted by $N \gg 1$ atoms, as well as of the collective frequency shift induced by the light-matter interaction. In addition, we promote the idea that the eigenvalue distribution of the Green's matrix (eventually complemented with a distribution of the inverse participation ratio of the eigenvectors) can serve as a 'map' on which signatures of various regimes of disorder can be distinguished (ballistic, diffusive, localized, effective medium, and superradiance regimes), providing therefore a simple 'visual' and unified picture of these regimes. The distribution of eigenvalues in the complex plane may also be used to test 'visually' various approximations such as the diffusion approximation, a possibility that was never realized before.

Finally, we combine microscopic equations of motion introduced in chapters 2 and 3 with analytic results derived in chapter 6 for the random Green's matrix to study the problem of random lasing in a ensemble of a large number of identical atoms that both scatter and amplify light (chapter 7). We obtain analytic results for the lasing threshold (section 7.1) and the emitted intensity above threshold in the semiclassical limit, as well as for the spectrum of light emitted below threshold taking into account quantum effects (section 7.2.2). The case of more 'standard' random lasers in which scattering centers are embedded in an amplifying homogenous medium is briefly discussed as well (section 7.3).

In this thesis, a special effort was made to confront, combine or merge different concepts or theoretical tools shaped in various fields of physics (atomic physics and quantum optics, mesoscopic and statistical physics of disordered systems, random matrix theory, laser theory). Although we believe that the potential interest of this thesis comes from the confrontation of these different ways to look at the same problem, it may be helpful to suggest a 'non-exhaustive' way of reading this manuscript. For a reader interested in random laser physics exclusively, in a spirit following the lines of section 1.2, it is to some extent sufficient to read section 4.2 and chapter 7, eventually complemented with section 6.4.2 where we point out the link between the statistical properties of the Green's matrix and those of effective Hamiltonian used to analyze open chaotic systems. To get some insight into the properties of the Green's matrix, we could suggest to read sections 2.5, 6.5, and 6.6. In particular, we attract the attention of the reader to section 6.6, where we study the signatures of Anderson localization in the statistical properties of the Green's matrix. The reader more interested in quantum aspects of the light-matter

interaction may find basic and more advanced notions in chapters 2 and 3. Although chapters 5 and 6 are the most 'mathematical' chapters of this thesis, we try to introduce the reader to the field of random matrix theory and emphasize simple physical pictures whenever possible, as illustrated by the mapping to the Dyson gas (sections 5.3 and 6.3.1). Finally, inasmuch as the results discussed in this thesis are in some sense nicely 'visual', a lazy reader might still learn something by just looking at the figures of the manuscript.

Chapter 2

Light-matter interaction in a quantum framework

2.1 General Hamiltonian

Before discussing in details the coupled dynamics of the electromagnetic field and atoms, it is suitable to remind what are the cornerstones of electrodynamics that we will need. All the work presented in this manuscript deals with a system of charged spinless particles interacting with the field in the non-relativistic limit, and described by the so-called 'standard Lagrangian' [41]. This Lagrangian is built in such a way that Lagrange equations exactly reproduce the Maxwell-Lorentz equations. Then, redundant degrees of freedom are eliminated by fixing the gauge. For example, in the Coulomb gauge, the component of the electric field parallel to the propagation wave-vector is not an independent quantity. And finally, the identification of independent parameters allows to proceed to a canonical quantization of the light-matter field.

The Hamiltonian associated with the standard Lagrangian in the Coulomb gauge reads:

$$H = \sum_{\alpha} \frac{1}{2m_\alpha} \left[\mathbf{p}_\alpha - q_\alpha \mathbf{A}(\mathbf{r}_\alpha)\right]^2 + V^{Coul} + H_R, \tag{2.1}$$

where the sum runs over all the particles α in the system, of mass m_α, charge q_α, and momentum $\mathbf{p}_\alpha$. The first term, that in particular involves the magnetic vector potential $\mathbf{A}$, is the kinetic energy of the particles, whereas the second and the third are respectively the energy of the longitudinal and the transverse components of the field:

$$V^{Coul} = \sum_{\alpha} \left[\epsilon_\alpha^{Coul} + \frac{1}{8\pi\epsilon_0} \sum_{\beta\neq\alpha} \frac{q_\alpha q_\beta}{|\mathbf{r}_\alpha - \mathbf{r}_\beta|} \right], \tag{2.2}$$

$$H_R = \epsilon_0 \int \mathrm{d}^3\mathbf{r} \left[\mathbf{E}_\perp^2(\mathbf{r}) + c^2\mathbf{B}^2(\mathbf{r})\right] = \sum_{\mathbf{k}\boldsymbol{\epsilon}} \hbar\omega_{\mathbf{k}} (a_{\mathbf{k}\boldsymbol{\epsilon}}^+ a_{\mathbf{k}\boldsymbol{\epsilon}} + \frac{1}{2}). \tag{2.3}$$

The Coulomb energy of each particle, ϵ_α^{Coul}, formally diverges because the standard Lagrangian fails to describe properly the interaction of the particles with the relativistic modes of the field. Therefore, it is usually regularized with a cut-off $\hbar\omega_c \ll m_\alpha c^2$. Quantization is achieved by promoting the properly normalized independent variables to

operators. Provided we impose standard equal-time commutation relations, Heisenberg equations of motion of these variables lead to a quantum version of the Maxwell-Lorentz equations. The choice of the independent variables used to quantize the field depends very much on the geometry. For example, in free space (or in a cubic box of volume $\mathcal{V}$ with periodic boundary conditions), it is convenient to promote the spatial Fourier components of the field, which become the annihilation and creation operators, $a_{\mathbf{k}\epsilon}$ and $a^+_{\mathbf{k}\epsilon}$ of the modes $|\mathbf{k},\epsilon\rangle$. In such a basis, the energy of the transverse field has the standard form (2.3), where $\omega_{\mathbf{k}} = c|\mathbf{k}|$.

So far, we have not specified how the charged particles are spatially distributed. We will suppose that they are packed to form N identical atoms located at positions $\mathbf{r}_i$ $(i = 1, ..., N)$, whose spatial extent (a few Bohr radii) is much smaller than both the interatomic distance and the relevant wavelengths of the field that will propagate among them later on. Thus, the interatomic Coulomb interaction in $V^{Coul} = \sum_{i=1}^N V_i^{Coul} + \sum_{i\neq j}^N V_{i,j}^{Coul}$, can be approximated by a dipole-dipole coupling:

$$V_{i,j}^{Coul} \simeq V_{i,j}^{dip} + \frac{1}{3\epsilon_0}\mathbf{D}_i \cdot \mathbf{D}_j \delta(\mathbf{r}_i - \mathbf{r}_j), \tag{2.4}$$

where $\mathbf{D}_i = \sum_{\alpha_i} q_{\alpha_i}(\mathbf{r}_{\alpha_i} - \mathbf{r}_i)$ is the dipole operator of the atom i. The delta function carries the essential information about the actual finite charge distribution of the atoms. Its purpose is to yield the correct volume integral of the electric field radiated by the point-like dipoles [42].

To simplify further the problem, a unitary transformation $U = e^{-\mathrm{i}\sum_{i=1}^N \mathbf{D}_i\cdot\mathbf{A}(\mathbf{r}_i)/\hbar}$ is usually applied to the resulting Hamiltonian [41]. It modifies $\mathbf{p}_{\alpha_i} - q_{\alpha_i}\mathbf{A}(\mathbf{r}_i)$ in $\mathbf{p}_{\alpha_i}$, and the transverse electric field $\mathbf{E}_\perp(\mathbf{r})$ in $\mathbf{E}_\perp(\mathbf{r}) - \mathbf{P}(\mathbf{r})/\epsilon_0$, where $\mathbf{P}(\mathbf{r})$ is the polarization operator :

$$\mathbf{P}(\mathbf{r}) = \sum_{i=1}^N \mathbf{D}_i \delta(\mathbf{r} - \mathbf{r}_i). \tag{2.5}$$

Under this unitary transformation, the energy H_R of the free field becomes

$$H_R \to H_R - \sum_{i=1}^N \mathbf{D}_i \cdot \mathbf{E}_\perp(\mathbf{r}_i) + \sum_{i=1}^N \epsilon_i^{dip} - \sum_{i,j<i}^N V_{i,j}^{dip} + \frac{2}{3\epsilon_0}\sum_{i,j<i}^N \mathbf{D}_i \cdot \mathbf{D}_j \delta(\mathbf{r}_i - \mathbf{r}_j). \tag{2.6}$$

In this expression, ϵ_i^{dip} is again a diverging quantity :

$$\epsilon_i^{dip} = \frac{1}{2\epsilon_0\mathcal{V}}\sum_{\mathbf{k}\epsilon}(\epsilon\cdot\mathbf{D}_i)^2 = \frac{1}{2\epsilon_0\mathcal{V}}\mathbf{D}_i \cdot \sum_{\mathbf{k}} \mathbf{\Delta}_{\mathbf{k}}^\perp \mathbf{D}_i = \frac{1}{3\epsilon_0}\delta(\mathbf{0})\mathbf{D}_i^2, \tag{2.7}$$

where we have used the properties of the $\mathbf{k}$-transverse projector:

$$\mathbf{\Delta}_{\mathbf{k}}^\perp = \mathbf{I} - \frac{\mathbf{k}\otimes\mathbf{k}}{k^2} = \sum_{\epsilon\perp\mathbf{k}} \epsilon\otimes\epsilon. \tag{2.8}$$

Interestingly, the dipole coupling $V_{i,j}^{dip}$ appearing in Eq. (2.6) exactly compensates the regular component of $V_{i,j}^{Coul}$ in Eq. (2.4).

Collecting all the remaining terms, the Hamiltonian (2.1) is finally simplified into $H = H_0 + V$, where

$$H_0 = \sum_{i=1}^{N} \left(H_i^{at} + \epsilon_i^{dip} \right) + H_R, \tag{2.9}$$

$$V = -\sum_{i=1}^{N} \mathbf{D}_i \cdot \mathbf{E}_\perp(\mathbf{r}_i) + \frac{1}{2\epsilon_0} \sum_{i \neq j} \mathbf{D}_i \cdot \mathbf{D}_j \delta(\mathbf{r}_i - \mathbf{r}_j). \tag{2.10}$$

In H_0, H_i^{at} is the usual monoatomic Hamiltonian that contains external and internal degrees of freedom of an atom: $H_i^{at} = p_i^2/2m + \sum_{\alpha_i}(p_{\alpha_i}^2/2m_{\alpha_i} + \epsilon_{\alpha_i}^{Coul}) + V_i^{Coul}$. Equations (2.9) and (2.10) deserve three comments:

- In several textbooks and publications [43, 44], the δ contributions, ϵ_i^{dip} in Eq. (2.9) and the contact term in Eq. (2.10), are omitted. It is usually assumed that they only give rise to either divergent contributions that somehow can be incorporated in the Lamb shift, or do not play any physical role. In the following sections, we will see that it is not always true, especially when many modes of the field have to be taken into account to catch the relevant physics of light-matter interaction.

- Contrary to some common and naive belief, $H_R = \sum_{\mathbf{k}\boldsymbol{\epsilon}} \hbar\omega_{\mathbf{k}}(a_{\mathbf{k}\boldsymbol{\epsilon}}^+ a_{\mathbf{k}\boldsymbol{\epsilon}} + \frac{1}{2})$ in Eq. (2.9), is not the observable that represents the energy of the free field. This was only true in Eq. (2.1) before application of the unitary transformation. In the new picture, the free field is represented by the observable (2.6), that *seems* to mix atomic and electromagnetic degrees of freedom.

- In the same manner, the observable $\mathbf{E}_\perp$, which couples with the dipole i through $-\mathbf{D}_i \cdot \mathbf{E}_\perp(\mathbf{r}_i)$, does not stand for the free electric field. The free field is

$$\mathbf{E}(\mathbf{r}) = \mathbf{E}_\perp(\mathbf{r}) - \frac{1}{\epsilon_0}\mathbf{P}(\mathbf{r}). \tag{2.11}$$

  Despite the fact that $\mathbf{E}$ differs from $\mathbf{E}_\perp$ only at the atomic positions, it obeys a very different dynamical equation, as we will show in section 2.3.1.

It is important to insist on the two latter points. Whereas it is true that the Hamiltonian (2.9) is the observable for the atomic and electromagnetic energies without interaction, adding the coupling (2.10) means that the unitary transform U has been applied, and therefore Eq. (2.9) loses its simple interpretation. Saying that the interaction between field and atoms is represented by (2.10) is an oversimplified picture.

The state space $\mathcal{E}$ that supports the Hamiltonian given by Eqs. (2.9) and (2.10) contains the internal and external degrees of freedom of the N atoms, as well as those of the radiation, $\mathcal{E} = \otimes_{i=1}^{N} \left(\mathcal{E}_i^{A,in} \otimes \mathcal{E}_i^{A,ex} \right) \otimes \mathcal{E}^R$. Needless to say, we will explore only a very tiny part of this space, whose structure is tremendously complex. Since the physical motivation of this thesis is the comprehension of the emergence of a collective behaviour in the light-matter interaction, we would like to avoid the detailed description of some of the features of a realistic situation. We will mainly work within the following restrictions:

- We will treat the N atoms as distinguishable particles, and therefore disregard their bosonic or fermionic statistics.

- We will neglect effects due to atomic motion, such as the Doppler effect. This can be achieved either by fixing the atoms in a solid matrix or a tight trap, or by cooling the atoms to a sufficiently low temperature. Typically, for atoms with rms velocity $\sqrt{\langle v^2 \rangle}$ and interacting with light through a two-level transition of frequency $\omega_0 = ck_0$, this requires at least that $k_0\sqrt{\langle v^2 \rangle} \ll \Gamma_0$, with Γ_0 the natural linewidth of the transition. We will also neglect the atomic collisions. In practice, all external degrees of freedom will be disregarded.

- In the same spirit, the atomic structure will be assumed as simple as possible. We will consider hydrogen-like atoms, whose dipoles have the simple form $\mathbf{D}_i = -e\mathbf{R}_i$, with essentially two relevant levels g and e separated by a bare atomic frequency ω_0. For an atomic transition between a ground state g with angular momentum $J_g = 0$ and an excited state e with $J_e = 1$, we can show that $\epsilon_i^{dip} = \delta(\mathbf{0})\mathbf{D}_i^2/3\epsilon_0$ reduces to $(2d^2\delta(\mathbf{0})/3\epsilon_0\hbar)|e_{i,m}\rangle\langle e_{i,m}|$, where m labels the magnetic quantum number of the excited state, and $d = \langle e||\mathbf{D}||g\rangle/\sqrt{2J_e+1}$ [45, 46]. Restricting further the excited subspace to only one m value, $|e_{i,m}\rangle \equiv |e_i\rangle$, we end up with an effective two-level model without degeneracy that obeys:

$$H_i^{at} + \epsilon_i^{dip} = \hbar\left(\omega_0 + \delta\omega_0^{(1)}\right)|e_i\rangle\langle e_i|, \tag{2.12}$$

$$\delta\omega_0^{(1)} = \frac{2d^2}{3\epsilon_0\hbar}\delta(\mathbf{0}). \tag{2.13}$$

  To allow for a laser effect in this two-level model, we will have to specify a mechanism that creates a population inversion between the excited and the ground states. To this end, we will introduce in chapter 3 an auxiliary third level. We will show how such three-level atoms can nevertheless be reduced to effective two-level atoms.

2.2 Choice of a formalism

Consider N atoms at rest at random positions in free space, interacting with the electromagnetic field through the Hamitlonian given by Eqs. (2.9) , (2.10), and (2.12), and eventually excited by an auxiliary pump (described in chapter 3). The naive question we would like to address is formally well defined: what are the properties of the light emitted by this atomic system? Because different physical communities have been dealing with this question, it has a rather long and rich history.

In the 'atomic physics' community were developed, almost simultaneously in the fifties, two ideas that give an answer to our question : the *superradiance* and the *laser*. Indeed, the classical paper by Dicke on collective spontaneous emission [47] was published in 1954. And in 1955, Townes proposed a new device producing coherent microwaves based on the stimulated emission, the maser [48]. In their original forms these two new concepts were not related to the problem of multiple scattering of light.

At about the same time, in the late fifties, much attention was paid to the multiple scattering, not of light but of electrons in solids. In particular the concept of *Anderson localization* emerged in 1958 [9]. Roughly speaking, it took then almost twenty years for these new ideas related to multiple scattering to move from the 'condensed matter physics' community to the 'optical physics' community. Although the multiple scattering of light has become, since the eighties, an active area of research, the bridge with the quantum 'atomic physics' is still under construction [49].

The purpose of this section — and more generally of this manuscript — is to discuss how we can merge into a single formalism the tools of quantum atomic physics and those of mesoscopic physics. To fix the ideas, suppose we want to calculate the intensity $I(t)$ produced by the atomic cloud at time t. As we shall see in chapter 3, the intensity can be expressed as a combination of atomic operators, generically denoted by $O_A(t)$. Hence, the quantum expectation value of the intensity is obtained by tracing those operators $O_A(t)$ over all the degrees of freedom in the space state $\mathcal{E} = \mathcal{E}^A \otimes \mathcal{E}^R$:

$$\langle O_A(t)\rangle = \mathrm{Tr}_{A,R}\left[\sigma(t)O_A\right] = \mathrm{Tr}_A\left[\mathrm{Tr}_R[\sigma(t)]O_A\right] = \mathrm{Tr}_A\left[\sigma_A(t)O_A\right], \tag{2.14}$$

where $\sigma(t)$ is the density operator for the complete system 'atoms+radiation', and $\sigma_A(t) = \mathrm{Tr}_R[\sigma(t)]$ is the reduced density operator for the atomic subsytem. Eq. (2.14) shows us that, to infer the averaged intensity $\langle I(t)\rangle$, we simply need to calculate $\sigma_A(t)$.

When the radiation can be regarded as a reservoir (or bath) containing many degrees of freedom, $\sigma_A(t)$ is usually calculated within the framework of the 'system and bath' formalism [50–53]. Generally speaking, this approach is well adapted if the reservoir (here the radiation) R is not affected essentially by the presence of the atomic system A, whereas A, subject to bath kicks, evolves at two different time scales: a relaxation time T_R associated with a damping due to the averaged kicks, and a much smaller correlation time τ_c, characteristic of kick fluctuations. Formally, the dynamics has to fulfill the condition:

$$\tau_c \ll \left|\frac{\sigma_A(t)}{\mathrm{d}\sigma_A/\mathrm{d}t}\right| \lesssim T_R. \tag{2.15}$$

For a generic coupling of the form $V = O_A O_R$, τ_c is the typical width of the correlation function $g(t-t') = \langle O_R(t)O_R(t')\rangle$, whereas a rough estimation of T_R is [52]

$$T_R \sim \frac{\hbar^2}{\tau_c\,\langle V^2\rangle}. \tag{2.16}$$

For example, for a single two-level atom interacting with the vacuum modes, $\tau_c \sim \lambda_0/c$ and $T_R \sim 1/\Gamma_0$. The condition (2.15) allows to perform the so-called *Born-Markov approximation*, which is essentially a first-order expansion of the dynamics of $\sigma_A(t)$ with respect to the parameter $\sqrt{\langle V^2\rangle}\tau_c/\hbar$. At the evolution time-scale of $\sigma_A(t)$, all memory concerning the fluctuating kicks should be lost (it is a Markov process), as well as all quantum correlations with the bath (consequence of the Born approximation).

We would like to know if this density matrix approach can be used to describe a random laser. To make the discussion clear, we will first show how this formalism applies in both cases of collective spontaneous emission in the absence of pump (when the system size is small compared with the atomic wavelength, this process is called superradiance), and laser.

First, we consider N two-level atoms in free space, initially in their excited state, in the presence of the field in its vacuum state. We do not impose any restriction on the size of the volume containing the N atoms. The equation describing the transient dynamics of the reduced density matrix $\sigma_A(t)$ controlled by the Hamiltonian (2.9) and (2.10) was derived, wihtin the Born-Markov approximation, in 1970, independently by

Agarwal [54] and Lehmberg [55] :

$$\frac{\mathrm{d}\sigma_A}{\mathrm{d}t} = -\mathrm{i}\,\omega_0 \sum_{i=1}^{N} \left[S_i^+ S_i^-, \sigma_A\right] - \mathrm{i} \sum_{i\neq j}^{N} \Delta_{ij} \left[S_i^+ S_j^-, \sigma_A\right]$$
$$- \sum_{i,j}^{N} \Gamma_{ij} \left(S_i^+ S_j^- \sigma_A + \sigma_A S_i^+ S_j^- - 2 S_j^- \sigma_A S_i^+\right), \tag{2.17}$$

where $S_i^+ = |e_i\rangle\langle g_i|$ and $S_i^- = |g_i\rangle\langle e_i|$ are the atomic raising and lowering operators that define the two-level dipole operators $\mathbf{D}_i = \mathbf{d}_i(S_i^+ + S_i^-)$. This equation is rederived and discussed in great details in two very instructive reviews, in 1974 again by Agarwal [43], and in 1982 by Gross and Haroche [56]. In these publications, as well as in a couple of following ones in the nineties (see, *e.g.*, various papers studying in detail the case $N = 2$ [57–59]) or even very recently in 2008 [60], the coupling term Δ_{ij} is presented as a dipole-dipole interaction arising from the virtual photon exchange between pairs of atoms and Γ_{ij} as a source of collective damping. Actually, as it will become transparent in section 2.3, Δ_{ij} is simply the real part of the free-space Green's function of the Helmholtz equation propagating the field from atom i to atom j, whereas Γ_{ij} is its imaginary part [61].

A natural question arises: is the Born-Markov approximation, used to derive Eq. (2.17), valid for any number N of atoms and any size R or dimensionnality of the volume where atoms are confined? In other words, is the condition (2.15) satisfied? In the small sample limit $k_0 R \lesssim 1$ where 'perfect' superradiance occurs [47], since the maximum energy available is N times the single-atom excitation $\hbar\omega_0$, the temporal width of the transient superradiant (or superfluorescent) pulse must be inversionaly proportional to N, $T_R \sim 1/N\Gamma_0$. Actually, we can even show that $\min|\sigma_A/(\mathrm{d}\sigma_A/\mathrm{d}t)| \sim 1/N^2\Gamma_0$ [56]. Because $\tau_c \sim \lambda_0/c$, the condition (2.15) becomes $N \lesssim \sqrt{c/\lambda_0\Gamma_0}$, which is still roughly valid for $k_0 R > 1$, at least in a quasi-one-dimensional sample [56]. This imposes an upper limit to the number of atoms of the order of 10^4 ($\lambda_0 \sim 10^{-6}$ m, $\Gamma_0 \sim 10^8$ s^{-1}).

Another severe restriction follows from (2.15) if we imagine that an intense and quasi-monochromatic wave propagates or is generated in the atomic sample. For a coherent wave of spectral width $\Delta\omega$ and intensity I, we shall have $\tau_c \sim 1/\Delta\omega$ and $T_R \sim 1/I$, leading to a breakdown of the Born-Markov approximation. Hence, at first sight, it seems impossible to describe in such a way a laser, and *a fortiori* a random laser, where coherent modes do exist. In fact, a laser description in a 'system-bath' approach can still be achieved, provided we consider the laser modes as part of the system and not of the bath. Suppose that we study an ensemble of N two-level atoms pumped by a strong field and placed inside a cavity, the modes of which are well known. The Hamiltonian of such a system can be formally written as $H = H_{sys} + H_{sys/bath}$, with

$$H_{sys} = H^{at} + H^{modes} + V^{at/pump} + V^{at/modes}, \tag{2.18}$$
$$H_{sys/bath} = H_R + V^{at/R} + H_{R'} + V^{modes/R'}. \tag{2.19}$$

H_{sys} contains all degrees of freedom that we are interested in: those of atoms (H^{at}) interacting with the optical pump ($V^{at/pump}$) and the laser modes ($H^{modes} + V^{at/modes}$). On the other hand, we have put in $H_{sys/bath}$ all degrees of freedom that we want to trace out: all cavity modes that do not participate in the lasing process and constitute a bath (H_R) acting on the atoms ($V^{at/R}$), as well as a contribution that is purely phenomenological, a fictitious bath ($H_{R'}$) coupled to the laser modes ($V^{modes/R'}$). Clearly, there is

no such a term in the true 'atoms-field' Hamiltonian (2.9) and (2.10). It is introduced by hand to take care of the net effect, mediated by the atoms, of the bath of cavity modes on the laser field operators. The space state is therefore $\mathcal{E} = \mathcal{E}^S \otimes \mathcal{E}^R \otimes \mathcal{E}^{R'}$, with $\mathcal{E}^S = \mathcal{E}^A \otimes \mathcal{E}^{modes}$. The dynamics of the density matrix reduced to $\mathcal{E}^S$, σ_S, is then obtained again with a Born-Markov approximation:

$$\frac{\mathrm{d}\sigma_S}{\mathrm{d}t} = -\frac{\mathrm{i}}{\hbar}\left[H_{sys}, \sigma_S\right] + L^{at}\sigma_S + L^{modes}\sigma_S, \tag{2.20}$$

where the Lindblad operators, L^{at} and L^{modes}, are calculated as if the two baths were independent [23, 52, 62]:

$$L^{at}\sigma_S = -\sum_{i=1}^{N}\frac{\Gamma_0}{2}\left(S_i^+S_i^-\sigma_S + \sigma_S S_i^+S_i^- - 2S_i^-\sigma_S S_i^+\right), \tag{2.21}$$

$$L^{modes}\sigma_S = -\sum_{m=1}^{M}\kappa_m\left(a_m^+a_m^-\sigma_S + \sigma_S a_m^+a_m^- - 2a_m^-\sigma_S a_m^+\right), \tag{2.22}$$

with $a_m^\pm$ the annihilation and creation operators of the M cavity laser modes, and κ_m their respective damping rates. Within the master equation approach, Eqs. (2.20), (2.21), and (2.22) are, still today, the cornerstones of multimode laser theories [63–65].

Can we generalize the superradiant and laser master equations, (2.17) and (2.20), to describe a random laser? So far, we have formulated the following objections. First, we can doubt that the Born-Markov approximation is valid for a large number N of atoms, as we discussed for superradiance. Second, to apply this approach in the presence of coherent and intense modes, we have to know their structure in advance, as it is the case in a standard laser, where the modes are those of the cavity. In a random laser the problem is that the nature of the modes cannot be guessed because there is precisely no cavity. The introduction of a fictitious bath for hypothetic laser modes is a completely uncontrolled procedure in this context.

A more general objection can be formulated against a master equation approach. In general, the density matrix $\sigma_A(t)$ is a huge mathematical quantity with 2^{2N} elements (for two-level atoms), which gives the clue for the evaluation of any dipole correlation at equal times. Actually, if we are only interested in the intensity, we do not need that much information. Rather than writing the quantum expectation value of an atomic operator in the form (2.14), we can also express it in the Heisenberg picture as

$$\langle O_A(t)\rangle = \mathrm{Tr}_{A,R}\left[\sigma(0)O_A(t)\right]. \tag{2.23}$$

Hence, we can settle for calculating $O_A(t)$. Interestingly, moving from Schrödinger to Heisenberg picture is not as innocent as it may seem. Not only it will allow us to formulate random laser equations without any strong or uncontrolled approximations, but also it will recast the problem in a form for which semiclassical approximation becomes very intuitive. In this change of perspective, a simple equation for a complicated quantity, $\sigma_A(t)$, will be replaced by a set of coupled nonlinear equations for simple quantities, the atomic dipoles. This alternative between Schrödinger and Heisenberg pictures, which is to some extent similar to the duality between Fokker-Planck and Langevin equations in classical physics, clearly appears in the laser [23, 50, 53], as well as in the superradiance litterature [56]. More recently, it was also discussed in the study of coherent backscattering of light from cold atoms [66].

Our plan will be, therefore, as follows. First, we will derive Heisenberg equations, for the electric field as well as for atomic operators, that somehow generalize the well-known Maxwell-Bloch equations. And then, we will try to solve them in the presence of disorder, using tools developed either in mesoscopic or in statistical physics.

Before closing this section, it is important to mention a third option, different from the master equation and Heisenberg approaches, that can be followed to calculate the intensity radiated by the atomic system. It is the quantum scattering formalism, where the concept of effective Hamiltonian emerges rigorously. This will be briefly discussed at the end of section 2.4.2 .

2.3 Heisenberg equations of motion

In this section, we work with the Hamiltonian given by Eqs. (2.9), (2.10), and (2.12), that describes the dynamics of N two-level atoms (without degeneracy) interacting with the electromagnetic field, in the Coulomb gauge and the dipole approximation. We reproduce its expression for the reader's convenience:

$$H = \sum_{i=1}^{N} \hbar \left(\omega_0 + \delta\omega_0^{(1)}\right) |e_i\rangle\langle e_i| + \sum_{\mathbf{k},\boldsymbol{\epsilon}} \hbar\omega_{\mathbf{k}} \left(a^\dagger_{\mathbf{k}\boldsymbol{\epsilon}} a_{\mathbf{k}\boldsymbol{\epsilon}} + \frac{1}{2}\right)$$
$$- \sum_{i=1}^{N} \mathbf{D}_i \cdot \mathbf{E}_\perp(\mathbf{r}_i) + \frac{1}{2\epsilon_0} \sum_{i\neq j} \mathbf{D}_i \cdot \mathbf{D}_j \delta(\mathbf{r}_i - \mathbf{r}_j), \tag{2.24}$$

where the dipole operators have, in the two non-degenerate level approximation, the simple form:

$$\mathbf{D}_i = \mathbf{D}_i^+ + \mathbf{D}_i^- = \mathbf{d}_i(S_i^+ + S_i^-) = \mathbf{d}_i(|e_i\rangle\langle g_i| + |g_i\rangle\langle e_i|), \tag{2.25}$$

and the field operator $\mathbf{E}_\perp$ writes [41]:

$$\mathbf{E}_\perp(\mathbf{r}) = \mathrm{i} \sum_{\mathbf{k},\boldsymbol{\epsilon}} \mathcal{E}_{\mathbf{k}} \left(a_{\mathbf{k}\boldsymbol{\epsilon}} \boldsymbol{\epsilon}\, e^{\mathrm{i}\mathbf{k}\cdot\mathbf{r}} - a^\dagger_{\mathbf{k}\boldsymbol{\epsilon}} \boldsymbol{\epsilon}\, e^{-\mathrm{i}\mathbf{k}\cdot\mathbf{r}}\right), \tag{2.26}$$

where $\mathcal{E}_{\mathbf{k}} = \sqrt{\frac{\hbar\omega_{\mathbf{k}}}{2\epsilon_0 \mathcal{V}}}$ with $\mathcal{V}$ the quantization volume, and $\boldsymbol{\epsilon}$ a unit polarization vector orthogonal to $\mathbf{k}$ (we drop the corresponding subscript to simplify the notation). Once again, we stress that $\mathbf{E}_\perp$ is not the electric field. Instead, it stands for the electric displacement operator $\epsilon_0 \mathbf{E}_\perp$ [41], whereas the electric field is given by Eq. (2.11). Choosing the modes of a box of volume $\mathcal{V}$ to quantize the field is very convenient when the physical problem under study involves only a small number of these modes. This is particularly the case when we study a laser in a plane parallel resonator (a Fabry-Perot). For confocal resonators however, a quantization in terms of gaussian modes would be more appropriate [1, 2]. A question immediately shows up: is there a suitable basis for the random laser? In a naive picture, we can see the N atoms randomly distributed in space as a collection of more or less small cavities of various shapes. Hence, we expect that many modes $|\mathbf{k}, \boldsymbol{\epsilon}\rangle$ participate in the random lasing process. And there is practically no way to guess a basis that could be more adapted than another, since there is no spatial symmetry in the problem (see chapters 1 and 7 for a discussion about the modes of random lasers).

Therefore, the best strategy is, according to us, to abandon any modal decomposition at this stage. In other words, rather than looking at the interaction of each atom with each mode $|\mathbf{k},\epsilon\rangle$, we can directly focus on the interaction of each atom with the total electric field operator $\mathbf{E}$. This procedure is detailed in section 2.3.2. In the same manner, rather than looking at the dynamics of each mode separately, we can settle for the electric field dynamics. As we pointed out in section 2.1, the commutation relations adopted in the quantization procedure of the field are such that Heisenberg equations of motion lead to a quantum version of the Maxwell-Lorentz equations. With this in mind, we expect the field to obey a quantum version of the Helmholtz equation, with a source term involving the polarization (2.5). The explicit derivation of such equation is the subject of section 2.3.1.

2.3.1 Electric field dynamics

The idea consists in solving the Heisenberg equations of motion for operators $a_{\mathbf{k}\boldsymbol{\epsilon}}$,

$$\frac{\mathrm{d}a_{\mathbf{k}\boldsymbol{\epsilon}}}{\mathrm{d}t} = -\frac{\mathrm{i}}{\hbar}\left[a_{\mathbf{k}\boldsymbol{\epsilon}}(t), H\right] = -\mathrm{i}\,\omega_{\mathbf{k}} a_{\mathbf{k}\boldsymbol{\epsilon}}(t) + \frac{1}{\hbar}\sum_{i=1}^{N}\mathcal{E}_{\mathbf{k}}\mathbf{D}_i(t)\cdot\boldsymbol{\epsilon}e^{-\mathrm{i}\mathbf{k}\cdot\mathbf{r}_i}, \tag{2.27}$$

in order to express the transverse field $\mathbf{E}_\perp$ defined by Eq. (2.26) in terms of atomic dipoles only. By doing so in the frequency domain, the retarded transverse field, $\mathbf{E}_\perp(r,\omega_L) = \lim_{\eta\to 0^+}\int_{-\infty}^{\infty} dt e^{\mathrm{i}(\omega_L+\eta)t}\mathbf{E}_\perp(r,t)$, reads

$$\mathbf{E}_\perp(r,\omega_L) = \mathbf{E}_0(r,\omega_L) - \frac{1}{\hbar}\sum_{i=1}^{N}\sum_{\mathbf{k},\boldsymbol{\epsilon}}\mathcal{E}_{\mathbf{k}}^2\left(\frac{e^{\mathrm{i}\mathbf{k}\cdot(\mathbf{r}-\mathbf{r}_i)}}{\omega_L-\omega_{\mathbf{k}}+\mathrm{i}\eta} + \frac{e^{-\mathrm{i}\mathbf{k}\cdot(\mathbf{r}-\mathbf{r}_i)}}{-\omega_L-\omega_{\mathbf{k}}-\mathrm{i}\eta}\right)\left[\boldsymbol{\epsilon}_{\mathbf{k}}\otimes\boldsymbol{\epsilon}_{\mathbf{k}}\right]\mathbf{D}_i(\omega_L), \tag{2.28}$$

where $\mathbf{E}_0(r,\omega_L)$ is the Fourier transform of the free component of the electric field. In the absence of atoms, all modes contribute to the field $\mathbf{E}_0(r,t)$, oscillating according to their natural frequencies:

$$\mathbf{E}_0(\mathbf{r},t) = \mathrm{i}\sum_{\mathbf{k},\boldsymbol{\epsilon}}\mathcal{E}_{\mathbf{k}}\left(a_{\mathbf{k}\boldsymbol{\epsilon}}\boldsymbol{\epsilon}\,e^{\mathrm{i}(\mathbf{k}\cdot\mathbf{r}-\omega t)} - a^\dagger_{\mathbf{k}\boldsymbol{\epsilon}}\boldsymbol{\epsilon}\,e^{-i(\mathbf{k}\cdot\mathbf{r}-\omega t)}\right). \tag{2.29}$$

Inasmuch as we would like to show that the electric field is the solution of a propagation equation, it is convenient to rewrite Eq. (2.28) in the form

$$\mathbf{E}_\perp(\mathbf{r},\omega_L) = \mathbf{E}_0(\mathbf{r},\omega_L) + \frac{1}{\epsilon_0}\sum_{i=1}^{N}\mathbf{g}^\perp(\mathbf{r}-\mathbf{r}_i,\omega_L)\mathbf{D}_i(\omega_L), \tag{2.30}$$

with

$$\begin{aligned}
\mathbf{g}^\perp(\mathbf{r},\omega_L) &= -\sum_{\mathbf{k},\boldsymbol{\epsilon}}\frac{\omega_{\mathbf{k}}}{2\mathcal{V}}\left(\frac{e^{\mathrm{i}\mathbf{k}\cdot\mathbf{r}}}{\omega_L-\omega_{\mathbf{k}}+\mathrm{i}\eta} + \frac{e^{-\mathrm{i}\mathbf{k}\cdot\mathbf{r}}}{-\omega_L-\omega_{\mathbf{k}}-\mathrm{i}\eta}\right)\left[\boldsymbol{\epsilon}_{\mathbf{k}}\otimes\boldsymbol{\epsilon}_{\mathbf{k}}\right] \\
&= \int\frac{d\mathbf{k}}{(2\pi)^3}e^{\mathrm{i}\mathbf{k}\cdot\mathbf{r}}\frac{\omega_{\mathbf{k}}}{2}\left(\frac{1}{\omega_L-\omega_{\mathbf{k}}+\mathrm{i}\eta} + \frac{1}{-\omega_L-\omega_{\mathbf{k}}-\mathrm{i}\eta}\right)\boldsymbol{\Delta}^\perp_{\mathbf{k}} \\
&= \int\frac{d\mathbf{k}}{(2\pi)^3}e^{\mathrm{i}\mathbf{k}\cdot\mathbf{r}}\frac{-k^2}{k_L^2+\mathrm{i}\eta-k^2}\boldsymbol{\Delta}^\perp_{\mathbf{k}},
\end{aligned} \tag{2.31}$$

where $k_L = \omega_L/c$ and $\mathbf{\Delta}_{\mathbf{k}}^{\perp}$ is the $\mathbf{k}$-transverse projector (2.8). Anticipating what is to come, we mention that $\mathbf{g}^{\perp}$ is the Green's function of an equation satisfied by the transverse field $\mathbf{E}_{\perp}$.

We are now able to infer the equation obeyed by the total electric field given, according to Eq. (2.11), by:

$$\mathbf{E}(\mathbf{r}) = \mathbf{E}_{\perp}(\mathbf{r}) - \frac{1}{\epsilon_0}\sum_{i=1}^{N}\mathbf{D}_i\delta(\mathbf{r}-\mathbf{r}_i). \tag{2.32}$$

Inserting the expression (2.30) of the transverse field into this equation leads us to introduce a function $\mathbf{g}$, similar to $\mathbf{g}^{\perp}$, such that

$$\mathbf{E}(\mathbf{r},\omega_L) = \mathbf{E}_0(\mathbf{r},\omega_L) + \frac{1}{\epsilon_0}\sum_{i=1}^{N}\mathbf{g}(\mathbf{r}-\mathbf{r}_i,\omega_L)\mathbf{D}_i(\omega_L). \tag{2.33}$$

The spatial Fourier transform of the kernel function $\mathbf{g}$ is

$$\begin{aligned}\mathbf{g}(\mathbf{k},\omega_L) &= \mathbf{g}^{\perp}(\mathbf{k},\omega_L) - \mathbf{I}\\ &= \frac{-k^2}{k_L^2 + \mathrm{i}\eta - k^2}\mathbf{\Delta}_{\mathbf{k}}^{\perp} - \mathbf{I}\\ &= \frac{-k_L^2}{k_L^2 + \mathrm{i}\eta - k^2\mathbf{\Delta}_{\mathbf{k}}^{\perp}}.\end{aligned} \tag{2.34}$$

Since $k^2\mathbf{\Delta}_{\mathbf{k}}^{\perp}$ behaves in the reciprocal $\mathbf{k}$-space as does the operator $\nabla\times\nabla\times$ in real space, Eq. (2.34) shows that $\mathbf{g}(\mathbf{r},\omega_L)$ is, as expected, the retarded Green's function of the Helmholtz equation:

$$\left(-\nabla\times\nabla\times + k_L^2 + \mathrm{i}\eta\right)\mathbf{g}(\mathbf{r},\omega_L) = -k_L^2\mathbf{I}\,\delta(\mathbf{r}). \tag{2.35}$$

It is relatively easy to show that the solution of Eq. (2.35) in three-dimensionnal space reads

$$\mathbf{g}(\mathbf{r},\omega_L) = -\frac{1}{3}\delta(\mathbf{r})\mathbf{I} + k_L^2\frac{e^{\mathrm{i}k_L r}}{4\pi r}\left[P(\mathrm{i}k_L r)\mathbf{I} + Q(\mathrm{i}k_L r)\frac{\mathbf{r}\otimes\mathbf{r}}{r^2}\right], \tag{2.36}$$

with

$$\begin{aligned}P(x) &= 1 - \frac{1}{x} + \frac{1}{x^2},\\ Q(x) &= -1 + \frac{3}{x} - \frac{3}{x^2}.\end{aligned} \tag{2.37}$$

In particular, in the far-field, the radiation becomes $\mathbf{r}$-transverse:

$$\mathbf{g}(\mathbf{r},\omega_L) \underset{r\to\infty}{\sim} k_L^2\frac{e^{\mathrm{i}k_L r}}{4\pi r}\mathbf{\Delta}_{\mathbf{r}}^{\perp}. \tag{2.38}$$

Finally, combining the solution (2.33) with Eq. (2.35), we infer the dynamical equation satisfied by the electric field operator:

$$\nabla\times\nabla\times\mathbf{E}(\mathbf{r},t) + \frac{1}{c^2}\partial_t^2\mathbf{E}(\mathbf{r},t) = -\frac{1}{\epsilon_0 c^2}\partial_t^2\mathbf{P}(\mathbf{r},t), \tag{2.39}$$

where $P(\mathbf{r},t)$ is the polarization associated with the N atomic point-like dipoles, already defined in Eq. (2.5). Note that Eq. (2.39) can equivalently be rewritten as

$$\Delta\mathbf{E}(\mathbf{r},t) - \frac{1}{c^2}\partial_t^2\mathbf{E}(\mathbf{r},t) = \frac{1}{\epsilon_0 c^2}\partial_t^2\mathbf{P}(\mathbf{r},t) - \frac{1}{\epsilon_0}\nabla\otimes\nabla\mathbf{P}(\mathbf{r},t). \tag{2.40}$$

Interestingly, although the Green's function $\mathbf{g}_\perp$ characterizing the transverse field $\mathbf{E}_\perp$ in Eq. (2.30) differs trivially from $\mathbf{g}$, the dynamics of $\mathbf{E}_\perp$ is substantially different from that of $\mathbf{E}$. In particular, the source term in the equation for $\mathbf{E}_\perp$ does not involve any temporal derivative of the polarization:

$$\Delta\mathbf{E}_\perp(\mathbf{r},t) - \frac{1}{c^2}\partial_t^2\mathbf{E}_\perp(\mathbf{r},t) = -\frac{1}{\epsilon_0}\Delta\mathbf{P}_\perp(\mathbf{r},t), \tag{2.41}$$

where $\mathbf{P}_\perp$ is the transverse component of the polarization:

$$\mathbf{P}_\perp(\mathbf{r},t) = \int\frac{d\mathbf{k}}{(2\pi)^3}e^{\mathrm{i}\mathbf{k}\cdot\mathbf{r}}\boldsymbol{\Delta}_\mathbf{k}^\perp\mathbf{P}(\mathbf{k},t). \tag{2.42}$$

Note also that the transverse field $\mathbf{E}_\perp$ does not coincide with the transverse component of the electric field $\mathbf{E}$, because the polarization, that makes the link between them in Eq. (2.32), is not longitudinal.

The propagation equation (2.39) is the quantum version of the standard wave equation in classical optics [42]. In its full quantum form, it rarely appears in the literature, presumably because the study of optical quantum properties in a medium without simple spatial symmetry (like a regular cavity) is not a very popular topic. That said, equations similar to (2.39) show up in some studies devoted, for example, to superradiance [56, 67] (where $\mathbf{E}_\perp$ and $\mathbf{E}$ are often confused), to the quantized motion of atoms in laser field [68], or to the propagation of quantum fields under conditions of the electromagnetically induced transparency [69].

2.3.2 Dynamics of atomic variables

2.3.2.a Rotating wave approximation

To calculate the evolution of atomic variables we will slightly simplify the Hamiltonian (2.24) by means of the so-called Rotating wave approximation (RWA). Its justification requires decomposition of the electric field in its positive and negative frequency parts [70, 71], $\mathbf{E}(\mathbf{r},t) = \mathbf{E}^+(\mathbf{r},t) + \mathbf{E}^-(\mathbf{r},t)$, with

$$\mathbf{E}^+(\mathbf{r},t) = \int_0^\infty\frac{\mathrm{d}\omega_L}{2\pi}\mathbf{E}(\mathbf{r},\omega_L)e^{-\mathrm{i}\omega_L t}, \tag{2.43}$$

and $\mathbf{E}^-(\mathbf{r},t) = [\mathbf{E}^+(\mathbf{r},t)]^\dagger$, or equivalently $\mathbf{E}^-(\mathbf{r},\omega) = [\mathbf{E}^+(\mathbf{r},-\omega)]^\dagger$ since $\mathbf{E}$ is Hermitian. In the same manner, we define $\mathbf{E}_\perp^+$ and $\mathbf{E}_\perp^-$, as well as $\mathbf{E}_0^+$ and $\mathbf{E}_0^-$. We now observe that, because of Eq. (2.29), the positive frequency part of the free field is given, in the plane-wave basis, by

$$\mathbf{E}_0^+(\mathbf{r},t) = \mathrm{i}\sum_{\mathbf{k},\boldsymbol{\epsilon}}\mathcal{E}_\mathbf{k}a_{\mathbf{k}\boldsymbol{\epsilon}}\boldsymbol{\epsilon}\,e^{\mathrm{i}(\mathbf{k}\cdot\mathbf{r}-\omega t)}. \tag{2.44}$$

We will assume that such a relation also holds in the presence of atoms, which means that

$$\mathbf{E}_\perp^+(\mathbf{r},t) = \mathrm{i}\sum_{\mathbf{k},\boldsymbol{\epsilon}}\mathcal{E}_\mathbf{k}a_{\mathbf{k}\boldsymbol{\epsilon}}(t)\boldsymbol{\epsilon}\,e^{\mathrm{i}\mathbf{k}\cdot\mathbf{r}}. \tag{2.45}$$

Furthermore, in Eq. (2.25) we introduced the atomic raising and lowering operators, which, logically, define the raising and lowering components of the polarization (2.5):

$$\mathbf{P}^+(\mathbf{r},t) = \sum_{i=1}^{N} \mathbf{D}_i^+(t)\delta(\mathbf{r}-\mathbf{r}_i), \tag{2.46}$$

and $\mathbf{P}^-(\mathbf{r},t) = [\mathbf{P}^+(\mathbf{r},t)]^\dagger$. Unfortunately, this notation does not coincide with the definition of the frequency components that we used for the field. Actually, as it will soon become clear from atomic Heisenberg equations, $\mathbf{P}^+(\mathbf{r},t)$ turns out to be the negative frequency component of the polarization. This is true when atoms evolve freely, and again we will assume that this holds in the presence of interaction with the field. Therefore, the positive frequency part of the total electric field (2.11) reads

$$\mathbf{E}^+(\mathbf{r},t) = \mathbf{E}_\perp^+(\mathbf{r}) - \frac{1}{\epsilon_0}\sum_{i=1}^{N} \mathbf{D}_i^-(t)\delta(\mathbf{r}-\mathbf{r}_i). \tag{2.47}$$

Moreover, the positive frequency part of the propagation equation (2.39) leads to the analog of Eq. (2.33):

$$\mathbf{E}^+(r,\omega_L) = \mathbf{E}_0^+(r,\omega_L) + \frac{1}{\epsilon_0}\sum_{i=1}^{N} \mathbf{g}(\mathbf{r}-\mathbf{r}_i,\omega_L)\mathbf{D}_i^-(\omega_L), \tag{2.48}$$

where, we recall, $\mathbf{g}$ is the retarded Green's function of the Helmholtz equation (2.35).

We are now able to introduce RWA. It consists in neglecting highly oscillatory terms that appear in the two contributions $(\mathbf{D}_i^+ + \mathbf{D}_i^-)\cdot\left[\mathbf{E}_\perp^+(\mathbf{r}_i) + \mathbf{E}_\perp^-(\mathbf{r}_i)\right]$ and $(\mathbf{D}_i^+ + \mathbf{D}_i^-)\cdot(\mathbf{D}_i^+ + \mathbf{D}_i^-)$ of the Hamiltonian (2.24). Provided that the typical frequencies ω_L of the field which will contribute to the random laser process are close to the atomic frequency ($|\omega_L - \omega_0| \ll \omega_0$), we can simplify the Hamiltonian (2.24) into a form where non-resonant contributions have been disregarded:

$$\begin{aligned} H = &\sum_{i=1}^{N} \hbar\left(\omega_0 + \delta\omega_0^{(1)}\right)|e_i\rangle\langle e_i| + \sum_{\mathbf{k},\boldsymbol{\epsilon}} \hbar\omega_{\mathbf{k}}(a_{\mathbf{k}\boldsymbol{\epsilon}}^\dagger a_{\mathbf{k}\boldsymbol{\epsilon}} + \frac{1}{2}) \\ &- \sum_{i=1}^{N}\left[\mathbf{D}_i^+\cdot\mathbf{E}_\perp^+(\mathbf{r}_i) + \mathbf{D}_i^-\cdot\mathbf{E}_\perp^-(\mathbf{r}_i)\right] + \frac{1}{\epsilon_0}\sum_{i\neq j}^{N} \mathbf{D}_i^+\cdot\mathbf{D}_j^-\delta(\mathbf{r}_i-\mathbf{r}_j). \end{aligned} \tag{2.49}$$

It is worth noting that we did not made use of the RWA to derive the quantum wave equation (2.39). If we selected only the resonant term of the positive frequency part in Eq. (2.28), we would have found a solution of the form (2.48), but with the Green's function $\mathbf{g}$ replaced by its imaginary part. This means that non-resonant contributions are essential as far as the field is concerned: without them we would not be able to recover the standard wave equation in the semiclassical limit.

2.3.2.b Dipole and population imbalance dynamics

Internal degrees of freedom of N two-level atoms without degeneracy are entirely characterized by a set of $2N$ operators. We can choose, for example, the dipole raising operator and the population imbalance of each atom:

$$\begin{aligned} &\mathbf{D}_i^+ = \mathbf{d}_i S_i^+ = \mathbf{d}_i|e_i\rangle\langle g_i| = d\,\widetilde{\mathbf{D}}_i^+ = d\,\widetilde{\mathbf{d}}_i|e_i\rangle\langle g_i|, \\ &\Pi_i = |e_i\rangle\langle e_i| - |g_i\rangle\langle g_i|. \end{aligned} \tag{2.50}$$

When computing Heisenberg equations of motion for these operators we shall keep in mind that, whereas any atomic operator commutes at equal time with the components $\mathbf{E}^{\pm}_{\perp q}$ of the transverse field (2.26), it is not always the case for the electric field (2.11):

$$\begin{aligned} \left[\mathbf{D}_i^{\pm}(t), \mathbf{E}^{\pm}_{\perp q}(\mathbf{r},t)\right] &= 0, & \left[\Pi_i(t), \mathbf{E}^{\pm}_{\perp q}(\mathbf{r},t)\right] &= 0, \\ \left[\mathbf{D}_i(t), \mathbf{E}_q(\mathbf{r},t)\right] &= 0, & \left[\Pi_i(t), \mathbf{E}_q(\mathbf{r},t)\right] &\neq 0, \\ \left[\mathbf{D}_i^{\pm}(t), \mathbf{E}^{\pm}_q(\mathbf{r},t)\right] &\neq 0, & \left[\Pi_i(t), \mathbf{E}^{\pm}_q(\mathbf{r},t)\right] &\neq 0. \end{aligned} \tag{2.51}$$

Under the action of the Hamiltonian (2.49), the dipole raising operator of atom i oscillates according to

$$\frac{\mathrm{d}\mathbf{D}_i^+}{\mathrm{d}t} = \mathrm{i}(\omega_0 + \delta\omega_0^{(1)})\mathbf{D}_i^+ + \frac{\mathrm{i}}{\hbar}\left[\mathbf{d}_i \otimes \mathbf{d}_i\right]\mathbf{E}_\perp^-(\mathbf{r}_i)\Pi_i - \frac{\mathrm{i}}{\epsilon_0\hbar}\left[\mathbf{d}_i \otimes \mathbf{d}_i\right]\sum_{j\neq i}^{N}\mathbf{D}_j^+\delta(\mathbf{r}_i - \mathbf{r}_j)\Pi_i. \tag{2.52}$$

In this equation we can force the field $\mathbf{E}^-$ to appear by expressing it through $\mathbf{E}_\perp^-$ using Eq. (2.47). In this operation, a new diverging frequency shift $\delta\omega_0^{(2)}$ emerges:

$$\frac{\mathrm{d}\mathbf{D}_i^+}{\mathrm{d}t} = \mathrm{i}(\omega_0 + \delta\omega_0^{(1)} + \delta\omega_0^{(2)})\mathbf{D}_i^+ + \frac{\mathrm{i}}{\hbar}\left[\mathbf{d}_i \otimes \mathbf{d}_i\right]\mathbf{E}^-(\mathbf{r}_i)\Pi_i, \tag{2.53}$$

with

$$\delta\omega_0^{(2)} = -\frac{d^2}{\epsilon_0\hbar}\delta(\mathbf{0}). \tag{2.54}$$

Note that we have chosen to write Eq. (2.53) in the normal order [71], namely with $\mathbf{E}^-$ appearing on the left side of Π_i. Actually, as we will see in the following, this choice is the most convenient to get the semiclassical limit of Heisenberg equations [72]. With the antinormal order, the shift $\delta\omega_0^{(2)}$ would be replaced by its opposite in Eq. (2.53):

$$\frac{\mathrm{d}\mathbf{D}_i^+}{\mathrm{d}t} = \mathrm{i}(\omega_0 + \delta\omega_0^{(1)} - \delta\omega_0^{(2)})\mathbf{D}_i^+ + \frac{\mathrm{i}}{\hbar}\Pi_i(\mathbf{d}_i \otimes \mathbf{d}_i)\mathbf{E}^-(\mathbf{r}_i). \tag{2.55}$$

On the other hand, the Heisenberg equation satisfied by the population imbalance is

$$\frac{\mathrm{d}\Pi_i}{\mathrm{d}t} = \frac{2\mathrm{i}}{\hbar}\left[\mathbf{D}_i^+ \cdot \mathbf{E}_\perp^+(\mathbf{r}_i) - \mathbf{E}_\perp^-(\mathbf{r}_i)\cdot\mathbf{D}_i^-\right] + \frac{2\mathrm{i}}{\epsilon_0\hbar}\sum_{j\neq i}^{N}\left(\mathbf{D}_i^+\cdot\mathbf{D}_j^- - -\mathbf{D}_j^+\cdot\mathbf{D}_i^-\right), \tag{2.56}$$

which takes a simpler form if we express it in terms of the electric field :

$$\frac{\mathrm{d}\Pi_i}{\mathrm{d}t} = \frac{2\mathrm{i}}{\hbar}\left[\mathbf{D}_i^+ \cdot \mathbf{E}^+(\mathbf{r}_i) - \mathbf{E}^-(\mathbf{r}_i)\cdot\mathbf{D}_i^-\right]. \tag{2.57}$$

Again, we choose here the normal order. However, although $\left[\mathbf{D}_i^{\pm}(t), \mathbf{E}^{\pm}_q(\mathbf{r},t)\right] \neq 0$, this equation looks formally the same in the antinormal order because the two commutators compensate each other.

There are reasons for not being entirely satisfied by the dynamical equations of motion (2.53) and (2.57). First, because we would like to get rid of diverging shifts $\delta\omega_0^{(1)}$ and $\delta\omega_0^{(2)}$. Second, because we would like to see explicitly the relaxation rate of atomic operators that we are familiar with. In fact, all this information is implicitly contained in the electric field, as we now show.

2.3.2.c Own radiation field, Lamb shift and spontaneous emission

As it is clear from expression (2.33), the electric field contains a contribution generated by the N atoms. In particular, each atom radiates a field towards all atoms including himself. The latter contribution $\mathbf{g}(\mathbf{0})\mathbf{D}_i/\epsilon_0$ is apparently pathologic since it diverges. Because we want to emphasize its role in equations of motion, we define a 'smoothed' electric field:

$$\mathbf{E}_s(r,\omega_L) = \mathbf{E}(r,\omega_L) - \frac{1}{\epsilon_0}\mathbf{g}(\mathbf{0},\omega_L)\sum_{i=1}^{N}\mathbf{D}_i(\omega_L)\delta_{\mathbf{r},\mathbf{r}_i}, \tag{2.58}$$

so that, at the position $\mathbf{r}_i$ of atom i, it becomes

$$\mathbf{E}_s^+(r_i,\omega_L) = \mathbf{E}_0^+(r_i,\omega_L) + \frac{1}{\epsilon_0}\sum_{j\neq i}^{N}\mathbf{g}(\mathbf{r}-\mathbf{r}_i,\omega_L)\mathbf{D}_j^-(\omega_L). \tag{2.59}$$

Assuming that $\mathbf{g}(\mathbf{0},\omega_L) \simeq \mathbf{g}(\mathbf{0},\omega_0)$ (which is consistent with RWA), we replace in Eqs. (2.53) and (2.57) the field $\mathbf{E}(r_i,t)$ by its decomposition inferred from Eq. (2.58). We obtain

$$\frac{\mathrm{d}\mathbf{D}_i^+}{\mathrm{d}t} = \mathrm{i}\left[\omega_0 + \delta\omega_0^{(1)} + \delta\omega_0^{(2)} - \frac{d^2}{\epsilon_0\hbar}\mathbf{g}^*(\mathbf{0},\omega_0)\right]\mathbf{D}_i^+ + \frac{\mathrm{i}}{\hbar}\left[\mathbf{d}_i\otimes\mathbf{d}_i\right]\mathbf{E}_s^-(\mathbf{r}_i)\Pi_i, \tag{2.60}$$

$$\frac{\mathrm{d}\Pi_i}{\mathrm{d}t} = \frac{2\mathrm{i}}{\hbar}\left[\mathbf{D}_i^+\cdot\mathbf{E}_s^+(\mathbf{r}_i) - \mathbf{E}_s^-(\mathbf{r}_i)\cdot\mathbf{D}_i^-\right] - \frac{2d^2}{\epsilon_0\hbar}\mathrm{Im}\left[\mathbf{g}(\mathbf{0},\omega_0)\right](\Pi_i+1). \tag{2.61}$$

We now take advantage of the relation between the singularity of the Green's function, $\mathbf{g}(\mathbf{0},\omega_0)$, and the monoatomic Lamb shift $\Delta\omega_0$ and natural line width Γ_0 calculated in the gauge '$\mathbf{A}\cdot\mathbf{p}$' without the RWA [45, 52]:

$$-\frac{d^2}{\epsilon_0\hbar}\mathbf{g}^*(\mathbf{0},\omega_0) = \Delta\omega_0 + \mathrm{i}\frac{\Gamma_0}{2} + \delta\omega_0^{(3)}, \tag{2.62}$$

with

$$\delta\omega_0^{(3)} = \frac{d^2}{3\epsilon_0\hbar}\delta(\mathbf{0}). \tag{2.63}$$

Therefore, apart from the Lamb shift $\Delta\omega_0$, the diverging contributions in Eq. (2.60) are $\delta\omega_0^{(1)}$, $\delta\omega_0^{(2)}$ and $\delta\omega_0^{(3)}$. Their explicit expressions given by Eqs. (2.13), (2.54), and (2.63) reveal that they nicely compensate each other:

$$\delta\omega_0^{(1)} + \delta\omega_0^{(2)} + \delta\omega_0^{(3)} = 0. \tag{2.64}$$

This is an indirect proof of the consistency of our approach. Thanks to the decomposition (2.58) we evacuate all monoatomic quantum subtleties that could bother us later. We finally obtain the atomic equations of motion in their useful form

$$\frac{\mathrm{d}\mathbf{D}_i^+}{\mathrm{d}t} = \mathrm{i}(\omega_0+\Delta\omega_0)\mathbf{D}_i^+ - \frac{\Gamma_0}{2}\mathbf{D}_i^+ + \frac{\mathrm{i}}{\hbar}\left[\mathbf{d}_i\otimes\mathbf{d}_i\right]\mathbf{E}_s^-(\mathbf{r}_i)\Pi_i, \tag{2.65}$$

$$\frac{\mathrm{d}\Pi_i}{\mathrm{d}t} = -\Gamma_0(\Pi_i+1) + \frac{2\mathrm{i}}{\hbar}\left[\mathbf{D}_i^+\cdot\mathbf{E}_s^+(\mathbf{r}_i) - \mathbf{E}_s^-(\mathbf{r}_i)\cdot\mathbf{D}_i^-\right]. \tag{2.66}$$

We recall that these equations are written in the normal order. Equivalent equations in the antinormal order look less intuitive. For example, Eq. (2.66) is formally the same as

$$\frac{\mathrm{d}\Pi_i}{\mathrm{d}t} = \Gamma_0(\Pi_i-1) + \frac{2\mathrm{i}}{\hbar}\left[\mathbf{E}_s^+(\mathbf{r}_i)\cdot\mathbf{D}_i^+ - \mathbf{D}_i^-\cdot\mathbf{E}_s^-(\mathbf{r}_i)\right], \tag{2.67}$$

where it *seems* that the population imbalance spontaneously diverges instead of decaying as it is the case in Eq. (2.66). To clarify this point, let us consider the somehow trivial situation where only one atom interacts with the field. In that case the smoothed field reduces to its free component, $\mathbf{E}_s^{\pm} = \mathbf{E}_0^{\pm}$. Suppose also the radiation initially in its vacuum state $|0_R\rangle$. Since, according to Eq. (2.29), $\langle 0_R|\mathbf{E}_0^- = 0$ and $\mathbf{E}_0^+|0_R\rangle = 0$, $\mathbf{E}_0^{\pm}$ does not contribute to the quantum expectation value of Eqs. (2.65) and (2.66) in the vacuum state. Consequently, in the normal order picture, spontaneous emission as well as the Lamb shift *seem* exclusively due to the own radiation field — as indicated by Eq. (2.62) — and not to the 'vacuum fluctuations'. However, this interpretation breaks down in the antinormal order picture, where terms involving $\mathbf{E}_0^{\pm}$ do not vanish. For example, in the expectation value of (2.67), the vacuum fluctuations (namely $\mathbf{E}_0^{\pm}$) are primordial to restore the proper decay rate. As pointed out in [73], the two interpretations are "merely two sides of the same quantum-mechanical coin, with each [...] being an oversimplification motivated by the ordering scheme adopted". We finally report that in [72], Cohen-Tannoudji proposes to use neither the normal nor the antinormal but the symmetric picture, where both the own radiation field and the vacuum fluctuations are responsible for the Lamb shift and spontaneous emission.

Atomic equations of motion (2.65) and (2.66) — or Eqs. (2.53) and (2.57) — together with Eq. (2.39) — or Eq. (2.59) — form a closed set that contains all the information necessary to infer the dynamics of both the field and the internal atomic degrees of freedom. Equations of this type are sometimes called 'Maxwell-Bloch equations' [56, 67]. We stress again that the field coupled to atoms in Eqs. (2.65) and (2.66) is not the total electric field $\mathbf{E}$ that appears in the wave equation (2.39), but only its smoothed part $\mathbf{E}_s$. In the computation of the atomic polarizability in chapter 4, we shall see that this seemingly technical detail might have non trivial consequences. The physical content of these coupled equations as well as the strategy to solve them is the subject of the next section.

2.4 Microscopic and mesoscopic pictures

Generally speaking, when looking at the interaction between atoms and light, we can adopt two points of view. In the perspective of mesoscopic transport, we focus on light behavior without paying very much attention to matter, whereas in a microscopic treatment we try to integrate out the radiative degrees of freedom to highlight atomic excitations [49]. While in the first picture we wish to follow the light in its dynamics, in the second we adopt a much more static glance that leads us to *interpret* manifestations of the light-matter interaction in terms of many-body physics, emergence of collective properties, or phase transitions. This alternative is somehow reminiscent of Lagrangian and Eulerian specifications of a flow field: either we sit in the boat and drift down the river, or we prefer its bank and watch the water pass. It is instructive to make a link with our discussion of section 2.2 about Schrödinger and Heisenberg pictures. In the master equation approach (Schrödinger picture), often used in atomic physics, we always consider the radiation as a reservoir that we try to integrate out. In this perspective, the master equation formalism clearly belongs to the microscopic picture. Situation is more versatile in the Heisenberg picture for we are free to choose between mesoscopic and microscopic points of view. Indeed, on the one hand we have the wave equation (2.39) for the electric field operator, and on the other atomic equations of motion (2.65) and

(2.66). At our convenience, we can formally eliminate the atomic or the field variables.

2.4.1 Microscopic excitations

First, we adopt the microscopic picture and eliminate the field variables. Rigorously, we have to insert the smoothed field solution (2.59) rewritten in the time domain in atomic Eqs. (2.65) and (2.66). One can verify that the resulting equations simplify provided that the atomic level spacing is well defined ($\Gamma_0 \ll \omega_0$) and that the time of flight through the sample of typical size R is negligible ($\Gamma_0 \ll c/R$). In that case we can simply replace $\mathbf{g}(\mathbf{r}_i - \mathbf{r}_j, \omega_L)$ by $\mathbf{g}(\mathbf{r}_i - \mathbf{r}_j, \omega_0)$ in Eq. (2.59). Note that it is only possible because the free space Green's function $\mathbf{g}$ has no resonance in the frequency domain where atoms scatter strongly (namely in the vicinity of ω_0). If atoms were surrounded with a cavity of high finesse, the frequency pattern of $\mathbf{g}$ would contain sharp peaks representing cavity modes, and our simplification scheme would break down. Having said that, here we obtain

$$\frac{\mathrm{d}\widetilde{\mathbf{D}}_i^+}{\mathrm{d}t} = \left(\mathrm{i}\omega_0 - \frac{\Gamma_0}{2}\right)\widetilde{\mathbf{D}}_i^+ + \frac{\mathrm{i}d^2}{\epsilon_0\hbar}\frac{k_0^3}{6\pi}\boldsymbol{\Delta}_i^{\parallel}\sum_j^N \mathbf{G}_{ij}^*(\omega_0)\widetilde{\mathbf{D}}_j^+\Pi_i + \frac{\mathrm{i}d}{\hbar}\boldsymbol{\Delta}_i^{\parallel}\mathbf{E}_0^-(\mathbf{r}_i)\Pi_i, \tag{2.68}$$

$$\frac{\mathrm{d}\Pi_i}{\mathrm{d}t} = -\Gamma_0\left(\Pi_i + 1\right) - \frac{d^2}{\epsilon_0\hbar}\frac{2k_0^3}{3\pi}\mathrm{Im}\left[\widetilde{\mathbf{D}}_i^+ \cdot \sum_j^N \mathbf{G}_{ij}(\omega_0)\widetilde{\mathbf{D}}_j^-\right] - \frac{4d}{\hbar}\mathrm{Im}\left[\widetilde{\mathbf{D}}_i^+ \cdot \mathbf{E}_0^+(\mathbf{r}_i)\right], \tag{2.69}$$

where we use a slightly loose operator notation $\mathrm{Im}O = (O - O^\dagger)/2\mathrm{i}$, and the Lamb shift $\Delta\omega_0$ has been absorbed in the definition of the atomic frequency ω_0; $\boldsymbol{\Delta}_i^{\parallel} = \tilde{\mathbf{d}}_i \otimes \tilde{\mathbf{d}}_i$ is the projection operator (on the dipole $\tilde{\mathbf{d}}_i$), and $\tilde{\mathbf{d}}_i$ and $\widetilde{\mathbf{D}}_i^{\pm}$ are defined in Eq. (2.50). Finally, the coupling coefficient $\mathbf{G}_{ij}(\omega_0)$ is the dimensionless free space Green's function:

$$\mathbf{G}_{ij}(\omega_0) = \frac{6\pi}{k_0^3}(1 - \delta_{ij})\mathbf{g}(\mathbf{r}_i - \mathbf{r}_j, \omega_0). \tag{2.70}$$

Next, thanks to the definition of the spontaneous decay rate,

$$\Gamma_0 = \frac{2\pi}{\hbar^2}\sum_{\mathbf{k},\boldsymbol{\epsilon}} \mathcal{E}_{\mathbf{k}}^2|\mathbf{d}\cdot\boldsymbol{\epsilon}|^2\delta(\omega_0 - \omega_{\mathbf{k}}) = \frac{d^2k_0^3}{3\pi\epsilon_0\hbar}, \tag{2.71}$$

Eqs. (2.68) and (2.69) reduce to

$$\frac{\mathrm{d}\widetilde{\mathbf{D}}_i^+}{\mathrm{d}t} = \left(\mathrm{i}\frac{\omega_0}{\Gamma_0} - \frac{1}{2}\right)\widetilde{\mathbf{D}}_i^+ + \frac{\mathrm{i}}{2}\boldsymbol{\Delta}_i^{\parallel}\sum_j^N \mathbf{G}_{ij}^*(\omega_0)\widetilde{\mathbf{D}}_j^+\Pi_i - \frac{\mathrm{i}}{2}\boldsymbol{\Delta}_i^{\parallel}\boldsymbol{\Omega}_0^-(\mathbf{r}_i)\Pi_i, \tag{2.72}$$

$$\frac{\mathrm{d}\Pi_i}{\mathrm{d}t} = -\left(\Pi_i + 1\right) - 2\mathrm{Im}\left[\widetilde{\mathbf{D}}_i^+ \cdot \sum_j^N \mathbf{G}_{ij}(\omega_0)\widetilde{\mathbf{D}}_j^-\right] + 2\mathrm{Im}\left[\widetilde{\mathbf{D}}_i^+ \cdot \boldsymbol{\Omega}_0^+(\mathbf{r}_i)\right], \tag{2.73}$$

where the time is from now on in units of Γ_0^{-1}, and $\boldsymbol{\Omega}_0^{\pm}$ is the dimensionless Rabi frequency associated with the free field, $\boldsymbol{\Omega}_0^{\pm} = -2d\mathbf{E}_0^{\pm}/\hbar\Gamma_0$ [52].

Equations (2.72) and (2.73) describe the matter-field dynamics in the microscopic picture. Quite interestingly, we did not need to make any strong approximation to get them. Actually, we only used two simplifications: the RWA for internal degrees of freedom and

the approximation $\mathbf{G}_{ij}(\omega_L) \simeq \mathbf{G}_{ij}(\omega_0)$. Both of them can be relaxed: equations would only look a bit more complicated, and would involve convolution products. In particular, we emphasize that we did not invoke any approximation of the Born-Markov type, as it it is necessary in the master equation approach.

It is also worth noting that equations similar to (2.72) and (2.73) were derived quite a long time ago, in the seventies, by Lehmberg [55] and Agarwal [43]. Nevertheless the spirit of their derivation differs substantially. Indeed, the key to our derivation lies in the clear division of the matter-field dynamics into a wave equation (2.39) and atomic equations (2.53) and (2.57), so that the origin of the coupling $\mathbf{G}_{ij}$ in Eqs. (2.72) and (2.73) is obvious. Conversely, the authors of [43, 55] looked at the interaction of each atom with each mode of the field $|\mathbf{k}, \epsilon\rangle$ and then summed up the contributions of all the modes. Because of this blurring summation (and also because the authors did not use the complete Hamiltonian (2.24), and made no difference between $\mathbf{E}$ and $\mathbf{E}_\perp$), they apparently overlooked the fact that the coupling tensor $\mathbf{G}$ was simply the Green's function of the Helmholtz equation. Having this point in mind clarifies the situation. For example, it allows for a straightforward generalization of Eqs. (2.72) and (2.73) to the case where atoms are embedded in a homogeneous medium or surrounded by a cavity.

Before discussing the physical content of equations (2.72) and (2.73), we would like to show what they become when we neglect the vectorial nature of the field. In this procedure, the dipolar coupling $\mathbf{D}_i \cdot \mathbf{E}_\perp(\mathbf{r}_i)$ in the Hamiltonian (2.24) is approximated by $dS_i E_\perp(\mathbf{r}_i)$, all summations over polarizations, like in Eq. (2.26), are omitted, and projectors onto dipoles, $\mathbf{\Delta}_i^{\parallel} = \widetilde{\mathbf{d}}_i \otimes \widetilde{\mathbf{d}}_i$, are simply replaced by the identity operator. Moreover, the scalar electric field operator E obeys the scalar wave equation

$$\Delta E(\mathbf{r}, t) - \frac{1}{c^2}\partial_t^2 E(\mathbf{r}, t) = \frac{1}{\epsilon_0 c^2}\partial_t^2 P(\mathbf{r}, t). \tag{2.74}$$

Its retarded Green's function g in reciprocal space,

$$g(\mathbf{k}, \omega_L) = \frac{-k_L^2}{k_L^2 + \mathrm{i}\eta - k^2}, \tag{2.75}$$

is nothing but the transverse component of the dyadic Green's function $\mathbf{g}$ (2.34),

$$\mathbf{g}(\mathbf{k}, \omega_L) = -\mathbf{\Delta}_{\mathbf{k}}^{\parallel} + g(\mathbf{k}, \omega_L)\mathbf{\Delta}_{\mathbf{k}}^{\perp}. \tag{2.76}$$

Finally, note that in the scalar approximation the value of the spontaneous emission rate is different from (2.71):

$$\Gamma_0 = \frac{2\pi}{\hbar^2}\sum_{\mathbf{k}} \mathcal{E}_{\mathbf{k}} d^2 \delta(\omega_0 - \omega_{\mathbf{k}}) = \frac{d^2 k_0^3}{2\pi\epsilon_0\hbar} \qquad \text{(scalar field)}. \tag{2.77}$$

Hence, the scalar version of Eqs. (2.68) and (2.69) is

$$\frac{\mathrm{d}S_i^+}{\mathrm{d}t} = \left(\mathrm{i}\frac{\omega_0}{\Gamma_0} - \frac{1}{2}\right) S_i^+ + \frac{\mathrm{i}}{2}\Pi_i \sum_j G_{ij}^*(\omega_0) S_j^+ - \frac{\mathrm{i}}{2}\Omega_0^-(\mathbf{r}_i)\Pi_i, \tag{2.78}$$

$$\frac{\mathrm{d}\Pi_i}{\mathrm{d}t} = -(\Pi_i + 1) - 2\mathrm{Im}\left[S_i^+ \sum_j G_{ij}(\omega_0) S_j^-\right] + 2\mathrm{Im}\left[S_i^+ \Omega_0^+(\mathbf{r}_i)\right], \tag{2.79}$$

where $G_{ij}(\omega_0)$ is the ij element of a $N \times N$ non-Hermitian matrix, which we will call in this manuscript the scalar *Green's matrix*:

$$G_{ij}(\omega_0) = \frac{4\pi}{k_0^3}(1-\delta_{ij})g(\mathbf{r}_i - \mathbf{r}_j, \omega_0). \tag{2.80}$$

Note that the normalization coefficient is not the same as in Eq. (2.70). It is chosen such that the average of $\mathbf{G}_{ij}(\omega_0)$ over the solid angle $\mathrm{d}\Omega_{ij} = \mathrm{d}\mathbf{r}_{ij}/r_{ij}^2 \mathrm{d}r_{ij}$ coincides with $G_{ij}(\omega_0)$:

$$\frac{1}{4\pi}\int \mathrm{d}\Omega_{ij}\mathbf{G}_{ij}(\omega_0) = G_{ij}(\omega_0). \tag{2.81}$$

In three dimensional space, it has the form

$$G_{ij}(\omega_0) = (1-\delta_{ij})\frac{e^{\mathrm{i}k_0|\mathbf{r}_i-\mathbf{r}_j|}}{k_0|\mathbf{r}_i-\mathbf{r}_j|}. \tag{2.82}$$

For future use, we also introduce the dimensionless smoothed field $\mathbf{\Omega}_s^+ = -2d\mathbf{E}_s^+/\hbar\Gamma_0$ and its scalar version $\Omega_s^+ = -2dE_s^+/\hbar\Gamma_0$. With Eqs. (2.59), (2.70), (2.71), (2.77), and (2.80), we obtain

$$\mathbf{\Omega}_s^+(\mathbf{r}_i,\omega_L) = \mathbf{\Omega}_0^+(\mathbf{r}_i,\omega_L) - \left(\frac{\omega_L}{\omega_0}\right)^3 \sum_{j\neq i}^{N} \boldsymbol{G}_{ij}(\omega_L)\widetilde{\boldsymbol{D}}_j^-(\omega_L), \tag{2.83}$$

$$\Omega_s^+(\mathbf{r}_i,\omega_L) = \Omega_0^+(\mathbf{r}_i,\omega_L) - \left(\frac{\omega_L}{\omega_0}\right)^3 \sum_{j\neq i}^{N} G_{ij}(\omega_L)S_j^-(\omega_L). \tag{2.84}$$

Coupled nonlinear quantum equations (2.78) and (2.79) deserve a few comments:

- Both of them contain three contributions: (1) a monoatomic part that corresponds to the well-known Bloch equations of atomic physics [52], (2) a part due to interatomic coupling, the kernel of which is the matrix G, (3) the action of the free field $E_0^\pm$ on each atom. The information about an eventual optical pump is not contained in these operatorial equations but in the state of the field that we will use to take their expectation value later on. If, for the time being, we average over $|0_R\rangle$, the terms containing $\Omega_0^\pm$ vanish. To some extent (that is detailed in section 3.3), and with respect to $|0_R\rangle$, these terms behave as Langevin forces, and for this reason are called quantum Langevin forces [52, 66, 74].

- Atom i is coupled to atom j through G_{ij} that propagates the field from one to the other. This is not surprising inasmuch as the same occurs for classical dipoles: G_{ij} is a classical quantity. Less trivially, this coupling does not vanish in the absence of photons, given that vacuum expectation values of interatomic terms in Eqs. (2.78) and (2.79) are nonzero. Just as the Lamb shift and the spontaneous decay rate are related to the the own radiation field through $\mathbf{g}_{ii}$ — see Eq. (2.62) — a 'collective Lamb shift' and van der Waals forces arise from the real and imaginary parts of the interatomic coupling G_{ij}. As they do not need the presence of external photons to build up, they are sometimes said to be due to virtual photon exchange between atoms [49, 52, 60, 75]. Note that the vacuum fluctuations depicted by the quantum Langevin forces *seem* here not necessary to explain these effects. As we discussed in section 2.3.2.c, this is only because Eqs. (2.78) and (2.79) are written in the normal order.

- As we will show later on, Eqs. (2.78) and (2.79) admit a semiclassical limit, where quantum Langevin forces are disregarded and the remaining operators, $S_i^{\pm}$ and Π_i, are replaced by c-numbers. In this limit, Eqs. (2.78) and (2.79) feature the dynamics of classical dipoles with long-range coupling coefficient G_{ij}. They correspond to an effective Hamiltonian — see, for example, Eq. (2.98) — which is strongly reminiscent of the Hamiltonian of topologically disordered systems, such as spin glasses. The latter are alloys in which magnetic impurities substitute atoms at random positions. They are well described by a randomized version of the Ising model such as the Sherrington-Kirkpatrick model [76]. The Hamiltonian of this model is $H = -\sum_i h_i S_i - \sum_{i\neq j} J_{ij} S_i S_j$, where h_i is the local external magnetic field and J_{ij} is the interaction between impurities. In a metal, localized magnetic moments interact indirectly via polarization of conduction electrons through the Ruderman-Kittel-Kasuya-Yosida (RKKY) potential. In three dimensional space the latter is of the form [77]

$$J_{ij} = J\frac{\cos\left(2k_F|\mathbf{r}_i - \mathbf{r}_j|\right)}{|\mathbf{r}_i - \mathbf{r}_j|^3}, \tag{2.85}$$

  where k_F is the Fermi wave vector. J_{ij} in a spin glass plays the same role as G_{ij} in an ensemble of atoms. Moreover, as we will see in chapter 3, the local magnetic field for spins is well mimicked by the incoherent local pump for atomic dipoles. Loosely speaking, we can therefore consider a random laser as a kind of optical spin glass. Transposing to random lasers the rich physics of spin glasses, as well as the theoretical toolbox promoted to describe them [76], is potentially fruitful. For example, we can expect (at zero temperature) a phase transition to occur depending on the respective strength of the pump and the interaction: this is precisely the threshold of the random laser.

2.4.2 Toward mesoscopic transport

The formulation of matter-field interaction in terms of light transport consists in eliminating the atomic degrees of freedom that appear in the coupled equations (2.39), (2.65), and (2.66). Ideally, this could be achieved by expressing the polarization as a function of the electric field only. However, contrary to the microscopic picture, such operation cannot be performed exactly. To understand where the problem comes from, we reformulate atomic equations (2.65) and (2.66) in the frequency domain:

$$\mathbf{D}_i^-(\omega_L) = \frac{1}{\omega_L - \omega_0 + \mathrm{i}\Gamma_0/2}\int\frac{\mathrm{d}\omega'}{2\pi\hbar}\,\Pi_i(\omega_L-\omega')\left[\mathbf{d}_i\otimes\mathbf{d}_i\right]\mathbf{E}_s^+(\mathbf{r}_i,\omega'), \tag{2.86}$$

$$\begin{aligned}\Pi_i(\omega_L) = &-\frac{2\mathrm{i}\pi\Gamma_0}{\omega_L+\mathrm{i}\Gamma_0}\delta(\omega_L) + \frac{2}{\omega_L+\mathrm{i}\Gamma_0}\int\frac{\mathrm{d}\omega'\mathrm{d}\omega''}{(2\pi\hbar)^2}\\ &\left[\frac{\left[\mathbf{d}_i\otimes\mathbf{d}_i\right]\mathbf{E}_s^-(\mathbf{r}_i,\omega'')\cdot\Pi_i(\omega_L-\omega'-\omega'')\mathbf{E}_s^+(\mathbf{r}_i,\omega')}{\omega_L-\omega'+\omega_0+\mathrm{i}\Gamma_0/2} + h.c.(\omega'\leftrightarrow\omega'')\right].\end{aligned} \tag{2.87}$$

With Eq. (2.86), the quantum wave equation (2.39) becomes

$$\left[\nabla\times\nabla\times - k_L^2\right]\mathbf{E}^+(\mathbf{r},\omega_L) = \int\frac{\mathrm{d}\omega'}{2\pi\epsilon_0\hbar}\left[\sum_{i=1}^N\frac{k_L^2\Pi_i(\omega_L-\omega')}{\omega_L-\omega_0+\mathrm{i}\Gamma_0/2}\left[\mathbf{d}_i\otimes\mathbf{d}_i\right]\delta(\mathbf{r}-\mathbf{r}_i)\right]\mathbf{E}_s^+(\mathbf{r},\omega'). \tag{2.88}$$

Equations (2.87) and (2.88) form a closed set from which population imbalance Π_i cannot be easily eliminated. Simple observation of these equations reveals that population imbalance is responsible for both inelastic scattering ($\omega_L \to \omega'$) and nonlinear response of the atomic medium to the field. Despite these subtleties, if we assume that a stationary regime exists in which the population imbalance is time independent, Eq. (2.88) can be reduced to an effective propagation equation of the form

$$\left[k_L^2 - H^f\right] \mathbf{E}^+(\mathbf{r}, \omega_L) = 0, \tag{2.89}$$

with

$$H^f = H_0^f + V^f = (\nabla \times \nabla \times) + \sum_{i=1}^{N} v_i \delta(\mathbf{r} - \mathbf{r}_i), \tag{2.90}$$

where v_i is an effective potential, the explicit form of which will be discussed and used in chapter 4. In a standard manner, we can interpret $\mathbf{E}^+(\mathbf{r})$ as the real-space representation of a ket $|\mathbf{E}^+\rangle$ embedded in a fictitious Hilbert space $\mathcal{E}^f$, and whose dynamics is governed by the fictitious Hamiltonian H^f. In this framework, the elementary building block that characterizes the behavior of the field is therefore the resolvent[1] of the Hamiltonian H^f, $\mathcal{G}^f = 1/(k_L^2 - H^f) = \mathcal{G}_0^f + \mathcal{G}_0^f V^f \mathcal{G}^f$, with $\mathcal{G}_0^f = 1/(k_L^2 - H_0^f)$. In order to avoid any confusion, we stress that $\langle \mathbf{r}|\mathbf{E}^+\rangle$ is at the same time a component of $|\mathbf{E}^+\rangle$ in $\mathcal{E}^f$, and an operator that acts in the true Hilbert space $\mathcal{E} = \mathcal{E}^A \otimes \mathcal{E}^R$. Moreover, H^f should not be confused with the matter-field Hamiltonian H (2.24) that we used to derive Eqs. (2.89) and (2.90). In particular, H^f is not Hermitian, contrary to H. For the study of light propagation in the presence of gain within the framework of mesoscopic scattering formalism [using Eqs. (2.89) and (2.90)], we refer the reader to chapter 4.

Obviously, we can argue that the scattered field may also be computed by directly using the resolvent $\mathcal{G}(z) = 1/(z - H)$ of the Hamiltonian $H = H_0 + V$ given by Eq. (2.24). In this approach, scattering of $|\mathbf{E}^+\rangle$ in $\mathcal{E}^f$ is replaced by scattering of matter-field excitations $|\psi_A\rangle|\psi_R\rangle$ in $\mathcal{E} = \mathcal{E}^A \otimes \mathcal{E}^R$. It is *a priori* much more difficult to keep track of $|\psi_A\rangle|\psi_R\rangle$ under the repeated action of V than of $|\mathbf{E}^+\rangle$ under the action of V^f. This explains why publications devoted to such quantum microscopic scattering formalism restrict themselves to the study of propagation of a single photon $|\psi_R\rangle = |\mathbf{k}\boldsymbol{\epsilon}\rangle$, in the presence of N atoms in their ground state $|\psi_A\rangle = |N : g\rangle$ [78–83]. It is interesting to illustrate this fact because this provides an occasion to introduce the concept of effective Hamiltonian properly. For this purpose, let us calculate the matrix element $\langle O|\mathcal{T}|I\rangle$ of the $\mathcal{T}$ operator, $\mathcal{T} = V + V\mathcal{G}V$, where $|I\rangle$ and $|O\rangle$ are eigenstates of H_0 containing one photonic excitation, $|I\rangle = |N : g\rangle|\mathbf{k}_{in}\boldsymbol{\epsilon}_{in}\rangle$ and $|O\rangle = |N : g\rangle|\mathbf{k}_{out}\boldsymbol{\epsilon}_{out}\rangle$:

$$\langle O|\mathcal{T}(E_I + \mathrm{i}\eta)|I\rangle = \langle O|V\mathcal{G}(E_I + \mathrm{i}\eta)V|I\rangle = \langle O|VP\mathcal{G}(E_I + \mathrm{i}\eta)PV|I\rangle, \tag{2.91}$$

where $E_I = \langle I|H_0|I\rangle = \hbar\omega_{in} = \hbar\omega_0$ (photon on resonance), and P is the projector on the subspace formed by the eigenstates of H_0 containing one atomic excitation:

$$P = \sum_{j=1}^{N} |j\rangle\langle j| \quad \text{with} \quad |j\rangle = |(N-1) : g, j : e\rangle|0_R\rangle. \tag{2.92}$$

[1] In this manuscript we use the term 'resolvent' rather than 'Green's function' to avoid any confusion with the Green's matrix (2.82).

The projected resolvent $P\mathcal{G}(E_I + \mathrm{i}\eta)P$ appearing in Eq. (2.91) is given by a very general expression that follows from simple algebra (see, for example, Ref. [84]):

$$P\mathcal{G}(E_I + \mathrm{i}\eta)P = \frac{P}{E_I + \mathrm{i}\eta - H^e(E_I + \mathrm{i}\eta)}. \tag{2.93}$$

The effective Hamiltonian H^e is nontrivial inasmuch as it is different from PHP:

$$H^e = PH_0P + PR(E_I + \mathrm{i}\eta)P, \tag{2.94}$$

with $R(z)$ defined as

$$R(z) = V + V\frac{Q}{z - QHQ}V = V + V\sum_{n=0}^{\infty}\left[\frac{Q}{z - QH_0Q}V\right]^n \frac{Q}{z - QH_0Q}V, \tag{2.95}$$

where $Q = 1 - P$. For the particular projector (2.92), we have to calculate $R_{jj} = \langle j|R(E_I + \mathrm{i}\eta)|j\rangle$ and $R_{jj'}$ $(j \neq j')$. For simplicity we give them for a scalar field. According to the explicit form of H_0 and V — see Eq. (2.24) — they are

$$R_{jj} = \sum_k \frac{V_{jk}V_{kj}}{E_I + \mathrm{i}\eta - E_k} = \hbar\Delta\omega_0 - \mathrm{i}\hbar\Gamma_0/2, \tag{2.96}$$

$$R_{jj'} = \sum_k \frac{V_{jk}V_{kj'}}{E_I + \mathrm{i}\eta - E_k} = \frac{\hbar\Gamma_0}{2}\frac{e^{\mathrm{i}k_0|\mathbf{r}_i - \mathbf{r}_j|}}{k_0|\mathbf{r}_i - \mathbf{r}_j|}, \tag{2.97}$$

where the label k refers to states with a single photonic excitation, $|k\rangle = |N : g\rangle|\mathbf{k}\rangle$, or $|k\rangle = |(N-2) : g, 2 : e\rangle|\mathbf{k}\rangle$ (non-resonant processes). Therefore, the effective Hamiltonian (2.94) becomes

$$H^e = \sum_{i=1}^{N}\hbar\left(\omega_0 - \mathrm{i}\frac{\Gamma_0}{2}\right)|e_i\rangle\langle e_i| - \frac{\hbar\Gamma_0}{2}\sum_{i\neq j}^{N} G_{ij}(\omega_0)S_i^+S_j^-, \tag{2.98}$$

where the Lamb shift has been absorbed in ω_0 and $G_{ij}(\omega_0)$ is given by Eq. (2.82). We emphasize that this effective Hamiltonian is *a priori* valid only with respect to the single-excitation subspace characterized by the projector P (2.92), contrary to Eqs. (2.87) and (2.88) valid for any quantum state of the matter-field. The eigenvalues of H^e define the excitation spectrum for light coupled to scatterers. Incidentally, note that H^e is a non-Hermitian operator, that must not be confused with the fictitious Hamiltonian H^f (2.90) of the mesoscopic scattering approach. This effective Hamiltonian H^e was explicitly used by several groups. Recently, in 2008, Akkermans *et al.* [79] used it to study the interplay of photon localization and Dicke superradiance in a collection of atoms at rest at random positions. And in 2009, Antezza and Castin [85] made used of H^e by taking into account the vectorial nature of light, as well as external atomic degrees of freedom (each atom harmonically trapped), to calculate the spectrum of light in a periodic structure (no disorder).

Although we will not adopt the microscopic scattering approach in the rest of this manuscript, we signal that the combination of equations (2.98) and (2.93) clearly allows to solve the scattering problem (2.91).

2.5 The Green's matrix in the literature

Microscopic equations (2.72) and (2.73), or their mesoscopic version (2.87) and (2.88), potentially contain an impressive amount of optical phenomena such as superradiance, collective spontaneous emission, subradiance, laser, inelastic scattering, nonlinear optics, quantum interferences, or Anderson localization. And in these equations, all information about disorder and interaction, *i.e.* about positions of scatterers and the way they couple to each other, is contained in $\mathbf{G}_{ij}(\omega_0)$ defined in Eq. (2.70). This means that all classical information related to the emergence of collective behavior is somehow hidden in the properties of the Green's matrix. In this section, we briefly review the recent works where the Green's matrix has been encountered. Most of them can be formulated and understood as various simplifications of Eqs. (2.72) and (2.73).

2.5.1 Cooperative emission of large atomic samples

A basic problem of traditional and modern quantum optics is the 'single-photon superradiance': a photon is stored in an ensemble of (cold) atoms, and one studies the properties (frequency, direction of propagation, etc.) of the photon re-emitted by the atoms at a later time. It is a specific case of the superradiance protocol, with only one photon and no restriction concerning the size of the system. Theoretically, this problem has been addressed a long time ago, in 1969, by Ernst [86], but has been popularized only very recently by the group of Scully [60, 75, 81–83, 87–90], as well as by Manassah and Friedberg (see for example [91] and references therein). The reason for this renewed interest is probably the recent development of experimental setups where cooperative emission can be observed without obscuring effects (*e.g.*, Doppler effect or near field atom-atom interactions), either with cold atoms or with ultrathin solid samples [92]. Another reason is the development of memories based on storage of photons in atomic media [93, 94], with in particular the implementation of quantum repeaters and long-distance quantum cryptography networks [95, 96]. The theoretical framework of the underlying physics is a linearized version of scalar equations (2.72) and (2.73), and is strictly equivalent to the one-photon scattering formalism associated to the effective Hamiltonian (2.98). Namely, Scully and coworkers study the dynamics, in the Schrödinger picture, of a pure state of the form

$$\begin{aligned} |\Psi(t)\rangle &= \sum_{j=1}^{N} \beta_j(t)|(N-1):g,j:e\rangle|0_R\rangle + \sum_{\mathbf{k}} \gamma_{\mathbf{k}}(t)|N:g\rangle|\mathbf{k}\rangle \\ &+ \sum_{i<j}^{N}\sum_{\mathbf{k}} \alpha_{ij\mathbf{k}}|(N-2):g,i:e,j:e\rangle|\mathbf{k}\rangle, \end{aligned} \tag{2.99}$$

where the last sum, that describes states with atoms i and j in their excited states in the presence of one 'virtual' photon, is necessary to capture non-resonant processes that give rise to the real part of the Green's matrix[2]. The evolution equation for the vector $\boldsymbol{\beta} = (\beta_1, .., \beta_N)$ reads [88, 90]:

$$\frac{\mathrm{d}\boldsymbol{\beta}}{\mathrm{d}t} = -\boldsymbol{\beta}(t) + \mathrm{i}G(\omega_0)\boldsymbol{\beta}(t), \tag{2.100}$$

[2]See sections 2.3.1, 2.3.2.a, or 2.4.2 for related discussions.

where the time is in units of Γ_0^{-1} and $G(\omega_0)$ is the scalar Green's matrix (2.82). According to this equation, an eigenvector of G associated with the eigenvalue Λ_k decays with a rate $\Gamma = \Gamma_0(1 + \mathrm{Im}\Lambda_k)$ and experiences a frequency shift $-\Gamma_0 \mathrm{Re}\Lambda_k$. Both the decay rate and the frequency shift were studied in [88, 90] in the limit of a very dense atomic cloud ($\rho\lambda_0^3 \to \infty$), where the summation $[G\beta(t)]_i = \sum_{j=1}^N G_{ij}\beta_j(t)$ can be replaced by integration in the last term on the r.h.s. of Eq. (2.100). It is important to realize that replacing summation by integration is equivalent to averaging this equation over all possible configurations $\{\mathbf{r}_i\}$ of atoms. It leads, therefore, to the neglect of the statistical nature of the initial problem. As a consequence, the authors of [88, 90] find deterministic eigenvalues Λ_k. Besides, with this approximation all subradiant states of the Green's matrix, the importance of which was already pointed out in the original paper by Ernst [86], are lost. This quite subtle effect seems to be overlooked by the authors of [88, 90], presumably because they are essentially interested in superradiant states. For a detailed discussion of this effect, we refer the reader to chapter 6. Moreover, although these deterministic results are interesting, atomic clouds of moderate density $\rho\lambda_0^3 \lesssim 1$ are readily created in modern laboratories (see, *e.g.*, [97, 98]). It is therefore important to extend the analysis to dilute atomic clouds. Such extension is discussed in great details in chapters 6 and 7.

We also point out that in Ref. [79], Akkermans *et al.* claimed that properties of the decay rate Γ can be understood, at least qualitatively, by dropping the real part of the Green's matrix, inasmuch as the latter is expected to be responsible for the collective Lamb shift (or Van der Waals dephasing). We believe that this picture is not entirely correct, because this shift is related to the real part of the eigenvalues of G, and not to the real part of the matrix itself. Nevertheless, we will see in chapters 5 and 6 that in certain regimes of disorder $\Lambda_k(\mathrm{Im}G)$ and $\mathrm{Im}\Lambda_k(G)$ have indeed some similarities. The advantage of such approximation is that $\mathrm{Im}G$ is an Hermitian matrix, contrary to G, and for this reason much easier to deal with. The authors of [79] observed that the decay rate γ only depends on what they called the 'disorder strength', a quantity proportional to the on-resonance optical thickness of the atomic cloud. We will properly justify this dependence in chapter 5.

Finally, we mention the recent works of Pierrat and Carminati who studied the statistics of the fluorescence decay rate of a single dipole emitter embedded in a strongly scattering medium [99, 100]. The key quantity of their numerical approach is the $3N \times 3N$ vectorial Green's matrix (2.70). Since the decay rate is proportional to the local density of states, understanding its statistics is important to improve imaging techniques.

2.5.2 Anderson localization in an open medium

The phenomenon of Anderson localization is common for all waves in random media [9, 101, 102]. It consists in a transition from extended (over the whole available sample volume) to exponentially localized eigenstates of a wave (or Schrödinger) equation with a randomly fluctuating potential, at a sufficiently strong randomness. A paradigm system in which Anderson localization can be studied for classical waves is a random arrangement of N identical point-like scatterers in a volume V. In such an open system of finite size the wave energy can leak to the outside and one expects Anderson localization to have an impact on decay of physical observables such as, *e.g.*, the intensity of the wave emerging from the random system.

Several authors studied the distribution of dimensionless decay rates $\gamma = \Gamma/\Gamma_0$ in

open random media and, in particular, promoted the idea of using its probability distribution $p(\gamma)$ as a criterion for Anderson localization [103, 104]. To be precise, $p(\gamma)$ is expected to decay as $1/\gamma$ in the localized regime (see section 6.6.1). In point-like dipole models, as it is clear from Eq. (2.100), the relevant decay rates are related to the imaginary part of the eigenvalues Λ_k of the non-Hermitian matrix G (2.82), $\gamma_k = 1 + \mathrm{Im}\Lambda_k$ [105]. Pinheiro *et al.* [104] observed this decay $p(\mathrm{Im}\Lambda) \propto 1/(1 + \mathrm{Im}\Lambda)$ in numerical simulations at high density and claimed that it was a signature of Anderson localization. In chapter 6, we will provide some analytical and numerical evidence that this tendency is actually present as soon as the regime of multiple scattering (large optical thickness) is established, and does not seem to require Anderson localization.

In addition, motivated by the recent advances in the manipulation of ultracold gases, Castin and coworkers [106, 107] numerically investigated the localization of a matter wave in a disordered potential made of atoms pinned at random positions of an optical lattice. The kernel of their calculation is, again, the Green's matrix (2.82). The main difference with optical waves is the possibility for the matter wave to have negative energy E, *i.e.* discrete bound states that are trapped without being necessarily of Anderson type. In particular in three dimensional systems, authors of Ref. [107] identify for $E > 0$ the existence of a mobility edge for a positive effective scattering length of the order of the mean distance between scatterers.

In chapter 6 we will identify eventual signatures of Anderson localization in the spectrum of the eigenvalues of G, as well as in its eigenvectors. Two quantities that shall manifest such signatures are the Thouless number and the inverse participation ratio of eigenstates of G. For the reader who might be doubtful about the link between the eigenvectors of H (2.24) (whose number is infinite) and those of the $N \times N$ matrix G, we recall that most physical properties are sensitive not directly to the true Hermitian Hamiltonian H but to effective Hamiltonians, similar to H^e defined in Eq. (2.98). And the eigenstates $|\Psi_\alpha\rangle$ of (2.98) are directly related to the eigenstates of G. Indeed, if we denote $\mathbf{\Psi}_\alpha = (\Psi_{\alpha 1}, .., \Psi_{\alpha N})$ where $\Psi_{\alpha i} = \langle (N-1) : g, i : e|\Psi_\alpha\rangle$, the equation $H^e|\Psi_\alpha\rangle = E_\alpha|\Psi_\alpha\rangle$ becomes

$$\hbar(\omega_0 - \mathrm{i}\Gamma_0/2)\mathbf{\Psi}_\alpha - \hbar\Gamma_0 G\mathbf{\Psi}_\alpha/2 = E_\alpha \mathbf{\Psi}_\alpha. \tag{2.101}$$

Hence, the eigenstates of G coincide with those of H^e that evolve in the one-excitation subspace defined by the projector P (2.92).

2.5.3 Optical instabilities and random lasers

Nonlinear disordered systems, such as the ensemble of atoms described by Eqs. (2.72) and (2.73), can exhibit speckle instabilities: if the nonlinearity is strong enough, there is no stationary state at long time so that the speckle patterns generated by point scatterers fluctuate in time. Grémaud and Wellens investigated in [108] these instabilities by considering an intensity-dependent scattering matrix

$$t(I) = -\frac{2\mathrm{i}\pi}{k_0}\left(1 + e^{\mathrm{i}\nu I}\right), \tag{2.102}$$

where I is the intensity of light on the scatterer and ν is a phenomenological nonlinear coefficient. For small ν, Eq. (2.102) reduces to a general $\chi^{(3)}$ nonlinearity (Kerr effect), and for real values of ν, the optical theorem is fulfilled, ensuring energy conservation (see chapter 4). The atomic dynamics is described by a scalar and semiclassical version of

Eqs. (2.65) and (2.66) where the population imbalance has been eliminated:

$$\frac{\mathrm{d}S_i^+}{\mathrm{d}t} = \mathrm{i}\left(\frac{\omega_0}{\Gamma_0} - \frac{1}{2}\right) S_i^+ - \frac{k_0}{8\pi} t(I_{s,i})\Omega_s^-(\mathbf{r}_i). \tag{2.103}$$

Here $\Omega_s^-(\mathbf{r}_i)$ is the dimensionless electric field defined by Eq. (2.84), that also gives rise to the intensity $I_{s,i} = |\Omega_s^+(\mathbf{r}_i)\Omega_s^-(\mathbf{r}_i)|^2$. Stationary, time-independent solutions lose their stability and the system starts to exhibit complex, spontaneous dynamic behavior when the nonlinear coefficient ν exceeds a critical value ν_{inst} proportional to $[1+\min(\mathrm{Im}\Lambda_k)]^{3/2}$. In chapter 6 we will see that eigenvalues of G with the smallest imaginary part belong to spiral branches of the statistical distribution $p(\Lambda)$ in the complex plane Λ. They are not related to the diffusion of light in the bulk of the random sample but originate from sub-radiant states localized on pairs of mutually close scatterers [108]. In chapter 6 we will provide an analytic derivation of the statistical distribution $p[1 + \min(\mathrm{Im}\Lambda)]$.

The average value $1 + \langle\min(\mathrm{Im}\Lambda_k)\rangle$ was also studied numerically by Pinheiro and Sampaio in the context of random lasers [109]. They considered an ensemble of point-like scatterers randomly distributed in a volume filled with some continuous amplifying medium that provides a constant amplification rate γ_{ampl}. They assumed that lasing should start when γ_{ampl} becomes larger than the minimum loss rate $\gamma_{\min} = 1 + \min(\mathrm{Im}\Lambda_k)$. Therefore, the average value of $\min(\mathrm{Im}\Lambda_k)$ defines the average random laser threshold: $\langle\gamma_{\text{ampl}}^{\text{th}}\rangle = 1 + \langle\min(\mathrm{Im}\Lambda_k)\rangle$. It turns out that both this threshold criterion and the physical interpretation of its value in terms of the diffusion theory of light scattering might be incorrect. This will be discussed in chapters 6 and 7.

Chapter 3

How much quantum is the radiation process ?

3.1 Intensity and spectrum of light emitted by a cloud of atoms

Let us consider a photodetector located at $\mathbf{r}_d$ and illuminated by the light emitted by N atoms, at rest in a volume of typical size R, described by the Hamiltonian H (2.24). The probability for this detector (made of atoms itself) to be excited during the time interval Δt can be calculated using the second order perturbation theory and reads [52, 71]

$$P_{exc}(\Delta t) = \frac{1}{\hbar^2}\int_0^{\Delta t} \mathrm{d}t' \int_0^{\Delta t} \mathrm{d}t'' \mathcal{C}_D(t'-t'')\mathcal{C}_R(t',t''), \tag{3.1}$$

where $\mathcal{C}_D(t'-t'')$ and $\mathcal{C}_R(t',t'')$ are the correlations function of the detector and the radiation, respectively[1]. The explicit form of the latter is

$$\mathcal{C}_R(t',t'') = \langle \mathbf{E}(\mathbf{r}_d,t')\cdot\mathbf{E}(\mathbf{r}_d,t'')\rangle = \mathrm{Tr}_{\mathcal{E}}\left[\rho(0)\mathbf{E}(\mathbf{r}_d,t')\cdot\mathbf{E}(\mathbf{r}_d,t'')\right], \tag{3.2}$$

where ρ is the density matrix of the coupled system 'atoms+field' that evolves in the Hilbert space $\mathcal{E} = \mathcal{E}_A \otimes \mathcal{E}_R$. For the moment, external atomic degrees of freedom are voluntarily disregarded: 'disorder' will be discussed later. The expression (3.2) is commonly simplified by decomposing the field into its positive and negative frequency parts. Assuming the spectral width $\Delta\omega_D$ of the detector to be much larger than the characteristic frequency difference $\Delta\omega_R$ for which the field correlation function decays significantly, only one of the four resulting terms contributes significantly to P_{exc}, which then becomes [52]

$$P_{exc}(\Delta t) = \mathcal{N}\int_0^{\Delta t} \mathrm{d}t \langle \mathbf{E}^-(\mathbf{r}_d,t)\cdot\mathbf{E}^+(\mathbf{r}_d,t)\rangle, \tag{3.3}$$

where the factor $\mathcal{N}$ quantifies the detector efficiency. Hence we can define a measurable dimensionless light intensity

$$I(\mathbf{r}_d,t) = \langle \mathbf{\Omega}^-(\mathbf{r}_d,t)\cdot\mathbf{\Omega}^+(\mathbf{r}_d,t)\rangle = \mathrm{Tr}_{\mathcal{E}}\left[\rho(t)\mathbf{\Omega}^-(\mathbf{r}_d,0)\cdot\mathbf{\Omega}^+(\mathbf{r}_d,0)\right]. \tag{3.4}$$

[1] In the following we will not make use of the explicit form of $\mathcal{C}_D$. However, for a curious reader, we indicate how it looks like for a simple model of detector — an atom with a ground state $|a\rangle$ and excited states $|c\rangle$: $\mathcal{C}_D(t-t') = \sum_c |\langle a|D|c\rangle|^2 e^{-\mathrm{i}\omega_{ca}(t-t')}$, where ω_{ca} is the frequency difference between levels c and a, and D the component of the dipole operator of the detector parallel to the incoming field [52].

Here $\mathbf{\Omega}^{\pm}(\mathbf{r},t)$ is the dimensionless electric field operator:

$$\mathbf{\Omega}^{\pm}(\mathbf{r},t) = -\frac{2d\mathbf{E}^{\pm}(\mathbf{r},t)}{\hbar\Gamma_0}. \tag{3.5}$$

The power spectrum S is usually calculated by assuming the field emitted by the atoms to be a stationary random process. Then, it is related to the autocorrelation function (3.2) by the Wiener-Khintchine theorem. Its main component is

$$S(\mathbf{r}_d,\omega_L) = \int_{-\infty}^{\infty} \mathrm{d}\tau e^{-\mathrm{i}\omega_L\tau}\langle \mathbf{\Omega}^{-}(\mathbf{r}_d,t_s+\tau)\cdot\mathbf{\Omega}^{+}(\mathbf{r}_d,t_s)\rangle. \tag{3.6}$$

Here the time t_s is large enough for the system to be in the stationary regime. Note that assuming a steady spectrum is nontrivial: for a large assembly of atoms where light dynamics may exhibit chaos or random lasing, this hypothesis cannot be always valid.

Our purpose is to calculate the spectrum (3.6) as well as the intensity (3.4) for an arbitrary number of atoms. As it is suggested by the two different but equivalent expressions of the intensity in Eq. (3.4), we can use either the Schrödinger or the Heisenberg picture. In the former, the forward time evolution operator $U(t)$ that defines $\rho(t) = U(t)\rho(0)U^{\dagger}(t)$ is expressed as the Fourier transform of the retarded resolvent $\mathcal{G}(z) = (z - H + i\eta)^{-1}$, so that the intensity reads

$$I(\mathbf{r}_d,t) = \int_{-\infty}^{\infty}\frac{\mathrm{d}\omega}{2\pi}\int_{-\infty}^{\infty}\frac{\mathrm{d}\Delta\omega}{2\pi}e^{-\mathrm{i}\Delta\omega t}\mathrm{Tr}_{\mathcal{E}}\left[\rho(0)\mathcal{G}^{\dagger}(\omega-\frac{\Delta\omega}{2})\mathbf{\Omega}_0^{-}(\mathbf{r}_d)\cdot\mathbf{\Omega}_0^{+}(\mathbf{r}_d)\mathcal{G}(\omega+\frac{\Delta\omega}{2})\right]. \tag{3.7}$$

This expression is formally equivalent to the square modulus of Eq. (2.91), and for this reason can be reasonably calculated only for a few photons in the initial state $\rho(0) = \rho_A(0)\otimes\rho_R(0)$. For one photon, *i.e.* for $\rho_R(0) = |\mathbf{k}_{in}\boldsymbol{\epsilon}_{in}\rangle\langle\mathbf{k}_{in}\boldsymbol{\epsilon}_{in}|$, the integrand of Eq. (3.7) is proportional to a sum of propagation kernels, the generic form of which is $\mathrm{Tr}_{\mathcal{E}_A}\left[\rho_A(0)\langle\mathbf{k}_{in}\boldsymbol{\epsilon}_{in}|\mathcal{G}(\omega+\frac{\Delta\omega}{2})|\mathbf{k}\boldsymbol{\epsilon}\rangle\langle\mathbf{k}'\boldsymbol{\epsilon}'|\mathcal{G}^{\dagger}(\omega-\frac{\Delta\omega}{2})|\mathbf{k}_{in}\boldsymbol{\epsilon}_{in}\rangle\right]$. Such quantity can be computed within a diagrammatic framework, where usually only ladder and maximally crossed diagrams are considered [78].

Another option is the Heisenberg picture, in which we have the possibility to choose between the mesoscopic and the microscopic representations. As we have seen in section 2.4, this corresponds to eliminate either the atomic variables or the field. The mesoscopic representation is suitable if we can reduce the wave equation to the effective set of equations (2.89) and (2.90). In that case we write $\mathbf{\Omega}^{\pm}(\mathbf{r}_d,t) = \langle\mathbf{r}_d|\mathbf{\Omega}^{\pm}(t)\rangle$ with $|\mathbf{\Omega}^{\pm}(t)\rangle$ that belongs to the fictitious Hilbert space $\mathcal{E}^f$defined in section 2.4.2. The intensity (3.4) takes a form similar to Eq. (3.7), where the integrand has to be replaced by $\langle\langle\mathbf{\Omega}^{+}(\omega-\frac{\Delta\omega}{2})|\mathbf{r}_d\rangle\langle\mathbf{r}_d|\mathbf{\Omega}^{+}(\omega+\frac{\Delta\omega}{2})\rangle\rangle$. With the help of the Lippman-Schwinger equation, the field $|\mathbf{\Omega}^{+}(\omega)\rangle$ is then expanded in terms of the resolvent $\mathcal{G}^f$, $|\mathbf{\Omega}^{+}(\omega)\rangle = |\mathbf{\Omega}_0^{+}(\omega)\rangle + \mathcal{G}^f(\omega)V^f|\mathbf{\Omega}_0^{+}(\omega)\rangle$ (see section 2.4.2). Hence, again, the calculation reduces to evaluating the intensity propagator kernel, $\langle\mathcal{G}^f(\omega+\frac{\Delta\omega}{2})\otimes\mathcal{G}^{f\dagger}(\omega-\frac{\Delta\omega}{2})\rangle$, which now involves the operator $\mathcal{G}^f$ rather than $\mathcal{G}$. The dynamics of this quantity in the presence of gain will be discussed in chapter 4.

In the present chapter we shall concentrate on the microscopic representation of the Heisenberg picture. This is achieved by making use of the solution of the quantum wave equation (2.39). According to Eq. (2.48), the solution for the dimensionless electric field (3.5) is

$$\mathbf{\Omega}^{+}(\mathbf{r},\omega_L) = \mathbf{\Omega}_0^{+}(\mathbf{r},\omega_L) - \sum_{i=1}^{N}\mathbf{G}(\mathbf{r}-\mathbf{r}_i,\omega_L)\widetilde{\mathbf{D}}_i^{-}(\omega_L), \tag{3.8}$$

where all notations have been already defined in section 2.4.1. For future use we also introduce the scalar version of Eq. (3.8),

$$\Omega^+(\mathbf{r},\omega_L) = \Omega_0^+(\mathbf{r},\omega_L) - \sum_{i=1}^{N} G(\mathbf{r}-\mathbf{r}_i,\omega_L) S_i^-(\omega_L). \tag{3.9}$$

As we did in section 2.4.1, in free space and with $\Gamma_0 \ll \omega_0, c/R$, we approximate the Green's function in (3.8) as $\mathbf{G}(\mathbf{r}-\mathbf{r}_i,\omega_L) \simeq \mathbf{G}(\mathbf{r}-\mathbf{r}_i,\omega_0)$. Inserted into Eq. (3.4), this leads to four terms of which the most interesting is the one that is nonzero in the absence of photons ($\rho_R(0) = |0_R\rangle\langle 0_R|$):

$$I(\mathbf{r}_d,t) = \sum_{i,j}^{N} \mathrm{Tr}_{(3)} \left[\mathbf{G}^*(\mathbf{r}_d-\mathbf{r}_i,\omega_0) \langle \widetilde{\mathbf{D}}_i^+(t) \otimes \widetilde{\mathbf{D}}_j^-(t)\rangle \mathbf{G}(\mathbf{r}_d-\mathbf{r}_j,\omega_0) \right], \tag{3.10}$$

where $\mathrm{Tr}_{(3)}$ indicates the dyadic trace of a 3×3 tensor. Because we would like to get rid of all dependence on the position of the detector, we place the latter in the far-field $k_0|\mathbf{r}_d-\mathbf{r}_i| \gg 1$, such that, with Eq. (2.38), $\mathbf{G}(\mathbf{r}_d-\mathbf{r}_i,\omega_0) \simeq 3\mathbf{\Delta}_{\mathbf{r}_d}^{\perp} e^{\mathrm{i}k_0|\mathbf{r}_d-\mathbf{r}_i|}/2k_0 r_d$. Intensity (3.10) becomes

$$I(\mathbf{r}_d,t) \simeq \left(\frac{3}{2k_0 r_d}\right)^2 \sum_{i,j}^{N} e^{\mathrm{i}k_0(\mathbf{r}_i-\mathbf{r}_j)\cdot\mathbf{r}_d/r_d} \mathrm{Tr}_{(3)} \left[\mathbf{\Delta}_{\mathbf{r}_d}^{\perp} \langle \widetilde{\mathbf{D}}_i^+(t) \otimes \widetilde{\mathbf{D}}_j^-(t)\rangle \right]. \tag{3.11}$$

Using Eq. (3.9), we also get the scalar version of Eq. (3.11),

$$I(\mathbf{r}_d,t) \simeq \frac{1}{(k_0 r_d)^2} \sum_{i,j}^{N} e^{\mathrm{i}k_0(\mathbf{r}_i-\mathbf{r}_j)\cdot\mathbf{r}_d/r_d} \langle S_i^+(t) S_j^-(t)\rangle \qquad \text{(scalar field)}. \tag{3.12}$$

After integrating over the direction of $\mathbf{r}_d$, we obtain

$$I(r_d,t) \simeq \frac{4\pi}{(k_0 r_d)^2} \sum_{i,j}^{N} \frac{\sin k_0|\mathbf{r}_i-\mathbf{r}_j|}{k_0|\mathbf{r}_i-\mathbf{r}_j|} \langle S_i^+(t) S_j^-(t)\rangle. \tag{3.13}$$

Following exactly the same line, the spectrum (3.6) of a scalar field takes, in the far-field, the form

$$S(r_d,\omega_L) \simeq \frac{8\pi}{(k_0 r_d)^2} \sum_{i,j}^{N} \frac{\sin k_0|\mathbf{r}_i-\mathbf{r}_j|}{k_0|\mathbf{r}_i-\mathbf{r}_j|} \mathrm{Re}\left[\int_{-\infty}^{\infty} \mathrm{d}\tau e^{-\mathrm{i}\omega_L\tau} \langle S_i^+(t_s+\tau) S_j^-(t_s)\rangle \Theta(\tau) \right]. \tag{3.14}$$

From now on, we will drop the geometric prefactor $4\pi/(k_0 r_d)^2$ that appears in I and S.

At this stage, we need to introduce a couple of notations. First, for future purpose, we define new operators

$$s_i^{\pm}(t) = e^{\mp\mathrm{i}\omega_a t} S_i^{\pm}(t), \tag{3.15}$$

where ω_a is an auxiliary tunable parameter that will be useful in the next section to move in the rotating frame of an optical pump. Moreover, it is convenient to introduce two $N\times N$ matrices

$$\mathcal{S}_{ij} = \frac{\sin k_0|\mathbf{r}_i-\mathbf{r}_j|}{k_0|\mathbf{r}_i-\mathbf{r}_j|}, \tag{3.16}$$

$$\mathcal{C}_{ij}(\tau) = \langle s_i^+(t_s+\tau) s_j^-(t_s)\rangle \Theta(\tau), \tag{3.17}$$

so that the spectrum (3.14) takes the compact form $S(\omega_L) = 2\mathrm{Tr}_{(N)}\left[\mathcal{S}\mathrm{Re}\,\mathcal{C}(\omega_a - \omega_L)\right]$. It is worth noting that the presence of the matrix $\mathcal{S}$ in Eq. (3.13) or Eq. (3.14) is not in any way related to the interactions between different atoms. It is simply a consequence of the fact that signals are measured in the far-field, while the information about decay rates is entirely, and only, contained in the dipole correlator $\langle S_i^+(t_s+\tau)S_j^-(t)\rangle$. We also define a matrix $\mathcal{Y}$ of size $N' \times N$,

$$\mathcal{Y}_{kj}(\tau) = \langle x_k(t_s+\tau)s_j^-(t_s)\rangle, \tag{3.18}$$

where x_k designates the N operators s_i^+ as well as any atomic operator coupled to them in equations of motion. Hence $N' > N$. Furthermore, let us assume that this matrix obeys a linear differential equation,

$$\frac{\mathrm{d}}{\mathrm{d}\tau}\mathcal{Y} = \mathcal{M}\mathcal{Y} + \mathcal{R}, \tag{3.19}$$

where $\mathcal{M}$ and $\mathcal{R}$ are time-independent matrices of sizes $N' \times N'$ and $N' \times N$, respectively. Then, using definitions (3.17) and (3.18), and Eq. (3.19), we readily obtain an expression for the spectrum (in units of Γ_0^{-1}) in terms of $\mathcal{M}$, $\mathcal{R}$ and $\mathcal{Y}(0)$:

$$\begin{aligned} S(\omega_L) = &-2\pi\,\mathrm{Tr}_{(N)}\left[\mathcal{S}P\mathrm{Re}\left[\mathcal{M}^{(-1)}\mathcal{R}\right]\right]\delta\left[(\omega_L-\omega_p)/\Gamma_0\right] \\ &+2\,\mathrm{Tr}_{(N)}\left[\mathcal{S}P\mathrm{Re}\left[\left[\mathrm{i}(\omega_L-\omega_p)\mathrm{I}_{N'}/\Gamma_0 - \mathcal{M}\right]^{-1}\left[\mathcal{Y}(0)+\mathcal{M}^{(-1)}\mathcal{R}\right]\right]\right], \end{aligned} \tag{3.20}$$

where $\mathrm{I}_{N'}$ is the $N' \times N'$ identity matrix and P is a $N \times N'$ matrix that represents the projector on the subspace generated by the N operators S_i^+. In this formula the unknown quantities are $\mathcal{Y}(0)$, $\mathcal{M}$ and $\mathcal{R}$. The first is defined in Eq. (3.18), and the two others were supposed to characterize the dynamics of $\mathcal{Y}$ in Eq. (3.19). Such dynamics exists if the quantum fluctuation-regression theorem is fulfilled [110, 111]. In that case $\mathcal{M}$ is defined as the kernel of the evolution of the vector $\mathbf{x} = (\langle x_1\rangle, ..., \langle x_{N'}\rangle)$,

$$\frac{\mathrm{d}}{\mathrm{d}\tau}\mathbf{x} = \mathcal{M}\mathbf{x} + \boldsymbol{\lambda}. \tag{3.21}$$

The free parameter ω_a that is contained in the definition of $\mathbf{x}$ is chosen such that the matrix $\mathcal{M}$ is effectively time-independent. If it is not possible to write the dynamics of $\mathbf{x}$ in the form (3.21), then the spectrum is not given by (3.20). The matrix $\mathcal{R}$ is related to $\boldsymbol{\lambda}$ according to

$$\mathcal{R}_{kj} = \lambda_k\langle s_j^-(t_s)\rangle. \tag{3.22}$$

In order to infer the spectrum (3.20) we simply need to find the matrix $\mathcal{M}$, and calculate $\mathcal{Y}(0)$ and $\mathcal{R}$ from $\mathbf{x}(t_s)$. This will be illustrated in the two following sections. Eq. (3.20) nicely shows us that the N' eigenvalues of $\mathcal{M}$ are the resonances of the spectrum: imaginary parts give their frequencies and real parts their spectral widths. Besides, note that the general structure (3.20) holds for a vectorial field as well. Indeed, it is sufficient to replace the product of operators that appears in Eq. (3.13) by the tensor product of Eq. (3.11). All matrices of size $N \times N$ or $N' \times N$, like $\mathcal{Y}$, become $3N \times 3N$ or $N' \times 3N$, and the matrix $\mathcal{S}$ reads now $\mathcal{S}_{ij} = \boldsymbol{S}(\mathbf{r}_i - \mathbf{r}_j)$, where

$$\boldsymbol{S}(\mathbf{r}) = \frac{3\sin k_0 r}{2k_0 r}\boldsymbol{\Delta}_{\mathbf{r}}^{\perp} + \frac{3}{2(k_0 r)^2}\left(\cos k_0 r - \frac{\sin k_0 r}{k_0 r}\right)\left(\mathbf{I} - 3\frac{\mathbf{r}\otimes\mathbf{r}}{r^2}\right) \tag{3.23}$$

is nothing but the imaginary part of the dyadic Green's matrix $\mathbf{G}_{ij}(\omega_0)$, see Eqs. (2.36) and (2.70).

Signals (3.13) and (3.14) contain classical and quantum contributions. To emphasize this fact we isolate the deviation of each quantum operator from its quantum expectation value

$$S_i^{\pm} = \langle S_i^{\pm} \rangle + \delta S_i^{\pm}, \tag{3.24}$$

such that the correlation function of S_i^+ and S_j^- can be written as a sum of 'classical' and 'quantum' contributions:

$$\langle S_i^+(t+\tau) S_j^-(t) \rangle = \langle S_i^+(t+\tau) \rangle \langle S_j^-(t) \rangle + \langle \delta S_i^+(t+\tau) \delta S_j^-(t) \rangle. \tag{3.25}$$

Within the stationary spectrum hypothesis, classical terms give rise to the monochromatic contribution in Eq. (3.20), while quantum terms account for the second term on its r.h.s. In the same manner, the classical part of the stationary intensity (3.13) is

$$I^c = \sum_{i,j}^{N} \frac{\sin k_0 |\mathbf{r}_i - \mathbf{r}_j|}{k_0 |\mathbf{r}_i - \mathbf{r}_j|} \langle S_i^+(t_s) \rangle \langle S_j^-(t_s) \rangle, \tag{3.26}$$

and its quantum part $I^q = I - I^c$ reads

$$I^q = \sum_{i,j}^{N} \frac{\sin k_0 |\mathbf{r}_i - \mathbf{r}_j|}{k_0 |\mathbf{r}_i - \mathbf{r}_j|} \langle \delta S_i^+(t_s) \delta S_j^-(t_s) \rangle. \tag{3.27}$$

One goal of this chapter is to understand the role and the origin of these two contributions. In particular, we would like to assess the importance of quantum interatomic correlations, $\langle \delta S_i^+(t+\tau) \delta S_j^-(t) \rangle$ for $i \neq j$, when we increase the number N of atoms. Inasmuch as the answer very much depends on the pumping scheme, we will make a distinction between coherent and incoherent pumps.

3.2 Introduction of a pumping mechanism

3.2.1 Coherent pump

Let us consider the light initially prepared in a coherent state, $\rho_R(0) = |\alpha_p\rangle\langle\alpha_p|$, associated with the mode $\mathbf{k}_p \boldsymbol{\epsilon}_p$ [see Fig. 3.1 (a)]. In atomic physics it is well known [52] that a unitary transform can be applied to the Hamiltonian (2.24) such that the initial state becomes $|0_R\rangle$ and the free field $\mathbf{E}_0^+(\mathbf{r}, t)$ acquires a new component

$$\mathbf{E}_p^+(\mathbf{r}, t) = E_p \boldsymbol{\epsilon}_p e^{\mathrm{i}(\mathbf{k}_p \cdot \mathbf{r} - \omega_p t)}, \tag{3.28}$$

with $E_p = \alpha_p \sqrt{\hbar \omega_p / 2\epsilon_0 \mathcal{V}}$. Taking into account this new classical and coherent field, we replace in equations of motions (2.72) and (2.73) the operator $\mathbf{\Omega}_0^{\pm}(\mathbf{r}, t)$ with $\mathbf{\Omega}_0^{\pm}(\mathbf{r}, t) + \mathbf{\Omega}_p^{\pm}(\mathbf{r}) e^{\mp \mathrm{i}\omega_p t}$, where $\mathbf{\Omega}_p^{\pm}(\mathbf{r}) = -2dE_p \boldsymbol{\epsilon}_p e^{\pm \mathrm{i}\mathbf{k}_p \cdot \mathbf{r}} / \hbar\Gamma_0$. Moreover, terms that involve $\mathbf{\Omega}_0^{\pm}$ behave now as Langevin forces since all quantum expectations values are taken with respect to $|0_R\rangle$ (see section 2.4.1 for details). Explicitly, in the rotating frame of the

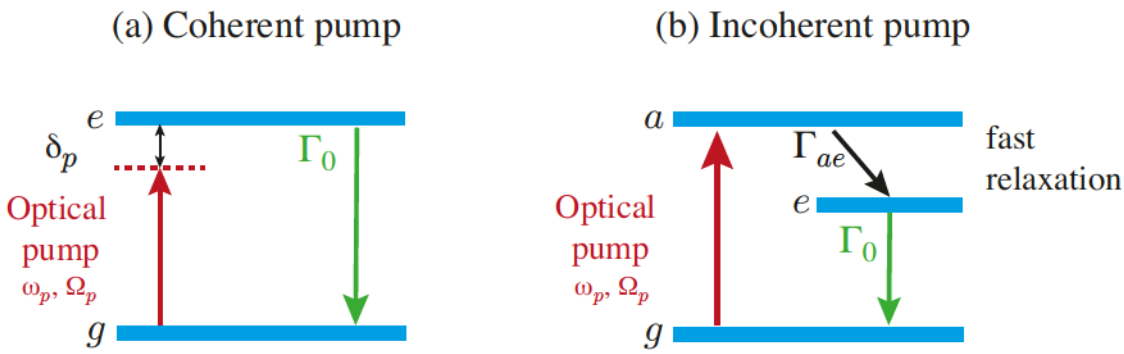

Figure 3.1: (a) Coherent optical pump (amplitude Ω_p, frequency $\omega_p = \omega_0 + \Gamma_0\Delta_p$) near resonance ($|\omega_p - \omega_0| \ll \omega_0$). (b) Effective incoherent pump: the optical pump is on resonance with an auxiliary level a, and $\Gamma_{ae} \gg \Gamma_0, \Gamma_0\Omega_p$.

pump, Eqs. (2.72) and (2.73) read now

$$\frac{\mathrm{d}\tilde{\tilde{\mathbf{D}}}_i^+}{\mathrm{d}t} = -\left(\mathrm{i}\Delta_p + \frac{1}{2}\right)\tilde{\tilde{\mathbf{D}}}_i^+ + \frac{\mathrm{i}}{2}\boldsymbol{\Delta}_i^{\parallel}\sum_{j\neq i}\mathbf{G}_{ij}^*(\omega_0)\tilde{\tilde{\mathbf{D}}}_j^+\Pi_i - \frac{\mathrm{i}}{2}\boldsymbol{\Delta}_i^{\parallel}\boldsymbol{\Omega}_p^-(\mathbf{r}_i)\Pi_i + \boldsymbol{\mathcal{F}}_i^+(t), \tag{3.29}$$

$$\frac{\mathrm{d}\Pi_i}{\mathrm{d}t} = -(\Pi_i + 1) - 2\mathrm{Im}\left[\tilde{\tilde{\mathbf{D}}}_i^+ \cdot \sum_{j\neq i}\mathbf{G}_{ij}(\omega_0)\tilde{\tilde{\mathbf{D}}}_j^-\right] + 2\mathrm{Im}\left[\tilde{\tilde{\mathbf{D}}}_i^+ \cdot \boldsymbol{\Omega}_p^+(\mathbf{r}_i)\right] + \mathcal{F}_i^{\Pi}(t). \tag{3.30}$$

Here $\tilde{\tilde{\mathbf{D}}}_i^{\pm} = e^{\mp\mathrm{i}\omega_p t}\tilde{\mathbf{D}}_i^{\pm}$, $\Delta_p = (\omega_p - \omega_0)/\Gamma_0$, the time t is in units of Γ_0^{-1}, and Langevin forces are

$$\boldsymbol{\mathcal{F}}_i^+(t) = -\frac{\mathrm{i}}{2}\boldsymbol{\Delta}_i^{\parallel}\boldsymbol{\Omega}_0^-(\mathbf{r}_i, t)\Pi_i(t)e^{-\mathrm{i}\omega_p t}, \tag{3.31}$$

$$\mathcal{F}_i^{\Pi}(t) = \mathrm{i}\boldsymbol{\Omega}_0^-(\mathbf{r}_i, t)\cdot\tilde{\mathbf{D}}_i^-(t) - \mathrm{i}\tilde{\mathbf{D}}_i^+(t)\cdot\boldsymbol{\Omega}_0^+(\mathbf{r}_i, t). \tag{3.32}$$

The scalar version of Eqs. (3.29) and (3.30) is straightforward to obtain from Eqs. (2.78) and (2.79).

Before discussing the spectrum that we can infer from Eqs. (3.29) and (3.30), we would like to show what these equations become when the pump is not coherent.

3.2.2 Incoherent pump

The first idea we can have to mimic an incoherent pump is to introduce a phenomenological stationary value of the atomic population imbalance $\Pi_i^{eq} \neq -1$. Eqs. (2.65) and (2.66) would transform into

$$\frac{\mathrm{d}\mathbf{D}_i^+}{\mathrm{d}t} = \mathrm{i}\omega_0\mathbf{D}_i^+ - \frac{\Gamma_0}{2}\mathbf{D}_i^+ + \frac{\mathrm{i}}{\hbar}\left[\mathbf{d}_i \otimes \mathbf{d}_i\right]\mathbf{E}_s^-(\mathbf{r}_i)\Pi_i, \tag{3.33}$$

$$\frac{\mathrm{d}\Pi_i}{\mathrm{d}t} = -\Gamma_0\left(\Pi_i - \Pi_i^{eq}\right) + \frac{2\mathrm{i}}{\hbar}\left[\mathbf{D}_i^+ \cdot \mathbf{E}_s^+(\mathbf{r}_i) - \mathbf{E}_s^-(\mathbf{r}_i)\cdot\mathbf{D}_i^-\right]. \tag{3.34}$$

In the absence of interatomic interactions, Π_i^{eq} is the stationary value of the population imbalance controlled by the pump. This apparently reasonable procedure, which is commonly used in the standard laser theory [23], and also in nonlinear optics [112], does not lead to any contradiction as long as we work with a single atom. However, already for two atoms, the solution of Eqs. (3.33) and (3.34) reveals that the quantum expectation values $\langle \Pi_i \rangle$ are no more restricted to $[-1, 1]$, as they physically have to. Therefore, to get rid of unphysical results, we shall proceed to a microscopic and well controlled description of the incoherent pump.

The simplest microscopic scheme of an effective incoherent pump for a two-level atom is a coherent field on resonance with an auxiliary third level $|a\rangle$ [see Fig. 3.1 (b)]. The atomic response to such a pump was studied recently in details by Savels *et al.* within the master-equation formalism [113, 114]. Here we use the Heisenberg picture. Dealing with three-level atoms without degeneracy, description of internal degrees of freedom requires to write the dynamical equations of motion for $5N$ operators (instead of $2N$ for two-level atoms). Without giving their lengthy derivations, we present here the main steps. First, we express the $5N$ Heisenberg equations of motion in terms of the total electric field $\mathbf{E}$, as we did in section 2.3.2.b. Next, we isolate the own radiation fields to reveal the spontaneous decay rates. Third, we decompose the smoothed field $\mathbf{E}_s$ in three parts: its free component that features Langevin forces, a coherent classical field $\mathbf{E}_p$ of type (3.28) associated with the coherent state of the pump, and the field radiated by atoms — see Eq. (2.59). And finally, we simplify the resulting equations under the following assumptions:

$$|\omega_p - \omega_{ag}| \ll \omega_{ag}, \tag{3.35}$$

$$\Gamma_{ag} \ll \Gamma_0, \Gamma_0 \Omega_p \ll \Gamma_{ae} \ll \omega_{ag},\ \omega_{ae},\ \omega_0. \tag{3.36}$$

The assumption (3.35) indicates that the optical pump is quasi-resonant with the auxiliary level, and (3.36) means that all levels are not excessively broad and each excitation generated by the pump from $|g\rangle$ to $|a\rangle$ is transferred to $|e\rangle$ almost instantaneously [see Fig. 3.1 (b)]. With these assumptions, it is possible to reduce the $5N$ equations to effective $2N$ equations that only involve the levels $|g\rangle$ and $|e\rangle$. The strength of the pump on atom i is controlled by a single dimensionless parameter

$$W_i = \frac{\Gamma_0 |\Omega_{p,i}|^2}{\Gamma_{ae}}, \tag{3.37}$$

where $\Omega_{p,i} = -2\mathbf{d}_{ga,i} \cdot \mathbf{E}_p^+(\mathbf{r}_i)/\hbar\Gamma_0$ with $\mathbf{d}_{ga,i}$ the dipole moment for the $|g_i\rangle \to |a_i\rangle$ transition. In the leading order, the pump only affects the monoatomic parts of dynamical equations: atomic interactions contained in the smoothed field (2.59) concern the two level transition and thus are essentially unaffected by the pump that efficiently triggers the auxiliary level only. Furthermore, as was the case for the coherent pump, all information about photons that are initially injected into the atomic medium is transferred into a classical pump field, meaning that quantum expectation values have now to be taken with respect to $|0_R\rangle$: action of the free field reduces to a Langevin force. Dynamical

equations of motion (2.72) and (2.73) in the presence of incoherent pump become

$$\frac{\mathrm{d}\widetilde{\mathbf{D}}_i^+}{\mathrm{d}t} = \left[\mathrm{i}\frac{\omega_0}{\Gamma_0} - \frac{1}{2}(1+W_i)\right]\widetilde{\mathbf{D}}_i^+ + \frac{\mathrm{i}}{2}\boldsymbol{\Delta}_i^{\parallel}\sum_j \mathbf{G}_{ij}^*(\omega_0)\widetilde{\mathbf{D}}_j^+\Pi_i + \boldsymbol{\mathcal{F}}_i^+(\mathbf{r}_i,t), \tag{3.38}$$

$$\frac{\mathrm{d}\Pi_i}{\mathrm{d}t} = -(1+W_i)\,\Pi_i + W_i - 1 - 2\mathrm{Im}\left[\widetilde{\mathbf{D}}_i^+\cdot\sum_j \mathbf{G}_{ij}(\omega_0)\widetilde{\mathbf{D}}_j^-\right] + \mathcal{F}_i^{\Pi}(\mathbf{r}_i,t). \tag{3.39}$$

Because the effective pump is incoherent, we do not need to move in the rotating frame of the pump field. Consequently, the Langevin forces are defined by Eqs. (3.31) and (3.32) with $\omega_p = 0$.

If we just look at the monoatomic part of Eqs. (3.38) and (3.39), the pump modifies the Bloch equations in two ways. It changes the value of the population imbalance at equilibrium, and it renormalizes the spontaneous emission rate of each atom:

$$\Pi_i^{eq} = \frac{W_i - 1}{W_i + 1}, \tag{3.40}$$

$$\Gamma_i = (1+W_i)\Gamma_0. \tag{3.41}$$

For $W_i = 1$, the population imbalance vanishes at equilibrium, meaning that independent atoms excited by such an incoherent process are transparent for external radiation. However, this simple picture must be reconsidered as soon as we take into account interatomic coupling.

In the following, we will sometimes neglect the vectorial nature of the field. In that case, we shall work with equations similar to Eqs. (2.78) and (2.79), which become in the presence of the pump

$$\frac{\mathrm{d}S_i^+}{\mathrm{d}t} = \left[\mathrm{i}\frac{\omega_0}{\Gamma_0} - \frac{1}{2}(1+W_i)\right]S_i^+ + \frac{\mathrm{i}}{2}\Pi_i\sum_j G_{ij}^*(\omega_0)S_j^+ + \mathcal{F}_i^+(t), \tag{3.42}$$

$$\frac{\mathrm{d}\Pi_i}{\mathrm{d}t} = -(1+W_i)\,\Pi_i + W_i - 1 - 2\mathrm{Im}\left[S_i^+\sum_j G_{ij}(\omega_0)S_j^-\right] + \mathcal{F}_i^{\Pi}(t), \tag{3.43}$$

where the time t is in units of Γ_0^{-1}, and the Langevin forces are

$$\mathcal{F}_i^+(t) = -\frac{\mathrm{i}}{2}\Omega_0^-(\mathbf{r}_i,t)\Pi_i(t), \tag{3.44}$$

$$\mathcal{F}_i^{\Pi}(t) = \mathrm{i}\Omega_0^-(\mathbf{r}_i,t)S_i^-(t) - \mathrm{i}S_i^+(t)\Omega_0^+(\mathbf{r}_i,t). \tag{3.45}$$

Equations (3.38) and (3.39) — or their scalar version (3.42) and (3.43) — contain all the information we need to describe an atomic random laser. The semiclassical threshold depends on the respective strength of the pump parameters $\{W_i\}$ and the interaction coefficients $\{\mathbf{G}_{ij}\}$, while all quantum effects are embedded in the fact that operators do not commute and in the quantum Langevin forces.

We also point out that it is not *a priori* straightforward to infer dynamical equations of motion of $\langle S_i^+(t)\rangle = \langle 0_R|S_i^+(t)|0_R\rangle$ and $\langle\Pi_i(t)\rangle$ from the previous equations. When taking the quantum expectation value of those equations with respect to $|0_R\rangle$, we do not get a close set since $\langle S_i^+(t)\rangle$ and $\langle\Pi_i(t)\rangle$ are coupled to the unknown quantities $\langle\Pi_i(t)S_j^+(t)\rangle$ and $\langle S_i^+(t)S_j^-(t)\rangle$. The quantum Langevin forces, the expectation value

	Coherent pump	Incoherent pump
$\boldsymbol{\lambda}$	$(0,-1,0)$	$(0,-1+W,0)$
$\mathcal{M}$	$-\begin{pmatrix} \mathrm{i}\delta_p+\frac{1}{2} & \frac{\mathrm{i}\Omega_p}{2} & 0 \\ \frac{\mathrm{i}\Omega_p}{2} & 1 & -\frac{\mathrm{i}\Omega_p}{2} \\ 0 & -\frac{\mathrm{i}\Omega_p}{2} & -i\delta_p+\frac{1}{2} \end{pmatrix}$	$-\begin{pmatrix} -\frac{\mathrm{i}\omega_0}{\Gamma_0}+\frac{1+W}{2} & 0 & 0 \\ 0 & 1+W & 0 \\ 0 & 0 & \frac{\mathrm{i}\omega_0}{\Gamma_0}+\frac{1+W}{2} \end{pmatrix}$
$I^c=\langle S^+\rangle\langle S^-\rangle$	$\frac{(1+4\delta_p^2)\Omega_p^2}{(1+4\delta_p^2+2\Omega_p^2)^2}$	0
$I=\frac{1+\langle\Pi\rangle}{2}$	$\frac{\Omega_p^2}{1+4\delta_p^2+2\Omega_p^2}$	$\frac{W}{W+1}$
$I^q=I-I^c$	$\frac{2\Omega_p^4}{(1+4\delta_p^2+2\Omega_p^2)^2}$	$\frac{W}{W+1}$

Table 3.1: $\boldsymbol{\lambda}$ and $\mathcal{M}$ are quantities that are useful to compute the spectrum (3.20) of light emitted by a single atom. $\mathbf{x}(t_s)=-\mathcal{M}^{(-1)}\boldsymbol{\lambda}=(x_1,x_2,x_3)$, in terms of which $\mathcal{Y}(0)=(1/2+x_2/2,-x_3,0)$ and $\mathcal{R}=x_3\boldsymbol{\lambda}$. Different contributions of the stationary intensiy depend only on $\mathbf{x}(t_s)$: $I^c=|x_1|^2$ and $I=(1+x_2)/2$.

of which is zero, actually contain the information that is necessary to reconstruct the complete dynamics. In this manuscript we call semi-classical the approximation that consists in replacing the quantum expectation value of the product of any quantum operators X_i and Y_j by the product of their quantum expectations values:

$$\langle 0_R|X_i(t)Y_j(t)|0_R\rangle \simeq \langle 0_R|X_i(t)|0_R\rangle\langle 0_R|Y_j(t)|0_R\rangle. \tag{3.46}$$

Intuitively, this approximation is expected to hold in the limit $N\to\infty$. It is very useful because now we only need $2N$ equations to close the set where appear $\langle S_i^+(t)\rangle$ and $\langle\Pi_i(t)\rangle$. But regarding spectrum properties, it amounts to neglecting quantum terms in Eq. (3.25).

3.2.3 One atom spectrum: coherent vs incoherent pump

Let us calculate the spectrum of light in the simple case of a single atom placed at $\mathbf{r}=\mathbf{0}$. Then, the terms that couple different atoms in Eqs. (3.29) and (3.30), as well as in Eqs. (3.38) and (3.39), disappear. The vector $\mathbf{x}$ defined in section 3.1 has only $N'=3$ components, $\mathbf{x}=(\langle s^+\rangle,\langle\Pi\rangle,\langle s^-\rangle)$, with $\omega_a=\omega_p$ for the coherent pump and $\omega_a=0$ for the incoherent pump. In Table 3.1, we give explicit expressions for the vector $\boldsymbol{\lambda}$ and the matrix $\mathcal{M}$ defined in Eq. (3.21). With a single atom, it is straightforward to verify that the matrix $\mathcal{Y}$ defined in Eq. (3.18) obeys Eq. (3.19). It means that the quantum fluctuation-regression theorem holds and, therefore, we can compute the spectrum from Eq. (3.20).

The main features of the monoatomic emission spectrum induced by a coherent pump are depicted in Fig. 3.2. On the one hand, the classical and monochromatic component of (3.20) is elastic with respect to the incident field ($\omega_L=\omega_p$). It is used to define, at small Ω_p, the elastic cross-section. When the intensity of the incident field is increased, the elastic response becomes nonlinear and is eventually suppressed at large Ω_p [see Fig. 3.2(b)]. On the other hand, when we increase Ω_p, the quantum contribution to the

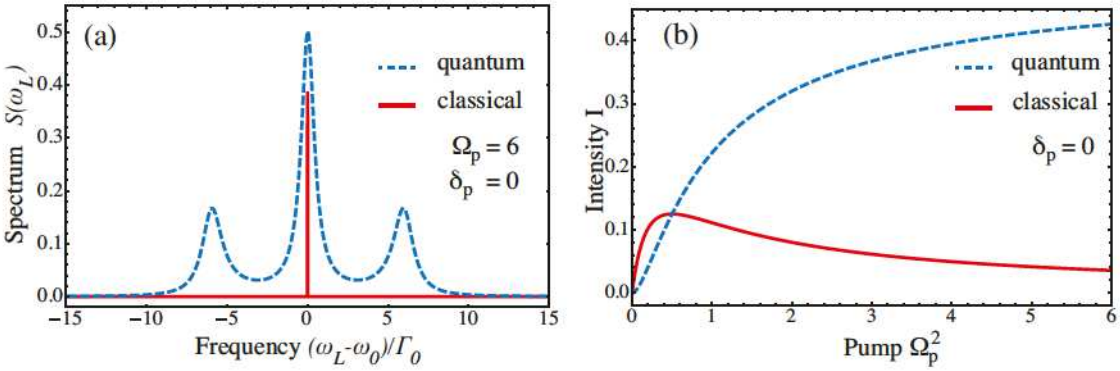

Figure 3.2: Spectrum and intensity of light emitted by an atom in the field of a coherent on-resonance pump ($\delta_p = 0$). (a) Classical and quantum contributions of the spectrum (3.20). (b) Stationary intensity $I = \int_{-\infty}^{\infty} d\omega_L S(\omega_L)/2\pi$. The classical and quantum components, I^c and I^q, are defined by Eqs. (3.26) and (3.27).

spectrum (3.20) becomes more and more important. The three different eigenvalues of the matrix $\mathcal{M}$ define three resonances that constitute the well-known 'Mollow-triplet' [115, 116]. The quantum contribution gives rise, therefore, to inelastic scattering.

The situation is completely different with the incoherent pump. Now, in the stationary regime atomic dipoles are zero, and thus the classical part of the spectrum vanishes. Furthermore, eigenvalues of $\mathcal{M}$ give rise to only one fluorescence-like resonance centered at $\omega_L = \omega_0$. As shown in Fig. 3.3(a), its width is controlled by Γ defined in Eq. (3.41). Finally, contrary to the coherent case, it is possible to get a population inversion ($\langle\Pi\rangle > 1$) for $W > 1$, so that $I = (1 + \langle\Pi\rangle)/2 > 0.5$ [compare Figs. 3.2(b) and 3.3(b)].

In the prospect of a description of a random laser composed of a large number N of atoms, there are reasons to prefer the incoherent scheme to the coherent one. First, it is close to the historical description of the standard cavity laser [23]. Second, we can properly define and detect a threshold as the point where classical dipoles become nonzero in the stationary regime. Third, the quantum part of the spectrum is simpler, inasmuch as we have only one monoatomic resonance and not three. This explains why, from here on, we shall concentrate ourselves on the incoherent scheme. We will return to the coherent pump later in chapters 4 and 7.

3.3 Properties of quantum Langevin forces

The purpose of this section is to present basic properties of the Langevin forces (3.44) and (3.45) that are necessary to compute the spectrum emitted by $N > 1$ atoms.

First of all, using $\Omega_0^+|0_R\rangle = 0$ and $\langle 0_R|\Omega_0^- = 0$, we note that quantum expectation values of the Langevin forces with respect to $|0_R\rangle$, as well as some of their time correlation functions, are zero:

$$\begin{aligned} \langle \mathcal{F}_i^{\pm}(t)\rangle &= 0, & \langle \mathcal{F}_i^{\Pi}(t)\rangle &= 0, \\ \left\langle \mathcal{F}_i^{\pm}(t)\mathcal{F}_j^{\pm}(t')\right\rangle &= 0, & \left\langle \mathcal{F}_i^{+}(t)\mathcal{F}_j^{-}(t')\right\rangle &= 0, \\ \left\langle \mathcal{F}_i^{+}(t)\mathcal{F}_j^{\Pi}(t')\right\rangle &= 0, & \left\langle \mathcal{F}_i^{\Pi}(t)\mathcal{F}_j^{-}(t')\right\rangle &= 0. \end{aligned} \tag{3.47}$$

Other time correlation functions essentially depend on the two time commutator

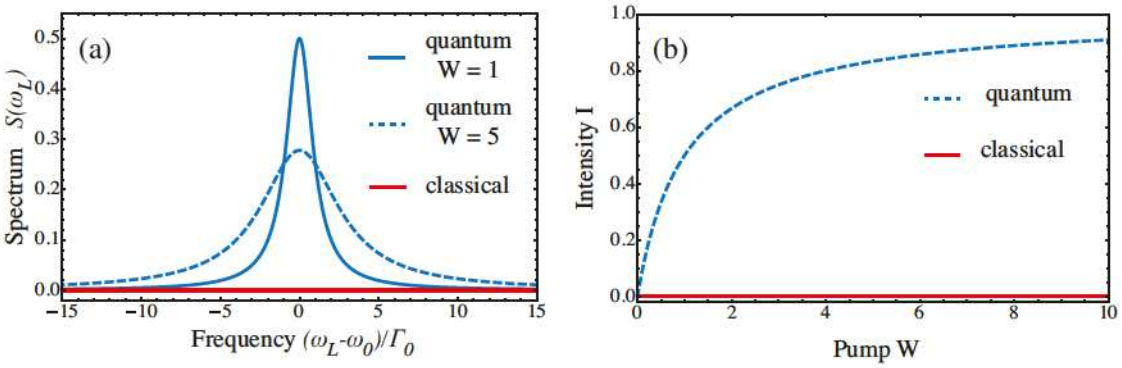

Figure 3.3: Spectrum and intensity of light emitted by an atom in the field of an incoherent pump. (a) and (b): same as in Fig. 3.2.

$[\Omega_0^+(\mathbf{r}_i,t),\Omega_0^-(\mathbf{r}_j,t')]$, where the vacuum field $\Omega_0^\pm = -2dE_0^\pm/\hbar\Gamma_0$ is proportional to the solution of the Helmholtz equation in the absence of atoms. Thus, by definition, correlation properties of $\Omega_0^\pm$ are such that two points in space-time, $(\mathbf{r}_i,t)$ and $(\mathbf{r}_j,t')$, that cannot be connected by light signals, are not correlated [52, 74]. Explicitly, with the scalar version of Eq. (2.44), we get

$$\begin{aligned}[\Omega_0^+(\mathbf{r}_i,t),\Omega_0^-(\mathbf{r}_j,t')] &= \left(\frac{2d}{\hbar\Gamma_0}\right)^2 \sum_{\mathbf{k}} \mathcal{E}_{\mathbf{k}}^2 e^{\mathrm{i}[\mathbf{k}\cdot(\mathbf{r}_i-\mathbf{r}_j)-\omega(t-t')]} \\ &= \frac{2}{\Gamma_0^2} f(\mathbf{r}_i-\mathbf{r}_j,t-t'). \end{aligned} \tag{3.48}$$

The function $f(\mathbf{r},\tau)$ has two maxima at $\tau=\pm r/c$. In the frequency domain,

$$[\Omega_0^+(\mathbf{r}_i,\omega_L),\Omega_0^-(\mathbf{r}_j,\omega_L')] = \frac{4\pi}{\Gamma_0^2} f(\mathbf{r}_i-\mathbf{r}_j,\omega_L)\delta(\omega_L+\omega_L'), \tag{3.49}$$

with

$$f(\mathbf{r}_i-\mathbf{r}_j,\omega_L) = \Gamma(k_L)\frac{\sin k_L|\mathbf{r}_i-\mathbf{r}_j|}{k_L|\mathbf{r}_i-\mathbf{r}_j|}, \tag{3.50}$$

and $\Gamma(k_L) = d^2k_L^3/2\pi\epsilon_0\hbar$. For frequencies ω_L such that $|\omega_L-\omega_0| \ll \omega_0$, we use $f(\mathbf{r},\omega_L)\simeq f(\mathbf{r},\omega_0)$, so that Eq. (3.48) becomes

$$[\Omega_0^+(\mathbf{r}_i,t),\Omega_0^-(\mathbf{r}_j,t')] \simeq \frac{2}{\Gamma_0}\frac{\sin k_0|\mathbf{r}_i-\mathbf{r}_j|}{k_0|\mathbf{r}_i-\mathbf{r}_j|}\delta(t-t'). \tag{3.51}$$

In the same approximation, we also have

$$[S_i^+(t),\Omega_0^-(\mathbf{r}_j,t')] = 0, \tag{3.52}$$

$$[S_i^+(t),\Omega_0^+(\mathbf{r}_j,t')] = G_{ij}^\perp(\omega_0)\Pi_i(t)\delta_{t,t'}, \tag{3.53}$$

$$[\Pi_i(t),\Omega_0^+(\mathbf{r}_j,t')] = -2G_{ij}^\perp(\omega_0)S_i^-(t)\delta_{t,t'}, \tag{3.54}$$

where $G_{ij}^\perp(\omega_0) = G_{ij}(\omega_0)+\delta(\mathbf{0})\delta_{ij}$ is the scalar form of the transverse Green's function defined by Eq. (2.34). A very simple way to derive Eqs. (3.52), (3.53), and (3.54) for

$t = t'$ consists in expressing $\Omega_0^+(\mathbf{r}_j, t)$ in terms of the solution (2.30) of the propagation equation for the transverse field $\Omega_\perp^+(\mathbf{r}_j, t) = -2dE_\perp^+(\mathbf{r}_j, t)/\hbar\Gamma_0$:

$$\Omega_0^+(\mathbf{r}_j, t) = \Omega_\perp^+(\mathbf{r}_j, t) + \sum_{l=1}^{N} G_{jl}^\perp(\omega_0) S_l^-(t). \tag{3.55}$$

For any atomic operator $X_i(t)$, $[X_i(t), a_\mathbf{k}(t)] = 0$ and thus, according to Eq. (2.45), $\left[X_i(t), \Omega_\perp^+(\mathbf{r}_j, t)\right] = 0$. Eq. (3.55) yields

$$\left[X_i(t), \Omega_0^+(\mathbf{r}_j, t)\right] = G_{ij}^\perp(\omega_0) \left[X_i(t), S_i^-(t)\right], \tag{3.56}$$

from which we get Eqs. (3.52), (3.53) and (3.54) for $t = t'$. For $t \neq t'$, it is more suitable to come back to the definition (2.44) of the field, as we did in Eq. (3.48).

It is now easy to evaluate time correlation functions that do not vanish:

$$\begin{aligned}
\left\langle \mathcal{F}_i^\Pi(t) \mathcal{F}_j^\Pi(t') \right\rangle &= \left\langle S_i^+(t) \Omega_0^+(\mathbf{r}_i, t) \Omega_0^-(\mathbf{r}_j, t') S_j^-(t') \right\rangle \\
&= \left\langle S_i^+(t) \left[\Omega_0^+(\mathbf{r}_i, t), \Omega_0^-(\mathbf{r}_j, t')\right] S_j^-(t') \right\rangle \\
&\simeq \frac{2}{\Gamma_0} \frac{\sin k_0 |\mathbf{r}_i - \mathbf{r}_j|}{k_0 |\mathbf{r}_i - \mathbf{r}_j|} \left\langle S_i^+(t) S_j^-(t) \right\rangle \delta(t - t'),
\end{aligned} \tag{3.57}$$

where we have successively used Eqs. (3.52) and (3.51). In the same manner, we obtain

$$\begin{aligned}
\left\langle \mathcal{F}_i^-(t) \mathcal{F}_j^+(t') \right\rangle &= \frac{1}{4} \left\langle \Pi_i(t) \Omega_0^+(\mathbf{r}_i, t) \Omega_0^-(\mathbf{r}_j, t') \Pi_j(t') \right\rangle \\
&\simeq \frac{1}{4} \left\langle \Pi_i(t) \left[\Omega_0^+(\mathbf{r}_i, t), \Omega_0^-(\mathbf{r}_j, t')\right] \Pi_j(t') \right\rangle \\
&\simeq \frac{1}{2\Gamma_0} \frac{\sin k_0 |\mathbf{r}_i - \mathbf{r}_j|}{k_0 |\mathbf{r}_i - \mathbf{r}_j|} \left\langle \Pi_i(t) \Pi_j(t) \right\rangle \delta(t - t'),
\end{aligned} \tag{3.58}$$

and

$$\begin{aligned}
\left\langle \mathcal{F}_i^\Pi(t) \mathcal{F}_j^+(t') \right\rangle &= -\frac{1}{2} \left\langle S_i^+(t) \Omega_0^+(\mathbf{r}_i, t) \Omega_0^-(\mathbf{r}_j, t') \Pi_j(t') \right\rangle \\
&\simeq -\frac{1}{2} \left\langle S_i^+(t) \left[\Omega_0^+(\mathbf{r}_i, t), \Omega_0^-(\mathbf{r}_j, t')\right] \Pi_j(t') \right\rangle \\
&\simeq -\frac{1}{\Gamma_0} \frac{\sin k_0 |\mathbf{r}_i - \mathbf{r}_j|}{k_0 |\mathbf{r}_i - \mathbf{r}_j|} \left\langle S_i^+(t) \Pi_j(t) \right\rangle \delta(t - t').
\end{aligned} \tag{3.59}$$

Here we have neglected the contributions due to Eqs. (3.53) and (3.54) that are dominated, at $t = t'$, by the contribution (3.51). Not surprisingly, correlation functions (3.57), (3.58), and (3.59) between operators corresponding to two different atoms i and j depend on the distance between them.

3.4 Semiclassical treatment of two atoms

Before considering full quantum Eqs. (3.42) and (3.43) — or Eqs. (3.38) and (3.39) — for $N = 2$ atoms, it is instructive to study their semiclassical approximation:

$$\frac{\mathrm{d}S_1^+}{\mathrm{d}t} = \left[\mathrm{i}\frac{\omega_0}{\Gamma_0} - \frac{1}{2}(1 + W_1)\right] S_1^+ + \frac{\mathrm{i}}{2} \Pi_1 G_{12}^*(\omega_0) S_2^+, \tag{3.60}$$

$$\frac{\mathrm{d}\Pi_1}{\mathrm{d}t} = -(1 + W_1)\Pi_1 + W_1 - 1 - 2\mathrm{Im}\left[S_1^+ G_{12}(\omega_0) S_2^-\right], \tag{3.61}$$

where all operators are now considered as simple c-numbers[2]. If we take into account the vectorial nature of the field, we have to specify the orientation of the dipoles $\mathbf{d}_1$ and $\mathbf{d}_2$ with respect to $\mathbf{r}_{12} = \mathbf{r}_1 - \mathbf{r}_2$. For simple configurations it just amounts to replace the Green's function $G_{12}(\omega_0)$ in Eqs. (3.60) and (3.61) by an effective Green's function $G_{12}^{eff}(\omega_0)$. For example,

$$\mathbf{d}_1 = \mathbf{d}_2 \perp \mathbf{r}_{12} \quad \Longrightarrow \quad G_{12}^{eff}(\omega_0) = \frac{3}{2}\frac{e^{\mathrm{i}k_0 r_{12}}}{k_0 r_{12}} P(\mathrm{i}k_0 r_{12}), \tag{3.62}$$

$$\mathbf{d}_1 = \mathbf{d}_2 \parallel \mathbf{r}_{12} \quad \Longrightarrow \quad G_{12}^{eff}(\omega_0) = \frac{3}{2}\frac{e^{\mathrm{i}k_0 r_{12}}}{k_0 r_{12}} \left[P(\mathrm{i}k_0 r_{12}) + Q(\mathrm{i}k_0 r_{12})\right], \tag{3.63}$$

where $P(x)$ and $Q(x)$ are defined in Eq. (2.37).

If the interatomic distance is sufficiently large or the pump parameters W_1 and W_2 are sufficiently small, the stationary solutions of Eqs. (3.60) and (3.61) are unaffected by the interatomic interaction:

$$S_1^{\pm}(t_s) = 0, \qquad S_2^{\pm}(t_s) = 0, \tag{3.64}$$

$$\Pi_1(t_s) = \Pi_1^{eq}, \quad \Pi_2(t_s) = \Pi_2^{eq}, \tag{3.65}$$

with Π_i^{eq} defined by Eq. (3.40). If now we increase the strength of the pump or if the atoms get closer, we can look for an eventual lasing threshold. It is found from the stability analysis of the nonlinear system formed by Eqs. (3.60), (3.61) and equations obtained by the label inversion $1 \leftrightarrow 2$. Following standard semiclassical theories [23], we will associate the instability of its trivial solution with reaching the lasing threshold. Formally, this system is of the form $d\mathbf{Z}/dt = \mathcal{F}(\mathbf{Z})$ where $\mathbf{Z} = \left(S_1^+, S_2^+, S_1^-, S_2^-, \Pi_1, \Pi_2\right)$. We introduce $\delta\mathbf{Z} = \mathbf{Z} - \mathbf{Z}^{(0)}$ where $\mathbf{Z}^{(0)}$ is the stationary solution in the absence of interaction and, since $\mathcal{F}(\mathbf{Z}^{(0)}) = 0$, we obtain

$$\frac{\mathrm{d}}{\mathrm{d}t}\delta\mathbf{Z} = \frac{\partial\mathcal{F}}{\partial\mathbf{Z}}\Big|_{Z^{(0)}}\delta\mathbf{Z}. \tag{3.66}$$

Here the 6×6 Jacobian matrix $\partial\mathcal{F}/\partial\mathbf{Z}|_{\mathbf{Z}^{(0)}}$ is block-diagonal. Hence, we restrict ourselves to the study of the 2×2 block governing the time evolution of $\delta\mathbf{S}^+ = \left(\delta S_1^+, \delta S_2^+\right)$. It is convenient to introduce a 2×2 matrix $\mathcal{N}$ defined by the relation

$$\frac{\mathrm{d}}{\mathrm{d}t}\delta\mathbf{S}^+ = \left(\mathrm{i}\frac{\omega_0}{\Gamma_0} - \frac{1}{2}\right)\delta\mathbf{S}^+ - \frac{\mathrm{i}}{2}\mathcal{N}^*\delta\mathbf{S}^+. \tag{3.67}$$

According to Eq. (3.66), the matrix $\mathcal{N}$ is

$$\mathcal{N} = \begin{bmatrix} \mathrm{i}W_1 & -\Pi_1^{eq}G_{12}(\omega_0) \\ -\Pi_2^{eq}G_{12}(\omega_0) & \mathrm{i}W_2 \end{bmatrix}, \tag{3.68}$$

so that, in the absence of pump, it is identical to the 2×2 Green's matrix $G(\omega_0)$. If $\delta\mathbf{S}^+(0)$ is an eigenstate of $\mathcal{N}$ associated with an eigenvalue Λ, then $\delta\mathbf{S}^+(t) \sim e^{-\Gamma_0(1+\mathrm{Im}\Lambda)t/2}$. It is thus clear that the linear description (3.67) breaks down and lasing starts when the imaginary part of at least one of the two eigenvalues of $\mathcal{N}$ becomes less than -1. This is possible if the condition $\Pi_1^{eq}\Pi_2^{eq} < 0$ is fulfilled, in agreement with [114]. Like for the standard cavity laser, a population inversion is necessary to reach the threshold, but here

[2]For brevity, in this section the quantum expectation value of any operator $\langle X_i\rangle$ is denoted by X_i.

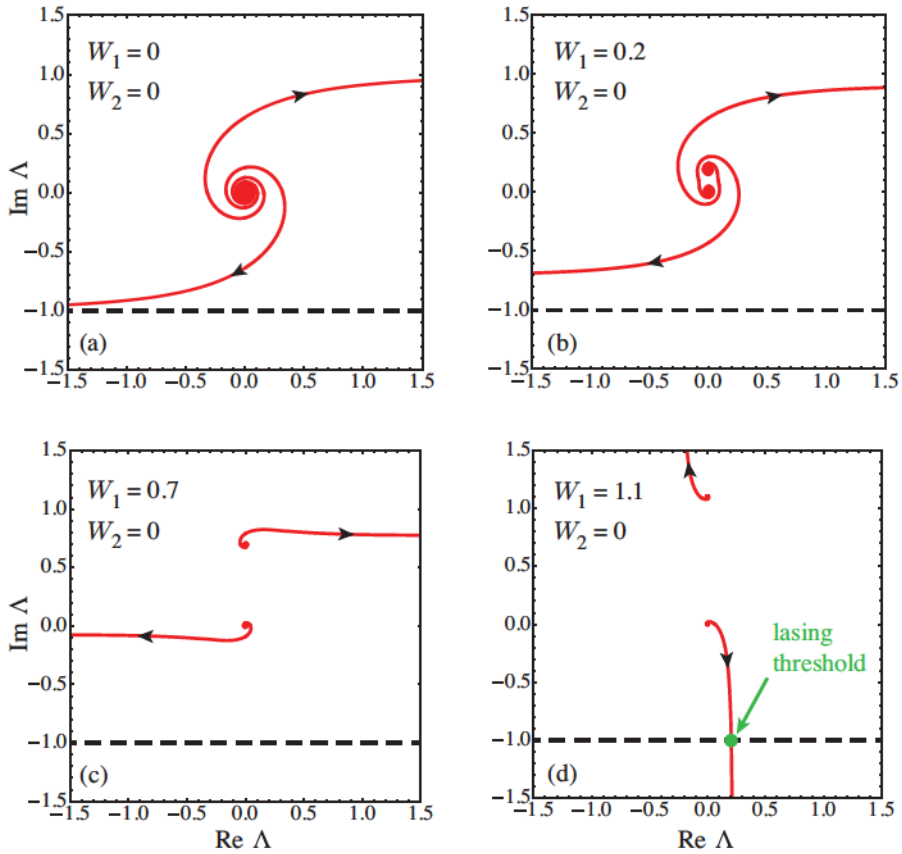

Figure 3.4: Trajectories in the complex-Λ plane of the two eigenvalues of the matrix $\mathcal{N}$ defined by Eq. (3.68), as interatomic distance $k_0 r_{12}$ decreases from ∞ to 0. From (a) to (d), the pump W_1 of one atom is progressively increased, while the other atom is not pumped.

only one of the two atoms has to be in this regime. In particular, if the two atoms are excited with the same pump power, the lasing transition does not occur. This restriction is specific to the case $N = 2$. In chapter 7 we will see that it is perfectly possible to get a semiclassical threshold for a large number of atoms which are all excited with the same pump power.

Figure 3.4 shows, for different pump parameters, the trajectories of the two eigenvalues of $\mathcal{N}$ when the interatomic distance r_{12} is progressively decreased. In the absence of pump, the eigenvalues of $\mathcal{N} = G(\omega_0)$ are $\Lambda_\pm = \pm G_{12}(\omega_0)$. They are localized on two hyperbolic spirals, $|\Lambda| = 1/\arg\Lambda$ and its reflection through the origin. Λ_+ and Λ_-, which are almost degenerated when the two atoms are far from each other, split into a subradiant and superradiant branches when the atoms get closer [Fig. 3.4 (a)]. This simple picture is modified when we add pump [Figs. 3.4 (b), (c), (d)]. As soon as the condition $\Pi_1^{eq}\Pi_2^{eq} < 0$ is satisfied, there exists a critical distance r_{12}^c such that, for $r_{12} < r_{12}^c$, lasing starts. The fact that only two scatterers can behave as a cavity is quite remarkable. Naively we could think that such a bad cavity is too leaky. Here we recover a sufficient quality factor because all modes of the field participate, through the free-space Green's function, to the scattering process. Actually, it is worth noting that there is no general restriction for lasing to occur in a given medium, provided that we can bring enough

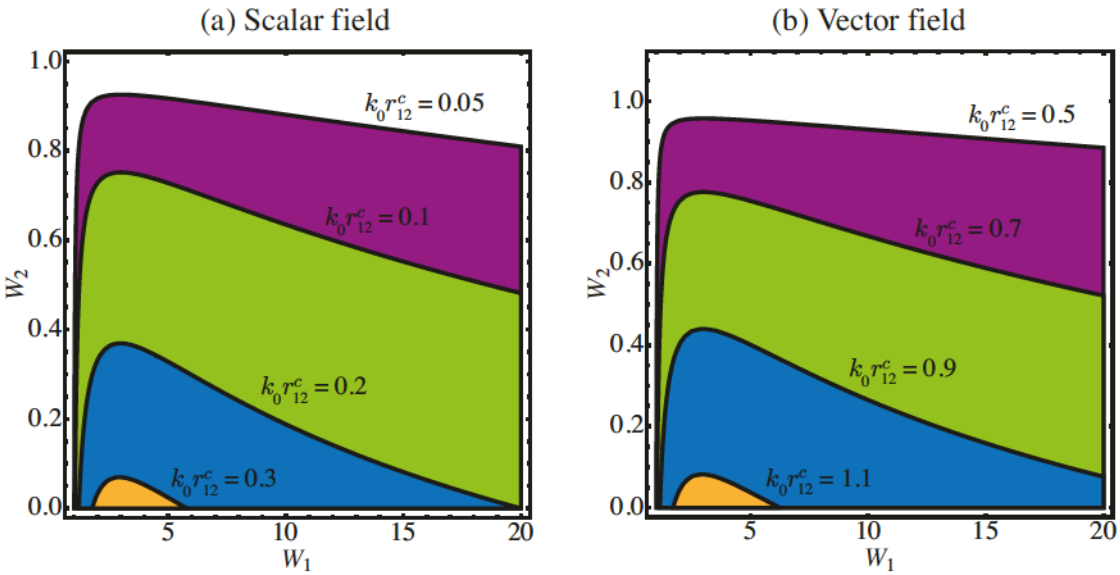

Figure 3.5: Domain of existence of the laser solution in the pump parameter space (W_1, W_2). (a) For a scalar field $G_{12}(\omega_0) = \frac{e^{ik_0 r_{12}}}{k_0 r_{12}}$. (b) For a vector field in the configuration $\mathbf{d}_1 = \mathbf{d}_2 \parallel \mathbf{r}_{12}$, see Eq. (3.63). A necessary condition for lasing to occur is $W_1 > 1$ (population inversion) and $W_2 < 1$. Here the symmetric domain corresponding to the label inversion $1 \leftrightarrow 2$ is not shown.

gain. In Fig. 3.5 (a), we present contour lines of equal r_{12}^c in the plane (W_1, W_2). Because $k_0 r_{12}^c < 1$, it is important to compare these results with a rigorous treatment of the vectorial nature of the field. From Fig. 3.5 (b), that corresponds to the situation considered in Eq. (3.63), we conclude that the lasing threshold still exists, although the results are quantitatively modified. For given values W_1 and W_2, the critical value $k_0 r_{12}^c$ is larger in the vectorial case than in the scalar one because, in the near field $k_0 r_{12} < 1$, the interaction coefficient $G_{12}^{eff}(\omega_0) \sim 1/(k_0 r_{12})^3 \gg G_{12}(\omega_0) \sim 1/k_0 r_{12}$.

Let us now consider the dynamics above threshold. In the stationary regime, it is possible to solve exactly the nonlinear system formed by Eqs. (3.60) and (3.61) and the corresponding equations obtained by the label inversion $1 \leftrightarrow 2$. Stationary solutions are of the form

$$S_i^+(t) = s_i e^{i(\omega_L t + \phi_i)}, \tag{3.69}$$

$$\Pi_i(t) = \Pi_i(t_s). \tag{3.70}$$

We remind that in our notation, t_s is a time that is long enough for the system to reach stationary regime. We found that the two dipoles oscillate at the same frequency given by

$$\omega_L = \omega_0 - \frac{\Gamma_0}{2} \frac{(1+W_1)(1+W_2)}{2+W_1+W_2} \tan(2\phi_{12}) \frac{2}{1+\sqrt{1+\frac{4(1+W_1)(1+W_2)}{(2+W_1+W_2)^2}\tan(2\phi_{12})^2}}, \tag{3.71}$$

where $\phi_{12} = \arg[G_{12}(\omega_0)]$. In Fig. 3.6 we show this solution for $W_1 = 3$ and $W_2 = 0$. Depending on the orientation of the atomic dipole moments, we get either a negative or a positive frequency shift with respect to the atomic frequency. Expressions of s_i, ϕ_i,

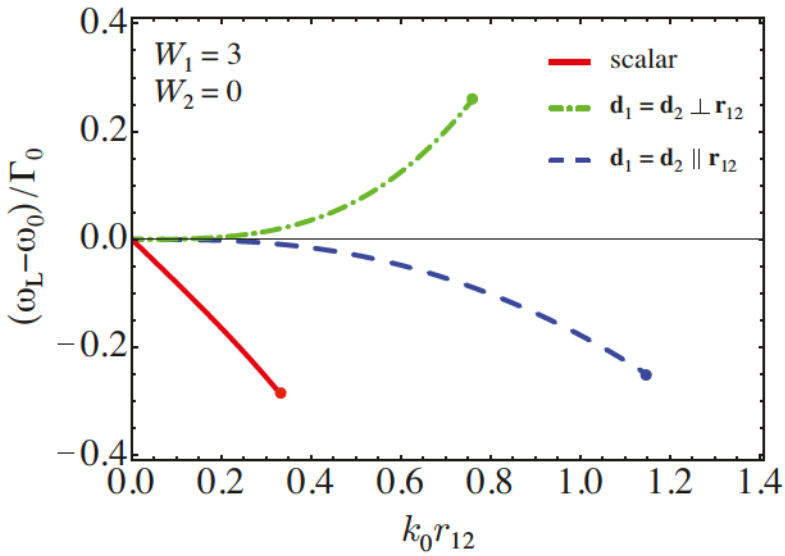

Figure 3.6: Laser frequency above threshold in the stationary regime, with only 1 atom pumped. Dots at extremities of the lines correspond to the laser thresholds.

and $\Pi_i(t_s)$ are lengthy and not particularly instructive. We shall simply illustrate them in Figs. 3.8 and 3.9, where the solution for the semiclassical laser intensity (solid red line) is compared with the full quantum solution.

Inasmuch as we found a laser threshold occuring at very short distance ($k_0 r_{12} \lesssim 1$), there are good reasons to think that quantum correlations may strongly modify this semiclassical result. A detailed comparison with the correct quantum description is the subject of the next section. Nonetheless, the results that we have presented here may still be valid for pairs of 'mesoscopic' dipoles, such as coupled quantum dots, for which external dissipative effects may eventually destroy the quantum correlations. To our knowledge, such a two-dipole laser, where all **k**-components of the field participate efficiently (through the free-space Green's function) to the lasing process, has not been experimentally observed. For the incoherent scheme, we have seen that the laser exists only when the pump is different for the two dipoles ($W_1 \neq W_2$), which is a rather severe experimental limitation, given a small distance $r_{12} \ll \lambda_0$ between them. However, we will see in chapter 7 that another pumping scheme can lead to the two-dipole laser while keeping the same pump power on each scatterer. Furthermore, we note that in the absence of pump, resonances of pairs of scatterers have been experimentally reported in [117]. It was shown that two resonant s-wave scatterers placed close together produce two resonances in the spectrum of the combined system, a broad s-wave resonance and an extremely narrow p-wave resonance. The latter was called 'proximity' resonance [118, 119], and in our context, it corresponds to the lower branch of Fig. 3.4(a) [120].

3.5 Quantum treatment of two atoms

Let us now calculate the spectrum of light emitted by two atoms, pumped in the incoherent way (section 3.2.2). We follow the same procedure as the one proposed in section 3.2.3. First, we need to find the closed set of equations that contains the dipoles $\langle S_1^+(t)\rangle$ and $\langle S_2^+(t)\rangle$. Simple observation of Eqs. (3.42) and (3.43) reveals that they are coupled

to $\langle S_1^+(t)\Pi_2(t)\rangle$ and $\langle S_2^+(t)\Pi_1(t)\rangle$. Dynamical equations for those quantities directly follow from Eqs. (3.42) and (3.43):

$$\frac{\mathrm{d}\left(S_2^+\Pi_1\right)}{\mathrm{d}t} = -\frac{1}{2}(3+2W_1+W_2)S_2^+\Pi_1 + (W_1-1)S_2^+ - \mathrm{Im}G_{12}(\omega_0)S_1^+\Pi_2 + \frac{\mathrm{i}}{2}G_{12}(\omega_0)S_1^+ + \mathcal{F}_2^+\Pi_1 + S_2^+\mathcal{F}_1^\Pi, \tag{3.72}$$

and label inversion $1 \leftrightarrow 2$ gives the equation for $S_1^+\Pi_2$. Then we take the expectation value of Eqs. (3.42) and (3.72) with respect to $|0_R\rangle$. Using Eq. (3.52), we easily verify that all terms that contain Langevin forces vanish. The vector $\mathbf{x}$ defined in section 3.1 has now $N' = 4$ components, $\mathbf{x} = \left(\langle S_1^+\rangle, \langle S_1^+\Pi_2\rangle, \langle S_2^+\rangle, \langle S_2^+\Pi_1\rangle\right)$, and the matrix $\mathcal{M}$ defined in Eq. (3.21) reads

$$\mathcal{M} = \begin{bmatrix} \frac{\mathrm{i}\omega_0}{\Gamma_0} - \frac{1+W_1}{2} & 0 & 0 & \frac{\mathrm{i}}{2}G_{12}^*(\omega_0) \\ W_2 - 1 & -\frac{1}{2}(3+2W_2+W_1) & \frac{\mathrm{i}}{2}G_{12}(\omega_0) & -\mathrm{Im}G_{12}(\omega_0) \\ 0 & \frac{\mathrm{i}}{2}G_{12}^*(\omega_0) & \frac{\mathrm{i}\omega_0}{\Gamma_0} - \frac{1+W_2}{2} & 0 \\ \frac{\mathrm{i}}{2}G_{12}(\omega_0) & -\mathrm{Im}G_{12}(\omega_0) & W_1 - 1 & -\frac{1}{2}(3+2W_1+W_2) \end{bmatrix}. \tag{3.73}$$

Furthermore, the vector $\boldsymbol{\lambda}$ and the matrix $\mathcal{R}$, introduced in Eqs. (3.21) and (3.22), are zero. Real parts of the four eigenvalues of the block symmetric matrix $\mathcal{M}$ are strictly negative for all values of the independent parameters W_1, W_2, and $k_0|\mathbf{r}_1 - \mathbf{r}_2|$, ensuring, in the stationary regime, $\mathbf{x}(t_s) = 0$. In particular, $\langle S_1^+(t_s)\rangle = 0$ and $\langle S_2^+(t_s)\rangle = 0$. Consequently, the laser transition, defined here as the phase transition in the parameters space between $\langle S_{1,2}^\pm(t_s)\rangle = 0$ and $\langle S_{1,2}^\pm(t_s)\rangle \neq 0$, never occurs for two incoherently pumped atoms. This is an importance difference with the semiclassical description formulated in the previous section. To make the link with the perturbative semiclassical equation (3.67), we define the matrix $\mathcal{N}^q = -2\mathrm{i}\mathcal{M}^* - \mathrm{i}I_4$ (I_4 is the 4×4 identity matrix), such that Eq. (3.21) becomes

$$\frac{\mathrm{d}\mathbf{x}}{\mathrm{d}t} = \left(\mathrm{i}\frac{\omega_0}{\Gamma_0} - \frac{1}{2}\right)\mathbf{x} - \frac{\mathrm{i}}{2}\mathcal{N}^{q*}\mathbf{x}. \tag{3.74}$$

Trajectories of the four eigenvalues of the matrix $\mathcal{N}^q$ are represented in Fig. 3.7, where we have chosen the same pump parameters, W_1 and W_2, as in Fig. 3.4. In the passive case [Fig. 3.7 (a)], two extra branches appear with respect to the semiclassical case [Fig. 3.4 (a)]. When one atom is pumped, the two pairs of spirals interact with each other, in such a way that lasing threshold does not occur, even for $W_1 > 1$. Therefore Fig. 3.7 (d) is quite different from Fig. 3.4 (d).

Using Eq. (3.52), it is not difficult to verify that the quantum regression theorem is satisfied, *i.e.* that the matrix $\mathcal{Y}$ defined in Eq. (3.18) obeys Eq. (3.19). In order to compute the spectrum (3.20), we have to evaluate

$$\mathcal{Y}(0) = \begin{bmatrix} \frac{1+\langle\Pi_1(t_s)\rangle}{2} & \langle S_1^+S_2^-(t_s)\rangle \\ \frac{\langle\Pi_2(t_s)\rangle+\langle\Pi_1\Pi_2(t_s)\rangle}{2} & -\langle S_1^+S_2^-(t_s)\rangle \\ \langle S_1^-S_2^+(t_s)\rangle & \frac{1+\langle\Pi_2(t_s)\rangle}{2} \\ -\langle S_1^-S_2^+(t_s)\rangle & \frac{\langle\Pi_1(t_s)\rangle+\langle\Pi_1\Pi_2(t_s)\rangle}{2} \end{bmatrix}, \tag{3.75}$$

and therefore to find a closed set of equations for $\langle\Pi_1(t)\rangle$, $\langle\Pi_2(t)\rangle$, $\langle\Pi_1\Pi_2(t)\rangle$, $\langle S_1^+S_2^-(t)\rangle$,

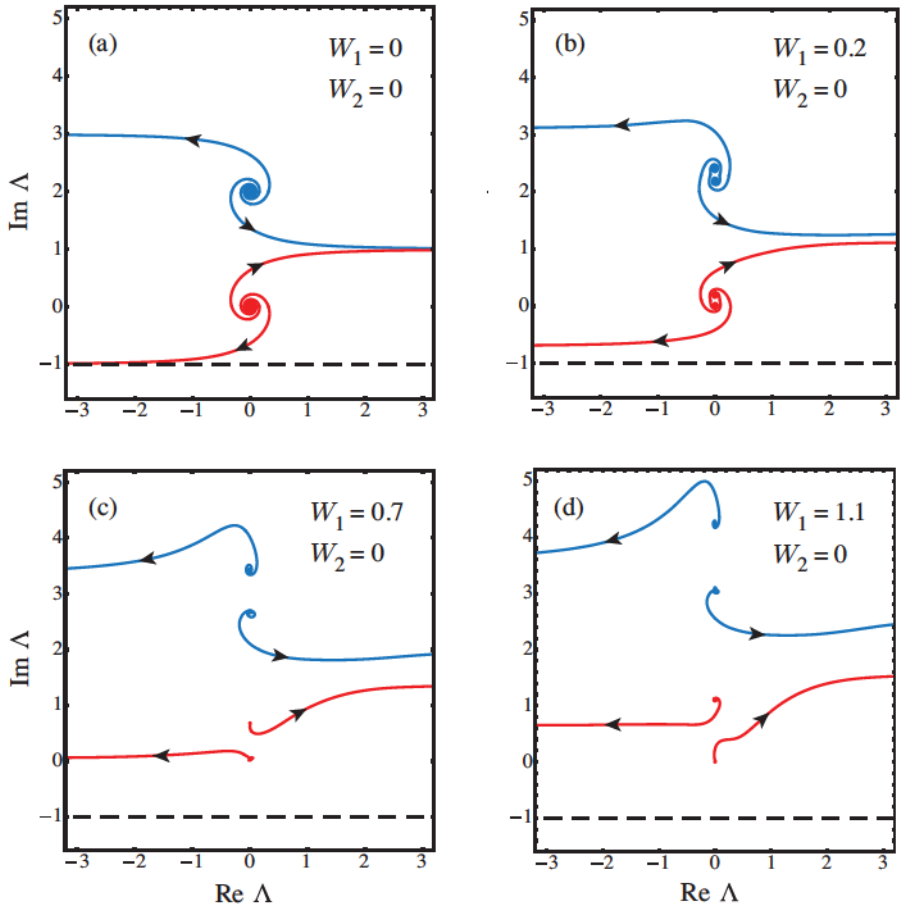

Figure 3.7: Trajectories in the complex-Λ plane of the four eigenvalues of the matrix $\mathcal{N}^q = -2i\mathcal{M}^* - iI_4$, with $\mathcal{M}$ given by Eq. (3.73), as interatomic distance $k_0 r_{12}$ decreases from ∞ to 0. From (a) to (d), the pump W_1 of the first atom is progressively increased, while the second atom is not pumped.

and $\langle S_1^- S_2^+(t)\rangle$. From Eqs. (3.42) and (3.43), we obtain

$$\begin{aligned}\frac{\mathrm{d}\,(\Pi_1\Pi_2)}{\mathrm{d}t} &= -(2+W_1+W_2)\Pi_1\Pi_2 + (W_2-1)\Pi_1 + (W_1-1)\Pi_2 \\ &\quad + 2\mathrm{Im}G_{12}(\omega_0)\left(S_2^+S_1^- - S_1^+S_2^-\right) + \mathcal{F}_1^{\Pi}\Pi_2 + \Pi_1\mathcal{F}_2^{\Pi}, \end{aligned} \tag{3.76}$$

$$\begin{aligned}\frac{\mathrm{d}\left(S_1^-S_2^+\right)}{\mathrm{d}t} &= -\left(1+\frac{W_1+W_2}{2}\right)S_1^-S_2^+ + \frac{1}{2}\mathrm{Im}G_{12}(\omega_0)\Pi_1\Pi_2 \\ &\quad + \frac{\mathrm{i}}{4}\left[G_{12}^*(\omega_0)\Pi_2 - G_{12}(\omega_0)\Pi_1\right] + \mathcal{F}_2^+S_1^- + S_2^+\mathcal{F}_1^-. \end{aligned} \tag{3.77}$$

When taking the expectation value of these equations, the terms with the Langevin forces vanish in Eq. (3.77) but not in Eq. (3.76). Indeed,

$$\begin{aligned}\langle\mathcal{F}_1^{\Pi}(t)\Pi_2(t)\rangle &= -\mathrm{i}\langle S_1^+(t)\Omega_0^+(\mathbf{r}_1,t)\Pi_2(t)\rangle \\ &= -\mathrm{i}\langle S_1^+(t)\left[\Omega_0^+(\mathbf{r}_1,t),\Pi_2(t)\right]\rangle \\ &= -2\mathrm{i}G_{12}(\omega_0)\langle S_1^+(t)S_2^-(t)\rangle, \end{aligned} \tag{3.78}$$

where we made use of the property (3.54). Similarly,

$$\langle \Pi_1(t)\mathcal{F}_2^{\Pi}(t)\rangle = 2\mathrm{i}G_{12}^*(\omega_0)\langle S_1^+(t)S_2^-(t)\rangle. \tag{3.79}$$

Hence, Eqs. (3.76) and (3.77) become

$$\begin{aligned}\frac{\mathrm{d}\langle \Pi_1\Pi_2\rangle}{\mathrm{d}t} &= -(2+W_1+W_2)\langle \Pi_1\Pi_2\rangle + (W_2-1)\langle \Pi_1\rangle + (W_1-1)\langle \Pi_2\rangle \\ &\quad + 2\mathrm{Im}G_{12}(\omega_0)\left(\langle S_2^+S_1^-\rangle + \langle S_1^+S_2^-\rangle\right), \end{aligned}\tag{3.80}$$

$$\begin{aligned}\frac{\mathrm{d}\langle S_1^-S_2^+\rangle}{\mathrm{d}t} &= -\left(1+\frac{W_1+W_2}{2}\right)\langle S_1^-S_2^+\rangle + \frac{1}{2}\mathrm{Im}G_{12}(\omega_0)\langle \Pi_1\Pi_2\rangle \\ &\quad + \frac{\mathrm{i}}{4}\left[G_{12}^*(\omega_0)\langle \Pi_2\rangle - G_{12}(\omega_0)\langle \Pi_1\rangle\right]. \end{aligned}\tag{3.81}$$

We clearly see here that quantum Langevin forces are essential to recover the correct dynamics of $\langle \Pi_1\Pi_2\rangle$. In particular, they ensure that $\langle \Pi_1\Pi_2\rangle$ is real.

Using Eqs. (3.80), (3.81), and the expection value of Eq. (3.43), we found, after some algebra, the analytical expressions for the stationary values that determine the intensity defined in Eqs. (3.26) and (3.27). For two atoms,

$$I = \frac{1+\langle \Pi_1(t_s)\rangle}{2} + \frac{1+\langle \Pi_2(t_s)\rangle}{2} + 2\mathrm{Im}G_{12}(\omega_0)\mathrm{Re}\langle S_1^+(t_s)S_2^-(t_s)\rangle, \tag{3.82}$$

where

$$\langle \Pi_1(t_s)\rangle = \frac{(W_1-W_2)f(W_2,W_1) + 2\left[\overline{W}^2 - 1 + \mathrm{Im}G_{12}^2(\omega_0)\frac{1-\overline{W}}{1+\overline{W}}\right]g(W_2,W_1)}{f(W_2,W_1)g(W_1,W_2) + f(W_1,W_2)g(W_2,W_1)}, \tag{3.83}$$

$$\mathrm{Re}\langle S_1^+(t_s)S_2^-(t_s)\rangle = \frac{\mathrm{Im}G_{12}(\omega_0)}{8}\frac{(3W_2+W_1)\langle \Pi_1(t_s)\rangle + (3W_1+W_2)\langle \Pi_2(t_s)\rangle}{(1+\overline{W})^2 - \mathrm{Im}G_{12}^2(\omega_0)}, \tag{3.84}$$

with

$$\overline{W} = \frac{W_1+W_2}{2}, \tag{3.85}$$

$$f(W_1,W_2) = (1+\overline{W})(1+W_1) + \mathrm{Im}G_{12}^2(\omega_0)\left(1+\frac{W_2-W_1-2}{1+\overline{W}}\right), \tag{3.86}$$

$$g(W_1,W_2) = 1+W_1+\frac{\mathrm{Re}G_{12}^2(\omega_0)}{1+\overline{W}}. \tag{3.87}$$

From Eq. (3.83), and with the label inversion $1 \leftrightarrow 2$, we also obtain $\langle \Pi_2(t_s)\rangle$. Solutions (3.83) and (3.84) were obtained without any approximation. They characterize light-matter interaction for any coupling $G_{12}(\omega_0)$, at arbitrary distance r_{12}, and for any values W_1 and W_2 of the pump. For a homogeneous pump, $W_1 = W_2 = W$, Eqs. (3.83) and (3.84) take a simpler form:

$$\langle \Pi_1(t_s)\rangle = \frac{(W-1)\left[(W+1)^2 - \mathrm{Im}G_{12}^2(\omega_0)\right]}{(W+1)^3 + (W-1)\mathrm{Im}G_{12}^2(\omega_0)}, \tag{3.88}$$

$$\mathrm{Re}\langle S_1^+(t_s)S_2^-(t_s)\rangle = \frac{W(W-1)\mathrm{Im}G_{12}(\omega_0)}{(W+1)^3 + (W-1)\mathrm{Im}G_{12}^2(\omega_0)}. \tag{3.89}$$

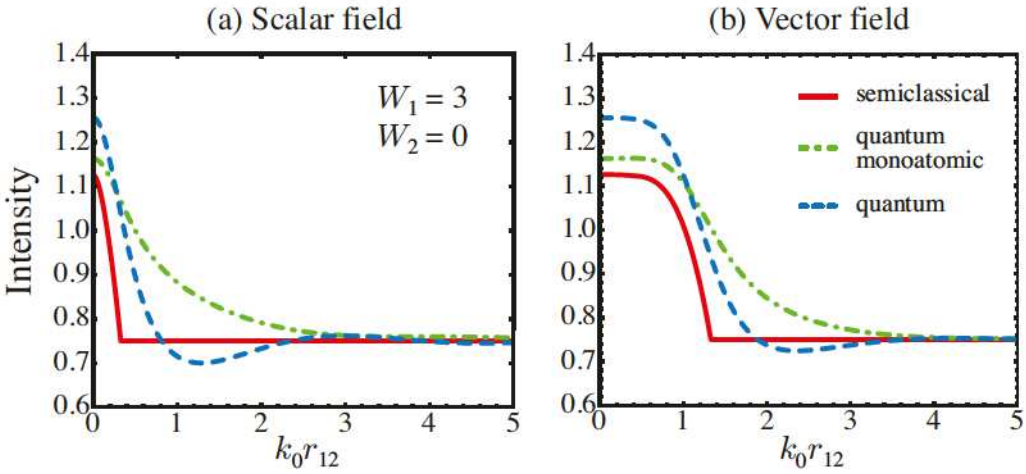

Figure 3.8: Stationary intensity emitted in the far field by two atoms excited with an incoherent pump ($W_1 = 3$ and $W_2 = 0$), versus the interatomic distance. The dashed line corresponds to the full quantum solution (3.82), the dot-dashed line to the first two terms of Eq. (3.82), and the solid line to the semiclassical approximation (3.92). In (a) the field is scalar, $G_{12}(\omega_0) = \frac{e^{ik_0 r_{12}}}{k_0 r_{12}}$, and in (b) the field is vectorial with the dipoles parallel to $\mathbf{r}_{12}$ ($\mathbf{d}_1 = \mathbf{d}_2 \parallel \mathbf{r}_{12}$), see Eq. (3.63).

The coupling between atoms, described by the Green's matrix $G_{12}(\omega_0)$, modifies the stationary values of the population imbalances with respect to the situation in the absence of interaction. For example, in the limit of $k_0 r_{12} \to \infty$ we have

$$\langle \Pi_1(t_s) \rangle = \Pi_1^{eq} + 2\frac{(W_2 - W_1)\mathrm{Re}G_{12}^2(\omega_0) + (W_1 + W_2 - 2W_1W_2)\mathrm{Im}G_{12}^2(\omega_0)}{(1+W_1)^2(1+W_2)(2+W_1+W_2)} + \mathcal{O}(G_{12}^4(\omega_0)), \tag{3.90}$$

where Π_1^{eq} is the solution (3.40) in the absence of interactions. And in the near-field $k_0 r_{12} \ll 1$, the two atoms become indistinguishable with the same population imbalance:

$$\lim_{k_0 r_{12} \to 0} \langle \Pi_1(t_s) \rangle = \lim_{k_0 r_{12} \to 0} \langle \Pi_2(t_s) \rangle = \frac{(W_1 + W_2 + 1)^2 - 9}{(W_1 + W_2 + 3)^2 + 7}. \tag{3.91}$$

Quite remarkably, the limit (3.91) is independent of the Green's matrix, and therefore has no singularity, while $G_{12}(\omega_0) \to \infty$ for $k_0 r_{12} \to 0$.

In Figure 3.8 we compare the full quantum solution (3.82) (dashed line) with its semiclassical approximation (solid line):

$$I^{sc} = \frac{1 + \langle \Pi_1(t_s) \rangle^{sc}}{2} + \frac{1 + \langle \Pi_2(t_s) \rangle^{sc}}{2} + 2\mathrm{Im}G_{12}(\omega_0)\mathrm{Re}\left[\langle S_1^+(t_s) \rangle^{sc} \langle S_2^-(t_s) \rangle^{sc}\right], \tag{3.92}$$

where the different terms were evaluated in section 3.4. At first sight, it seems that an effect reminiscent of the semiclassical threshold persists in the quantum description too. Indeed, the quantum intensity is substantially higher above the semiclassical threshold than below, even if the average dipoles $\langle S_i^{\pm} \rangle$ are always zero within the quantum formalism. Nevertheless, this interpretation is somehow suspicious because the semiclassical laser phase precisely coincides with the near-field regime. Consequently, the growth of the quantum intensity is essentially due to the divergence of the Green's function $G_{12}(\omega_0)$

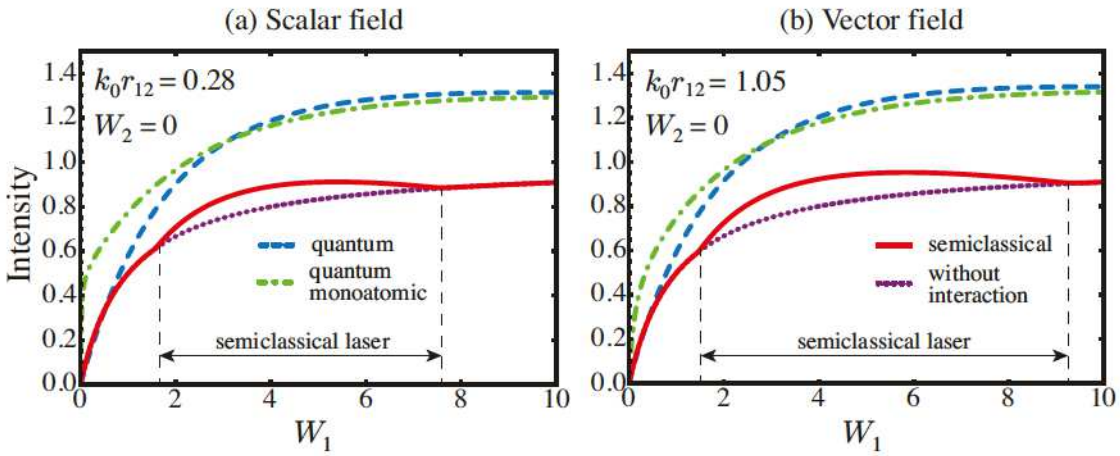

Figure 3.9: Stationary intensity emitted in the far field versus the pump W_1 of the first atom ($W_2 = 0$). Solid, dashed, and dot-dashed lines are defined in Fig. 3.8.

in the limit $k_0r_{12} \to 0$. Fig. 3.9, that shows the dependence of the intensity on the pump, reveals no clear and obvious signature of a threshold in the quantum intensity (dashed line).

By comparing the dashed and dot-dashed lines in Fig. 3.8, we note that the interatomic contribution — the third term of Eq. (3.82) — is responsible for a non-monotonic decay of the intensity (long range tail). This effect is not simply related to the trivial term $\mathrm{Im}G_{12}(\omega_0)$ appearing in Eq. (3.82) — which is due to the fact that we consider the far-field intensity averaged over a 4π solid angle, — but it is really due to the quantum interatomic coupling $\langle S_1^+(t_s)S_2^-(t_s)\rangle$. And, as it is clear from Eq. (3.84), this term is roughly proportional to $\mathrm{Im}G_{12}(\omega_0)$. This implies that purely quantum matter-field correlations can subsist over relatively long ranges in an atomic system.

An analytical expression for the spectrum of emitted light can be obtain by substituting Eqs. (3.73), (3.75), (3.80), (3.83), and (3.84) for $\mathcal{M}$ and $\mathcal{Y}(0)$ into Eq. (3.20). Figure 3.10(a) shows how the spectrum evolves when the interatomic distance k_0r_{12} is varied from ∞ to 0.1. The four eigenvalues of $\mathcal{N}^q = -2\mathrm{i}\mathcal{M}^* - \mathrm{i}I_4$ control the central frequencies and spectral widths of the four Lorentzians that contribute to the spectrum, as illustrated in Fig. 3.10(b). And the matrix $\mathcal{Y}(0)$ determines their spectral weights. A study of the spectral width as a function of the pump strength W does not reveal a significant spectral narrowing at high pump, that could have been interpreted as a signature of the semiclassical laser threshold.

More interestingly, we note that only two modes are well resolved in Fig. 3.10(a). In the regime $k_0r_{12} \gtrsim 1$, these modes are controlled by the two lower branches of Fig. 3.10(b). It is worth recalling that these branches correspond, in the absence of pump, to the eigenvalues of the Green's matrix [see Figs. 3.4(a) and 3.7(a)]. This seems to indicate that the spectral properties of the $N \times N$ Green's matrix somehow characterize the main features of the spectrum. In the next section, we propose to develop this idea in the large N limit.

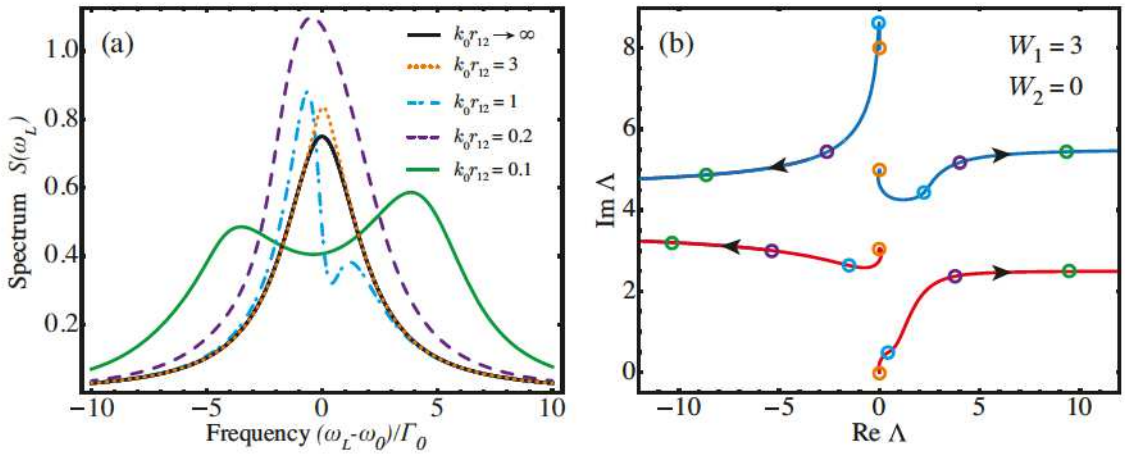

Figure 3.10: (a) Far-field angle-averaged spectrum emitted by two atoms, with $W_1 = 3$ and $W_2 = 0$, coupled by a scalar field. The interatomic distance k_0r_{12} is varied from ∞ to 0.1. (b) Trajectories in the complex-Λ plane of the four eigenvalues of the matrix $\mathcal{N}^q = -2\mathrm{i}\mathcal{M}^* - \mathrm{i}I_4$, with $\mathcal{M}$ given by Eq. (3.73), as the interatomic distance k_0r_{12} decreases from ∞ to 0. For each value of k_0r_{12} chosen in (a), we indicate with open circles (same color) the positions of the four corresponding eigenvalues Λ. Each of them eventually gives rise to a Lorentzian centered at $\omega_L = \omega_0 + \Gamma_0\mathrm{Re}\Lambda/2$, with a width at half-maximum of $\Gamma_0(1 + \mathrm{Im}\Lambda)$.

3.6 Increasing the number of atoms

In the literature dedicated to the light emitted by a collection of N atoms in the absence of cavity, the dynamics of atomic operators is most of the time described by a master equation, such as (2.17). Then, unequal-time correlations of atomic operators are reduced to equal-time expectation values by using the quantum fluctuation-regression theorem [110, 111], and field correlations are calculated, usually numerically, from atomic correlation functions. Quite strikingly, most of the papers deal with no more than two atoms, exposed either to thermal [57, 121] or monochromatic field [58, 59, 122–125], and only rarely analytical expressions are derived. The case of an incoherent pump is less popular. It was numerically studied by Steudel for two and three atoms [126], and much more recently for up to five atoms by Savels *et al.* [61]. The drawback of the master equation approach is the necessity to inverse and diagonalize a $2^{2N} \times 2^{2N}$ matrix, limiting its practical use to a small number of atoms [61]. Moreover, an analytical inspection of the main features of the spectrum is difficult to achieve with this approach. For example, we know that the spectrum can be expressed as a sum of $(2N)!/(N+1)!(N-1)!$ Lorentzians [126], but their relative spectral weight are not really understood. As a consequence, no clear picture has emerged so far about the essential features of the spectrum of light emitted by N atoms in the large N limit.

In the previous sections we followed a different path and used quantum Langevin equations. This allowed us to understand the role of quantum Langevin forces, to check explicitly the validity of the quantum regression theorem, and to compare the quantum results with the semiclassical approximation. For $N > 2$ atoms, rather than trying to compute the spectrum exactly, with the same procedure as in section 3.5, we would like to take advantage of the pleasant form of the Langevin equations to perform a perturbative

expansion valid in the case where atoms are weakly coupled by the dipole interaction, *i.e.* in the regime where $|G_{ij}(\omega_0)| \lesssim 1$. This correspond to $k_0 r_{ij} \gtrsim 1$, or in terms of the density $\rho = N/V$, $\rho\lambda_0^3 \lesssim 10$. A similar approach was proposed by Grémaud *et al.* in the study of the coherent backscattering by 2 atoms [66]. The authors treated the electromagnetic field radiated by one atom onto the other as a perturbation with respect to the incident laser field, thanks to an expansion of the stationary solutions for atomic operators in powers of the Green's function $G_{12}(\omega_0)$.

Let us consider Eqs. (3.42) and (3.43). The first correction with respect to the situation where dipole interactions are zero, is obtained by replacing the operator $\Pi_i(t)$ in Eq. (3.42) by its expectation value in the absence of interaction, Π_i^{eq}. Within this approximation, the equations for the N expectations values $\langle S_i^+(t)\rangle$ form a closed set. Therefore, by definition of $\mathbf{x}$ in Eq. (3.21), we have $\mathbf{x} = (\langle S_1\rangle^+, ..., \langle S_N\rangle^+)$, $\lambda = 0$, and

$$\mathcal{M} = \mathrm{i}\frac{\omega_0}{\Gamma_0} I_N - B + \mathrm{i}AG(\omega_0)^*, \tag{3.93}$$

where we introduced $N \times N$ diagonal matrices

$$A = \frac{1}{2}\mathrm{diag}\left(\frac{W_i - 1}{W_i + 1}\right), \tag{3.94}$$

$$B = \frac{1}{2}\mathrm{diag}\left(W_i + 1\right), \tag{3.95}$$

and I_N is the $N \times N$ identity matrix. Multiple scattering of light, such as independent or dependent scattering (see chapter 4), is fully included in Eq. (3.93). What we neglect are essentially field nonlinearities. We also stress that the expression (3.93) results only from a perturbative expansion, and not from a semiclassical approximation. This ensures that the present analysis can go beyond the semiclassical one.

The power spectrum (3.20) takes a simpler form

$$S(\omega_L) = 2\,\mathrm{Tr}_{(N)}\left\{\mathcal{S}\cdot\mathrm{Re}\left[\left(\mathrm{i}\frac{\omega_L}{\Gamma_0}\mathrm{I}_N - \mathcal{M}\right)^{-1}\cdot\mathcal{Y}(0)\right]\right\}, \tag{3.96}$$

where the ij element of the $N \times N$ matrix $\mathcal{Y}(0)$ is now

$$\mathcal{Y}_{ij}(0) = \langle S_i^+(t_s)S_j^-(t_s)\rangle. \tag{3.97}$$

This matrix is also calculated perturbatively. Using again Eqs. (3.42) and (3.43), we easily show that

$$\langle S_i^+(t_s)S_i^-(t_s)\rangle = \frac{1 + \langle\Pi_i(t_s)\rangle}{2} = \frac{1 + \Pi_i^{eq}}{2} + \mathcal{O}(G^2(\omega_0)), \tag{3.98}$$

$$\langle S_i^+(t_s)S_j^-(t_s)\rangle = \frac{\mathrm{i}G_{ij}^*(\omega_0)\Pi_i^{eq} - \mathrm{i}G_{ij}(\omega_0)\Pi_j^{eq} + 2\mathrm{Im}G_{ij}(\omega_0)\Pi_i^{eq}\Pi_j^{eq}}{2(2 + W_i + W_j)} + \mathcal{O}(G^2(\omega_0)), \tag{3.99}$$

in agreement, in the case $N = 2$, with Eqs. (3.83) and (3.84). Restricting ourselves to the lowest order, we take

$$\mathcal{Y}(0) \simeq \frac{1}{2}I_N + A = \mathrm{diag}\left(\frac{W_i}{W_i + 1}\right). \tag{3.100}$$

In terms of the stationary intensity,

$$I = \int \frac{\mathrm{d}\omega_L}{2\pi} S(\omega_L) = \mathrm{Tr}_{(N)} \left[\mathcal{S} \cdot \mathrm{Re} \left[\mathcal{Y}(0) \right] \right], \tag{3.101}$$

the approximation (3.100) is quite strong since it brings us back to the trivial solution in the absence of interaction, $I = \sum_{i=1}^{N} (1 + \Pi_i^{eq})/2$. However, as far as the spectrum is concerned, Eq. (3.100) is sufficient to capture the dominant collective effects.

Equations (3.93), (3.100), and (3.96) yield an analytical expression for the power spectrum, that is essentially controlled by the properties of the $N \times N$ Green's matrix $G(\omega_0)$. Among the $(2N)!/(N+1)!(N-1)!$ possible Lorentzians, we now have shown that only N dominate the spectrum in the weak-scattering regime $\rho\lambda_0^3 \lesssim 10$. Note that the quantum Langevin forces, discussed in section 3.3, do not play a dominant role here to evaluate the quantum spectrum. This is radically different from standard laser theory where phenomenological quantum Langevin forces for cavity modes are necessary to compute the spectrum of light below and above threshold [23].

To check the validity of the perturbative expression (3.96), we can compare, for $N = 2$, its prediction with the exact result calculated in section 3.5. Figure 3.11 shows a good agreement as long as $k_0 r_{12} \gtrsim 1$. Interestingly, this agreement is improved when W_1 and W_2 get closer, and is almost perfect for $W_1 = W_2$. All this is not completely obvious because (3.96) and the exact result do not have exactly the same perturbative expansion in $G_{12}(\omega_0)$ in the limit $k_0 r_{12} \to \infty$. Nevertheless, our result (3.96) is valid as long as the dipole coupling is weak. In particular, since it is based on a linear expansion in $G(\omega_0)$, it is properly justified below an eventual random laser threshold. We will see in chapter 7 that a description of the laser above threshold requires to keep at least the terms cubic in $G(\omega_0)$.

In the case of a uniform pump ($W_i = W$), it is convenient to express the trace in Eq. (3.96) in the bi-orthogonal basis of right R_n and left L_n eigenvectors of the non-Hermitian matrix $G(\omega_0)$:

$$G(\omega_0) R_n = \Lambda_n R_n \qquad \text{and} \qquad G(\omega_0)^\dagger L_n = \Lambda_n^* L_n. \tag{3.102}$$

We normalize R_n and L_n such that

$$\sum_{i=1}^{N} L_n^{i*} R_m^i = \delta_{nm}, \tag{3.103}$$

and here $L_n = R_n^*$ because $G(\omega_0)$ is a symmetric matrix. Then, the spectrum (3.96) becomes

$$S(\omega_L) = \frac{2W}{1+W} \sum_{n=1}^{N} \mathrm{Re} \left[\frac{c_n}{\mathrm{i}\left[(\omega_L - \omega_0)/\Gamma_0 - A(W)\mathrm{Re}\Lambda_n\right] + B(W) - A(W)\mathrm{Im}\Lambda_n} \right], \tag{3.104}$$

where

$$A(W) = \frac{1}{2}\frac{W-1}{W+1}, \tag{3.105}$$

$$B(W) = \frac{W+1}{2}, \tag{3.106}$$

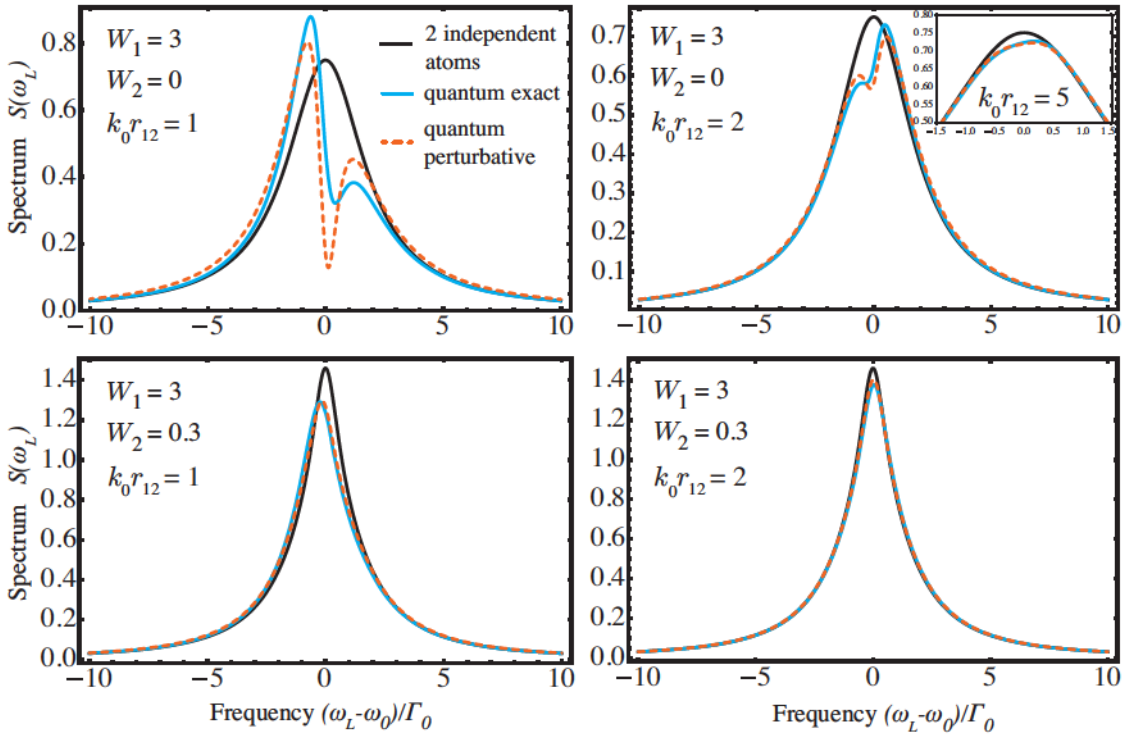

Figure 3.11: Far-field angle-averaged spectrum emitted by two atoms, with $W_1 = 3$, and $W_2 = 0$ or $W_2 = 0.3$. The perturbative result (3.96) (dashed line) is compared with the exact formula of section 3.5 (solid blue line, see also Fig. 3.10) for $k_0 r_{12} = 1, 2$, and 5.

and the c-numbers c_n depend on eigenstates L_n and R_n,

$$c_n = \langle L_n | \mathcal{S} | R_n \rangle = \sum_{i,j}^{N} \frac{\sin k_0 |\mathbf{r}_i - \mathbf{r}_j|}{k_0 |\mathbf{r}_i - \mathbf{r}_j|} R_n^i R_n^{j*}. \tag{3.107}$$

If $\mathrm{Im}\,(c_n) \ll \mathrm{Re}\,(c_n)$, $S(\omega_L)$ is a sum of N Lorentzians centered at

$$\omega_n = \omega_0 + \frac{\Gamma_0}{2} \frac{W-1}{W+1} \mathrm{Re}\Lambda_n, \tag{3.108}$$

and having widths at half-maximum given by

$$\Gamma_n = \frac{\Gamma_0}{2} \left(W + 1 - \frac{W-1}{W+1} \mathrm{Im}\Lambda_n \right). \tag{3.109}$$

To illustrate how the spectrum (3.104) evolves with N, we consider N atoms randomly distributed in a sphere of radius R, at a given density $\rho = 3N/4\pi R^3$ such that $\rho\lambda_0^3 = 1$. By numerical diagonalization, we find eigenvalues Λ_n and eigenstates R_n of $G(\omega_0)$, and use them to evaluate $S(\omega_L)$. Results are presented in Fig. 3.12(a). In the regime $\rho\lambda_0^3 < 10$, the modes strongly overlap, *i.e.* $|\mathrm{Re}\Lambda_n - \mathrm{Re}\Lambda_{n+1}| \ll |\mathrm{Im}\Lambda_n|$, so that they cannot be distinguished in the spectrum. This is further illustrated in Fig. 3.12(b), where we show the eigenvalues Λ_n that we used to evaluate $S(\omega_L)$ for $N = 1000$. The shape of the eigenvalue domain as well as the eigenvalue density of the Green's matrix will be discussed in great details in chapter 6. Here we just mention, as it is indicated

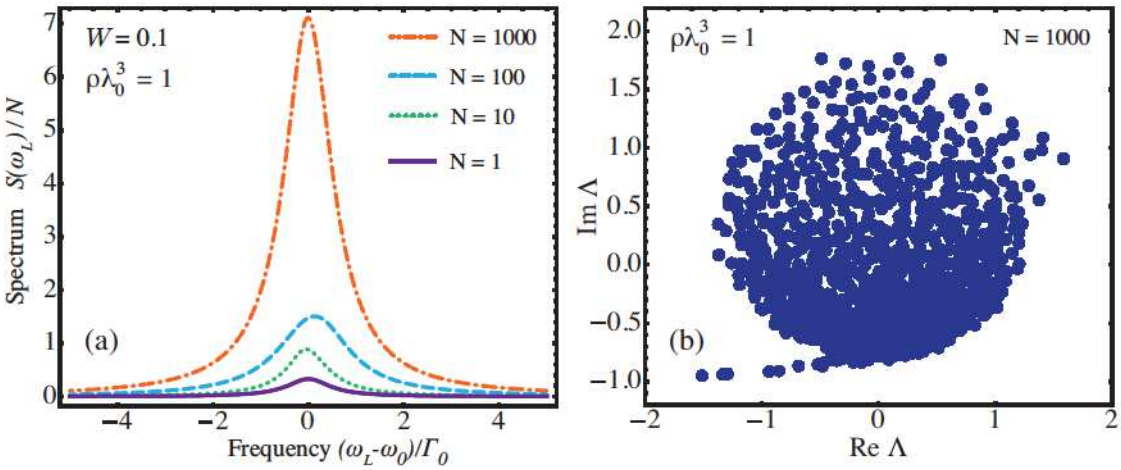

Figure 3.12: (a) Far-field angle-averaged spectrum emitted by N atoms randomly distributed in a sphere, with $W_i = 0.1$ $(i = 1, ..., N)$. N is varied from 1 to 1000 at fixed density $\rho\lambda_0^3 = 1$. (b) Eigenvalues of the $N \times N$ Green's matrix $G(\omega_0)$ for a single random configuration of $N = 1000$ points, used to compute the corresponding power spectrum in (a) (dot-dashed line).

by Eqs. (3.108) and (3.109), that the spectral extent of the eigenvalue distribution may control the shape of $S(\omega_L)$. In particular, all modes contribute to the spectrum, which is in contrast with the behavior above threshold, as we shall see in chapter 7. In addition, we stress that the smooth curves of Fig. 3.12(a) were obtained for a single spatial configuration of the N atoms, indicating that $S(\omega_L)$ seems to be a self-averaging quantity in the limit $N \to \infty$.

Calculating analytically the quantum many-body quantity $S(\omega_L)$ is *a priori* a complicated task. Quite interestingly, we will see in chapter 7 that $S(\omega_L)$ is related to the resolvent associated with the Green's matrix, for which we will develop a complete analytical theory in chapter 6. We therefore refer the reader interested in the random laser physics to chapter 7, where theoretical tools developed in chapters 5 and 6 will find a natural and elegant application.

CHAPTER 4

Multiple-scattering of light in the presence of gain: a mesoscopic description

4.1 Fictitious Hamiltonian and scattering building blocks

4.1.1 Atomic polarizability

In the previous chapter, we provided a formulation of matter-field interaction in terms of microscopic excitations. We are now interested in the alternative picture, where atomic degrees of freedom are eliminated. We extend the 'mesoscopic' formulation briefly introduced in section 2.4.2 to the case where atoms are excited by an optical pump. For simplicity, we concentrate on the incoherent pumping scheme described in section 3.2.2. The pump strength on atom i, W_i, is defined by Eq. (3.37). In the presence of pump, Eqs. (2.86) and (2.87) become

$$\mathbf{D}_i^-(\omega_L) = \frac{1}{\omega_L - \omega_0 + \mathrm{i}(1+W_i)\Gamma_0/2} \int \frac{\mathrm{d}\omega'}{2\pi\hbar}\, \Pi_i(\omega_L - \omega')\, [\mathbf{d}_i \otimes \mathbf{d}_i]\, \mathbf{E}_s^+(\mathbf{r}_i, \omega'), \tag{4.1}$$

$$\begin{aligned}\Pi_i(\omega_L) = {} & \frac{2\mathrm{i}\pi\,(W_i - 1)\,\Gamma_0}{\omega_L + \mathrm{i}\,(1+W_i)\,\Gamma_0}\delta(\omega_L) + \frac{2}{\omega_L + \mathrm{i}\Gamma_0}\int \frac{\mathrm{d}\omega'\mathrm{d}\omega''}{(2\pi\hbar)^2} \\ & \left[\frac{[\mathbf{d}_i \otimes \mathbf{d}_i]\,\mathbf{E}_s^-(\mathbf{r}_i, \omega'') \cdot \Pi_i(\omega_L - \omega' - \omega'')\mathbf{E}_s^+(\mathbf{r}_i, \omega')}{\omega_L - \omega' + \omega_0 + \mathrm{i}(1+W_i)\Gamma_0/2} + h.c.(\omega' \leftrightarrow \omega'')\right],\end{aligned} \tag{4.2}$$

where $\mathbf{E}_s^+(\mathbf{r}_i, \omega')$ is the smoothed field (2.59). With Eq. (4.1), the quantum wave equation (2.39) reads

$$\begin{aligned}&\nabla \times \nabla \times \mathbf{E}^+(\mathbf{r}, \omega_L) - k_L^2 \mathbf{E}^+(\mathbf{r}, \omega_L) = \\ &\int \frac{\mathrm{d}\omega'}{2\pi\epsilon_0\hbar}\left[\sum_{i=1}^{N} \frac{k_L^2 \Pi_i(\omega_L - \omega')}{\omega_L - \omega_0 + \mathrm{i}(1+W_i)\Gamma_0/2}\,[\mathbf{d}_i \otimes \mathbf{d}_i]\,\delta(\mathbf{r} - \mathbf{r}_i)\right]\mathbf{E}_s^+(\mathbf{r}, \omega').\end{aligned} \tag{4.3}$$

Quantum equations of motion (4.1), (4.2) and (4.3) were derived with almost no approximation: we used RWA for internal degrees of freedom (see section 2.3.2), and we omitted the terms involving the values of atomic operators at the initial time (see the discussion below). As it is known in the semiclassical laser theory, where similar equations for classical fields show up [23, 32], such coupled equations can be solved in all orders in the electric field only if we neglect the time dependence of the population inversion Π_i.

This is often well justified for lasers of interest, for which the polarization relaxes at a phenomenological rate $\gamma_\perp$ much greater than the relaxation rate $\gamma_\parallel$ of the population inversion. Such lasers are sometimes referred to as lasers of class B. The condition $\gamma_\perp \gg \gamma_\parallel$ is not satisfied for independent atoms in free space, for which $\gamma_\perp = \Gamma_0/2$ and $\gamma_\parallel = \Gamma_0$. Nevertheless, the situation can be radically modified by the pump and interactions. In particular, we will show in chapter 7 that the inversion may be approximated as stationary in the vicinity of the random laser threshold. Suppose, for the time being, that such a stationary approximation is meaningful in our context:

$$\Pi_i(\omega_L) \simeq 2\pi \Pi_i(t_s)\delta\left(\omega_L\right), \tag{4.4}$$

where t_s is a time that is long enough for the system to reach stationary regime. From Eq. (4.2), we readily get

$$\Pi_i(t_s) = \frac{\Pi_i^{eq}}{1+s_i}, \tag{4.5}$$

with Π_i^{eq} the solution (3.40) in the absence of interatomic interactions, and s_i a saturation parameter defined by

$$s_i = 2\int \frac{\mathrm{d}\omega'\mathrm{d}\omega''}{(2\pi\hbar)^2} \frac{\left[\mathbf{d}_i \otimes \mathbf{d}_i\right] \mathbf{E}_s^-(\mathbf{r}_i,\omega'') \cdot \mathbf{E}_s^+(\mathbf{r}_i,\omega')}{\left(\omega'-\omega_0\right)^2 + (1+W_i)^2\Gamma_0^2/4}. \tag{4.6}$$

Such a saturation parameter accounts for infinite-order nonlinear spatial 'hole burning'. It is well known in standard laser theory [23], and has attracted recent attention in the context of multimode laser action in open and irregular systems [21, 22, 33].

Using the assumption (4.4) in Eq. (4.1), we find the atomic polarizability $\alpha(\omega_L)$ that relates each dipole to the local electric field:

$$\mathbf{D}_i^-(\omega_L) = \epsilon_0 \alpha_i(\omega_L) \mathbf{\Delta}_i^{\parallel} \mathbf{E}_s^+(\mathbf{r}_i,\omega_L), \tag{4.7}$$

where $\mathbf{\Delta}_i^{\parallel} = \tilde{\mathbf{d}}_i \otimes \tilde{\mathbf{d}}_i$ is the projection operator (on the dipole $\tilde{\mathbf{d}}_i$), and the polarizability reads

$$\alpha_i(\omega_L) = \frac{d^2}{\epsilon_0\hbar}\left(\frac{1}{1+s_i}\right)\frac{\Pi_i^{eq}}{\omega_L-\omega_0+\mathrm{i}(1+W_i)\Gamma_0/2}. \tag{4.8}$$

For later convenience, we introduce the dimensionless polarizability,

$$\tilde{\alpha}_i(\omega_L) = \frac{\Pi_i^{eq}}{1+s_i}\frac{\Gamma_0/2}{\omega_L-\omega_0+\mathrm{i}(1+W_i)\Gamma_0/2}, \tag{4.9}$$

such that, according to Eqs. (2.71), (2.77), and (4.8),

$$\alpha_i(\omega_L) = \begin{cases} \frac{6\pi}{k_0^3}\tilde{\alpha}_i(\omega_L) & \text{(vector field)} \\ \\ \frac{4\pi}{k_0^3}\tilde{\alpha}_i(\omega_L) & \text{(scalar field)} \end{cases}. \tag{4.10}$$

It is worth noting that the polarizability defined in Eq. (4.7) relates the dipole $\mathbf{D}_i^-$ not to the total electric field $\mathbf{E}^+(\mathbf{r}_i)$ but only to its smooth part $\mathbf{E}_s^+(\mathbf{r}_i)$. This means that α_i features the response of atom i to the field radiated by all atoms except itself.

4.1.2 Fictitious Hamiltonian

In order to obtain a closed equation for the the total electric field $\mathbf{E}^+(\mathbf{r})$ from Eq. (4.3), we have to express $\mathbf{E}_s^+(\mathbf{r}_i)$ in terms of $\mathbf{E}^+(\mathbf{r}_i)$. Using its definition (2.58) and the relation (4.7), we find

$$\begin{aligned}\mathbf{E}_s^+(\mathbf{r}_i,\omega_L) &= \mathbf{E}^+(\mathbf{r}_i,\omega_L) - \frac{1}{\epsilon_0}\mathbf{g}(\mathbf{0},\omega_L)\mathbf{D}_i^-(\omega_L) \\ &= \frac{1}{1+\mathbf{g}(\mathbf{0},\omega_L)\alpha_i(\omega_L)\mathbf{\Delta}_i^{\parallel}}\mathbf{E}^+(\mathbf{r}_i,\omega_L). \end{aligned} \tag{4.11}$$

With the help of Eqs. (4.4) and (4.11), Eq. (4.3) can be rewritten as an effective propagation equation:

$$\left[k_L^2 - H^f\right]|\mathbf{E}^+(\omega_L)\rangle = 0, \tag{4.12}$$

where we use the notation $\mathbf{E}^+(\mathbf{r},\omega_L) = \langle\mathbf{r}|\mathbf{E}^+(\omega_L)\rangle$, with $|\mathbf{E}^+(\omega_L)\rangle$ that belongs to the fictitious Hilbert space $\mathcal{E}^f$ defined in section 2.4.2. The fictitious Hamiltonian H^f is

$$H^f = H_0^f + V^f = (\nabla\times\nabla\times) + \sum_{i=1}^{N} v_i, \tag{4.13}$$

where v_i is the effective potential[1]

$$v_i = \tilde{v}_i\mathbf{\Delta}_i^{\parallel}\delta(\hat{\mathbf{r}}-\mathbf{r}_i), \tag{4.14}$$

$$\tilde{v}_i = \frac{-k_L^2\alpha_i(\omega_L)}{1+\mathbf{g}(\mathbf{0},\omega_L)\alpha_i(\omega_L)}. \tag{4.15}$$

The fictitious Hamiltonian H^f is non-Hermitian because $\tilde{v}_i$ is a complex quantity.

Eq. (4.12) implies that all scattering is elastic. This is a direct consequence of the approximation (4.4). Inelastic scattering induced by an eventual non-stationary value of population imbalance in Eq. (4.3) must not be confused with the inelastic scattering of purely quantum origin considered in the previous chapter. To make clear the difference, it is sufficient to consider the spectrum of light emitted by a single atom. We recall that for the incoherent pump, the only nonzero contribution to the spectrum of light (3.20) is a term proportional to $\mathcal{Y}(0) = (\langle S^+(t_s)S^-(t_s)\rangle, \langle\Pi(t_s)S^-(t_s)\rangle, \langle S^-(t_s)S^-(t_s)\rangle)$ (see section 3.2.3 for details). Such a contribution, responsible for the 'quantum' part of the spectrum, is not contained in Eqs. (4.1), (4.2) and (4.3), because we omitted in those equations the values of atomic operators at time t_s. Taking them into account amounts to adding a new source term in the propagation equation (4.12), that does not vanish in the approximation (4.4). It is exactly the idea that we used in section 3.6. Rigorously speaking, Eqs. (4.1), (4.2), (4.3), and (4.12), are exact provided that we replace quantum operators with their expectation value with respect to $|0_R\rangle$. This is the semiclassical approximation that we defined in section 3.2.2, and it will be used in the following. For brevity, we will keep the operator-like notation, *i.e.* for any operator A acting in $\mathcal{E}$, we note

$$\langle 0_R|A|0_R\rangle \equiv A. \tag{4.16}$$

[1]For simplicity, we add hats to operators that act in $\mathcal{E}^f$ only if confusion is possible. For example, we note v_i and H^f rather than $\hat{v}_i$ and $\hat{H}^f$.

4.1.3 Atomic t-operator

Formally, the scattering amplitude $\tilde{v}_i$ that appears in Eq. (4.14) is zero because $\mathbf{g}(\mathbf{0}, \omega_L)$ in Eq. (4.15) is infinite. At first sight, the singularity of $\mathbf{g}(\mathbf{0}, \omega_L)$ is problematic. However, if we consider scattering quantities like the t-operator of a single atom, this divergence disappears, as we now show. We define the retarded free-space Green's operator associated with H_0^f:

$$\mathcal{G}_0^f = \frac{1}{k_L^2 + \mathrm{i}\epsilon - H_0^f}. \tag{4.17}$$

According to Eq. (2.35), in the $\mathbf{r}$-representation, it is proportional to the free-space Green's function $\mathbf{g}$ (2.36):

$$\langle \mathbf{r}|\mathcal{G}_0^f|\mathbf{r}'\rangle = -\frac{c^2}{\omega_L^2}\mathbf{g}(\mathbf{r}-\mathbf{r}', \omega_L). \tag{4.18}$$

In terms of $\mathcal{G}_0^f$, the t-operator of an atom i reads [127]

$$\begin{aligned} t_i &= v_i + v_i \mathcal{G}_0^f t_i \\ &= v_i + v_i \mathcal{G}_0^f v_i + v_i \mathcal{G}_0^f v_i \mathcal{G}_0^f v_i + \dots \end{aligned} \tag{4.19}$$

For a potential v_i of the form (4.14) associated with point-like particles, the Born series (4.19) can be easily summed exactly:

$$t_i = \tilde{t}_i \mathbf{\Delta}_i^{\parallel} \delta(\hat{\mathbf{r}} - \mathbf{r}_i), \tag{4.20}$$

$$\tilde{t}_i = \frac{\tilde{v}_i}{1 - \tilde{v}_i \langle \mathbf{r}|\mathcal{G}_0^f|\mathbf{r}\rangle}, \tag{4.21}$$

where $\langle \mathbf{r}|\mathcal{G}_0^f|\mathbf{r}\rangle = -\mathbf{g}(\mathbf{0}, \omega_L)/k_L^2$ is infinite. In the literature devoted to multiple scattering by point scatterers (see, *e.g.*, the two reviews [128] and [129]), $\langle \mathbf{r}|\mathcal{G}_0^f|\mathbf{r}\rangle$ is often replaced by a regularized function to retain a physical nonzero t-operator. We show here that such a regularization is not necessary. Indeed, inserting the explicit expression (4.15) into Eq. (4.21), we obtain

$$\tilde{t}_i = -k_L^2 \alpha_i(\omega_L) \simeq \begin{cases} -\frac{6\pi}{k_0}\tilde{\alpha}_i(\omega_L) & \text{(vector field)} \\ -\frac{4\pi}{k_0}\tilde{\alpha}_i(\omega_L) & \text{(scalar field)} \end{cases}, \tag{4.22}$$

that has no singularity. To get the last equality of Eq. (4.22), we used Eq. (4.10) with the very reasonable approximation $k_L \simeq k_0$ ($|k_L - k_0| \ll k_0$) for the prefactor. The consistency of our approach comes from the fact that the polarizability in Eq. (4.7) is rigorously related to the smoothed field and not to the total electric field. To recover the same expression (4.22), authors of [128] and [129] first introduced a large-momentum cutoff in the Green's function, that is then phenomenologically related to the linewidth Γ_0.[2] The singularity of v_i is not a problem because v_i is not a physical observable. Generally speaking, all quantities related to multiple scattering among point-like scatterers must contain, if they are properly calculated, t_i and not v_i as a building block.

[2] Note also that, ironically, if we make the incorrect choice $\tilde{v}_i = -k_L^2 \alpha_i(\omega_L)$, and restrict the evaluation of $\tilde{t}_i$ given by Eq. (4.19) to the unjustified second-order Born approximation, we also get the correct result (4.22).

Note finally that the monoatomic t-operator associated with H^f coincides with the one associated with the Hamiltonian H (2.24). In the absence of pump, the proof is straightforward; it is given by Eqs. (2.91), (2.93), and (2.98) where we set $N = 1$ (see also [78]). However, as soon as several photons are considered, the microscopic scattering approach becomes more involved (see, *e.g.*, [130]).

4.1.4 Scattering cross-section and optical theorem

Let us now recall how the t-operator and the polarizability α are related to the monatomic scattering cross-section, defined as the ratio between the scattered flux and the incoming flux density (per unit of area) [49, 131]. For a single atom i located at $\mathbf{r} = 0$ and illuminated by an incident wave $|\mathbf{E}^+_{in}(\omega_L)\rangle$, Eq. (4.12) can be formally rewritten as the Lippman-Schwinger equation

$$|\mathbf{E}^+(\omega_L)\rangle = |\mathbf{E}^+_{in}(\omega_L)\rangle + \mathcal{G}^f_0 v_i |\mathbf{E}^+(\omega_L)\rangle, \tag{4.23}$$

that becomes, with Eq. (4.19),

$$|\mathbf{E}^+(\omega_L)\rangle = |\mathbf{E}^+_{in}(\omega_L)\rangle + \mathcal{G}^f_0 t_i |\mathbf{E}^+_{in}(\omega_L)\rangle. \tag{4.24}$$

In the far-field, using the approximation (2.38) of the Green's function, we obtain

$$\mathbf{E}^+(\mathbf{r},\omega_L) = \mathbf{E}^+_{in}(\mathbf{r},\omega_L) - \tilde{t}_i \frac{e^{\mathrm{i}k_L r}}{4\pi r} \mathbf{\Delta}^{\parallel}_i \mathbf{\Delta}^{\perp}_{\mathbf{r}} \mathbf{E}^+_{in}(\mathbf{0},\omega_L). \tag{4.25}$$

For a scalar field, projectors $\mathbf{\Delta}^{\parallel}_i$ and $\mathbf{\Delta}^{\perp}_{\mathbf{r}}$ disappear. We can define a scattering amplitude

$$f_i = \begin{cases} -\frac{\tilde{t}_i}{4\pi} \mathbf{\Delta}^{\parallel}_i \mathbf{\Delta}^{\perp}_{\mathbf{r}} & \text{(vector field)} \\ -\frac{\tilde{t}_i}{4\pi} & \text{(scalar field)} \end{cases}, \tag{4.26}$$

from which we find the total scattering cross-section by integrating over the solid angle:

$$\sigma_i = \int \mathrm{d}\Omega |f_i|^2 = \begin{cases} \frac{|\tilde{t}_i|^2}{6\pi} \simeq \frac{6\pi}{k_0^2} |\tilde{\alpha}_i|^2 & \text{(vector field)} \\ \frac{|\tilde{t}_i|^2}{4\pi} \simeq \frac{4\pi}{k_0^2} |\tilde{\alpha}_i|^2 & \text{(scalar field)} \end{cases}, \tag{4.27}$$

where we used Eqs. (4.22) and (4.10) with $k_L \simeq k_0$ for the prefactors.

If energy is conserved, the so-called S-matrix of a single atom, $S_i = \hat{1} + \mathcal{G}^f_0 t_i$, is unitary. In optics, this result is known as the optical theorem [49, 132] and reads

$$|\tilde{t}_i|^2 = \begin{cases} -\frac{6\pi}{k_L} \mathrm{Im} \tilde{t}_i & \text{(vector field)} \\ -\frac{4\pi}{k_L} \mathrm{Im} \tilde{t}_i & \text{(scalar field)} \end{cases} \quad \text{(if energy is conserved)}, \tag{4.28}$$

which is simpler in terms of $\tilde{\alpha}_i$:

$$\mathrm{Im}\left[\frac{1}{\tilde{\alpha}_i(\omega_L)}\right] = -1 \qquad \text{(if energy is conserved)}. \tag{4.29}$$

For the specific model (4.9), the optical theorem is fulfilled in the absence of pump ($W_i = 0$) and field nonlinearities ($s_i = 0$), as it could be expected [113].

4.2 A simple but universal semiclassical laser threshold

Now we would like to establish a very simple and general condition for lasing in any system of point-like scatterers — atoms, in the present context. It is based on two basic ingredients: on the one hand, the equation of propagation (2.39) that relates the field to atoms (through the Green's matrix), and on the other hand, the microscopic response of atoms to the field (through the polarizability).

4.2.1 Threshold condition

Below threshold, we can assume linear response of atoms to the field. This implies that the polarizability in Eq. (4.7) does not depend on the field. For instance, if we consider the model (4.9) of incoherent pump, it amounts to take $s_i = 0$. We rewrite (4.7) in terms of the dimensionless polarizability $\tilde{\alpha}_i$ (4.8) and the dimensionless electric field $\mathbf{\Omega}_s^+$ (3.5):

$$\begin{aligned} \tilde{\mathbf{D}}_i^-(\omega_L) &= -\tilde{\alpha}_i(\omega_L)\mathbf{\Delta}_i^{\parallel}\mathbf{\Omega}_s^+(\mathbf{r}_i,\omega_L) \quad \text{(vector field)} \\ S_i^-(\omega_L) &= -\tilde{\alpha}_i(\omega_L)\Omega_s^+(\mathbf{r}_i,\omega_L) \qquad \text{(scalar field)} \end{aligned} , \tag{4.30}$$

and for later convenience, we define the diagonal matrix[3]

$$\mathcal{A}(\omega_L) = \begin{cases} \operatorname{diag}\left[\tilde{\alpha}_i(\omega_L)\mathbf{\Delta}_i^{\parallel}\right] & 3N \times 3N \quad \text{(vector field)} \\ \operatorname{diag}\left[\tilde{\alpha}_i(\omega_L)\right] & N \times N \quad \text{(scalar field)} \end{cases} . \tag{4.31}$$

On the other hand, the smoothed field, solution of the equation of propagation, is given by Eqs. (2.83) and (2.84):

$$\begin{aligned} \mathbf{\Omega}_s^+(\mathbf{r}_i,\omega_L) &= -\left(\tfrac{\omega_L}{\omega_0}\right)^3 \textstyle\sum_{j\neq i}^N \boldsymbol{G}_{ij}(\omega_L)\tilde{\boldsymbol{D}}_j^-(\omega_L) \quad \text{(vector field)} \\ \Omega_s^+(\mathbf{r}_i,\omega_L) &= -\left(\tfrac{\omega_L}{\omega_0}\right)^3 \textstyle\sum_{j\neq i}^N G_{ij}(\omega_L)S_j^-(\omega_L) \quad \text{(scalar field)} \end{aligned} . \tag{4.32}$$

Here the free component $\mathbf{\Omega}_0^+$ of the field vanishes because, as explained in the previous section, all operators considered in the present chapter are implicitly averaged with respect to $|0_R\rangle$.

It then follows immediately from the combination of Eqs. (4.30) and (4.32) that the linear description breaks down and the lasing starts as soon as at least one eigenvalue λ_k of the product of the Green's matrix and $\mathcal{A}(\omega_L)$ is equal to $(\omega_0/\omega_L)^3$:

$$\text{lasing threshold:} \quad \left(\frac{\omega_0}{\omega_L}\right)^3 = \begin{cases} \lambda_k\left\{\boldsymbol{G}(\omega_L)\mathcal{A}(\omega_L)\right\} & \text{(vector field)} \\ \lambda_k\left\{G(\omega_L)\mathcal{A}(\omega_L)\right\} & \text{(scalar field)} \end{cases} . \tag{4.33}$$

This condition contains no approximation. It is valid for any dimensionality of space, any atomic polarizability, any number and configuration of atoms, and any form of the Green's matrix that, in particular, can account for an external cavity and amplification or absorption of light in the space between the atoms.

[3]For a vector field, $\mathcal{A}(\omega_L)$ is (3×3)-block diagonal.

The case of an ensemble of passive atoms embedded in an amplifying matrix will be discussed in chapter 7. For the time being, suppose that the atoms are confined to an empty volume of typical size R, without external cavity. As we discussed in section 2.4, for $\Gamma_0 \ll \omega_0, c/R$, we can safely replace $\boldsymbol{G}(\omega_L)$ by $\boldsymbol{G}(\omega_0)$, and $(\omega_0/\omega_L)^3$ by one. Obviously, we cannot replace ω_L by ω_0 in $\tilde{\alpha}_i(\omega_L)$ because the latter has a resonance in ω_0. For $N = 2$ and the polarizability (4.9), the laser condition (4.33) becomes then equivalent to the semiclassical lasing threshold found in section 3.4. From here on, we will be interested in the large N limit. The simplest case that we can look at is the situation where the pump is uniform ($\tilde{\alpha}_i = \tilde{\alpha}$), and the dipoles $\tilde{\mathbf{d}}_i$ are all oriented in the same direction. The condition (4.33) is then rewritten only in terms of the eigenvalues Λ_k of the Green's matrix, either the $3N \times 3N$ matrix $\boldsymbol{G}(\omega_0)$ (2.70) or the $N \times N$ matrix $G(\omega_0)$ (2.80):

$$\Lambda_k(\omega_0) = \frac{1}{\tilde{\alpha}(\omega_L)}. \tag{4.34}$$

This equation illustrates that laser threshold results from an interplay of single-atom properties (described by the polarizability $\tilde{\alpha}$) and geometry-dependent collective effects (quantified by the eigenvalues Λ_k of the Green's matrix). If the N atoms are localized at random positions, the Green's matrix becomes a random matrix, and the threshold the one of a random laser. Clearly, the most difficult task in evaluating analytically the condition (4.34) is to compute the statistical properties of the eigenvalues Λ_k. To tackle this problem we have developed an analytic theory for non-Hermitian Euclidean random matrices that is presented in chapter 6. This theory will be applied to the case of the Green's matrix, and we will show, in chapter 7, that it is able to predict the random laser threshold all the way from weak ($\rho\lambda_0^3 \ll 1$) to strong ($\rho\lambda_0^3 \gg 1$) scattering regime.

We point out that for the condition (4.34) to be physically consistent, eigenvalues Λ_k necessarily have to satisfy the condition $\mathrm{Im}\Lambda_k > -1$ for any dimensionality of space and any number or configuration of atoms. The explanation is the following. We know from Eq. (4.29) that the line $\mathrm{Im}\,(1/\tilde{\alpha}_i) = -1$ in the complex plane corresponds to the domain where no energy is brought to the atomic system. Thus, if one eigenvalue Λ_k could cross this line, that would mean that lasing could occur without pump. Actually, as we shall see later, the property $\mathrm{Im}\Lambda_k > -1$ is a consequence of causality.

4.2.2 Polarizability models

An easy way to visualize the threshold condition (4.34) is to draw the two-dimensional domain $\mathcal{D}_\Lambda$ occupied by the complex eigenvalues of $\boldsymbol{G}$ (or G) and the region $\mathcal{D}_\alpha$ spanned by $1/\tilde{\alpha}$ when its free parameters — ω_L and W in the case of Eq. (4.9) — are varied on the complex plane. Lasing takes place when $\mathcal{D}_\Lambda$ and $\mathcal{D}_\alpha$ touch (threshold) or overlap. This is illustrated in chapter 7 for $N \gg 1$ atoms in a sphere of radius $R \gg \lambda_0$, with two gain mechanisms described by two different models of polarizability $\tilde{\alpha}$.

The first gain mechanism is given by Eq. (4.9). It features optical pumping of a three-level atom in a regime such that the latter can be reduced to an effective two-level atom pumped by an incoherent process [see section 3.2.2 and Fig. 3.1 (b)]. For $W > 1$, population inversion is achieved ($\Pi^{eq} > 0$), so that the atom amplifies incident light ($\mathrm{Im}t > 0$).

The second gain mechanism is probably the most simple that we can imagine for cold atoms. It involves a two-level atom (resonant frequency ω_0) in the field of a strong near-resonant coherent pump (Rabi frequency Ω_p, frequency $\omega_0 + \Gamma_0\Delta_p$), depicted in Fig.

3.1 (a). The driving field induces a population inversion in the dressed-state basis [52], so that a weak probe beam (frequency $\omega_L = \omega_0 + \Delta_p\Gamma_0 + \delta_L\Gamma_0$) can be amplified. The whole process can be also described in the bare-state basis by a three-photon transition from the ground state to the excited state via absorption of two pump photons. This phenomenon, first described by Mollow in 1972 [115] and observed soon afterwards [116], is relevant for current experiments with cold atoms [65]. Equations of motion for this system were introduced in section 3.2.1. Treating the probe as a perturbation with respect to the pump, we can easily show that the relation (4.30) holds with $\tilde{\alpha}$ given by [65, 112, 115]

$$\tilde{\alpha}(\delta_L) = -\frac{1}{2}\frac{1+4\Delta_p^2}{1+4\Delta_p^2+2\Omega_p^2} \times \frac{(\delta_L+\mathrm{i})(\delta_L-\Delta_p+\mathrm{i}/2)-\Omega_p^2\delta_L/(2\Delta_p-\mathrm{i})}{(\delta_L+\mathrm{i})\,(\delta_L-\Delta_p+\mathrm{i}/2)\,(\delta_L+\Delta_p+\mathrm{i}/2)-\Omega_p^2\,(\delta_L+\mathrm{i}/2)}. \tag{4.35}$$

Whereas we had, in the case of the incoherent gain (4.9), only two independent parameters (frequency of the probe ω_L and intensity of the pump W), we now have for the coherent gain (4.35), three parameters (frequency of the probe ω_L, intensity of the pump Ω_p, frequency of the pump ω_p). The main amplification feature of (4.35) appears for a pump-probe detuning $\delta_L = \mathrm{sgn}(\Delta_p)\sqrt{\Delta_p^2+\Omega_p^2}$.

We directly refer the reader interested in a discussion of the laser threshold using the criterion (4.34) to chapter 7. In the present chapter, we would like to discuss the random laser threshold in the terms used initially in 1968 by Letokhov [6], who was the first to consider the possibility of a 'photonic bomb', in a regime where the size of the system R exceeds the scattering mean free path. In the following sections we introduce the general tools necessary to compute such a threshold. We believe that this description has a double interest. First, it will present a derivation of a transport equation in the presence of gain, a situation that is not sufficiently well covered by the existing literature. Second, it will reveal explicitly all hypotheses that are necessary to evaluate the laser threshold within the diffusion approximation, and will allow for a direct comparison with the theoretical framework developed in chapter 6. In particular, a comparison of diagrammatic techniques used in both cases will turn out to be fruitful.

4.3 Extinction mean free path in a gas of pumped atoms

In a random medium described by the fictitious Hamiltonian (4.13), a complete solution of the wave equation (4.12) amounts to the knowledge of the Green's operator

$$\mathcal{G}^f = \frac{1}{k_L^2 - H^f}. \tag{4.36}$$

Averaged over disorder, it gives information about the effective medium as seen by the wave. Without pump, it exponentially decays in space, with a decay length defined as the extinction mean free path l_e. Beyond a few l_e, the average of the field amplitude vanishes. Transport dynamics are then contained in the second moment of $\mathcal{G}^f$, the average intensity. All this is correct if the effect of random scattering is effectively captured by configurational averaging. We should keep two points in mind: first, such a spatial average over many configurations is equivalent to infinite-time average only if

the system is ergodic; and second, for any given configuration, the expected behavior can deviate from the actual behavior. Such a deviation may be especially large when the number of scatterings is small.

For simplicity, we will neglect in the following the vectorial nature of the field, and assume that external degrees of freedom are the uncorrelated classical positions $\mathbf{r}_i$ ($i = 1, \ldots, N$). Average is performed by spatial integration over the volume V to which the atoms are confined[4]:

$$\langle \ldots \rangle = \int_V \prod_{i=1}^{N} \frac{\mathrm{d}^d \mathbf{r}_i}{V} (\ldots) . \tag{4.37}$$

We also temporarily assume that the gain is uniform ($\tilde{v}_i = \tilde{v}$), so that the disorder potential V^f reads:

$$V^f(\hat{\mathbf{r}}) = \tilde{v} \sum_{i=1}^{N} \delta(\hat{\mathbf{r}} - \mathbf{r}_i). \tag{4.38}$$

All information about $\langle \mathcal{G}^f \rangle$ is contained in the self-energy Σ^f defined by

$$\langle \mathcal{G}^f \rangle = \frac{1}{(\mathcal{G}_0^f)^{-1} - \Sigma^f} = \mathcal{G}_0^f + \mathcal{G}_0^f \Sigma^f \langle \mathcal{G}^f \rangle. \tag{4.39}$$

We can compute Σ^f in the $|\mathbf{k}\rangle$- or $|\mathbf{r}\rangle$- representations. The former is generally chosen if we wish to highlight the elementary excitations generated during the scattering process. In particular, $V^f(\hat{\mathbf{r}})$ breaks the translational invariance, and generates new excitations from an initial wave vector $\mathbf{k}$. On the other hand, the $|\mathbf{r}\rangle$-representation is advantageous to keep track of the propagation in space, where changes of positions are induced by $\mathcal{G}_0^f$, and not by the one-body potential $V^f(\hat{\mathbf{r}})$. Indeed, $V^f(\hat{\mathbf{r}})$ is necessarily local:

$$\langle \mathbf{r} | V^f(\hat{\mathbf{r}}) | \mathbf{r}' \rangle = V^f(\mathbf{r}) \delta(\mathbf{r} - \mathbf{r}'). \tag{4.40}$$

Before calculating Σ^f, we will derive its relation to the extinction mean free path l_e. To define properly the latter, some assumptions are necessary. First, we assume space to be translationally invariant (it is true only in the limit $V \to \infty$), so that Σ^f becomes diagonal in $\mathbf{k}$-space. Besides, $\langle \mathbf{k} | \Sigma^f | \mathbf{k} \rangle$ for point scatterers has only a weak dependence on $\mathbf{k}$, as we will see later. Neglecting this dependence, we write

$$\langle \mathbf{k} | \Sigma^f | \mathbf{k}' \rangle \simeq \Sigma_0 \, \delta_{\mathbf{k},\mathbf{k}'}, \tag{4.41}$$

and in $\mathbf{k}$-space, Eq. (4.39) becomes

$$\langle \mathcal{G}^f(\mathbf{k}, \mathbf{k}') \rangle = \langle \langle \mathbf{k} | \mathcal{G}^f | \mathbf{k}' \rangle \rangle = \frac{1}{k_L^2 - k^2 - \Sigma_0} \delta_{\mathbf{k},\mathbf{k}'}. \tag{4.42}$$

We then define l_e by the relation

$$\sqrt{k_L^2 - \Sigma_0} = \tilde{k}_L + \frac{\mathrm{i}}{2 l_e} \quad \text{with} \quad \tilde{k}_L > 0, \tag{4.43}$$

[4]The same notation $\langle \ldots \rangle$ was used in previous chapters for the quantum expectation value with respect to degrees of freedom of the field. In the present chapter, we recall that this averaging with respect to $|0_R\rangle$ has already been performed in section 4.1.1. Hence, we hope that no confusion is possible.

so that, in three-dimensional space, the retarded Green's function is

$$\langle \mathcal{G}^f(\mathbf{r},\mathbf{r}')\rangle = -\frac{e^{-|\mathbf{r}-\mathbf{r}'|/2l_e}}{4\pi|\mathbf{r}-\mathbf{r}'|}e^{\mathrm{i}\tilde{k}_L|\mathbf{r}-\mathbf{r}'|}. \tag{4.44}$$

Without pump, l_e is a positive decay length. However, in the presence of a gain mechanism, l_e may eventually become negative. In that case there is amplification[5]. For $|\mathrm{Re}\Sigma_0|, |\mathrm{Im}\Sigma_0| \ll k_L^2$,

$$\tilde{k}_L \simeq k_L\ , \quad \text{and} \quad l_e \simeq \frac{-k_L}{\mathrm{Im}\Sigma_0}. \tag{4.45}$$

Let us now evaluate Σ^f. Different diagrammatic strategies can be adopted. First, in the limit $\tilde{v} \to 0$ obeyed by (4.15), we notice that all cummulants of (4.38) are zero, except the second one [79]. Therefore, $V^f(\mathbf{r})$ can be assumed to be a Gaussian random field. It is convenient to define

$$\tilde{V}^f = V^f - \langle V^f\rangle = V^f - \rho\tilde{v}, \tag{4.46}$$

and expand $\langle \mathcal{G}^f\rangle$ in series of the shifted propagator $\tilde{\mathcal{G}}_0^f = \left(k_L^2 + \langle V^f\rangle - H_0^f\right)^{-1}$:

$$\mathcal{G}^f = \tilde{\mathcal{G}}_0^f + \tilde{\mathcal{G}}_0^f\tilde{V}^f\tilde{\mathcal{G}}_0^f + \tilde{\mathcal{G}}_0^f\tilde{V}^f\tilde{\mathcal{G}}_0^f\tilde{V}^f\tilde{\mathcal{G}}_0^f + \dots \tag{4.47}$$

The result of averaging Eq. (4.47), written in the $|\mathbf{r}\rangle$-representation, can be expressed through pairwise contractions

$$\langle \tilde{V}^f(\mathbf{r})\tilde{V}^f(\mathbf{r}')\rangle = \rho\tilde{v}^2\delta(\mathbf{r}-\mathbf{r}'). \tag{4.48}$$

The shifted self-energy $\tilde{\Sigma}^f = \tilde{\mathcal{G}}_0^{f-1} - \mathcal{G}^{f-1}$ is the sum of all one-particle irreducible diagrams (*i.e.* those that cannot be separated into two independent diagrams linked by the propagator $\tilde{\mathcal{G}}_0^f$) contained in $\tilde{\mathcal{G}}_0^{f-1}\langle\mathcal{G}^f\rangle\tilde{\mathcal{G}}_0^{f-1}$. Selecting the simplest class of diagrams, it is straightforward to get

$$\begin{aligned}\langle\mathbf{r}|\tilde{\Sigma}^f|\mathbf{r}'\rangle &= \langle\tilde{V}^f(\mathbf{r})\tilde{V}^f(\mathbf{r}')\rangle\langle\mathbf{r}|\mathcal{G}^f|\mathbf{r}'\rangle \\ &= \rho\tilde{v}^2\langle\mathbf{r}|\mathcal{G}^f|\mathbf{r}\rangle\delta(\mathbf{r}-\mathbf{r}').\end{aligned} \tag{4.49}$$

This result is known as the self-consistent Born approximation. It it not satisfactory for two reasons. First Eq. (4.49) is subject to the singularity of $\langle\mathbf{r}|\mathcal{G}^f|\mathbf{r}\rangle$. Second, the result for $\langle\mathcal{G}^f(\mathbf{r},\mathbf{r}')\rangle = \langle\langle\mathbf{r}|\mathcal{G}^f|\mathbf{r}'\rangle\rangle$ is expressed in terms of $\tilde{v}$, that contains, for the case (4.15), also a singularity. While the first singularity can probably be regularized by taking into account more diagrams [133], the second one is more problematic. As we argued in the previous section, all physical observable like $\langle\mathcal{G}^f\rangle$, must be expressed in terms of $\tilde{t}$ instead of $\tilde{v}$.

To see $\tilde{t}$ in the expansion of the self-energy, we must adopt another strategy. We introduce the collective $\mathcal{T}^f$ operator defined as

$$\mathcal{T}^f = V^f + V^f\mathcal{G}^fV^f, \tag{4.50}$$

$$= V^f + V^f\mathcal{G}_0^f\mathcal{T}^f. \tag{4.51}$$

[5]Note that if we calculate $\langle\mathcal{G}^f(\mathbf{r},\mathbf{r}')\rangle$ from Eq. (4.42), we only find the retarded solution $e^{-\mathrm{sgn}(l_e)|\mathbf{r}-\mathbf{r}'|/2l_e}e^{\mathrm{i}\tilde{k}_L|\mathbf{r}-\mathbf{r}'|}/4\pi|\mathbf{r}-\mathbf{r}'|$. The reason is that the other solution of the propagation equation, $e^{-|\mathbf{r}-\mathbf{r}'|/2l_e}e^{\mathrm{i}\tilde{k}_L|\mathbf{r}-\mathbf{r}'|}/4\pi|\mathbf{r}-\mathbf{r}'|$ with $l_e < 0$, is not integrable, and thus its Fourier transform does not exist.

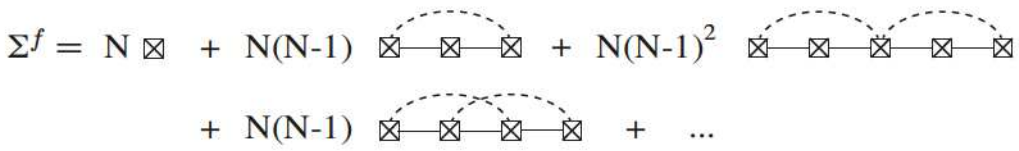

Figure 4.1: Diagrammatic expansion of the self energy Σ^f in terms of $\langle t_i \rangle = \boxtimes = \tilde{t}/V$. A straight line represents the free-space Green's function $\mathcal{G}_0^f$, and dashed lines indicate that scattering takes place from the same atom i.

Equations (4.50) and (4.39) show that

$$\langle \mathcal{T}^f \rangle = \Sigma^f + \Sigma^f \mathcal{G}_0^f \langle \mathcal{T}^f \rangle. \tag{4.52}$$

Therefore, Σ^f is the sum of all one-particle irreducible diagrams contained in the expansion of $\langle \mathcal{T}^f \rangle$. We now take advantage of the form $V^f = \sum_{i=1}^N v_i$, to express $\mathcal{T}^f$ in terms of the t_i's (4.19) of individual atoms [127]

$$\mathcal{T}^f = \sum_i t_i + \sum_i \sum_{j \neq i} t_i \mathcal{G}_0^f t_j + \sum_i \sum_{j \neq i} \sum_{k \neq j} t_i \mathcal{G}_0^f t_j \mathcal{G}_0^f t_k + \ldots, \tag{4.53}$$

and we proceed to average Eq. (4.53) according to the spatial integration (4.37). In the case of a uniform pump ($\tilde{t}_i = \tilde{t}$), irreducible diagrams are represented in Fig. 4.1. For a dilute medium ($\rho \lambda_0^3 \ll 1$), it is sufficient to truncate this expansion to the first order in density:

$$\Sigma^f \simeq N \boxtimes = \rho \tilde{t}\, \hat{\mathbf{1}}. \tag{4.54}$$

This result is known as the independent scattering approximation (ISA)[6]. It is of the form (4.41), meaning that Eqs. (4.43) and (4.44) are relevant. For $\rho \lambda_0^3 \ll 1$, the approximation (4.45) is valid, and with Eqs. (4.54) and (4.22), the extinction mean free path becomes

$$l_e \simeq -\frac{k_L}{\rho \mathrm{Im} \tilde{t}} \tag{4.55}$$

$$\simeq \frac{k_0^2}{4\pi\rho} \frac{1}{\mathrm{Im} \tilde{\alpha}(\omega_L)}. \tag{4.56}$$

Note that Eq. (4.55) is also true for a vector field. If we consider the incoherent pump (4.9) on resonance, we get

$$l_e(\omega_L = \omega_0) = \frac{k_0^2}{4\pi\rho} \frac{(1+W)^2}{1-W}. \tag{4.57}$$

As expected, the wave is amplified ($l_e < 0$) for $W > 1$ (population inversion).

In Fig. 4.1, terms different from (4.54) correspond to 'dependent' scattering, meaning that the scattering from an atom depends on other atoms in its local environment [49]. This dependent scattering can be important when the particles scatter strongly, as it is the case for atoms on resonance [133]. Whereas it is impossible to calculate all diagrams exactly, it is feasible to take into account, without much extra effort, all higher order terms of a certain class. Before discussing such an extension, we would like to make the link between the scattering formalism and Euclidean random matrices, for which similar diagrammatic will be performed in chapters 5 and 6.

[6]The same result can be obtained with the expansion (4.47), provided we shift the potential V^f with respect to $\rho\tilde{t}$ rather than to $\langle V^f \rangle$, and take the lowest order $\tilde{\Sigma}^f = 0$. This shift is sometimes used to define the coherent potential approximation (CPA) [127].

4.4 Mapping to the Green's matrix properties

In the $|\mathbf{r}\rangle$-representation with t_i given by Eq. (4.20), the operator $\mathcal{T}^f$ (4.53) becomes

$$\begin{aligned}\langle\mathbf{r}|\mathcal{T}^f|\mathbf{r}'\rangle &= \sum_i \delta(\mathbf{r}-\mathbf{r}_i)\tilde{t}_i\boldsymbol{\Delta}_i^{\parallel}\delta(\mathbf{r}_i-\mathbf{r}') + \sum_i\sum_{j\neq i}\delta(\mathbf{r}-\mathbf{r}_i)\tilde{t}_i\boldsymbol{\Delta}_i^{\parallel}\langle\mathbf{r}_i|\mathcal{G}_0^f|\mathbf{r}_j\rangle\tilde{t}_j\boldsymbol{\Delta}_j^{\parallel}\delta(\mathbf{r}_j-\mathbf{r}') \\ &+ \sum_i\sum_{j\neq i}\sum_{k\neq j}\delta(\mathbf{r}-\mathbf{r}_i)\tilde{t}_i\boldsymbol{\Delta}_i^{\parallel}\langle\mathbf{r}_i|\mathcal{G}_0^f|\mathbf{r}_j\rangle\tilde{t}_j\boldsymbol{\Delta}_j^{\parallel}\langle\mathbf{r}_j|\mathcal{G}_0^f|\mathbf{r}_k\rangle\tilde{t}_k\boldsymbol{\Delta}_k^{\parallel}\delta(\mathbf{r}_k-\mathbf{r}') + \dots\end{aligned} \tag{4.58}$$

This series is conveniently rewritten as

$$\mathcal{T}^f = \sum_{i=1}^N\sum_{j=1}^N\left[\frac{t^m}{I-\mathcal{G}_0^m t^m}\right]_{ij}|\mathbf{r}_i\rangle\langle\mathbf{r}_j|, \tag{4.59}$$

where I is the identity matrix, and t^m and $\mathcal{G}_0^m$ are given by

$$[t^m]_{ij} = \delta_{ij}\tilde{t}_i\boldsymbol{\Delta}_i^{\parallel}, \tag{4.60}$$

$$[\mathcal{G}_0^m]_{ij} = (1-\delta_{ij})\mathcal{G}_0^f(\mathbf{r}_i,\mathbf{r}_j). \tag{4.61}$$

These matrices are of size $3N\times 3N$ for a vector field and $N\times N$ for a scalar field (the projector $\boldsymbol{\Delta}_i^{\parallel}$ then disappears). In the same manner, combining Eqs. (4.50) and (4.59), we express $\mathcal{G}^f$ in terms of the inverse of the Green's matrix $\mathcal{G}_0^m$:

$$\langle\mathbf{r}_i|\mathcal{G}^f|\mathbf{r}_j\rangle = \left[\frac{1}{(\mathcal{G}_0^m)^{-1}-t^m}\right]_{ij}. \tag{4.62}$$

It is worth noting that Eqs. (4.59) and (4.62) express $\mathcal{T}^f$ and $\mathcal{G}^f$, that both act in the fictitious Hilbert space $\mathcal{E}^f$ of infinite dimension and both depend on disorder $\{\mathbf{r}_i\}$, only in terms of a finite size matrix that is built from the free-space Green's function. This is a specific feature of the disordered system composed of point-like particles.

From here on, let us concentrate ourselves on uniformly pumped atoms ($\tilde{t}_i = \tilde{t}$), interacting with a scalar field. Equation (4.59) is simplified into

$$\mathcal{T}^f = \sum_{i=1}^N\sum_{j=1}^N\left[\frac{1}{1/\tilde{t}-\mathcal{G}_0^m}\right]_{ij}|\mathbf{r}_i\rangle\langle\mathbf{r}_j|, \tag{4.63}$$

$$= -\frac{4\pi}{k_0}\sum_{i=1}^N\sum_{j=1}^N\left[\frac{1}{1/\tilde{\alpha}(\omega_L)-G(\omega_0)}\right]_{ij}|\mathbf{r}_i\rangle\langle\mathbf{r}_j|. \tag{4.64}$$

We used $\omega_L \simeq \omega_0$ in Eq. (4.64). This equation deserves a few comments:

- In the absence of pump, the operator $\mathcal{T}^f$ (4.64) coincides with the operator $\mathcal{T}$ of the quantum scattering approach, given by Eqs. (2.91), (2.93) and (2.98). This is intuitively what we might expect, if we think in terms of scattering of a weak probe. However, it is not as trivial as it seems inasmuch as $\mathcal{T}^f$ and $\mathcal{T}$ are associated with two Hamiltonian, H^f and H, given by Eqs. (4.13) and (2.24) respectively, that look quite different.

- Expression (4.64) of $\mathcal{T}^f$ can be used to simulate the scattering cross-section of the atomic cloud numerically, since one simply needs to generate the Green's matrix $G(\omega_0)$ (for a given configuation of points) and to invert $1/\tilde{\alpha}(\omega_L) - G(\omega_0)$. Such an approach was used recently by Sokolov *et al.* to study light scattering from a dense ultracold atomic gas [80].

- The poles of the scattering matrix $\mathcal{S}^f = \hat{\mathbf{1}} + \mathcal{G}_0^f \mathcal{T}^f$ coincide with the zeros of $1/\tilde{\alpha}(\omega_L) - G(\omega_0)$. Hence, an eigenvector of $G(\omega_0)$ that satisfies the laser threshold condition (4.34) is also an eigenstate of $\mathcal{S}^f$ associated with an infinite eigenvalue. Besides, in the absence of pump and according to causality, the poles $\omega_L \in \mathbb{C}$ of $\mathcal{S}^f$ must be located in the lower half-plane. Using (4.29), we thus recover the fact that the eigenvalues Λ_k of $G(\omega_0)$ must satisfy $\mathrm{Im}\Lambda_k > -1$.

We would like to make the link between scattering operators such as $\mathcal{T}^f$ in the form (4.63), and some mathematical quantities that we will study in chapters 5 and 6 within the framework of random matrix theory. One of them is the averaged operator

$$O_A(z) = \left\langle \sum_{i=1}^{N} \sum_{j=1}^{N} \left[\frac{1}{z - A} \right]_{ij} |\mathbf{r}_i\rangle\langle\mathbf{r}_j| \right\rangle, \tag{4.65}$$

where A is an arbitrary $N \times N$ Euclidean random matrix. By definition of such a matrix, its elements are given by a deterministic function f of positions of pairs of points: $A_{ij} = f(\mathbf{r}_i, \mathbf{r}_j) = \langle \mathbf{r}_i | \hat{A} | \mathbf{r}_j \rangle$, where we introduced an operator $\hat{A}$ associated with the matrix A. Another object of interest is the resolvent

$$g(z) = \frac{1}{N} \left\langle \mathrm{Tr} \frac{1}{z - A} \right\rangle, \tag{4.66}$$

where Tr designates the usual trace of a $N \times N$ matrix. Taking the expectation value of (4.65) with respect to $|\mathbf{k}\rangle$, with $\langle \mathbf{r}|\mathbf{k}\rangle = e^{i\mathbf{k}\cdot\mathbf{r}}/\sqrt{V}$, we find a simple relation between $g(z)$ and $O_A(z)$:

$$\rho g(z) = \lim_{k\to\infty} \langle \mathbf{k} | O_A(z) | \mathbf{k} \rangle. \tag{4.67}$$

For $\hat{A} = \mathcal{G}_0^f$, *i.e.* for $A = \mathcal{G}_0^m$ given by Eq. (4.61), and for $z = 1/\tilde{t}$, O_A is equal to the operator $\langle \mathcal{T}^f \rangle$:

$$\langle \mathcal{T}^f \rangle = O_{\mathcal{G}_0^m}(1/\tilde{t}) = -\frac{4\pi}{k_0} O_{G(\omega_0)}(1/\tilde{\alpha}) \tag{4.68}$$

In addition, Eq. (4.52) shows that $\lim_{k\to\infty} \langle \mathcal{T}^f(\mathbf{k},\mathbf{k}) \rangle = \lim_{k\to\infty} \Sigma^f(\mathbf{k},\mathbf{k})$, because $\lim_{k\to\infty} \mathcal{G}_0^f(\mathbf{k},\mathbf{k}) = 0$. Therefore, with $A = \mathcal{G}_0^m$, Eqs. (4.67) and (4.68) yield

$$\rho g(z) = \lim_{k\to\infty} \Sigma^f(\mathbf{k},\mathbf{k}). \tag{4.69}$$

Let us take advantage of the relation (4.68) to calculate $\langle \mathcal{T}^f \rangle$ from $O_A(z)$. A standard way to calculate $O_A(z)$ [Eq. (4.65)] is to use its series expansion in $1/z$. Although this series is only convergent in the vicinity of $|z| \to \infty$, we can use its analytic continuation in the holomorphic domain of $O_A(z)$, *i.e.* in the region of the complex plane z where A has no eigenvalues. If A is Hermitian, its eigenvalues lie on segments of the real axis, so that the analytic continuation allows us to reconstruct $O_A(z)$ for any $z \in \mathbb{C}$. For a non-Hermitian matrix A, however, the eigenvalues are complex and $O_A(z)$ loses its

analyticity inside a two-dimensional domain $\mathcal{D}$ on the complex plane where eigenvalues are concentrated. In our present context, $A = \mathcal{G}_0^m$ is non-Hermitian, and thus $O_A(z)$ for $z \in \mathcal{D}$ cannot be assessed by the analytic continuation of its series expansion. In particular, by virtue of Eq. (4.68), this also applies to $\langle \mathcal{T}^f \rangle$: expansion presented in Fig. 4.1 is not valid for $1/\tilde{t} \in \mathcal{D}$. A consequence is that the expression for the self-energy Σ^f, and therefore for the extinction mean free path l_e, might be dramatically affected when $1/\tilde{t}$ reaches $\mathcal{D}$. The question then arises as to what the condition $1/\tilde{t} \in \mathcal{D}$ physically means. Quite interestingly, the random laser threshold (4.34) shows that it exactly corresponds to the domain where random lasing occurs. Furthermore, we know that, in this regime, the linear model — given by Eq. (4.12) where the saturation parameter s_i (4.6), implicitly contained in V^f, is set to zero — breaks down, and field nonlinearities come into play (see chapter 7 for a statistical treatment). For sure, this will affect the self-energy and the extinction mean free path. However, we stress that it is not the only change: to calculate Σ^f in this regime properly, adding nonlinearities to the diagrams of Fig. 4.1 is not sufficient; we also have to take into account the breakdown of holomorphic symmetry of $\langle \mathcal{T}^f \rangle$. Technically, a way to circumvent this problem is to duplicate the matrix size of operators like Σ^f. This point is discussed in details in chapter 6. For the time being, suppose we are interested in the regime below threshold. Then, we use the solution found in chapter 5 for $O_A(z)$ restricted to its holomorphic domain ($z \notin \mathcal{D}$):

$$O_A(z) = \rho \frac{g(z)}{1 - g(z)\hat{T}}, \tag{4.70}$$

where $\hat{T} = \rho \hat{A}$, and the the resolvent g is given by

$$g(z) = \frac{1}{z - \sigma(z)}, \tag{4.71}$$

$$\sigma(z) = \frac{g(z)}{N} \mathrm{Tr} \frac{\hat{T}^2}{1 - g(z)\hat{T}}. \tag{4.72}$$

Here Tr designates the trace of an operator (and not of a $N \times N$ matrix). Choosing $A = \mathcal{G}_0^m$, Eq. (4.68) becomes

$$\langle \mathcal{T}^f \rangle = \frac{\rho g(1/\tilde{t})}{1 - \rho g(1/\tilde{t}) \mathcal{G}_0^f}, \tag{4.73}$$

and the comparison with Eq. (4.52) gives us the self-energy

$$\Sigma^f = \rho g(1/\tilde{t}) \hat{\mathbf{1}}. \tag{4.74}$$

This result is consistent with Eq. (4.69). Eq. (4.72) reads now

$$\begin{aligned} \sigma(1/\tilde{t}) &= \frac{1}{N} \mathrm{Tr} \frac{\rho^2 g(1/\tilde{t}) (\mathcal{G}_0^f)^2}{1 - \rho g(1/\tilde{t}) \mathcal{G}_0^f} \\ &= \frac{1}{V} \mathrm{Tr} \frac{\mathcal{G}_0^f \Sigma^f \mathcal{G}_0^f}{1 - \Sigma^f \mathcal{G}_0^f} \\ &= \frac{1}{V} \mathrm{Tr} \left[\mathcal{G}_0^f \Sigma^f \langle \mathcal{G}^f \rangle \right], \end{aligned} \tag{4.75}$$

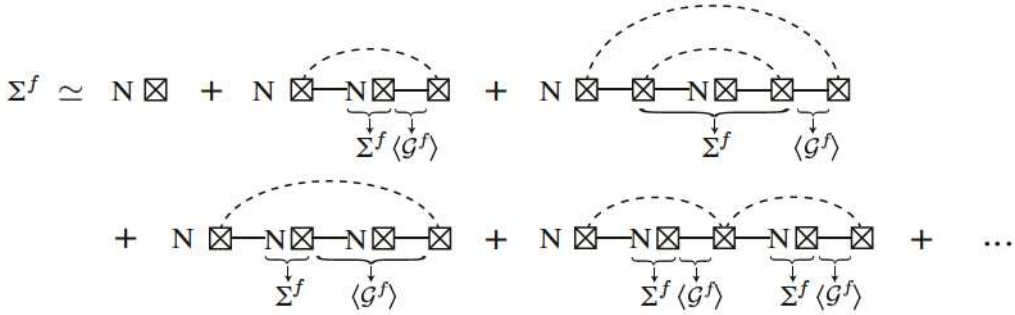

Figure 4.2: Selection of diagrams in the series expansion of the self energy Σ^f, in the limit $N \to \infty$. Braces with arrows denote parts of diagrams that are the beginnings of diagrammatic expansions of the quantities to which the arrows point. Other notations are defined in Fig. 4.1.

where we used successively Eqs. (4.74) and (4.39). Inserting (4.75) into (4.71), the self-energy (4.74) is finally expressed only in terms of scattering operators. With Eq. (4.39), it forms the following closed set

$$\langle\mathcal{G}^f\rangle = \frac{1}{(\mathcal{G}_0^f)^{-1} - \Sigma^f}, \tag{4.76}$$

$$\Sigma^f = \frac{\rho\tilde{t}}{1 - \frac{\tilde{t}}{V}\mathrm{Tr}\left[\mathcal{G}_0^f \Sigma^f \langle\mathcal{G}^f\rangle\right]}\hat{\mathbf{1}} \equiv \Sigma_0\hat{\mathbf{1}}. \tag{4.77}$$

The non-perturbative result (4.77) goes beyond ISA. Contrary to (4.54), it is not restricted to the low density regime $\rho\lambda_0^3 \ll 1$, and takes into account dependent scattering as we discuss below. Moreover, it was derived without any assumption about the volume V. In particular we did not assume translational invariance[7]. In a sphere for example, the trace appearing in Eq. (4.77) can be calculated exactly. It allows to find Σ^f and therefore l_e without introducing an iterative and perturbative scheme. Moreover, no divergency appears in this solution (see chapter 5).

It is now interesting to identify the diagrams of Fig. 4.1 that are necessary to recover the result (4.77). We propose to consider the diagrams represented in Fig. 4.2. To calculate explicitly their sum, we express Σ^f in the $|\mathbf{r}\rangle$-representation. After summation of diagrams that appear under each loop (dashed lines), we obtain

$$\begin{aligned}\langle\mathbf{r}|\Sigma^f|\mathbf{r}'\rangle &= \rho\tilde{t}\int_V \mathrm{d}^d\mathbf{r}_1\delta(\mathbf{r}-\mathbf{r}_1)\left[1 + \langle\mathbf{r}_1|\mathcal{G}_0^f\Sigma^f\langle\mathcal{G}^f\rangle|\mathbf{r}_1\rangle + \langle\mathbf{r}_1|\mathcal{G}_0^f\Sigma^f\langle\mathcal{G}^f\rangle|\mathbf{r}_1\rangle^2 + \dots\right]\delta(\mathbf{r}_1-\mathbf{r}') \\ &= \frac{\rho\tilde{t}}{1 - \langle\mathbf{r}|\mathcal{G}_0^f\Sigma^f\langle\mathcal{G}^f\rangle|\mathbf{r}\rangle}\delta(\mathbf{r}-\mathbf{r}'),\end{aligned} \tag{4.78}$$

and in the $|\mathbf{k}\rangle$-representation, Eq. (4.78) becomes[8]

$$\langle\mathbf{k}|\Sigma^f|\mathbf{k}'\rangle = \rho\tilde{t}\int_V \mathrm{d}^d\mathbf{r}\frac{e^{-\mathrm{i}(\mathbf{k}-\mathbf{k}')\cdot\mathbf{r}}}{1 - \langle\mathbf{r}|\mathcal{G}_0^f\Sigma^f\langle\mathcal{G}^f\rangle|\mathbf{r}\rangle}. \tag{4.79}$$

[7]In a finite volume V, operators such as $\mathcal{G}_0^f$ are not diagonal in the $|\mathbf{k}\rangle$-representation. For example, in three dimensional space, $\mathcal{G}_0^f(\mathbf{k},\mathbf{k}') = -\int_V\int_V \mathrm{d}^3\mathbf{r}\mathrm{d}^3\mathbf{r}' e^{-\mathrm{i}(\mathbf{k}\cdot\mathbf{r}-\mathbf{k}'\cdot\mathbf{r}')}e^{\mathrm{i}k_0|\mathbf{r}-\mathbf{r}'|}/4\pi|\mathbf{r}-\mathbf{r}'|$.

[8]Note that the expression (4.79) is similar but not identical to the k-independent part of the self-energy Σ^f discussed by van Tiggelen *et al.* [133].

To recover (4.77) from (4.78), we have to replace $\langle \mathbf{r}|\mathcal{G}_0^f \Sigma^f \langle \mathcal{G}^f \rangle|\mathbf{r}\rangle$ by $\mathrm{Tr}[\mathcal{G}_0^f \Sigma^f \langle \mathcal{G}^f \rangle]/V$. This is rigorously exact only if we temporarily assume translational invariance ($V \to \infty$). This small difference with (4.78) comes from the Gaussian hypothesis used to derive Eqs. (4.70), (4.71) and (4.72) in chapter 5. In this sense, (4.78) is a slightly better estimate of Σ^f than (4.77).

Furthermore, we now understand which dependent scattering diagrams are not contained in the result (4.77). They are all diagrams contained in Fig. 4.1 but not in Fig. 4.2, and correspond to scattering by clusters of atoms. The simplest example is the last diagram represented in Fig. 4.1, that corresponds to the scattering sequence $\mathbf{r}_1 \to \mathbf{r}_2 \to \mathbf{r}_1 \to \mathbf{r}_2 \to$ etc. It stands for a 'cavity' formed by only two atoms, associated with the two resonances that we studied (non-perturbatively) in section (3.4) (see, in particular, the two eigenvalues of the matrix $\mathcal{N}$ represented in Fig. 3.4). Other diagrams correspond to the various sequences that can propagate in cavites formed by a number of atoms larger than 2. All of them participate to the formation of 'subradiant' eigenstates — of the Green's matrix, and therefore also of the effective Hamiltonian (2.98), — that may play a crucial role in the limit of large density $\rho\lambda_0^3 \gg 1$. For further discussion about these states we refer the reader to chapters 5 and 6. As soon as we take into account some of these extra dependent scattering diagrams, $\langle \mathbf{k}|\Sigma^f|\mathbf{k}\rangle$ acquires a $\mathbf{k}$-dependence [133]. It is not the case for Eqs. (4.77) and (4.79), because point-like scatterers do no exhibit any typical length scale or geometric structure, as long as we stick to the 'mean-field' picture, which is not sufficient to describe scattering by clusters of particles of a typical size λ_0.

4.5 Transport equation in the presence of gain

4.5.1 Definition of notation

Let us reconsider the dimensionless light intensity that we introduced in chapter 3:

$$I(\mathbf{r},t) = \langle \mathbf{\Omega}^-(\mathbf{r},t) \cdot \mathbf{\Omega}^+(\mathbf{r},t)\rangle, \tag{4.80}$$

where $\mathbf{\Omega}^\pm$ is the dimensionless electric field (3.5). Although we use the same notation as in Eq. (3.4), Eq. (4.80) is different from (3.4) because averaging in Eq. (4.80) is defined with respect to external degrees of freedom, and not with respect to those of the radiation. As explained earlier, we use here the semiclassical approximation (3.46) together with the simplifying notation (4.16). To evaluate $I(\mathbf{r},t)$, it is convenient to work in the frequency representation:

$$I(\mathbf{r},t) = \int \frac{\mathrm{d}\omega_L}{2\pi}\frac{\mathrm{d}\Delta\omega_L}{2\pi} e^{-\mathrm{i}\Delta\omega_L t} I(\mathbf{r},\omega_L^+,\omega_L^-), \tag{4.81}$$

where

$$\begin{aligned} I(\mathbf{r},\omega_L^+,\omega_L^-) &= \langle \mathbf{\Omega}^+(\mathbf{r},\omega_L^+) \cdot \mathbf{\Omega}^+(\mathbf{r},\omega_L^-)^*\rangle, \\ &= \langle \langle \mathbf{r}|\mathbf{\Omega}^+(\omega_L^+)\rangle \cdot \langle \mathbf{\Omega}^+(\omega_L^-)|\mathbf{r}\rangle\rangle, \end{aligned} \tag{4.82}$$

and $\omega_L^\pm = \omega_L \pm \Delta\omega_L/2$. According to Eqs. (4.12), (4.36), and (4.50), $|\mathbf{\Omega}^+(\omega_L)\rangle$ is given by

$$|\mathbf{\Omega}^+(\omega_L)\rangle = |\mathbf{\Omega}_{in}^+(\omega_L)\rangle + \mathcal{G}^f(\omega_L)V^f(\omega_L)|\mathbf{\Omega}_{in}^+(\omega_L)\rangle, \tag{4.83}$$

$$= |\mathbf{\Omega}_{in}^+(\omega_L)\rangle + \mathcal{G}_0^f(\omega_L)\mathcal{T}^f(\omega_L)|\mathbf{\Omega}_{in}^+(\omega_L)\rangle, \tag{4.84}$$

where $|\mathbf{\Omega}_{in}^{+}(\omega_L)\rangle$ represents an incident wave packet, that we assume to be initially localized in space around $\mathbf{r}_{in}$. Far enough from the source ($|\mathbf{r}-\mathbf{r}_{in}| \gg l_e$), only the second term of Eq. (4.83) contributes significantly to the average of the intensity (4.82). After averaging, it is proportional to a sum of propagation kernels that have the generic form

$$\begin{aligned}\mathcal{I}(\mathbf{r},\mathbf{r}',\Delta\omega_L) &= \langle \mathcal{G}^f(\mathbf{r},\mathbf{r}',\omega_L^+)\mathcal{G}^f(\mathbf{r},\mathbf{r}',\omega_L^-)^*\rangle, \\ &= \langle\langle \mathbf{r}|\mathcal{G}^f(\omega_L^+)|\mathbf{r}'\rangle\langle\mathbf{r}'|\mathcal{G}^f(\omega_L^-)^\dagger|\mathbf{r}\rangle\rangle.\end{aligned} \tag{4.85}$$

It represents the intensity measured at point $\mathbf{r}$ due to a source at $\mathbf{r}'$, and is the physical quantity that we will study in the remainder of this chapter. In particular, we will see that it obeys a transport equation[9]. We omit the dependence of $\mathcal{I}$ on the carrier frequency ω_L because the latter is fixed (elastic scattering), contrary to the modulation frequency $\Delta\omega_L$ that is the Fourier conjugated variable of time t [see Eq. (4.81)]. The stationary regime is recovered for $\Delta\omega_L \to 0$. To simplify further the expressions, we note

$$\begin{aligned}\mathcal{G}^+ &= \mathcal{G}^f(\omega_L^+), \\ \mathcal{G}^- &= \mathcal{G}^f(\omega_L^-)^\dagger,\end{aligned} \tag{4.86}$$

and for reasons that will become clear later, we will work in this section in the momentum representation. We define succesively

$$\Phi_{\mathbf{k}\mathbf{k}'}(\Delta\mathbf{k},\Delta\mathbf{k}',\Delta\omega_L) = \langle\langle \mathbf{k}^+|\mathcal{G}^+|\mathbf{k}'^+\rangle\langle\mathbf{k}'^-|\mathcal{G}^-|\mathbf{k}^-\rangle\rangle, \tag{4.87}$$

$$\Phi_{\mathbf{k}}(\Delta\mathbf{k},\Delta\mathbf{k}',\Delta\omega_L) = \sum_{\mathbf{k}'}\Phi_{\mathbf{k}\mathbf{k}'}(\Delta\mathbf{k},\Delta\mathbf{k}',\Delta\omega_L), \tag{4.88}$$

$$\mathcal{I}(\Delta\mathbf{k},\Delta\mathbf{k}',\Delta\omega_L) = \sum_{\mathbf{k}}\Phi_{\mathbf{k}}(\Delta\mathbf{k},\Delta\mathbf{k}',\Delta\omega_L), \tag{4.89}$$

$$\mathbf{J}(\Delta\mathbf{k},\Delta\mathbf{k}',\Delta\omega_L) = \sum_{\mathbf{k}}\Phi_{\mathbf{k}}(\Delta\mathbf{k},\Delta\mathbf{k}',\Delta\omega_L)\mathbf{k}, \tag{4.90}$$

where $\mathbf{k}^\pm = \mathbf{k} \pm \Delta\mathbf{k}/2$. The intensity (4.85) is simply the Fourier transform of (4.89):

$$\mathcal{I}(\mathbf{r},\mathbf{r}',\Delta\omega_L) = \sum_{\Delta\mathbf{k}}\sum_{\Delta\mathbf{k}'}\frac{e^{\mathrm{i}(\Delta\mathbf{k}\cdot\mathbf{r}-\Delta\mathbf{k}'\cdot\mathbf{r}')}}{V^2}\mathcal{I}(\Delta\mathbf{k},\Delta\mathbf{k}',\Delta\omega_L). \tag{4.91}$$

In the infinite medium with translational invariance, the intensity is nonzero if the momentum is conserved. It implies $\Delta\mathbf{k} = \Delta\mathbf{k}'$. Thus, it is clear from Eq. (4.91) that $|\mathbf{r}-\mathbf{r}'| \to \infty$ limit corresponds to $|\Delta\mathbf{k}| \to 0$.

In the following we will use standard notations for the outer product of two second-rank tensors A and B [127]:

$$\begin{aligned}(A\otimes B)_{injm} &= \langle in|A\otimes B|jm\rangle \\ &= \langle i|A|j\rangle\langle m|B|n\rangle \\ &= A_{ij}B_{mn},\end{aligned} \tag{4.92}$$

[9]We could also express the intensity (4.82) in terms of the product of two operators $\mathcal{T}^f$ instead of two Green's operators $\mathcal{G}^f$, by using Eq. (4.84). We do not apply this procedure because $\langle\mathcal{T}^f(\mathbf{r},\mathbf{r}',\omega_L^+)\mathcal{T}^f(\mathbf{r},\mathbf{r}',\omega_L^-)^*\rangle$ does not obey a closed equation such as a transport equation, as we shall see below.

as well as for the inner product of two fourth-rank tensors:

$$(M : N)_{injm} = \sum_{lp} M_{inlp} N_{lpjm}, \tag{4.93}$$

so that we have the following property:

$$(AB) \otimes (CD) = (A \otimes D) : (B \otimes C). \tag{4.94}$$

With these notations, we finally define the fourth-rank intensity tensor:

$$\mathcal{I}(\Delta\omega_L) = \langle \mathcal{G}^+ \otimes \mathcal{G}^- \rangle, \tag{4.95}$$

related to the intensity (4.85) and to its equivalent in the momentum representation (4.87) by

$$\mathcal{I}(\mathbf{r}, \mathbf{r}', \Delta\omega_L) = \langle \mathbf{r}\mathbf{r} | \mathcal{I}(\Delta\omega_L) | \mathbf{r}'\mathbf{r}' \rangle, \tag{4.96}$$

$$\Phi_{\mathbf{k}\mathbf{k}'}(\Delta\mathbf{k}, \Delta\mathbf{k}', \Delta\omega_L) = \langle \mathbf{k}^+\mathbf{k}^- | \mathcal{I}(\Delta\omega_L) | \mathbf{k}'^+\mathbf{k}'^- \rangle. \tag{4.97}$$

4.5.2 From Bethe-Salpeter equation to Boltzmann equation

In complete analogy with the self-energy defined for the averaged Green's function in Eq. (4.39), we introduce the irreducible vertex $U(\Delta\omega_L)$ as

$$\mathcal{I}(\Delta\omega_L) = \frac{1}{\langle \mathcal{G}^+ \rangle^{-1} \otimes \langle \mathcal{G}^- \rangle^{-1} - U(\Delta\omega_L)} \tag{4.98}$$

$$= \langle \mathcal{G}^+ \rangle \otimes \langle \mathcal{G}^- \rangle + \langle \mathcal{G}^+ \rangle \otimes \langle \mathcal{G}^- \rangle : U(\Delta\omega_L) : \mathcal{I}(\Delta\omega_L). \tag{4.99}$$

This equation is known as the Bethe-Salpeter equation. Formally, it looks like the Dyson equation (4.39), but for fourth-rank tensors. In the study of point-like particles, we have seen in section 4.3 that it is suitable to work with the expansion of $\mathcal{T}^f$ rather than $\mathcal{G}^f$, inasmuch as the physical building block is the t-operator of one atom. Therefore, in analogy with $\langle \mathcal{T}^f \rangle$ in Eq. (4.52), we also define the reducible vertex $\Gamma(\Delta\omega_L)$ as

$$\Gamma(\Delta\omega_L) = U(\Delta\omega_L) + U(\Delta\omega_L) : \langle \mathcal{G}^+ \rangle \otimes \langle \mathcal{G}^- \rangle : \Gamma(\Delta\omega_L). \tag{4.100}$$

Using the definitions (4.50), (4.99), and (4.100), we relate $\Gamma(\Delta\omega_L)$ to $\langle \mathcal{T}^+ \otimes \mathcal{T}^- \rangle$:

$$\begin{aligned} \Gamma(\Delta\omega_L) = & \langle \mathcal{G}^+ \rangle^{-1} \mathcal{G}_0^+ \otimes \mathcal{G}_0^- \langle \mathcal{G}^- \rangle^{-1} : \\ & \left[\langle \mathcal{T}^+ \otimes \mathcal{T}^- \rangle - \langle \mathcal{T}^+ \rangle \otimes \langle \mathcal{T}^- \rangle \right] : \mathcal{G}_0^+ \langle \mathcal{G}^+ \rangle^{-1} \otimes \langle \mathcal{G}^- \rangle^{-1} \mathcal{G}_0^-, \end{aligned} \tag{4.101}$$

where $\mathcal{G}_0^\pm$ and $\mathcal{T}^\pm$ are defined as $\mathcal{G}^\pm$ in Eq. (4.86). $\Gamma(\Delta\omega_L)$ is not exactly equal to $\langle \mathcal{T}^+ \otimes \mathcal{T}^- \rangle - \langle \mathcal{T}^+ \rangle \otimes \langle \mathcal{T}^- \rangle$ because the propagator in the expansion of $\langle \mathcal{G}^f \rangle$ and $\langle \mathcal{T}^f \rangle$ is $\mathcal{G}_0$, whereas it is $\langle \mathcal{G}^+ \rangle \otimes \langle \mathcal{G}^- \rangle$ for $\mathcal{I}$ and Γ. The latter is defined in the effective medium, while the former is not. We will neglect this slight difference, and consider that $U(\Delta\omega_L)$ is the sum of all irreducible diagrams contained in the expansion of $\langle \mathcal{T}^+ \otimes \mathcal{T}^- \rangle - \langle \mathcal{T}^+ \rangle \otimes \langle \mathcal{T}^- \rangle$.[10]

[10] In a more rigorous treatment, we can introduce a new $\mathcal{T}$-operator defined in the effective medium. The main effect of this operation would be the dressing of the t-operator of each scatterer, as discussed by Sheng [127]. It is called the coherent potential approximation (CPA).

Leaving aside the calculation of U for the moment, let us discuss the physical meaning of the Bethe-Salpeter equation (4.99). In the momentum representation, it becomes

$$\begin{aligned}\Phi_{\mathbf{k}}(\Delta\mathbf{k},\Delta\mathbf{k}',\Delta\omega_L) &= \sum_{\mathbf{k}'}\langle\mathcal{G}^+(\mathbf{k}^+,\mathbf{k}'^+)\rangle\langle\mathcal{G}^-(\mathbf{k}'^-,\mathbf{k}^-)\rangle + \\ &\sum_{\mathbf{k}_1\mathbf{k}_2\mathbf{k}_3\mathbf{k}_4}\langle\mathcal{G}^+(\mathbf{k}^+,\mathbf{k}_1)\rangle\langle\mathcal{G}^-(\mathbf{k}_2,\mathbf{k}^-)\rangle U_{\mathbf{k}_1\mathbf{k}_2\mathbf{k}_3\mathbf{k}_4}(\Delta\omega_L)\Phi_{\frac{\mathbf{k}_3+\mathbf{k}_4}{2}}(\mathbf{k}_3-\mathbf{k}_4,\Delta\mathbf{k}',\Delta\omega_L),\end{aligned} \tag{4.102}$$

where $\Phi_{\mathbf{k}}(\Delta\mathbf{k},\Delta\mathbf{k}',\Delta\omega_L)$ is defined by Eqs. (4.88) and (4.97). Assuming the medium to be infinite with translational invariance, we note

$$\begin{aligned}\langle\mathcal{G}^\pm(\mathbf{k}_1,\mathbf{k}_2)\rangle &= \langle\mathcal{G}^\pm(\mathbf{k}_1)\rangle\delta_{\mathbf{k}_1,\mathbf{k}_2},\\ U_{\mathbf{k}^+\mathbf{k}^-\mathbf{k}_1^+\mathbf{k}_1^-}(\Delta\omega_L) &= U_{\mathbf{k}\mathbf{k}_1}(\Delta\mathbf{k},\Delta\omega_L)\delta_{\Delta\mathbf{k},\Delta\mathbf{k}_1},\\ \Phi_{\mathbf{k}}(\Delta\mathbf{k},\Delta\mathbf{k}',\Delta\omega_L) &= \Phi_{\mathbf{k}}(\Delta\mathbf{k},\Delta\omega_L)\delta_{\Delta\mathbf{k},\Delta\mathbf{k}'},\end{aligned} \tag{4.103}$$

and rewrite Eq. (4.102) as

$$\Phi_{\mathbf{k}}(\Delta\mathbf{k},\Delta\omega_L) = \langle\mathcal{G}^+(\mathbf{k}^+)\rangle\langle\mathcal{G}^-(\mathbf{k}^-)\rangle\left[1+\sum_{\mathbf{k}_1}U_{\mathbf{k}\mathbf{k}_1}(\Delta\mathbf{k},\Delta\omega_L)\Phi_{\mathbf{k}_1}(\Delta\mathbf{k},\Delta\omega_L)\right]. \tag{4.104}$$

We are interested in the behavior of the intensity $\sum_{\mathbf{k}}\Phi_{\mathbf{k}}$ in the limit of $\Delta\omega_L$, $|\Delta\mathbf{k}|\to 0$, that corresponds to the long-time and large-travel-distance limit. It is only in this regime that we expect to obtain a transport equation. For the time being, let us expand only the prefactor of Eq. (4.104), $\langle\mathcal{G}^+(\mathbf{k}^+)\rangle\langle\mathcal{G}^-(\mathbf{k}^-)\rangle$, according to

$$\langle\mathcal{G}^+(\mathbf{k}^+)\rangle\langle\mathcal{G}^-(\mathbf{k}^-)\rangle = \frac{\langle\mathcal{G}^+(\mathbf{k}^+)\rangle-\langle\mathcal{G}^-(\mathbf{k}^-)\rangle}{\langle\mathcal{G}^-(\mathbf{k}^-)\rangle^{-1}-\langle\mathcal{G}^+(\mathbf{k}^+)\rangle^{-1}}, \tag{4.105}$$

$$\simeq \frac{\Delta\mathcal{G}_{\mathbf{k}}(\Delta\mathbf{k},\Delta\omega_L)}{-2k_L\Delta k_L+2\mathbf{k}\cdot\Delta\mathbf{k}+\Delta\Sigma_{\mathbf{k}}(\Delta\mathbf{k},\Delta\omega_L)}, \tag{4.106}$$

where $\Delta\mathcal{G}_{\mathbf{k}}(\Delta\mathbf{k},\Delta\omega_L) = \langle\mathcal{G}^+(\mathbf{k}^+)\rangle-\langle\mathcal{G}^-(\mathbf{k}^-)\rangle$ and $\Delta\Sigma_{\mathbf{k}}(\Delta\mathbf{k},\Delta\omega_L) = \Sigma^+(\mathbf{k}^+)-\Sigma^-(\mathbf{k}^-)$. To obtain (4.106) from (4.105), we performed a Taylor expansion of the denominator of (4.105) in the limit $\Delta\omega_L$, $|\Delta\mathbf{k}|\to 0$, using $\langle\mathcal{G}^f(\mathbf{k})\rangle^{-1} = k_L^2-k^2-\Sigma^f(\mathbf{k})$. At this stage, a somehow technical but nevertheless important comment is necessary. If we continue expanding (4.106) such that the fraction disappears, as it is done, for example, in [129] in the **r**-representation, all terms proportional to $\Phi_{\mathbf{k}}$ in Eq. (4.104) would also be proportional to the irreducible vertex U, except for the l.h.s. of Eq. (4.104). On the contrary, if we insert (4.106) into (4.104) without further approximation, we also get a term of the form $\Delta\Sigma_{\mathbf{k}}\Phi_{\mathbf{k}}$. The two approaches are equivalent in the absence of pump, when the self-energy Σ^f and the irreducible vertex U are related by a Ward identity (see below), but they are not equivalent when atoms are pumped. In our situation, it is therefore important to avoid expanding the denominator of Eq. (4.106).[11] Hence, the Bethe-Salpeter equation (4.104) may be rewritten as

$$\begin{aligned}&\left[-2k_L\Delta k_L+2\mathbf{k}\cdot\Delta\mathbf{k}+\Delta\Sigma_{\mathbf{k}}(\Delta\mathbf{k},\Delta\omega_L)\right]\Phi_{\mathbf{k}}(\Delta\mathbf{k},\Delta\omega_L)\\ &= \Delta\mathcal{G}_{\mathbf{k}}(\Delta\mathbf{k},\Delta\omega_L)\left[1+\sum_{\mathbf{k}_1}U_{\mathbf{k}\mathbf{k}_1}(\Delta\mathbf{k},\Delta\omega_L)\Phi_{\mathbf{k}_1}(\Delta\mathbf{k},\Delta\omega_L)\right].\end{aligned} \tag{4.107}$$

[11] This also justifies *a posteriori* the use of the **k**-representation and not of the **r**-representation. Using **r**-representation is advantageous only when the denominator of Eq. (4.106) is further expanded in series [129].

This equation can be regarded as a generalized Boltzmann equation, where the building block of the collision integral is the irreducible vertex U [49].

If we approximate Σ^f and U by their lowest order in density — ISA (4.54) for Σ^f and Boltzmann approximation for U (see below) — all interferences are neglected. To be consistent with energy conservation, all time correlations also have to be disregarded: it amounts to neglect the width of the spectral function that is proportional to the source term $\Delta\mathcal{G}_{\mathbf{k}}(\Delta\mathbf{k}, \Delta\omega_L)$ [49]. The resulting equation is a Boltzmann equation for light, also named the radiative transfer equation (RTE).

4.5.3 Diffusion equation

In the present study, we would like to avoid approximations that neglect spatial and time correlations in the generalized Boltzmann equation, and keep Eq. (4.107) as general as possible, by taking into account the fact that scattering is provided by point-like particles, eventually responsible for absorption or amplification. As usual with a microscopic Boltzmann-like equation, we can derive a continuity equation for the intensity (4.89), as well as a constitutive equation that makes the link between the current (4.90) and $\Phi_{\mathbf{k}}$. To do so, on the one hand we sum Eq. (4.107) with respect to $\mathbf{k}$, and on the other hand we multiply (4.107) with $\mathbf{k}$ and sum over $\mathbf{k}$. The continuity equation is:

$$\begin{aligned}&-\Delta k_L \mathcal{I}(\Delta\mathbf{k}, \Delta\omega_L) + \frac{\Delta\mathbf{k}\cdot\mathbf{J}(\Delta\mathbf{k}, \Delta\omega_L)}{k_L}\\ &-\mathrm{i}\sum_{\mathbf{k}}\left[\frac{1}{l_e(\mathbf{k}, \Delta\mathbf{k}, \Delta\omega_L)} - \frac{1}{l_s(\mathbf{k}, \Delta\mathbf{k}, \Delta\omega_L)}\right]\Phi_{\mathbf{k}}(\Delta\mathbf{k}, \Delta\omega_L) = \frac{1}{2k_L}\sum_{\mathbf{k}}\Delta\mathcal{G}_{\mathbf{k}}(\Delta\mathbf{k}, \Delta\omega_L),\end{aligned} \tag{4.108}$$

and the constitutive equation reads:

$$\begin{aligned}\Delta k_L \mathbf{J}(\Delta\mathbf{k}, \Delta\omega_L) + \mathrm{i}\sum_{\mathbf{k}}\frac{\Phi_{\mathbf{k}}(\Delta\mathbf{k}, \Delta\omega_L)\mathbf{k}}{l_e(\mathbf{k}, \Delta\mathbf{k}, \Delta\omega_L)} - \sum_{\mathbf{k}}\frac{\Delta\mathbf{k}\cdot\mathbf{k}}{k_L}\Phi_{\mathbf{k}}(\Delta\mathbf{k}, \Delta\omega_L)\mathbf{k}\\ = \sum_{\mathbf{k}}\left[-\frac{1}{2k_L}\Delta\mathcal{G}_{\mathbf{k}}(\Delta\mathbf{k}, \Delta\omega_L) + \mathrm{i}\frac{\Phi_{\mathbf{k}}(\Delta\mathbf{k}, \Delta\omega_L)\mathbf{k}}{l_s(\mathbf{k}, \Delta\mathbf{k}, \Delta\omega_L)}\right]\mathbf{k}.\end{aligned} \tag{4.109}$$

Here l_e and l_s are the (generalized) extinction and scattering mean free paths, that depend on the self-energy Σ^f and the irreducible vertex U, respectively:

$$\frac{1}{l_e(\mathbf{k}, \Delta\mathbf{k}, \Delta\omega_L)} = \frac{\mathrm{i}}{2k_L}\Delta\Sigma_{\mathbf{k}}(\Delta\mathbf{k}, \Delta\omega_L), \tag{4.110}$$

$$\frac{1}{l_s(\mathbf{k}, \Delta\mathbf{k}, \Delta\omega_L)} = \frac{\mathrm{i}}{2k_L}\sum_{\mathbf{k}'}\Delta\mathcal{G}_{\mathbf{k}'}(\Delta\mathbf{k}, \Delta\omega_L)U_{\mathbf{k}'\mathbf{k}}(\Delta\mathbf{k}, \Delta\omega_L). \tag{4.111}$$

It is clear from Eq. (4.108) that, in the absence of external pump, (4.110) and (4.111) must be equal in the stationary regime $\Delta\omega_L \to 0$ to insure energy conservation at fixed carrier frequency ω_L (elastic scattering). This identity is called Ward identity [127].

We now simplify Eqs. (4.108) and (4.109) by assuming $\Delta\Sigma_{\mathbf{k}}(\Delta\mathbf{k}, \Delta\omega_L) \equiv \Delta\Sigma_0(\Delta\omega_L)$ and $U_{\mathbf{k}'\mathbf{k}}(\Delta\mathbf{k}, \Delta\omega_L) \equiv U_0(\Delta\omega_L)$ independent of the wavevectors $\mathbf{k}$ and $\mathbf{k}'$. As far as the self-energy is concerned, this simplification is correct for point-like particles at least as long as we can neglect scattering by clusters of particles (see section 4.4). We expect the same to be true for the irreducible vertex, if we disregard maximally crossed diagrams

that account, in particular, for coherent backscattering (see below). The fact that $U_{\mathbf{k}'\mathbf{k}}$ is independent of the angle between $\mathbf{k}$ and $\mathbf{k}'$ means that scattering is isotropic, which is true for a single point-like scatterer. Consequently, l_e and l_s become independent of $\mathbf{k}$. The continuity equation (4.108) is now given by

$$-\left[\Delta k_L + \frac{\mathrm{i}}{l_e(\Delta\omega_L)} - \frac{\mathrm{i}}{l_s(\Delta\mathbf{k},\Delta\omega_L)}\right]\mathcal{I}(\Delta\mathbf{k},\Delta\omega_L) + \frac{\Delta\mathbf{k}\cdot\mathbf{J}(\Delta\mathbf{k},\Delta\omega_L)}{k_L} = \frac{1}{2k_L}\sum_{\mathbf{k}}\Delta\mathcal{G}_{\mathbf{k}}(\Delta\mathbf{k},\Delta\omega_L), \tag{4.112}$$

and by multiplying the constitutive equation (4.109) with $\Delta\mathbf{k}$, we obtain

$$\frac{\Delta\mathbf{k}\cdot\mathbf{J}(\Delta\mathbf{k},\Delta\omega_L)}{k_L} = \frac{\Delta k^2\sum_{\mathbf{k}}(\widehat{\Delta\mathbf{k}}\cdot\mathbf{k})^2\Phi_{\mathbf{k}}(\Delta\mathbf{k},\Delta\omega_L)}{k_L^2[\Delta k_L + \mathrm{i}/l_e(\Delta\omega_L)]}, \tag{4.113}$$

where $\widehat{\Delta\mathbf{k}} = \Delta\mathbf{k}/\Delta k$. Note that the r.h.s. of Eq. (4.109) is zero for isotropic scatterers, so that $\Delta\mathbf{k}\cdot\mathbf{J}(\Delta\mathbf{k},\Delta\omega_L)$ depends only on Σ^f through l_e and not on U. The last term of the r.h.s. of Eq. (4.109) would bring a correction for anisotropic scatterers, responsible for the difference between the transport mean free path l_{tr} and the scattering mean free path l_s. In our context, l_{tr} and l_s are equal. We now replace $\Phi_{\mathbf{k}}$ appearing in (4.113) by its expansion in terms of irreducible moments [127] that can be inferred from (4.107), $\Phi_{\mathbf{k}} = \Phi_{\mathbf{k}}^{(0)} + \Phi_{\mathbf{k}}^{(1)} + \ldots$. The truncation of such an expansion to its first terms insures that the continuity equation becomes a diffusion-like equation. It is the main difference with a RTE-like equation where all moments are conserved. $\Phi_{\mathbf{k}}^{(1)}$ is proportional to $\mathbf{k}$ and thus does not contribute to (4.113). $\Phi_{\mathbf{k}}^{(0)}$ is given by

$$\Phi_{\mathbf{k}}^{(0)} = \frac{\Delta\mathcal{G}_{\mathbf{k}}(\Delta\mathbf{k},\Delta\omega_L)}{\sum_{\mathbf{k}'}\Delta\mathcal{G}_{\mathbf{k}'}(\Delta\mathbf{k},\Delta\omega_L)}\mathcal{I}(\Delta\mathbf{k},\Delta\omega_L). \tag{4.114}$$

Hence the numerator of the r.h.s. of Eq. (4.113) is proportional to

$$\sum_{\mathbf{k}}(\widehat{\Delta\mathbf{k}}\cdot\mathbf{k})^2\Delta\mathcal{G}_{\mathbf{k}}(\Delta\mathbf{k},\Delta\omega_L) = \frac{1}{3}\sum_{\mathbf{k}}k^2\Delta\mathcal{G}_{\mathbf{k}}(\Delta\mathbf{k},\Delta\omega_L), \tag{4.115}$$

$$\simeq \frac{k_L^2}{3}\sum_{\mathbf{k}}\Delta\mathcal{G}_{\mathbf{k}}(\Delta\mathbf{k},\Delta\omega_L), \tag{4.116}$$

where we used the fact that $\Delta\mathcal{G}_{\mathbf{k}}(\Delta\mathbf{k},\Delta\omega_L)$ has a resonance at $k \simeq k_L$ in the limit $|\Delta\mathbf{k}|, \Delta\omega_L \to 0$. What remains in (4.113) is

$$\frac{\Delta\mathbf{k}\cdot\mathbf{J}(\Delta\mathbf{k},\Delta\omega_L)}{k_L} = \frac{\Delta k^2\mathcal{I}(\Delta\mathbf{k},\Delta\omega_L)}{3[\Delta k_L + \mathrm{i}/l_e(\Delta\omega_L)]}. \tag{4.117}$$

For simplicity, we set the source term of the continuity equation — the r.h.s. of Eq. (4.112) — to 0, and insert (4.117) into (4.112). We obtain:

$$-\Delta k_L^2\mathcal{I}(\Delta\mathbf{k},\Delta\omega_L) - \mathrm{i}\Delta k_L\left[\frac{2}{l_e(\Delta\omega_L)} - \frac{1}{l_s(\Delta\mathbf{k},\Delta\omega_L)}\right]\mathcal{I}(\Delta\mathbf{k},\Delta\omega_L) + \frac{\Delta k^2}{3}\mathcal{I}(\Delta\mathbf{k},\Delta\omega_L) + \frac{1}{l_e(\Delta\omega_L)}\left[\frac{1}{l_e(\Delta\omega_L)} - \frac{1}{l_s(\Delta\mathbf{k},\Delta\omega_L)}\right]\mathcal{I}(\Delta\mathbf{k},\Delta\omega_L) = 0. \tag{4.118}$$

We now have to be extremely cautious when further simplifying Eq. (4.118). The first idea we could have is to neglect the term $-\Delta k_L^2 \mathcal{I}(\Delta\mathbf{k}, \Delta\omega_L)$ in Eq. (4.118). It turns out that this approximation leads to a diffusion equation in the presence of gain that predicts unphysical results. A much better approximation consists in neglecting the second time derivative of the 'dressed' intensity: $\tilde{\mathcal{I}}(\Delta\mathbf{k}, t) = e^{-ct/l_g}\mathcal{I}(\Delta\mathbf{k}, t)$, where $1/l_g = 1/l_s - 1/l_e$ is the gain length ($l_g < 0$ in the case of absorption).[12] Indeed, according to Eq. (4.118), $\tilde{\mathcal{I}}$ obeys an equation that does not contain the extinction length l_e:

$$-\Delta k_L^2 \tilde{\mathcal{I}}(\Delta\mathbf{k}, \Delta\omega_L) - \frac{\mathrm{i}\Delta k_L}{l_s(\Delta\mathbf{k}, \Delta\omega_L)}\tilde{\mathcal{I}}(\Delta\mathbf{k}, \Delta\omega_L) + \frac{\Delta k^2}{3}\tilde{\mathcal{I}}(\Delta\mathbf{k}, \Delta\omega_L) = 0. \tag{4.119}$$

The intensity $\tilde{\mathcal{I}}$ propagates as if there were no absorption or gain in the medium. Neglecting $\Delta k_L^2 \tilde{\mathcal{I}}(\Delta\mathbf{k}, \Delta\omega_L)$ in Eq. (4.119), we obtain

$$\begin{aligned} &-\frac{\mathrm{i}\Delta k_L}{l_s(\Delta\mathbf{k}, \Delta\omega_L)}\mathcal{I}(\Delta\mathbf{k}, \Delta\omega_L) + \frac{\Delta k^2}{3}\mathcal{I}(\Delta\mathbf{k}, \Delta\omega_L) \\ &+ \frac{1}{l_s(\Delta\omega_L)}\left[\frac{1}{l_e(\Delta\omega_L)} - \frac{1}{l_s(\Delta\mathbf{k}, \Delta\omega_L)}\right]\mathcal{I}(\Delta\mathbf{k}, \Delta\omega_L) = 0. \end{aligned} \tag{4.120}$$

Note the rather subtle but important difference with Eq. (4.118). Finally, we expand $1/l_e(\Delta\omega_L)$ and $1/l_s(\Delta\mathbf{k}, \Delta\omega_L)$ as $1/l_e(0) + \Delta k_L \partial_{\Delta k_L}(1/l_e)(0) + \mathcal{O}(\Delta\omega_L)$ and $1/l_s(0,0) + \Delta k_L \partial_{\Delta k_L}(1/l_s)(0,0) + \mathcal{O}(\Delta\mathbf{k}, \Delta\omega_L)$, respectively. Equation (4.120) takes now the form of a diffusion equation:

$$-\mathrm{i}\Delta\omega_L \mathcal{I}(\Delta\mathbf{k}, \Delta\omega_L) + D\Delta k^2 \mathcal{I}(\Delta\mathbf{k}, \Delta\omega_L) + v\left[\frac{1}{l_e} - \frac{1}{l_s}\right]\mathcal{I}(\Delta\mathbf{k}, \Delta\omega_L) = 0, \tag{4.121}$$

where $l_e = l_e(0)$, $l_s = l_s(0,0)$, v is the transport velocity,

$$v = \frac{c}{1+\delta}, \tag{4.122}$$

$$\delta = \partial_{\mathrm{i}\Delta k_L}\left(\frac{1}{l_s}\right)(0,0) - \partial_{\mathrm{i}\Delta k_L}\left(\frac{1}{l_e}\right)(0), \tag{4.123}$$

and D is the diffusion coefficient,

$$D = \frac{1}{3} l_s v. \tag{4.124}$$

δ can be interpreted as the ratio between the 'dwell' time and the scattering time l_s/c [49, 129]. For atoms on resonance ($\omega_L = \omega_0$) and without pump, we can verify, using ISA (4.55) and $l_e = l_s$, that the dwell time is roughly equal to the inverse of the spontaneous decay rate Γ_0, so that $v \simeq \Gamma_0 l_s$ [78]. According to Eqs. (4.110) and (4.111), l_e and l_s are given by

$$\frac{1}{l_e} = -\frac{1}{k_L}\mathrm{Im}\Sigma_0(\Delta\omega_L = 0), \tag{4.125}$$

$$\frac{1}{l_s} = \frac{V}{4\pi} U_0(\Delta\omega_L = 0). \tag{4.126}$$

We recall that we did not make any assumption concerning $\Sigma_0(\Delta\omega_L) = \Sigma_{\mathbf{k}}(\Delta\mathbf{k}, \Delta\omega_L)$ and $U_0(\Delta\omega_L) = U_{\mathbf{k}'\mathbf{k}}(\Delta\mathbf{k}, \Delta\omega_L)$, except that they are independent of the wavevectors $\mathbf{k}$ and $\mathbf{k}'$. In the next section, we examine the irreducible vertex U and give expressions for the laser threshold inferred either from the diffusion equation (4.121), or directly from the Bethe-Salpeter equation (4.99).

[12] Here we temporarily omit the frequency dependence of l_e and l_s. If we take it into account, we should consider $\tilde{\mathcal{I}}(\Delta\mathbf{k}, t) = e^{-vt/l_g}\mathcal{I}(\Delta\mathbf{k}, t)$, where v is the transport velocity (see below).

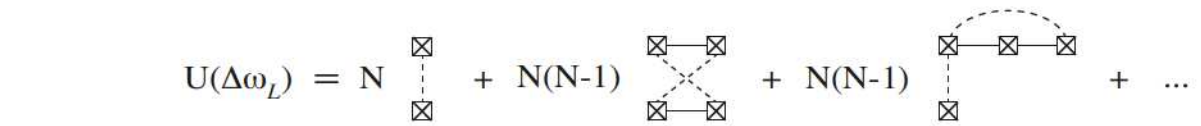

Figure 4.3: Diagrammatic expansion of the irreducible vertex $U(\Delta\omega_L)$. In the upper line $\boxtimes$ involves $t_i(\omega_L^+)$, and in the lower line $t_i(\omega_L^-)$. Other notations are defined in Fig. 4.1.

4.6 Laser threshold from transport equation

As announced above, $U(\Delta\omega_L)$ is the sum of all irreducible diagrams contained in the expansion of $\langle \mathcal{T}^+ \otimes \mathcal{T}^- \rangle - \langle \mathcal{T}^+ \rangle \otimes \langle \mathcal{T}^- \rangle$, where $\mathcal{T}^+ = \mathcal{T}^f(\omega_L^+)$ and $\mathcal{T}^- = \mathcal{T}^f(\omega_L^-)^\dagger$. Using the expansion (4.53) for $\mathcal{T}^f$, $U(\Delta\omega_L)$ is given by the series represented in Fig. 4.3. In the weak-scattering regime ($\rho\lambda_0^3 \ll 1$), $U(\Delta\omega_L)$ is commonly approximated by the first term $N\langle \boxtimes \otimes \boxtimes \rangle$.[13] In the momentum representation,

$$U_{\mathbf{k}\mathbf{k}'}(\Delta\mathbf{k}, \Delta\omega_L) \simeq \rho \frac{\tilde{t}(\omega_L^+)\tilde{t}(\omega_L^-)}{V} \tag{4.127}$$

is, as expected, independent of $\mathbf{k}$, $\mathbf{k}'$, and $\Delta\mathbf{k}$. The scattering mean free path (4.126) is then given by

$$l_s \simeq \frac{4\pi}{\rho|\tilde{t}(\omega_L)|^2} \simeq \frac{l_0}{|\tilde{\alpha}(\omega_L)|^2}, \tag{4.128}$$

with l_0 the on-resonance scattering mean free path in the absence of pump [see, *e.g.* (4.9), with $W = 0$]:

$$l_0 = \frac{k_0^2}{4\pi\rho}. \tag{4.129}$$

Eq. (4.127) is known as the Boltzmann approximation, sometimes also called 'ladder' approximation because it leads to the reducible vertex (4.100) that looks like a sum of ladders. It neglects interferences and corresponds to the same degree of approximation as ISA (4.54) for Σ^f. With ISA and Boltzmann approximation, the albedo is

$$a = \frac{l_e}{l_s} = \frac{k_L|\tilde{t}(\omega_L)|^2}{4\pi \mathrm{Im}[\tilde{t}(\omega_L)]} = -\frac{1}{\mathrm{Im}[1/\tilde{\alpha}(\omega_L)]}, \tag{4.130}$$

so that the Ward identity in the stationary regime, $1/l_e = 1/l_s$, reduces to the optical theorem (4.29) obeyed by a single scatterer, and it is satisfied only in the absence of pump. Combining Eqs. (4.56) and (4.128), the diffusion equation (4.121) now becomes

$$-\partial_t \mathcal{I}(\mathbf{r}, t) + D\Delta_{\mathbf{r}}\mathcal{I}(\mathbf{r}, t) = Q\mathcal{I}(\mathbf{r}, t), \tag{4.131}$$

with

$$D = \frac{v l_0}{3|\tilde{\alpha}(\omega_L)|^2}, \tag{4.132}$$

$$Q = \frac{v}{l_0}\left[|\tilde{\alpha}(\omega_L)|^2 - \mathrm{Im}[\tilde{\alpha}(\omega_L)]\right]. \tag{4.133}$$

[13] By convention, each diagram is the outer product of the upper line read from left to right, and the lower line read from right to left. After using the property (4.94), it becomes an inner product of four-rank tensors read from left to right.

Hence, we recover the diffusion equation discussed in [129], and implicitly used in the recent literature [134].

The second term of Eq. (4.131) describes attenuation of the radiation due to diffusion spreading, and the third term absorption and/or amplification. As pointed out already by Letokhov in 1968, in his seminal paper about 'generation of light by a scattering medium with negative resonance absorption' [6], there obviously exists a threshold at which the radiation losses are compensated by the gain. To find this threshold, we write the general solution of Eq. (4.131) in the basis of the eigenstates ψ_n of the Laplacian, $\Delta_{\mathbf{r}}\psi_n(\mathbf{r}) = -\kappa_n^2\psi_n(\mathbf{r})$, as

$$\mathcal{I}(\mathbf{r},t) = \sum_n a_n\psi_n(\mathbf{r})e^{-(D\kappa_n^2-Q)t}, \tag{4.134}$$

where a_n are constants determined by the distribution of intensity at $t = 0$. Therefore, the first (linear) lasing mode ψ_{n_0} is the one associated with the eigenvalue $\kappa_{n_0}^2 = \min(\kappa_n^2)$ that satifies the threshold condition

$$\frac{Q}{D\kappa_{n_0}^2} = 1. \tag{4.135}$$

Although we derived the diffusion equation (4.131) by assuming the medium to be infinite with translational invariance, it is still possible to take into account the boundary conditions. For example, if the region occupied by atoms is a sphere of radius R we have to set $\psi_n(R + r_0) = 0$, where r_0 is the extrapolation length [129, 135],

$$\begin{aligned} r_0 &= \frac{2}{3}l_s\frac{1}{1+2l_s/3R}, \\ &= \frac{R}{1+3b_0|\tilde{\alpha}(\omega_L)|^2/4}, \end{aligned} \tag{4.136}$$

with $b_0 = 2R/l_0$ the on-resonance optical thickness of the medium. κ_{n_0} is then given by

$$\kappa_{n_0} = \frac{\pi}{R+r_0}. \tag{4.137}$$

The threshold condition is obtained by substituting Eqs. (4.132) and (4.133), together with Eqs. (4.136) and (4.137), into (4.135):

$$\frac{\sqrt{3}}{2\pi}b_0|\tilde{\alpha}(\omega_L)|\sqrt{|\tilde{\alpha}(\omega_L)|^2 - \mathrm{Im}\tilde{\alpha}(\omega_L)}\left(1+\frac{1}{1+3b_0|\tilde{\alpha}(\omega_L)|^2/4}\right) = 1. \tag{4.138}$$

This condition, that involves only one disorder parameter, the optical thickness b_0, applies for any polarizability $\tilde{\alpha}(\omega_L)$, and thus does not depend on a particular pumping mechanism or atomic model. It was recently used to address the problem of achieving a random laser with a cloud of cold atoms [134].

Let us now show how a threshold condition that is even more general than (4.138) may actually be obtained without much effort. In section 4.2, we saw that the exact laser threshold, valid for each spatial configuration of atoms, is given by Eq. (4.34). It means that finding the threshold is equivalent, on average, to finding the boundary of the support of the eigenvalue density for the Green's matrix (4.61). In chapter 6, we

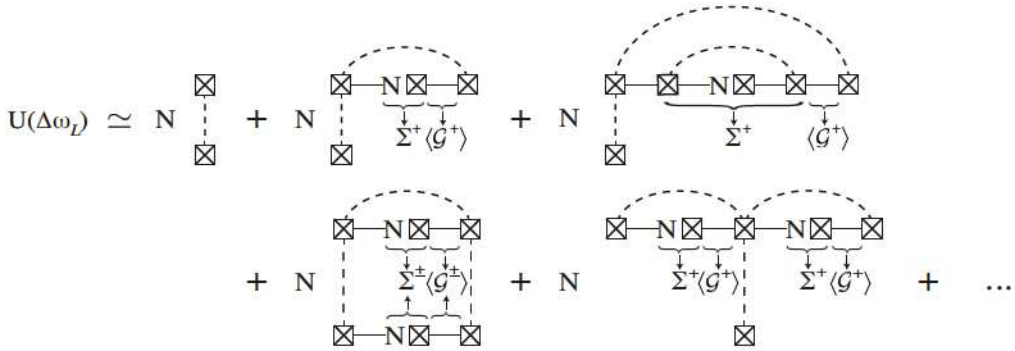

Figure 4.4: Selection of diagrams in the series expansion of the irreducible vertex $U(\Delta\omega_L)$, in the limit $N \to \infty$. Notations are defined in Figs. 4.2 and 4.3. We recognize in the upper line $\Sigma^+ = \Sigma^f(\omega_L^+)$ and in the lower line $\Sigma^- = \Sigma^f(\omega_L^-)^\dagger$, with Σ^f given by the diagrams of Fig. 4.2.

shall derive the following equation for the borderline z of the eigenvalue domain of the Green's matrix:

$$\frac{|g(z)|^2}{N}\mathrm{Tr}\left[\frac{\hat{T}}{1-g(z)\hat{T}}\frac{\hat{T}^\dagger}{1-g(z)^*\hat{T}^\dagger}\right] = 1. \tag{4.139}$$

This has to be solved self-consistently with Eqs. (4.71) and (4.72). $\hat{T}$ and $g(z)$ are defined in section 4.4. Combining this equation with the threshold condition $z = 1/\tilde{t}$ gives

$$\frac{|\Sigma_0|^2}{N}\mathrm{Tr}\left[\langle\mathcal{G}^f\rangle\langle\mathcal{G}^{f\dagger}\rangle\right] = 1, \tag{4.140}$$

that has, in turn, to be solved self-consistently with Eqs. (4.76) and (4.77), where Σ_0 is defined. To derive (4.140), we used the relation (4.74) that makes the link between quantities defined for non-Hermitian matrices and scattering operators. A question shows up immediately: can we recover the result (4.140) thanks to a direct analysis of the Bethe-Salpeter equation (4.99)? According to the definition (4.98) of the irreducible vertex $U(\Delta\omega_L)$ the average intensity tensor $\mathcal{I}(\Delta\omega_L)$ diverges for

$$U(\Delta\omega_L) : \langle\mathcal{G}^+\rangle \otimes \langle\mathcal{G}^-\rangle = \hat{\mathbf{1}} \otimes \hat{\mathbf{1}}. \tag{4.141}$$

This condition can be interpreted as a generic random laser threshold for the average intensity $\mathcal{I}(\Delta\omega_L)$. Better is the estimation of Σ^f and U, better will be the prediction for the threshold. We propose to retain in Σ^f the diagrams represented in Fig. 4.2, leading to the result (4.77). And as far as U is concerned, we consider the diagrams of Fig. 4.4, where we recognize in the upper and lower lines, the outer product of diagrams identical to those of Fig. 4.2. Consequently, in the momentum representation, the irreducible vertex has now the form

$$\begin{aligned} U_{\mathbf{k}_1\mathbf{k}_2\mathbf{k}_3\mathbf{k}_4}(\Delta\omega_L) &= U_0(\Delta\omega_L)\delta_{\mathbf{k}_2-\mathbf{k}_1+\mathbf{k}_3-\mathbf{k}_4}, \\ U_0(\Delta\omega_L) &= \frac{1}{N}\Sigma_0(\omega_L^+)\Sigma_0(\omega_L^-)^*. \end{aligned} \tag{4.142}$$

Taking the trace of (4.141), in which we insert the result (4.142), we exactly recover, in the stationary regime $\Delta\omega_L \to 0$, the threshold condition (4.140). This means that

Eq. (4.139), derived in chapter 6, for the borderline of the eigenvalue domain of the Green's matrix can be interpreted in terms of the scattering events represented in Fig. 4.4.

The threshold equation (4.140) is more precise than (4.138) for three reasons. Firstly, it goes beyond ISA and Boltzmann approximation by taking into account a special class of dependent scattering discussed in section 4.4. It is thus not limited to the weak-scattering regime $\rho\lambda_0^3 \ll 1$. Secondly, it does not assume translational invariance. For instance, $\langle \mathcal{G}^f \rangle$ is not diagonal in the $\mathbf{k}$-representation, and has to be found self-consistently. Thirdly, it does not rely on any expansion that would correspond to the limit $|\Delta\mathbf{k}| \to 0$. Therefore, it can be applied even outside the diffusive regime ($R/l_s \gg 1$). We refer the reader interested in a quantitative evaluation of Eq. (4.140) to chapter 7, where it will be used for atoms in a sphere, and compared with brute-force numerical analysis.

Let us conclude this chapter with two important comments. The expansion of the irreducible vertex $U(\Delta\omega_L)$ such as presented in Fig. 4.3 is not valid for all values of the scattering amplitude $\tilde{t}$. As it was already pointed out in section 4.4, it is meaningful only in the holomorphic domain of $\langle \mathcal{T}^f \rangle$, *i.e.* below the laser threshold. Above threshold, apart from nonlinearities, we have to take care of the holomorphic symmetry breaking. This can be done by duplicating the dimensionality of the space in which the irreducible vertex is defined (see chapter 6).

In addition, we mention that diagrams of Fig. 4.4 do not contain the so-called maximally crossed diagrams, like, *e.g.*, the second diagram of Fig. 4.3. It is well known that such diagrams are the microscopic building blocks that explain weak localization of light [127, 131, 136]. We point out that it is *a priori* not difficult to include them in the generic threshold condition (4.141), and thus also to check how they contribute to the eigenvalue domain of the non-Hermitian Green's matrix.

Chapter 5

Hermitian Euclidean random matrix theory

Random matrix theory (RMT) is a powerful tool of modern theoretical physics [137]. Its main goal is to calculate the statistical properties of eigenvalues or eigenvectors for large matrices. First introduced by Wishart in 1928 [138] and then used by Wigner in 1950's to describe the statistics of energy levels in complex nuclei [139], random matrices are nowadays omnipresent in physics [140–143]. The majority of works — including the seminal papers by Wigner [139] and Dyson [144–146] — deal with Hermitian matrices. Hermitian matrices are of special importance in physics because of the Hermiticity of operators associated with observables in quantum mechanics.

A special class of random matrices are the so-called Euclidean random matrices (ERMs) [147]. The elements A_{ij} of a $N \times N$ Euclidean random matrix A are given by a deterministic function f of positions of pairs of points that are randomly distributed in a finite region V of Euclidean space: $A_{ij} = f(\mathbf{r}_i, \mathbf{r}_j)$, $i = 1, \ldots, N$. Hermitian ERM models play an important role in the theoretical description of supercooled liquids [147–153], disordered superconductors [154], relaxation in glasses and scalar phonon localization [155]. They have been used as a playground to study Anderson localization [156, 157]. A number of analytic approaches were developed to deal with Hermitian ERMs [147–157]. The principal difficulties that one encounters when trying to develop a theory for ERMs stem from the nontrivial statistics of their elements and the correlations between them. Both are not known analytically and are often difficult to calculate. This is in contrast with standard approaches [137, 141] in which the joint probability distribution of the elements of the random matrix under study is the starting point of analysis.

The main goal of this chapter is to study eigenvalue distributions of various large ERMs that appear in problems of wave propagation in random media. One of the most interesting ERM in this context is probably the Green's matrix $\mathbf{G}(\omega_0)$, that plays a central role in many important physical situations already mentioned in section 2.5. $\mathbf{G}(\omega_0)$ is non-Hermitian, its eigenvalues are complex, and their probability distribution is difficult to access (see chapter 6). This is why in several works dealing with superradiance [79, 82, 87, 88, 90] the imaginary part of the scalar Green's matrix $G(\omega_0)$, a matrix with elements $\sin(k_0|\mathbf{r}_i - \mathbf{r}_j|)/k_0|\mathbf{r}_i - \mathbf{r}_j|$, was considered. This real symmetric matrix is much easier to study and in many situations it still contains some of the important aspects of the full problem. Similarly, the real part of $G(\omega_0)$, a matrix with elements

$\cos(k_0|\mathbf{r}_i-\mathbf{r}_j|)/k_0|\mathbf{r}_i-\mathbf{r}_j|$, is relevant for understanding the collective Lamb shifts in dense atomic systems [83, 90]. Despite the importance of these matrices, little is known about statistical properties of their eigenvalues. Some analytical results are available only in the limit of high density of points $\mathbf{r}_i$, $\rho = N/V \to \infty$, when the summation in the eigenvalue equation $\sum_j A_{ij}\psi_j = \Lambda\psi_i$ can be replaced by integration [87, 88, 90]. We would like to fill this gap by considering eigenvalue distributions of the matrices above at finite densities ρ, with the distances between neighboring points $\mathbf{r}_i$ that are larger than, comparable, or smaller than the wavelength $\lambda_0 = 2\pi/k_0$. This situation is of particular importance in the context of wave propagation in random media because in order to observe phenomena due to scattering of waves on the heterogeneities of the medium, the density of scattering centers should be neither too low (in this case the scattering is negligible), nor too high (in this case the medium responds as an effective homogeneous medium). The most interesting phenomena for waves in an ensemble of point-like scattering centers are known to take place at densities $\rho\lambda_0^3 \gtrsim 1$, when interference effects become important, eventually leading to Anderson localization [9, 101, 102].

The chapter is organized as follows. In section 5.1, we introduce well-known ensembles of random matrices that play an important role in our context, the Gaussian and Wishart ensembles. We also propose a representation of ERMs, that will be the cornerstone of further treatments. In section 5.2, we define basic tools of RMT, such as the resolvent, the Blue function, and the $\mathcal{R}$-transform, and indicate how they are related to the statical properties of random matrices. Then, we present four different methods to deal with Hermitian ERMs: a mapping to the so-called Dyson gas (section 5.3), a field-theoretical approach (section 5.4), a direct diagrammatic treatment (section 5.5), and a method based on the free probability theory (section 5.6). We think that each of these methods shines an original light on the problem, based on a deep and specific physical picture. Comparison of these approaches clearly reveals the power of RMT[1]. Finally, we apply the results presented in previous sections to the two ERMs $\mathrm{Im}G(\omega_0)$ (section 5.7) and $\mathrm{Re}G(\omega_0)$ (section 5.8).

5.1 Random matrix ensembles of interest

5.1.1 Gaussian matrices

The best known random matrix ensembles are probably the Gaussian ensembles. They are ensembles of $N \times N$ Hermitian matrices $A = A^\dagger$, that have independent and identically distributed (i.i.d.) zero-mean Gaussian entries. The probability distribution of A is

$$P(A) = C_N e^{-\frac{\beta N}{4}\mathrm{Tr}A^2}, \tag{5.1}$$

where C_N is a normalization constant, and β is the symmetry index, that counts the number of degrees of freedom in the matrix elements.

For our purpose, it is sufficient to consider matrices A with entries being either real or complex numbers ($\beta = 1$ or 2). Let us first analyze the case of complex elements, for which $\beta = 2$. Since the transformation $A \to UAU^{-1}$, with U unitary, leaves $P(A)$ invariant, the ensemble is called 'Gaussian unitary ensemble' (GUE). From Eq. (5.1), we

[1] Obviously, the set of techniques developed in RMT includes many approaches that will not be used in this manuscript. For instance, we will not deal with the method of orthogonal polynomials, which is one of the oldest methods developed in RMT [137].

easily verify that the second moments of A_{ij} take the values

$$\langle A_{ij}A_{kl}\rangle = \tfrac{1}{N}\delta_{il}\delta_{jk} \qquad \text{GUE } (\beta = 2). \tag{5.2}$$

On the other hand, if elements of A are reals numbers, $\beta = 1$, and the transformation $A \to UAU^{-1}$ leaves $P(A)$ invariant for U orthogonal. The ensemble is called 'Gaussian orthogonal ensemble' (GOE), and the second moments are given by

$$\langle A_{ij}A_{kl}\rangle = \tfrac{1}{N}(\delta_{il}\delta_{jk} + \delta_{ik}\delta_{jl}) \qquad \text{GOE } (\beta = 1). \tag{5.3}$$

As we shall see later, the density of eigenvalues of a Gaussian matrix A converges, in the limit $N \to \infty$, to the so-called 'semicircle' law, first discovered by Wigner in the 1950's [139].

5.1.2 Wishart matrices

Another ensemble of particular interest for us is the Wishart ensemble, that is as old as RMT itself [138]. It is useful in many contexts, such as neural networks, image processing, or wireless communications, where Wishart matrices naturally arise to characterize the singular values of 'channel matrices' [143]. A $N \times N$ Wishart matrix A is of the form

$$A = HH^\dagger, \tag{5.4}$$

where H is a rectangular $N \times M$ matrix, with columns that are zero-mean independent real/complex Gaussian vectors with covariance matrix $\mathbf{\Sigma}$ [143]. In this chapter, we will work with H complex and $\mathbf{\Sigma}$ proportional to the identity matrix I_N. In this case, entries of H are zero-mean i.i.d. complex Gaussian random numbers. The probability distribution of the non-Hermitian matrix H is

$$P(H) = C_{N,M}e^{-N\mathrm{Tr}HH^\dagger}, \tag{5.5}$$

so that the second-moments of H obey

$$\langle H_{i\alpha}H^\dagger_{\beta j}\rangle = \frac{1}{N}\delta_{ij}\delta_{\alpha\beta} = \langle H^\dagger_{\alpha i}H_{j\beta}\rangle. \tag{5.6}$$

For $c = N/M < 1$, Wishart showed that the probability distribution of (5.4) is given by [138, 143]

$$P(A) = C'_{N,M}\det A^{M-N}e^{-N\mathrm{Tr}A}. \tag{5.7}$$

Quite surprisingly, no such explicit formula was known for $c > 1$ ('anti-Wishart case') until recently [158]. However, as far as the eigenvalue distribution of A is concerned, it is straightforward to obtain the result for $c > 1$ from the one for $c < 1$ (see section 5.3.4).

In section 5.3.4, we will see that the eigenvalues distribution of $A = HH^\dagger$ converges, in the limit $N, M \to \infty$ with $c = N/M$ fixed, to the so-called 'Marchenko-Pastur' law. It was first established in 1967 in a remarkable paper [159], and then rediscovered several times [143].

5.1.3 Euclidean random matrices

As explained in the introduction, ERMs are matrices with elements A_{ij} defined with the help of some deterministic function f of positions of pairs of points:

$$A_{ij} = f(\mathbf{r}_i, \mathbf{r}_j) = \langle \mathbf{r}_i | \hat{A} | \mathbf{r}_j \rangle. \tag{5.8}$$

Here the N points $\mathbf{r}_i$ are randomly distributed inside some region V of d-dimensional space with a uniform density $\rho = N/V$, and we introduced an operator $\hat{A}$ associated with the matrix A. Contrary to Gaussian or Wishart matrices, the probability distribution $P(A)$ is not known analytically. Averaging $\langle \dots \rangle$ is not performed with respect to $P(A)$, but by spatial integration over the volume V where points are confined, according to Eq. (4.37).

It is worth noting that the property $\sum_j A_{ij} = 0$ is not imposed in our definition (5.8). Such a condition is required when studying, for instance, vibration modes of an amorphous solid, instantaneous normal modes of a liquid, or random master equations [147]. It expresses global translational invariance (conservation of momentum in the case of propagating excitations), and is encoded in the fact that a vector with identical components is an eigenvector associated with zero eigenvalue. Such a property is absent for ERMs relevant for wave propagation in random media.

We now propose a very useful trick to study statistical properties of (5.8), that consists in changing the basis from $\{\mathbf{r}_i\}$ to $\{\psi_\alpha\}$, which is orthogonal in V. Inserting the closure relation $\hat{\mathbf{1}} = \sum_\alpha |\psi_\alpha\rangle\langle\psi_\alpha|$ into Eq. (5.8), we obtain for arbitrary V:

$$A = HTH^\dagger, \tag{5.9}$$

where

$$H_{i\alpha} = \frac{1}{\sqrt{\rho}} \langle \mathbf{r}_i | \psi_\alpha \rangle, \tag{5.10}$$

$$T_{\alpha\beta} = \rho \, \langle \psi_\alpha | \hat{A} | \psi_\beta \rangle. \tag{5.11}$$

In Eq. (5.10) and (5.11), the prefactor ρ is introduced for later convenience. In a rectangular box, for example, $|\psi_\alpha\rangle = |\mathbf{k}_\alpha\rangle$ with $\langle \mathbf{r} | \mathbf{k}_\alpha \rangle = \exp(i\mathbf{k}_\alpha \mathbf{r})/\sqrt{V}$, so that $T_{\alpha\beta}$ are simply the Fourier coefficients of $f(\mathbf{r}_i, \mathbf{r}_j)$:

$$T_{\alpha\beta} = N \iint_V \frac{\mathrm{d}^d \mathbf{r}_i}{V} \frac{\mathrm{d}^d \mathbf{r}_j}{V} f(\mathbf{r}_i, \mathbf{r}_j) \exp[-\mathrm{i}(\mathbf{k}_\alpha \cdot \mathbf{r}_i - \mathbf{k}_\beta \cdot \mathbf{r}_j)]. \tag{5.12}$$

The advantage of the representation (5.9) lies in the separation of two different sources of complexity: the matrix H is random but independent of the function f, whereas the matrix T depends on f but is not random.

Furthermore, we assume that

$$\int_V \mathrm{d}^d \mathbf{r} \; \psi_\alpha(\mathbf{r}) = 0, \tag{5.13}$$

which in a box is obeyed for all α except when $\mathbf{k}_\alpha = 0$. We readily find that $H_{i\alpha}$ are

identically distributed random variables with zero mean and variance equal to $1/N$:

$$\langle H_{i\alpha}\rangle = \frac{1}{\sqrt{\rho}}\int_V \frac{\mathrm{d}^d\mathbf{r}_i}{V}\psi_\alpha(\mathbf{r}_i) = 0, \tag{5.14}$$

$$\begin{aligned}\langle H_{i\alpha}H^*_{j\beta}\rangle &= \frac{1}{\rho}\iint_V \frac{\mathrm{d}^d\mathbf{r}_i}{V}\frac{\mathrm{d}^d\mathbf{r}_j}{V}\psi_\alpha(\mathbf{r}_i)\psi^*_\beta(\mathbf{r}_j) \quad (i\neq j),\\ &= \langle H_{i\alpha}\rangle\langle H^*_{j\beta}\rangle = 0,\end{aligned} \tag{5.15}$$

$$\langle H_{i\alpha}H^*_{i\beta}\rangle = \frac{1}{\rho}\int_V \frac{\mathrm{d}^d\mathbf{r}_i}{V}\psi_\alpha(\mathbf{r}_i)\psi^*_\beta(\mathbf{r}_i) = \frac{1}{N}\delta_{\alpha\beta}. \tag{5.16}$$

Eq. (5.15) and (5.16) show that H satisfies the property (5.6), reproduced here for clarity:

$$\langle H_{i\alpha}H^\dagger_{\beta j}\rangle = \frac{1}{N}\delta_{ij}\delta_{\alpha\beta} = \langle H^\dagger_{\alpha i}H_{j\beta}\rangle. \tag{5.17}$$

It means that the covariance matrix of the columns of H is $\mathbf{\Sigma} = I_N/N$. If $H_{i\alpha}$ were Gaussian random variables, then the property (5.17) would be sufficient to conclude that $H_{i\alpha}$ are independent. However, they are not Gaussian and hence not necessarily independent. For example, the cumulant $\langle A_{ij}A_{ji}A_{ij}\rangle_c$ is not zero. It turns out that neglecting these complications and assuming $H_{i\alpha}$ Gaussian i.i.d. amounts to disregarding the class of 'dependent scattering' events corresponding to the formation of 'cavities' by clusters of points $\mathbf{r}_i$ (see the discussion at the end of section 4.4).

In section 5.5, we will explicitly assume that $H_{i\alpha}$ are independent Gaussian random variables. This assumption largely simplifies calculations but may limit applicability of our results at high densities of points ρ, at least for certain types of Euclidean matrices, as we will see later. Within this assumption, the only but crucial difference between an ERM (5.9) and a Wishart matrix (5.4) is the matrix T that contains all information about the function f defining the ERM. It can modify the eigenvalue distribution in a non-trivial way and lead to transitions between topologically different supports $\mathcal{D}$ of the eigenvalue density. Illustrations of such transitions are given by the examples considered in sections 5.7 and 5.8.

5.2 Resolvent, Blue function, and $\mathcal{R}$-transform

Eigenvalues Λ_n of a $N\times N$ Hermitian matrix A are real. Their density,

$$p(\Lambda) = \frac{1}{N}\left\langle \sum_{n=1}^N \delta(\Lambda-\Lambda_n)\right\rangle, \tag{5.18}$$

can be obtained from the (one-point) resolvent

$$g(z) = \frac{1}{N}\left\langle \mathrm{Tr}\frac{1}{z-A}\right\rangle = \frac{1}{N}\left\langle \sum_{n=1}^N \frac{1}{z-\Lambda_n}\right\rangle. \tag{5.19}$$

Using the standard relation $\lim_{\epsilon\to 0^+} 1/(\Lambda+\mathrm{i}\epsilon) = \mathrm{P}1/\Lambda - \mathrm{i}\pi\delta(\Lambda)$ (P is the Principal value), Eq. (5.19) becomes

$$g(\Lambda+\mathrm{i}\epsilon) = \mathrm{P}\int_{-\infty}^{\infty}\mathrm{d}\Lambda'\frac{p(\Lambda')}{\Lambda-\Lambda'} - \mathrm{i}\pi p(\Lambda), \tag{5.20}$$

so that $p(z)$ may be reconstructed either from the imaginary part or the real part of $g(\Lambda + \mathrm{i}\epsilon)$[2]:

$$p(\Lambda) = -\frac{1}{\pi} \lim_{\epsilon \to 0^+} \mathrm{Im} g(\Lambda + \mathrm{i}\epsilon), \tag{5.21}$$

$$\mathrm{P} \int_{-\infty}^{\infty} \mathrm{d}\Lambda' \frac{p(\Lambda')}{\Lambda - \Lambda'} = \mathrm{Re}\, g(\Lambda + \mathrm{i}\epsilon). \tag{5.22}$$

To calculate $p(\Lambda)$, Eq. (5.21) is much more popular than the integral equation (5.22). However, the inversion of the latter — named Fredholm integral equation of the first kind — sometimes gives the solution in a very efficient manner. Indeed, if $p(\Lambda)$ has a finite support $[a, b]$, the solution of Eq. (5.22) is given by Tricomi's theorem [160]:

$$p(\Lambda) = \frac{1}{\pi^2 \sqrt{(\Lambda - a)(b - \Lambda)}} \left[\pi - \mathrm{P} \int_a^b \mathrm{d}\Lambda' \frac{\sqrt{(\Lambda' - a)(b - \Lambda')}}{\Lambda' - \Lambda} \mathrm{Re} g(\Lambda' + \mathrm{i}\epsilon) \right]. \tag{5.23}$$

Such an expression for $p(\Lambda)$ turns out to be particularly useful within the framework of the Dyson gas model (see section 5.3).

In order to compute $g(z)$, we can rewrite it in different forms. Each of them is the starting point of a specific analysis developed in the following sections. First, we note that

$$\sum_{n=1}^{N} \frac{1}{z - \Lambda_n} = \partial_z \ln \left[\prod_{n=1}^{N} (z - \Lambda_n) \right], \tag{5.24}$$

and express the resolvent (5.19) as

$$g(z) = \frac{1}{N} \partial_z \left\langle \ln \det(z - A) \right\rangle. \tag{5.25}$$

This expression will be used in the field-theoretical approach presented in section 5.4. Another interesting expression for $g(z)$ is a decomposition in terms of the moments of $p(\Lambda)$,

$$\langle \Lambda^n \rangle = \int_{-\infty}^{\infty} \mathrm{d}\Lambda p(\Lambda) \Lambda^n = \frac{1}{N} \langle \mathrm{Tr} A^n \rangle. \tag{5.26}$$

For Hermitian matrices, $g(z)$ is a holomorphic function of $z \in \mathbb{C}$ except for some cuts of the real axis where eigenvalues of A are concentrated. Therefore, we can reconstruct $g(z)$ for all z by analytical continuation of its series expansion

$$g(z) = \sum_{n=0}^{\infty} \frac{\langle \Lambda^n \rangle}{z^{n+1}}, \tag{5.27}$$

which is in general convergent only in the vicinity of $|z| \to \infty$. We will work with the representation (5.27) in section 5.5, to perform a diagrammatic computation of $g(z)$. In this perspective, it is also convenient to define the self-energy $\sigma(z)$, that contains all irreducible diagrams in Eq. (5.27):

$$g(z) = \frac{1}{z - \sigma(z)}. \tag{5.28}$$

[2]Physically, $g(\Lambda + \mathrm{i}\epsilon)$ is the Fourier transform of the causal propagator $e^{-\mathrm{i}At}\Theta(t)$, and therefore its real and imaginary parts obey Kramers-Kronig relations.

Other important objects for us are the functional inverse of $g(z)$, also named Blue function, and the $\mathcal{R}$-transform:

$$\mathcal{B}(z) = g^{-1}(z), \tag{5.29}$$

$$\mathcal{R}(z) = \mathcal{B}(z) - \frac{1}{z}. \tag{5.30}$$

Both of them are fundamental objects of the free random variable theory, discussed in section 5.6. In particular, $\mathcal{R}(z)$ is the generating function of the 'free cumulants' (see section 5.6 for more details). According to Eq. (5.28), $\mathcal{B}(z)$ and $\mathcal{R}(z)$ are related to the self-energy $\sigma(z)$ by

$$\sigma(z) = \mathcal{R}[g(z)], \tag{5.31}$$

$$\mathcal{B}(z) = \frac{1}{z} + \sigma[\mathcal{B}(z)]. \tag{5.32}$$

Let us now mention a couple of properties useful for further analysis. The functions $g(z)$, $\mathcal{B}(z)$, and $\mathcal{R}(z)$ obey the following scaling relations:

$$\begin{aligned} g_{\alpha A}(z) &= \frac{1}{\alpha} g_A(\frac{z}{\alpha}), \\ \mathcal{B}_{\alpha A}(z) &= \alpha \mathcal{B}_A(\alpha z), \\ \mathcal{R}_{\alpha A}(z) &= \alpha \mathcal{R}_A(\alpha z), \end{aligned} \tag{5.33}$$

where $\alpha \in \mathbb{C}^*$. Besides, the moments $\langle \Lambda^n \rangle$ can be obtained from $g(z)$, $\mathcal{B}(z)$, and $\mathcal{R}(z)$. Using Eqs. (5.27), (5.29), and (5.30), we easily show that

$$\langle \Lambda^n \rangle = \frac{1}{(n+1)!} \frac{d^{n+1} g(z)}{d(1/z)^{n+1}} \bigg|_{z\to\infty}, \tag{5.34}$$

$$\langle \Lambda^n \rangle = \frac{1}{(n+1)!} \left[-\frac{\mathcal{B}^2(z)}{\mathcal{B}'(z)} \frac{d}{dz} \right]^n \left[-\frac{\mathcal{B}^2(z)}{\mathcal{B}'(z)} \right] \bigg|_{z\to 0}, \tag{5.35}$$

$$\langle \Lambda \rangle = \mathcal{R}(0), \tag{5.36}$$

$$\mathrm{var}\Lambda = \langle (\Lambda - \langle \Lambda \rangle)^2 \rangle = \mathcal{R}'(z)|_{z\to 0}, \tag{5.37}$$

where $\mathcal{B}'(z) = \mathrm{d}\mathcal{B}(z)/\mathrm{d}z$ and $\mathcal{R}'(z) = \mathrm{d}\mathcal{R}(z)/\mathrm{d}z$. Finally, we note that the boundaries Λ_* of the domain of existence of eigenvalues, $p(\Lambda_*) = 0$, are given by the following simple relations [161]:

$$g'(\Lambda_*) = \infty, \tag{5.38}$$

$$\mathcal{B}'(\Lambda_*) = 0. \tag{5.39}$$

5.3 Mapping to the Dyson gas

5.3.1 Dyson gas picture

Observing that the electric field created by a point charge in two dimensions is inversely proportional to the distance from the charge, the resolvent (5.19) can be interpreted as the electric field created, at point z in the complex plane, by charges ($q = +1$) situated at positions Λ_n on the real axis. This suggests an analogy between the statistical properties

of random matrices and those of a gas of charged particles restricted to move in one dimension, the so-called Dyson gas [137, 144–146].

For a large class of random matrices A, the distribution of the eigenvalues Λ_n can be seen as the equilibrium distribution of fictitious point charges repealing each other by Coulomb interaction, and submitted to an external one-body potential determined by the precise form of the probability distribution $P(A)$. In particular, this statement is true for the Wigner-Dyson ensemble defined as

$$P(A) = C_N e^{-\beta N \mathrm{Tr} V^g(A)}, \tag{5.40}$$

where $V^g(A)$ is arbitrary, provided existence of the partition function C_N^{-1}. If V^g is quadratic, we recover the Gaussian ensemble (5.1). To justify the Dyson gas picture, it is sufficient to consider the (joint) probability distribution of the eigenvalues (for the proof, see section 5.3.2):

$$P(\{\Lambda_n\}) = C'_N e^{-\beta H^g(\{\Lambda_n\})}, \tag{5.41}$$

$$H^g(\{\Lambda_n\}) = N \sum_{n=1}^{N} V^g(\Lambda_n) - \sum_{n<m} \ln|\Lambda_n - \Lambda_m|. \tag{5.42}$$

We recognize the Boltzmann-Gibbs distribution of a classical gas in thermal equilibrium at temperature $T = 1/\beta$. The logarithmic pair-wise repulsion

$$V^{int}(z) = -\sum_{n=1}^{N} \ln|z - \Lambda_n| \tag{5.43}$$

is the Coulomb interaction in 2D, associated with the electric field $\mathbf{g} = (\mathrm{Re}g, \mathrm{Im}g)$ represented by the resolvent (5.19):

$$N\mathbf{g}(z = x + \mathrm{i}y) = -\nabla_{x,y} V^{int} = \sum_{n=1}^{N} \left(\frac{x - \mathrm{Re}\Lambda_n}{|z - \Lambda_n|^2}, \frac{y - \mathrm{Im}\Lambda_n}{|z - \Lambda_n|^2} \right). \tag{5.44}$$

For Hermitian matrices, the Dyson gas is a two-dimensional Coulomb gas, experiencing the one-body potential V^g, with the kinematic restriction that the charges move along the real line ($\mathrm{Im}\Lambda_n = 0$).[3]

The main advantage of the Dyson gas picture is that it allows to apply methods of statistical mechanics to calculate distributions and correlations of eigenvalues, giving therefore a physical intuition about the statistical properties of the eigenvalues. In particular, it is clear that the shape of the overall density will strongly depend on the one-body potential V^g, while the correlations in the relative positions of eigenvalues are affected by the interaction V^{int} and are generally insensitive to V^g.

5.3.2 Brownian motion of eigenvalues

Before exploiting further the Dyson gas mapping, let us justify the form of $P(\{\Lambda_n\})$ (5.41) in two ways.

Mathematically, Eq. (5.41) can be obtained from (5.40) by changing the integration variables from the independent matrix elements of A to parameters related to eigenvalues

[3] This kinematic restriction is suppressed for non-Hermitian matrices (see chapter 6).

and eigenvectors of A. The Jacobian of the transformation contains, in particular, a factor $|\mathcal{V}(\{\Lambda_n\})|^\beta$, where

$$\mathcal{V}(\{\Lambda_n\}) = \prod_{n<m} (\Lambda_n - \Lambda_m) \tag{5.45}$$

is a Vandermonde determinant, that is the source of the logarithmic repulsion in H^g. Integrating over the parameters related to the eigenvectors, one obtains Eqs. (5.41) and (5.42) [137].

The distribution (5.41) can also be proved elegantly using physical arguments, in the following way. Interpreting Eq. (5.40) as the stationary solution of a Fokker-Planck equation [137, 162], it is easy to infer the associated Langevin equation that controls the fictitious dynamics, parametrized by the fictitious time τ, of the independent matrix elements $A_\eta(\tau)$[4], as well as the drift and diffusion coefficients of the matrix elements A_η:

$$M_1(A_\eta) = \lim_{\Delta\tau\to 0} \frac{\langle \Delta A_\eta \rangle}{\Delta\tau} = -NV^{g'}(A_\eta), \tag{5.46}$$

$$M_2(A_\eta) = \lim_{\Delta\tau\to 0} \frac{\langle \Delta A_\eta^2 \rangle}{2\Delta\tau} = \frac{1}{2\beta}\left[1 + \delta_{\eta,(m,m)}\right], \tag{5.47}$$

where $\langle ... \rangle$ denotes the ensemble-average over the fictitious Markov processes. This averaging must not be confused with averaging over matrix elements or point positions (4.37). The key point now is that we can calculate, by a second-order perturbative expansion at time τ, how the eigenvalues are modified during $\Delta\tau$:

$$\Delta\Lambda_n = \Delta A_{nn} + \sum_{m\neq n} \sum_{\mu=0}^{\beta-1} \frac{\Delta A_{mn}^{(\mu)2}}{\Lambda_m - \Lambda_n}. \tag{5.48}$$

Averaging (5.48) using Eqs. (5.46) and (5.47), and keeping only $\mathcal{O}(\Delta\tau)$ terms, we find $\langle \Delta\Lambda_n \rangle$ and $\langle \Delta\Lambda_n^2 \rangle$, and the related drift and diffusion coefficients for the eigenvalues :

$$M_1(\Lambda_n) = -NV'(\Lambda_n) + \sum_{m\neq n} \frac{1}{\Lambda_m - \Lambda_n}, \tag{5.49}$$

$$M_2(\Lambda_n) = \frac{1}{\beta}. \tag{5.50}$$

We recognize in the drift coefficient (5.49) the deterministic force driving the point charge located at Λ_n. In particular, we understand in a new way the origin of the electrostatic repulsion (5.43), since in the present context it arises from the second-order perturbative term in Eq. (5.48). Finally, from the coefficients (5.49) and (5.50), it is straightforward to reconstruct the Fokker-Planck equation obeyed by the fictitious time-dependent joint probability density of the eigenvalues, and its stationnary solution is precisely the desired result (5.41).

5.3.3 Mean field approximation

Once the probability distribution $P(\{\Lambda_n\})$ is known, the density of eigenvalues $p(\Lambda)$ can formally be recovered by integrating it $(N-1)$ times. Luckily, we can avoid this

[4] η labels independent elements of A. Alternatively, we can write $A_\eta = A_{mn}^{(\mu)}$, with $\mu = 0, \ldots, \beta - 1$, see Eq. (5.48).

cumbersome calculation by taking advantage of the Dyson gas picture. In a naive mean-field approach, the distribution of charges at equilibrium is found by minimizing the energy H^g (5.42). This is expressed by

$$-\partial_\Lambda V^{int}(\Lambda) = N\partial_\Lambda V^g(\Lambda). \tag{5.51}$$

Furthermore, since for Hermitian matrices $\mathrm{Im}\Lambda_n = 0$, Eqs. (5.43) and (5.44) yield

$$N\,\mathrm{Re}g(\Lambda + \mathrm{i}\epsilon) = \sum_{n=1}^{N} \frac{1}{\Lambda - \Lambda_n} = -\partial_\Lambda V^{int}(\Lambda), \tag{5.52}$$

so that the combination of Eqs. (5.51) and (5.52) allows to relate $\mathrm{Re}g(\Lambda' + \mathrm{i}\epsilon)$ with the one-body potential V^g. Inserting the result into Eq. (5.23), we obtain

$$p(\Lambda) = \frac{1}{\pi^2\sqrt{(\Lambda - a)(b - \Lambda)}}\left[\pi - \mathrm{P}\int_a^b \mathrm{d}\Lambda' \frac{\sqrt{(\Lambda' - a)(b - \Lambda')}}{\Lambda' - \Lambda}\partial_{\Lambda'} V^g(\Lambda')\right]. \tag{5.53}$$

Let us justify this mean-field result in a different way. In the large N limit, we can perform a coarse-graining of the energy functional H^g (5.42):

$$H^g(p) \simeq N^2 \int_{-\infty}^{\infty} \mathrm{d}\Lambda p(\Lambda) V^g(\Lambda) - \frac{N^2}{2}\iint_{-\infty}^{\infty} \mathrm{d}\Lambda \mathrm{d}\Lambda' p(\Lambda) p(\Lambda') \ln|\Lambda - \Lambda'|. \tag{5.54}$$

Rigorously, when changing the integration variables from $\{\Lambda_n\}$ to the density 'field' p in the partition function, a Jacobian appears, which physically takes into account the entropy associated with the 'field' p. We neglect all corresponding sub-leading terms of order $\ln N/N$ [162][5]. The equilibrium of the Dyson gas is given by the extremum of this functional. Note that we also have to take into account the normalization constraint of p, which can be done by introducing a Lagrange multiplier c. We thus find:

$$V^g(\Lambda) - \int_{-\infty}^{\infty} \mathrm{d}\Lambda' p(\Lambda') \ln|\Lambda - \Lambda'| + c = 0. \tag{5.55}$$

Differentiating Eq. (5.55) with respect to Λ we get

$$\mathrm{P}\int_{-\infty}^{\infty} \mathrm{d}\Lambda' \frac{p(\Lambda')}{\Lambda - \Lambda'} = \partial_\Lambda V^g(\Lambda), \tag{5.56}$$

which admits the solution (5.53) for p defined on the compact support $[a, b]$, as expected.

The mean-field approach used to infer the eigenvalue distribution $p(\Lambda)$ from the joint probability distribution $P(\{\Lambda_n\})$ is general and can be applied to any ensemble, provided that $P(\{\Lambda_n\})$ is known. Actually, $P(\{\Lambda_n\})$ can be found for a larger class of matrices than the Wigner-Dyson ensemble (5.40). It is straightforward for any distribution $P(A)$ that is simply expressed in terms of the eigenvalues of A, *e.g.* through $\mathrm{Tr}A$ or $\det A$: $P(\{\Lambda_n\})$ is then obtained by multiplying $P(A)$ by the Vandermonde-type Jacobian $|\mathcal{V}(\{\Lambda_n\})|^\beta$ responsible for the logarithmic repulsion between eigenvalues.

[5] This is justified when the confining potential V^g is 'strong'. In the case of 'weak' confining potential explicit examples of the failure of Eq. (5.54) can be found in [163].

5.3.4 Examples of application

We start by considering the Gaussian ensemble (5.1), that corresponds to $V^g(x) = x^2/4$ in (5.40). Using Eq. (5.53) with $a = -b$ found by the normalization condition $\int_{-b}^{b} \mathrm{d}\Lambda p(\Lambda) = 1$, we readily obtain the celebrated Wigner semicircle law[6] [139]:

$$p(\Lambda) = \frac{1}{2\pi}\left(4 - \Lambda^2\right)^{1/2}. \tag{5.57}$$

It states that for large N and on average, the N eigenvalues lie within a finite interval $[-2, 2]$, sometimes referred to as the 'Wigner sea'. Within this sea, the eigenvalue distribution has a semicircular form.

The second example is the Wishart ensemble defined by Eqs. (5.4) and (5.5). Let us focus on $P(A)$ given by Eq. (5.7) that corresponds to the the case $c = N/M < 1$. As explained above, $P(\{\Lambda_n\})$ follows by adding the Jacobian $|\mathcal{V}(\{\Lambda_n\})|^2$ to (5.7):

$$P(\{\Lambda_n\}) = C''_{N,M} e^{-2H^g(\{\Lambda_n\})}, \tag{5.58}$$

$$H^g(\{\Lambda_n\}) = \frac{1}{2}\sum_{n=1}^{N}\left[N\Lambda_n - (M-N)\ln\Lambda_n\right] - \sum_{n<m}\ln|\Lambda_n - \Lambda_m|. \tag{5.59}$$

This result has the same form as Eqs. (5.41) and (5.42), with the one-body potential

$$V^g(x) = \frac{1}{2}\left[x - \left(\frac{1}{c} - 1\right)\ln x\right], \tag{5.60}$$

which is repulsive in the limit $x \to 0^+$. The linear and logarithmic contributions come from $\mathrm{Tr}A$ and $\det A$ in Eq. (5.7), respectively. Note the difference with H entering in the definition of $A = HH^\dagger$, for which the joint distribution of eigenvalues exhibits harmonic potential due to the term $\mathrm{Tr}HH^\dagger$ in Eq. (5.5). Inserting the potential (5.60) into Eq. (5.53), the eigenvalue density of A takes the form

$$p(\Lambda) = \frac{1}{2\pi\Lambda}\sqrt{(\Lambda_+ - \Lambda)(\Lambda - \Lambda_-)}, \tag{5.61}$$

which is defined on the compact support $[\Lambda_-, \Lambda_+]$ with

$$\Lambda_\pm = \left(\frac{1}{\sqrt{c}} \pm 1\right)^2. \tag{5.62}$$

This result was derived for $c < 1$. It is easy to find the solution for $c > 1$, by noting that, according to its definition (5.19), g is the average of

$$\mathrm{Tr}_{(N)}\frac{1}{z - HH^\dagger} = \mathrm{Tr}_{(M)}\frac{1}{z - H^\dagger H} + \frac{N-M}{z}, \tag{5.63}$$

where we used the cyclic permutation of the trace operator. From Eq. (5.21), it is thus clear that the case $c > 1$ is obtained by adding $N - M$ zero eigenvalues to $p(\Lambda)$. For arbitrary c, the latter has the generic form[7]

$$p(\Lambda) = \left(1 - \frac{1}{c}\right)^+ \delta(\Lambda) + \frac{1}{2\pi\Lambda}\sqrt{(\Lambda_+ - \Lambda)^+(\Lambda - \Lambda_-)^+}, \tag{5.64}$$

[6] Note that if the quadratic V^g is multiplied by an arbitrary constant α, the eigenvalue density is found by a simple rescaling of variables: $p_\alpha(\Lambda) = \sqrt{\alpha}p_{\alpha=1}(\sqrt{\alpha}\Lambda)$.

[7] If (5.5) is modified into $P_\alpha(H) = C_{N,M}e^{-\alpha N \mathrm{Tr}HH^\dagger}$, a rescaling of variables shows that $p_\alpha(\Lambda) = \alpha\, p_{\alpha=1}(\alpha\Lambda)$.

where $x^+ = \max(x, 0)$. The result (5.64) is the famous Marchenko-Pastur law [143, 159].

It would be fruitful to apply the Dyson gas picture to ERMs. This requires to find $P(\{\Lambda_n\})$ in a form similar to Eqs. (5.58) and (5.59). The problem is that, in order to derive $P(\{\Lambda_n\})$ with standard tools of RMT, we need $P(A)$, which is unfortunately unknown for ERMs. However, as we discussed in section 5.1.3, any ERM A can be rewritten as $A = HTH^\dagger$, with entries $H_{i\alpha}$ that approximately behave as i.i.d. Gaussian random variables. The probability distribution of H is then given by Eq. (5.5). Hence, following the original Wishart's idea [138], we expect $P(A)$ to be of the form

$$P(A) = C_{N,M}(T) \det A^{M-N} e^{-N \mathrm{Tr}(H\, T^{-1} H^\dagger)}, \tag{5.65}$$

where the size M of the matrix T can be arbitrary, and in fact it will be infinite for the majority of function $f(\mathbf{r}_i, \mathbf{r}_j)$. In Eq. (5.65), we assume $N < M$ and $C_{N,M}(T)$ is a normalization coefficient that depends on the matrix T. For $T = I_M$, we recover the Wishart case (5.7). This shows that the eigenvalue density of the ERM associated with the simplest matrix T yields already a non-trivial result, the Marchenko-Pastur law (5.64). An explicit example of ERM that obeys this law is given in section 5.7. For arbitrary T, inferring $P(\{\Lambda_n\})$ from Eq. (5.65) is *a priori* not easy, inasmuch as the argument $\mathrm{Tr}(H\, T^{-1} H^\dagger)$ cannot be expressed in terms of the eigenvalues of A. Therefore, integration over the independent parameters related to the eigenvectors of A may be complicated. At the time of writing this thesis, we have not found $P(\{\Lambda_n\})$. We believe, however, that the Dyson gas picture is promising for ERMs, in particular to study more complicated quantities than just the density of eigenvalues. $P(\{\Lambda_n\})$ could be used, for example, to characterize two-point correlations of the eigenvalue density, that play a role in the study of Anderson localization (see section 6.6.3).

We finally mention that the Dyson gas picture is also a powerful tool to study rare events in the distribution of eigenvalues. For instance, considering the Gaussian ensemble, the semicircle law provides only a global information about how the eigenvalues are typically distributed. Unfortunately it does not contain enough information to answer a number of questions about eigenvalues, like, for example: what is the probability that all the eigenvalues are larger than, say, x? Using tools of statistical mechanics, we know that it is equal to $Z(x)/Z(-\infty)$, where $Z(x) = \int_x^\infty \prod_{n=1}^N \mathrm{d}\Lambda_n e^{-\beta H^g(\{\Lambda_n\})} \propto \int \mathcal{D}[p_x] e^{-\beta H^g(p_x)}$ is the restricted partition function of the Dyson gas. $H^g(p_x)$ is given by the coarse-grained functional (5.54), where the unknown density 'field' p_x is such that it minimizes the energy $H^g(p_x)$, and satisfies $p_x(\Lambda) = 0$ for $\Lambda < x$. The field p_x obeys the integral equation (5.56), where the lower bound of the integral is replaced by x. Inverting the latter with Tricomi's theorem, we can find p_x and $Z(x)$. Such an approach was used recently by Majumdar and coworkers to study large deviations of extreme eigenvalues of Gaussian and Wishart matrices, in a series of interesting papers [164–167]. This reveals once again the interest of developing the Dyson gas picture for ERMs, inasmuch as it would allow us to characterize the statistics of rare events for a large variety of disordered systems.

5.4 Field representation

In this section we discuss a field-theoretical representation of the resolvent $g(z)$. The starting point is the expression (5.25), that we rewrite as

$$g(z) = -\frac{2}{N} \partial_z \left\langle \ln \det(z - A)^{-1/2} \right\rangle. \tag{5.66}$$

The determinant $\det(z-A)^{-1/2}$ can be represented as a canonical partition function:

$$\mathcal{Z}(z) = \det(z-A)^{-1/2} = \int \frac{\mathrm{d}\phi_1}{\sqrt{2\pi}} ... \frac{\mathrm{d}\phi_N}{\sqrt{2\pi}} \exp\left[-\frac{1}{2}\Phi^T \left(zI_N - A\right)\Phi\right], \tag{5.67}$$

where Φ^T is the transpose of the vector $\Phi = (\phi_1, ..., \phi_N)$. In this way, we recast the calculation of the resolvent $g(z)$ into a statistical mechanics problem of N interacting particles ϕ_i with a Hamiltonian

$$\mathcal{H}(\Phi, z) = \frac{z}{2}\sum_{i=1}^{N} \phi_i^2 - \frac{1}{2}\sum_{i\neq j=1}^{N} A_{ij}\phi_i\phi_j. \tag{5.68}$$

The corresponding Boltzmann-Gibbs distribution is

$$P(\Phi, z) = \frac{1}{\mathcal{Z}(z)} e^{-\mathcal{H}(\Phi,z)}, \tag{5.69}$$

so that the resolvent (5.66) is proportional to the derivative of the average thermodynamic free energy, $-\ln \mathcal{Z}(z)$:

$$g(z) = -\frac{2}{N}\partial_z \left\langle \ln \mathcal{Z}(z)\right\rangle = -\frac{1}{N}\left\langle \sum_{i=1}^{N} \left\langle \phi_i^2 \right\rangle_z \right\rangle, \tag{5.70}$$

where $\langle ... \rangle_z$ denotes the field-average with respect to $P(\Phi, z)$ defined by Eq. (5.69). In order to compute $\langle \ln \mathcal{Z}(z)\rangle$, we apply the replica method based on a smart use of the identity

$$\ln x = \lim_{n\to 0} \frac{x^n - 1}{n}. \tag{5.71}$$

The idea is to compute the right-hand-side for finite and integer n and then perform the analytic continuation to $n \to 0$.[8] Eq. (5.70) becomes

$$g(z) = -\frac{2}{N}\partial_z \left[\lim_{n\to 0} \frac{1}{n}\left\langle \mathcal{Z}^n(z)\right\rangle\right]. \tag{5.72}$$

The quantity that we now want to evaluate is $\langle \mathcal{Z}^n(z)\rangle$, that contains n copies (replicas) of the original system (5.67):

$$\left\langle \mathcal{Z}^n(z)\right\rangle = \left(\frac{1}{2\pi}\right)^{Nn/2} \int (\mathrm{d}\phi_1^1 ... \mathrm{d}\phi_1^n) ... (\mathrm{d}\phi_N^1 ... \mathrm{d}\phi_N^n) \left\langle \exp\left[-\frac{1}{2}\sum_{\alpha=1}^{n} \Phi^{\alpha T}\left(zI_N - A\right)\Phi^\alpha\right]\right\rangle. \tag{5.73}$$

In Eq. (5.73), the averarge $\langle ... \rangle$ can be performed in different ways, depending on what we know about A. In the standard RMT, $P(A)$ is known and averaging is directly performed over the distribution of A. Without entering into details, let us formulate the two main steps of the calculation of (5.73) in this case. First, we perform two algebraic manipulations: we integrate over the matrix elements (which is possible, in practice, for Gaussian-like distributions), and we introduce auxiliary fields such that integration over replica variables can be carried out. We thus get a new integral form that depends

[8] For some models, the analytic continuation may not be unique, and the replica trick may break down. In a more rigorous treatment, we have to use the supersymmetric approach [168, 169].

only on these new fields. Second, in the $N \to \infty$ limit, we find the relevant values of these fields by making a saddle point approximation. This method was originally applied to the Gaussian ensemble (5.1) in Ref. [170] by Edwards and Jones who rederived the semicircle law (5.57). More recently, it was also applied to Wishart matrices (5.4) (with arbitrary covariance matrix), and the Marchenko-Pastur law (5.64) was recovered [171].

For Hermitian ERMs of the form $f(\mathbf{r}_i, \mathbf{r}_j) = f(\mathbf{r}_i - \mathbf{r}_j)$, the field-theoretical approach was first proposed by Mézard, Parisi and Zee in Ref. [147]. Let us review some details of their approach. For $A_{ij} = f(\mathbf{r}_i - \mathbf{r}_j)$, Eq. (5.73) becomes:

$$\langle \mathcal{Z}^n(z) \rangle \propto \int (\mathrm{d}\phi_1^1 \ldots \mathrm{d}\phi_1^n) \ldots (\mathrm{d}\phi_N^1 \ldots \mathrm{d}\phi_N^n)$$
$$\int \frac{\mathrm{d}^d \mathbf{r}_1}{V} \ldots \frac{\mathrm{d}^d \mathbf{r}_N}{V} \exp\left[-\frac{z}{2} \sum_{\alpha=1}^{n} \sum_{i=1}^{N} (\phi_i^\alpha)^2 + \frac{1}{2} \sum_{\alpha=1}^{n} \sum_{i,j=1}^{N} f(\mathbf{r}_i - \mathbf{r}_j) \phi_i^\alpha \phi_j^\alpha \right]. \quad (5.74)$$

As explained just above, in order to perform the Gaussian integration over the replica fields, we introduce two sets of auxiliary (bosonic) fields ψ^α and $\hat{\psi}^\alpha$, *i.e.* we insert into Eq. (5.74) the relation

$$\int \prod_{\alpha=1}^{n} \mathrm{D}[\psi^\alpha] \, \delta_F \left[\psi^\alpha(\mathbf{r}) - \sum_{i=1}^{N} \phi_i^\alpha \delta(\mathbf{r} - \mathbf{r}_i) \right], \quad (5.75)$$

where δ_F stands for the functional Dirac delta:

$$\delta_F[\psi] = \int \mathrm{D}[\hat{\psi}] \exp\left[\mathrm{i} \int \mathrm{d}^d \mathbf{r} \; \psi(\mathbf{r}) \hat{\psi}(\mathbf{r}) \right]. \quad (5.76)$$

We then integrate out the ϕ variables to obtain a field representation of the partition function

$$\langle \mathcal{Z}^n(z) \rangle = \frac{1}{z^{Nn/2}} \int D[\psi^\alpha, \hat{\psi}^\alpha] A^N e^{\mathcal{S}_0}, \quad (5.77)$$

where

$$A = \int \mathrm{d}^d \mathbf{r} \exp\left[-\frac{1}{2z} \sum_{\alpha=1}^{n} \hat{\psi}^\alpha(\mathbf{r})^2 \right],$$
$$\mathcal{S}_0 = \mathrm{i} \sum_{\alpha=1}^{n} \int \mathrm{d}^d \mathbf{r} \; \psi^\alpha(\mathbf{r}) \hat{\psi}^\alpha(\mathbf{r}) + \frac{1}{2} \sum_{\alpha=1}^{n} \int \mathrm{d}^d \mathbf{r} \mathrm{d}^d \mathbf{r}' \psi^\alpha(\mathbf{r}) f(\mathbf{r} - \mathbf{r}') \psi^\alpha(\mathbf{r}'). \quad (5.78)$$

Finally, integrating out the ψ fields, we get an expression which is a good starting point for different approximations:

$$\langle \mathcal{Z}^n(z) \rangle = \int D[\hat{\psi}^\alpha] e^{\mathcal{S}_1}, \quad (5.79)$$

with

$$\mathcal{S}_1 = N \ln \left[z^{-n/2} \int \mathrm{d}^d \mathbf{r} e^{-\frac{1}{2z} \sum_{\alpha=1}^{n} \hat{\psi}^\alpha(\mathbf{r})^2} \right] + \frac{1}{2} \sum_{\alpha=1}^{n} \int \mathrm{d}^d \mathbf{r} \mathrm{d}^d \mathbf{r}' \hat{\psi}^\alpha(\mathbf{r}) f^{-1}(\mathbf{r} - \mathbf{r}') \hat{\psi}^\alpha(\mathbf{r}'), \quad (5.80)$$

and f^{-1} is the operator inverse of f considered as an integral operator:

$$\int \mathrm{d}^d\mathbf{r}'' f^{-1}(\mathbf{r}-\mathbf{r}'')f(\mathbf{r}''-\mathbf{r}') = \delta(\mathbf{r}-\mathbf{r}'). \tag{5.81}$$

Suppose now that we can expand the logarithmic term in Eq. (5.80). We omit terms independent of ψ and apply the Wick rotation $\hat{\psi} \to i\hat{\psi}$, so that the action $\mathcal{S}_1$ becomes:

$$\mathcal{S}_1 \simeq \rho z^{-n/2} \int \mathrm{d}^d\mathbf{r} \exp\left[\frac{1}{2z}\sum_{\alpha=1}^{n} \hat{\psi}^\alpha(\mathbf{r})^2\right] - \frac{1}{2}\sum_{\alpha=1}^{n} \int \mathrm{d}^d\mathbf{r}\mathrm{d}^d\mathbf{r}' \hat{\psi}^\alpha(r) f^{-1}(\mathbf{r}-\mathbf{r}')\hat{\psi}^\alpha(\mathbf{r}'). \tag{5.82}$$

In the high density limit $\rho = N/V \to \infty$, Mézard *et al.* proposed to expand the exponential term of the action (5.82), at z/ρ fixed. Inserting the result into Eq. (5.79), we obtain:

$$g(z) = \frac{1}{\rho}\int \frac{\mathrm{d}^d\mathbf{k}}{(2\pi)^d}\frac{1}{z-\rho f_0(\mathbf{k})}, \tag{5.83}$$

where

$$f_0(\mathbf{k}) = \int \mathrm{d}^d\mathbf{r} f(\mathbf{r}) e^{\mathrm{i}\mathbf{k}\cdot\mathbf{r}} \tag{5.84}$$

is the Fourier transform of $f(\mathbf{r})$. The corresponding density of eigenvalues (5.21) is

$$p(\Lambda) = \frac{1}{\rho}\int \frac{\mathrm{d}^d\mathbf{k}}{(2\pi)^d}\, \delta\left[\Lambda - \rho f_0(\mathbf{k})\right]. \tag{5.85}$$

Alternatively, this result can actually be derived from the following simple argument. For any ERM A, we can always formally write: $\sum_{j=1}^{N} A_{ij}\Phi_j(\mathbf{k}) = \Lambda_i(\mathbf{k})\Phi_i(\mathbf{k})$ with $\Phi_i(\mathbf{k}) = e^{-\mathrm{i}\mathbf{k}.\mathbf{r}_i}$ and

$$\Lambda_i(\mathbf{k}) = \sum_{j=1}^{N} e^{\mathrm{i}\mathbf{k}\cdot(\mathbf{r}_i-\mathbf{r}_j)} f(\mathbf{r}_i-\mathbf{r}_j). \tag{5.86}$$

Suppose now the density large enough that the phase $\mathrm{i}\mathbf{k}\cdot(\mathbf{r}_i-\mathbf{r}_j)$ does not oscillate too much between neighboring points. This is roughly satisfied for $k \ll \rho^{1/d}$. The sum in Eq. (5.86) can then be approximated by an integral, so that $\Lambda_i(\mathbf{k})$ does not depend anymore on i, becoming an eigenvalue of A, $\Lambda(\mathbf{k}) = \rho f_0(\mathbf{k})$, associated with the eigenvector $(e^{-\mathrm{i}\mathbf{k}\cdot\mathbf{r}_1}, .., e^{-\mathrm{i}\mathbf{k}\cdot\mathbf{r}_N})$. Summing over the different eigenvalues labelled by $\mathbf{k}$, we reconstruct the spectrum (5.85).

In order to obtain an expression for the resolvent $g(z)$ valid beyond the high density regime, Mézard *et al.* [147] looked for the best quadratic action $\mathcal{S}_v$ that approximates the full interacting problem (5.82):

$$\mathcal{S}_v = -\frac{1}{2}\int \mathrm{d}^d\mathbf{r}\mathrm{d}^d\mathbf{r}' \hat{\Psi}^T(\mathbf{r}) K^{-1}(\mathbf{r},\mathbf{r}')\hat{\Psi}(\mathbf{r}'), \tag{5.87}$$

where $\hat{\Psi}^T = (\hat{\psi}^1, ..., \hat{\psi}^n)$. The $n \times n$ matrix $K^{-1}(\mathbf{r},\mathbf{r}')$ is obtained by minimizing the variational free energy $F_v = \langle \mathcal{S}_1 \rangle_v - \ln \mathcal{Z}_v$, where $\mathcal{Z}_v = \int \mathrm{D}[\hat{\Psi}] e^{\mathcal{S}_v}$ and $\langle ... \rangle_v$ is defined with respect to the measure $P_v = e^{\mathcal{S}_v}/\mathcal{Z}_v$. This yields to the following self-consistent

equations for the resolvent $g(z)$ [147] [9]:

$$g(z) = \frac{1}{z - \sigma(z)}, \tag{5.88}$$

$$\sigma(z) = \int \frac{\mathrm{d}^d\mathbf{k}}{(2\pi)^d} \frac{f_0(\mathbf{k})}{1 - \rho f_0(\mathbf{k}) g(z)}. \tag{5.89}$$

This result assumes implicitly that the function $f(\mathbf{r})$ decays fast enough for large r, to recover translational invariance in the limit $V \to \infty$ at fixed density $\rho = N/V$. Consequently, the resolvent $g(z)$ and the density of eigenvalues $p(\Lambda)$ depend only on the density ρ. We shall see in the following that this assumption does not apply to ERMs relevant for wave propagation in random media. In section 5.5 we will derive equations for the resolvent that generalize Eqs. (5.88) and (5.89) to physical problems in which ρ is not the only parameter that controls the shape of $p(\Lambda)$. In addition, our (subjective) belief is that the diagrammatic proof that we propose in section 5.5 is somewhat more transparent than the field method discussed in the present section, inasmuch as it can be entirely interpreted in terms of multiple scattering of waves by an ensemble of point-like scattering centers.

5.5 Diagrammatic approach

5.5.1 From Gaussian and Wishart ensembles to ERMs

Before discussing in details the diagrammatic treatment of Hermitian ERMs, we briefly review the results for Gaussian and Wishart matrices. The starting point of a diagrammatic computation of the resolvent (5.19) is its series expansion (5.27). For Gaussian-like ensembles, the result of averaging can be expressed through pairwise contractions, such as (5.2). The different terms (diagrams) arising from this calculation are conveniently collected in the self-energy $\sigma(z)$ defined by Eq. (5.28). By construction, $\sigma(z)$ is the sum of all irreducible diagrams contained in the expansion of $g(z)$, *i.e.* those that cannot be separated into two independent diagrams linked by the propagator $1/z$. Concerning Gaussian and Wishart ensembles, we do not detail the diagrammatic representation of $\sigma(z)$, because these ensembles can be considered as special cases of ERMs, for which a diagrammatic calculation is given below.

It is easy to show, using the pairwise contractions (5.2) for GUE and (5.3) for GOE, that the self-energy $\sigma(z)$ of the Gaussian ensemble (5.1) is given by

$$\sigma(z) = g(z). \tag{5.90}$$

A detailed proof for GUE[10] can be found, *e.g.*, in Ref. [172]. Inserting (5.90) into Eq. (5.28), we find the resolvent:

$$g(z) = \frac{1}{2}\left(z - \sqrt{z^2 - 4}\right), \tag{5.91}$$

which leads, via Eq. (5.21), to the semicircle law (5.57).

[9] Eqs. (5.88) and (5.89) do not appear explicitly in [147]. It is however straightforward to obtain them from the results presented in [147].

[10] The GOE case is slightly more involved since (5.3) generates two types of diagrams rather than one in (5.2). However, in the large N limit, the second term of (5.3) does not contribute to $\sigma(z)$ because it gives rise to non-planar diagrams only (for the definition of these diagrams, see section 5.5.3).

The self-energy $\sigma(z)$ of Wishart matrices (5.4) is obtained in a similar way. The main difference with the Gaussian case is that we now have to distinguish, when manipulating pairwise contractions (5.6), indices $i = 1, \ldots, N$ and $\alpha = 1, \ldots, M$. For $c = N/M < 1$, the self-energy is [172]:

$$\sigma(z) = \frac{1}{c}\frac{1}{1 - g(z)}. \tag{5.92}$$

Eqs. (5.28) and (5.92) lead to a quadratic equation for $g(z)$, that has the normalizable solution

$$g(z) = \frac{1}{2z}\left[z + 1 - \frac{1}{c} - \sqrt{(z - \Lambda_+)(z - \Lambda_-)}\right], \tag{5.93}$$

with $\Lambda_\pm$ given by Eq. (5.62). From Eq. (5.21), we recover the Marchenko-Pastur function (5.61).

Historically, neither the Wigner semicircle law (5.57) nor the Marchenko-Pastur law (5.64) were derived by calculating diagrammatically the self-energy $\sigma(z)$. Wigner's original proof [173] is based on an explicit calculation of the moments $\langle \Lambda^n \rangle$ that appear in the series expansion (5.27) of the resolvent. This is somewhat surprising inasmuch as the counting procedure required to evaluate the moments is more complicated than a direct evaluation of the self-energy (5.90). Odd moments of the symmetric semicircle law are zero, and even moments are the Catalan numbers:

$$\langle \Lambda^{2p} \rangle = \frac{(2p)!}{p!(p+1)!}. \tag{5.94}$$

A calculation of the Marchenko-Pastur law from its moments can also be performed [174]. The procedure is quite tricky, as we can imagine by looking at the result for the moments:

$$\langle \Lambda^n \rangle = \frac{1}{c^n}\sum_{k=0}^{n} \frac{n!(n-1)!}{(n+1-k)!(n-k)!\,[(k-1)!]^2}\frac{c^{k-1}}{k}. \tag{5.95}$$

The first six moments read explicitly :

$$\begin{array}{l|l} \langle \Lambda \rangle = 1/c & \langle \Lambda^4 \rangle = (1 + 6c + 6c^2 + c^3)/c^4 \\ \langle \Lambda^2 \rangle = (1 + c)/c^2 & \langle \Lambda^5 \rangle = (1 + 10c + 20c^2 + 10c^3 + c^4)/c^5 \\ \langle \Lambda^3 \rangle = (1 + 3c + c^2)/c^3 & \langle \Lambda^6 \rangle = (1 + 15c + 50c^2 + 50c^3 + 15c^4 + c^5)/c^6. \end{array}$$

Undoubtedly, if we are interested in the full distribution $p(\Lambda)$ the counting procedure for evaluating the moments is less appropriate than a diagrammatic self-consistent calculation of the self-energy. The same remark holds for ERMs, as we will see shortly.

In the following analysis dedicated to Hermitian ERMs, we are interested in the calculation of the following operator

$$\hat{O}(z) = \left\langle \sum_{i=1}^{N}\sum_{j=1}^{N}\left[\frac{1}{z - A}\right]_{ij} |\mathbf{r}_i\rangle\langle\mathbf{r}_j| \right\rangle, \tag{5.96}$$

where A is an ERM. For later convenience, we also define

$$\begin{aligned} g_{\mathbf{k}}(z) &= \frac{1}{\rho}\langle \mathbf{k}|\hat{O}(z)|\mathbf{k}\rangle, \\ &= \frac{1}{N}\left\langle \sum_{i=1}^{N}\sum_{j=1}^{N} e^{\mathrm{i}\mathbf{k}\cdot(\mathbf{r}_i - \mathbf{r}_j)}\left[\frac{1}{z - A}\right]_{i,j} \right\rangle. \end{aligned} \tag{5.97}$$

Since in the limit $k \to \infty$ only terms $i = j$ contribute significantly in Eq. (5.97), $g_{\mathbf{k}}(z)$ is related to the resolvent (5.19) by

$$g(z) = \lim_{k\to\infty} g_{\mathbf{k}}(z). \tag{5.98}$$

Similarly to $g(z)$, $g_{\mathbf{k}}(z)$ admits the following series expansion in its holomorphic domain:

$$g_{\mathbf{k}}(z) = \sum_{n=0}^{\infty} \frac{\langle \Lambda^n \rangle_{\mathbf{k}}}{z^{n+1}}, \tag{5.99}$$

$$\langle \Lambda^n \rangle_{\mathbf{k}} = \frac{1}{N} \left\langle \sum_{i=1}^{N} \sum_{j=1}^{N} e^{\mathrm{i}\mathbf{k}\cdot(\mathbf{r}_i - \mathbf{r}_j)} \left[A^n\right]_{ij} \right\rangle. \tag{5.100}$$

The rest of this section is organized as follows. First, in subsection 5.5.2, we briefly present a perturbative calculation, in the limit $\rho \to \infty$, of the moments $\langle \Lambda^n \rangle_{\mathbf{k}}$, that was developed in the pioneering works of Grigera, Parisi and coworkers [148–151, 153]. Unfortunately, the combinatory procedure proposed by the authors becomes involved when high orders $1/\rho^n$ $(n > 2)$ in the expansion of $\langle \Lambda^n \rangle_{\mathbf{k}}$ have to be considered, as it is the case for regimes of disorder relevant for wave propagation in disordered media. For this reason, we have developed our own diagrammatic approach, in a spirit similar to the self-consistent calculation of the self-energy for Gaussian and Wishart ensembles. This is the subject of subsection 5.5.3.

5.5.2 ERM: high density expansion

The aim of this section is to present a perturbative calculation of the resolvent (5.97) by a direct evaluation of the moments (5.100) for ERMs of the form $A_{ij} = f(\mathbf{r}_i, \mathbf{r}_j) = f(\mathbf{r}_i - \mathbf{r}_j)$. This method is directly inspired by Refs. [149, 153]. Moments (5.100),

$$\langle \Lambda^n \rangle_{\mathbf{k}} = \frac{1}{N} \left\langle \sum_{i_1=1}^{N} \cdots \sum_{i_{n+1}=1}^{N} e^{\mathrm{i}\mathbf{k}\cdot(\mathbf{r}_{i_1} - \mathbf{r}_{i_{n+1}})} A_{i_1,i_2} A_{i_2,i_3} \ldots A_{i_{n-1},i_n} A_{i_n,i_{n+1}} \right\rangle, \tag{5.101}$$

can be expressed as sums of n terms characterized by the number of repeating indices. The term with all indices different is

$$\langle \Lambda^n \rangle_{\mathbf{k}}^{(n)} = N^n \int_V \frac{\mathrm{d}^d \mathbf{r}_1}{V} \ldots \frac{\mathrm{d}^d \mathbf{r}_{n+1}}{V} e^{\mathrm{i}\mathbf{k}\cdot(\mathbf{r}_{i_1} - \mathbf{r}_{i_{n+1}})} f(\mathbf{r}_1 - \mathbf{r}_2) \ldots f(\mathbf{r}_n - \mathbf{r}_{n+1}) f(\mathbf{r}_{n+1} - \mathbf{r}_1). \tag{5.102}$$

Assuming translational invariance, we can eliminate one integral in Eq. (5.102), showing that $\langle \Lambda^n \rangle_{\mathbf{k}}^{(n)} \sim \rho^n$. When two indices are equal in Eq. (5.101), we have a missing N factor from the sum and a missing $1/V$ factor from the average, leading to $\langle \Lambda^n \rangle_{\mathbf{k}}^{(n-1)} \sim \rho^{n-1}$. Therefore, $\langle \Lambda^n \rangle_{\mathbf{k}}$ has the following density expansion:

$$\langle \Lambda^n \rangle_{\mathbf{k}} = \sum_{i=1}^{n} \langle \Lambda^n \rangle_{\mathbf{k}}^{(i)} \quad \text{with} \quad \langle \Lambda^n \rangle_{\mathbf{k}}^{(i)} \sim \rho^i. \tag{5.103}$$

Let us compute explicitly the two first leading terms in the high density regime, $\langle \Lambda^n \rangle_{\mathbf{k}}^{(n)}$ and $\langle \Lambda^n \rangle_{\mathbf{k}}^{(n-1)}$. We replace all terms $f(\mathbf{r}_i - \mathbf{r}_j)$ in Eq. (5.102) by $\int \mathrm{d}^d\mathbf{k} f_0(\mathbf{k}) e^{-\mathrm{i}\mathbf{k}\cdot(\mathbf{r}_i - \mathbf{r}_j)}/(2\pi)^d$,

and perform the n spatial integrations. For points $\mathbf{r}_i$ in a box ($V = L^d$), $\langle \Lambda^n \rangle_{\mathbf{k}}^{(n)}$ becomes

$$\langle \Lambda^n \rangle_{\mathbf{k}}^{(n)} = \frac{N^n}{(2\pi)^{nd}} \int \mathrm{d}^d\mathbf{k}_1 \ldots \mathrm{d}^d\mathbf{k}_n \operatorname{sinc}\left[\frac{\mathbf{k}-\mathbf{k}_1}{2/L}\right] \ldots \\ \operatorname{sinc}\left[\frac{\mathbf{k}_{n-1}-\mathbf{k}_n}{2/L}\right] \operatorname{sinc}\left[\frac{\mathbf{k}_n-\mathbf{k}}{2/L}\right] f_0(\mathbf{k}_1)\ldots f_0(\mathbf{k}_n), \tag{5.104}$$

where $\operatorname{sinc}[\mathbf{k}] = \operatorname{sinc}[k^x]\operatorname{sinc}[k^y]\operatorname{sinc}[k^z]$ (for $d = 3$). Assuming $f_0(\mathbf{k})$ centered around, say, $\mathbf{k}_a$, with a width Δk_a such that $k_a L, \Delta k_a L \ll 1$, we use $\operatorname{sinc}[(\mathbf{k}_i - \mathbf{k}_j)L/2] \simeq (2\pi)^d \delta(\mathbf{k}_i - \mathbf{k}_j)/L^d$ and obtain

$$\langle \Lambda^n \rangle_{\mathbf{k}}^{(n)} = [\rho f_0(\mathbf{k})]^n . \tag{5.105}$$

Inserting this into Eq. (5.99), we obtain the crudest approximation that we can imagine for the resolvent, $g_{\mathbf{k}}(z) \simeq g_{\mathbf{k}}^0(z)$, where

$$g_{\mathbf{k}}^0(z) = \frac{1}{z - \rho f_0(\mathbf{k})} \tag{5.106}$$

is the 'bare' propagator that does not capture any fluctuations of A (indeed, it means that $g(z)$ is approximated by $g^0(z) = \lim_{k\to\infty} g_{\mathbf{k}}^0(z) = 1/z$). We then calculate the next contribution $\langle \Lambda^n \rangle_{\mathbf{k}}^{(n-1)}$, which contains two equal indices. There are two differences with the calculation of $\langle \Lambda^n \rangle_{\mathbf{k}}^{(n)}$. First, we can choose the two positions of the equal indices. Second, for given positions such that we have $\beta + 2$ functions f between the two equal indices[11], we replace $\beta + 1$ sinc terms by δ-functions. The result reads

$$\langle \Lambda^n \rangle_{\mathbf{k}}^{(n-1)} = \frac{1}{\rho} \sum_{\alpha+\beta+\gamma=n-2} [\rho f_0(\mathbf{k})]^\alpha \left[\int \frac{\mathrm{d}^d\mathbf{q}}{(2\pi)^d} [\rho f_0(\mathbf{q})]^{(\beta+2)}\right] [\rho f_0(\mathbf{k})]^\gamma . \tag{5.107}$$

Summing over n to get the corresponding resolvent (5.99), $g_{\mathbf{k}}(z) \simeq g_{\mathbf{k}}^1(z)$, suppresses the restriction imposed on α, β, γ :

$$g_{\mathbf{k}}^1(z) = \left[\frac{1}{z - \rho f_0(\mathbf{k})}\right] \left[\frac{1}{\rho} \int \frac{\mathrm{d}^d\mathbf{q}}{(2\pi)^d} \frac{1}{z - \rho f_0(\mathbf{q})} [\rho f_0(\mathbf{q})]^2\right] \left[\frac{1}{z - \rho f_0(\mathbf{k})}\right], \tag{5.108}$$

which is of the form $g_{\mathbf{k}}^0(z)\sigma^1(z)g_{\mathbf{k}}^0(z)$. The first irreducible diagram contained in the self-energy $\sigma_{\mathbf{k}}(z) = 1/g_{\mathbf{k}}^0(z) - 1/g_{\mathbf{k}}(z)$ is therefore independent of $\mathbf{k}$ and reads

$$\sigma^1(z) = \frac{1}{\rho} \int \frac{\mathrm{d}^d\mathbf{q}}{(2\pi)^d} [\rho f_0(\mathbf{q})]^2 g_{\mathbf{q}}^0(z). \tag{5.109}$$

If now we restrict the density expansion of the self-energy to the first order (5.109), $\sigma_{\mathbf{k}}(z) \simeq \sigma^1(z)$, the resolvent (5.97) is given by

$$g_{\mathbf{k}}(z) = \frac{1}{z - \rho f_0(\mathbf{k}) - \sigma^1(z)}, \tag{5.110}$$

[11] $\beta \in [0, n-2]$ is an integer that should not be confused with the symmetry index defined in section 5.1.1.

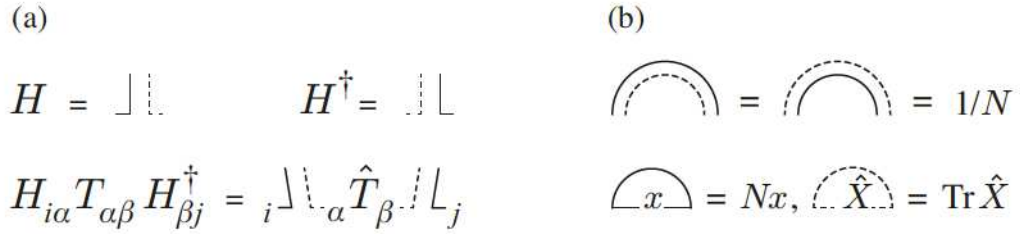

Figure 5.1: (a) Diagrammatic representations of the matrices H, $H^\dagger$, and $A = HTH^\dagger$. Full and dashed lines propagate in the bases $\{\mathbf{r}_i\}$ and $\{\psi_\alpha\}$, respectively, defined in section 5.1.3; $\hat{T} = \rho\hat{A}$. (b) Diagrammatic notation for pairwise contractions (5.17) and loop diagrams for any scalar x in the basis $\{\mathbf{r}_i\}$, and for any operator $\hat{X}$ in an arbitrary basis $\{\psi_\alpha\}$.

and, from Eqs. (5.21) and (5.98), the density of eigenvalues takes the form

$$p(\Lambda) = \frac{\mathrm{Im}\sigma^1(\Lambda + \mathrm{i}\epsilon)}{[\Lambda - \mathrm{Re}\sigma^1(\Lambda + \mathrm{i}\epsilon)]^2 + [\mathrm{Im}\sigma^1(\Lambda + \mathrm{i}\epsilon)]^2}. \tag{5.111}$$

For $|\Lambda| \gg |\mathrm{Re}\sigma^1(\Lambda + \mathrm{i}\epsilon)|, |\mathrm{Im}\sigma^1(\Lambda + \mathrm{i}\epsilon)|$, $p(\Lambda) \simeq \mathrm{Im}\sigma^1(\Lambda + \mathrm{i}\epsilon)/\Lambda^2$. Using the explicit form (5.109) of σ_1, we recover the result (5.85).[12] This indicates that the more diagrams we take into account into $\sigma_{\mathbf{k}}(z)$, the more accurate is $p(\Lambda)$ at small $|\Lambda|$. Note also that a simple way to improve the result (5.109) is to replace in this equation the bare propagator $g^0_{\mathbf{q}}(z)$ by $g_{\mathbf{q}}(z)$. This improved form of the self-energy was used in Ref. [148] to characterize the vibrational spectrum of topologically disordered systems.

Applying essentially the same procedure as for the calculation of $\sigma^1(z)$, it is also possible to compute higher contributions $\sigma^i_{\mathbf{k}}$ $(i > 1)$ of order $1/\rho^i$ to the self-energy $\sigma_{\mathbf{k}}(z) = \sigma^1(z) + \sigma^2_{\mathbf{k}}(z) + \ldots$, but the combinatorial rules presented in the very recent literature [152, 153] seem quite involved. We present in the next subsection an efficient diagrammatic representation of ERMs based on the identity (5.9), that has the advantage to apply at any density ρ, and does not assume implicitly that ρ is the only relevant parameter, as it is the case in the expansion (5.103).

5.5.3 ERM: self-consistent equations

The purpose of this section is to derive self-consistent equations for the operator (5.96), using the representation $A = HTH^\dagger$ for ERM $A_{ij} = f(\mathbf{r}_i, \mathbf{r}_j) = \langle \mathbf{r}_i|\hat{A}|\mathbf{r}_j\rangle$. We recall that the matrix H is random but independent of the function f, whereas the matrix T depends on f but is not random (see section 5.1.3).

We start by expanding the resolvent (5.19) in series in $1/z$:

$$g(z) = \frac{1}{N}\left\langle \mathrm{Tr}\left[\frac{1}{z} + \frac{1}{z}A\frac{1}{z} + \frac{1}{z}A\frac{1}{z}A\frac{1}{z} + \ldots\right]\right\rangle, \tag{5.112}$$

where averaging $\langle\ldots\rangle$ is performed over the ensemble of matrices H. As explained in section 5.1.3, we assume that H has i.i.d. complex entries distributed according to the

[12] Another way to recover Eq. (5.85) is to compute the series (5.27), with $\langle\Lambda^n\rangle \simeq \langle\Lambda^n\rangle^{(n)}$ calculated with the same procedure as for $\langle\Lambda^n\rangle^{(n)}_{\mathbf{k}}$.

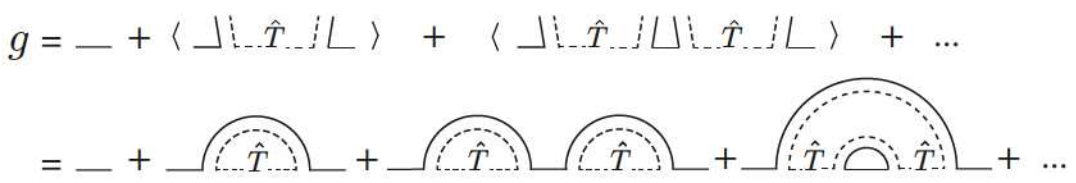

Figure 5.2: Diagrammatic expansion of the resolvent $g(z)$. A horizontal straight line reprepresents the propagator $1/z$.

Gaussian law (5.5). Using the properties of Gaussian random variables (such as the Wick theorem), the result of averaging in Eq. (5.112) can be expressed through pairwise contractions (5.17). To evaluate efficiently the weight of different terms that arise in the calculation, it is convenient to introduce diagrammatic notations. The matrices H, $H^\dagger$, and A will be represented as shown in Fig. 5.1(a).

Each contraction (5.17) brings a factor $1/N$, and each loop corresponding to taking the trace of a matrix brings a factor N, see Fig. 5.1(b). In the limit $N \to \infty$, only the diagrams that contain as many loops as contractions will survive. These diagrams are those where full and dashed lines do not cross. Therefore, the leading order expansion of the resolvent (5.112) involves only diagrams which are planar and look like rainbows, see Fig. 5.2 where we show the beginning of the expansion of $g(z)$. Note that the prefactor $1/N$ of Eq. (5.112) does not appear in Fig. 5.2 because it is compensated by the external trace. An example of a non-planar diagram is represented in Fig. 5.3. It vanishes in the limit $N \to \infty$.

The self-energy $\sigma(z)$ is the sum of all one-particle irreducible diagrams contained in $zg(z)z$. The first dominant terms that appear in the expansion of $\sigma(z)$ are represented in Fig. 5.4. Under a pairwise contraction, we recognize $g(z)$ depicted in Fig. 5.2. After summation of all planar rainbow diagrams in the expansion of Fig. 5.4 and application of 'Feynman' rules defined in Fig. 5.1(b), the self-energy becomes

$$\sigma(z) = \frac{1}{N}\mathrm{Tr}\left[\frac{\hat{T}}{1-g(z)\hat{T}}\right] \tag{5.113}$$

$$= \frac{\mathrm{Tr}\hat{T}}{N} + \frac{g(z)}{N}\mathrm{Tr}\frac{\hat{T}^2}{1-g(z)\hat{T}}. \tag{5.114}$$

where $\hat{T} = \rho\hat{A}$, and Tr denotes the trace of an operator. Inserting Eq. (5.113) into

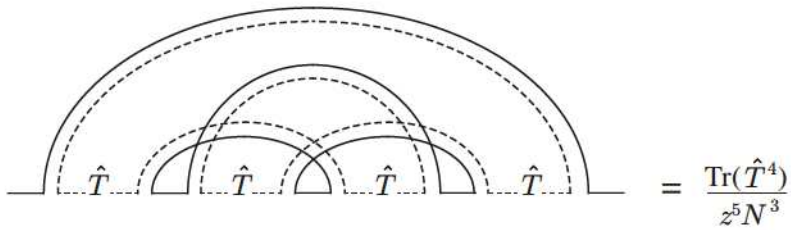

Figure 5.3: A typical non-planar diagram appearing in the expansion of the resolvent $g(z)$. Its value follows after application of 'Feynman' rules defined in Fig. 5.1(b). It does not survive in the limit $N \to \infty$.

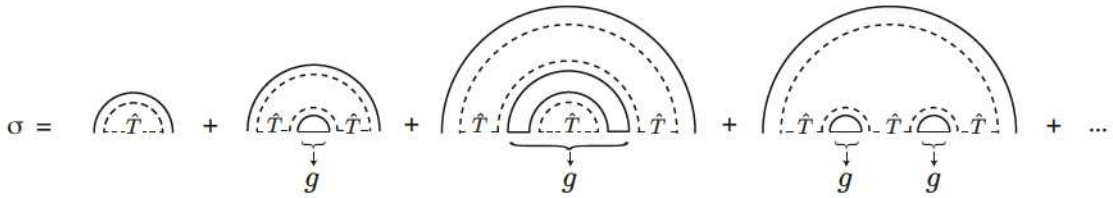

Figure 5.4: Diagrammatic expansion of the self-energy $\sigma(z)$. Braces with arrows denote parts of diagrams that are the beginning of the diagrammatic expansion of the resolvent $g(z)$.

Eq. (5.28), we obtain:

$$z = \frac{1}{g(z)} + \frac{1}{N}\mathrm{Tr}\left[\frac{\hat{T}}{1-g(z)\hat{T}}\right], \tag{5.115}$$

that allows one to solve for $g(z)$ and $p(\Lambda)$. Noting that[13]

$$\mathrm{Tr}\hat{T} = \rho\mathrm{Tr}\hat{A} = \langle \mathrm{Tr}_N A\rangle = N\langle\Lambda\rangle, \tag{5.116}$$

we conclude that $\mathrm{Tr}\hat{T}/N$ in Eq. (5.114) leads to a shift in the distribution of eigenvalues $p(\Lambda)$.

Before commenting on the result (5.113), let us see how the operator (5.96) can be expressed through the solution $g(z)$ and $\hat{T}$. In the basis $\{\psi_\alpha\}$, (5.96) reads

$$O_{\alpha\beta} = \langle\psi_\alpha|\hat{O}|\psi_\beta\rangle = \rho\sum_{i=1}^{N}\sum_{j=1}^{N} H^\dagger_{\alpha i}\left[\frac{1}{z} + \frac{1}{z}A\frac{1}{z} + \frac{1}{z}A\frac{1}{z}A\frac{1}{z} + \dots\right]_{ij} H_{j\beta}, \tag{5.117}$$

where we used the definition (5.10) of the matrix H. In Fig. 5.5, we represent the beginning of the expansion of $O_{\alpha\beta}/\rho$ with the diagrammatic notations of Fig. 5.1(a). Note that all diagrams in Fig. 5.5 are irreducible. As it was the case for $\sigma(z)$, we recognize the expansion of $g(z)$ under pairwise contractions. After summation of planar diagrams, the operator $\hat{O}(z)$ is finally given by:

$$\hat{O}(z) = \rho\frac{g(z)}{1-g(z)\hat{T}} \tag{5.118}$$

$$= \rho\frac{1}{z-\hat{T}-\sigma(z)}. \tag{5.119}$$

Equations (5.115) and (5.118) were derived for Hermitian ERMs. They also apply for non-Hermitian ERMs as long as z belongs to the holomorphic (or analytic) domain of $g(z)$ and $\hat{O}(z)$. In section 4.4, the result (5.118) is applied to the scalar Green's matrix (2.80). In that case, $\hat{O}(z)$ is proportional to the average $\mathcal{T}^f$-operator of the scattering problem (4.12), see Eqs. (4.50) and (4.68).

The solution (5.113) admits two simple limits. First, if the operator $\hat{T}$ is identity, *i.e.* if $T = I_M$ (M is the number of functions in the basis $\{\psi_\alpha\}$), then we recover the solution (5.92), that yields to the Marchenko-Pastur law (5.64). Second, without loss

[13] From here on, we denote by Tr_N the trace of a $N\times N$ matrix when confusion is possible with the trace of an operator.

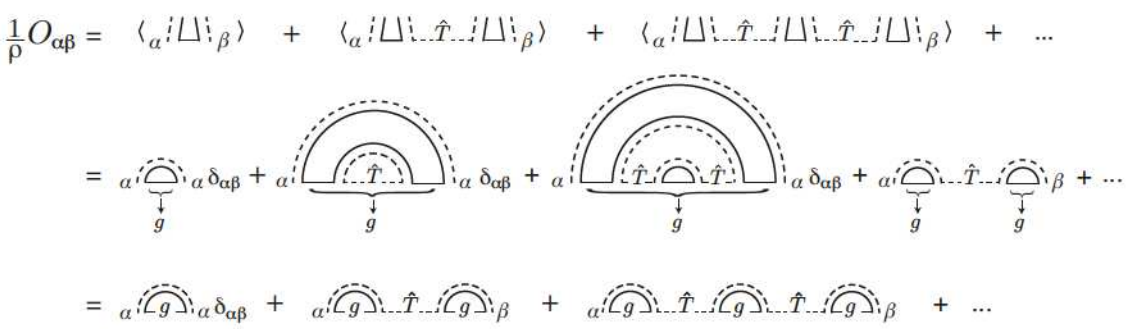

Figure 5.5: Diagrammatic expansion of $O_{\alpha\beta}/\rho$. Braces with arrows denote parts of diagrams that are the beginning of the expansion depicted in Fig. 5.2.

of generality, let us assume that the diagonal elements of the matrix A are all equal, $A_{ii} = \langle\Lambda\rangle$. At low density $\rho \to 0$, an approximation of the self-energy (5.113) can be obtained by neglecting the term $g(z)\hat{T}$ in the denominator[14]:

$$\sigma(z) \simeq \frac{\mathrm{Tr}(\hat{T})}{N} + \frac{\mathrm{Tr}(\hat{T}^2)}{N} g(z) = \langle\Lambda\rangle + \mathrm{Var}\Lambda\, g(z). \tag{5.120}$$

The last equality of Eq. (5.120) follows from

$$\mathrm{Tr}(\hat{T}^2) = \rho^2 \iint_V \mathrm{d}^d\mathbf{r}\, \mathrm{d}^d\mathbf{r}' \left|f(\mathbf{r},\mathbf{r}')\right|^2 = \langle \mathrm{Tr}_N(A^2)\rangle - \frac{\langle \mathrm{Tr}_N(A)\rangle^2}{N} = N\mathrm{Var}\Lambda. \tag{5.121}$$

The implication of Eq. (5.120) is that the eigenvalue density of any Hermitian ERM $A_{ij} = f(\mathbf{r}_i, \mathbf{r}_j)$ is identical, in the low density regime, to the one of a Gaussian matrix[15]. It obeys the Wigner semicircle law

$$p(\Lambda) = \frac{1}{2\pi\mathrm{Var}\Lambda}\sqrt{4\mathrm{Var}\Lambda - (\Lambda - \langle\Lambda\rangle)^2}, \tag{5.122}$$

with the variance $\mathrm{Var}\Lambda$ given by Eq. (5.121).

Finally, let us show how the various approximations found in the previous sections, for $g(z)$, $\sigma(z)$, and $g_{\mathbf{k}}(z)$ associated with ERMs $A_{ij} = f(\mathbf{r}_i - \mathbf{r}_j)$, can be recovered from Eqs. (5.113) and (5.118). We need to assume that

$$f(\mathbf{k},\mathbf{k}') = \langle\mathbf{k}|\hat{A}|\mathbf{k}'\rangle = \frac{1}{V}\iint_V \mathrm{d}^d\mathbf{r}\, \mathrm{d}^d\mathbf{r}' e^{-\mathrm{i}(\mathbf{k}\cdot\mathbf{r} - \mathbf{k}'\cdot\mathbf{r}')} f(\mathbf{r}-\mathbf{r}') \tag{5.123}$$

is diagonal, $f(\mathbf{k},\mathbf{k}') \simeq \langle\mathbf{k}|\hat{A}|\mathbf{k}\rangle\delta_{\mathbf{k}\mathbf{k}'} \equiv f(\mathbf{k})\delta_{\mathbf{k}\mathbf{k}'}$, which is not exact in a finite volume V. In the momentum representation, Eqs. (5.113) and (5.119) read now

$$\sigma(z) \simeq \int \frac{\mathrm{d}^d\mathbf{k}}{(2\pi)^d} \frac{f(\mathbf{k})}{1 - \rho f(\mathbf{k}) g(z)}, \tag{5.124}$$

$$\langle\mathbf{k}|\hat{O}(z)|\mathbf{k}\rangle = g_{\mathbf{k}}(z) \simeq \frac{1}{z - \rho f(\mathbf{k}) - \sigma(z)}, \tag{5.125}$$

[14]For ERMs such as $\mathrm{Re}G(\omega_0)$ or $\mathrm{Im}G(\omega_0)$, it corresponds to the regime $\rho\lambda_0^3 \ll 1$. Rigorously, this condition is necessary but not entirely sufficient to justify the approximation (5.120): see, for example, the study of $\mathrm{Re}G(\omega_0)$ in section 5.8.

[15]Some 'pathological' ERMs may not follow this prediction. Actually, an implicit assumption of our proof is that the number m of non-zero eigenvalues of the operator $\hat{T}$ is large, see section 5.6.3. An example of 'pathological' ERM is $A_{ij} = \cos k_0|\mathbf{r}_i - \mathbf{r}_j|$, for which $m = 2$.

where $f(\mathbf{k}) = \langle \mathbf{k}|\hat{A}|\mathbf{k}\rangle$ can be further approximated by $f_0(\mathbf{k})$ defined in Eq. (5.84). Hence, Eq. (5.124) becomes identical to Eq. (5.89). If the integrand of Eq. (5.124) is expanded in series in ρ, Eq. (5.125) becomes consistent with Eqs. (5.109) and (5.110). This means that the approximate self-energy (5.109) corresponds to a truncation of the expansion depicted in Fig. 5.4 after the second diagram.

5.5.4 Solving Eq. (5.115) in practice

The solution of Eq. (5.115) for a given matrix A can be greatly facilitated by a suitable choice of the basis in which the trace appearing in this equation is expressed. In addition to $\{\mathbf{r}\}$ and $\{\mathbf{k}\}$, a basis of eigenvectors $|\mathcal{R}_\alpha\rangle$ of $\hat{T}$ can be quite convenient. The eigenvector $|\mathcal{R}_\alpha\rangle$ obeys

$$\langle \mathbf{r}|\hat{T}|\mathcal{R}_\alpha\rangle = \rho \int_V \mathrm{d}^d\mathbf{r}' f(\mathbf{r},\mathbf{r}')\mathcal{R}_\alpha(\mathbf{r}') = \mu_\alpha \mathcal{R}_\alpha(\mathbf{r}), \tag{5.126}$$

where μ_α is the eigenvalue corresponding to the eigenvector $|\mathcal{R}_\alpha\rangle$. In this basis, Eq. (5.115) becomes

$$z = \frac{1}{g(z)} + \frac{1}{N}\sum_\alpha \frac{\mu_\alpha}{1-g(z)\mu_\alpha}. \tag{5.127}$$

For matrices $\mathrm{Im}G(\omega_0)$ and $\mathrm{Re}G(\omega_0)$, with points $\mathbf{r}_i$ distributed in a sphere, Eqs. (5.126) and (5.127) can be solved exactly, see sections 5.7 and 5.8.

In the following, we will be particularly interested in ERMs $A_{ij} = f(|\mathbf{r}_i - \mathbf{r}_j|)$ with points $\mathbf{r}_i$ randomly distributed inside a three-dimensionnal space, either a cube of side L, or a sphere of radius R. To evaluate integrals of type (5.121), we will make use of the following auxiliary result:

$$\iint_V \frac{\mathrm{d}^3\mathbf{r}}{V}\frac{\mathrm{d}^3\mathbf{r}'}{V} H(|\mathbf{r}-\mathbf{r}'|) = \begin{cases} \iiint_{-\infty}^{\infty} \mathrm{d}x\mathrm{d}y\mathrm{d}z H\left(L\sqrt{x^2+y^2+z^2}\right) w(x,y,z) & \text{(cube)} \\ 24\int_0^1 \mathrm{d}x H(2Rx)s(x)x^2 & \text{(sphere)} \end{cases} \tag{5.128}$$

where H is an arbitrary function, and

$$w(x,y,z) = (1-|x|)^+(1-|y|)^+(1-|z|)^+, \tag{5.129}$$

$$s(x) = 1 - \frac{3x}{2} + \frac{x^3}{2}, \tag{5.130}$$

with $x^+ = \max(x,0)$. To derive Eq. (5.128) for a sphere, we define new variables $\mathbf{x} = (\mathbf{r}-\mathbf{r}')/2R$ and $\mathbf{y} = (\mathbf{r}+\mathbf{r}')/2R$. The conditions $r \le R, r' \le R$ become $x^2+y^2+2xyt \le 1$, with $0 \le t \le 1$, so that

$$\iint_{V(R)} \frac{\mathrm{d}^3\mathbf{r}}{V}\frac{\mathrm{d}^3\mathbf{r}'}{V}(...) = \frac{18}{\pi}\int_{V(1)} \mathrm{d}^3\mathbf{x}\int_0^1 \mathrm{d}t \int_0^{y_M(t,x)} \mathrm{d}y\, y^2(...), \tag{5.131}$$

where $V(R) = 4\pi R^3/3$ and $y_M(t,x) = \sqrt{1+(t^2-1)x^2} - tx$. Evaluation of all integrals except one in Eq. (5.131) leads to Eq. (5.128). For points distributed in a cube, the proof of Eq. (5.128) is straightforward. Note that $w(x,y,z)$ is non-zero only within a cube of side 2 centered at the origin.

For example, the variance $\mathrm{Var}\Lambda$ of $p(\Lambda)$, given by Eq. (5.121), reads now

$$\mathrm{Var}\Lambda = \begin{cases} N \iiint_{-\infty}^{\infty} \mathrm{d}x\mathrm{d}y\mathrm{d}z \left| f\left(L\sqrt{x^2+y^2+z^2}\right)\right|^2 w(x,y,z) & \text{(cube)} \\ \\ 24N \int_0^1 \mathrm{d}x |f(2Rx)|^2 s(x) x^2 & \text{(sphere)} \end{cases} . \tag{5.132}$$

In order to derive Eq. (5.115), we assumed that the matrix H, entering in the representation $A = HTH^\dagger$, has i.i.d. complex Gaussian entries. We investigate the role of the Gaussian hypothesis in the next section, thanks to the powerful mathematical arsenal of the so-called free random variable theory.

5.6 Free probability theory

5.6.1 Theoretical framework

The term 'free probability theory' designates a discipline founded by Voiculescu in the 1980's [175, 176] in order to solve the following problem: can we say anything about the spectral properties of the sum of of two matrices, $X_1 + X_2$, when the spectral properties of the summands, X_1 and X_2, are known? Unless the two matrices commute, knowing their eigenvalues is, in general, not enough to find the eigenvalues of the sum. However, free probability identifies a certain sufficient condition, called asymptotic freeness, under which this problem can be tackled, without involving the eigenvectors of the matrices. The notion of asymptotic freeness is equivalent to the notion of statistical independence that we are familiar with for random variables. It is a generalization of the latter to the case where the variables — here, the matrices — do not commute.

Let us briefly recall basic properties of independent variables. We denote by p_x the probability density of the variable x, by $g_x(z) \equiv \langle e^{zx} \rangle = \sum_{n\geqslant 0} \langle x^n \rangle z^n/n!$ its characteristic function, and by $r_x(z) \equiv \ln g_x(z) = \sum_{n\geqslant 0} c_{x,n} z^n$ its cumulant generating function. For two independent real random variables x_1 and x_2, the following relations hold:

$$\langle x_1 x_2 \rangle = \langle x_1 \rangle \langle x_2 \rangle , \tag{5.133}$$

$$p_{x_1+x_2} = p_{x_1} * p_{x_2}, \tag{5.134}$$

$$r_{x_1+x_2} = r_{x_1} + r_{x_2}. \tag{5.135}$$

We will see that these relations find their equivalents for asymptotically free matrices.

By definition, two Hermitian matrices X_1 and X_2 are asymptotically free if for all $l \in \mathbb{N}$ and for all polynomials p_i and q_i $(1 \leq i \leq l)$, we have [143]

$$\langle p_i(X_1) \rangle_\Lambda = \langle q_i(X_2) \rangle_\Lambda = 0 \;\Rightarrow\; \langle p_1(X_1) q_1(X_2) \ldots p_l(X_1) q_l(X_2) \rangle_\Lambda = 0, \tag{5.136}$$

where the expectation value $\langle ... \rangle_\Lambda$ is defined as

$$\langle X \rangle_\Lambda = \frac{1}{N} \langle \mathrm{Tr} X \rangle . \tag{5.137}$$

The interpretation of the formal definition (5.136) is the following: two matrices are free if their eigenbases are related to one another by a random rotation, or said differently, if their eigenvectors are almost surely orthogonal.

From the definition (5.136), it is easy to compute various mixed moments of X_1 and X_2. By considering the binomials $\tilde{X}_i = X_i - \langle X_i \rangle_\Lambda$ that obey $\langle \tilde{X}_1 \rangle_\Lambda = \langle \tilde{X}_2 \rangle_\Lambda = 0$, we obtain from Eq. (5.136):

$$\langle X_1 X_2 \rangle_\Lambda = \langle X_1 \rangle_\Lambda \langle X_2 \rangle_\Lambda \,. \tag{5.138}$$

Note that this last condition is not enough to define asymptotic freeness, since matrices do not commute. For example, from Eq. (5.136), forth moments read

$$\begin{aligned} \langle X_1 X_1 X_2 X_2 \rangle_\Lambda &= \langle X_1^2 \rangle_\Lambda \langle X_2^2 \rangle_\Lambda \,, \\ \langle X_1 X_2 X_1 X_2 \rangle_\Lambda &= \langle X_1^2 \rangle_\Lambda \langle X_2 \rangle_\Lambda^2 + \langle X_1 \rangle_\Lambda^2 \langle X_2^2 \rangle_\Lambda - \langle X_1 \rangle_\Lambda^2 \langle X_2 \rangle_\Lambda^2 \,. \end{aligned} \tag{5.139}$$

Free cumulants are defined such that the sum property (5.135) is preserved for the generating function of the free cumulants, the so-called $\mathcal{R}$-transform [143, 177]. Interestingly, the $\mathcal{R}$-transform is simply related, by Eq. (5.30), to the Blue function (5.29), the latter being the functional inverse of the resolvent $g(z)$[16]. The $\mathcal{R}$-transform of the sum of two asymptotically free matrices X_1 and X_2 obeys:

$$\mathcal{R}_{X_1+X_2}(z) = \mathcal{R}_{X_1}(z) + \mathcal{R}_{X_2}(z). \tag{5.140}$$

Hence, the problem of finding the eigenvalue distribution of the sum of two free random matrices is straightforward. Applying successively Eqs. (5.29), (5.30), and (5.140), one readily infers $g_{X_1+X_2}$ from g_{X_1} and g_{X_2}. The steps of the algorithm are:

$$g_{X_i} \;\rightarrow\; \mathcal{B}_{X_i} \;\rightarrow\; \mathcal{R}_{X_i} \;\rightarrow\; \mathcal{R}_{X_1+X_2} \;\rightarrow\; \mathcal{B}_{X_1+X_2} \;\rightarrow\; g_{X_1+X_2}. \tag{5.141}$$

There is an analogous result for the product of free matrices, which involves the so-called $\mathcal{S}$-transform [143]. If we define $\chi(z)$ as a solution of

$$\frac{1}{\chi(z)} g\left(\frac{1}{\chi(z)}\right) - 1 = z, \tag{5.142}$$

then the $\mathcal{S}$-transform is

$$\mathcal{S}(z) = \frac{1+z}{z}\chi(z). \tag{5.143}$$

Eqs. (5.142) and (5.143) are equivalent to the following implicit equation for $\mathcal{S}(z)$:

$$\mathcal{S}(z)\mathcal{R}[z\mathcal{S}(z)] = 1. \tag{5.144}$$

The $\mathcal{S}$-transform of the product of two asymptotically free matrices X_1 and X_2 satisfies [143]:

$$\mathcal{S}_{X_1X_2}(z) = \mathcal{S}_{X_1}(z)\mathcal{S}_{X_2}(z). \tag{5.145}$$

Therefore, the S-transform plays a role analogous to the $\mathcal{R}$-transform for products (instead of sums) of free matrices. The recipe to find the eigenvalue density of X_1X_2 is analogous to (5.141):

$$g_{X_i} \;\rightarrow\; \chi_{X_i} \;\rightarrow\; \mathcal{S}_{X_i} \;\rightarrow\; \mathcal{S}_{X_1X_2} \;\rightarrow\; \chi_{X_1X_2} \;\rightarrow\; g_{X_1X_2}. \tag{5.146}$$

[16] Note that $g(z)$ plays the role of a free characteristic function, see Eq. (5.26) and (5.27). See also Ref. [177] for a discussion about the relation between the free cumulants and the moments $\langle \Lambda^n \rangle$.

5.6.2 Application 1: Gaussian and Wishart ensembles revisited

A good attitude when searching for the eigenvalue density of a given matrix, is to look at a possible decomposition of the latter in a sum or product of free matrices, for which resolvents are known. Let us apply this idea to recover in a new manner the now familiar semicircle and Marchenko-Pastur laws.

Let us first consider a matrix A from the Gaussian orthogonal ensemble (GOE), with the probability distribution $P(A) = C_N e^{-\frac{N}{4}\mathrm{Tr}(A^2)}$. From Eq. (5.134), it is clear that the distribution of the variable $x_1 + x_2$, where x_1 and x_2 are independent Gaussian random variables of variance σ, is still Gaussian of variance $\sqrt{2}\sigma$. We can therefore decompose any Gaussian matrix A in a sum of two independent rescaled matrices A_1 and A_2 that obey the same law P, $A = \frac{1}{\sqrt{2}}(A_1 + A_2)$. In addition, two independent Gaussian matrices are asymptotically free. Indeed, since the measure $P(A)$ is invariant under orthogonal transformation, rotation matrices O_1 and O_2, diagonalizing A_1 and A_2 respectively, are random rotations over the orthogonal group. This means that the rotation $O_1^\dagger O_2$ from the eigenbasis of A_1 to that of A_2 is also random, which is precisely the intuitive definition of asymptotic freeness (for a formal proof, see Ref. [143]). The additive property of the $\mathcal{R}$-transform and the scaling property (5.33) yield:

$$\mathcal{R}_A(z) = \mathcal{R}_{\frac{A_1}{\sqrt{2}}}(z) + \mathcal{R}_{\frac{A_2}{\sqrt{2}}}(z) = \sqrt{2}\mathcal{R}_A\left(\frac{z}{\sqrt{2}}\right). \tag{5.147}$$

A solution of this equation is $\mathcal{R}_A(z) \propto z$. According to Eq. (5.37), $\mathcal{R}'(0) = \langle \Lambda^2 \rangle = \langle \mathrm{Tr} A^2 \rangle / N = 1$, so that

$$\mathcal{R}(z) = z. \tag{5.148}$$

This is, as expected, the $\mathcal{R}$-transform of the semicircle law, see Eqs. (5.31) and (5.90). Thus, we can claim that the semicircle law is the free counterpart of the Gaussian distribution in classical probability theory.

In order to use the the powerful arsenal of free probability for Wishart matrices, we decompose the $N \times N$ matrix $A = HH^\dagger$ as:

$$HH^\dagger = \sum_{\alpha=1}^{M} \mathbf{h}^{(\alpha)\dagger}\mathbf{h}^{(\alpha)} \quad \text{with} \quad \mathbf{h}^{(\alpha)} = (H_{1\alpha}^*, \ldots, H_{N\alpha}^*). \tag{5.149}$$

The spectrum of each matrix $\mathbf{h}^{(\alpha)\dagger}\mathbf{h}^{(\alpha)}$ is simple because it has only one nonzero eigenvalue $\Lambda_\alpha = \|\mathbf{h}^{(\alpha)}\|^2 = \sum_{i=1}^N |H_{i\alpha}|^2$, associated with the eigenvector $\mathbf{h}^{(\alpha)*}$. The $(N-1)$ other eigenvectors associated with zero eigenvalue form the basis of the hyperplane perpendicular to the vector $\mathbf{h}^{(\alpha)*}$. Since the vectors $\mathbf{h}^{(\alpha)}$ are uncorrelated, we can replace the resolvent of the matrix $\mathbf{h}^{(\alpha)\dagger}\mathbf{h}^{(\alpha)}$ by:

$$g_{\mathbf{h}^{(\alpha)\dagger}\mathbf{h}^{(\alpha)}}(z) = \frac{1}{N}\left[\frac{N-1}{z} + \frac{1}{z-1}\right], \tag{5.150}$$

where we used $\langle \Lambda_0 \rangle = 1$ ($\langle |H_{i\alpha}|^2 \rangle = 1/N$). Inverting this relation gives:

$$\begin{aligned}\mathcal{R}_{\mathbf{h}^{(\alpha)\dagger}\mathbf{h}^{(\alpha)}}(z) &= \frac{1}{2z}\left(z - 1 - \sqrt{(z-1)^2 + \frac{4z}{N}}\right) \\ &= \frac{1}{N}\frac{1}{1-z} + \mathcal{O}\left(\frac{1}{N^2}\right).\end{aligned} \tag{5.151}$$

For independent vectors $\mathbf{h}^{(\alpha)}$, that have independent entries with variances equal to $1/N$ and identical means, it can be shown that the matrices $\mathbf{h}^{(\alpha)\dagger}\mathbf{h}^{(\alpha)}$ are asymptotically free [143]. Thus,

$$\mathcal{R}_{HH^\dagger}(z) = \sum_{\alpha=1}^{M} \mathcal{R}_{\mathbf{h}^{(\alpha)\dagger}\mathbf{h}^{(\alpha)}}(z) \tag{5.152}$$

$$= \frac{1}{c}\frac{1}{1-z}, \tag{5.153}$$

where $c = N/M$. This is the $\mathcal{R}$-transform of the Marchenko-Pastur law, see Eqs. (5.31) and (5.92). It is interesting to note that, if we were to take the Nth classical convolution (by inverting the sum of cumulant-generating functions) of the distributions of the variables Λ_α, we would obtain asymptotically ($N, M \to \infty$, at fixed $c = N/M$) the Poisson distribution. However, the distribution that we obtain by taking the Nth free convolution (by inverting the sum of $\mathcal{R}$-transforms) is the Marchenko-Pastur law. The latter is therefore the free analog of the Poisson law in classical probability [143]. Another simple proof of this law, based on a product decomposition of the matrix $HH^\dagger$ and the $\mathcal{S}$-transform, can be found in Ref. [178].

5.6.3 Application 2: ERMs

From the previous result concerning the Wishart ensemble, it is straightforward to apply the toolbox of free probability to ERMs. We start with the decomposition $A = HTH^\dagger$, where the basis $\{\psi_\alpha\}$, that defines $H_{i\alpha}$ in Eq. (5.10), is assumed to be the eigenbasis of the operator $\hat{T}$, $\hat{T}|\psi_\alpha\rangle = \mu_\alpha|\psi_\alpha\rangle$. The matrix A is conveniently rewritten as:

$$HTH^\dagger = \sum_{\alpha=1}^{M} \mu_\alpha \mathbf{h}^{(\alpha)\dagger}\mathbf{h}^{(\alpha)}, \tag{5.154}$$

where $\mathbf{h}^{(\alpha)}$ is defined in Eq. (5.149). As explained above, the M matrices $\mathbf{h}^{(\alpha)\dagger}\mathbf{h}^{(\alpha)}$ are asymptotically free, as long as the vectors $\mathbf{h}^{(\alpha)}$ are independent. Hence,

$$\mathcal{R}_{HTH^\dagger}(z) = \sum_{\alpha=1}^{M} \mathcal{R}_{\mu_\alpha \mathbf{h}^{(\alpha)\dagger}\mathbf{h}^{(\alpha)}}(z) = \sum_{\alpha=1}^{M} \mu_\alpha \mathcal{R}_{\mathbf{h}^{(\alpha)\dagger}\mathbf{h}^{(\alpha)}}(\mu_\alpha z) \tag{5.155}$$

$$= \frac{1}{N}\sum_{\alpha=1}^{M} \frac{\mu_\alpha}{1-\mu_\alpha z} = \frac{1}{N}\mathrm{Tr}_M\left[\frac{T}{1-zT}\right] \tag{5.156}$$

$$= \frac{1}{N}\mathrm{Tr}\left[\frac{\hat{T}}{1-z\hat{T}}\right] \tag{5.157}$$

$$= \frac{1}{cz}\left[\frac{1}{z}g_T\left(\frac{1}{z}\right) - 1\right]. \tag{5.158}$$

Eq. (5.155) follows from the properties (5.140) and (5.33), Eq. (5.156) — from the result (5.151), and Eq. (5.158) — from $g_T(z) = \sum_{\alpha=1}^{M} 1/(z-\mu_\alpha)M$. Using the definition (5.143) of the $\mathcal{S}$-transform, one also easily shows that Eq. (5.158) is equivalent to

$$\mathcal{S}_{HTH^\dagger}(z) = \frac{1}{z+1/c}\mathcal{S}_T(cz). \tag{5.159}$$

For completeness, we now propose to derive the solution (5.159) by means of the property (5.145). From the definitions of the resolvent $g(z)$ and the $\mathcal{S}$-transform, one can check that, for arbitrary matrices A and B of size $N \times M$ and $M \times N$, respectively,

$$\mathcal{S}_{AB}(z) = \frac{z+1}{z+1/c}\mathcal{S}_{BA}(cz). \tag{5.160}$$

Applying this result for $A = HT$ and $B = H^\dagger$, we obtain

$$\begin{aligned}\mathcal{S}_{HTH^\dagger}(z) &= \frac{z+1}{z+1/c}\mathcal{S}_{H^\dagger HT}(cz),\\ &= \frac{z+1}{z+1/c}\mathcal{S}_{H^\dagger H}(cz)\mathcal{S}_T(cz).\end{aligned} \tag{5.161}$$

Eq. (5.161) follows from the fact that the deterministic matrix T and the random matrix $H^\dagger H$ are asymptotically free. Besides, the combination of Eq. (5.144) with $\mathcal{R}_{H^\dagger H}(z) = \mathcal{R}_{HH^\dagger}(z/c)/c = c/(c-z)$ gives

$$\mathcal{S}_{H^\dagger H}(z) = \frac{c}{c+z}. \tag{5.162}$$

From Eqs. (5.161) and (5.162), we finally recover (5.159).

The result (5.159), or equivalently its operator form (5.157), is in perfect agreement with the solution obtained by a diagrammatic approach in section 5.5.3. Indeed, the self-energy $\sigma(z) = \mathcal{R}[g(z)]$ inferred from Eq. (5.157) is exactly the result (5.113). It is worth recalling that (5.157) was obtained from the asymptotic freeness of the matrices $\mathbf{h}^{(\alpha)\dagger}\mathbf{h}^{(\alpha)}$, that holds as long as the elements $H_{i\alpha}$ are i.i.d. with a finite second moment [143]. In particular, it means that (5.113) is valid even if $H_{i\alpha}$ are not Gaussian variables: the Gaussian hypothesis, that largely simplified diagrammatic calculations in section 5.5.3, is not essential[17]. In particular, this remark holds for the Wigner semicircle and the Marchenko-Pastur laws[18], and justifies their large degree of universality.

As far as ERMs are concerned, we conclude that the only assumption that may limit the applicability of (5.113) at high density of points ρ is the independence of the vectors $\mathbf{h}^{(\alpha)}$. We know that their covariance matrix is proportional to the identity (see section 5.1.3), but this is not enough to insure their independence, precisely because $H_{i\alpha}$ are not Gaussian random variables. In the two following sections, we investigate the precision of the result (5.113) in the limit $N \to \infty$, with two examples of Hermitian ERMs that are particularly important in the study of wave propagation in random media.

5.7 ERM Im$G(\omega_0)$ in three-dimensional space

In this section, we study the real symmetric $N \times N$ Euclidean matrix $S(\omega_0) = \mathrm{Im}G(\omega_0) + I_N$ with elements defined through the cardinal sine (sinc) function:

$$S_{ij}(\omega_0) = f(\mathbf{r}_i - \mathbf{r}_j) = \frac{\sin(k_0|\mathbf{r}_i - \mathbf{r}_j|)}{k_0|\mathbf{r}_i - \mathbf{r}_j|}, \tag{5.163}$$

[17] A rigorous diagrammatic proof of (5.113), by just assuming a finite second moment of $H_{i\alpha}$, seems nontrivial.

[18] We are not aware of a diagrammatic proof of the Wigner semicircle and the Marchenko-Pastur laws, that would not invoke the Gaussian assumption.

that may play an important role for understanding the cooperative emission of atomic samples (see section 2.5.1).

A general property of the matrix $S(\omega_0)$ is the positiveness of its eigenvalues: $\Lambda_n > 0$. Indeed, the Fourier transform of the function $f(\Delta\mathbf{r})$ in (5.163) is positive and hence $f(\Delta\mathbf{r})$ is a function of positive type. An Euclidean matrix defined through a function of positive type is positive definite and hence has only positive eigenvalues. Note also that, for each realization of $S(\omega_0)$, $\sum_{i=1}^{N}\Lambda_i = N$, so that $\langle\Lambda\rangle = 1$.

5.7.1 Approximate solution for the eigenvalue density

Let us assume that the vectors $\mathbf{r}_i$ define positions of N randomly chosen points inside a three-dimensional cube of side L. A convenient set of basis functions $\{\psi_\alpha\}$ is then given by 'plane waves'

$$\psi_\alpha(\mathbf{r}) = \frac{1}{\sqrt{V}} e^{\mathrm{i}\mathbf{k}_\alpha\cdot\mathbf{r}}, \tag{5.164}$$

where $\mathbf{k}_\alpha = \{k_{\alpha_x}, k_{\alpha_y}, k_{\alpha_z}\}$, $k_{\alpha_x} = \alpha_x\Delta k$ with $\alpha_x = \pm1, \pm2, \ldots$ (and similarly for k_{α_y} and k_{α_z}), and $\Delta k = 2\pi/L$. $T_{\alpha\beta}$ is then simply a double Fourier transform of the function $f(\mathbf{r}_i, \mathbf{r}_j)$ in the box — see Eq. (5.12) — and the representation (5.9) stems from the Fourier series expansion of $f(\mathbf{r}_i, \mathbf{r}_j)$, without the harmonics corresponding to $\mathbf{k}_\alpha = 0$. Furthermore, the variance (5.132) of $p(\Lambda)$ is given by:

$$\langle\Lambda^2\rangle - 1 = \frac{N}{(k_0L)^2}\iiint_{-\infty}^{\infty}\mathrm{d}x\mathrm{d}y\mathrm{d}z\frac{\sin\left(k_0L\sqrt{x^2+y^2+z^2}\right)^2}{x^2+y^2+z^2}w(x,y,z) \tag{5.165}$$

$$\simeq \frac{2.8N}{(k_0L)^2} \equiv \gamma. \tag{5.166}$$

To obtain (5.166) from (5.165), we assumed $k_0L \gg 1$.

Our goal is to calculate $g(z)$, or equivalently $\mathcal{B}(z)$ or $\mathcal{R}(z) = \sigma[\mathcal{B}(z)]$. All these quantities depend on the matrix T, see, *e.g.*, Eq. (5.158). Unfortunately, it is impossible to calculate the double integral (5.12) exactly in a box. In the limit of large volume V, the integrations over $\Delta\mathbf{r} = \mathbf{r}_i - \mathbf{r}_j$ and $\mathbf{r}_i + \mathbf{r}_j$ can be approximatively decoupled, yielding

$$\begin{aligned} &T_{\alpha\beta} \simeq T_{\alpha\alpha}\delta_{\alpha\beta}, \\ &T_{\alpha\alpha} = \rho f(\mathbf{k}_\alpha) = N\iiint_{-\infty}^{\infty}\mathrm{d}x\mathrm{d}y\mathrm{d}z\, w(x,y,z)\frac{\sin(k_0\Delta r)}{k_0\Delta r}e^{\mathrm{i}\mathbf{k}_\alpha\cdot\Delta\mathbf{r}}, \end{aligned} \tag{5.167}$$

where $f(\mathbf{k}_\alpha)$ and $w(x,y,z)$ are defined by Eqs. (5.123) and (5.129), respectively, and (x,y,z) are the Cartesian coordinates of the vector $\Delta\mathbf{r}/L$.[19] Eq. (5.167) is still too involved to be useful. We propose in the following two different approximations of Eq. (5.167).

First, we approximate the function $w(x,y,z)$ by 1 for $\mathbf{r}$ in a sphere of radius $L/2\kappa_1$, with $\kappa_1 \sim 1$ a numerical constant to be fixed later, and 0 elsewhere:

$$\begin{aligned} T_{\alpha\alpha} &\simeq \rho\int\limits_{|\Delta\mathbf{r}|<L/2\kappa_1}\mathrm{d}^3\Delta\mathbf{r}\,\frac{\sin(k_0\Delta r)}{k_0\Delta r}\mathrm{e}^{\mathrm{i}\mathbf{k}_\alpha\cdot\Delta\mathbf{r}} \\ &= \rho\frac{2\pi^2}{k_0k_\alpha}\frac{L}{2\kappa_1\pi}\left\{\mathrm{sinc}\left[(k_\alpha-k_0)\frac{L}{2\kappa_1}\right] - \mathrm{sinc}\left[(k_\alpha+k_0)\frac{L}{2\kappa_1}\right]\right\}. \end{aligned} \tag{5.168}$$

[19] If the volume V is infinite, Eq. (5.167) can be simplified using $\lim_{L\to\infty} w(x,y,z) = 1$.

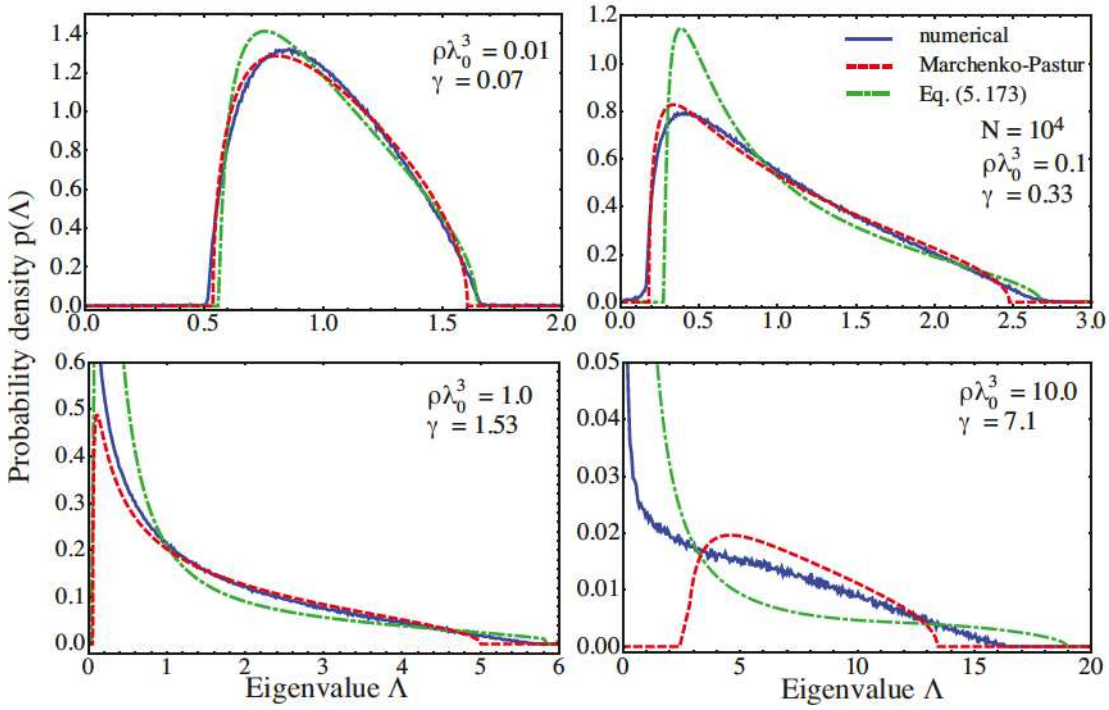

Figure 5.6: Probability density of eigenvalues of a square $N \times N$ Euclidean matrix $S(\omega_0)$ with elements $S_{ij}(\omega_0) = \sin(k_0|\mathbf{r}_i - \mathbf{r}_j|)/k_0|\mathbf{r}_i - \mathbf{r}_j|$, where the N points $\mathbf{r}_i$ are randomly chosen inside a 3D cube of side L. Numerical results (blue solid lines) obtained for $N = 10^4$ after averaging over 10 realizations are compared to the Marchenko-Pastur law (5.171) (red dashed lines), and to the approximation (5.173) (green dot-dashed line), with $\gamma = 2.8N/(k_0L)^2$ for several densities ρ of points ($\lambda_0 = 2\pi/k_0$).

In order to simplify this expression, we note that the second sinc function in Eq. (5.168) is always smaller than $2\kappa_1/k_0L$ (because $k_\alpha = |\mathbf{k}_\alpha| > 0$ and $k_0 > 0$) and hence can be dropped in the limit of large $k_0L \gg 1$ considered here. Furthermore, because the first sinc function in Eq. (5.168) is peaked around $q_\alpha = k_0$, we replace it by a boxcar function $\Pi[(k_\alpha - k_0)L/2\kappa_1\pi]$, where $\Pi(x) = 1$ for $|x| < 1/2$ and $\Pi(x) = 0$ otherwise. The coefficient in front of $(k_\alpha - k_0)$ in the argument of Π is chosen to ensure that the integral of the latter over k_α from 0 to ∞ is equal to the same integral of the sinc function. We then obtain

$$T_{\alpha\beta} \simeq \rho \frac{2\pi^2}{k_0^2} \frac{L}{2\kappa_1\pi} \Pi\left[(k_\alpha - k_0)\frac{L}{2\pi\kappa_1}\right] \delta_{\alpha\beta}, \tag{5.169}$$

which is different from zero only for $\mathbf{k}_\alpha$'s inside a spherical shell of radius k_0 and thickness $2\pi\kappa_1/L$. In addition, for all $\mathbf{k}_\alpha$'s inside the shell the value of $T_{\alpha\alpha}$ is the same and equal to $c = N/M$ with $M = \kappa_1(k_0L)^2/\pi \gg 1$ the number of $\mathbf{k}_\alpha$'s inside the shell:

$$T \simeq \frac{N}{M} I_M \quad \text{with} \quad M = \frac{\kappa_1(k_0L)^2}{\pi}. \tag{5.170}$$

Hence, the sinc matrix becomes a Wishart matrix: $S \simeq cHH^\dagger$. From Eqs. (5.153) and (5.33), we find $\mathcal{R}_A(z) = \mathcal{R}_{cHH^\dagger}(z) = 1/(1 - cz)$. By requiring that the variance of the distribution, $\mathrm{Var}\Lambda = \mathcal{R}'(0) = c$, coincides with (5.166), $c = \gamma$, we fix the value of

$\kappa_1 \simeq \pi/2.8 \simeq 1.12$. $\mathcal{R}_A(z)$ is the $\mathcal{R}$-transform of the rescaled Marchenko-Pastur law:

$$p(\Lambda) = \left(1 - \frac{1}{\gamma}\right)^+ \delta(\Lambda) + \frac{\sqrt{(\Lambda_+ - \Lambda)^+(\Lambda - \Lambda_-)^+}}{2\pi\gamma\Lambda}, \tag{5.171}$$

where $\Lambda_\pm = (1 \pm \sqrt{\gamma})^2$ and $x^+ = \max(x, 0)$. The distribution of eigenvalues of the matrix (5.163) is therefore parameterized by a single parameter γ equal to the variance of this distribution. To our knowledge, the fact that this distribution describes eigenvalues of the Euclidean matrix S was never noticed before.

In Fig. 5.6 we present a comparison of (5.171) with the results of direct numerical simulations. The latter amount to generate N random points $\mathbf{r}_i$ inside a three-dimensional cube, to use these points to define a random $N \times N$ matrix S according to Eq. (5.163), and to diagonalize S using the standard software package LAPACK [179]. The procedure is repeated several times and a histogram of all eigenvalues Λ is created. This histogram approximates the eigenvalue distribution $p(\Lambda)$. As we see from Fig. 5.6, the agreement between numerical results and the Marchenko-Pastur law (5.171) (dashed-line) is good for $\gamma < 1$, but (5.171) fails to describe $p(\Lambda)$ when γ becomes larger than unity. The reason for this is easy to understand if we go back to Eqs. (5.167), (5.168) and (5.169). Indeed, when we approximate the result of integration in (5.167) by (5.169), we reduce the infinite-size matrix T to a matrix of finite size $M \times M$. By definition, the rank of the latter matrix is inferior or equal to M. The rank of $S = HTH^\dagger$ cannot be larger than the rank of T and hence is also bounded by M from above when we use Eq. (5.169). When $\gamma > 1$, implying $M < N$, the representation (5.9) only gives us access to M of N eigenvalues of S, which is not sufficient to reconstruct the probability density $p(\Lambda)$. In order to access the regime of $\gamma > 1$ one needs to find another approximation to (5.167) than (5.169).

A second approximation to Eq. (5.167) consists in replacing $w(x, y, z)$ by $e^{-\kappa_2 r/L}$, with $\kappa_2 \sim 1$ a numerical constant to be fixed later:

$$\begin{aligned} T_{\alpha\alpha} &\simeq \rho \int \mathrm{d}^3\Delta\mathbf{r}\, \frac{\sin(k_0\Delta r)}{k_0\Delta r} e^{-\kappa_2 r/L} \mathrm{e}^{\mathrm{i}\mathbf{k}_\alpha\cdot\Delta\mathbf{r}} \\ &= \rho \frac{2\pi^2}{k_0 k_\alpha} \frac{\kappa_2 L}{\pi} \left[\frac{1}{(k_\alpha L - k_0 L)^2 + \kappa_2^2} - \frac{1}{(k_\alpha L + k_0 L)^2 + \kappa_2^2} \right]. \end{aligned} \tag{5.172}$$

Inserting $f(\mathbf{k}_\alpha) = T_{\alpha\alpha}/\rho$ into Eq. (5.124), the $\mathcal{R}$-transform $\mathcal{R}(z) = \sigma[\mathcal{B}(z)]$ becomes, after integration over $\mathbf{k}_\alpha$,

$$\mathcal{R}(z) = \frac{2\mathrm{i}\kappa_2}{\kappa_-(z) - \kappa_+(z)}, \tag{5.173}$$

$$\kappa_\pm(z) = \sqrt{(k_0 L)^2 - \kappa_2^2 \pm 2\sqrt{\kappa_2(2\pi N z - (k_0 L)^2 \kappa_2)}}. \tag{5.174}$$

The mean and the variance of $p(\Lambda)$ are thus given by

$$\langle\Lambda\rangle = \mathcal{R}(0) = 1, \tag{5.175}$$

$$\mathrm{Var}\Lambda = \mathcal{R}'(0) = \frac{\pi N}{\kappa_2(k_0^2 L^2 + \kappa_2^2)}. \tag{5.176}$$

In the limit $k_0 L \gg 1$, by requiring that the variance (5.176) is equal to γ defined by Eq. (5.166), we obtain $\kappa_2 \simeq \pi/2.8 \simeq 1.12$ $(= \kappa_1)$.

In Fig. 5.6, $p(\Lambda)$ following from Eq. (5.173) (dot-dashed line) is also compared with the results of numerical simulations. We find the resolvent $g(z)$ by solving $1/g(z) + \mathcal{R}[g(z)] = z$ numerically and then evaluate $p(\Lambda)$ with the help of Eq. (5.21). Contrary to Eq. (5.171) that applies only for $\gamma < 1$, Eq. (5.173) applies *a priori* for all γ. However, it turns out that the probability distribution of eigenvalues inferred from Eq. (5.173) is in less good agreement with numerical results than the Marchenko-Pastur law (5.171), meaning that (5.168) is a better approximation of the elements of T than (5.172).

In the following we propose another method to solve Eq. (5.115) for the resolvent $g(z)$ exactly.

5.7.2 Exact solution for the eigenvalue density

As explained in section 5.5.4, a general way to solve Eq. (5.115) is to express the latter in the eigenbasis of the operator $\hat{T}$. The resulting equation (5.127) is then formulated only in terms of the eigenvalues μ_α of the integral equation (5.126). The latter may be solved exactly if the volume V preserves the symmetry of its kernel $f(|\mathbf{r}-\mathbf{r}'|)$. From here on, we assume that the N points $\mathbf{r}_i$ are randomly chosen inside a three-dimensional sphere of radius R. In this case, the variance (5.132) becomes:

$$\begin{aligned}\langle\Lambda^2\rangle - 1 &= \frac{6N}{(k_0R)^2}\int_0^1 \mathrm{d}x \sin\left(2k_0Rx\right)^2 s(x) \\ &= \frac{9N}{(k_0R)^2}\frac{32(k_0R)^4 - 8(k_0R)^2 + 4k_0R\sin(4k_0R) + \cos(4k_0R) - 1}{256(k_0R)^4} \qquad (5.177)\\ &\simeq \frac{9N}{8(k_0R)^2} \equiv \gamma, \qquad (5.178)\end{aligned}$$

where we assumed $k_0R \gg 1$.

In order to solve the eigenvalue equation

$$\rho\int_V \mathrm{d}^3\mathbf{r}'\frac{\sin(k_0|\mathbf{r}-\mathbf{r}'|)}{k_0|\mathbf{r}-\mathbf{r}'|}\mathcal{R}_\alpha(\mathbf{r}') = \mu_\alpha\mathcal{R}_\alpha(\mathbf{r}), \qquad (5.179)$$

it is convenient to decompose its kernel in spherical harmonics [180]:

$$\frac{\sin(k_0|\mathbf{r}-\mathbf{r}'|)}{k_0|\mathbf{r}-\mathbf{r}'|} = 4\pi\sum_{l=0}^{\infty}\sum_{m=-l}^{l} j_l(k_0r)j_l(k_0r')Y_{lm}(\theta,\phi)Y_{lm}(\theta',\phi')^*, \qquad (5.180)$$

where θ and ϕ are the polar and azimuthal angles of the vector $\mathbf{r}$, respectively, j_l are spherical Bessel functions of the first kind, and Y_{lm} are spherical harmonics. Inserting the decomposition (5.180) into Eq. (5.179), we readily find that

$$\mathcal{R}_\alpha(\mathbf{r}) = \mathcal{R}_{lm}(\mathbf{r}) = \mathcal{A}_l j_l(k_0r)Y_{lm}(\theta,\phi), \qquad (5.181)$$

$$\begin{aligned}\mu_\alpha = \mu_l &= 4\pi\rho\int_0^R \mathrm{d}r' j_l(k_0r')^2 r'^2 \\ &= \frac{3}{2}N\left[j_l(k_0R)^2 - j_{l-1}(k_0R)j_{l+1}(k_0R)\right], \qquad (5.182)\end{aligned}$$

where $\mathcal{A}_l$ are normalization coefficients and $\alpha = \{l, m\}$. Eigenvalues μ_l are $(2l+1)$-times degenerated ($m \in [-l, l]$). Eq. (5.127) then becomes

$$z = \frac{1}{g(z)} + \frac{1}{N}\sum_l \frac{(2l+1)\mu_l}{1 - g(z)\mu_l}. \qquad (5.183)$$

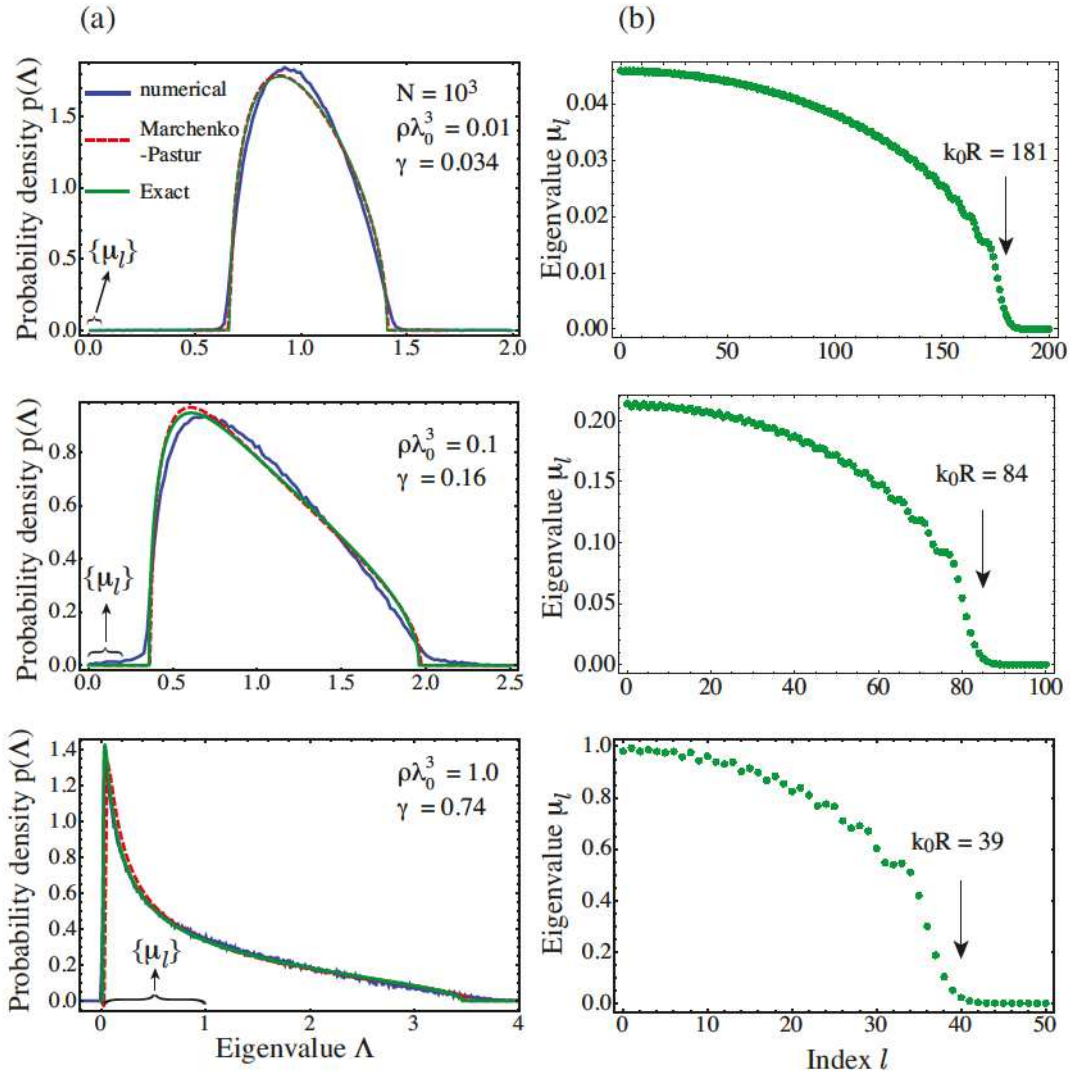

Figure 5.7: (a) Probability density of eigenvalues of the $N \times N$ ERM (5.163), where the N points $\mathbf{r}_i$ are randomly chosen inside a sphere of radius R. Numerical results (blue solid lines) obtained for $N = 10^3$ after averaging over 100 realizations are compared to the Marchenko-Pastur law (5.171) (red dashed lines), and to Eq. (5.183) (green solid lines), with $\gamma = 9N/8(k_0R)^2$ for several densities ρ of points ($\lambda_0 = 2\pi/k_0$). (b) Eigenvalues μ_l, given by Eq. (5.182) and used to compute $p(\Lambda)$ from Eq. (5.183) [green solid line in (a)], versus the index l. μ_l are non-zero for $l \lesssim k_0R$. The range covered by the eigenvalues μ_l is also indicated in (a) with braces.

In Figs. 5.7(a) and 5.8(a), $p(\Lambda)$ following from Eq. (5.183) is compared with results of numerical diagonalization, and with the Marchenko-Pastur law (5.171), where γ is now given by Eq. (5.178).[20] These figures deserve two comments:

- As long as $\gamma < 1$, results (5.183) and (5.171) are almost undistinguishable, and differ

[20] The reasoning leading to the representation (5.170) of the matrix T, for points distributed in a cubic box, holds for points distributed in a sphere as well, provided that we replace L by $2R$ in Eq. (5.168). The value of κ_1 is modified, but the property $N/M = \mathrm{Var}\Lambda = \gamma$ still holds.

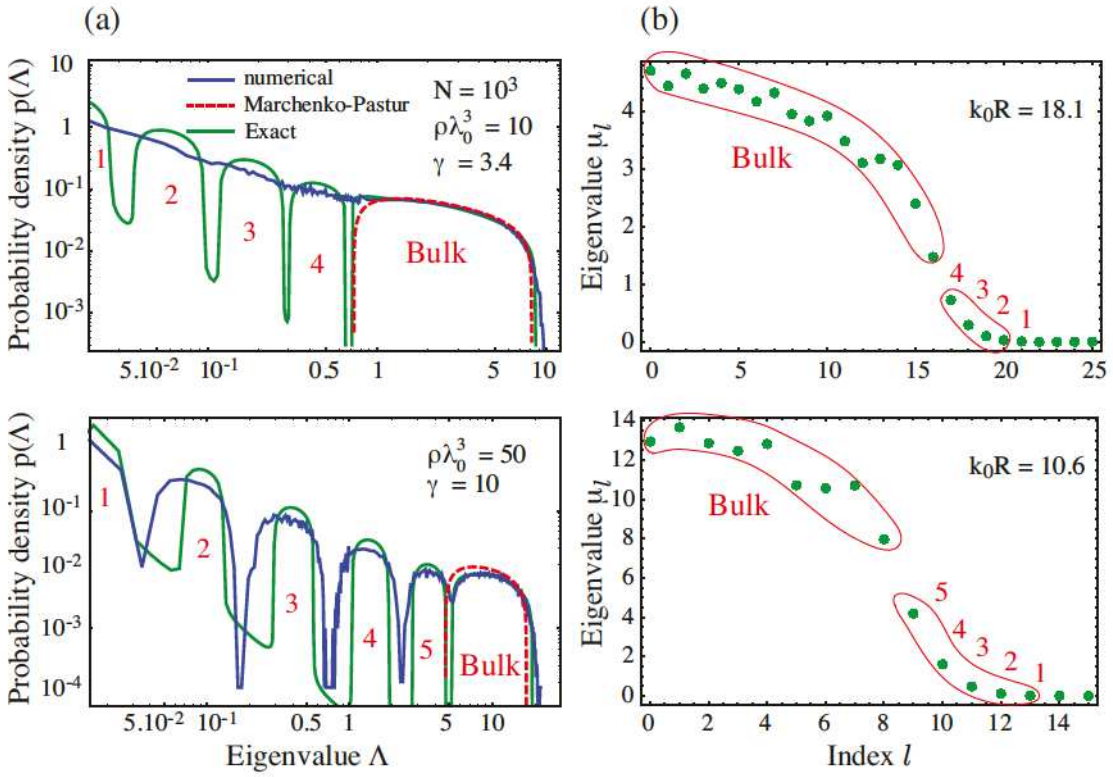

Figure 5.8: Same as Fig. 5.7 but for higher densities $\rho\lambda_0^3 = 10$ and 50. For $2R/\lambda_0 \lesssim 1$, the probability density $p(\Lambda)$ splits into sectors centered around the eigenvalues μ_l of $\hat{T}$.

slightly from the numerical simulation. As explained above, for $\gamma > 1$, Eq. (5.171) only gives us access to M of N eigenvalues of S, leading to a rough estimation [red dashed-lines in Fig. 5.8(a)] of the large-Λ part of the spectrum, denoted as the 'bulk' in Fig. 5.8(a), while Eq. (5.183) is still in good agreement with numerical results.

- For $R/\lambda_0 \lesssim 1$, the numerical spectrum splits into several domains [solid blue line of the lower panel of Fig. 5.8(a)]. To understand this effect, we have represented in Figs. 5.7(b) and 5.8(b) the eigenvalues μ_l (5.182) used to compute $p(\Lambda)$ from Eq. (5.183) [green solid line in (a)]. We observe that μ_l are non-zero for $l \lesssim k_0R$. At low density $\rho\lambda_0^3 \lesssim 10$, the support of $p(\Lambda)$ is larger than the range covered by the eigenvalues μ_l, and does not necessarily overlap with the latter [see braces in Fig. 5.7(a)]. At large density ($\rho\lambda_0^3 \gtrsim 10$ corresponding here to $R/\lambda_0 \lesssim 1$), $p(\Lambda)$ following from Eq. (5.183) splits into domains centered around some of the smallest values $\mu_l \neq 0$ (indicated with labels $1, \ldots, 5$ in Fig. 5.8). This splitting appears also in the numerical results but at slightly smaller values of k_0R: it is present in the lower panel, but not in the upper panel of Fig. 5.8(a). In addition, the widths of the islands found by numerical diagonalization are larger than those predicted by Eq. (5.183) (note the logarithmic scale). Such a 'smoothening' of the probability density of eigenvalues is typical of $p(\Lambda)$ computed at finite N [137]. Therefore, we believe that the difference with numerical results should disappear in the limit $N \to \infty$ that we assumed to derive Eq. (5.183). The observed splitting

of the eigenvalue domain means that, in the limit $\rho\lambda_0^3 \to \infty$, the eigenvalues Λ_n of the ERM S become equal to the eigenvalues $\mu_\alpha = \mu_l$ of $\hat{T}$, and the problem losses its statistical nature.

We conclude that the result (5.183) is in fare agreement with numerical results at all densities. In particular, it reveals that γ is not always the only parameter that governs the shape of $p(\Lambda)$. The density $\rho\lambda_0^3$ plays a role for $\gamma \gtrsim 1$, while k_0R is the relevant parameter for $k_0R \lesssim 1$. The drawback of (5.183) is that it does not give a compact form for the resolvent $g(z)$ or the distribution $p(\Lambda)$. For example, it is not obvious from Eq. (5.183) that the latter admits, with an excellent precision, the Marchenko-Pastur solution (5.171) for $\gamma < 1$.

Finally, it is worth noting that the eigenvalue distribution of the matrix S has been studied numerically by Akkermans *et al.* in the context of light propagation in atomic gases (see figure 1 of Ref. [79]) without proposing any analytical approximation to it. The parameter $\gamma \sim N/(k_0L)^2$ has been introduced in that work as a ratio of the number of atoms N to the number of transverse optical modes $N_\perp \propto (k_0L)^2$. The same parameter appeared in Refs. [83, 87, 88, 90] as a superradiant decay rate in a cold atomic gas (see section 2.5.1 for more details). Hence the results of this section complement and extend the works [79, 83, 87, 88, 90].

5.8 ERM Re$G(\omega_0)$ in three-dimensional space

Let us now consider the $N \times N$ Hermitian ERM $C(\omega_0) = \mathrm{Re}G(\omega_0)$, with elements defined using the cardinal cosine (cosc) function:

$$C_{ij}(\omega_0) = f(\mathbf{r}_i - \mathbf{r}_j) = (1 - \delta_{ij})\frac{\cos(k_0|\mathbf{r}_i - \mathbf{r}_j|)}{k_0|\mathbf{r}_i - \mathbf{r}_j|}. \tag{5.184}$$

This matrix is relevant, for example, for understanding the collective Lamb shift in atomic samples (see section 2.5.1).

Contrary to the matrix $S(\omega_0)$, the Fourier transform of the function $f(\Delta\mathbf{r})$ is not positive, and hence, the spectrum of $C(\omega_0)$ is not bounded from below. Besides, for each realization of $C(\omega_0)$, $\sum_{n=1}^{N} \Lambda_n = 0$, so that $\langle\Lambda\rangle = 0$.

5.8.1 Approximate solution for the eigenvalue density

We proceed exactly as in section 5.7.1. Assuming the points $\mathbf{r}_i$ randomly distributed inside a cube of side L, with $k_0L \gg 1$, the variance (5.132) of $p(\Lambda)$ is now given by:

$$\langle\Lambda^2\rangle = \frac{N}{(k_0L)^2}\iiint_{-\infty}^{\infty} \mathrm{d}x\mathrm{d}y\mathrm{d}z \frac{\cos\left(k_0L\sqrt{x^2+y^2+z^2}\right)^2}{x^2+y^2+z^2} w(x,y,z) \tag{5.185}$$

$$\simeq \frac{2.8N}{(k_0L)^2} \equiv \gamma. \tag{5.186}$$

In the plane wave basis $\{\mathbf{k}_\alpha\}$, we use the approximation $T_{\alpha\beta} = \langle \mathbf{k}_\alpha|\hat{T}|\mathbf{k}_\beta\rangle \simeq T_{\alpha\alpha}\delta_{\alpha\beta}$, with

$$T_{\alpha\alpha} = \rho f(\mathbf{k}_\alpha) = N \iiint_{-\infty}^{\infty} \mathrm{d}x\mathrm{d}y\mathrm{d}z \, \frac{\cos(k_0\Delta r)}{k_0\Delta r} w(x,y,z) e^{\mathrm{i}\mathbf{k}_\alpha\cdot\Delta\mathbf{r}} \tag{5.187}$$

$$\simeq \rho \int\limits_{|\Delta\mathbf{r}|<L/2\kappa_3} \mathrm{d}^3\Delta\mathbf{r} \, \frac{\cos(k_0\Delta r)}{k_0\Delta r} \mathrm{e}^{\mathrm{i}\mathbf{k}_\alpha\cdot\Delta\mathbf{r}} \tag{5.188}$$

$$\simeq \rho \frac{4\pi}{k_0} \frac{1}{k_\alpha^2 - k_0^2} \left\{ 1 - \Pi\left[(k_\alpha - k_0)\frac{L}{2\pi\kappa_3}\right]\right\}, \tag{5.189}$$

where κ_3 is a numerical constant that will be fixed later. To obtain Eq. (5.189) from Eq. (5.188), we excluded a shell of thickness $2\pi\kappa_3/L$ around $k_\alpha = k_0$ where $T_{\alpha\alpha}$ changes sign rapidly [181]. On the other hand, the $\mathcal{R}$-transform $\mathcal{R}(z) = \sigma[\mathcal{B}(z)]$, that is given by Eq. (5.114), is expressed in the basis $\{\mathbf{k}_\alpha\}$, using $\mathrm{Tr}\hat{T} = N\langle\Lambda\rangle = 0$:

$$\mathcal{R}(z) = \frac{z}{N}\sum_{\mathbf{k}_\alpha} \frac{T_{\alpha\alpha}^2}{1 - zT_{\alpha\alpha}}$$

$$\simeq \rho z \int \frac{\mathrm{d}^3\mathbf{k}_\alpha}{(2\pi)^3} \frac{f(\mathbf{k}_\alpha)^2}{1 - \rho z f(\mathbf{k}_\alpha)}. \tag{5.190}$$

After inserting Eq. (5.189) into Eq. (5.190), the integral can be evaluated yielding

$$\mathcal{R}(z) = -\frac{2}{\pi}\mathrm{arccoth}\frac{4\pi^3\gamma}{\rho\lambda_0^3} + \frac{2}{\pi}\sqrt{-1 - \frac{\rho\lambda_0^3}{2\pi^2}z}$$

$$\times \left[\arctan\frac{1 + \frac{\rho\lambda_0^3}{2\pi^3\gamma}}{\sqrt{-1 - \frac{\rho\lambda_0^3}{2\pi^2}z}} - \arctan\frac{1 - \frac{\rho\lambda_0^3}{2\pi^3\gamma}}{\sqrt{-1 - \frac{\rho\lambda_0^3}{2\pi^2}z}} - \frac{\pi}{2}\right], \tag{5.191}$$

that corresponds to the choice $\kappa_3 \simeq 4/2.8\pi \simeq 0.45$ ensuring, in the limit $k_0L \gg 1$, $\gamma = \mathrm{Var}\Lambda = \mathcal{R}'(0) = 4N/\kappa_3\pi(k_0L)^2$.

Before discussing the result (5.191), let us briefly introduce a second possible approximation of Eq. (5.187), where $w(x,y,z)$ is replaced by $e^{-\kappa_4 r/L}$:

$$T_{\alpha\alpha} \simeq \rho \int \mathrm{d}^3\Delta\mathbf{r} \, \frac{\cos(k_0\Delta r)}{k_0\Delta r} e^{-\kappa_4 r/L} \mathrm{e}^{\mathrm{i}\mathbf{k}_\alpha\cdot\Delta\mathbf{r}}$$

$$= \frac{\pi\rho\left[(k_\alpha L)^2 - (k_0L)^2 + \kappa_4^2\right]}{k_0^2 k_\alpha} \left[\frac{1}{(k_\alpha L - k_0L)^2 + \kappa_4^2} - \frac{1}{(k_\alpha L + k_0L)^2 + \kappa_4^2}\right]. \tag{5.192}$$

The corresponding $\mathcal{R}$-transform (5.190) reads now

$$\mathcal{R}(z) = \frac{\kappa_4}{k_0L} + \frac{1}{2(k_0L)^{3/2}}\left[\frac{p_1(z) + \mathrm{i}p_2(z)}{p_+(z)} + \frac{p_1(z) - \mathrm{i}p_2(z)}{p_-(z)}\right], \tag{5.193}$$

where the functions $p_1(z)$, $p_2(z)$, and $p_\pm(z)$ are defined as

$$p_1(z) = (k_0L)^3 + 4\pi Nz - k_0L\kappa_4^2, \tag{5.194}$$

$$p_2(z) = \frac{\pi Nz\left[(k_0L)^3 + 4\pi Nz\right] - 2(k_0L)^4\kappa_4^2 - \pi N k_0 L\kappa_4^2 z}{\sqrt{(k_0L)^4\kappa_4^2 - \pi^2N^2z^2}}, \tag{5.195}$$

$$p_\pm(z) = \sqrt{k_0L\kappa_4^2 - (k_0L)^3 - 2\pi Nz \pm 2\mathrm{i}\sqrt{(k_0L)^4\kappa_4^2 - \pi^2N^2z^2}}. \tag{5.196}$$

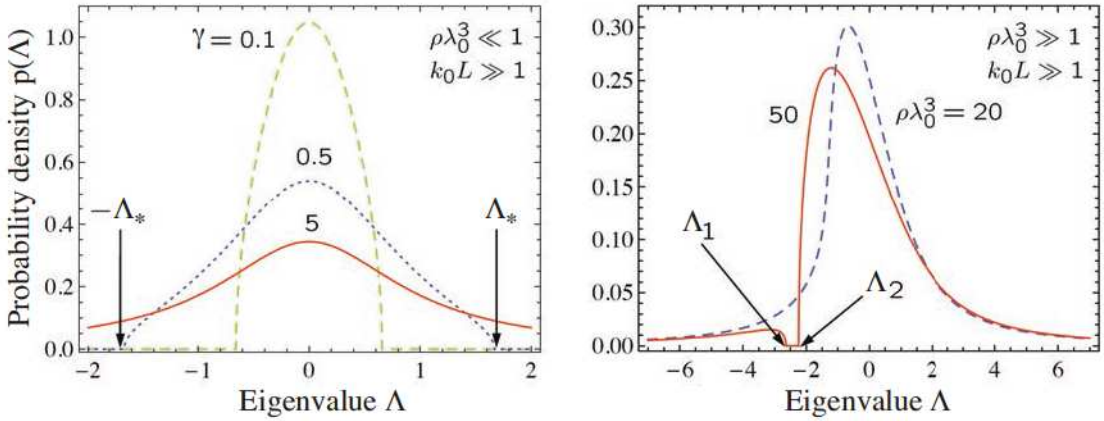

Figure 5.9: Probability density of eigenvalues of a square $N \times N$ Euclidean matrix $C(\omega_0)$ with elements $C_{ij}(\omega_0) = (1-\delta_{ij})\cos(k_0|\mathbf{r}_i - \mathbf{r}_j|)/k_0|\mathbf{r}_i - \mathbf{r}_j|$, where the N points $\mathbf{r}_i$ are randomly chosen inside a 3D cube of side L. The left panel corresponds to the low-density limit and is obtained using Eq. (5.197) with $\gamma = 0.1$, 0.5 and 5. The distributions are symmetric and vanish for $|\Lambda| > \Lambda_*$ with Λ_* given by Eq. (5.198). The right panel illustrates our equation (5.199) obtained in the high-density limit for two densities $\rho\lambda_0^3 = 20$ and 50. For $\rho\lambda_0^3 > 30.3905$ the distribution develops a gap in between Λ_1 and Λ_2 given by Eq. (5.200) and (5.201), respectively.

Eq. (5.193) satisfies $\langle\Lambda\rangle = \mathcal{R}(0) = 0$ and, in the limit $k_0L \gg 1$, $\gamma = \mathrm{Var}\Lambda = \mathcal{R}'(0) = \pi N/\kappa_4(k_0L)^2$, so that $\kappa_4 \simeq \pi/2.8 \simeq 1.12$ $(= \kappa_1 = \kappa_2)$. Although the two approximations (5.191) and (5.193) for the $\mathcal{R}$-transform look quite different, they may exhibit universal features in some limits.

Let us consider the low-density limit of Eq. (5.191), $\rho\lambda_0^3 \ll 1$. For large box size $L \gg 1/k_0$ the arguments of arctan functions in Eq. (5.191) are close to $-\mathrm{i}$. They can be thus expanded in series in the vicinity of this point. In the resulting expression we take the limits of $\rho\lambda_0^3 \to 0$ and $\rho\lambda_0^3/\gamma \sim 1/k_0L \to 0$ to obtain

$$\mathcal{R}(z) = -\frac{1}{\pi}\ln\frac{1-\frac{\pi}{2}\gamma z}{1+\frac{\pi}{2}\gamma z}, \quad \rho\lambda_0^3 \ll 1. \tag{5.197}$$

This expression has two important limits. For $\gamma \ll 1$ we find $\mathcal{R}(z) = \gamma z$ which is the $\mathcal{R}$-transform of the Wigner semi-circle law (5.122). In the opposite limit of $\gamma \gg 1$ we have $\mathcal{R}(z) = -\mathrm{i}$, which corresponds to the Cauchy distribution $p(\Lambda) = 1/[\pi(1+\Lambda^2)]$. Eq. (5.197) therefore describes a transition from the Wigner semi-circle law at $\gamma \ll 1$ to the Cauchy distribution at $\gamma \to \infty$. The eigenvalue distribution following from Eq. (5.197) is always symmetric with respect to $\Lambda = 0$ and vanishes for $|\Lambda| > \Lambda_*$ (see the left panel of Fig. 5.9). The latter can be found by using Eq. (5.39):

$$\Lambda_* = \sqrt{\gamma\left(1+\frac{\pi^2}{4}\gamma\right)} + \frac{2}{\pi}\mathrm{arccoth}\sqrt{1+\frac{4}{\pi^2\gamma}}. \tag{5.198}$$

This equation simplifies to $\Lambda_* = 2\sqrt{\gamma}$ for $\gamma \ll 1$ and to $\Lambda_* = \frac{\pi}{2}\gamma$ for $\gamma \gg 1$.

Another important limit of Eq. (5.191) is that of high density $\rho\lambda_0^3 \gg 1$ of points in a large box $L \gg 1/k_0$. In this limit, the arguments of arctan functions in Eq. (5.191) are

small and we can put $\arctan x \simeq x$. Taking the limit of $\rho\lambda_0^3/\gamma \sim 1/k_0L \to 0$, we then obtain

$$\mathcal{R}(z) = \mathrm{i}\sqrt{1 + \frac{\rho\lambda_0^3}{2\pi^2}z}, \quad \rho\lambda_0^3 \gg 1. \tag{5.199}$$

For $\rho\lambda_0^3$ below a critical value $(\rho\lambda_0^3)_c = 30.3905$, the eigenvalue distribution corresponding to Eq. (5.199) is asymmetric but bell-shaped, similarly to the case of low density. For $\rho\lambda_0^3 > (\rho\lambda_0^3)_c$, however, the distribution develops a gap: $p(\Lambda) = 0$ for $\Lambda_1 < \Lambda < \Lambda_2$, where $\Lambda_{1,2} = \mathcal{B}(z_{1,2})$ with $\mathcal{B}(z)$ being the Blue function of the matrix C and $z_{1,2}$ solutions of $\mathcal{B}'(z) = 0$ (see the right panel of Fig. 5.9). In the limit of $\rho\lambda_0^3 \gg (\rho\lambda_0^3)_c$ we have

$$\Lambda_1 \simeq -\frac{\rho\lambda_0^3}{2\pi^2} - \frac{\pi^2}{2\rho\lambda_0^3}, \tag{5.200}$$

$$\Lambda_2 \simeq -\frac{3}{2\pi^{2/3}}(\rho\lambda_0^3)^{1/3} + \frac{\pi^{2/3}}{2(\rho\lambda_0^3)^{1/3}} + \frac{\pi^2}{6\rho\lambda_0^3}. \tag{5.201}$$

Note finally that the result (5.199), valid in the limit of infinite volume $k_0L \to \infty$, can also be recovered by approximating $f(\mathbf{k}_\alpha)$ in Eq. (5.187) by the Fourier transform $f_0(\mathbf{k}_\alpha) = 4\pi/k_0(k_\alpha^2 - k_0^2)$ of $f(\Delta\mathbf{r})$.[21] Inserting the latter into Eq. (5.190), we readily obtain the solution (5.199), that depends only on the density $\rho\lambda_0^3$, as expected when translational invariance is preserved (see the discussion in section 5.5.2).

In Fig. 5.10 we compare $p(\Lambda)$ following from Eqs. (5.191) and (5.193) with the results of numerical simulations. We find the resolvent $g(z)$ by solving the equation $1/g(z) + \mathcal{R}[g(z)] = z$ numerically. When $\gamma \to 0$, the distribution $p(\Lambda)$ tends to the Wigner semi-circle law. In contrast, for large $\gamma > 1$ it resembles a Cauchy distribution. A good agreement between numerical results and Eqs. (5.191) and (5.193) is observed not only for $\gamma < 1$ (similarly to the case of sinc matrix in section 5.7) but for $\gamma > 1$ as well. The agreement is even better for the approximation (5.193) than for (5.191) (green dot-dashed lines are almost undistinguishable from numerical results). Note that in contrast to the Marchenko-Pastur law (5.171) parameterized by a single parameter γ, the $\mathcal{R}$-transform (5.191) or (5.193) and the corresponding probability distribution depend on two parameters γ and $\rho\lambda_0^3$. At densities $\rho\lambda_0^3 \gtrsim 30$, both expressions (5.191) and (5.193) reduce to (5.199). The corresponding probability distribution develops a gap (see Fig. 5.9) that is not present in numerical results (not shown). Interestingly, this gap in the probability distribution appears at the same density $\rho\lambda_0^3 \approx 30$ for all γ. In order to find out whether this gap is an artefact of our approximations for $\mathcal{R}(z)$, we propose to solve Eq. (5.115) exactly in the eigenbasis of the operator $\hat{T}$.

[21] This amounts to replacing $w(x, y, z)$ by 1 in Eq. (5.187).

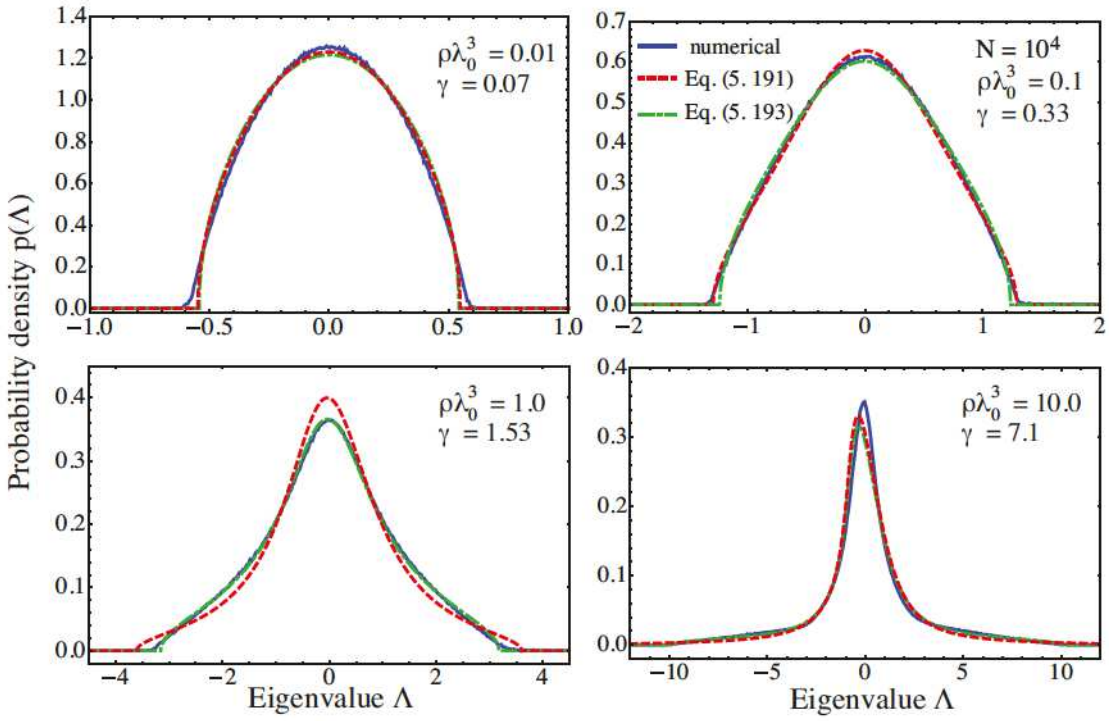

Figure 5.10: Probability density of eigenvalues of a square $N \times N$ Euclidean matrix C with elements $C_{ij} = (1-\delta_{ij})\cos(k_0|\mathbf{r}_i - \mathbf{r}_j|)/k_0|\mathbf{r}_i - \mathbf{r}_j|$, where the N points $\mathbf{r}_i$ are randomly chosen inside a 3D cube of side L. Numerical results (blue solid lines) obtained for $N = 10^4$ after averaging over 10 realizations are compared to Eqs. (5.191) (red dashed lines) and (5.193) (green dot-dashed lines) with $\gamma = 2.8N/(k_0L)^2$ for several densities ρ of points ($\lambda_0 = 2\pi/k_0$).

5.8.2 Exact solution for the eigenvalue density

Proceeding as in section 5.7.2, we now assume that the N points $\mathbf{r}_i$ are randomly distributed in a sphere of radius $R \gg k_0^{-1}$, so that the variance (5.132) reads:

$$\begin{aligned}
\mathrm{Var}\Lambda = \langle\Lambda^2\rangle &= \frac{6N}{(k_0R)^2}\int_0^1 \mathrm{d}x \cos\left(2k_0Rx\right)^2 s(x), \\
&= \frac{9N}{(k_0R)^2}\frac{32(k_0R)^4 + 8(k_0R)^2 - 4k_0R\sin(4k_0R) - \cos(4k_0R) + 1}{256(k_0R)^4}, \quad (5.202)\\
&\simeq \frac{9N}{8(k_0R)^2} \equiv \gamma. \quad (5.203)
\end{aligned}$$

In order to solve Eq. (5.127), we have to find the eigenvalues μ_α of the operator $\hat{T}$, solutions of the integral equation

$$\rho\int_V \mathrm{d}^3\mathbf{r}'\frac{\cos(k_0|\mathbf{r}-\mathbf{r}'|)}{k_0|\mathbf{r}-\mathbf{r}'|}\mathcal{R}_\alpha(\mathbf{r}') = \mu_\alpha\mathcal{R}_\alpha(\mathbf{r}). \quad (5.204)$$

For this purpose, we make use of the decomposition [180]

$$\frac{\cos(k_0|\mathbf{r}-\mathbf{r}'|)}{k_0|\mathbf{r}-\mathbf{r}'|} = -4\pi \sum_{l=0}^{\infty} \sum_{m=-l}^{l} j_l\left[k_0 \min(r,r')\right] n_l\left[k_0 \max(r,r')\right] Y_{lm}(\theta,\phi) Y_{lm}(\theta',\phi')^*, \tag{5.205}$$

where θ and ϕ are the polar and azimuthal angles of the vector $\mathbf{r}$, respectively, Y_{lm} are spherical harmonics, and j_l and n_l are spherical Bessel functions of the first and second kind, respectively. Inserting Eq. (5.205) into Eq. (5.204), and using standard properties of spherical harmonics and spherical Bessel functions [182], it is easy to show that the eigenvectors of $\hat{T}$ are necessarily of the form

$$\mathcal{R}_\alpha(\mathbf{r}) = \mathcal{R}_{lmp}(\mathbf{r}) = \mathcal{A}_{lp} j_l(\kappa_{lp} r) Y_{lm}(\theta,\phi), \tag{5.206}$$

where the coefficients κ_{lp} obey

$$\frac{\kappa_{lp}}{k_0} = \frac{j_l(\kappa_{lp}R)}{j_{l-1}(\kappa_{lp}R)} \frac{n_{l-1}(k_0R)}{n_l(k_0R)}. \tag{5.207}$$

Integer p labels the different solutions of this equation for a given l. κ_{lp} are either real or imaginary numbers, and the corresponding eigenvalues

$$\mu_\alpha = \mu_{lp} = \frac{\rho\lambda_0^3}{2\pi^2} \frac{1}{(\kappa_{lp}/k_0)^2 - 1} \tag{5.208}$$

are $(2l+1)$-times degenerate ($m \in [-l, l]$). In terms of the solutions μ_{lp} of Eqs. (5.207) and (5.208), Eq. (5.127) reads finally

$$z = \frac{1}{g(z)} + \frac{g(z)}{N} \sum_l \sum_p \frac{(2l+1)\mu_{lp}^2}{1 - g(z)\mu_{lp}}. \tag{5.209}$$

κ_{lp}, μ_{lp}, $g(z)$ and $p(\Lambda)$ are found numerically.

Figs. 5.11(a) and 5.12(a) show that Eqs. (5.191) and (5.209) are in good agreement with the results of numerical diagonalization for all γ and for $\rho\lambda_0^3 \lesssim 10$. As expected, the exact solution (5.209) is closer to numerical data than the approximation (5.191). Furthermore, two distinct phenomena are observed. First, in the small sample limit ($R/\lambda_0 \lesssim 1$), the eigenvalue distribution splits into disjoint domains [see Fig. 5.12(a)]. As it was the case for the sinc matrix in section 5.7.2, each eigenvalue μ_{lp} of the operator $\hat{T}$ contributes to a part of the spectrum in the vicinity of $\Lambda \simeq \mu_{lp}$. If eigenvalues μ_{lp} are far from each other, the different parts do not overlap and a splitting is observed in $p(\Lambda)$. This effect can be observed in the tails of $p(\Lambda)$ in Fig. 5.12(a), and is perfectly captured by Eq. (5.209). However, another mechanism affects notably the distribution $p(\Lambda)$ at high density $\rho\lambda_0^3 \gtrsim 30$. In the previous section we saw that $p(\Lambda)$ following from Eq. (5.191) develops a gap for $\rho\lambda_0^3 > (\rho\lambda_0^3)_c = 30.3905$: $p(\Lambda) = 0$ for $\Lambda_1 < \Lambda < \Lambda_2$ [see the right panel of Fig. 5.9, and the dashed red lines in Fig. 5.12(a)]. This gap is still present in $p(\Lambda)$ following from Eq. (5.209) [solid green lines in Figs. 5.12(a)], but is slightly different from $[\Lambda_1, \Lambda_2]$ because there are solutions μ_{lp} belonging to the interval $[-\rho\lambda_0^3/2\pi^2, 0] \simeq [\Lambda_1, \Lambda_2]$.[22] The latter are enough to fill the gap only for $\rho\lambda_0^3 \lesssim 30$ [see Fig. 5.11(a)]. In contrast, this gap is never observed in numerical simulations, meaning that

[22] Solutions $\mu_{lp} \in [-\rho\lambda_0^3/2\pi^2, 0]$ correspond to $\kappa_{lp} \in i\mathbb{R}$, see Eq. (5.208).

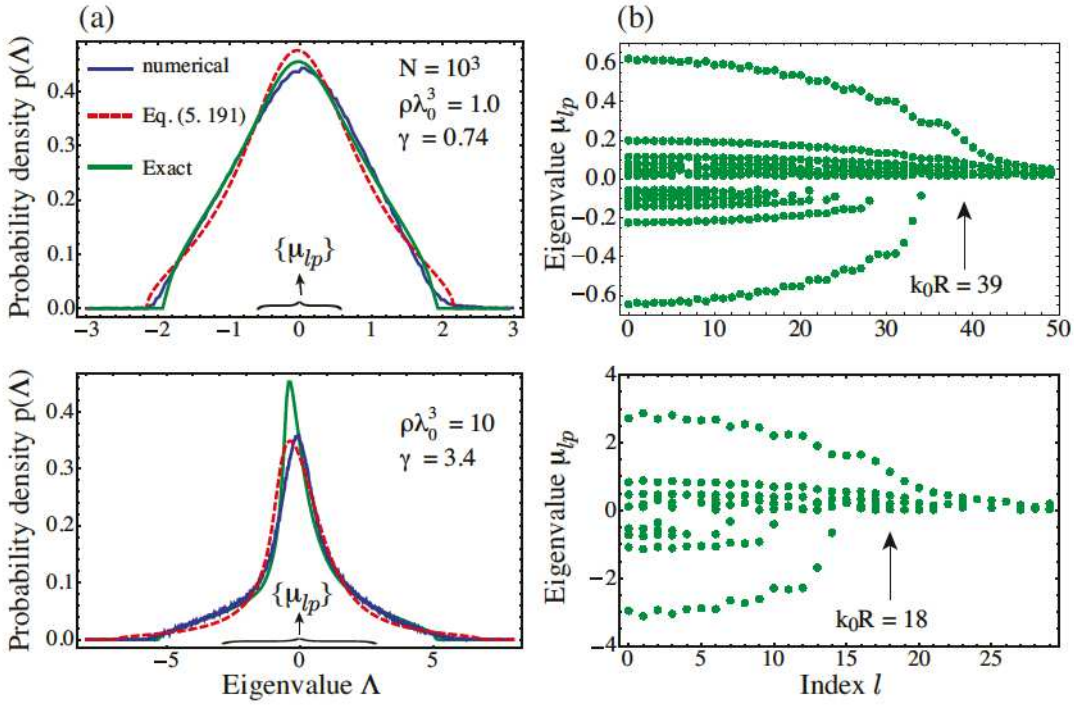

Figure 5.11: (a) Probability density of eigenvalues of the $N \times N$ ERM (5.184), where the N points $\mathbf{r}_i$ are randomly chosen inside a sphere of radius R. Numerical results (blue solid lines) obtained for $N = 10^3$ after averaging over 100 realizations are compared to Eq. (5.191) (red dashed lines), and to Eq. (5.209) (green solid lines), with $\gamma = 9N/8(k_0R)^2$ for several densities ρ of points ($\lambda_0 = 2\pi/k_0$). (b) Eigenvalues $\mu_{l,p}$, given by Eq. (5.208) and used to compute $p(\Lambda)$ from Eq. (5.209) [green solid line in (a)], versus the index l. $\mu_{l,p}$ are non-zero for $l \lesssim k_0R$. The range covered by the eigenvalues μ_{lp} is also indicated in (a) with braces.

our theoretical prediction (5.127) does not describe properly $p(\Lambda)$ for $\Lambda \in [-\rho\lambda_0^3/2\pi^2, 0]$.[23] To understand the origin of this difference, we analyze the degree of localization of the eigenvectors R_n of the matrix (5.184), by computing their inverse participation ratio (IPR):

$$\mathrm{IPR}_n = \frac{\sum_{i=1}^N |R_n(\mathbf{r}_i)|^4}{\left[\sum_{i=1}^N |R_n(\mathbf{r}_i)|^2\right]^2}. \tag{5.210}$$

An eigenvector extended over all N points is characterized by IPR $\sim 1/N$, whereas an eigenvector localized on a single point has IPR $= 1$. IPR_n associated with the eigenvalues Λ_n used to compute $p(\Lambda)$ in Fig. 5.12(a) are represented in Fig. 5.12(b).[24] Our numerical analysis of IPR reveals that three types of states can contribute to the spectrum. At low density $\rho\lambda_0^3 \lesssim 10$, IPR $\simeq 2/N$ for all eigenvectors except eigenvectors that are localized on pairs of points that are very close together, for which IPR $\simeq 1/2$. The

[23]Note also that the eigenvalues density following from Eq. (5.127) compensates for the existence of the gap by larger values of $p(\Lambda)$ near $\Lambda \simeq 0$, to satisfy the normalization condition $\int \mathrm{d}\Lambda p(\Lambda) = 1$ [see the lower panel of Fig. 5.11(a), and Fig. 5.12(a)].

[24]We do not not represent the average $\mathrm{IPR}(\Lambda) = \langle \sum_{n=1}^N \mathrm{IPR}_n\ \delta(\Lambda - \Lambda_n)\rangle / Np(\Lambda)$ in Fig. 5.12(b) because eigenvectors with very different IPR_n and almost the same Λ_n coexist in the the spectrum.

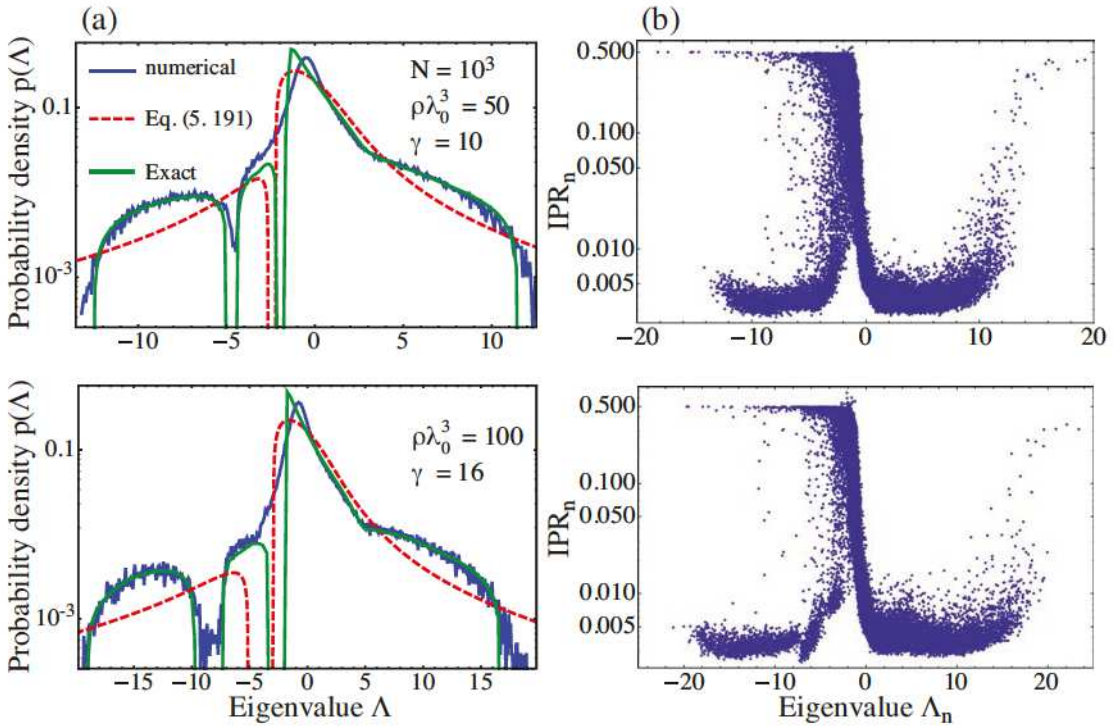

Figure 5.12: (a) Same as Fig. 5.11(a) but for higher densities $\rho\lambda_0^3 = 10$ and 50. For $R/\lambda_0 \lesssim 1$, the probability density $p(\Lambda)$ splits into sectors centered around the eigenvalues μ_{lp} of $\tilde{T}$. (b) Inverse participation ratio IPR_n (5.210) of eigenvectors R_n of the cosc matrix (5.184), versus eigenvalues Λ_n associated to R_n. Λ_n are used to compute the numerical spectrum $p(\Lambda)$ in (a) (solid blue line).

latter correspond to eigenvalues roughly equal to those of the matrix (5.184) for $N = 2$, $\Lambda = \pm C_{12}$. They are not described by our Eq. (5.127). The lack of these states in our theory can be traced back to he assumption of statistical independence of the matrix H in the representation $A = HTH^\dagger$ of ERMs (see sections 5.1.3 and 4.4). At large densities, the statistical weight of these states increases[25], and since most of them are associated with eigenvalues $\Lambda_n < 0$ [Fig. 5.12(b)], there is consequently no gap in $p(\Lambda)$ [Fig. 5.12(a)]. Finally, we note that IPR starts to grow in the vicinity of $\Lambda = 0$ for $\rho\lambda_0^3 \gtrsim 10$ [Fig. 5.12(b)]. Unfortunately, the part of the spectrum corresponding to those localized states almost overlaps with the one associated with states localized on pairs (or small cluster) of points. Hence, it is not very clear from Fig. 5.12(b) that two types of localized states coexist in the spectrum. Interestingly, such a distinction is much easier to make for non-Hermitian matrices, that have eigenvalues distributed in the complex plane and not on the real axis. Inspired by the analysis of localization signatures in the properties of the non-Hermitian Green's matrix performed in chapter 6, we believe that some states in the vicinity of $\Lambda = 0$, with IPR < 0.5, are localized due to disorder, and not simply because they are associated to clusters of points behaving as small 'cavities' independent of their environment. Understanding the way in which the two types of localized states influence each other requires a deeper analysis.

[25]More precisely, only the weight of the 'lower branch' $-C_{12}$ increases. For further discussion of this effect, we refer the reader to chapter 6.

In conclusion, the eigenvalue density of the cosc matrix (5.184) following from Eq. (5.209) is in good agreement with the numerical simulations for any γ (exhibiting, in the limit $\rho\lambda_0^3 \ll 1$, a transition from the Wigner semicircle law for $\gamma \ll 1$ to the Cauchy distribution for $\gamma \gg 1$), for any $k_0 R$ (exhibiting several splittings around the eigenvalues $\mu_l p$ of the operator $\hat{T}$ for $R/\lambda_0 \lesssim 1$), and for $\rho\lambda_0^3 \lesssim 30$. At large densities ($\rho\lambda_0^3 \gtrsim 30$), Eq. (5.209) predicts the existence of a gap (different from those appearing at $R/\lambda_0 \lesssim 1$), that is absent in numerical simulations because of states localized on clusters of points and associated with eigenvalues lying in the gap. These states are not described by our theory, and exist *a priori* for any ERM $A_{ij} = f(\mathbf{r}_i, \mathbf{r}_j)$. However, their effect on the shape of $p(\Lambda)$ very much depends on the function f. In the case of the sinc matrix (5.163), for example, all these states accumulate near $\Lambda = 0$, and therefore do not disturb the spectrum $p(\Lambda)$ too much even at high densities [see Fig. 5.8(a)].

5.9 Work in progress and perspectives

At the time of writing this thesis, we have in mind several extensions of the results presented in this chapter. We would like to mention them briefly.

The main result of this chapter are Eqs. (5.115) and (5.118) that apply to any ERM $A_{ij} = f(\mathbf{r}_i, \mathbf{r}_j)$ as long as the variable z belongs to the holomorphic domain of the resolvent $g(z)$. In particular, Eq. (5.115) is useful to compute the density of eigenvalues $p(\Lambda)$ of Hermitian ERMs. We applied the latter to the matrices $\mathrm{Re}G(\omega_0)$ and $\mathrm{Im}G(\omega_0)$, where $G(\omega_0)$ is the free-space Green's matrix that appears in problems of wave propagation in three-dimensional random media. A natural and straightforward extension of this study is to consider the same matrices but for propagation in two- and one- dimensional space. This modifies not only the finite region V of Euclidean space where points $\mathbf{r}_i$ are randomly distributed but also the deterministic function f of position of pairs of points. A second straightforward extension is to use Eq. (5.115) for others ERMs that appear in various physical problems. We can mention the study of RKKY interaction described by the ERM (2.85), or the relaxation in glasses described by an ERM $A_{ij} = e^{-|\mathbf{r}_i - \mathbf{r}_j|/\xi}$, recently studied in the low density limit [155].

Eq. (5.115) was derived thanks to the representation $A = HTH^\dagger$ by assuming uncorrelated disorder (uncorrelated $\mathbf{r}_i$). If disorder exhibits spatial correlations, the statistics of the matrix H is modified. Interestingly, it seems feasible to include spatial correlations in this representation — *e.g.*, by taking the covariance matrix of the columns of H different from identity — inasmuch as results exist in the literature for correlated Wishart matrices $HH^\dagger$ [143, 159, 171]. The problem then reduces to the generalization of the latter to the case where T is different from identity.

A great advantage of the representation $A = HTH^\dagger$ is that more advanced quantities than $p(\Lambda)$ can be calculated without much extra effort. For example, imagine we are interested in the mean square fluctuation of a physical quantity $q(A)$ defined by the trace of some function of A:

$$\langle q(A)^2 \rangle - \langle q(A) \rangle^2 = \int \mathrm{d}\Lambda \mathrm{d}\Lambda' p_c(\Lambda, \Lambda') q(\Lambda) q(\Lambda'), \tag{5.211}$$

with $p_c(\Lambda, \Lambda')$ the connected two-point correlation function:

$$p_c(\Lambda, \Lambda') = \frac{1}{N^2} \left\langle \sum_{n=1}^{N} \sum_{n'=1}^{N} \delta(\Lambda - \Lambda_n) \delta(\Lambda' - \Lambda_{n'}) \right\rangle_c , \tag{5.212}$$

where $\langle xy\rangle_c = \langle xy\rangle - \langle x\rangle\langle y\rangle$ for any x, y. $p_c(\Lambda, \Lambda')$ can be computed from the two-point resolvent

$$g_c(z, z') = \frac{1}{N^2}\left\langle \mathrm{Tr}\frac{1}{z-A}\mathrm{Tr}\frac{1}{z'-A}\right\rangle_c, \tag{5.213}$$

$$= \frac{1}{N^2}\partial_z\partial_{z'}\left\langle \mathrm{Tr}\log(z-A)\mathrm{Tr}\log(z'-A)\right\rangle_c, \tag{5.214}$$

invoking the relation [183]:

$$p_c(\Lambda, \Lambda') = -\frac{1}{4\pi^2}\left[g_c(+,+) + g_c(-,-) - g_c(+,-) - g_c(-,+)\right], \tag{5.215}$$

where we introduced the shorthand notation $g_c(\pm,\pm) = g_c(\Lambda \pm i\epsilon, \Lambda' \pm i\epsilon')$. Using an elegant diagrammatic approach, Brezin and Zee showed in Ref. [184] that $g_c(z, z')$ can be expressed as

$$g_c(z, z') = -\frac{1}{N^2}\partial_z\partial_{z'}\log\left[1 - U(z, z')g(z)g(z')\right], \tag{5.216}$$

where $U(z, z')$ is the irreducible vertex that contains the sum of all irreducible diagrams contained in the expansion of $g_c(z, z')$.[26] The authors also showed with simple arguments that $U(z, z')$ for the Wigner-Dyson ensemble (5.40) is given by [172, 184]

$$U_{WD}(z, z') = \frac{1}{g(z)g(z')} + \frac{g(z) - g(z')}{z - z'}. \tag{5.217}$$

For ERMs $A = HTH^\dagger$, by applying the diagrammatic method developed in section 5.5.3 it is quite easy to find $U(z, z')$ in the limit of large N where only planar rainbow-like diagrams survive. We obtain

$$U(z, z') = \frac{1}{N^2}\mathrm{Tr}\left[\frac{\hat{T}^2}{\left[1 - g(z)\hat{T}\right]\left[1 - g(z')\hat{T}\right]}\right], \tag{5.218}$$

where $g(z)$ is the solution of Eq. (5.115). Inserting Eq. (5.218) into Eq. (5.216) gives us finally the two-point correlation function (5.215).

Last but not least, we mentioned at the end of section 5.3.4 our interest in developing the very intuitive Dyson gas picture for ERMs. In a nutshell, this picture expresses that eigenvalues Λ_n behave as a Coulomb gas submitted to a one-body potential determined by $P(A)$. On the one hand, finding $P(\{\Lambda_n\})$ for $A = HTH^\dagger$ with i.i.d. elements $H_{i\alpha}$ would give us the one-body potential V_1 to which eigenvalues Λ_n are submitted; it also would be useful to calculate n-point correlation functions. On the other hand, the Dyson gas picture could help us to go beyond the assumption of independent $H_{i\alpha}$. Our reasoning is based on the following observations: 1) we briefly saw in the previous section that an important effect that we neglect with the latter hypothesis is the existence of eigenvectors of the $N \times N$ matrix A localized on clusters of very close points; 2) these eigenvectors are associated with eigenvalues that seem to distribute on the real axis as

[26] It is somewhat surprising that the proof of the relation between g_c and U for random matrices requires a lengthy demonstration [184], while in the scattering theory studied in section 4.5 the relation between the analogous quantities $\langle \mathcal{T}^+ \otimes \mathcal{T}^-\rangle - \langle \mathcal{T}^+\rangle \otimes \langle \mathcal{T}^-\rangle$ and U directly results from simple definitions, see Eqs. (4.98) and (4.100).

if they were submitted to a one-body potential V_2 similar to the one experienced by the smallest eigenvalue of A for $N = 2$. Hence, a possible idea to go beyond the assumption of independent $H_{i\alpha}$ would be to extract the potential V_2 from the case $N = 2$, and add it to V_1. Using the mean-field approximation of section 5.3.3, we then could find the modified distribution $p(\Lambda)$.

Chapter 6

Non-Hermitian Euclidean random matrix theory

Although the majority of works in RMT concern Hermitian random matrices, non-Hermitian random matrices have also attracted considerable attention [177, 178, 185–191]. They can be used to model such physical phenomena as scattering in dissipative or open systems [192–195], dynamics of neural networks [196, 197], diffusion in random velocity fields [198], or chiral symmetry breaking of the QCD Dirac operator [199, 200].

In contrast to Hermitian matrices, the eigenvalues of non-Hermitian matrices are not constrained to lie on the real axis and may invade the complex plain. Consequently, various methods developed for Hermitian matrices and based on the powerful constraints of analytic function theory are no longer applicable and require non-trivial modifications [177, 178, 186–188, 191].

Most of the literature on random non-Hermitian matrices has focused on Gaussian randomness. A paradigmatic example is the ensemble of $N \times N$ matrices A generated with the probability distribution $P(A) = C_N e^{-N \mathrm{Tr} AA^\dagger}$. Ginibre showed in 1965 that, in the limit $N \to \infty$, the eigenvalues of A are uniformly distributed within a disk of radius unity on the complex plane [201]. Twenty years later, Girko generalized this result to matrix elements A_{ij} that are i.i.d. with zero mean and variance $1/N$ [202]. This is commonly referred to as Girko's law. In this chapter we would like to tackle the problem of computing the density of eigenvalues of matrices that break away from this law: the non-Hermitian Euclidean random matrices (ERMs). Non-Hermitian ERMs appear in such important physical problems as Anderson localization of light [104, 105] and matter waves [106, 107], random lasing [109], propagation of light in nonlinear disordered media [108], and collective spontaneous emission of atomic systems [79, 86, 90]. However, no analytic theory is available to deal with these matrices, and our knowledge about their statistical properties is based exclusively on large-scale numerical simulations [104–109, 181].

This chapter is organized as follows. In section 6.1 we introduce new mathematical objects that allow to generalize the methods developed for Hermitian matrices to the non-Hermitian case. A diagrammatic theory for the density of eigenvalues of an arbitrary non-Hermitian ERM in the limit of large matrix size ($N \to \infty$) is developed in section 6.2. Alternative approaches are also briefly discussed (section 6.3). We illustrate our theory by applying it to the scalar random Green's matrix $G(\omega_0)$ that previously appeared in

Refs. [90, 104–109, 181] but was studied only numerically up to now (sections 6.5.1, 6.5.2, and 6.5.4). The difference between the statistical properties of $G(\omega_0)$ and those of effective Hamiltonians used to analyze open chaotic systems is pointed out in section 6.4, and the signatures of Anderson localization in the statistical properties of $G(\omega_0)$ are investigated in section 6.6. Note finally that we also consider the eigenvalue distribution of the dyadic random Green's matrix $\mathbf{G}(\omega_0)$ in section 6.5.3.

6.1 Foundations of the non-Hermitian random matrix theory

This section is devoted to the introduction of basic definitions and relations useful in the study of non-Hermitian matrices.

6.1.1 Eigenvalue density and Hermitization

Eigenvalues Λ_n of a $N \times N$ non-Hermitian A are, in general, complex. Their density is defined as

$$p(\Lambda) = \frac{1}{N} \left\langle \sum_{n=1}^{N} \delta^{(2)}(\Lambda - \Lambda_n) \right\rangle, \tag{6.1}$$

where we use the shorthand notation $\delta^{(2)}(\Lambda - \Lambda_n) = \delta(\mathrm{Re}\Lambda - \mathrm{Re}\Lambda_n)\delta(\mathrm{Im}\Lambda - \mathrm{Im}\Lambda_n)$. The relation between $p(\Lambda)$ and the resolvent

$$g(z = x + \mathrm{i}y) = \frac{1}{N} \left\langle \mathrm{Tr} \frac{1}{z - A} \right\rangle = \frac{1}{N} \left\langle \sum_{n=1}^{N} \frac{1}{z - \Lambda_n} \right\rangle \tag{6.2}$$

can be found using $\partial_{z^*}(1/z) = \pi\delta(x)\delta(y)$, with the standard notation $\partial_{z^*} = \frac{1}{2}(\partial_x + \mathrm{i}\partial_y)$ for $z = x + \mathrm{i}y$. We obtain:

$$p(\Lambda) = \frac{1}{\pi} \partial_{z^*} g(z) \Big|_{z=\Lambda} \tag{6.3}$$

$$= \frac{1}{2\pi} \left[\partial_x \mathrm{Re} g(z) - \partial_y \mathrm{Im} g(z) \right] \Big|_{z=\Lambda}. \tag{6.4}$$

Note that $\partial_y \mathrm{Re} g(z) = -\partial_x \mathrm{Im} g(z)$ because $p(\Lambda)$ is real. The r.h.s. of Eq. (6.4) vanishes if $g(z)$ obeys the Cauchy-Riemann conditions, *i.e.*, if it is an analytic function of the complex variable z. In general, the eigenvalues Λ_n occupy, on average, a two-dimensional domain $\mathcal{D}$ on the complex plane where $g(z)$ is non-analytic, and $p(\Lambda)$ describes the location and the amount of non-analyticity.

We now recall that the resolvent $g(z)$ can be interpreted as the electric field $\mathbf{g}(z)$ [Eq. (5.44)] created, at point z in the complex plane, by charges ($q = +1$) situated at positions Λ_n. Eq. (6.4) can thus be seen as the Gauss law $p(z) = \nabla_{x,y} \cdot \mathbf{g}(z)/2\pi$. Hence, we readily obtain a new relation between $p(\Lambda)$ and the logarithmic pair-wise repulsion $V^{int}(z)$ defined by $\mathbf{g}(z) = -\nabla_{x,y} V^{int}(z)$ [see Eq. (5.43)]:

$$p(\Lambda) = -\frac{1}{2\pi N} \Delta_{x,y} V^{int}(z) \Big|_{z=\Lambda}, \tag{6.5}$$

where $\Delta_{x,y} = 4\partial_z\partial_{z^*}$ is the Laplacian in the coordinates x and y. Clearly, Eq. (6.5) may be particularly useful within the framework of the Dyson gas model where V^{int} may be related to a one-body potential determined by the probability distribution $P(A)$ (see sections 5.3 and 6.3.1).

Inserting the explicit expression (5.43) of $V^{int}(z)$ into Eq. (6.5), we express $p(\Lambda)$ in an alternative form:

$$p(\Lambda) = \frac{1}{\pi N}\partial_z\partial_{z^*}\left\langle \mathrm{Tr}\ln(z-A)(z^*-A^\dagger)\right\rangle\Big|_{z=\Lambda} \tag{6.6}$$

$$= \frac{1}{\pi N}\partial_z\partial_{z^*}\left\langle \ln\det(z-A)(z^*-A^\dagger)\right\rangle\Big|_{z=\Lambda} \tag{6.7}$$

$$= \frac{1}{\pi N}\lim_{\epsilon\to 0}\partial_z\partial_{z^*}\left\langle \ln\det\left[\mathcal{H}_A(z) - i\epsilon I_{2N}\right]\right\rangle\Big|_{z=\Lambda}, \tag{6.8}$$

where I_{2N} is the $2N\times 2N$ identity matrix and $\mathcal{H}_A$ is the $2N\times 2N$ chiral Hermitian matrix

$$\mathcal{H}_A(z) = \begin{pmatrix} 0 & A-z \\ A^\dagger - z^* & 0 \end{pmatrix}. \tag{6.9}$$

Note that Eq. (6.6) can also be derived from Eq. (6.1) using $\partial_z\partial_{z^*}\ln zz^* = \pi\delta(x)\delta(y)$. Eq. (6.8) is generally used in field-theoretical approaches (section 6.3.2). In addition, since the matrix (6.9) is Hermitian, one can compute its resolvent with well-established Hermitian techniques, from which it is still possible to recover the eigenvalue density of A [188, 191]. This is the so-called 'Hermitization method'. In the following, we will use an alternative method which has various advantages: it is technically slightly simpler, it reveals a relation between $g(z)$ and the correlator of right and left eigenvectors of A, and finally it allows for a generalization of free probability calculus.

6.1.2 Quaternions and the eigenvector correlator

If A is Hermitian, the eigenvalues Λ_n lie, on average, on some intervals (cuts) of the real axis. Therefore, it is possible to reconstruct $g(z)$ by analytic continuation of its series expansion (5.27) performed in the vicinity of $|z|\to\infty$. The eigenvalue distribution $p(\Lambda)$ follows from the discontinuities of $g(z)$ on the real axis [see Eqs. (5.21) and (6.3)]. For a non-Hermitian matrix A however, $g(z)$ loses its analyticity inside the two-dimensional domain $\mathcal{D}$ where Λ_n are concentrated, meaning that $g(z)$ for $z\in\mathcal{D}$ cannot be simply assessed by analytic continuation of its series expansion. A way to circumvent this problem is based on the algebra of quaternions: while $p(\Lambda)$ for an Hermitian A is obtained by approaching the real axis from orthogonal directions (in the complex plane), $p(\Lambda)$ for a non-Hermitian A can be found by approaching two sides of $\mathcal{D}$ from directions 'orthogonal' to the complex plane (in the quaternion space) [177]. Doubling the size of the matrix under study, we now work with a new $2N\times 2N$ matrix,

$$A^D = \begin{pmatrix} A & 0 \\ 0 & A^\dagger \end{pmatrix} \tag{6.10}$$

and a quaternion resolvent matrix,

$$G(Q) = \frac{1}{N}\left\langle \mathrm{Tr}_N \frac{1}{Q\otimes I_N - A^D}\right\rangle. \tag{6.11}$$

The 2×2 matrix Q is an arbitrary quaternion in matrix representation,

$$Q = \begin{pmatrix} a & ib^* \\ ib & a^* \end{pmatrix} = x_0 I_2 + \mathrm{i}\mathbf{x} \cdot \boldsymbol{\sigma}, \tag{6.12}$$

where $\mathbf{x} = (x_1, x_2, x_3)$, $\boldsymbol{\sigma}$ is the triplet of usual Pauli matrices, $a = x_0 + \mathrm{i}x_3$, and $b = x_1 + \mathrm{i}x_2$. Tr_N in Eq. (6.11) denotes the block trace of an arbitrary $2N \times 2N$ matrix X. It is defined by separating X in four $N \times N$ blocks X_{11}, X_{12}, X_{21}, X_{22} and taking the trace of each of the latter separately:

$$\begin{aligned} \mathrm{Tr}_N X &= \mathrm{Tr}_N \begin{pmatrix} X_{11} & X_{12} \\ X_{21} & X_{22} \end{pmatrix} \\ &= \begin{pmatrix} \mathrm{Tr}X_{11} & \mathrm{Tr}X_{12} \\ \mathrm{Tr}X_{21} & \mathrm{Tr}X_{22} \end{pmatrix}. \end{aligned} \tag{6.13}$$

Algebraic properties of the quaternions are useful to generalize the free probability theory to non-Hermitan matrices (see section 6.3.3). However, if we wish to compute $g(z)$ by a diagrammatic approach, it is sufficient to consider the quaternion $Q = Z_\epsilon$:

$$Z_\epsilon = \begin{pmatrix} z & i\epsilon \\ i\epsilon & z^* \end{pmatrix}. \tag{6.14}$$

The generalized resolvent matrix $G(Z_\epsilon)$ is then safely equal to its series expansion in $1/Z_\epsilon$ [177, 186, 203]. By evaluating the block trace in Eq. (6.11) explicitly, one readily finds that

$$G(Z_\epsilon) = \begin{pmatrix} G_{11}^\epsilon & G_{12}^\epsilon \\ G_{12}^\epsilon & G_{11}^{\epsilon *} \end{pmatrix}, \tag{6.15}$$

with

$$G_{11}^\epsilon = \frac{1}{N} \left\langle \mathrm{Tr} \frac{z^* - A^\dagger}{(z - A)(z^* - A^\dagger) + \epsilon^2} \right\rangle, \tag{6.16}$$

$$G_{12}^\epsilon = -\frac{i\epsilon}{N} \left\langle \mathrm{Tr} \frac{1}{(z - A)(z^* - A^\dagger) + \epsilon^2} \right\rangle, \tag{6.17}$$

so that

$$\lim_{\epsilon \to 0} G(Z_\epsilon) = \begin{bmatrix} g(z) & c(z) \\ c(z) & g(z)^* \end{bmatrix}. \tag{6.18}$$

Interestingly, the off-diagonal elements $c(z) = \lim_{\epsilon \to 0} G_{12}^\epsilon$ yield the correlator of right $|R_n\rangle$ and left $|L_n\rangle$ eigenvectors of A [204, 205]:

$$\mathcal{C}(z) = -\frac{\pi}{N} \left\langle \sum_{n=1}^{N} \langle L_n | L_n \rangle \langle R_n | R_n \rangle \delta^{(2)}(z - \Lambda_n) \right\rangle = N c(z)^2. \tag{6.19}$$

This shows that $c(z)$ must vanish on the boundary $\delta\mathcal{D}$ of the support of the eigenvalue density $\mathcal{D}$. In order to obtain $p(\Lambda)$, we can compute $G(Z_\epsilon)$ at finite $\epsilon \in \mathbb{R}$ (by a diagrammatic or any other approach), then take the limit $\epsilon \to 0$ to extract $g(z)$ from the diagonal elements of (6.18), and finally apply Eq. (6.3).

6.1.3 Bi-orthogonal basis of left and right eigenvectors

For the sake of completeness, we recall here basic properties of right $|R_n\rangle$ and left $|L_n\rangle$ eigenvectors of a non-Hermitian matrix A (or operator $\hat{A}$). By definition,

$$A|R_n\rangle = \Lambda_n|R_n\rangle, \tag{6.20}$$

$$\langle L_n|A = \Lambda_n\langle L_n| \iff A^\dagger|L_n\rangle = \Lambda_n^*|L_n\rangle, \tag{6.21}$$

meaning that $|L_n\rangle$ are the right eigenvectors of $A^\dagger$. Obviously, A and $A^\dagger$ have complex conjugated eigenvalues for $\det(A - \Lambda_n I_n) = 0 = \det(A^\dagger - \Lambda_n^* I_n)$. Besides, $|L_n\rangle$ and $|R_m\rangle$ are necessarily orthogonal because $\langle L_n|A|R_m\rangle = \Lambda_n\langle L_n|R_m\rangle = \Lambda_m\langle L_n|R_m\rangle$. Assuming that the eigenvalues Λ_n are not degenerate, we normalize $|R_n\rangle$ and $|L_n\rangle$ such that:

$$\langle L_n|R_m\rangle = \sum_{i=1}^{N} L_n^{i*} R_m^i = \delta_{nm}, \tag{6.22}$$

Note that $\langle R_n|R_m\rangle \neq \delta_{nm}$. Finally, the following properties hold

$$I_N = \sum_n |R_n\rangle\langle L_n| = \sum_n |L_n\rangle\langle R_n|, \tag{6.23}$$

$$\mathrm{Tr}X = \sum_n \langle L_n|X|R_n\rangle, \tag{6.24}$$

where X is an arbitrary matrix.

6.2 Diagrammatic approach for non-Hermitian ERMs

Our goal is to derive equations for the resolvent $g(z)$ and the correlator $c(z)$ of an arbitrary $N \times N$ non-Hermitian ERM $A_{ij} = f(\mathbf{r}_i, \mathbf{r}_j) = \langle \mathbf{r}_i|\hat{A}|\mathbf{r}_j\rangle$ in the limit of $N \to \infty$. For this purpose, we make use of the representation $A = HTH^\dagger$ introduced in section 5.1.3, with the assumption that H has i.i.d. complex Gaussian entries satisfying the property (5.17). We recall that the Gaussian assumption simplifies diagrammatic calculations but is not essential, contrary to the assumption of independent elements that may limit the applicability of our results at high densities of points ρ (see the discussion in section 5.6.3). Since diagrammatic calculations presented here generalize those performed for Hermitian matrices, it may be helpful to read section 5.5.3 before proceeding further.

6.2.1 Derivation of self-consistent equations

We start by expanding the 2×2 resolvent matrix $G(Z_\epsilon)$ defined by Eqs. (6.11) and (6.14) in series in $1/\mathcal{Z}_\epsilon = (1/Z_\epsilon) \otimes I_N$:

$$G(Z_\epsilon) = \frac{1}{N}\left\langle \mathrm{Tr}_N\left[\frac{1}{\mathcal{Z}_\epsilon} + \frac{1}{\mathcal{Z}_\epsilon} A^D \frac{1}{\mathcal{Z}_\epsilon} + \dots\right]\right\rangle. \tag{6.25}$$

Inasmuch as $H_{i\alpha}$ are i.i.d. Gaussian entries, the result of averaging $\langle \dots \rangle$ over the ensemble of matrices H can be expressed through pairwise contractions (5.17) only. Diagrammatic notations, already introduced in section 5.5.3 to evaluate efficiently the weight of

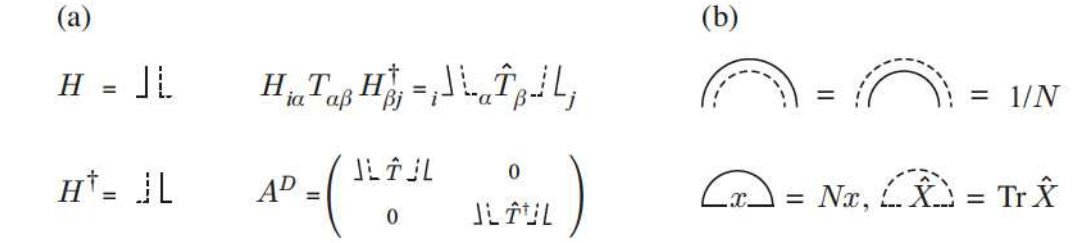

Figure 6.1: (a) Diagrammatic representations of the matrices H, $H^\dagger$, $A = HTH^\dagger$, and A^D. Full and dashed lines propagate in the bases $\{\mathbf{r}_i\}$ and $\{\psi_\alpha\}$, respectively (see section 5.1.3); $\hat{T} = \rho\hat{A}$. (b) Diagrammatic notation for pairwise contractions (5.17) and loop diagrams for any scalar x in the basis $\{\mathbf{r}_i\}$, and for any operator $\hat{X}$ in an arbitrary basis $\{\psi_\alpha\}$.

different terms arising in the calculation, are reproduced in Fig. 6.1(a) for clarity. The 'propagator' $1/Z_\epsilon$ will be depicted by

$$\frac{1}{Z_\epsilon} = \begin{pmatrix} \frac{1}{z} & -\frac{i\epsilon}{|z|^2} \\ -\frac{i\epsilon}{|z|^2} & \frac{1}{z^*} \end{pmatrix} = \begin{pmatrix} \overline{1\ 1} & \overline{1\ 2} \\ \overline{2\ 1} & \overline{2\ 2} \end{pmatrix}. \tag{6.26}$$

Since each contraction (5.17) brings a factor $1/N$, and each loop corresponding to taking the trace of a matrix brings a factor N [see Fig. 6.1(b)], only the planar rainbow-like diagrams, that contain as many loops as contractions, survive in the limit $N \to \infty$. Such diagrams appear, for example, in Fig. 6.2, where we show the beginning of the expansion of the two independent elements of $G(Z_\epsilon)$ defined by Eq. (6.15).

In the standard way, rather than summing the diagrams for the resolvent, we introduce the 2×2 self-energy matrix

$$\Sigma(Z_\epsilon) = Z_\epsilon - G(Z_\epsilon)^{-1} = \begin{pmatrix} \Sigma^\epsilon_{11} & \Sigma^\epsilon_{12} \\ \Sigma^\epsilon_{12} & \Sigma^{\epsilon *}_{11} \end{pmatrix}. \tag{6.27}$$

It is equal to the sum of all one-particle irreducible diagrams contained in

$$Z_\epsilon G(Z_\epsilon) Z_\epsilon = \frac{1}{N}\left\langle \mathrm{Tr}_N \left[A^D + A^D \frac{1}{\mathcal{Z}_\epsilon} A^D + \ldots \right] \right\rangle. \tag{6.28}$$

The first dominant terms that appear in the expansion of the two matrix elements Σ^ϵ_{11} and Σ^ϵ_{12} are represented in Fig. 6.3. In the two series of Fig. 6.3 we recognize, under a pairwise contraction, the matrix elements G^ϵ_{11} and G^ϵ_{12} depicted in Fig. 6.2, as well as the two operators $\hat{\Sigma}^\epsilon_{11}$ and $\hat{\Sigma}^\epsilon_{12}$ defined in Fig. 6.4. Equations obeyed by the operators

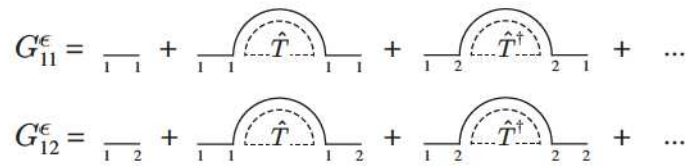

Figure 6.2: Diagrammatic expansion of the two independent elements of the matrix $G(Z_\epsilon)$.

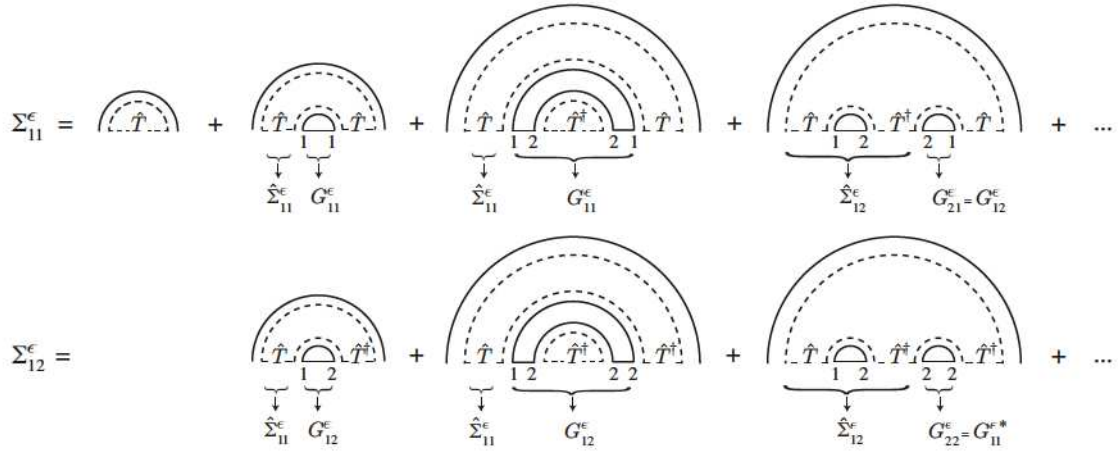

Figure 6.3: Diagrammatic expansion of the two independent elements of the self-energy $\Sigma(Z_\epsilon)$. Braces with arrows denote parts of diagrams that are beginning of diagrammatic expansions of the quantities which the arrows point to.

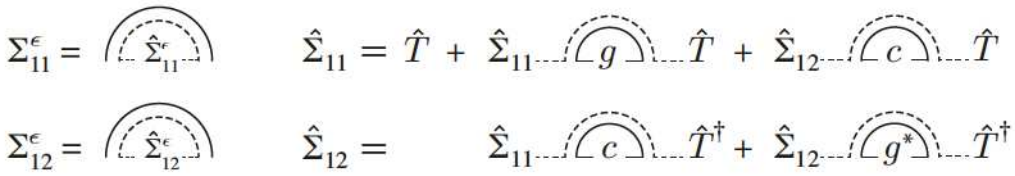

Figure 6.4: The elements Σ^ϵ_{11} and Σ^ϵ_{12} of the matrix $\Sigma(Z_\epsilon)$ can be written as traces of operators $\hat{\Sigma}^\epsilon_{11}$ and $\hat{\Sigma}^\epsilon_{12}$: $\Sigma^\epsilon_{11} = \mathrm{Tr}\hat{\Sigma}^\epsilon_{11}/N$ and $\Sigma^\epsilon_{12} = \mathrm{Tr}\hat{\Sigma}^\epsilon_{12}/N$. Operators $\hat{\Sigma}_{11} = \lim_{\epsilon\to 0^+}\hat{\Sigma}^\epsilon_{11}$ and $\hat{\Sigma}_{12} = \lim_{\epsilon\to 0^+}\hat{\Sigma}^\epsilon_{12}$ obey coupled equations, where $g = \lim_{\epsilon\to 0^+} G^\epsilon_{11}$ and $c = \lim_{\epsilon\to 0^+} G^\epsilon_{12}$ [see Eq. (6.18)].

$\hat{\Sigma}_{11} = \lim_{\epsilon\to 0^+}\hat{\Sigma}^\epsilon_{11}$ and $\hat{\Sigma}_{12} = \lim_{\epsilon\to 0}\hat{\Sigma}^\epsilon_{12}$ are obtained after summation of all planar rainbow diagrams in the expansion of Fig. 6.3 and taking the limit $\epsilon \to 0^+$.[1] The diagrammatic representation of these equations is shown in Fig. 6.4. Applying 'Feynman' rules defined in Fig. 6.1(b), we obtain:

$$\hat{\Sigma}_{11} = (1 + g\,\hat{\Sigma}_{11} + c\,\hat{\Sigma}_{12})\hat{T}, \tag{6.29}$$

$$\hat{\Sigma}_{12} = (c\,\hat{\Sigma}_{11} + g^*\,\hat{\Sigma}_{12})\hat{T}^\dagger, \tag{6.30}$$

where $\hat{T} = \rho\hat{A}$. After some algebra[2], $\Sigma_{11} = \mathrm{Tr}\hat{\Sigma}_{11}/N$ and $\Sigma_{12} = \mathrm{Tr}\hat{\Sigma}_{12}/N$ can be expressed as:

$$\Sigma_{11} = \frac{1}{N}\mathrm{Tr}\frac{(1 - g^*\hat{T}^\dagger)\hat{T}}{(1 - g^*\hat{T}^\dagger)(1 - g\hat{T}) - c^2\hat{T}^\dagger\hat{T}}, \tag{6.31}$$

$$\Sigma_{12} = \frac{c}{N}\mathrm{Tr}\frac{\hat{T}^\dagger\hat{T}}{(1 - g^*\hat{T}^\dagger)(1 - g\hat{T}) - c^2\hat{T}^\dagger\hat{T}}. \tag{6.32}$$

[1] As usual in such a procedure, summation must be performed before taking the limit $\epsilon \to 0$. Hence, the off-diagonal element of the propagator $1/Z_\epsilon$ gives rise to non-vanishing terms after summation, although it is zero in the limit $\epsilon \to 0$.

[2] Although $[\hat{T}, \hat{T}^\dagger] \neq 0$, this calculation is easily performed using cyclic permutations under the trace operator.

Furthermore, as follows from Eq. (6.18) and the definition (6.27) of the self-energy matrix, g and c are simply related to Σ_{11} and Σ_{12} by

$$\begin{bmatrix} g(z) & c(z) \\ c(z) & g(z)^* \end{bmatrix} = \begin{pmatrix} z - \Sigma_{11} & -\Sigma_{12} \\ -\Sigma_{12} & z^* - \Sigma_{11}^* \end{pmatrix}^{-1}. \tag{6.33}$$

Elimination of the self-energy from Eqs. (6.31), (6.32) and (6.33) leads to two self-consistent equations for the resolvent $g(z)$ and the eigenvector correlator $c(z)$:

$$z = \frac{g^*}{|g|^2 - c^2} + \frac{1}{N}\mathrm{Tr}\frac{(1 - g^*\hat{T}^\dagger)\hat{T}}{(1 - g^*\hat{T}^\dagger)(1 - g\hat{T}) - c^2\hat{T}^\dagger\hat{T}}, \tag{6.34}$$

$$\frac{1}{|g|^2 - c^2} = \frac{1}{N}\mathrm{Tr}\frac{\hat{T}^\dagger\hat{T}}{(1 - g^*\hat{T}^\dagger)(1 - g\hat{T}) - c^2\hat{T}^\dagger\hat{T}}. \tag{6.35}$$

At this final stage, it is convenient to define the following operators

$$\hat{S}_0 = \hat{S}(g) = \frac{\hat{T}}{1 - g\hat{T}}, \tag{6.36}$$

$$\hat{S}_1 = \hat{S}(g + c^2\hat{S}_0^\dagger) = \frac{(1 - g^*\hat{T}^\dagger)\hat{T}}{(1 - g^*\hat{T}^\dagger)(1 - g\hat{T}) - c^2\hat{T}^\dagger\hat{T}}, \tag{6.37}$$

in terms of which Eqs. (6.34) and (6.35) become

$$z = \frac{g^*}{|g|^2 - c^2} + \frac{1}{N}\mathrm{Tr}\hat{S}_1, \tag{6.38}$$

$$\frac{1}{|g|^2 - c^2} = \frac{1}{N}\mathrm{Tr}\hat{S}_1\hat{S}_0^\dagger. \tag{6.39}$$

Because $c(z)$ must vanish on the boundary $\delta\mathcal{D}$ of the support of the eigenvalue density $\mathcal{D}$, equations for $z \in \delta\mathcal{D}$ follow:

$$z = \frac{1}{g} + \frac{1}{N}\mathrm{Tr}\hat{S}_0, \tag{6.40}$$

$$\frac{1}{|g|^2} = \frac{1}{N}\mathrm{Tr}\hat{S}_0\hat{S}_0^\dagger. \tag{6.41}$$

6.2.2 Analysis of self-consistent equations

Equations (6.34), (6.35), (6.40) and (6.41) are the main results of this chapter. An equation for the borderline of the support of the eigenvalue density of a non-Hermitian ERM on the complex plane $z = \Lambda$ follows from Eqs. (6.40) and (6.41) upon elimination of g. The density of eigenvalues Λ inside its support $\mathcal{D}$ can be found by solving Eqs. (6.34) and (6.35) with respect to $g(z)$ and then applying Eq. (6.3).

Our analysis includes the result for Hermitian ERMs as a special case: if A is Hermitian, the support of the eigenvalue density shrinks to a segment on the real axis, meaning that $c(z) = 0$ for $z \in \mathbb{C}\setminus\mathbb{R}$ and Σ is diagonal. Indeed, from Eq. (6.32), $\Sigma_{12} = 0$. Equation (6.40) then allows one to solve for $g(z)$ with $z \in \mathbb{C} \setminus \mathbb{R}$, in agreement with Eq. (5.115) of the previous chapter.

At low density, we already know that, at least in the framework of our representation $A = HTH^\dagger$, the eigenvalue density of any Hermitian ERM obeys the Wigner semicircle

law; see Eq. (5.122).[3] A similar result exists for non-Hermitian ERMs as well. Indeed, using the approximation

$$\hat{S}_1 \simeq \hat{S}_0 \simeq \hat{T} \tag{6.42}$$

valid at low densities, Eqs. (6.40) and (6.41) for the borderline of the eigenvalue domain reduce to

$$\left| z - \frac{1}{N}\mathrm{Tr}\hat{T} \right|^2 = \frac{1}{N}\mathrm{Tr}\hat{T}\hat{T}^\dagger, \tag{6.43}$$

and Eqs. (6.38) and (6.39) for $g(z)$ and $c(z)$ with $z \in \mathcal{D}$ become

$$g(z) = \frac{z^* - \frac{1}{N}\mathrm{Tr}\hat{T}^\dagger}{\frac{1}{N}\mathrm{Tr}\hat{T}\hat{T}^\dagger}, \tag{6.44}$$

$$c(z) = \frac{1}{\frac{1}{N}\mathrm{Tr}\hat{T}\hat{T}^\dagger}\left[\frac{|z - \frac{1}{N}\mathrm{Tr}\hat{T}|^2}{\frac{1}{N}\mathrm{Tr}\hat{T}\hat{T}^\dagger} - 1\right]. \tag{6.45}$$

The term $\mathrm{Tr}\hat{T}/N$ that appears in Eqs. (6.43), (6.44), and (6.45), leads to a shift in the eigenvalue distribution equal to

$$\frac{\mathrm{Tr}\hat{T}}{N} = \frac{\mathrm{Tr}\hat{A}}{V} = \frac{\langle \mathrm{Tr}_N A\rangle}{N} = \langle \Lambda \rangle. \tag{6.46}$$

We assume from here on that $A_{ii} = 0$ $(i = 1, \ldots, N)$, so that, in particular, $\langle \Lambda \rangle = 0$. With this assumption, the term $\mathrm{Tr}\hat{T}\hat{T}^\dagger$ reads:

$$\mathrm{Tr}(\hat{T}\hat{T}^\dagger) = \rho^2 \mathrm{Tr}(\hat{A}\hat{A}^\dagger) = \rho^2 \iint_V \mathrm{d}^d\mathbf{r}\, \mathrm{d}^d\mathbf{r}' \left| f(\mathbf{r}, \mathbf{r}') \right|^2, \tag{6.47}$$

$$= \left\langle \mathrm{Tr}_N(AA^\dagger) \right\rangle = \left\langle \sum_{n=1}^{N}\sum_{m=1}^{N} \Lambda_n \Lambda_m^* \langle L_n | L_m \rangle \langle R_m | R_n \rangle \right\rangle, \tag{6.48}$$

$$\simeq \left\langle \sum_{n=1}^{N} |\Lambda_n|^2 \langle L_n | L_n \rangle \langle R_n | R_n \rangle \right\rangle, \tag{6.49}$$

$$\simeq 2\left\langle \sum_{n=1}^{N} |\Lambda_n|^2 \right\rangle = 2N \left\langle |\Lambda|^2 \right\rangle. \tag{6.50}$$

In Eqs. (6.49) and (6.50) we assumed that, at low densities, $\langle \mathbf{r}_i | L_n \rangle$ and $\langle \mathbf{r}_i | R_n \rangle$ behave as Gaussian random variables. Note that Eq. (6.50) differs from the Hermitian case (5.121) by a factor 2. This is because the eigenvector structure does not come into play in Eq. (5.121). Introducing the shorthand notation

$$\gamma = \frac{\mathrm{Tr}(\hat{T}\hat{T}^\dagger)}{2N} \simeq \langle |\Lambda|^2 \rangle, \tag{6.51}$$

we rewrite Eqs. (6.43), (6.44), and (6.45) as

$$|z|^2 = 2\gamma \quad (z \in \delta\mathcal{D}), \tag{6.52}$$

$$g(z) = \frac{z^*}{2\gamma} \quad (z \in \mathcal{D}), \tag{6.53}$$

$$c(z) = \frac{1}{2\gamma}\left[\frac{|z|^2}{2\gamma} - 1\right] \quad (z \in \mathcal{D}). \tag{6.54}$$

[3] We exclude rare ERMs for which the operator $\hat{T}$ has a small number of non-zero eigenvalues.

This shows that, in the limit $N \to \infty$ and $\rho \to 0$ at fixed γ, the eigenvalues of an arbitrary traceless non-Hermitian ERM are uniformly distributed within a disk of radius $\sqrt{2\gamma}$. Within the disk, $p(\Lambda) = 1/2\pi\gamma$. This is the famous Girko's law mentioned in the introduction of this chapter and first found by Ginibre for the complex Gaussian ensemble [201]. We recover this law because in the limit $N \to \infty$ and $\rho \to 0$, elements of A essentially behave as i.i.d. variables. In that case, $\Sigma_{11} = 0$ and $\Sigma_{12} = c(z)/2\gamma$.

If the ERM is of the form $A_{ij} = f(|\mathbf{r}_i - \mathbf{r}_j|)$, where the vectors $\mathbf{r}_i$ determine positions of N randomly chosen points inside a three-dimensional cube of side L or inside a sphere of radius R, γ is explicitly given by

$$\gamma = \begin{cases} \frac{N}{2} \iiint_{-\infty}^{\infty} \mathrm{d}x\mathrm{d}y\mathrm{d}z \left| f\left(L\sqrt{x^2+y^2+z^2}\right)\right|^2 w(x,y,z) & \text{(cube)} \\ \\ 12N \int_0^1 \mathrm{d}x |f(2Rx)|^2 s(x) x^2 & \text{(sphere)} \end{cases}, \tag{6.55}$$

where $w(x,y,z)$ and $s(x)$ are defined by Eqs. (5.129) and (5.130), respectively.

As was the case for Hermitian ERMs, the solution of Eqs. (6.34), (6.35), (6.40) and (6.41) for a given matrix A can be greatly facilitated by a suitable choice of the basis in which traces appearing in these equations are expressed. In addition to $\{\mathbf{r}\}$ and $\{\mathbf{k}_\alpha\}$, a bi-orthogonal basis of right $|\mathcal{R}_\alpha\rangle$ and left $|\mathcal{L}_\alpha\rangle$ eigenvectors of $\hat{T}$ can be quite convenient. We recall that the right eigenvector $|\mathcal{R}_\alpha\rangle$ obeys

$$\langle \mathbf{r}|\hat{T}|\mathcal{R}_\alpha\rangle = \rho \int_V \mathrm{d}^d\mathbf{r}' f(\mathbf{r},\mathbf{r}')\mathcal{R}_\alpha(\mathbf{r}') = \mu_\alpha \mathcal{R}_\alpha(\mathbf{r}), \tag{6.56}$$

where μ_α is the eigenvalue corresponding to the eigenvector $|\mathcal{R}_\alpha\rangle$. The traces appearing in Eqs. (6.40) and (6.41) can be expressed as

$$\mathrm{Tr}\hat{S}_0 = \sum_\alpha \langle \mathcal{L}_\alpha|\hat{S}_0|\mathcal{R}_\alpha\rangle = \sum_\alpha \frac{\mu_\alpha}{1-g\mu_\alpha}, \tag{6.57}$$

$$\mathrm{Tr}\hat{S}_0\hat{S}_0^\dagger = \sum_{\alpha,\beta} \frac{\mu_\alpha\mu_\beta^* \langle \mathcal{L}_\alpha|\mathcal{L}_\beta\rangle\langle\mathcal{R}_\beta|\mathcal{R}_\alpha\rangle}{(1-g\mu_\alpha)(1-g\mu_\beta)^*}, \tag{6.58}$$

respectively. Technically, the main difference with the study of Hermitian ERMs is that we now have to know the eigenvectors of $\hat{T}$ explicitly [compare Eqs. (6.58) and (5.127)].

6.3 Other approaches

6.3.1 Mapping to the Dyson gas

In this section we extend the mapping to the Dyson gas first discussed for Hermitian matrices (section 5.3) to the non-Hermitian case. Let us first consider the class of non-Hermitian random matrices originally introduced by Ginibre [201]. It is given by complex matrices A with Gaussian probability density:

$$P(A) = C_N e^{-N\mathrm{Tr}AA^\dagger}. \tag{6.59}$$

$P(A)$ is invariant under all unitary transformations, but not under the similarity transformation $A \to SAS^{-1}$ used to diagonalize $A = S^{-1}DS$ (D denotes a diagonal matrix with elements Λ_n, $n = 1\ldots N$). Hence, $P(A)$ depends explicitly on S and not only on

the eigenvalues of A. This feature is the main difference with the Gaussian ensemble (5.1) or the Wigner-Dyson ensemble (5.40). Hermitian matrices drawn from these two latter ensembles can be diagonalized by unitary matrices, so that $P(A)$ depends on Λ_n only. In order to obtain the joint probability density $P(\{\Lambda_n\})$ from Eq. (6.59), we must change variables from A_{ij} to parameters related to eigenvalues and eigenvectors of A. Since $\mathrm{Tr}AA^\dagger$ depends on eigenvectors, the new variables have to be chosen carefully to facilitate further manipulations. The result is the following [137, 201]:

$$P(\{\Lambda_n\}) = C'_N e^{-\beta H^g(\{\Lambda_n\})}, \tag{6.60}$$

$$H^g(\{\lambda_n\}) = N\sum_{n=1}^{N} V^g(\Lambda_n) - \sum_{n<m} \ln|\Lambda_n - \Lambda_m|, \tag{6.61}$$

$$\beta = 2, \quad V^g(z) = \frac{|z|^2}{2}. \tag{6.62}$$

This is the Boltzmann-Gibbs distribution of a Coulomb gas in thermal equilibrium at temperature $T = 1/\beta$. These equations have exactly the same form as Eqs. (5.41) and (5.42). As for Hermitian matrices, the logarithmic pairwise repulsion comes from the Vandermonde-type Jacobian $|\mathcal{V}(\{\Lambda_n\})|^\beta$.

In the limit $N \to \infty$, we can perform coarse-graining of the energy functional H^g [see Eq. (5.54)], and minimize it to obtain the equality

$$-\partial_z V^{int}(z) = N\partial_z V^g(z), \tag{6.63}$$

where $V^{int}(z)$ is the logarithmic pair-wise repulsion (5.43). Eq. (6.63) means that the force $N\partial_z V^g(z)$ experienced by each particle of the gas is compensated by the Coulomb repulsion by all other particles. The eigenvalue distribution (6.5) reads now:

$$p(\Lambda) = \frac{1}{2\pi}\Delta_{x,y} V^g(z)\Big|_{z=\Lambda}. \tag{6.64}$$

Note the difference with the result (5.53) for Hermitian matrices: Eq. (6.64) is local; the shape of the distribution at Λ depends on the profile of V^g in the vicinity of Λ only, while in Eq. (5.53) the shape of $p(\Lambda)$ strongly depends on the boundaries of the distribution, meaning that the influence of V^g on $p(\Lambda)$ is nonlocal. Note also that Eq. (6.64) contains no information about the borderline of the support of eigenvalues. If V^g is simple enough, the borderline can be obtained by the normalization constraint $\int \mathrm{d}\Lambda p(\Lambda) = 1$.[4] For $V^g(z) = |z|^2/2$, we find that the eigenvalues are uniformly distributed [$p(\Lambda) = 1/\pi$] inside a disk of radius 1. This is the celebrated Ginibre's result [201].

Obviously, Eqs. (6.60) and (6.61) apply also to any normal matrix A ($[A, A^\dagger] = 0$) with probability

$$P(A) = C_N e^{-N\mathrm{Tr}\mathcal{V}^g(AA^\dagger)}, \tag{6.65}$$

where $\mathcal{V}^g$ is arbitrary, for A can be diagonalized by a unitary matrix. The one-body potential appearing in Eq. (6.61) is then given by $V^g(z) = \mathcal{V}^g(|z|^2)$. A counter-intuitive result is that solutions (6.60) and (6.61) may completely break down for most of non-Hermitian matrices— *i.e.* for non-Hermitian matrices that are not normal or partially normal [191, 206] — distributed according to (6.65). In Ref. [187], Feinberg and Zee

[4] For complicated cases, the borderline may be found by inspection of Eq. (5.55) that is still valid for non-Hermitian matrices.

proved the 'single-ring theorem'. It stipulates that the shape of the eigenvalue distribution is either a disk or an annulus, whatever polynomial the potential $\mathcal{V}^g$ is. This is clearly in contradiction with what we could expect from Eqs. (6.60) and (6.61), that tell us that the number of domains occupied by the eigenvalues on the complex plain should grow with the number of minima of $V^g(z) = \mathcal{V}^g(|z|^2)$. The polynomial $\mathcal{V}^g \sim AA^\dagger$ that corresponds to the complex Gaussian ensemble (6.59) is actually the only polynomial for which Eqs. (6.60) and (6.61) are valid whatever the matrix A obeying (6.65) is. Remarkably, the authors of [187] also showed that the eigenvalue distribution of A can nevertheless be found from the resolvent of the Hermitian matrix $AA^\dagger$. This resolvent has already been known in the literature for arbitrary polynomial $\mathcal{V}^g$ [187].

As far as ERMs are concerned, comments given at the end of section 5.3.4 for Hermitian matrices still hold for non-Hermtian matrices. We believe that $P(\{\Lambda_n\})$ may be found using the representation $A = HTH^\dagger$, with entries $H_{i\alpha}$ approximated by i.i.d. Gaussian random variables. Although we have not been able to rigorously justify the Dyson gas picture for ERMs, the latter may be helpful to understand qualitatively the eigenvalue distribution obtained by numerical diagonalization. For example, in the study of the Green's matrix $G(\omega_0)$ (section 6.5), we observe that the support $\mathcal{D}$ of $p(\Lambda)$ deforms when the density is increased, going through a transition from a disk-like to an annulus-like shape, and eventually splitting into multiple disconnected domains at high density (see Fig. 6.6). It is difficult to refrain from interpreting such transitions as phase transitions for the Dyson gas due to modifications of a hypothetic one-body potential V^g.

6.3.2 Field representation

Let us now briefly explain how to compute the eigenvalue distribution of a non-Hermitian matrix A in the field-theoretical approach. We start with the expression (6.8) of $p(\Lambda)$, rewritten as:

$$p(\Lambda) = -\frac{1}{\pi N} \lim_{\epsilon\to 0} \partial_z \partial_{z^*} \left\langle \ln \mathcal{Z}^\epsilon(z) \right\rangle \Big|_{z=\Lambda}, \tag{6.66}$$

where we have introduced the partition function

$$\mathcal{Z}^\epsilon = \det \begin{bmatrix} \epsilon I_n & \mathrm{i}(z - A) \\ \mathrm{i}(z^* - A^\dagger) & \epsilon I_n \end{bmatrix}. \tag{6.67}$$

In order to evaluate $\langle \ln \mathcal{Z}^\epsilon(z) \rangle$, we follow the same procedure as in section 5.4, namely, we apply the replica trick,

$$\langle \ln \mathcal{Z}^\epsilon(z) \rangle = \lim_{n\to 0} \frac{\langle \mathcal{Z}^\epsilon(z)^n \rangle - 1}{n}, \tag{6.68}$$

together with the representation

$$\mathcal{Z}^\epsilon(z) \propto \int \mathrm{d}\phi_1 \ldots \mathrm{d}\phi_N e^{-\mathcal{H}(\Phi, z, \epsilon)}, \tag{6.69}$$

$$\mathcal{H}(\Phi, z, \epsilon) = \sum_{i=1}^N \phi_i^\dagger \left(\epsilon I_2 + \mathrm{i}x\sigma_x - \mathrm{i}y\sigma_y\right) \phi_i - \mathrm{i} \sum_{i,j=1}^N \phi_i^\dagger \left(A_{ij}^h \sigma_x - A_{ij}^s \sigma_y\right) \phi_i, \tag{6.70}$$

where the N fields ϕ_i are pairs of complex variables, σ_x and σ_y are Pauli matrices, $z = x + \mathrm{i}y$, and we have written $A = A^h + \mathrm{i}A^s$, with A^h and A^s Hermitian matrices.

This representation combined with the cavity method was used in the recent literature [207] to analyze the eigenvalue distribution of non-Hermitian sparse matrices. A slightly different representation of $p(\Lambda)$, also based on the replica trick, can be found in a nice review of RMT [208], where the Girko's law is easily recovered. As for Hermitian matrices, $\langle \mathcal{Z}^\epsilon(z)^n \rangle$ is found after integration over the matrix elements, introduction of auxiliary fields, integration over replica fields ϕ_i^α, and finally application of a saddle point approximation (see section 5.4).

For non-Hermitian ERMs of the form $f(\mathbf{r}_i, \mathbf{r}_j) = f(\mathbf{r}_i - \mathbf{r}_j)$, it seems feasible to generalize the field method proposed by Mézard, Parisi and Zee in Ref. [147] for Hermitian ERMs. Basically, it amounts to make the same approximations, in the calculation of $\langle \mathcal{Z}^\epsilon(z)^n \rangle$, as those presented in details in section 5.4. Although we have not performed this calculation explicitly, we believe that it would lead to equations that have the same degree of validity as Eq. (5.89) with respect to Eq. (5.113). For example, equations for the borderline of the eigenvalue domain are expected to be of the form:

$$z = \frac{1}{g(z)} + \int \frac{\mathrm{d}^d\mathbf{k}}{(2\pi)^d} \frac{f_0(\mathbf{k})}{1 - \rho f_0(\mathbf{k}) g(z)}, \tag{6.71}$$

$$\frac{1}{|g(z)|^2} = \int \frac{\mathrm{d}^d\mathbf{k}}{(2\pi)^d} \frac{\rho |f_0(\mathbf{k})|^2}{|1 - \rho f_0(\mathbf{k}) g(z)|^2}, \tag{6.72}$$

where $f_0(\mathbf{k})$ is the Fourier transform of $f(\mathbf{r})$. Eqs. (6.71) and (6.72) can be obtained from Eqs. (6.40) and (6.41) by using the approximation $\langle \mathbf{k}|\hat{A}|\mathbf{k}'\rangle \simeq \langle \mathbf{k}|\hat{A}|\mathbf{k}\rangle \delta_{\mathbf{k}\mathbf{k}'} \simeq f_0(\mathbf{k})\delta_{\mathbf{k}\mathbf{k}'}$. Contrary to Eqs. (6.40) and (6.41), Eqs. (6.71) and (6.72) depend on the density $\rho = N/V$ only.

6.3.3 Free probability

The extension of free probability theory, and in particular the generalization of the concept of Blue function, to non-Hermitian matrices is natural in quaternion space. It appeared recently in the mathematical literature [209]. The quaternion Blue matrix $B_X(Q)$ of any matrix X is the functional inverse of the the quaternion resolvent matrix (6.11):

$$G_X[B_X(Q)] = B_X[G_X(Q)] = Q, \tag{6.73}$$

where Q is a quaternion defined by Eq. (6.12). For convenience, we also introduce the quaternion R-transform:

$$R_X(Q) = B_X(Q) - \frac{1}{Q}. \tag{6.74}$$

For $Q = Z_\epsilon$ given by Eq. (6.14), $R_X(Z_\epsilon)$ is simply related to the self-energy matrix (6.27) by

$$R_X(Z_\epsilon) = \Sigma_X[B_X(Z_\epsilon)], \tag{6.75}$$

and therefore $R_X(z) = \lim_{\epsilon\to 0} R_X(Z_\epsilon)$ and $\Sigma_X(z) = \lim_{\epsilon\to 0} \Sigma_X(Z_\epsilon)$ are related through[5]

$$R_X(z) = \Sigma_X[\mathcal{B}_X(z)], \tag{6.76}$$

where $\mathcal{B}_X(z)$ is the usual Blue function (5.29). We now mention two important properties of the matrices $G_X(Q)$ and $R_X(Q)$. First, $G_X(Q)$ and $R_X(Q)$ obey the following scaling

[5] To obtain Eq. (6.76), we use $B[\mathrm{diag}(z, z^*)] = \mathrm{diag}[\mathcal{B}(z), \mathcal{B}(z^*)]$.

relations [177, 209]:

$$G_{\alpha X}(Q) = G_X\left[\begin{pmatrix} 1/\alpha & 0 \\ 0 & 1/\alpha^* \end{pmatrix} Q\right]\begin{pmatrix} 1/\alpha & 0 \\ 0 & 1/\alpha^* \end{pmatrix}, \tag{6.77}$$

$$R_{\alpha X}(Q) = \begin{pmatrix} \alpha & 0 \\ 0 & \alpha^* \end{pmatrix} R_X\left[Q\begin{pmatrix} \alpha & 0 \\ 0 & \alpha^* \end{pmatrix}\right], \tag{6.78}$$

where $\alpha \in \mathbb{C}^*$. Second, both $G_X(Q)$ and $R_X(Q)$ can be expressed in terms of the resolvent $g_X(z)$ and the $\mathcal{R}$-transform $\mathcal{R}_X(z)$ only [177, 209]:

$$G_X(Q) = \frac{1}{q-q^*}\left\{[qg_X(q) - q^* g_X(q^*)]\, I_2 - [g_X(q) - g_X(q^*)]\, Q^\dagger\right\}, \tag{6.79}$$

$$R_X(Q) = \frac{1}{q-q^*}\left\{[q\mathcal{R}_X(q) - q^* \mathcal{R}_X(q^*)]\, I_2 - [\mathcal{R}_X(q) - \mathcal{R}_X(q^*)]\, Q^\dagger\right\}, \tag{6.80}$$

where $q = x_0 + \mathrm{i}|\mathbf{x}|$ and q^* are two complex conjugated eigenvalues of Q.[6]

For arbitrary Q, we can use algebraic properties of the quaternions to show that the following addition law holds [177, 209]:

$$R_{X_1+X_2}(Q) = R_{X_1}(Q) + R_{X_2}(Q), \tag{6.81}$$

where X_1 and X_2 are two non-Hermitian, asymptotically free random matrices.[7] Therefore, applying successively Eqs. (5.29), (5.30), (6.80), (6.74) and (6.73) for $Q = Z_\epsilon$, we can infer $G_{X_1+X_2}(Z_\epsilon)$ from $g_{X_1}(z)$ and $g_{X_2}(z)$. The steps of the algorithm are:

$$g_{X_i} \to \mathcal{B}_{X_i} \to \mathcal{R}_{X_i} \to R_{X_i} \to R_{X_1+X_2} \to B_{X_1+X_2} \to G_{X_1+X_2}. \tag{6.82}$$

The resolvent $g_{X_1+X_2}(z)$ and the eigenvector correlator $c_{X_1+X_2}(z)$ are finally given by Eq. (6.18).

This algorithm is greatly simplified when we look for the eigenvalue distribution of a non-Hermitian matrix $X_1 + \mathrm{i}X_2$, where X_1 and X_2 are free Hermitian matrices with known $\mathcal{R}$-transforms. Jarosz and Nowak showed that the problem reduces to solving a simple system of three equations with three unknown variables, complex u, v, and real t [177, 209]:

$$\begin{aligned} \mathcal{R}_{X1}(u) &= x + \frac{t-1}{u}, \\ \mathcal{R}_{X2}(v) &= y - \frac{t}{v}, \\ |u| &= |v|, \end{aligned} \tag{6.83}$$

where $z = x + \mathrm{i}y$. From the two first equations, we express u and v via t, while t is computed from the third equation. The resolvent and the correlator are then given by

$$g_{X_1+\mathrm{i}X_2}(z) = \mathrm{Re}\, u - \mathrm{i}\mathrm{Re}\, v, \tag{6.84}$$

$$c_{X_1+\mathrm{i}X_2}(z) = (\mathrm{Re}\, u)^2 + (\mathrm{Re}\, v)^2 - |u|^2. \tag{6.85}$$

[6] The relation (6.80) between $R_X(Q)$ and $\mathcal{R}_X(q)$ holds also between $B_X(Q)$ and $\mathcal{B}_X(q)$ because $Q^{-1} = Q^\dagger/qq^*$.

[7] Surprisingly, a generalization of the concept of $\mathcal{S}$-transform for non-Hermitian matrices — in such a way that the property (5.145) could be preserved in quaternion space — does not seem to exist in the current literature.

Equation for the borderline $z \in \delta\mathcal{D}$ of the eigenvalue domain follows from $c_{X_1+\mathrm{i}X_2}(z) = 0$.[8] From this simplified algorithm it is straightforward to recover the Girko's law for Gaussian Hermitian matrices X_1 and X_2 [$\mathcal{R}_1(z) = \mathcal{R}_2(z) = z$, see Eq. (5.90)]. A less trivial application of this algorithm, with matrices X_1 and X_2 relevant for wave propagation in random media, is given in section 6.4.

At this stage, we formally have all the ingredients to apply the free probability theory to non-Hermtian ERMs. We briefly indicate how the R-transform of an arbitrary ERM A could be obtained. The starting point is once again the representation $A = HTH^\dagger$, rewritten as in Eq. (5.154):

$$HTH^\dagger = \sum_{\alpha=1}^{M} \mu_\alpha \mathbf{h}^{(\alpha)\dagger}\mathbf{h}^{(\alpha)}, \tag{6.86}$$

where μ_α are the complex eigenvalues of the operator $\hat{T} = \rho\hat{A}$. We assume that the M vectors $\mathbf{h}^{(\alpha)}$ are independent, such that the matrices $\mathbf{h}^{(\alpha)\dagger}\mathbf{h}^{(\alpha)}$ are free. Properties (6.81) and (6.78) yield

$$R_{HTH^\dagger}(Z_\epsilon) = \sum_{\alpha=1}^{M} R_{\mu_\alpha \mathbf{h}^{(\alpha)\dagger}\mathbf{h}^{(\alpha)}}(Z_\epsilon) \tag{6.87}$$

$$= \sum_{\alpha=1}^{M} \begin{pmatrix} \mu_\alpha & 0 \\ 0 & \mu_\alpha^* \end{pmatrix} R_{\mathbf{h}^{(\alpha)\dagger}\mathbf{h}^{(\alpha)}}\left[Z_\epsilon \begin{pmatrix} \mu_\alpha & 0 \\ 0 & \mu_\alpha^* \end{pmatrix}\right]. \tag{6.88}$$

We now have to use the relation (6.80), together with $\mathcal{R}_{\mathbf{h}^{(\alpha)\dagger}\mathbf{h}^{(\alpha)}}(z) = 1/N(1-z)$. We expect that the diagonal and off-diagonal elements of $R_A(Z_\epsilon)$ obey coupled equations, that lead, in the limit $\epsilon \to 0$ and according to Eq. (6.76), to an expression of $R_A(z) = \Sigma_A[\mathcal{B}_A(z)]$ in agreement with the self-energy $\Sigma_A(z)$ given by Eqs. (6.31) and (6.32). As was the case for Hermitian ERMs, this would show that Eqs. (6.31) and (6.32) are valid even if elements $H_{i\alpha}$ are not Gaussian variables. The essential assumption that limits the applicability of Eqs. (6.34), (6.35), (6.40) and (6.41) would then be the statistical independence of the vectors $\mathbf{h}_\alpha$.

6.4 Independent Re$G(\omega_0)$ and Im$G(\omega_0)$

We start our study of non-Hermitian ERMs by the case of a $N \times N$ matrix

$$X_{ij}(\omega_0) = f(\mathbf{r}_i - \mathbf{r}_j) = (1-\delta_{ij})\left[\frac{\cos(k_0|\mathbf{r}_i - \mathbf{r}_j|)}{k_0|\mathbf{r}_i - \mathbf{r}_j|} + \mathrm{i}\frac{\sin(k_0|\mathbf{r}'_i - \mathbf{r}'_j|)}{k_0|\mathbf{r}'_i - \mathbf{r}'_j|}\right], \tag{6.89}$$

where $\{\mathbf{r}_i\}$ and $\{\mathbf{r}'_i\}$ are two different and independent sets of points. We recognize in the real and imaginary parts of $X(\omega_0)$ the two Hermitian ERMs studied independently in the previous chapter, $C(\omega_0)$ and $S'(\omega_0)$. The matrix $X(\omega_0) = C(\omega_0) + \mathrm{i}[S'(\omega_0) - I_N]$ defined in this way is similar to the three dimensional free-space Green's matrix $G(\omega_0)$ defined by Eq. (2.82) except that it has no correlation between its real and imaginary parts.

[8] If we are just interested in the borderline $z \in \delta\mathcal{D}$, *i.e.* the boundary between the holomorphic and non-holomorphic domains of $g_{X_1+\mathrm{i}X_2}(z)$, it is also possible to use a conformal transformation that maps the cuts $t \in \mathbb{R}$ of $g_{X_1+X_2}(t)$ onto $\delta\mathcal{D}$. The equation $z = f(t)$ follows from $g_{X_1+\mathrm{i}X_2}(z) = g_{X_1+X_2}(t)$, see Refs. [177, 178].

Using the definition (5.136) of asymptotic freeness [143, 176] it is easy to check that the matrices $\hat{C}$ and $\hat{S}'$ are asymptotically free, in agreement with the intuitive definition of freeness as statistical independence.

One can easily show that for the same reason as the one that ensured positiveness of the eigenvalues of the matrix $S(\omega_0)$ in section 5.7, the complex eigenvalues Λ_n of the matrix $X(\omega_0)$ obey $\mathrm{Im}\Lambda_n > -1$. Besides, for each realization of $X(\omega_0)$, $\sum_{n=1}^{N} \Lambda_n = 0$, so that $\langle \Lambda \rangle = 0$.

6.4.1 Analytical solutions for the resolvent and the eigenvector correlator

Since $X(\omega_0)$ is of the form $X_1 + \mathrm{i}X_2$, where X_1 and X_2 are two asymptotically free Hermitian matrices, we can make use of Eqs. (6.83), (6.84) and (6.85) to calculate the resolvent $g(z)$ and the eigenvector correlator $c(z)$ of $X(\omega_0)$. In our case, $X_1 = C(\omega_0)$ and $X_2 = S'(\omega_0) - I_N$. In the limit of $\gamma \ll 1$, the $\mathcal{R}$-transforms of X_1 and X_2 are those of Gaussian and Wishart matrices, respectively: $\mathcal{R}_{X_1}(z) = \gamma z$ (section 5.8.1) and $\mathcal{R}_{X_2}(z) = 1/(1-\gamma z)$ (section 5.7.1). Solving Eqs. (6.83), (6.84) and (6.85), we find:

$$g(z = x + \mathrm{i}y) = \frac{x}{2\gamma} - \frac{\mathrm{i}}{2}\left[\frac{y}{\gamma(1+y)} + \frac{1}{2+y}\right], \tag{6.90}$$

$$c(z = x + \mathrm{i}y) = \left(\frac{x}{2\gamma}\right)^2 + \frac{1}{4}\left[\frac{y}{\gamma(1+y)} - \frac{1}{2+y}\right]^2 - \frac{1}{\gamma(1+y)(2+y)}. \tag{6.91}$$

The correlator (6.91) must vanish on the borderline $\delta\mathcal{D}$ of the eigenvalue domain. We therefore readily obtain an equation for the borderline $z \in \delta\mathcal{D}$ on the complex plane:

$$x^2 + \left(\frac{y}{1+y} - \frac{\gamma}{2+y}\right)^2 - \frac{4\gamma}{(1+y)(2+y)} = 0, \tag{6.92}$$

The probability density inside this domain is

$$\begin{aligned} p(x,y) &= \frac{1}{2\pi}\left[\partial_x \mathrm{Re}\, g(z) - \partial_y \mathrm{Im}\, g(z)\right] \\ &= \frac{1}{4\pi}\left[\frac{1}{\gamma} + \frac{1}{\gamma(1+y)^2} - \frac{1}{(2+y)^2}\right]. \end{aligned} \tag{6.93}$$

A better model for the $\mathcal{R}$-transform of the matrix $X_1 = C(\omega_0)$ is given by Eq. (5.197). If we use this equation instead of $\mathcal{R}_{X_1}(z) = \gamma z$ above, analytic calculation becomes impossible but we can still compute $g(z)$ and $c(z)$ numerically. The resulting borderline of the eigenvalue domain is shown in Fig. 6.5 (dashed lines) together with the eigenvalue distribution of the matrix $X(\omega_0) = C(\omega_0) + \mathrm{i}[S'(\omega_0) - I_N]$ found by the numerical diagonalization of a set of $10^4 \times 10^4$ random matrices. At the smallest density considered $\rho\lambda_0^3 = 0.01$, the borderline found using Eq. (5.197) is very close to Eq. (6.92). At higher densities the former describes numerical results much better than Eq. (6.92).

Eq. (6.92) predicts a splitting of the eigenvalue domain in two parts at $\gamma = 8$. The more accurate calculation using Eq. (5.197) makes a similar prediction (see the lower right panel of Fig. 6.5). However, the eigenvalues of the matrix $X(\omega_0)$ do not show such a splitting and form an 'inverted T' distribution on the complex plane instead. This is due to the fact that the Marchenko-Pastur law (5.171) fails to describe the eigenvalue distribution of the matrix $S'(\omega_0)$ at $\gamma > 1$ and hence the $\mathcal{R}$-transform $1/(1-\gamma z)$ that we assumed for $S'(\omega_0)$ is not a good approximation anymore.

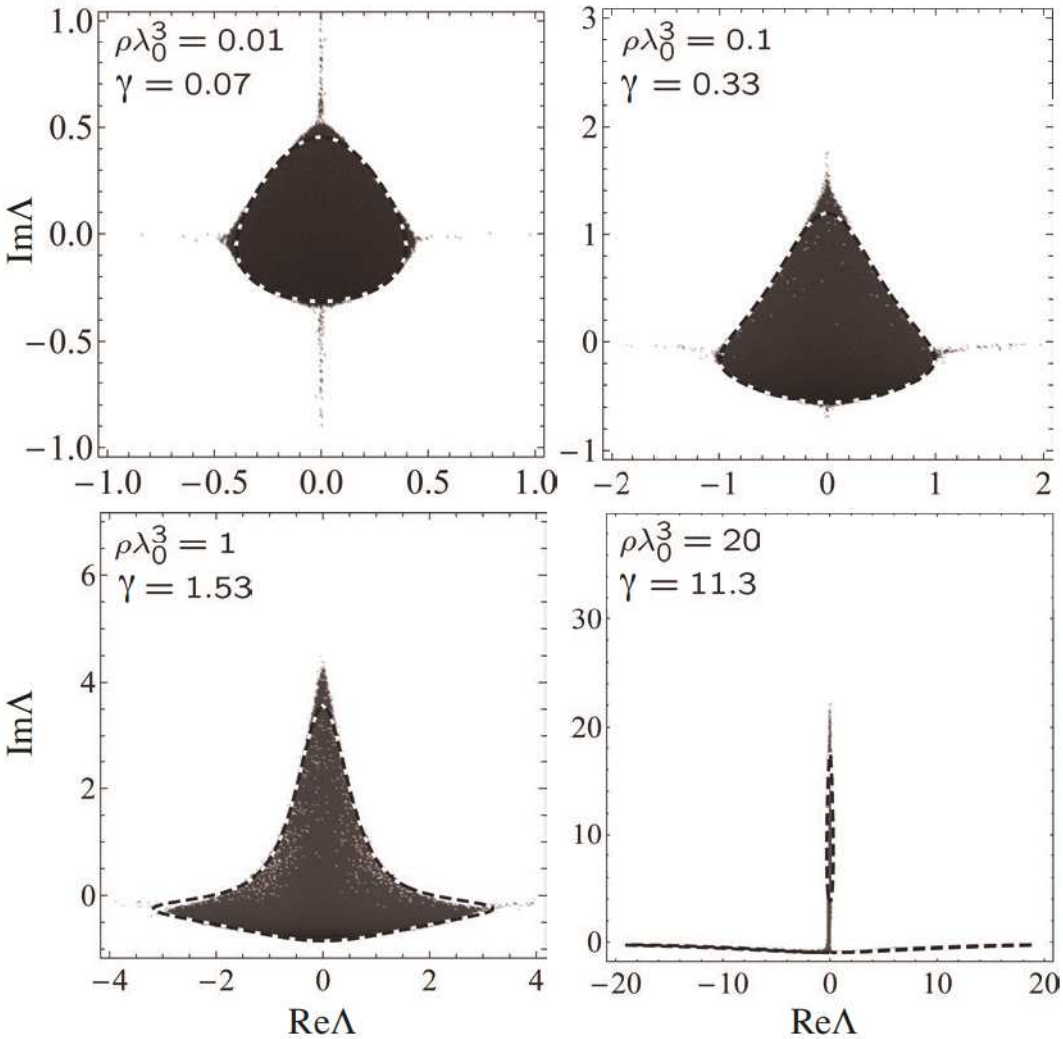

Figure 6.5: Density plot of the logarithm of the probability density of eigenvalues Λ_n of a square $N \times N$ Euclidean matrix $X(\omega_0)$ with elements $X(\omega_0)_{ij} = (1-\delta_{ij})[\cos(k_0|\mathbf{r}_i - \mathbf{r}_j|)/k_0|\mathbf{r}_i - \mathbf{r}_j| + \mathrm{i}\sin(k_0|\mathbf{r}'_i - \mathbf{r}'_j|)/k_0|\mathbf{r}'_i - \mathbf{r}'_j|]$ at 4 different densities ρ of points $\mathbf{r}_i$, $\mathbf{r}_i{}'$ per wavelength $\lambda_0 = 2\pi/k_0$ cube. $2N = 2 \times 10^4$ points $\mathbf{r}_i$ and $\mathbf{r}'_i$ $(i = 1, \ldots, N)$ are randomly chosen inside a 3D cube of side L; $\gamma = 2.8N/(k_0L)^2$ [see Eqs. (5.166) and (5.186)]. The probability distributions are estimated from 10 realizations of $\{\mathbf{r}_i\}$ and $\{\mathbf{r}'_i\}$. Dashed lines show the domain of existence of eigenvalues following from the free probability theory.

6.4.2 Scattering matrix and effective Hamiltonian

It is worthwhile to note that the statistical properties of our matrix $X(\omega_0)$ are strongly reminiscent of those of effective Hamiltonians used to characterize open chaotic systems [193, 195, 210, 211]. If we remind the physical meaning of the matrix under study, we understand that this analogy is not an accident, as we now explain. The random matrix model introduced by Mahaux and Weidenmüller for the $M \times M$ scattering matrix of an

open chaotic system is [210, 211]:

$$\mathcal{S}(\mathcal{E}) = I_M - \mathrm{i}aH^\dagger \frac{1}{\mathcal{E} - \tilde{H}^e} H, \tag{6.94}$$

$$\tilde{H}^e = H_0 - \frac{\mathrm{i}a}{2} HH^\dagger, \tag{6.95}$$

where H_0 is a Hermitian matrix that describes the closed part of the system under consideration, $\mathcal{E}$ is the energy of the incoming wave, H is a $N \times M$ matrix that contains entries coupling the N internal states to the M external channels, and $a > 0$ is an overall coupling parameter controlling the 'degree of non-Hermiticity' of the effective Hamiltonian $\tilde{H}^e$. Eqs. (6.94) and (6.95) are a direct consequence of the general expression (2.93) for the projection of an arbitrary resolvent. H_0 is commonly drawn from the Gaussian ensemble (5.1), and H is chosen such that $HH^\dagger$ is a Wishart matrix. Randomness in H_0 and $HH^\dagger$ is assumed to be independent, meaning that H_0 and $HH^\dagger$ are asymptotically free matrices. The eigenvalue distribution of $\tilde{H}^e$ was considered previously by Haake *et al.* [192] (with the help of the replica trick), Lehmann *et al.* [212] (using the supersymmetry method) and Janik *et al.* [178] (using the free probability theory). The splitting of the domain of existence of eigenvalues in two parts was observed when a was increased. This is slightly different from our matrix $X(\omega_0)$ that has elements with equal variances γ/N of real and imaginary parts (hence always the same degree of non-Hermiticity) but that still exhibits the splitting of the eigenvalue domain when γ is increased. To fully understand the origin of this similarity, let us consider a realistic scattering matrix $\mathcal{S}^f_{\alpha\beta} = \delta_{\alpha\beta} + \langle\psi_\alpha|\mathcal{G}^f_0\mathcal{T}^f|\psi_\beta\rangle$ $(\alpha = 1, \ldots, M)$, describing the propagation of light among N atoms with known polarizability (see chapters 2 and 3 for a microscopic derivation). According to Eq. (4.59), it is given by

$$\mathcal{S}^f(\omega_L) = I_M + TH^\dagger \frac{1}{\mathcal{A}(\omega_L)^{-1} - G(\omega_0)} H, \tag{6.96}$$

$$G(\omega_0) = HTH^\dagger, \tag{6.97}$$

where ω_L is the frequency of light, ω_0 the frequency of the active atomic transition, $\mathcal{A}(\omega_L)$ is the polarizability matrix (4.31), and H is defined by Eq. (5.10). To be concrete, let us now choose the polarizability (4.8) of a three-level atom under an incoherent pump. Eq. (6.96) becomes

$$\mathcal{S}^f(\omega_L) = I_M + TH^\dagger \frac{\Gamma_0}{\omega_L - H^e} D^{(1)} H, \tag{6.98}$$

$$H^e = \omega_0 I_N + \Gamma_0 D^{(1)} \mathrm{Re}G(\omega_0) - \frac{\mathrm{i}\Gamma_0}{2}\left[-2D^{(1)}\mathrm{Im}G(\omega_0) + I_N + D^{(2)}\right], \tag{6.99}$$

where $D^{(1)} = \mathrm{diag}[\Pi_i^{eq}/2(1+s_i)]$ and $D^{(2)} = \mathrm{diag}[W_i]$. In the absence of pump ($W_i = 0$) and field nonlinearities ($s_i = 0$), the effective Hamiltonian (6.99) reduces to

$$H^e = \omega_0 I_N - \frac{\Gamma_0}{2}\mathrm{Re}G(\omega_0) - \frac{\mathrm{i}\Gamma_0}{2}\left[\mathrm{Im}G(\omega_0) + I_N\right]. \tag{6.100}$$

As already noticed in section 4.4, this expression is identical to the effective Hamiltonian (2.98) obtained with the quantum scattering formalism. On the other hand, H^e reveals important differences with respect to the effective Hamitonian $\tilde{H}^e$ (6.95):

- In Eq. (6.100), the Hermitian part accounting for the closed system, $H_0 = \omega_0 I_N$, is not random, contrary to H_0 in Eq. (6.95), because we assumed that all atoms have the same internal frequency ω_0. Interestingly, we note that a random contribution can neverthesless appear in H_0 if we assume an inhomogeneous pump in such a way that $D^{(1)}$ and $D^{(2)}$ become random matrices, see Eq. (6.99).

- The Hermitian part of Eq. (6.100) contains also the random matrix $\mathrm{Re}G(\omega_0)$. We recall that it comes from non-resonant contributions (or 'off-shell processes') in the light-matter interaction, and represents the 'collective Lamb shift' [75, 83, 88, 90]. The latter is lost if RWA is used in the derivation of the wave equation (see sections 2.3.1 and 2.3.2.a). This shift is absent in the model (6.95) because it is generally assumed to be smaller than H_0 and its effect is therefore neglected[9] [210, 211]. In the study of multiple scattering, neglecting the real part of the Green's matrix largely simplifies the analysis of resonances but is not valid at high densities (see section 6.5.4). Interestingly, in the limit $\gamma \ll 1$, $\mathrm{Re}G(\omega_0)$ is well approximated by a Gaussian matrix, mimicking therefore the random Hamiltonian H_0 of Eq. (6.95). However, if it is well justified to consider H_0 independent from the anti-Hermitian part of $\tilde{H}^e$, it is clearly inaccurate to assume that $\mathrm{Re}G(\omega_0)$ and $\mathrm{Im}G(\omega_0)$ are independent (compare Figs. 6.5 and 6.6).

- The anti-Hermitian part of Eq. (6.100) is the sinc matrix $S(\omega_0) = \mathrm{Im}G(\omega_0) + I_N$, that is well approximated for $\gamma < 1$ by the Wishart matrix $\gamma HH^\dagger$. Hence, we recover the anti-Hermitian part of Eq. (6.95) with $a = \gamma = N/M$. This is not surprising inasmuch as the model (6.95) is obtained with exactly the same approximation as the one yielding to $S(\omega_0) \simeq \gamma HH^\dagger$.[10] This analogy suggests that the model (6.95) should not be completely sufficient when the number N of internal degrees of freedom exceeds the number M of channels. As discussed above, the splitting observed in the eigenvalue distribution for large γ is a consequence of this approximation. Hence, we believe that the splitting discussed in Ref. [178, 192, 212], and reported in the recent literature [211], is an artefact of the model (6.95) that fails to describe the correct effective Hamiltonian of the system under study, in all regimes of disorder[11].

6.5 Eigenvalue density of the random Green's matrix $G(\omega_0)$

Let us now illustrate the power of Eqs. (6.34), (6.35), (6.40), and (6.41) on the example of the $N \times N$ random Green's matrix

$$G(\omega_0)_{ij} = (1 - \delta_{ij}) \frac{\exp(\mathrm{i}k_0|\mathbf{r}_i - \mathbf{r}_j|)}{k_0|\mathbf{r}_i - \mathbf{r}_j|}, \tag{6.101}$$

where $k_0 = 2\pi/\lambda_0$ and λ_0 is the wavelength. We assume that the N points $\mathbf{r}_i$ are chosen randomly inside a three-dimensional ($d = 3$) volume V. This non-Hermitian ERM is of

[9] It amounts to neglecting the principal-value component of $R_{jj'}$ in Eq. (2.97).

[10] Starting from the representation (5.154), we recover $S(\omega_0) \simeq \gamma HH^\dagger$ by choosing $\mu_\alpha \simeq \rho f_0(\mathbf{k}_\alpha) = 2\pi^2 \rho \delta(k_\alpha - k_0)/k_0^2$ (see also section 5.7.1). On the other hand, Eq. (6.95) is obtained from Eq. (2.97) where the matrix V is nothing but the matrix H (up to a numerical prefactor).

[11] Note that splittings are, however, observed in the eigenvalue distribution of $S(\omega_0)$ (section 5.7.2) or $G(\omega_0)$ (section 6.5.1). The crucial point is that they do not occur for $\gamma \sim N/(k_0L)^2 \sim 1$, but for $k_0L \sim 1$. In particular, in the limit of very small sample $k_0L \ll 1$, the cloud of eigenvalues of $G(\omega_0)$ with the largest imaginary part describes the superradiance (see section 6.5.1).

special importance in the context of wave propagation in disordered media because its elements are proportional to the Green's function of Helmholtz equation, with $\mathbf{r}_i$ that may be thought of as positions of point-like scattering centers. It previously appeared in Refs. [86, 90, 104–106, 108, 109, 181], but was studied only by extensive numerical simulations, except in Ref. [90] where analytic results were obtained in the infinite density limit.

Similarly to the eigenvalues of $X(\omega_0)$ defined by Eq. (6.89) and for the same reasons, the eigenvalues Λ_n of the random matrix (6.101) obey, for each realization,

$$\sum_{n=1}^{N} \Lambda_n = 0, \quad \mathrm{Im}\Lambda_n > -1. \tag{6.102}$$

Very generally, the eigenvalue density of $G(\omega_0)$ depends on two dimensionless parameters: the number of points per wavelength cubed $\rho\lambda_0^3$ and the second moment of $|\Lambda|$ calculated in the limit of low density: $\langle|\Lambda|^2\rangle = \gamma = \mathrm{Tr}(\hat{T}\hat{T}^\dagger)/N$ [Eq. (6.51)]. Even though the latter result for $\langle|\Lambda|^2\rangle$ can be rigourously justified only in the limit of low density $\rho\lambda_0^3 \ll 1$ [see Eq. (6.50)], we checked numerically that it holds approximately up to densities as high as $\rho\lambda_0^3 \sim 100$. Eqs. (6.51), (6.50), and (5.121) show that the second moment of $|\Lambda|$ is related to the second moments of the eigenvalues of $\mathrm{Re}G(\omega_0)$ and $\mathrm{Im}G(\omega_0)$ according to

$$\begin{aligned}\gamma = \left\langle|\Lambda|^2\right\rangle_{G(\omega_0)} &= \left\langle(\mathrm{Re}\Lambda)^2\right\rangle_{G(\omega_0)} + \left\langle(\mathrm{Im}\Lambda)^2\right\rangle_{G(\omega_0)} \\ &= \frac{1}{2}\left\langle\Lambda^2\right\rangle_{\mathrm{Re}G(\omega_0)} + \frac{1}{2}\left\langle\Lambda^2\right\rangle_{\mathrm{Im}G(\omega_0)} \qquad (6.103)\\ &= \left\langle\Lambda^2\right\rangle_{\mathrm{Re}G(\omega_0)} = \left\langle\Lambda^2\right\rangle_{\mathrm{Im}G(\omega_0)}. \qquad (6.104)\end{aligned}$$

Eq. (6.104) holds for $k_0R \gg 1$ and $\rho\lambda_0^3 \lesssim 100$, whereas Eq. (6.103) is also valid for any k_0R and arbitrary non-Hermitian traceless ERM [provided that Eq. (6.50) holds]. We will see from the following that the two parameters $\rho\lambda_0^3$ and γ control different properties of the eigenvalue density.

6.5.1 Borderline of the eigenvalue domain

We first focus on the borderline of the support of eigenvalues which is easier to visualize. Our goal is to solve Eqs. (6.40) and (6.41). As was the case for the Hermitian matrices $\mathrm{Im}G(\omega_0)$ and $\mathrm{Re}G(\omega_0)$, this can be done exactly if the volume V preserves the symmetry of the function $f(|\mathbf{r}-\mathbf{r}'|)$. In this section, we assume that the N points are chosen inside a sphere of radius R. For arbitrary k_0R, the parameter γ (6.55) is then given by

$$\gamma = \frac{3N}{(k_0R)^2}\int_0^1 \mathrm{d}x s(x) = \frac{9N}{8(k_0R)^2}. \tag{6.105}$$

In Fig. 6.6 we present a comparison of the solutions of Eqs. (6.40) and (6.41) (see below for explanation) with results of numerical diagonalization of the matrix (6.101) for $k_0R \gg 1$.

6.5.1.a Approximate solution at low density

Let us show how an explicit equation for the borderline of the support of eigenvalue density of the random Green's matrix (6.101) can be derived in the low-density limit.

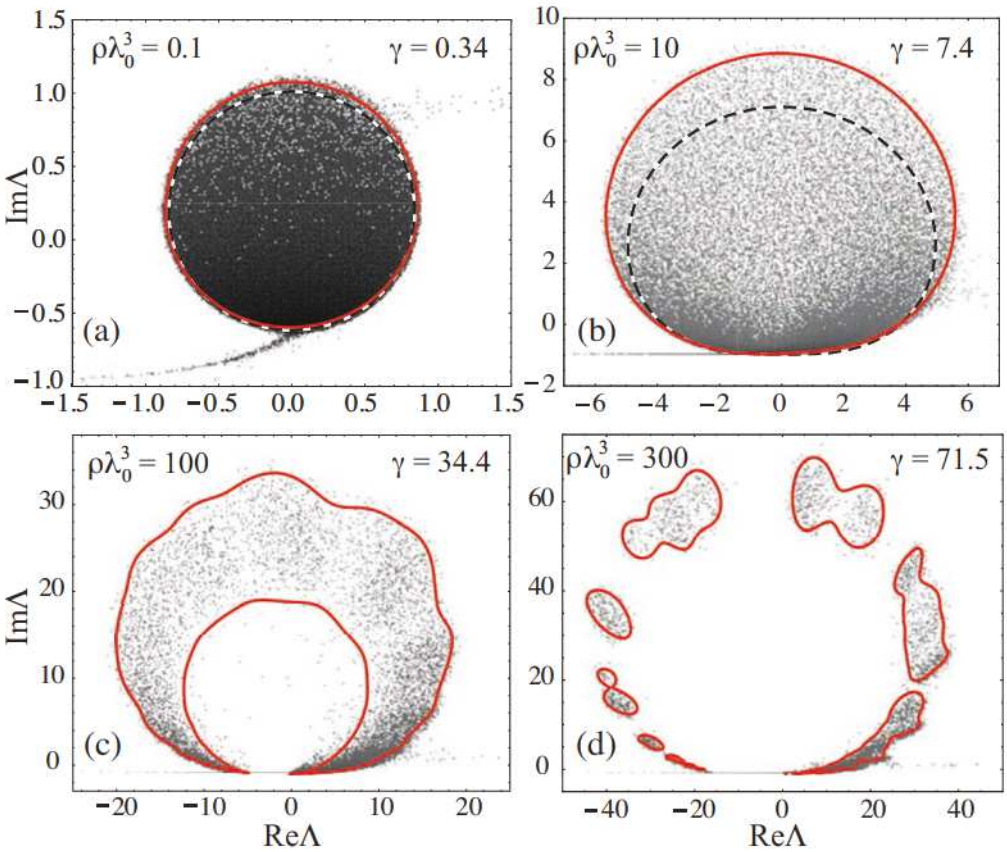

Figure 6.6: Density plots of the logarithm of eigenvalue density of the $N \times N$ random Green's matrix (6.101) obtained by numerical diagonalization of 10 realizations of the matrix for $N = 10^4$. Points $\mathbf{r}_i$ are randomly chosen inside a sphere of radius R. The solid red lines represent the borderlines of the support of eigenvalue density following from Eq. (6.117) in panels (a) and (b) and from Eqs. (6.135) and (6.136) in panels (c) and (d). The dashed lines show the diffusion approximation (6.121).

On the one hand, traces appearing in Eqs. (6.40) and (6.41) in the $|\mathbf{r}\rangle$-representation read

$$\begin{aligned}\mathrm{Tr}\hat{S}_0 &= \mathrm{Tr}\left(\frac{\hat{T}}{1-g\hat{T}}\right) = \mathrm{Tr}\left(\hat{T} + g\hat{T}\hat{S}_0\right) \\ &= g\iint_V \mathrm{d}^3\mathbf{r}\,\mathrm{d}^3\mathbf{r}'\,T(\mathbf{r},\mathbf{r}')S_0(\mathbf{r}',\mathbf{r}), \qquad (6.106)\\ \mathrm{Tr}\hat{S}_0\hat{S}_0^\dagger &= \iint_V \mathrm{d}^3\mathbf{r}\,\mathrm{d}^3\mathbf{r}'\,\left|S_0(\mathbf{r},\mathbf{r}')\right|^2, \qquad (6.107)\end{aligned}$$

where $T(\mathbf{r},\mathbf{r}') = \rho\langle\mathbf{r}|\hat{A}|\mathbf{r}'\rangle = \rho\exp(\mathrm{i}k_0|\mathbf{r}-\mathbf{r}'|)/k_0|\mathbf{r}-\mathbf{r}'|$ and in Eq. (6.106) we used the fact that $\mathrm{Tr}\hat{T} = \rho\mathrm{Tr}\hat{A} = 0$, as follows from Eq. (6.101). On the other hand, $S_0(\mathbf{r},\mathbf{r}') = \langle\mathbf{r}|\hat{S}_0|\mathbf{r}'\rangle$ obeys

$$S_0(\mathbf{r},\mathbf{r}') = T(\mathbf{r},\mathbf{r}') + g\int_V \mathrm{d}^3\mathbf{r}''T(\mathbf{r},\mathbf{r}'')S_0(\mathbf{r}'',\mathbf{r}'), \qquad (6.108)$$

as follows from the definition of $\hat{S}_0$. Noting that

$$\left(\Delta_{\mathbf{r}} + k_0^2 + \mathrm{i}\epsilon\right) T(\mathbf{r}, \mathbf{r}') = -\frac{4\pi\rho}{k_0}\delta^{(3)}(\mathbf{r} - \mathbf{r}'), \tag{6.109}$$

where $\epsilon \to 0^+$, we apply the operator $\Delta_{\mathbf{r}} + k_0^2 + \mathrm{i}\epsilon$ to Eq. (6.108) and obtain

$$\Delta_{\mathbf{r}} S_0(\mathbf{r}, \mathbf{r}') + k_0^2 \left[1 + g\frac{\rho\lambda_0^3}{2\pi^2}\Pi_V(\mathbf{r}) + \mathrm{i}\epsilon\right] S_0(\mathbf{r}, \mathbf{r}') = -\frac{4\pi\rho}{k_0}\delta^{(3)}(\mathbf{r} - \mathbf{r}'), \tag{6.110}$$

where $\Pi_V(\mathbf{r}) = 1$ for $\mathbf{r} \in V$ and 0 elsewhere. In the limit of low density $\rho\lambda_0^3 \to 0$, an approximate solution of this equation is obtained by neglecting 'reflections' of the 'wave' $S_0(\mathbf{r}, \mathbf{r}')$ on the boundaries of the volume V and thus setting $\Pi_V(\mathbf{r}) = 1$ everywhere. This yields

$$S_0(\mathbf{r}, \mathbf{r}') \simeq \rho\frac{\exp\left[\mathrm{i}\kappa(g)|\mathbf{r} - \mathbf{r}'|\right]}{k_0|\mathbf{r} - \mathbf{r}'|}, \tag{6.111}$$

$$\kappa(g) = k_0\sqrt{1 + \frac{g\rho\lambda_0^3}{2\pi^2}}. \tag{6.112}$$

We now plug the explicit expressions for $T(\mathbf{r}, \mathbf{r}')$ and $S_0(\mathbf{r}, \mathbf{r}')$ into Eqs. (6.106) and (6.107) and use the auxiliary result (5.128). This yields

$$\mathrm{Tr}\hat{S}_0 = 2\gamma N g h[-\mathrm{i}\kappa(g)R - \mathrm{i}k_0 R], \tag{6.113}$$

$$\mathrm{Tr}\hat{S}_0\hat{S}_0^\dagger = 2\gamma N h[2\mathrm{Im}\kappa(g)R], \tag{6.114}$$

with

$$h(x) = \frac{\int_0^1 \mathrm{d}u s(u) e^{-2ux}}{\int_0^1 \mathrm{d}u s(u)} = \frac{1}{6x^4}\left[3 - 6x^2 + 8x^3 - 3(1 + 2x)e^{-2x}\right]. \tag{6.115}$$

In the low-density limit, g can be eliminated from Eqs. (6.40) and (6.41) by neglecting $\mathrm{Tr}\hat{S}_0/N$ in Eq. (6.40) and substituting $g = 1/z$ into Eq. (6.114). This gives

$$|\Lambda|^2 = 2\gamma h\left[2\mathrm{Im}\kappa\left(1/\Lambda\right)R\right]. \tag{6.116}$$

If the argument of the function h in Eq. (6.116) is expanded in series in $\rho\lambda_0^3$, Eq. (6.116) becomes:

$$|\Lambda|^2 \simeq 2\gamma h\left(-8\gamma\frac{\mathrm{Im}\Lambda}{3|\Lambda|^2}\right). \tag{6.117}$$

By comparing Eq. (6.117) with the exact solution (see section 6.5.1.c and Fig. 6.6), we conclude that it is valid up to densities as high as $\rho\lambda_0^3 \simeq 10$.

For $\gamma \ll 1$, the density of eigenvalues is roughly uniform within a circular domain of radius $\sqrt{2\gamma}$, see Fig. 6.6(a). The domain grows in size and shifts up upon increasing γ. At $\gamma \gtrsim 1$ it starts to 'feel' the 'wall' $\mathrm{Im}\Lambda = -1$ and deforms [Fig. 6.6(b)]. Before considering the shape of the eigenvalue domain at higher densities, we would like to show how the scattering theory discussed in chapter 4 can also be used to derive an equation for its borderline.

6.5.1.b Mapping to the scattering theory

In section 4.4 we introduced a mapping between the problem of multiple scattering of waves by pointlike scatterers and the properties of the Green's matrix. In the stationary regime, the intensity at $\mathbf{r}_i$ of a wave emitted by a point source located at $\mathbf{r}_j$ is $I_{ij} = |\mathcal{G}^f_{ij}|^2$, where $\mathcal{G}^f_{ij} = \langle \mathbf{r}_i|\mathcal{G}^f|\mathbf{r}_j\rangle$ is the Green's operator [see Eqs. (4.36) and (4.85)]. Let us introduce $I(\tilde{t}) = \sum_{i\neq j} I_{ij}$, where we emphasize that I depends on $\tilde{t}$, the scattering strength of an individual scatterer [Eq. (4.20)]. With the help of Eq. (4.62), we rewrite $I(\tilde{t})$ as

$$I(\tilde{t}) = \mathrm{Tr}\frac{1}{[\tilde{t} - (\mathcal{G}^m_0)^{-1}][\tilde{t} - (\mathcal{G}^m_0)^{-1}]^\dagger}, \tag{6.118}$$

where the $N \times N$ matrix $\mathcal{G}^m_0$ is proportional to the Green's matrix, $\mathcal{G}^m_0 = -k_0 G(\omega_0)/4\pi$. This is to be compared with the expression for the correlator of right and left eigenvectors of an arbitrary matrix A, $c(z) = \lim_{\epsilon\to 0^+} G^\epsilon_{12}$, following from Eq. (6.17):

$$c(z) = -\lim_{\epsilon\to 0^+}\frac{i\epsilon}{N}\left\langle \mathrm{Tr}\frac{1}{(z-A)(z-A)^\dagger + \epsilon^2}\right\rangle. \tag{6.119}$$

For $A = (\mathcal{G}^m_0)^{-1}$ and $z = \tilde{t}$ we thus have

$$c(\tilde{t}) = -\lim_{\epsilon\to 0^+}\frac{i\epsilon}{N}\langle I(\tilde{t})\rangle. \tag{6.120}$$

This should become different from zero when $\tilde{t}$ enters the support of the eigenvalue density of $(\mathcal{G}^m_0)^{-1}$ or, equivalently, when $1/\tilde{t}$ enters the support of the eigenvalue density of $\mathcal{G}^m_0$. The only way to obtain $c(\tilde{t}) \neq 0$ for $\epsilon \to 0^+$ is to make $\langle I(\tilde{t})\rangle$ diverge. In the framework of our linear model of scattering, this can be achieved by realizing a random laser. We thus come to the conclusion that finding the borderline of the support of the eigenvalue density $p(\Lambda)$ of the $N \times N$ Green's matrix (6.101) is mathematically equivalent to calculating the random lasing threshold in an ensemble of N identical point-like scatterers with scattering strength $\tilde{t} = -4\pi/k_0\Lambda$. This conclusion can also be seen as a direct consequence of the more general threshold condition (4.34) valid for each realization of the Green's matrix, and not only on average. In the diffusion approximation, for example, the threshold of such a random laser is given by Eq. (4.138) with $\tilde{t} = -4\pi\tilde{\alpha}/k_0$. This leads to the following equation for the borderline :

$$|\Lambda|^2 = \frac{8\gamma}{\sqrt{3}\pi}\sqrt{1+\mathrm{Im}\Lambda}\left(1 + \frac{|\Lambda|^2}{|\Lambda|^2 + 4\gamma}\right). \tag{6.121}$$

We show this equation in Figs. 6.6(a) and (b) by dashed lines. As expected, it gives satisfactory results only in the weak scattering regime $\rho\lambda_0^3 \lesssim 10$ and at large optical thickness $b = 2R/l_s = 16\gamma/3|\Lambda|^2 \gg 1$, where $l_s = 4\pi/\rho|\tilde{t}|^2$ is the scattering mean free path [Eq. (4.128)]. In contrast, our Eqs. (6.40) and (6.41) apply at any $\rho\lambda_0^3$ and b. These equations can therefore serve as a benchmark for theories of multiple scattering.

6.5.1.c Exact solution at any density

The approximate equation (6.116) for the borderline of the support of eigenvalue density yields a closed line on the complex plane until $\rho\lambda_0^3 \simeq 30$, after which the line opens from below. This opening is reminiscent of the gap predicted by Eq. (5.199) for the eigenvalue

distribution of the matrix $\mathrm{Re}G(\omega_0)$. This signals that an important change in behavior might be expected at this density. And indeed, we observe that a 'hole' opens in the eigenvalue density for $\rho\lambda_0^3 \gtrsim 30$. As we see in Fig. 6.6(c), this hole is perfectly described by our Eqs. (6.40) and (6.41) which we now solve in the bi-orthogonal basis of right $|\mathcal{R}_\alpha\rangle$ and left $|\mathcal{L}_\alpha\rangle$ eigenvectors of the operator $\hat{T}$. These eigenvectors obey $\hat{T}|\mathcal{R}_\alpha\rangle = \mu_\alpha|\mathcal{R}_\alpha\rangle$ and $\hat{T}^\dagger|\mathcal{L}_\alpha\rangle = \mu_\alpha^*|\mathcal{L}_\alpha\rangle$. In this basis, Eqs. (6.40) and (6.41) read

$$z = \frac{1}{g} + \frac{g}{N}\sum_\alpha \frac{\mu_\alpha^2}{1-g\mu_\alpha}, \tag{6.122}$$

$$\frac{1}{|g|^2} = \frac{1}{N}\sum_{\alpha,\beta} \frac{\mu_\alpha\mu_\beta^*\langle\mathcal{L}_\alpha|\mathcal{L}_\beta\rangle\langle\mathcal{R}_\beta|\mathcal{R}_\alpha\rangle}{(1-g\mu_\alpha)(1-g\mu_\beta)^*}, \tag{6.123}$$

where we made use of the fact that $\mathrm{Tr}\hat{T} = 0$ and therefore $\mathrm{Tr}\hat{S}_0 = g\mathrm{Tr}\hat{T}\hat{S}_0$ [see Eq. (6.106)]. The problem essentially reduces to solving the eigenvalue equation

$$\rho\int_V \mathrm{d}^3\mathbf{r}' \frac{\exp(\mathrm{i}k_0|\mathbf{r}-\mathbf{r}'|)}{k_0|\mathbf{r}-\mathbf{r}'|}\mathcal{R}_\alpha(\mathbf{r}') = \mu_\alpha\mathcal{R}_\alpha(\mathbf{r}), \tag{6.124}$$

where $\mathbf{r} \in V$. As follows from Eq. (6.109), $\mathcal{R}_\alpha(\mathbf{r})$ is also an eigenvector of the Laplacian, $\Delta_\mathbf{r}\mathcal{R}_\alpha(\mathbf{r}) = -\kappa_\alpha^2\mathcal{R}_\alpha(\mathbf{r})$, with $\kappa_\alpha = \kappa(1/\mu_\alpha)$. In a sphere of radius R, using the decomposition of the kernel of Eq. (6.124) in spherical harmonics,

$$\frac{\exp(\mathrm{i}k_0|\mathbf{r}-\mathbf{r}'|)}{k_0|\mathbf{r}-\mathbf{r}'|} = 4\mathrm{i}\pi\sum_{l=0}^{\infty}\sum_{m=-l}^{l} j_l\left[k_0\min(r,r')\right] h_l^{(1)}\left[k_0\max(r,r')\right] Y_{lm}(\theta,\phi)Y_{lm}(\theta',\phi')^*, \tag{6.125}$$

it is quite easy to find that [90]

$$\mathcal{R}_\alpha(\mathbf{r}) = \mathcal{R}_{lmp}(\mathbf{r}) = \mathcal{A}_{lp}j_l(\kappa_{lp}r)Y_{lm}(\theta,\phi), \tag{6.126}$$

where θ and ϕ are the polar and azimuthal angles of the vector $\mathbf{r}$, respectively, j_l are spherical Bessel functions of the first kind, $h_l^{(1)}$ are spherical Hankel functions, Y_{lm} are spherical harmonics, $\mathcal{A}_{lp}$ are normalization coefficients, and $\alpha = \{l,m,p\}$. Furthermore, coefficients κ_{lp} obey [90]

$$\frac{\kappa_{lp}}{k_0} = \frac{j_l(\kappa_{lp}R)}{j_{l-1}(\kappa_{lp}R)}\frac{h_{l-1}^{(1)}(k_0R)}{h_l^{(1)}(k_0R)}. \tag{6.127}$$

Integer p labels the different solutions of this equation for a given l. Hence, eigenvalues

$$\mu_{lp} = \frac{\rho\lambda_0^3}{2\pi^2}\frac{1}{(\kappa_{lp}/k_0)^2-1} \tag{6.128}$$

are $(2l+1)$-times degenerate ($m \in [-l,l]$).

In the limit $k_0R \to \infty$, for $l \ll k_0R$ and $l \ll \kappa_{lp}R$, we can use asymptotic expressions for the spherical functions in Eq. (6.127) to obtain

$$\frac{\mathrm{i}}{2}\ln\left(\frac{\kappa_{lp}+k_0}{\kappa_{lp}-k_0}\right) = -\kappa_{lp}R + \left(\frac{l}{2}+p\right)\pi. \tag{6.129}$$

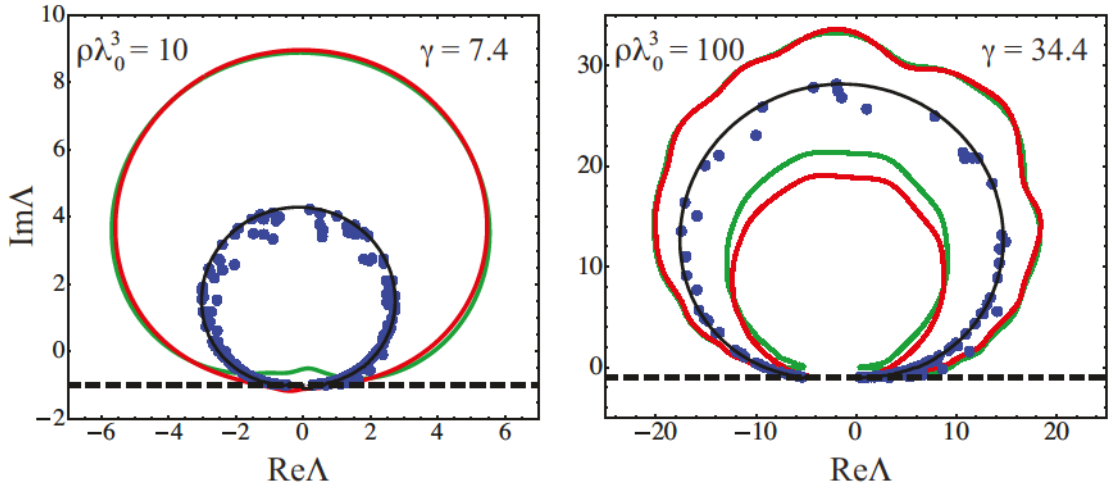

Figure 6.7: The solid red (green) line represents the borderline of the support of eigenvalue density following from Eq. (6.135) [Eq. (6.135) approximated by $z \simeq 1/g$, respectively] and Eq. (6.136); $N = 10^4$. Blue points represent $\mu_{lp} - \mathrm{i}$, with μ_{lp} the eigenvalues given by Eqs. (6.127) and (6.128). They are localized in the vicinity of a roughly circular black line following from Eq. (6.130). The horizontal dashed line corresponds to $\mathrm{Im}\Lambda = -1$.

In this limit, the eigenvalues μ_{lp} are therefore localized in the vicinity of a roughly circular line[12] in the complex plane given by

$$\left|\frac{\kappa(1/\mu) - k_0}{\kappa(1/\mu) + k_0}\right|^2 \left|e^{4\mathrm{i}\kappa(1/\mu)R}\right| = 1. \tag{6.130}$$

Let us now study the eigenvectors. Using standard properties of spherical harmonics and spherical Bessel functions [182], we can show that

$$\langle \mathcal{R}^*_{lmp} | \mathcal{R}_{l'm'p'} \rangle = (-1)^m \mathcal{A}^2_{lp} \frac{R^3}{2} \Big[j_l(\kappa_{lp}R)^2 - j_{l-1}(\kappa_{lp}R) j_{l+1}(\kappa_{lp}R) \Big] \delta_{l,l'} \delta_{m,-m'} \delta_{p,p'}. \tag{6.131}$$

From the normalization condition $\langle \mathcal{L}_{lmp} | \mathcal{R}_{l'm'p'} \rangle = \delta_{l,l'} \delta_{m,m'} \delta_{p,p'}$, we find that $\mathcal{L}_{lmp}(\mathbf{r}) = (-1)^m \mathcal{R}_{l(-m)p}(\mathbf{r})^*$ and

$$\mathcal{A}_{lp} = \sqrt{\frac{2}{R^3}} \frac{1}{\sqrt{j_l(\kappa_{lp}R)^2 - j_{l-1}(\kappa_{lp}R) j_{l+1}(\kappa_{lp}R)}}. \tag{6.132}$$

On the other hand, we also have

$$\langle \mathcal{R}_{lmp} | \mathcal{R}_{l'm'p'} \rangle = \frac{R^2 \mathcal{A}^*_{lp} \mathcal{A}_{lp'}}{\kappa^2_{lp'} - \kappa^{*2}_{lp}} \Big[\kappa^*_{lp} j_{l-1}(\kappa^*_{lp}R) j_l(\kappa_{lp'}R) - \kappa_{lp'} j_{l-1}(\kappa_{lp'}R) j_l(\kappa^*_{lp}R) \Big] \delta_{l,l'} \delta_{m,m'}, \tag{6.133}$$

[12] An equation of a circle can be found from Eq. (6.130) by expanding $\kappa(1/\mu)$ in series in $1/\rho\lambda_0^3$. The resulting equation is $(x + \rho\lambda_0^3/8\pi^2)^2 + (y - R/2 + 1)^2 = R^2$ with $R = 4\gamma/3W(4k_0R)$, $\mu = x + \mathrm{i}y$, and $W(t)$ the Lambert function (the inverse relation of the function $f(W) = We^W$); $W(t) \simeq \ln t$ for $|t| \gg 1$. Hence, $R \simeq 4\gamma/3\ln(4k_0R)$ for $k_0R \gg 1$.

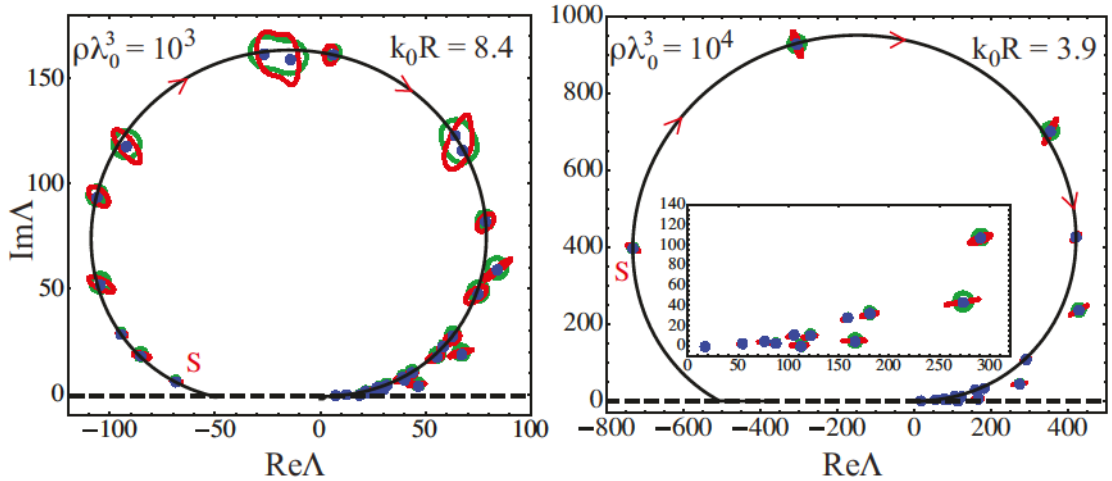

Figure 6.8: Same as Fig. 6.7 but for higher densities. Arrows indicate how the clouds of eigenvalues Λ_n centered around $\mu_{lp} - \mathrm{i}$ are moving along the roughly circular black line [Eq. (6.130)] when the density is increased at fixed $N = 10^4$, *i.e.*, when the size k_0R is decreased. Symbol S designates the cloud of eigenvalues that will give rise to superradiance in the limit of small sample $k_0R \to 0$.

and $\langle \mathcal{L}_{lmp} | \mathcal{L}_{l'm'p'} \rangle = \langle \mathcal{R}_{lmp} | \mathcal{R}_{lmp'} \rangle \delta_{l,l'} \delta_{m,m'}$. It is now convenient to introduce a new coefficient

$$C_{lpp'} = \frac{4\left[\kappa_{lp}^* R j_{l-1}(\kappa_{lp}^* R) j_l(\kappa_{lp'} R) - \kappa_{lp'} R j_{l-1}(\kappa_{lp'} R) j_l(\kappa_{lp}^* R)\right]^2}{\left[\kappa_{lp'}^2 R^2 - \kappa_{lp}^{*2} R^2\right]^2 \left[j_l(\kappa_{lp}^* R)^2 - j_{l-1}(\kappa_{lp}^* R) j_{l+1}(\kappa_{lp}^* R)\right] \left[j_l(\kappa_{lp'} R)^2 - j_{l-1}(\kappa_{lp'} R) j_{l+1}(\kappa_{lp'} R)\right]}, \tag{6.134}$$

in terms of which Eqs. (6.122) and (6.123) become

$$z = \frac{1}{g} + \frac{g}{N} \sum_l \sum_p \frac{(2l+1)\mu_{lp}^2}{1 - g\mu_{lp}}, \tag{6.135}$$

$$\frac{1}{|g|^2} = \frac{1}{N} \sum_l \sum_p \sum_{p'} \frac{(2l+1)\mu_{lp'} \mu_{lp}^* C_{lpp'}}{(1 - g\mu_{lp'})(1 - g\mu_{lp})^*}. \tag{6.136}$$

To find the borderline of the support of eigenvalue density of the matrix (6.101) — shown in Figs. 6.6(c), 6.6(d), 6.7 and 6.8 — we apply the following recipe. (1) Find solutions κ_{lp} of Eq. (6.127) numerically and then compute the corresponding μ_{lp}. (2) Compute the coefficients $C_{lpp'}$ using Eq. (6.134). (3) Find lines on the complex plane $1/g$ defined by Eq. (6.136) (solid green lines in Figs. 6.7 and 6.8). (4) Transform the lines on the complex plane $1/g$ into contours on the complex plane z using Eq. (6.135). The latter contours are the borderlines of the support of eigenvalue density $p(\Lambda)$.

At high density the crown formed by the eigenvalues blows up in spots centered around $\mu_\alpha - \mathrm{i}$, where μ_α are the eigenvalues of $\hat{T}$, as we show in Fig. 6.6(d). When the density is further increased, the clouds of eigenvalues of A turn clockwise along the circular line given by Eq. (6.130) and shrink in size. The eigenvalues Λ eventually become equal to $\mu_\alpha - \mathrm{i}$ (Fig. 6.8). They then fall on the circular line (6.130) and the problem

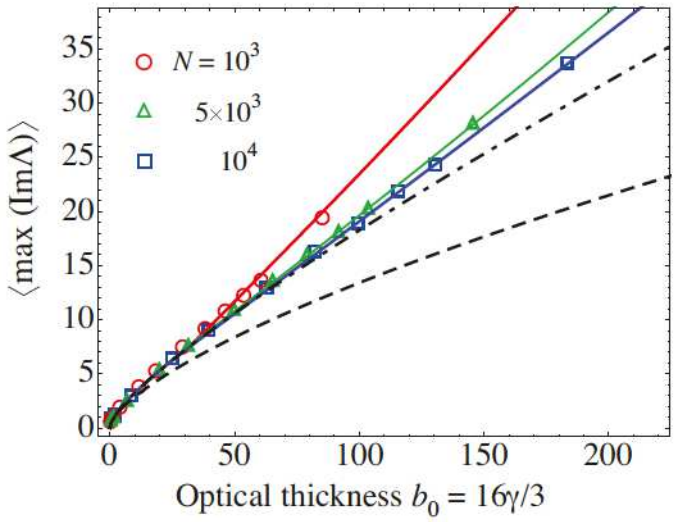

Figure 6.9: Mean maximum value of the imaginary part of eigenvalues Λ of the $N\times N$ random Green's matrix $G(\omega_0)$. Our analytic results (solid lines) following from Eqs. (6.135) and (6.136) are compared with the results of numerical diagonalization for three different matrix sizes N (symbols). Analytic results depend both on γ and $\rho\lambda_0^3$, except for $\rho\lambda_0^3 \lesssim 10$ when they reduce to Eq. (6.117) (dot-dashed line). The dashed line represents the prediction of the diffusion approximation (6.121).

looses its statistical nature. As follows from our analysis, the parameter γ controls the overall extent of the support of eigenvalue density $\mathcal{D}$ on the complex plane, whereas its structure depends also on the density $\rho\lambda_0^3$. At fixed γ, $\mathcal{D}$ goes through a transition from a disk-like to an annulus-like shape, and eventually splits into multiple disconnected spots upon increasing $\rho\lambda_0^3$. The transition from disk-like to the annulus-like shape is reminiscent of the disk-annulus transition in the eigenvalue distribution of rotationally invariant non-Hermitian random matrix ensembles [187] (see the discussion at the end of section 6.3.1).

Quite remarkably, our formalism captures properly the transition to the continuous medium regime (high density) and to the small sample regime (low k_0R). To illustrate this point, we calculated $\langle\max(\mathrm{Im}\Lambda)\rangle$ from Eqs. (6.135) and (6.136), and found excellent agreement with numerical results at all values of parameters, including high densities $\rho\lambda_0^3$, see Fig. 6.9.[13] In addition, in the regime of high density, we are able to identify the cloud of eigenvalues (symbol S in Fig. 6.8) that will give rise, in the limit $k_0R \to 0$, to superradiance, *i.e.* the eigenvalues that will have the largest decay rate $\mathrm{Im}\Lambda \simeq N$ [82, 90]. This identification is possible because the different clouds of eigenvalues are well separated and evolve smoothly and continuously when the density is increased. At the present time, we have no physical interpretation for the trajectory followed by the cloud S. It is somewhat compelling that eigenvalues with the smallest $\mathrm{Im}\Lambda$ evolve in such a way that, at the end of the day, they have the largest $\mathrm{Im}\Lambda$ and are well separated, in the complex plane, from all other (subradiant) states.

[13]We show $\max(\mathrm{Im}\Lambda)$ because it is the quantity that controls the threshold of a random laser in an ensemble of atoms in free space (see chapter 7). It is also worth noting that Eqs. (6.135) and (6.136) do not give an accurate estimate of $\min(\mathrm{Im}\Lambda)$, see section 6.5.2.

6.5.2 Hyperbolic spiral branches and subradiant states

An important additional feature of the numerical results in Fig. 6.6 that is not described by our Eqs. (6.40) and (6.41) is the eigenvalues that concentrate around the two hyperbolic spirals, $|\Lambda| = 1/\arg\Lambda$ and its reflection through the origin. These spirals correspond to the two eigenvalues $\pm A_{12}$ of the matrix (6.101) for $N = 2$. We already encountered these spirals in the study of light emitted by two atoms, see Fig. 3.4(a) in section 3.4. The eigenvectors corresponding to these eigenvalues are localized on pairs of very close points $|\mathbf{r}_i - \mathbf{r}_j| \ll \lambda_0$. These are the super- and sub-radiant states of a pair of atoms. In the limit of $\rho\lambda_0^3 \to \infty$, we observe that the lower branch is much more populated than the upper one. A rough model that partially mimics this behavior is given by the $N \times N$ matrix:

$$\tilde{G}(\omega_0) = G(\omega_0)_{12} \begin{pmatrix} 0 & 1 & \dots & 1 \\ 1 & \ddots & \ddots & \vdots \\ \vdots & \ddots & \ddots & 1 \\ 1 & \dots & 1 & 0 \end{pmatrix}, \tag{6.137}$$

where $G(\omega_0)_{12} = e^{\mathrm{i}k_0|\mathbf{r}_1-\mathbf{r}_2|}/k_0|\mathbf{r}_1 - \mathbf{r}_2|$, and $\mathbf{r}_1$ and $\mathbf{r}_2$ are randomly chosen points inside the sphere of radius R. This matrix has two different eigenvalues: the non-degenerate eigenvalue $\Lambda = (N-1)G(\omega_0)_{12}$ corresponds to the superradiant state $(1,\dots,1)/\sqrt{N}$; and the $(N-1)$-degenerate eigenvalue $\Lambda = -G(\omega_0)_{12}$ corresponds to subradiant states localized on pairs of points $(1,0,\dots,0,-1,0,\dots,0)/\sqrt{2}$. In the limit $N \to \infty$, only subradiant states contribute significantly to the eigenvalue distribution of $\tilde{G}(\omega_0)$. Using the definition (6.1) and Eq. (5.128), we easily show that the latter is then given by:

$$p(\Lambda) = \frac{3}{(k_0R)^3}\frac{1}{|\Lambda|^2}\, s\left(\frac{1}{2k_0R|\Lambda|}\right)\delta\left(\arg\Lambda + \frac{1}{|\Lambda|}\right), \tag{6.138}$$

where $s(x)$ is defined by Eq. (5.130). Loosely speaking, the true eigenvalue distribution of the Green's matrix $G(\omega_0)$ is a superposition of Eqs. (6.34) and (6.35), and Eq. (6.138). With the qualitative picture of the Dyson gas in mind, we could say that the lower 'branch' $|\Lambda| = -1/\arg\Lambda$ plays the role of a channel for the gas of eigenvalues, through which the latter can escape from the bulk predicted by our Eqs. (6.40) and (6.41). This effect is more pronounced at high density because the eigenvalues accumulate near the axis $\mathrm{Im}\Lambda = -1$, so that the repulsive interaction between eigenvalues forces the latter to flow into the lower branch. Strikingly, the vicinity of $\Lambda = 0$ on the complex plane is also the place where some states start to become localized for $\rho\lambda_0^3 \gtrsim 10$ (since these states are localized due to disorder, they may be identified as 'Anderson' states, see section 6.6.2). This indicates that two different types of localized states coexist in the spectrum near $\Lambda = 0$, and therefore suggests that subradiance and Anderson localization might be two competitive phenomena. The competition between Anderson localization and sub- and superradiance was recently discussed in Ref. [79].

From numerical results for $N \leq 10^4$, we estimate the statistical weight of subradiant states to be important at large densities, of the order of $1 - \mathrm{const}/(\rho\lambda_0^3)^p$ with $p \sim 1$. This is consistent with the estimation of the number of subradiant states in a large atomic cloud by Ernst [86].[14] At large densities, the absolute majority of the eigenvalues

[14] Physically, this seems to indicate that most of the states are localized due to subradiance in the effective medium limit $\rho\lambda_0^3 \to \infty$. This could be used for information storage on subradiant states in a disordered and dense ensemble of atoms.

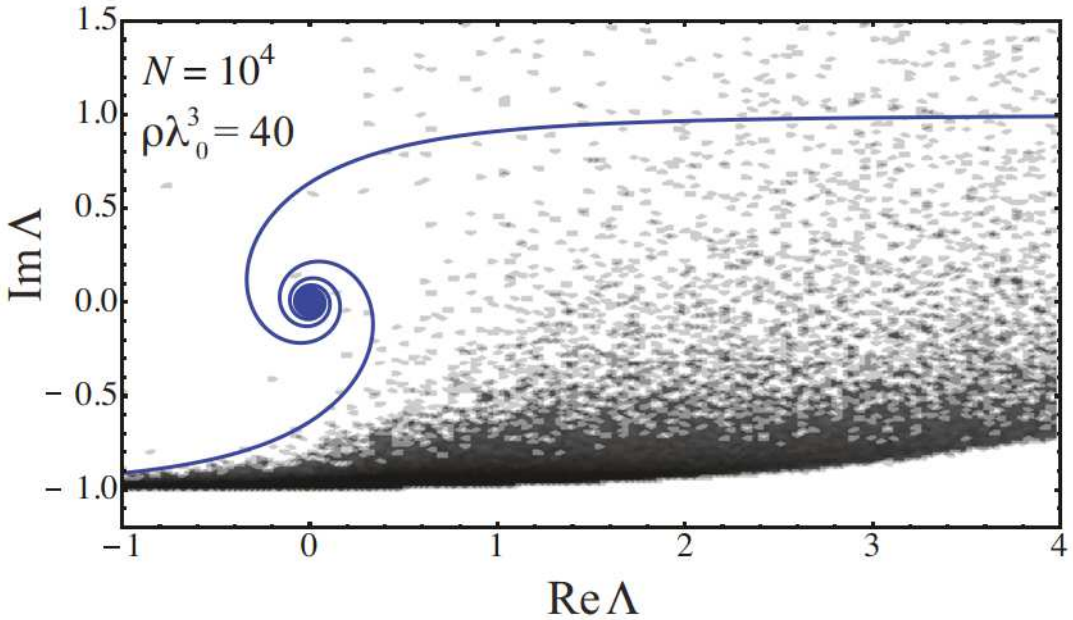

Figure 6.10: Zoom of the density plot of the logarithm of eigenvalue density of the $N \times N$ random Green's matrix (6.101) obtained by numerical diagonalization of 10 realizations of the matrix for $N = 10^4$ and $\rho\lambda_0^3 = 40$. Solid lines represent the pair of subradiant and superradiant branches discussed in the text.

that lack in our model (6.38), (6.39), fall very close to the axis $\mathrm{Im}\Lambda = -1$, in the 'gap' that opens in the eigenvalue distribution following from our theory on the left from $\mathrm{Re}\Lambda = 0$ [see Figs. 6.6(c), 6.6(d), 6.7, 6.8, and 6.10]. The same effect was observed for the Hermitian matrix $\mathrm{Re}G(\omega_0)$, see section 5.8.2.

As explained earlier, the lack of the spiral branches of $p(\Lambda)$ in our theory can be traced back to the assumption of statistical independence of elements of the matrix H in the representation $A = HTH^\dagger$. It does not affect the excellent agreement of the borderline of the rest of the eigenvalue domain with numerical results.

An important implication of the existence of the hyperbolic spiral branches is that quantities such as $\langle \min(\mathrm{Re}\Lambda)\rangle$ or $\langle \min(\mathrm{Im}\Lambda)\rangle$, that are *a priori* difficult to calculate, can be found from 2-body interactions only. $\langle \min(\mathrm{Re}\Lambda)\rangle$ and $\langle \min(\mathrm{Im}\Lambda)\rangle$ are directly related to physical observables. The former may control the threshold of a random laser (see chapter 7), while the latter defines the average threshold for dynamic instabilities in nonlinear media. Instabilities appear when the nonlinear coefficient ν defined in Eq. (2.102) exceeds a critical value ν_{inst} (see section 2.5.3). In Ref. [108] it was found numerically that the average value of the instability threshold scales as $\langle \nu_{inst}\rangle \propto [1 + \langle \min(\mathrm{Im}\Lambda)\rangle]^{3/2}$, with $1 + \langle \min(\mathrm{Im}\Lambda)\rangle \propto (N\rho\lambda_0^3)^{-2/3}$. We now provide simple arguments to derive the full distributions of $\min(\mathrm{Re}\Lambda)$ and $\min(\mathrm{Im}\Lambda)$ analytically, based on the knowledge of the two eigenvalues $\Lambda_\pm = \pm G_{12}(\omega_0)$ of the 2×2 Green's matrix. The smallest values of $\mathrm{Re}\Lambda$ and $\mathrm{Im}\Lambda$ are achieved for small distance $k_0\Delta r = k_0|\mathbf{r}_1 - \mathbf{r}_2|$ when

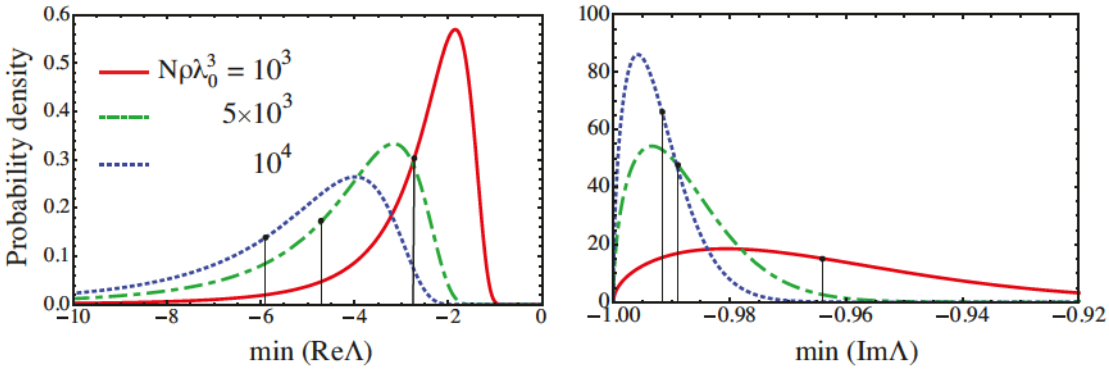

Figure 6.11: Analytic predictions (6.143) and (6.144) for the probability density of the minimum of the real and imaginary parts of the eigenvalues of the Green's matrix (6.101). Vertical lines show the positions of the means given by Eqs. (6.145) and (6.146).

we can write

$$\mathrm{Re}\Lambda_- = -\frac{\cos(k_0\Delta r)}{k_0\Delta r} = -\frac{1}{k_0\Delta r} + \mathcal{O}(k_0\Delta r), \tag{6.139}$$

$$\mathrm{Im}\Lambda_- = -\frac{\sin(k_0\Delta r)}{k_0\Delta r} = -1 - \frac{(k_0\Delta r)^2}{6} + \mathcal{O}(k_0\Delta r^4). \tag{6.140}$$

Hence, the statistical distributions of min(ReΛ) and min(ImΛ) are directly related to the statistical distribution $p(\Delta r_{\min})$ of the minimal distance $\Delta r_{\min}$ between any 2 points among N points in the sphere of radius R. The distribution $p(\Delta r_{\min})$ is easily obtained from the probability to find two points separated by a distance $\Delta r > xR$:

$$\begin{aligned} p(\Delta r > xR) &= \left[1 - \int_0^{xR} \mathrm{d}\Delta r' p(\Delta r')\right]^{N(N-1)/2} \\ &= \left[1 - x^3\left(1 - \frac{9x}{16} + \frac{x^3}{32}\right)\right]^{N(N-1)/2}, \end{aligned} \tag{6.141}$$

where the probability to find two points separated by a distance $\Delta r'$, $p(\Delta r') = 4(\Delta r')^2 s(\Delta r'/2R)/R^3$, follows from Eq. (5.128). The probability $p(\Delta r_{\min})$ is then

$$p(\Delta r_{\min}) = \frac{1}{R}\frac{\mathrm{d}}{\mathrm{d}x}\left[1 - p(\Delta r > xR)\right]|_{x=\Delta r_{\min}/R}. \tag{6.142}$$

The combination of Eqs. (6.139), (6.140), (6.141) and (6.142) yields the distributions $p[\min(\mathrm{Re}\Lambda)]$ and $p[\min(\mathrm{Im}\Lambda)]$. In the limit $N \to \infty$ and $k_0R \gg 1$, these distributions reduce to

$$p[\min(\mathrm{Re}\Lambda) = x] = \frac{N\rho\lambda_0^3}{4\pi^2x^4}\exp\left(\frac{N\rho\lambda_0^3}{12\pi^2x^3}\right), \tag{6.143}$$

$$p[\min(\mathrm{Im}\Lambda) = y] = \frac{9N\rho\lambda_0^3}{2\sqrt{6}\pi^2}\sqrt{y+1}\exp\left(-\frac{\sqrt{6}}{2\pi^2}N\rho\lambda_0^3(y+1)^{3/2}\right), \tag{6.144}$$

which both depend on the parameter $N\rho\lambda_0^3$ only. They are represented in Fig. 6.11.

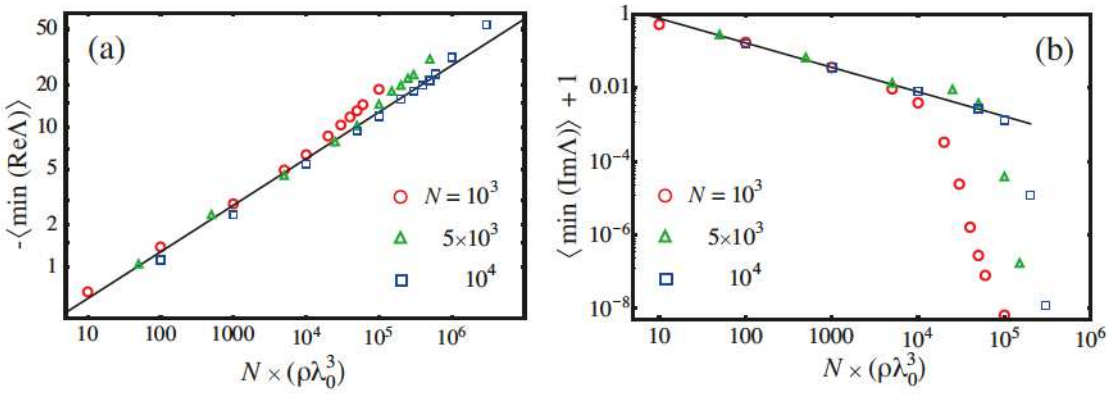

Figure 6.12: Mean minimum value of the real part (a) and the imaginary part (b) of the eigenvalues of the $N \times N$ random Green's matrix (6.101). Analytic results (6.145) and (6.146) (solid lines) are compared with the results of numerical diagonalization for three different matrix sizes N (symbols). Analytic results are valid for $\rho\lambda_0^3 \lesssim 10$.

Their means are given by

$$\langle \min(\mathrm{Re}\Lambda)\rangle = -\Gamma(2/3)\left(\frac{N\rho\lambda_0^3}{12\pi^2}\right)^{1/3}, \tag{6.145}$$

$$\langle \min(\mathrm{Im}\Lambda)\rangle = -1 + \Gamma(5/3)\left(\frac{2\pi^2}{\sqrt{6}N\rho\lambda_0^3}\right)^{2/3}, \tag{6.146}$$

where $\Gamma(x)$ is the Gamma function. Contrary to $\min(\mathrm{Im}\Lambda)$, $\min(\mathrm{Re}\Lambda)$ presents large fluctuations in the limit $N\rho\lambda_0^3 \to \infty$. This can be seen in the variances:

$$\mathrm{Var}[\min(\mathrm{Re}\Lambda)] = [\Gamma(1/3) - \Gamma(2/3)^2]\left(\frac{N\rho\lambda_0^3}{12\pi^2}\right)^{2/3}, \tag{6.147}$$

$$\mathrm{Var}[\min(\mathrm{Im}\Lambda)] = \left(\frac{2\pi^2}{\sqrt{6}N\rho\lambda_0^3}\right)^{4/3}\left\{\frac{4}{9}\Gamma(1/3) - \Gamma(5/3)^2 + [2\Gamma(5/3) - \frac{6}{5}\Gamma(8/3)]\left(\frac{\sqrt{6}N\rho\lambda_0^3}{2\pi^2}\right)^{2/3}\right\}. \tag{6.148}$$

Analytic results (6.145) and (6.146) are compared with numerical simulations in Fig. 6.12. Good agreement is seen as long as $\rho\lambda_0^3 \lesssim 10$, confirming the scaling with $N\rho\lambda_0^3$. At higher densities, $\langle \min(\mathrm{Re}\Lambda)\rangle$ and $\langle \min(\mathrm{Im}\Lambda)\rangle$ are smaller than predicted by Eqs. (6.145) and (6.146), signaling that $\min(\mathrm{Re}\Lambda)$ and $\min(\mathrm{Im}\Lambda)$ are not dominated by the eigenvalues corresponding to eigenvectors localized on pairs of points anymore. And indeed, we observe in the numerical simulations at $\rho\lambda_0^3 \gtrsim 10$ that $\langle \min(\mathrm{Im}\Lambda)\rangle$ is imposed by the lower bound of the bulk of eigenvalues [see Fig. 6.6(b) and 6.12(b)]. Our equations (6.135) and (6.136) that describe the bulk of eigenvalues seem not accurate enough to capture this effect [note the logarithmic scale in Fig. 6.12(b)]. In fact, the bulk and the lower branch cannot be considered independently for $\rho\lambda_0^3 \gtrsim 10$. This can be inferred from Fig. 6.12(a) where $\langle \min(\mathrm{Re}\Lambda)\rangle$ is smaller than predicted by Eq. (6.145) because eigenvalues from the

bulk invade the lower branch and therefore 'push' the eigenvalues from the branch away. Further work is needed to explain these observations quantitatively.

The scalar random Green's matrix (6.101) is the relevant matrix to study light propagation in disordered media as long as the vector nature of the electromagnetic field can be neglected. In particular, if points $\mathbf{r}_i$ are in a near-field configuration $k_0|\mathbf{r}_i - \mathbf{r}_j| \ll 1$ — as it is the case when considering eigenvalues in the spiral branches — the scalar approximation is not justified. Hence, the spiral branches of the scalar Green's matrix cannot quantitatively describe effects such as subradiance in the light-matter interaction. We reconsider this problem in the next section by studying the eigenvalue distribution of the Dyadic random Green's matrix.

6.5.3 Dyadic random Green's matrix

We now consider the $3N \times 3N$ dyadic random Green's matrix $\mathbf{G}(\omega_0)$. This matrix is made of N^2 blocks of size 3×3 defined as

$$\mathbf{G}_{ij}(\omega_0) = \frac{3}{2}(1-\delta_{ij})\frac{\exp(\mathrm{i}k_0 r_{ij})}{k_0 r_{ij}}\left[P(\mathrm{i}k_0 r_{ij})I_3 + Q(\mathrm{i}k_0 r_{ij})\frac{\mathbf{r}_{ij}\otimes\mathbf{r}_{ij}}{r_{ij}^2}\right], \tag{6.149}$$

where $\mathbf{r}_{ij} = \mathbf{r}_i - \mathbf{r}_j$, I_3 is the 3×3 identity matrix, and $P(x)$ and $Q(x)$ are defined by Eq. (2.37). We recall that $\mathbf{G}(\omega_0)$ emerges naturally from the description of light-matter interaction (chapter 2). It is proportional to the Green's function of the propagation equation for the electric field; see Eqs. (2.36), (2.39), and (2.70). This matrix was considered in chapter 3 to compute the spectrum of light emitted by a cloud of atoms, and in chapter 4 to study elastic scattering in the presence of gain. In particular, we recall that eigenvalues of $\mathbf{G}(\omega_0)$ control the lasing threshold according to Eqs. (4.33) and (4.34).

We first want to show that the statistical properties of $\mathbf{G}(\omega_0)$ are related, in the low-density regime $\rho\lambda_0^3 \lesssim 10$, to those of the scalar Green's matrix (6.101) in a simple way. For this purpose, we rexpress $\mathbf{G}_{ij}(\omega_0)$ in terms of the entries of $G(\omega_0)$ as:

$$\mathbf{G}_{ij}(\omega_0) = G_{ij}(\omega_0)D(\mathbf{r}_{ij}), \tag{6.150}$$

where D is the 3×3 matrix:

$$D(\mathbf{r}) = \frac{3}{2}\left[P(\mathrm{i}k_0 r)I_3 + Q(\mathrm{i}k_0 r)\frac{\mathbf{r}\otimes\mathbf{r}}{r^2}\right]. \tag{6.151}$$

On average, $D(\mathbf{r})$ is equal to the identity matrix:

$$\langle D(\mathbf{r})\rangle = \int_V \frac{\mathrm{d}^3\mathbf{r}}{V} D(\mathbf{r}) = I_3. \tag{6.152}$$

In view of Eq. (6.150), we propose to approximate $\mathbf{G}(\omega_0)$ as

$$\mathbf{G}(\omega_0) \simeq G(\omega_0) \otimes D(\mathbf{r}_1' - \mathbf{r}_2'), \tag{6.153}$$

i.e. as the Kronecker product of the $N \times N$ random matrix $G(\omega_0)$ with the 3×3 random matrix $D(\mathbf{r}_1' - \mathbf{r}_2')$. The two points $\mathbf{r}_1'$ and $\mathbf{r}_2'$ are randomly chosen inside the volume V, and in the limit $N \gg 1$, they are assumed to be independent of the N points $\{\mathbf{r}_i\}$. Eq. (6.153) means that the eigenvalues of $\mathbf{G}(\omega_0)$ and $G(\omega_0)$ are related according to

$$\Lambda_{\mathbf{G}(\omega_0)} = \Lambda_{G(\omega_0)}\Lambda_{D(\mathbf{r}_1'-\mathbf{r}_2')}, \tag{6.154}$$

where the eigenvalues $\Lambda_{D(\mathbf{r})}$ of the matrix $D(\mathbf{r})$ are

$$\{\Lambda_{D(\mathbf{r})}\} = \frac{3}{2}\left\{P(\mathrm{i}k_0 r), P(\mathrm{i}k_0 r), P(\mathrm{i}k_0 r) + Q(\mathrm{i}k_0 r)\right\}. \tag{6.155}$$

In the regime of low densities $\rho\lambda_0^3 \lesssim 10$, we showed that the borderline of the eigenvalue domain of the scalar Green's matrix (6.101) depends essentially on $\gamma = \langle|\Lambda_{G(\omega_0)}|^2\rangle$, see Eq. (6.117).[15] If we assume that this property holds for the dyadic Green's matrix, the problem reduces to calculate the second moment $\langle|\Lambda_{\mathbf{G}(\omega_0)}|^2\rangle$. According to Eq. (6.154), the latter is given by

$$\left\langle|\Lambda_{\mathbf{G}(\omega_0)}|^2\right\rangle = \left\langle|\Lambda_{G(\omega_0)}|^2\right\rangle \left\langle|\Lambda_{D(\mathbf{r}'_1-\mathbf{r}'_2)}|^2\right\rangle. \tag{6.156}$$

For $\rho\lambda_0^3 \lesssim 10$ and $k_0 R \gg 1$, it is sufficient to take

$$\{\Lambda_{D(\mathbf{r})}\} \simeq \frac{3}{2}\{1, 1, 0\}, \tag{6.157}$$

so that Eq. (6.156) becomes

$$\left\langle|\Lambda_{\mathbf{G}(\omega_0)}|^2\right\rangle \simeq \frac{3}{2}\left\langle|\Lambda_{G(\omega_0)}|^2\right\rangle. \tag{6.158}$$

Therefore, an equation for the borderline of the eigenvalue domain of $\mathbf{G}(\omega_0)$ follows from equations derived in section 6.5.1.a by replacing the variance γ by $3\gamma/2$. From Eq. (6.117), we obtain:

$$|\Lambda|^2 \simeq 3\gamma h\left(-4\gamma\frac{\mathrm{Im}\Lambda}{|\Lambda|^2}\right). \tag{6.159}$$

The borderline corresponding to Eq. (6.159) is compared with results of numerical diagonalization in Fig. 6.13. As expected, the agreement is satisfactory as long as $\rho\lambda_0^3 \lesssim 10$.

In Fig. 6.13, we also show two pairs of sub- and superradiant branches. They correspond to the six eigenvalues of the $3N \times 3N$ matrix $\mathbf{G}(\omega_0)$ for $N = 2$. In this simple case, the representation (6.153) is exact with $\mathbf{r}'_1 = \mathbf{r}_1$ and $\mathbf{r}'_2 = \mathbf{r}_2$. The eigenvalues of $\mathbf{G}(\omega_0)$ follow therefore from the combination of Eqs. (6.154) and (6.155):

$$\{\Lambda_{\mathbf{G}(\omega_0)}\} = \pm\frac{3}{2}\frac{\exp(\mathrm{i}k_0 r_{12})}{k_0 r_{12}}\left\{P(\mathrm{i}k_0 r_{12}), P(\mathrm{i}k_0 r_{12}), P(\mathrm{i}k_0 r_{12}) + Q(\mathrm{i}k_0 r_{12})\right\}. \tag{6.160}$$

There are two different eigenvalues that are two-times degenerate, and correspond to eigenvectors that can be seen as pairs of 'dipoles' oriented perpendicularly to $\mathbf{r}_{12}$, see Fig. 6.13. The two other eigenvalues are located on a pair of subradiant and superradiant branches, qualitatively similar to those of the scalar Green's matrix. They are, however, quantitatively different. In the limit $k_0\Delta r = k_0 r_{12} \to 0$, the subradiant branch $\Lambda_- = -3e^{\mathrm{i}k_0\Delta r}(1/k_0\Delta r - \mathrm{i})/(k_0\Delta r)^2$ is expanded in series as

$$\mathrm{Re}\Lambda_- = -\frac{3}{(k_0\Delta r)^3} + \mathcal{O}\left(\frac{1}{k_0\Delta r}\right), \tag{6.161}$$

$$\mathrm{Im}\Lambda_- = -1 + \frac{(k_0\Delta r)^2}{10} + \mathcal{O}(k_0\Delta r^4). \tag{6.162}$$

[15] In section 6.5.4 we will also show that γ controls the full distribution $p(\Lambda)$ for $\rho\lambda_0^3 \lesssim 10$.

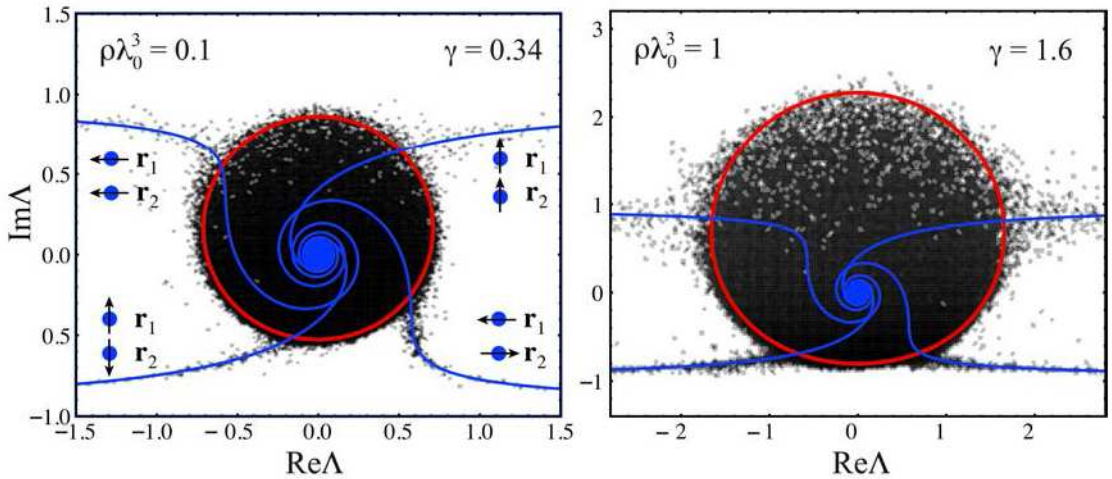

Figure 6.13: Density plots of the logarithm of eigenvalue density of the $3N \times 3N$ random Green's matrix (6.149) obtained by numerical diagonalization of 10 realizations of the matrix for $N = 2 \times 10^3$. Points $\mathbf{r}_i$ are randomly chosen inside a sphere of radius R. The solid red lines represent the borderlines of the support of eigenvalue density following from Eq. (6.159). The four branches follow from Eq. (6.160). Eigenvectors of $\mathbf{G}(\omega_0)$ corresponding to eigenvalues situated in the branches are represented as pairs of dipoles localized on pairs of points $\mathbf{r}_1$ and $\mathbf{r}_2$, with different orientation with respect to the direction $\mathbf{r}_1 - \mathbf{r}_2$.

Note that $[\mathrm{Im}\Lambda_- + 1]_{\mathrm{vector}} = \frac{3}{5}[\mathrm{Im}\Lambda_- + 1]_{\mathrm{scalar}}$ [see Eq. (6.140)]. The distributions $p[\min(\mathrm{Re}\Lambda)]$ and $p[\min(\mathrm{Im}\Lambda)]$ of the $3N \times 3N$ matrix $\mathbf{G}(\omega_0)$ follow from Eqs. (6.141), and (6.142). In the limit $N \to \infty$ and $k_0 R \gg 1$, we find

$$p[\min(\mathrm{Re}\Lambda) = x] = \frac{N\rho\lambda_0^3}{4\pi^2 x^2} \exp\left(\frac{N\rho\lambda_0^3}{4\pi^2 x}\right), \tag{6.163}$$

$$p[\min(\mathrm{Im}\Lambda) = y] = \frac{5\sqrt{10}N\rho\lambda_0^3}{4\pi^2}\sqrt{y+1}\exp\left(-\frac{5\sqrt{10}}{6\pi^2}N\rho\lambda_0^3(y+1)^{3/2}\right). \tag{6.164}$$

The mean and the variance of $\min(\mathrm{Re}\Lambda)$ are not defined, and the mean of $\min(\mathrm{Im}\Lambda)$ is

$$\langle\min(\mathrm{Im}\Lambda)\rangle = -1 + \frac{3}{5}\Gamma(5/3)\left(\frac{2\pi^2}{\sqrt{6}N\rho\lambda_0^3}\right)^{2/3}. \tag{6.165}$$

6.5.4 $G(\omega_0)$: eigenvalue density profile and projections

Let us now analyze the shape of the eigenvalue density $p(\Lambda)$ of the $N \times N$ scalar Green's matrix (6.101) inside its support $\mathcal{D}$. This analysis can be done analytically by solving Eqs. (6.38) and (6.39).

But before using Eqs. (6.38) and (6.39), we would like to mention an interesting relation between the statistical properties of the non-Hermitian matrix $G(\omega_0)$ and those of the Hermitian matrices $S(\omega_0)$ and $C(\omega_0)$ studied in the previous chapter 5. Because the matrices $S(\omega_0)$ and $C(\omega_0)$ represent the imaginary and real parts of the matrix

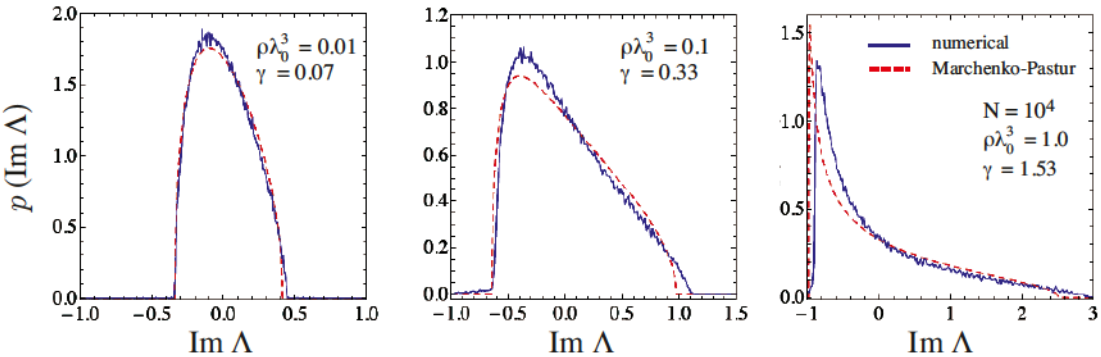

Figure 6.14: Marginal probability density of the imaginary part of eigenvalues Λ of the $N \times N$ random Green's matrix (6.101) compared to the Marchenko-Pastur law (5.171) with Λ replaced by $\mathrm{Im}\Lambda+1$ and γ replaced by $\gamma/2$ (dashed red line). Points are randomly chosen inside a cube of side L; $\gamma = 2.8N/(k_0L)^2$, see Eqs. (5.166) and (5.186).

$G(\omega_0)$, respectively, one might expect some links between the probability distribution of eigenvalues of $S(\omega_0)$ and $C(\omega_0)$ and the marginal probability distributions of the real and imaginary parts of the eigenvalues of $G(\omega_0)$, $p[\mathrm{Re}\Lambda_{G(\omega_0)}]$ and $p[\mathrm{Im}\Lambda_{G(\omega_0)}]$. To elaborate on this issue, we make two observations. First, at low densities $\rho\lambda_0^3 \lesssim 1$, the eigenvalue distribution of $G(\omega_0)$ depends on the second moment $\gamma = \langle|\Lambda|^2\rangle$ only. It is thus also the case for $p[\mathrm{Re}\Lambda_{G(\omega_0)}]$ and $p[\mathrm{Im}\Lambda_{G(\omega_0)}]$. Second, Eqs. (6.103) and (6.104) suggest that

$$\gamma = \langle\Lambda^2\rangle_{\mathrm{Re}G(\omega_0)} = 2\left\langle(\mathrm{Re}\Lambda)^2\right\rangle_{G(\omega_0)}, \tag{6.166}$$

$$= \langle\Lambda^2\rangle_{\mathrm{Im}G(\omega_0)} = 2\left\langle(\mathrm{Im}\Lambda)^2\right\rangle_{G(\omega_0)}, \tag{6.167}$$

as long as $k_0R \gg 1$ and the density is not too high. We now recall that the eigenvalue distributions of $\mathrm{Im}G(\omega_0)$ and $\mathrm{Re}G(\omega_0)$ depend as well on γ only, for $\rho\lambda_0^3 \lesssim 1$. It is therefore reasonable to conjecture that $p[\mathrm{Im}\Lambda_{G(\omega_0)}]$ and $p[\mathrm{Re}\Lambda_{G(\omega_0)}]$ may be described by equations for $p[\Lambda_{\mathrm{Im}G(\omega_0)}]$ and $p[\Lambda_{\mathrm{Re}G(\omega_0)}]$ with γ replaced by $\gamma/2$:

$$p\left[\mathrm{Im}\Lambda_{G(\omega_0)}, \gamma\right] \simeq p\left[\Lambda_{\mathrm{Im}G(\omega_0)}, \frac{\gamma}{2}\right], \tag{6.168}$$

$$p\left[\mathrm{Re}\Lambda_{G(\omega_0)}, \gamma\right] \simeq p\left[\Lambda_{\mathrm{Re}G(\omega_0)}, \frac{\gamma}{2}\right]. \tag{6.169}$$

Figures 6.14 and 6.15 show, indeed, that numerical marginal distributions are nicely described by the laws following from Eqs. (5.171) and (5.191) where we replaced γ by $\gamma/2$. The marginal distribution $p[\mathrm{Im}\Lambda_{G(\omega_0)}]$ is well approximated by the Marchenko-Pastur law (5.171) as long as $\gamma/2 \lesssim 1$ (Fig. 6.14), and Eq. (5.191) is a good estimate of $p[\mathrm{Re}\Lambda_{G(\omega_0)}]$ for $\rho\lambda_0^3 \lesssim 10$ (Fig. 6.15).

Let us now investigate the shape of $p(\Lambda)$ with the help of Eqs. (6.38) and (6.39). Very generally, $p(\Lambda)$ is roughly symmetric with respect to the line $\mathrm{Re}\Lambda = 0$ and decays with $\mathrm{Im}\Lambda$. In the regime of low densities $\rho\lambda_0^3 \lesssim 1$, an approximation of Eqs. (6.38) and (6.39) can be obtained by replacing the operator $\hat{S}_1$ by $\hat{S}_0$. This amounts to neglecting the term $c^2\hat{T}\hat{T}^\dagger$ in the denominator of Eq. (6.37). Then, Eqs. (6.38) and (6.39) reduce to

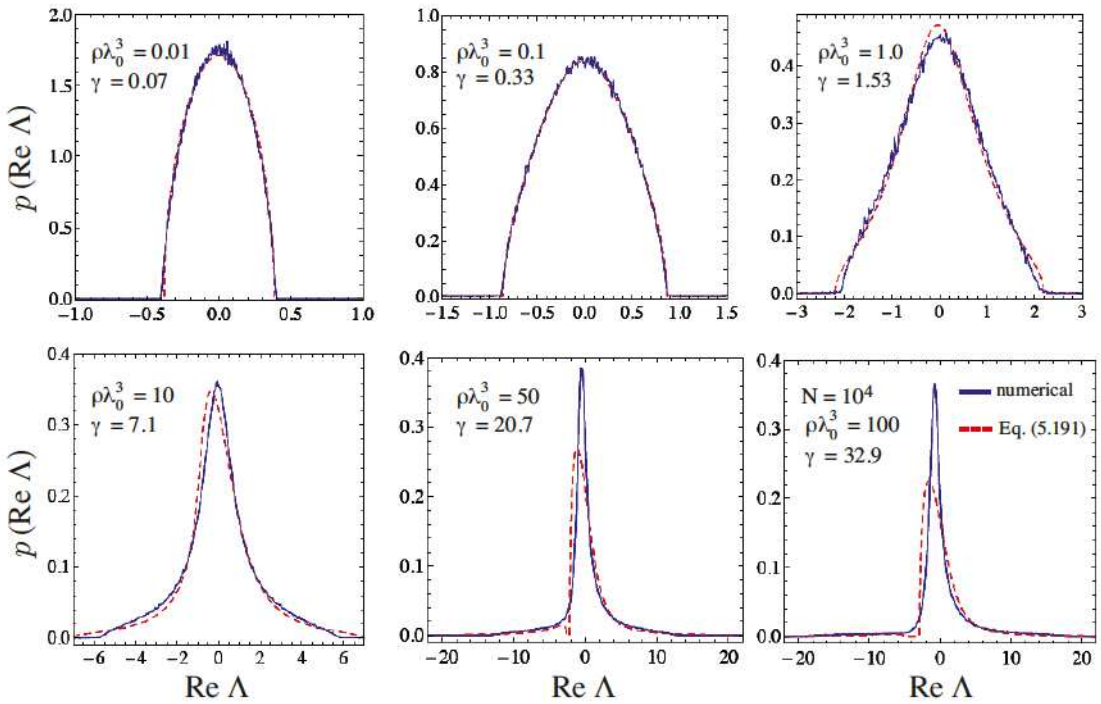

Figure 6.15: Marginal probability density of the real part of eigenvalues Λ of the $N \times N$ random Green's matrix (6.101) compared to Eq. (5.191) with Λ replaced by ReΛ and γ replaced by $\gamma/2$ (dashed red line). Points are randomly chosen inside a cube of side L; $\gamma = 2.8N/(k_0L)^2$, see Eqs. (5.166) and (5.186).

two equations where the resolvent $g(z)$ and the eigenvector correlator $c(z)$ are decoupled:

$$g(z) = \frac{z^* - \frac{1}{N}\mathrm{Tr}\hat{S}_0^\dagger}{\frac{1}{N}\mathrm{Tr}\hat{S}_0\hat{S}_0^\dagger}, \tag{6.170}$$

$$c(z)^2 = |g(z)|^2 - \frac{N}{\mathrm{Tr}\hat{S}_0\hat{S}_0^\dagger}. \tag{6.171}$$

Assuming explicitly that the N points are distributed in a sphere of radius R, we can make use of the results of section 6.5.1.a to compute traces in these equations, so that Eqs. (6.170) and (6.171) become

$$g(z) = \frac{z^* - 2\gamma g(z)^* h\left(\mathrm{i}\kappa[g(z)]^* R + \mathrm{i}k_0 R\right)}{2\gamma h\left(2\,\mathrm{Im}\kappa[g(z)]R\right)}, \tag{6.172}$$

$$c(z)^2 = |g(z)|^2 - \frac{1}{2\gamma h\left(2\,\mathrm{Im}\kappa[g(z)]R\right)}, \tag{6.173}$$

where the functions $\kappa(g)$ and $h(x)$ are defined by Eqs. (6.112) and (6.115), respectively. We find the resolvent $g(z)$ by solving Eq. (6.172) numerically and then evaluate the eigenvalue density $p(\Lambda)$ with the help of Eq. (6.4). Note that Eq. (6.172) applies only within the eigenvalue domain $\mathcal{D}$ given by Eq. (6.116). Figure 6.16 shows the full distribution $p(\Lambda)$ obtained in this way for $N = 10^4$ and $\rho\lambda_0^3 = 1$, together with the result of numerical diagonalization.

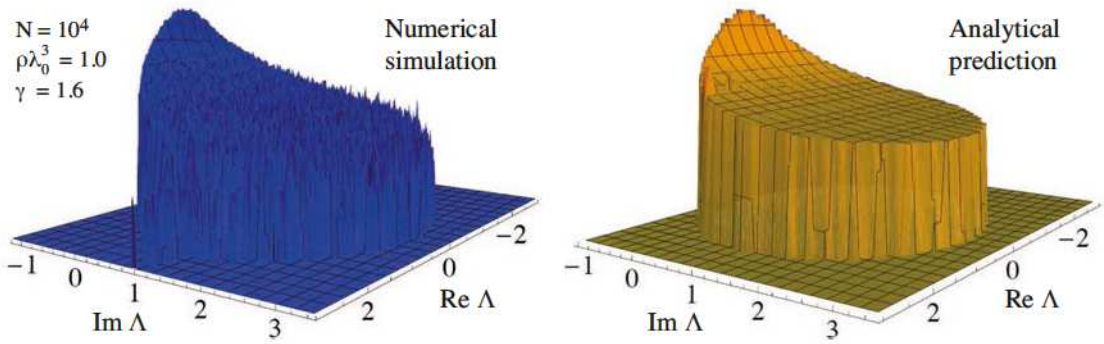

Figure 6.16: Logarithm of the eigenvalue density of the $N \times N$ random Green's matrix (6.101). Numerical results obtained by diagonalization of 10 realizations of the matrix for $N = 10^4$ (left) are compared with the solution of Eq. (6.172) (right). Points $\mathbf{r}_i$ are chosen randomly inside a sphere of radius R; $\gamma = 9N/8(k_0R)^2$. For a quantitive comparison, see Fig. 6.17.

The marginal probability distributions of the imaginary and real parts are finally obtained after projection of $p(\Lambda)$ on the imaginary and real axes. A good quantitative agreement is found with numerical simulations presented in Fig. 6.17 for $\rho\lambda_0^3 = 0.1$ and $\rho\lambda_0^3 = 1$. At higher densities $\rho\lambda_0^3 \gtrsim 1$, Eq. (6.172) is not a good approximation of Eqs. (6.38) and (6.39) anymore. Eqs. (6.38) and (6.39) are difficult to solve exactly for two reasons: $g(z)$ and $c(z)$ are coupled, and $\mathrm{Tr}\hat{S}_1\hat{S}_0^\dagger$ has no 'simple' expression in the bi-orthogonal basis of eigenvectors of the operator $\hat{T}$, contrary to $\mathrm{Tr}\hat{S}_0\hat{S}_0^\dagger$ [see Eqs. (6.57), (6.58), (6.135), and (6.136).] Further work is needed to be able to deduce the eigenvalue distribution $p(\Lambda)$ from Eqs. (6.38) and (6.39) at high densities $\rho\lambda_0^3 \gtrsim 1$.

6.6 Green's matrix and Anderson localization in a finite and open medium

Rigorously, Anderson localization is a phenomenon that is well defined in an infinite medium. In a three-dimensional system, in the absence of gain or absorption, and for a given disorder strength, a wave is expected to be exponentially suppressed at a large distance from its source (and therefore localized) if its frequency ω_L is below the so-called mobility edge ω_c.[16] Said differently, and probably more precisely, all 'modes' (or states, or eigenfunctions) are expected to be exponentially localized for $\omega_L < \omega_c$ and delocalized for $\omega_L > \omega_c$. From these two pictures have emerged two different types of criteria to identify the Anderson localization.

First, we can look at the solution of the transport equation for the average intensity, without invoking the underlying mode structure. One of the first microscopic theories of Anderson localization is the diagrammatic self-consistent theory proposed in the 1980's by Volhardt and Wölfe [136]. To illustrate this theory, let us reconsider the elastic scattering of light in a random arrangement of N identical point-like scatterers (atoms) studied in chapter 4. In the simplest case, we can think of the Bethe-Salpeter equation (4.104) in the absence of pump ($l_e = l_s$) and for atoms on resonance ($\omega_L = \omega_0$), simplified

[16] A detailed consideration shows that there may be several (at least two for light, see Ref. [213]) mobility edges.

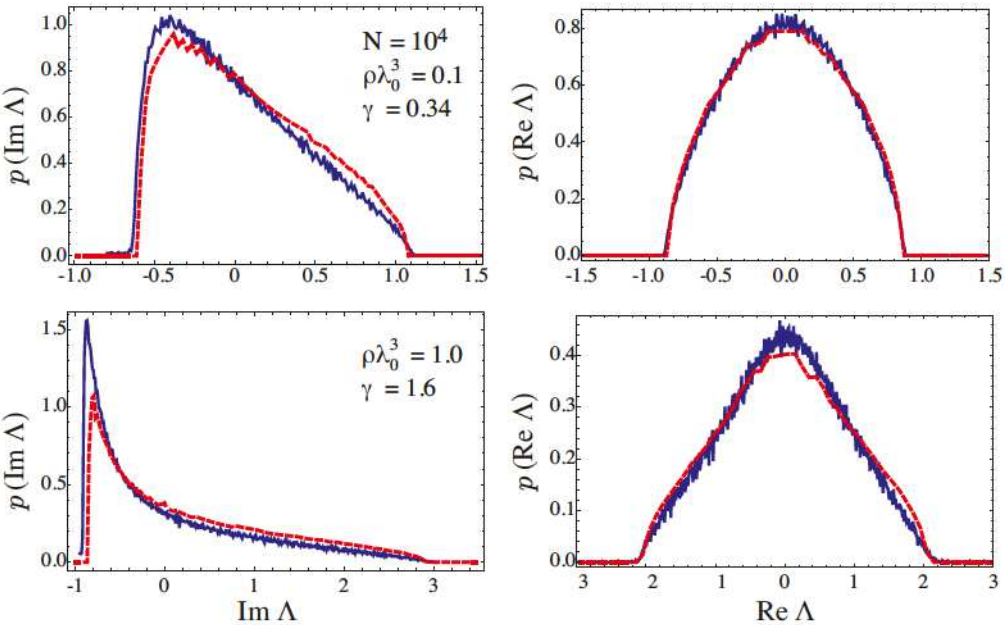

Figure 6.17: Marginal probability density of the imaginary part (left column) and the real part (right column) of eigenvalues Λ of the $N \times N$ random Green's matrix (6.101), where the N points $\mathbf{r}_i$ are randomly chosen inside a sphere of radius R; $\gamma = 9N/8(k_0R)^2$. Results of numerical diagonalization (blue solid lines) obtained for $N = 10^4$ after averaging over 10 realizations are compared to the solution of Eq. (6.172) (red dot-dashed line).

with the ISA (4.54) and the Boltzmann approximation (4.127). It yields a diffusion equation for the average intensity with a diffusion constant $D_B = l_0 v/3$, where v is the transport velocity and l_0 the on-resonance scattering mean free path (4.129) [see Eqs. (4.121), (4.124) and (4.128)]. Localization corrections to this result are obtained by taking into account maximally crossed diagrams in the irreducible vertex depicted in Fig. 4.3. The diffusion equation becomes self-consistently coupled to an equation for the diffusion coefficient D. The latter involves the 'return probability', *i.e.* the average intensity that goes back to the source [136]. In the 'weak scattering' regime $k_0 l_0 \gg 1$, the diffusion coefficient reduces to

$$D \simeq D_B \left[1 - \frac{1}{(k_0 l_0)^2}\right]. \tag{6.174}$$

This simple expression shows that transport cancels ($D \simeq 0$) for

$$k_0 l_0 = \frac{k_0^3}{4\pi\rho} \simeq 1 \iff \rho\lambda_0^3 \simeq 20. \tag{6.175}$$

This is the so-called Ioffe-Regel criterion for Anderson localization [101]. For $k_0 l_0 \lesssim 1$, interference effects are so strong that they occur during the scattering process and may lead to localization of eigenstates.

An alternative picture consists in looking at the 'modes' of the disordered system under study. As already discussed in sections 2.5.2, 4.4, and 6.4, the modes (or 'quasi-modes' or 'resonances') of a system of N point-like scatterers interacting with light

in a finite and open volume V are the eigenvectors of the effective Hamiltonian H^e (6.100), which are also the eigenvectors R_n of the Green's matrix $G(\omega_0)$. In this context, Anderson localization formally refers to the localized nature of eigenvectors R_n in space due to disorder. We investigate the degree of localization of these eigenvectors in section 6.6.2. On the other hand, one also expects Anderson localization to have an impact on the statistics of the eigenvalues E_n of H^e:

$$E_n = \omega_n - \mathrm{i}\frac{\Gamma_n}{2}, \tag{6.176}$$

$$\omega_n = \omega_0 - \frac{\Gamma_0}{2}\mathrm{Re}\Lambda_n, \tag{6.177}$$

$$\Gamma_n = \Gamma_0\left(1 + \mathrm{Im}\Lambda_n\right), \tag{6.178}$$

where Λ_n are the eigenvalues of the Green's matrix $G(\omega_0)$. Γ_n controls the decay rate of physical observables, such as the intensity of the wave emerging from the random system. Indeed, from the linear analysis of section 4.2, it is straightforward to write the positive frequency part electric field measured at point $\mathbf{r}$ as

$$E^+(\mathbf{r}, \omega_L) = \sum_{n=1}^{N} \frac{a_n(\mathbf{r})}{\Gamma_n/2 - \mathrm{i}(\omega_L - \omega_n)}, \tag{6.179}$$

where $a_n(\mathbf{r})$ is a function that depends on the eigenvector R_n of the Green's matrix and the spatial distribution of the field at the initial time. Signatures of different transport regimes may be traced back to the statistics of eigenvalues Λ_n in various ways. Two options are considered in the following. In section 6.6.1 we study the behavior of $p(\Lambda)$ as a function of $\mathrm{Im}\Lambda$, and in section 6.6.2 we concentrate on the behavior of the Thouless number g. The latter is the ratio between the mean spectral width $\delta\omega$ of the modes and their mean level spacing $\Delta\omega$.[17] Intuitively, one expects Anderson localization to occur when the modes cease to overlap. This criterion,

$$g = \frac{\delta\omega}{\Delta\omega} = g_c \simeq 1, \tag{6.180}$$

is known as the Thouless criterion for Anderson localization in a finite open medium [101, 214]. $\delta\omega^{-1}$ is called the Thouless time, and $\Delta\omega^{-1}$ the Heisenberg time. The Thouless number g can be shown to be equal to the dimensionless conductance of a disordered sample, and it is the only relevant parameter in the scaling theory of Anderson localization [215]. In section 6.6.2 we present preliminary results concerning the calculation of the scaling function $\beta(g)$ from the eigenvalues Λ_n of the Green's matrix.

6.6.1 Statistics of resonances of the random Green's matrix

The generic behavior of the distribution of decay rates $p(\Gamma)$ in a disordered open system may be estimated thanks to the following simple argument [103, 104]. Loosely speaking, the probability of finding a spectral width Γ' smaller than Γ is

$$p(\Gamma' < \Gamma) \sim \frac{[R - r(\Gamma)]^d}{R^d}, \tag{6.181}$$

[17] See section 6.6.2 for a precise definition of $\delta\omega$ and $\Delta\omega$ in terms of the eigenvalues Λ_n.

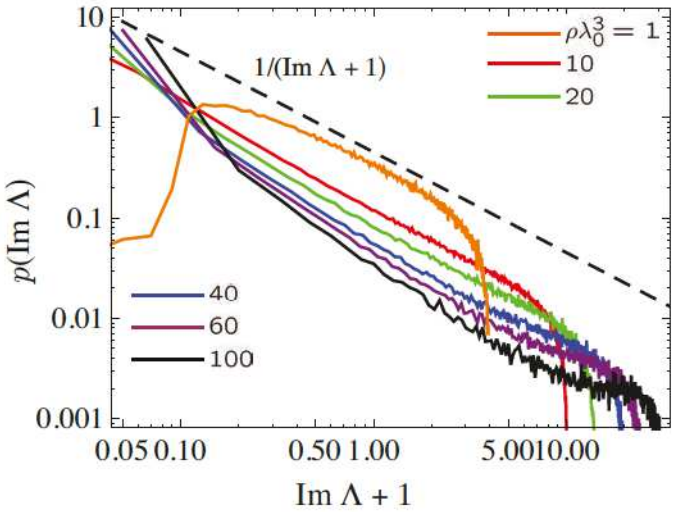

Figure 6.18: Numerical marginal distribution of the imaginary part of the eigenvalues of the $N \times N$ Green's matrix (6.101), where the N points $\mathbf{r}_i$ are randomly chosen inside a cube of side L. Results at densities $\rho\lambda_0^3 = 1, 10, 20, 40, 60$ and 100 (curves from top to bottom) for $N = 10^4$ are compared with the asymptotic law $1/(\mathrm{Im}\Lambda + 1)$ shown by the dashed line.

where R^d is the typical volume of the d-dimensional system and $r(\Gamma)$ is the typical distance (from boundaries) travelled by the waves leaving the system in a time Γ^{-1}. Then, the distribution of decay rates is given by

$$p(\Gamma) = \frac{\mathrm{d}\,p(\Gamma' < \Gamma)}{\mathrm{d}\Gamma'} = -\frac{\mathrm{d}r(\Gamma)}{\mathrm{d}\Gamma} d \left[1 - \frac{r(\Gamma)}{R}\right]^{d-1} \sim -\frac{\mathrm{d}r(\Gamma)}{\mathrm{d}\Gamma}. \tag{6.182}$$

For ballistic and diffusive motions, we obtain:

$$r(\Gamma) = \frac{v}{\Gamma} \quad \Longrightarrow \quad p(\Gamma) \sim \frac{1}{\Gamma^2} \quad \text{(ballistic)}, \tag{6.183}$$

$$r(\Gamma) = \sqrt{\frac{D}{\Gamma}} \quad \Longrightarrow \quad p(\Gamma) \sim \frac{1}{\Gamma^{3/2}} \quad \text{(diffusive)}. \tag{6.184}$$

In the localized regime, modes are exponentially localized, $|\psi(r)| \sim e^{-r/\xi}$ (ξ is the localization length), so that leakage $\Gamma \sim |\psi(r)|^2$ is essentially due to states localized near the system boundaries. This yields

$$\Gamma(r) \sim e^{-2r/\xi} \quad \Longrightarrow \quad p(\Gamma) \sim \frac{1}{\Gamma} \quad \text{(localized)}. \tag{6.185}$$

It is worth noting that the three power laws (6.183), (6.184), and (6.185) apply for one-, two-, or three-dimensional random media. The reason is that $r(\Gamma)$ in Eq. (6.182) is independent of the dimensionality of space.

Pinheiro *et al.* [104] studied numerically the marginal distribution $p(\mathrm{Im}\Lambda)$ of the scalar Green's matrix, and observed $p(\mathrm{Im}\Lambda) \propto 1/(\mathrm{Im}\Lambda + 1)$ at high densities of points. Our numerical results also exhibit such a behavior (see Fig. 6.18). Based on the qualitative prediction (6.185), the authors of [104] conjectured that the power law $p(\mathrm{Im}\Lambda) \propto$

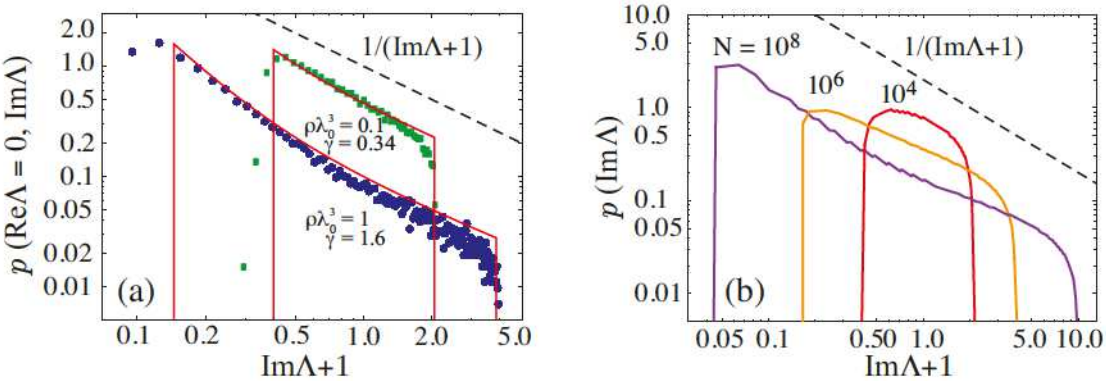

Figure 6.19: (a) Cuts of the eigenvalue density $p(\Lambda)$ of the $N \times N$ Green's matrix (6.101) along the imaginary axis $\mathrm{Re}\Lambda = 0$. $N = 10^4$ points $\mathbf{r}_i$ are randomly chosen inside a sphere of radius R; $\gamma = 9N/8(k_0R)^2$. Results of numerical diagonalization (symbols) are compared with the solution of Eq. (6.172) (solid red lines). (b) Marginal probability density of the imaginary part of eigenvalues of (6.101). Solutions of Eq. (6.172) (solid lines) at $N = 10^4$ ($\gamma = 0.34$), 10^6 ($\gamma = 1.6$), and 10^8 ($\gamma = 7.4$) for $\rho\lambda_0^3 = 0.1$ are compared with the asymptotic law $1/(\mathrm{Im}\Lambda + 1)$ (dashed line).

$1/(\mathrm{Im}\Lambda+1)$ was a signature of Anderson localization of waves in the corresponding point-scatterer model. To test this conjecture, we analyze $p(\Lambda)$ computed from Eq. (6.172) at low densities $\rho\lambda_0^3 \lesssim 1$, for which no Anderson localization is expected, according to the (qualitative) Ioffe-Regel criterion (6.175). In Fig. 6.19(a), we show cuts of $p(\Lambda)$ along the imaginary axis $\mathrm{Re}\Lambda = 0$. We clearly observe that $p(\mathrm{Re}\Lambda = 0, \mathrm{Im}\Lambda)$ decays as $1/(\mathrm{Im}\Lambda + 1)$, even though the density of points $\rho\lambda_0^3$ is too low to bring the system to the Anderson localization transition. For $\gamma \lesssim 1$, although $p(\Lambda) \propto 1/(\mathrm{Im}\Lambda + 1)$, the marginal distribution $p(\mathrm{Im}\Lambda)$ follows the Marchenko Pastur law [see Fig. 6.14] due to the circluar shape of the support of $p(\Lambda)$. Incidentally, we now understand in a new fashion why $p(\mathrm{Im}\Lambda)$ follows the Marchenko Pastur law for $\gamma \lesssim 1$: the latter can be seen as the projection of a two-dimensional distribution $p(\Lambda)$ on the imaginary axis $\mathrm{Im}\Lambda$, provided that $p(\Lambda)$ is different from zero inside a circle of radius $\sqrt{2\gamma}$ centered at $(0, \gamma/2)$ and that $p(\Lambda) \propto 1/(\mathrm{Im}\Lambda + 1)$.[18] The power-law decay becomes visible in the marginal distribution $p(\mathrm{Im}\Lambda)$ [see Fig. 6.18] only when the support of $p(\mathrm{Im}\Lambda)$ is sufficiently wide, *i.e.* for $\gamma \gtrsim 1$. Because the condition $\gamma \gtrsim 1$ can be obeyed at any, even very low density by just increasing the number of points N, it seems that no direct link can be established between the power-law decay of $p(\mathrm{Im}\Lambda)$ and Anderson localization. This also seems to be confirmed by our theoretical prediction for $p(\mathrm{Im}\Lambda)$ computed at large values $N > 10^4$ (that are inaccessible for numerical simulations) and low density $\rho\lambda_0^3 = 0.1$, see Fig. 6.19(b).

Our conclusion is that it is not clear *a priori* if any sign of Anderson localization should (and could) be visible in the density of eigenvalues $p(\Lambda)$, in the marginal distributions $p(\mathrm{Im}\Lambda)$ and $p(\mathrm{Re}\Lambda)$, or in the modifications observed in the shape of the eigenvalue domain when the density is increased (see section 6.5.1). To elaborate on this issue, we analyze in the next section the eigenvectors of the matrix (6.101).

[18] Equation for a circle can be found from Eq. (6.116), and $p(\Lambda) \propto 1/(\mathrm{Im}\Lambda + 1)$ from Eq. (6.172), in the regime $\rho\lambda_0^3 \ll 1$ and $\gamma \lesssim 1$.

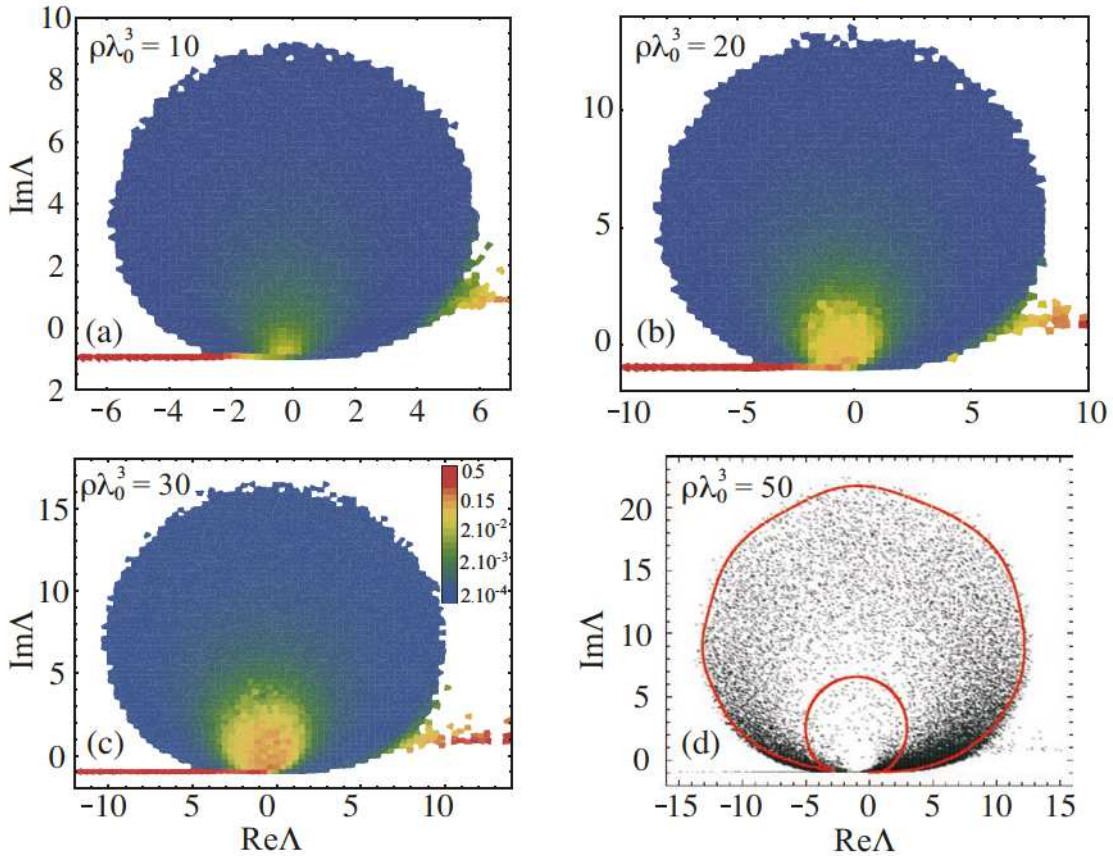

Figure 6.20: (a), (b) and (c) Density plots of the logarithm of the average inverse participation ratio of eigenvectors of the Green's matrix (6.101). For each of these plots, we found eigenvalues of 10 different random realizations of $10^4 \times 10^4$ Green's matrix numerically (with points $\mathbf{r}_i$ randomly chosen inside a sphere of radius R), computed their IPRs using Eq. (6.186), and then determined IPR(Λ) by integrating Eq. (6.187) over a small area $(\Delta\Lambda)^2$ around Λ, for a grid of Λ's on the complex plane. (d) Density plot of the logarithm of the eigenvalue density of (6.101). The solid red line represents the borderline of the support of eigenvalue density following from Eqs. (6.135) and (6.136).

6.6.2 Inverse participation ratio

To determine if an eigenvector $R_n = \{R_n(\mathbf{r}_1), \ldots, R_n(\mathbf{r}_N)\}$ of the Green's matrix (6.101) is localized or not, we compute its inverse participation ratio (IPR), already introduced in section 5.8.2:

$$\mathrm{IPR}_n = \frac{\sum_{i=1}^{N} |R_n(\mathbf{r}_i)|^4}{\left[\sum_{i=1}^{N} |R_n(\mathbf{r}_i)|^2\right]^2}. \tag{6.186}$$

We recall that an eigenvector extended over all N points is characterized by IPR $\sim 1/N$, whereas an eigenvector localized on a single point has IPR $= 1$. The average value of IPR corresponding to eigenvectors with eigenvalues in the vicinity of Λ can be defined as

$$\mathrm{IPR}(\Lambda) = \frac{1}{Np(\Lambda)} \left\langle \sum_{n=1}^{N} \mathrm{IPR}_n \, \delta^2(\Lambda - \Lambda_n) \right\rangle, \tag{6.187}$$

where averaging is over all possible configurations of N points in a sphere. Our numerical analysis of the average IPR defined by this equation reveals the following scenario. At low density $\rho\lambda_0^3 \lesssim 10$, IPR $\simeq 2/N$ for all eigenvectors except those corresponding to the eigenvalues that belong to spiral branches [see Fig. 6.6(a) and (b) and section 6.5.2] for which IPR $\simeq \frac{1}{2}$. These states are localized on pairs of points that are very close together and correspond to proximity resonances [105] that do not require a large optical thickness to build up. The prefactor 2 in the result for IPR of extended eigenvectors is due to the Gaussian statistics of eigenvectors at low densities. For $\rho\lambda_0^3 \gtrsim 10$ [Fig. 6.20(a) and (b)], IPR starts to grow in a roughly circular domain in the vicinity of $\Lambda = 0$ and reaches maximum values ~ 0.1 at $\rho\lambda_0^3 \simeq 30$ [Fig. 6.20(c)]. Contrary to common belief [105], neither localized states necessarily have $\mathrm{Im}\Lambda$ close to -1, nor states with $\mathrm{Im}\Lambda \simeq -1$ are always localized, as can be seen from Fig. 6.20(c). For $\rho\lambda_0^3 > 30$, the localized states start to disappear and a hole opens in the eigenvalue density. As can be seen from the comparison of Fig. 6.20(c) and (d), it is quite remarkable that the opening of the hole in $p(\Lambda)$ [Fig. 6.20(d)] proceeds by disappearance of localized states [*i.e.*, of states with IPR $\gg 1/N$ in Fig. 6.20(c)]. Further work is needed to give a definitive physical interpretation of this scenario. At present, two speculative conjectures can be formulated, that might be the two sides of the same coin. The opening of the hole might be a signature of Anderson localization, meaning that the states localize due to interference effects; or it could be interpreted as a signature of a transition towards an effective medium regime, and in that case localized states could be reminiscent to those that one can observe, *e.g.*, inside a band gap of a periodic structure due to localized defects.

6.6.3 Scaling theory and the Green's matrix

The purpose of the scaling theory of Anderson localization is to capture features that are important on macroscopic scales but insensitive to microscopic details of disorder. In particular, it assumes that transport properties at large scales depend only on one parameter, the Thouless number $g = \delta\omega/\Delta\omega$. From Eq. (6.177), we can express the mean level spacing $\Delta\omega$ in terms of the properties of the Green's matrix as

$$\Delta\omega = \langle \omega_{n-1} - \omega_n \rangle = \frac{\Gamma_0}{2} \langle \mathrm{Re}\Lambda_n - \mathrm{Re}\Lambda_{n-1} \rangle \,, \tag{6.188}$$

where the eigenvalues Λ_n are ordered by their real part. On the other hand, it is worth noting that the mean spectral width of the modes cannot be defined as $\delta\omega = \langle \Gamma_n \rangle$, with Γ_n given by Eq. (6.178), because $\langle \mathrm{Im}\Lambda_n \rangle = 0$ ($\sum_{n=1}^{N} \Lambda_n = 0$ for each realization). Therefore, we define $\delta\omega$ as the inverse of the mean Thouless time:

$$\delta\omega = \left\langle \frac{2}{\Gamma_n} \right\rangle^{-1} = \frac{\Gamma_0}{2} \left\langle \frac{1}{\mathrm{Im}\Lambda_n + 1} \right\rangle^{-1} . \tag{6.189}$$

The definitions (6.188) and (6.189) are consistent with the very recent work of Wang and Genack [216], that shows that it is experimentally possible to measure the set (ω_n, Γ_n) that define the modes of an open random medium. The authors assumed that the electric field $E^+(\mathbf{r})$ has the decomposition (6.179) and found (ω_n, Γ_n) from measurements of microwave spectra at many points $\mathbf{r}$. They could evaluate experimentally the Thouless number $g = \delta\omega/\Delta\omega$ with $\Delta\omega$ and $\delta\omega$ defined as in Eqs. (6.188) and (6.189), and were

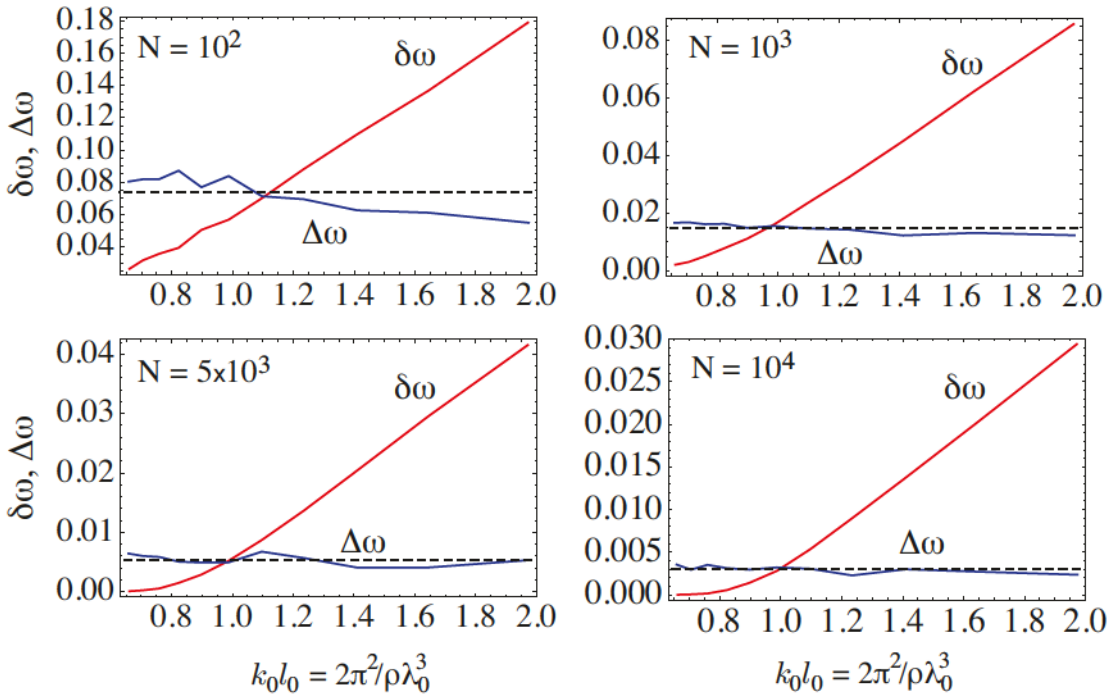

Figure 6.21: Mean spectral width $\delta\omega$ (6.189) and mean level spacing $\Delta\omega$ (6.188) (both normalized by $\Gamma_0/2$) evaluated numerically from the eigenvalues of the $N \times N$ Green's matrix (6.101) for $N = 10^2$, 10^3, 5×10^3 and 10^4, and at 11 different densities $\rho\lambda_0^3 = 10, 12, \ldots, 28, 30$. For $N \gtrsim 10^3$, $\Delta\omega$ is almost constant in the vicinity of $k_0 l_0 \simeq 1$ (dashed lines represent its mean value over the range $k_0 l_0 \in [0.6, 2]$), and $\delta\omega \simeq \Delta\omega$ for $k_0 l_0 \simeq 1$ [see also Fig. 6.22(a)].

able to compare its value to the ensemble average of the transmittance (the analog of the dimensionless conductance for classical waves) [216].

The elegance of the scaling theory comes from the fact that universal features of Anderson localization are captured by the simple scaling function

$$\beta(g) = \frac{\partial \ln g}{\partial \ln k_0 R}. \tag{6.190}$$

This function tells us how g evolves with system size R: $\beta(g) < 0$ means that increasing the system size leads to exponentially small g, and therefore corresponds to the localized regime, while for $\beta(g) > 0$, the 'renormalization flow' leads to delocalized regimes (diffusive and ballistic regimes). In the strongly localized regime $R \gg \xi$, $g \sim e^{-R/\xi}$ and $\beta(g) \sim \ln g$, while in the diffusive regime $R \gg l_0$, $g(R) \sim R^{d-2}$ and $\beta(g) \sim d - 2$. This shows that all states are localized for $d \leq 2$. Assuming that the shape of $\beta(g)$ interpolates smoothly between the two previous asymptotics, one predicts, for $d \geq 3$, the existence of an unstable fixed point g_c defined by $\beta(g_c) = 0$. To the critical point corresponds also a critical frequency ω_c. According to the Thouless criterion of localization (6.180), $g_c \sim 1$. To be consistent with the Ioffe-Regel criterion (6.175), one also should have $k_c l_0 \sim 1$. Using the linearized form $\beta(g) = \ln(g/g_c)/\nu$ around the fixed point g_c, we find after an elementary calculation[19] that the localization length diverges close to the transition for

[19]For a pedagogical introduction to scaling theory of Anderson localization, see, *e.g.*, Ref. [217].

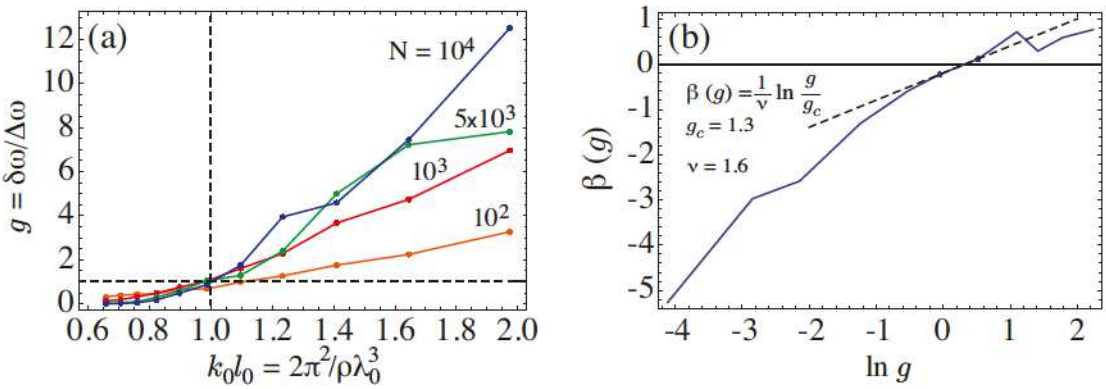

Figure 6.22: (a) Thouless number $g = \delta\omega/\Delta\omega$ evaluated from the data of Fig. 6.21. Curves for different N cross at the critical point $k_0 l_0 \simeq g \simeq 1$. (b) Scaling function $\beta(g) = \partial \ln g / \partial \ln k_0 R$ computed from the results of (a). The slope at the critical point g_c yields the critical exponent $\nu \simeq 1.6$.

$\omega_0 < \omega_c$ as $\xi \sim |\omega_0 - \omega_c|^{-\nu}$, and the diffusion constant vanishes algebraically for $\omega_0 > \omega_c$ as $D \sim (\omega_0 - \omega_c)^{\nu}$. The critical exponent ν is determined by the slope of the scaling function $\beta(g)$ at the transition. From extensive numerical simulations we know today that $\nu = 1.58 \pm 0.01$ [218, 219]. Note that no analytic theory has been able to predict this value so far.

Our goal is to revisit the scaling theory through the statistical properties of the eigenvalues Λ_n of the Green's matrix. In Fig. 6.21, we show numerical computations of $\Delta\omega$ and $\delta\omega$. We diagonalized the Green's matrix (6.101) for different matrix size N and for different values of the disorder parameter $k_0 l_0 = 2\pi^2/\rho\lambda_0^3$, and evaluated $\Delta\omega$ and $\delta\omega$ with Eqs. (6.188) and (6.189), respectively. We nicely observe that $\Delta\omega$ and $\delta\omega$ become equal when $k_0 l_0 \simeq 1$, meaning that the Thouless criterion (6.180) is perfectly consistent with the Ioffe-Regel criterion (6.175) in an open three-dimensional medium. This is further illustrated in Fig. 6.22(a), where we plot the Thouless number g as a function of $k_0 l_0$. Note that within the accuracy of our simulations, $\Delta\omega$ remains roughly constant in the considered range of $k_0 l_0$, at a fixed N. From the results of Fig. 6.22(a) we evaluated the scaling function (6.190), which is represented in Fig. 6.22(b). We clearly see that $\beta(g)$ is positive for $g > g_c \simeq 1.3$, and takes values in agreement with the theoretical prediction $\lim_{g\to\infty} \beta(g) = d - 2 = 1$. If we start increasing the size from some $g > g_c$, the 'renormalization flow' drives the system toward the stable fixed point $g = \infty$. On the other hand, if we start with $g < g_c$, the flow $\beta(g)$ leads to the 'insulating' stable fixed point $g = 0$. Moreover, $\beta(g)$ behaves smoothly in the vicinity of the unstable fixed point g_c. From the slope at the critical point g_c, we roughly estimated the critical exponent of the Anderson transition as $\nu \simeq 1.6$, which is consistent with the result of extensive numerical simulations in other systems [218, 219]. Even if we found ν very close to the expected result, it happened by chance. The quality of numerical results in Figs. 6.21 and 6.22 is clearly insufficient to estimate ν with acceptable precision.

In order to obtain a better estimate of the critical exponent ν, we could diagonalize the $N \times N$ Green's matrix with $N > 10^4$, which is a painful numerical work. However, our purpose was not to provide a precise numerical description of the scaling function $\beta(g)$, but rather to verify that the statistical properties of the Green's matrix indeed

contain information related to Anderson localization. In particular, our numerical analysis confirms that the scaling function can be computed from the definitions (6.188) and (6.189). The challenge becomes therefore to calculate $\Delta\omega$ and $\delta\omega$, and thus $\beta(g)$, from Eqs. (6.188) and (6.189) analytically. At the time of writing this thesis, we are working in this direction. In principle, our analytical equations (6.38) and (6.39) allow to solve for the eigenvalue density $p(\Lambda)$, and therefore for the mean spectral width (6.189) as well.

Chapter 7

Euclidean matrix theory of random lasing

Recent theoretical models of random lasers rely on expansions of the laser field in terms of overlapping modes of 'random cavities' formed by the heterogeneities of the active medium [21, 32–34, 36, 40, 220]. Alternative approaches consist in solving Maxwell-Bloch equations numerically [22, 28, 30, 31] or within the diffusion approximation [6, 134, 221]. The latter has the advantage of yielding a simple criterion for the lasing threshold (section 4.6) but it lacks rigorous justification, does not capture the mode structure of the random laser, and breaks down in the strong scattering regime [3].

In the present chapter we develop a new approach to the problem of random lasing that does rely neither on the expansion of the laser field in terms of cavity modes, nor on the diffusion approximation. It is based on our analytic results for the random Green's matrix derived in chapter 6. To demonstrate the power of this new approach, we will mainly consider random lasing in an ensemble of a large number N of identical atoms in free space, a problem of recent interest [61, 65, 134]. Our microscopic starting point is the dynamic equations of motion, derived in chapters 2 and 4, for N atoms that both scatter and amplify light. We obtain analytic results for the lasing threshold (section 7.1) and the average emitted intensity (section 7.2) in the semiclassical limit, thus achieving an important progress with respect to previous works on similar systems by Savels *et al.* (who treated lasing in ensembles of $N \leq 5$ three-level atoms) [61] and Froufe-Pérez *et al.* (who dealt with $N \gg 1$ two-level atoms but in the diffusion approximation) [134]. The spectrum of light emitted below threshold is computed analytically in section 7.2.1 by taking into account quantum effects. Our approach can be extended to deal with more 'standard' random lasers in which scattering centers ('particles') are embedded in an amplifying homogeneous matrix (section 7.3).

7.1 Threshold in a cloud of cold atoms

7.1.1 Threshold condition

Let us first consider the incoherent pump model introduced in section 3.2.2. In this model, a gas of N three-level atoms at random positions $\mathbf{r}_i$ $(i = 1, \ldots, N)$ in free three-dimensional space is subject to a strong external pump field resonant with the transition from the ground state $|g_i\rangle$ to the upper auxiliary level $|a_i\rangle$ of each atom. The atoms rapidly decay to the upper level $|e_i\rangle$ of the laser transition at a rate $\Gamma_{ae} \gg \Gamma_{eg} = \Gamma_0 \gg \Gamma_{ag}$

[see Fig. 3.1(b)]. Interaction of atoms with the electromagnetic field which is near-resonant with the transition from $|e_i\rangle$ to $|g_i\rangle$ (energy difference $\hbar\omega_0$) is described by $5N$ equations of motion for atomic operators that are coupled to the quantum propagation equation (2.39) for the electric field. After elimination of the electric field, these equations can be reduced to Eqs. (3.42) and (3.43) for atomic raising operators $\hat{S}_i^+ = |e_i\rangle\langle g_i|$ and population imbalances $\hat{\Pi}_i = |e_i\rangle\langle e_i| - |g_i\rangle\langle g_i|$ (see section 3.2.2 for details). We reproduce these equations here for clarity:

$$\frac{\mathrm{d}\hat{S}_i^+}{\mathrm{d}t} = \left[\mathrm{i}\frac{\omega_0}{\Gamma_0} - \frac{1}{2}(1+W_i)\right]\hat{S}_i^+ + \frac{\mathrm{i}}{2}\hat{\Pi}_i\sum_j G_{ij}^*(\omega_0)\hat{S}_j^+ + \hat{\mathcal{F}}_i^+(t), \tag{7.1}$$

$$\frac{\mathrm{d}\hat{\Pi}_i}{\mathrm{d}t} = -(1+W_i)\,\hat{\Pi}_i + W_i - 1 - 2\mathrm{Im}\left[\hat{S}_i^+\sum_j G_{ij}(\omega_0)\hat{S}_j^-\right] + \hat{\mathcal{F}}_i^{\Pi}(t). \tag{7.2}$$

Time t is in units of Γ_0^{-1}, W_i is the pumping rate (3.37) and $G(\omega_0)$ is the $N\times N$ Green's matrix (6.101) that couples different atoms[1]. The Langevin forces $\hat{\mathcal{F}}_i^+(t)$ and $\hat{\mathcal{F}}_i^{\Pi}(t)$ describe the quantum fluctuations of the vacuum field (see section 3.3). Equations (7.1) and (7.2) are derived in the scalar approximation for the electromagnetic field and assuming $\Gamma_0 \ll \omega_0$, c/R, where R is the size of the atomic cloud (see section 2.4.1). They can be regarded as a generalization of the optical Bloch equation [41, 55] to an ensemble of identical, incoherently pumped atoms. In the absence of coupling between atoms, they describe an isolated atom and have the stationary solution

$$\langle 0_R|\hat{\Pi}_i|0_R\rangle = \frac{W_i - 1}{W_i + 1} \equiv \Pi_i^{eq}, \tag{7.3}$$

$$\langle 0_R|\hat{S}_i^{\pm}|0_R\rangle = 0, \tag{7.4}$$

where $|0_R\rangle$ is the vacuum field state. This shows that population inversion $\Pi_i^{eq} > 0$ can be achieved for $W_i > 1$. This threshold for achieving population inversion, as well as the power broadening of the transition (the natural line-width Γ_0 is increased by a factor $1 + W_i$), are due to sharing of the same ground state by the pump and the lasing transitions.

Equations (7.1) and (7.2) provide a quantum description of the problem of random lasing in an ensemble of three-level atoms. The intensity and the spectrum of the emitted light can be obtained from quantum correlation functions $\langle 0_R|\hat{S}_i^+(t)\hat{S}_j^-(t')|0_R\rangle$ (see section 3.1). In the present section we limit ourselves to the semiclassical picture that is sufficient to analyze the lasing threshold and the average emitted intensity. The semiclassical approximation of Eqs. (7.1) and (7.2) is obtained by replacing all operators $\hat{O}$ by their quantum expectation values $O = \langle 0_R|\hat{O}|0_R\rangle$. In particular, Langevin forces vanish in this approximation: $\mathcal{F}_i^{\Pi} = 0$ and $\mathcal{F}_i^+ = 0$, see Eq. (3.47). Equations (7.1) and (7.2) become

$$\frac{\mathrm{d}S_i^+}{\mathrm{d}t} = \left[\mathrm{i}\frac{\omega_0}{\Gamma_0} - \frac{1}{2}(1+W_i)\right]S_i^+ + \frac{\mathrm{i}}{2}\Pi_i\sum_j G_{ij}^*(\omega_0)S_j^+, \tag{7.5}$$

$$\frac{\mathrm{d}\Pi_i}{\mathrm{d}t} = -(1+W_i)\,\Pi_i + W_i - 1 - 2\mathrm{Im}\left[S_i^+\sum_j G_{ij}(\omega_0)S_j^-\right]. \tag{7.6}$$

[1] In this chapter, hats are explicitly added to quantum operators. Besides, we use the loose operator notation $\mathrm{Im}\hat{O} = (\hat{O} - \hat{O}^\dagger)/2\mathrm{i}$.

When coupling between different atoms is at work, the stationary solution $S_i^{\pm} = 0$ of Eqs. (7.5) and (7.6) may lose its stability for a sufficiently strong pump. Following standard semiclassical laser theories [23], we will associate this instability with reaching the lasing threshold. The stability analysis is identical to the one performed in section 3.4 for $N = 2$ atoms. Equations (7.5) and (7.6) are rewritten as $d\mathbf{Z}/dt = \mathcal{F}(\mathbf{Z})$ where $\mathbf{Z} = \left(S_1^+, \ldots, S_N^+, S_1^-, \ldots, S_N^-, \Pi_1, \ldots, \Pi_N\right)$. We introduce $\delta\mathbf{Z} = \mathbf{Z} - \mathbf{Z}^{(0)}$ where $\mathbf{Z}^{(0)}$ is the stationary solution in the absence of interaction. $\delta\mathbf{Z}$ obeys

$$\frac{\mathrm{d}}{\mathrm{d}t}\delta\mathbf{Z} = \frac{\partial\mathcal{F}}{\partial\mathbf{Z}}\Big|_{Z^{(0)}}\delta\mathbf{Z}. \tag{7.7}$$

Since the $3N \times 3N$ Jacobian matrix $\partial\mathcal{F}/\partial\mathbf{Z}|_{\mathbf{Z}^{(0)}}$ is block-diagonal, we restrict ourselves to the study of the $N \times N$ block governing the time evolution of $\delta\mathbf{S}^- = \left(\delta S_1^-, \ldots, \delta S_N^-\right)$. It is convenient to introduce a $N \times N$ matrix $\mathcal{N}$ defined by the relation

$$\frac{\mathrm{d}}{\mathrm{d}t}\delta\mathbf{S}^- = \left(-\mathrm{i}\frac{\omega_0}{\Gamma_0} - \frac{1}{2}\right)\delta\mathbf{S}^- + \frac{\mathrm{i}}{2}\mathcal{N}\delta\mathbf{S}^-. \tag{7.8}$$

According to Eq. (7.7), the matrix $\mathcal{N}$ is

$$\mathcal{N} = \begin{pmatrix} \mathrm{i}W_1 & -\Pi_1^{eq}G_{12}(\omega_0) & \ldots & -\Pi_1^{eq}G_{1N}(\omega_0) \\ -\Pi_2^{eq}G_{21}(\omega_0) & \ddots & \ddots & \vdots \\ \vdots & \ddots & \ddots & -\Pi_{N-1}^{eq}G_{(N-1)N}(\omega_0) \\ -\Pi_N^{eq}G_{N1}(\omega_0) & \ldots & -\Pi_N^{eq}G_{N(N-1)}(\omega_0) & \mathrm{i}W_N \end{pmatrix}, \tag{7.9}$$

so that, in the absence of pump ($W_i = 0$), it is identical to the $N \times N$ Green's matrix $G(\omega_0)$. If $\delta\mathbf{S}^-(0)$ is a (right) eigenvector of $\mathcal{N}$ associated with an eigenvalue λ, then $\delta\mathbf{S}^-(t) \sim e^{-\Gamma_0(1+\mathrm{Im}\lambda)t/2}$. This shows that the linear description (7.8) breaks down and lasing starts when the imaginary part of at least one of the eigenvalues of $\mathcal{N}$ becomes less than -1. For uniform pump $W_i = W$, this condition reduces to

$$\frac{2W}{1+W}\mathrm{Im}\Lambda_n > (1+W) + \mathrm{Im}\Lambda_n, \tag{7.10}$$

where Λ_n is an eigenvalue of $G(\omega_0)$. The left-hand side of this condition can be regarded as gain that depends on both the pumping rate W and scattering (through Λ_n), whereas the right-hand side contains pump-dependent losses due to spontaneous emission $(1+W)$ and leakage out of the system ($\mathrm{Im}\Lambda_n$). As counterintuitive as it may seem, it follows from Eq. (7.10) that random lasing takes place when $\mathrm{Im}\Lambda_n$ (that quantifies losses due to open boundaries in the absence of pump) *exceeds* $(1+W)^2/(W-1)$ and $W > 1$.

It is worth noting that the threshold condition (7.10) is a specific case of the condition

$$\Lambda_n(\omega_0) = \frac{1}{\tilde{\alpha}(\omega_L)} \tag{7.11}$$

derived in section 4.2. In Eq. (7.11), $\tilde{\alpha}(\omega_L)$ is the dimensionless atomic polarizability [Eq. (4.10)] at frequency ω_L that may feature an arbitrary pumping scheme. If we substitute the polarizability (4.9) (and neglect the field nonlinearities so that $s_i = 0$) into Eq. (7.11), we recover Eq. (7.10). But Eq. (7.11) is more general than Eq. (7.10) and is not restricted to lasing in a system of three-level atoms. We can also apply it,

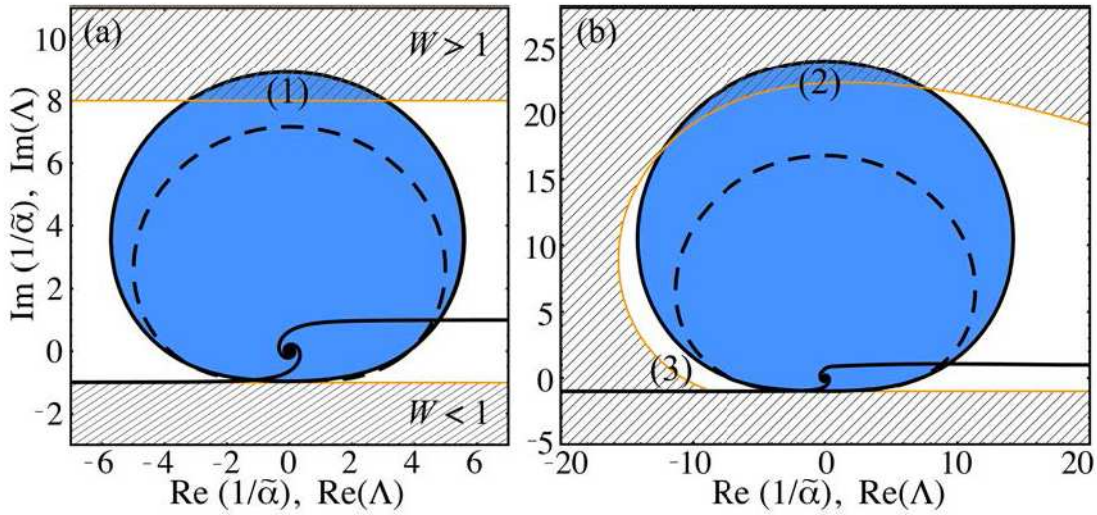

Figure 7.1: The domain $\mathcal{D}_\alpha$ (hatched) spanned by $1/\tilde{\alpha}$ and the domain $\mathcal{D}_\Lambda$ (blue area delimited by the solid line) occupied by the eigenvalues Λ of the random Green's matrix (6.101). (a) Incoherent gain $\tilde{\alpha}(\omega_L, W)$, see Eq. (4.9). (b) Coherent Mollow gain $\tilde{\alpha}(\delta_L, \Delta_p, \Omega_p)$ [Eq. (4.35)] with $\Delta_p = 1$. Lasing occurs when $\mathcal{D}_\alpha$ and $\mathcal{D}_\Lambda$ overlap: regions (1), (2), (3). The borderline of $\mathcal{D}_\Lambda$ is given by Eq. (7.12) with the optical thickness $b_0 = 40$ in (a) and $b_0 = 140$ in (b). The dashed lines show the borderline of $\mathcal{D}_\Lambda$ following from the diffusion approximation [Eq. (6.121)].

for example, to an ensemble of two-level atoms (resonant frequency ω_0) in the field of a strong near-resonant coherent pump (frequency $\omega_0 + \Gamma_0\Delta_p$, Rabi frequency $\Gamma_0\Omega_p$). When illuminated by a weak probe light at a frequency $\omega_0 + \Gamma_0\Delta_p + \Gamma_0\delta_L$, each atom behaves as if it had the effective polarizability (4.35) [see section 4.2.2 and Fig. 3.1(a)]. Optical gain in such a system is sometimes referred to as 'Mollow gain' [115].

As explained in section 4.2.2, the threshold condition (7.11) is easily visualized by drawing the two-dimensional domain $\mathcal{D}_\Lambda$ occupied by the eigenvalues of $G(\omega_0)$ and the region $\mathcal{D}_\alpha$ spanned by $1/\tilde{\alpha}$ when its free parameters — ω_L and W in the case of Eq. (4.9), and δ_L, Δ_p, and Ω_p in the case of Eq. (4.35) — are varied, on the complex plane. Random lasing takes place when $\mathcal{D}_\Lambda$ and $\mathcal{D}_\alpha$ touch (threshold) or overlap. This is illustrated in Fig. 7.1 for $N \gg 1$ atoms in a sphere of radius $R \gg \lambda_0$. In this figure, we adjusted the parameters for the random laser to be slightly above threshold: $\mathcal{D}_\Lambda$ and $\mathcal{D}_\alpha$ barely overlap. Whereas $\mathcal{D}_\alpha$ is easy to determine when $\tilde{\alpha}$ is known as a function of its parameters, finding $\mathcal{D}_\Lambda$ is much less trivial. Here we make use of our results for the eigenvalue distribution of the Green's matrix (6.101) in the limit of large N (chapter 6). The distribution and the boundary of its support $\mathcal{D}_\Lambda$ on the complex plane depend on two dimensionless parameters: the number of atoms per wavelength cubed $\rho\lambda_0^3$ and the on-resonance optical thickness $b_0 = 2R/l_0$, where ρ is the number density of atoms and $l_0 = k_0^2/4\pi\rho$ is the on-resonance scattering mean free path in the absence of the pump [see Eqs. (4.128) and (4.129)]. Note that b_0 is proportional to the second moment $\gamma = \langle|\Lambda|^2\rangle$ of the eigenvalues of $G(\omega_0)$, $b_0 = 16\gamma/3$ [Eq. (6.105)]. At a moderate density $\rho\lambda_0^3 \lesssim 10$, the eigenvalue domain $\mathcal{D}_\Lambda$ consists of two parts: a (roughly circular) 'bulk' and a pair of spiral branches (see section 6.5.1 and Fig. 6.6). Depending on the particular model of atomic polarizability $\tilde{\alpha}$, either the bulk or the branches may touch $\mathcal{D}_\alpha$, as we

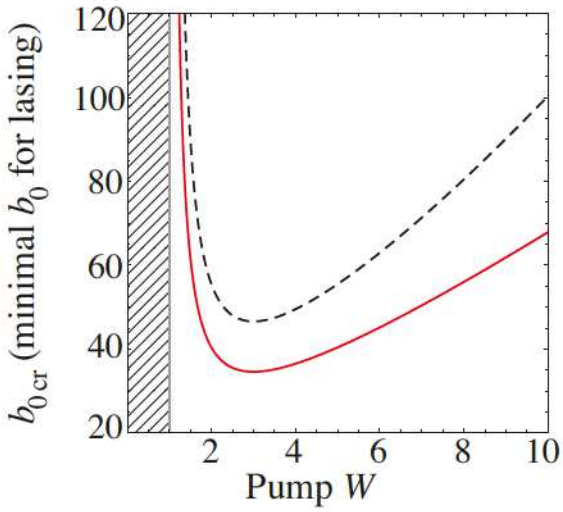

Figure 7.2: The minimal (critical) optical thickness $b_{0\mathrm{cr}}$ necessary for lasing in the incoherent pump model, following from our Euclidean matrix theory (7.12) (solid line) and from the diffusion approximation (4.138) (dashed line).

now discuss.

7.1.2 Threshold due to the 'bulk' of eigenvalues

We first focus on the lasing threshold due to the bulk of eigenvalues. Combining the analytic equation (6.117) for the borderline of $\mathcal{D}_\Lambda$ at low density $\rho\lambda_0^3 \lesssim 10$ and Eq. (7.11) results in a threshold condition that depends on the optical thickness b_0 but not on the density $\rho\lambda_0^3$:

$$\frac{3}{8}b_0|\tilde{\alpha}|^2 h\left(\frac{1}{2}b_0\mathrm{Im}\tilde{\alpha}\right) = 1, \tag{7.12}$$

where $h(x)$ is given by Eq. (6.115). Note that for both gain mechanisms considered in this section, the threshold condition (7.12) involves the eigenvalue with the largest imaginary part, as can be seen from Fig. 7.1. We calculated $\langle\max(\mathrm{Im}\Lambda)\rangle$ based on our non-Hermitian random matrix theory (section 6.5.1.c) and found excellent agreement with numerical results, see Fig. 6.9. It is quite remarkable that the agreement is present at all values of parameters, including high densities $\rho\lambda_0^3 \gg 1$ that were necessary to reach large optical thicknesses $b_0 \gg 1$ in numerical calculations with moderate $N \leq 10^4$. Because it is $\langle\max(\mathrm{Im}\Lambda)\rangle$ that controls the laser threshold, we conclude that our theory applies to random lasing all the way from weak ($\rho\lambda_0^3 \ll 1$) to strong ($\rho\lambda_0^3 \gg 1$) scattering regime.

It is interesting to compare the threshold condition (7.12) with the one obtained in the diffusion approximation. The latter amounts to solve the diffusion equation for the average intensity of light in the presence of gain [see section 4.5, and in particular Eq. (4.131)]. The threshold is reached when the solution diverges. This yields the threshold condition (4.138). The latter is similar to our result (7.12) at large optical thickness $b = b_0|\tilde{\alpha}|^2 \gg 1$ [Eq. (4.128)] but deviates significantly at $b \lesssim 1$, as can be seen from Fig. 7.1. Consequently, the predictions of Eq. (4.138) for the laser threshold (that is reached at $b < 1$, see Fig. 7.1) turn out to be inaccurate. In particular, our Eq. (7.12)

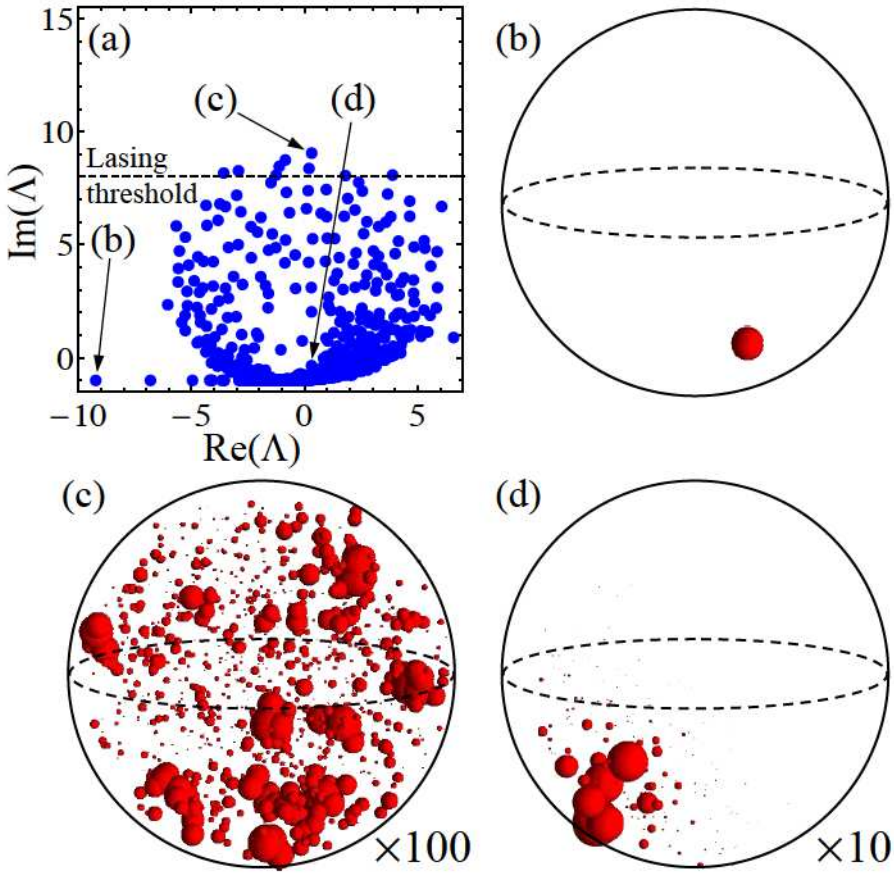

Figure 7.3: (a) Eigenvalues Λ of a single random realization of the Green's matrix $G(\omega_0)$ (dots) for a cloud of optical thickness $b_0 = 40$, composed of $N = 10^3$ atoms. (b)–(d) Intensities $|R_n^i|^2$ corresponding to the mode in the subradiant branch, localized on a pair of atoms (b), the mode with the largest ImΛ (c) and the mode corresponding to the smallest $|\Lambda|$ (d). A mode $\mathbf{R}_n = \{R_n^1, R_n^2, \ldots, R_n^N\}$ is represented by spheres centered at positions of atoms $\mathbf{r}_i$ and having radii equal to $1\times$ (b), $100\times$ (c), and $10 \times |R_n^i|^2$ (d).

predicts that the minimum on-resonance optical thicknesses required for random lasing are $b_{0\mathrm{cr}} \simeq 35$ for the incoherent (Fig. 7.2) and $b_{0\mathrm{cr}} \simeq 110$ for the coherent pump. This is significantly less than 50 and 200, respectively, following from Eq. (6.121).

Analysis of the right eigenvectors $\mathbf{R}_n$ (modes) of the matrix $G(\omega_0)$ shows that at all densities $\rho\lambda_0^3$, the mode that reaches the threshold first is extended over the whole atomic cloud [see Fig. 7.3(c), and Fig. 6.20 for a statistical analysis of the inverse participation ratio], even when the system may support localized modes as well [see modes (b) and (d) in Fig. 7.3, and Fig. 6.20]. This is specific for the models considered here in which, in particular, scattering and gain are due to the same atoms, and in contrast with systems where gain and scattering are independent and (pre-)localized modes may be better candidates for lasing [18, 22, 222] (see also section 7.3).

In the high-density limit $\rho\lambda_0^3 \to \infty$, the eigenvalues of $G(\omega_0)$ that have large imaginary parts collapse on a line (Fig. 6.8) described by the simple equation (6.130) which, combined with Eq. (7.11), yields the lasing threshold condition for a continuous medium

with a refractive index $n(\tilde{\alpha}) = (1 + \tilde{\alpha}\rho\lambda_0^3/2\pi^2)^{1/2}$:

$$\left|\frac{n(\tilde{\alpha}) - 1}{n(\tilde{\alpha}) + 1}\right|^2 \left|e^{4in(\tilde{\alpha})k_0 R}\right| = 1. \tag{7.13}$$

In this limit the problem looses its statistical nature and the random laser turns into a 'standard' laser with the feedback due to (partial) reflections at the boundaries of a homogeneous amplifying medium.

7.1.3 Threshold due to the 'subradiant branch'

Let us now analyze the role of the spiral branches of $\mathcal{D}_\Lambda$. As we illustrate in Fig. 7.3(b), the eigenvalues belonging to these branches correspond to eigenvectors (modes) localized on pairs of very close points $|\mathbf{r}_i - \mathbf{r}_j| \ll \lambda_0$ (see also Fig. 6.20). These are the super- and subradiant states of a pair of atoms (section 6.5.2). For the uniform incoherent gain (4.9), the branches do not overlap with $\mathcal{D}_\alpha$ [Fig. 7.1(a)], whereas the lower, 'subradiant' branch overlaps with $\mathcal{D}_\alpha$ for the coherent Mollow gain [Fig. 7.1(b), region (3)]. Thus, in the latter case the solution $S_i^\pm = 0$ of Eqs. (7.5) and (7.6) may lose its stability due to the eigenvalue with the smallest real part belonging to this branch. In section 6.5.2, we calculated $\langle \min(\mathrm{Re}\Lambda)\rangle$ and showed that the result [Eq. (6.145)] scales with $(N\rho\lambda_0^3)^{1/3}$, in good agreement with numerical simulations as long as $\rho\lambda_0^3 \lesssim 10$ [Fig. 6.12(a)]. When $(-\mathrm{Re}\Lambda)$ exceeds a critical value, a pair of closely located atoms on which the eigenvector (mode) associated with the eigenvalue Λ is localized, starts to emit coherent light. On average, the threshold for this effect is given by the condition $\langle \min(\mathrm{Re}\Lambda)\rangle - \mathrm{i} = 1/\tilde{\alpha}$ that reduces to

$$-\Gamma(2/3)\left(\frac{N\rho\lambda_0^3}{12\pi^2}\right)^{1/3} = \frac{1}{\tilde{\alpha}} + \mathrm{i}, \tag{7.14}$$

where $\Gamma(x)$ is the Gamma function. Formally, this emission of light by a pair of pumped atoms may be called 'laser', especially given the fact that one-atom cavity lasers [223] and few-atom random lasers [114] were already discussed in the literature. It is very different from the collective laser mechanism leading to Eqs. (7.12) and (7.13) and associated with eigenvectors extended over the whole atomic system. Whereas Eqs. (7.12) and (7.13) are good estimates of the threshold even for a *single* atomic configuration, the threshold for light emission by a pair of atoms is expected to fluctuate strongly around its typical value given by Eq. (7.14) [see Fig. 6.11(a) and Eq. (6.147)]. In the full vector model, fluctuations are even stronger than those predicted by Eq. (6.147), because the spiral branches of the distribution are sensitive to the vector nature of light: taking into account this correction yields the distribution (6.163) for $\min(\mathrm{Re}\Lambda)$ (and therefore also for the threshold), for which the variance is not defined. In addition, the light emission is expected to be strongly affected by quantum effects that wash out the sharp threshold obtained in the semiclassical framework, see section 3.5 and Fig. 3.9.

It is finally worthwhile to stress that lasing due to subradiant states cannot be predicted from the theory based on the diffusion approximation and leading to Eq. (4.138). Because the emission of the subradiant laser is due to only two atoms, it remains to be seen if this phenomenon can be detected in an experiment or if it will be overwhelmed by the amplified spontaneous emission of the rest of the atomic cloud.

7.2 Behavior below and above threshold

In this section, we briefly discuss the spectrum of light below threshold (subsection 7.2.1), and then calculate the intensity of laser emission above threshold in the semiclassical approximation (subsections 7.2.2, 7.2.3 and 7.2.4).

7.2.1 Spectrum below threshold

Our goal is to compute the spectrum of light (3.6) emitted by N incoherently pumped atoms described by the quantum Langevin equations (7.1) and (7.2). In section 3.1, we showed that a spectrum of the form (3.6) can formally be rewritten as (3.20), where the matrices $\mathcal{Y}(0)$, $\mathcal{M}$ and $\mathcal{R}$ depend on the specific equations of motion of the system under study. For equations of motion (7.1) and (7.2), we proposed, in section 3.6, a simple perturbative scheme that allowed us to approximate the spectrum by

$$S(\omega_L) = \frac{2W}{1+W}\sum_{n=1}^{N}\mathrm{Re}\left[\frac{c_n}{\mathrm{i}\left[(\omega_L-\omega_0)/\Gamma_0 - A(W)\mathrm{Re}\Lambda_n\right] + B(W) - A(W)\mathrm{Im}\Lambda_n}\right], \tag{7.15}$$

where Λ_n are the eigenvalues of the Green's matrix (6.101), and $A(W)$, $B(W)$, and c_n are defined bys Eqs. (3.105), (3.106), and (3.107), respectively. Since Eq. (7.15) was derived by neglecting field nonlinearities, it is assumed to be valid below the random lasing threshold and for moderate densities $\rho\lambda_0^3$. The result (7.15) is conveniently rewritten in terms of the atomic polarizability $\tilde{\alpha}(\omega_L)$ [Eq. (4.9)] as:

$$S(\omega_L) = 2\left(1+\frac{1}{\Pi^{eq}}\right)\sum_{n=1}^{N}\mathrm{Im}\left[\frac{c_n}{1/\tilde{\alpha}(\omega_L)-\Lambda_n}\right], \tag{7.16}$$

where Π^{eq} is the population imbalance in the absence of coupling between atoms [Eq. (7.3)]. The result (7.16) is reminiscent of the scattering matrix (6.96) that describes scattering of light by N atoms with polarizability $\tilde{\alpha}(\omega_L)$. This is not surprising because both Eqs. (7.16) and (6.96) characterize the properties of the scattered light in a regime where field nonlinearities are neglected. However, despite these similarities, it is worth noting that Eq. (7.16) describes quantum inelastic scattering while Eq. (6.96) features classical elastic scattering. We recall that the classical counterpart of the spectrum (7.16) emitted by incoherently pumped atoms is zero in the stationary regime (see section 3.6), while the non-vansihing quantum contribution to the spectrum (7.16) comes from the term $\mathcal{Y}(0)$ in Eq. (3.96).

Expression (7.16) applies for arbitrary spatial configuration of the N atoms. We now assume that N is large, and that the positions $\mathbf{r}_i$ of the N atoms are randomly chosen inside a sphere of radius R. In order to compute the average spectrum $\langle S(\omega_L)\rangle$, we have to evaluate the coefficients c_n that appear in Eq. (7.16) and are defined by Eq. (3.107). We recall that the latter do not contain any information about the interaction between atoms, but rather come from the fact that light signal is measured in the far-field (see section 3.1). Besides, we numerically checked that coefficients c_n are self-averaging quantities in the limit $N \gg 1$: $c_n \simeq \langle c\rangle$. Therefore, we propose to focus our attention on the following normalized spectrum, averaged over disorder:

$$\langle s(\omega_L)\rangle = \frac{\langle S(\omega_L)\rangle}{N\langle c\rangle}. \tag{7.17}$$

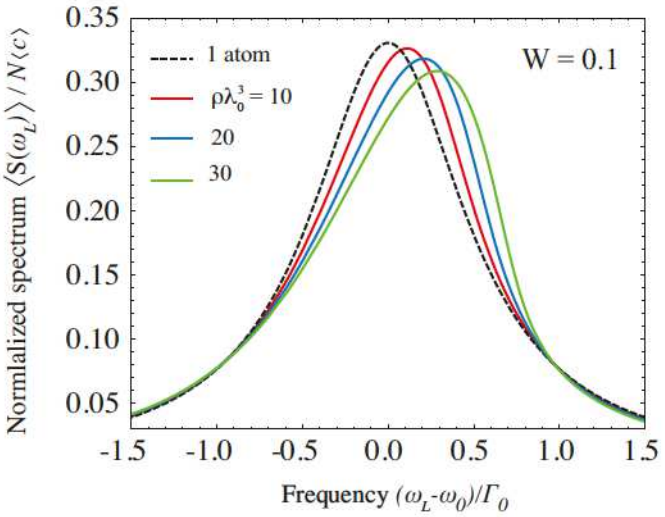

Figure 7.4: Analytic prediction for the normalized average spectrum (7.17) emitted by N incoherently pumped atoms ($W = 0.1$), randomly distributed in a sphere ($k_0R = 10$). Results following from Eqs. (7.18) and (7.20) at different densities $\rho\lambda_0^3 = 10$, 20 and 30 (solid lines) are compared with the spectrum in the absence of coupling between atoms (dashed line).

According to Eq. (7.16), it is given by

$$\begin{aligned}\langle s(\omega_L)\rangle &= 2\left(1+\frac{1}{\Pi^{eq}}\right)\mathrm{Im}\left\langle\frac{1}{N}\sum_{n=1}^{N}\frac{1}{1/\tilde{\alpha}(\omega_L)-\Lambda_n}\right\rangle \\ &= 2\left(1+\frac{1}{\Pi^{eq}}\right)\mathrm{Im}\, g\left[\frac{1}{\tilde{\alpha}(\omega_L)}\right],\end{aligned} \tag{7.18}$$

where $g(z)$ is the resolvent (6.2) of the Green's matrix (6.101). If $1/\tilde{\alpha}(\omega_L)$ belongs to the non-holomorphic domain $\mathcal{D}$ of the resolvent $g(z)$, the latter is solution of Eqs. (6.38) and (6.39); otherwise, $g(z)$ can be found from Eq. (6.40). At moderate densities $\rho\lambda_0^3$, these equations reduce to [see Eq. (6.172)]

$$g(z) = \frac{z^* - 2\gamma g(z)^* h\left(-\mathrm{i}\kappa[g(z)]R - \mathrm{i}k_0R\right)^*}{2\gamma h\left(2\,\mathrm{Im}\kappa[g(z)]R\right)} \quad (z\in\mathcal{D}), \tag{7.19}$$

$$g(z) = \frac{1}{z - 2\gamma g(z) h\left(-\mathrm{i}\kappa[g(z)]R - \mathrm{i}k_0R\right)} \quad (z\notin\mathcal{D}), \tag{7.20}$$

where the functions $\kappa(g)$ and $h(x)$ are defined by Eqs. (6.112) and (6.115), respectively. Solutions $g(z)$ of Eqs. (7.19) and (7.20) are equal on the borderline $z \in \delta\mathcal{D}$ of the eigenvalue domain of the Green's matrix. Since on the one hand, Eq. (7.18) represents the spectrum of light below the random laser threshold only, and on the other hand, the condition $1/\tilde{\alpha}(\omega_L) \in \mathcal{D}$ refers to the regime above threshold, Eq. (7.18) can rigorously be used to evaluate the spectrum only in the range of parameters where $1/\tilde{\alpha}(\omega_L) \notin \mathcal{D}$.

For the incoherent pump model (4.9), lasing may occur at some frequency ω_L if both the pumping rate W and the on-resonance optical thickness b_0 are sufficiently large: $W > 1$ and $b_0 \gtrsim 35$ (see section 7.1.2). We compute the spectrum (7.18) for $W < 1$, ensuring that lasing never starts, whatever the density of atoms. Using the holomorphic

solution $g[1/\tilde{\alpha}(\omega_L)]$ of Eq. (7.20), we find that the spectrum (7.18) depends on the density $\rho\lambda_0^3$ but not on b_0, if the system size is large enough ($k_0R \gtrsim 10$). This is somewhat surprising for the spectral extent of the eigenvalue distribution of the Green's matrix depends on b_0 only [see Eq. (6.117)]. In fact, the eigenvalues with large real parts $|\mathrm{Re}\Lambda_n|$ also have small imaginary parts $|\mathrm{Im}\Lambda_n|$, and therefore give rise to Lorentzian components in the spectrum (7.15) that have small spectral weights. Note also that the spectrum emitted by N uncoupled atoms is recovered if we approximate $g(z)$ in Eq. (7.20) by $1/z$. Figure 7.4 shows that the exact solution differs notably from this non-interacting case for $\rho\lambda_0^3 \gtrsim 1$. The blue-detuning of the maximum of $\langle s(\omega_L)\rangle$ is reminiscent of the asymmetry of the marginal probability density of $\mathrm{Re}\Lambda$ [see Fig. 6.15], that represents the probability distribution of the 'collective Lamb shift' [75, 83, 88, 90].

7.2.2 Non-linear dynamics of laser emission and rate equations

Let us now study the dynamics of laser emission slightly above threshold. The questions that we would like to address are: What is the intensity of laser emission in the stationary regime? How many modes of the 'passive' cavity can coexist above threshold? To answer these questions in the limit $N \gg 1$, it is sufficient to limit ourselves to the semiclassical picture, in which quantum operators are replaced by their quantum expectation values. Our starting point is therefore the set of Eqs. (7.5) and (7.6). The simplest intensity signal that we can compute is the square modulus of the smoothed electric field (4.32). In the absence of external cavity, the latter is well approximated, in the time-domain, by (see section 2.4.1 for details):

$$\Omega_s^+(\mathbf{r}_i, t) = -\sum_{j\neq i}^{N} G_{ij}(\omega_0) S_j^-(t). \tag{7.21}$$

In the following, we will use vector notations $\mathbf{\Omega} = \{\Omega_s^+(\mathbf{r}_i,), \ldots, \Omega_s^+(\mathbf{r}_N,)\}$, and $\mathbf{S} = (S_1^-, \ldots, S_N^-)$, so that Eq. (7.21) reads $\mathbf{\Omega} = -G(\omega_0)\mathbf{S}$.

In the vicinity of threshold, population imbalances Π_i can be adiabatically eliminated from Eqs. (7.5) and (7.6) because the dipoles (and therefore the field) evolve slowly with respect to Π_i. Indeed, slightly below threshold, $\mathbf{S}^-(t) \sim e^{-\Gamma_0(1+\mathrm{Im}\lambda)t/2}$, where the eigenvalue λ of the matrix (7.9) satisfies $\mathrm{Im}\lambda \simeq -1$ (by definition of the threshold), while $\Pi_i(t) \sim e^{-\Gamma_0(1+W_i)t}$. The lowest-order non-linear approximation of Eqs. (7.5) and (7.6) is then found by applying a standard iterative procedure [23]

$$\Pi_i^{(0)}(t) = \Pi_i^{eq}, S_i^{(0)-}(t) = S_i^-(0)e^{-i\omega_0 t} \;\rightarrow\; S_i^{(1)-}(t) \;\rightarrow\; \Pi_i^{(1)}(t) \;\rightarrow\; S_i^{(2)-}(t), \tag{7.22}$$

meaning that at each step of the calculation, the solution $\Pi_i^{(j)}(t)$ or $S_i^{(j)}(t)$ is found by inserting solutions found at the previous step into Eqs. (7.5) and (7.6).

The resulting equation for the field $\mathbf{\Omega}(t) = -G(\omega_0)\mathbf{S}^{(2)}(t)$ is

$$\frac{\mathrm{d}\mathbf{\Omega}}{\mathrm{d}t} = -\left[\mathrm{i}\left(\frac{\omega_0}{\Gamma_0} + G(\omega_0)A - G(\omega_0)C|\mathbf{\Omega}|^2\right) + G(\omega_0)BG(\omega_0)^{-1}\right]\mathbf{\Omega}, \tag{7.23}$$

where we introduced $N \times N$ diagonal matrices

$$A = \frac{1}{2}\mathrm{diag}\left(\frac{W_i - 1}{W_i + 1}\right), \tag{7.24}$$

$$B = \frac{1}{2}\mathrm{diag}\left(W_i + 1\right), \tag{7.25}$$

$$C = \mathrm{diag}\left[\frac{W_i - 1}{(W_i + 1)^3}\right], \tag{7.26}$$

$$|\mathbf{\Omega}|^2 = \mathrm{diag}[|\Omega_i|^2]. \tag{7.27}$$

Note that the eigenvectors of the linear kernel of Eq. (7.23) coincide with the right eigenvectors $\mathbf{R}_k$ of the Green's matrix $G(\omega_0)$ that play the role of eigenmodes of the 'cold cavity' only if the pump is uniform: $W_i = W$.

Restricting further consideration to the latter case ($W_i = W$), we express the field in the basis of right eigenvectors $\mathbf{R}_k$ of $G(\omega_0)$, $\mathbf{\Omega}(t) = \sum_{n=1}^{N} b_k(t)\mathbf{R}_k$. Since $G(\omega_0)$ is a symmetric matrix, left eigenvectors are $\mathbf{L}_k = \mathbf{R}_k^*$. The eigenvectors can be normalized to satisfy

$$\langle \mathbf{L}_k | \mathbf{R}_n \rangle = \sum_{i=1}^{N} R_k^i R_n^i = \delta_{kn}, \tag{7.28}$$

where $R_k^i = \langle \mathbf{r}_i | \mathbf{R}_k \rangle$ are the components of $\mathbf{R}_n$. Multiplying the component i of Eq. (7.23) by R_k^i and summing over i, we obtain

$$\frac{\mathrm{d}b_k}{\mathrm{d}t} = -\left[\mathrm{i}\left(\frac{\omega_0}{\Gamma_0} + A\Lambda_k\right) + B\right] b_k + \mathrm{i}C\Lambda_k \sum_{m,n,l} \alpha_{mnlk} b_m b_n^* b_l, \tag{7.29}$$

where $\alpha_{mnlk} = \sum_{i=1}^{N} R_k^i R_m^i R_n^{i*} R_l^i$, and A, B and C are the elements of matrices defined above (we keep the same notation for simplicity). We now introduce the ansatz $b_k(t) = a_k(t)e^{-\mathrm{i}\omega_k t}$, where 'envelopes' $a_k(t)$ are weakly time dependent [23]. In other words, the field is decomposed as

$$\mathbf{\Omega}(t) = \sum_{k=1}^{N} a_k(t) e^{-\mathrm{i}\omega_k t} \mathbf{R}_k \quad \text{with} \quad \left|\frac{1}{a_k}\frac{da_k}{dt}\right| \ll \omega_k. \tag{7.30}$$

If we multiply Eq. (7.29) by b_k^*, the last term of the r.h.s. of the resulting equation is proportional to

$$\sum_{m,n,l} \alpha_{mnlk} b_m b_n^* b_l b_k^* = \sum_{m,n,l} \alpha_{mnlk} a_m a_n^* a_l a_k^* e^{-\mathrm{i}(\omega_m - \omega_n + \omega_l - \omega_k)t}. \tag{7.31}$$

In this sum, terms that are weakly time-dependent correspond to three different combinations:

$$\begin{aligned} &(1) \quad \omega_m = \omega_n \quad \text{and} \quad \omega_l = \omega_k, \\ &(2) \quad \omega_m = \omega_k \quad \text{and} \quad \omega_n = \omega_l, \\ &(3) \quad \omega_m + \omega_l = \omega_n + \omega_k. \end{aligned}$$

The case (3) represents 'phase locking' that can play an important role in standard lasers where a few modes can coexist [23]. Such an effect may also occur in a random laser,

but we will not considered it here, *i.e.* we will confine our analysis to a free-running situation where phases of the oscillations are uncoupled. Hence, we multiply Eq. (7.29) by $b_k^*\langle \mathbf{R}_k|\mathbf{R}_k\rangle$, and keep, in the sum (7.31), the terms of types (1) and (2) only. The imaginary part of the resulting equation gives laser frequencies of modes k:

$$\omega_k = \omega_0 + \Gamma_0 A \mathrm{Re}\Lambda_k - 2\Gamma_0 C \sum_n \mathrm{Re}\left(\Lambda_k \eta_{nk}\right) I_n, \tag{7.32}$$

while the real part yields rate equations for mode intensities $I_k = |a_k|^2\langle \mathbf{R}_k|\mathbf{R}_k\rangle$:

$$\frac{\mathrm{d}I_k}{\mathrm{d}t} = -2\kappa_k I_k + \sum_n \mathcal{W}_{nk} I_n I_k, \tag{7.33}$$

where

$$\kappa_k = \frac{\Gamma_0}{2}\left(W + 1 - \frac{W-1}{W+1}\mathrm{Im}\Lambda_k\right), \tag{7.34}$$

$$\mathcal{W}_{nk} = -4\Gamma_0 \frac{W-1}{(W+1)^3}\mathrm{Im}(\Lambda_k \eta_{nk}), \tag{7.35}$$

$$\eta_{nk} = \frac{\sum_{i=1}^N (R_k^i)^2 |R_n^i|^2}{\sum_{i=1}^N |R_n^i|^2}. \tag{7.36}$$

The threshold for the mode k is given by the condition $\kappa_k = 0$ [we recover Eq. (7.10)] and depends only on the eigenvalue Λ_k, whereas the mode competition above the threshold involves the overlap of eigenvectors η_{nk}. It is worth noting that although rate equations similar to Eq. (7.33) appeared in previous works on random lasers [21, 36, 40, 220], loss rates κ_k and nonlinear couplings $\mathcal{W}_{nk}$ were most often assumed to follow from *ad hoc* random matrix models [36–38], except in one-dimensional systems where they could be calculated with a reasonable effort [40]. We, in contrast, provide explicit general expressions for these quantities and show that they are determined by the eigenvalues Λ_k and eigenvectors $\mathbf{R}_k$ of the random Green's matrix. The link between κ_k, $\mathcal{W}_{nk}$ and Λ_k, $\mathbf{R}_k$ is independent of the geometry or dimensionality of the problem.

7.2.3 Stationary solutions

Let us now analyze the stationary solutions of rate equations (7.33). In Eq. (7.33), the sum over n runs from 1 to N_L, where N_L is the number of lasing modes that has to be found self-consistently, requiring that all intensities I_k ($k = 1, \ldots, N_L$) are positive. Before studying the general case of multimode lasing, it is instructive to consider the single-mode situation, where only one mode k_1 is excited ($N_L = 1$). Then, the solution of Eq. (7.33) is

$$I_{k_1} = \frac{1}{\eta_{k_1k_1}}\frac{(W+1)^2}{4}\left(1 - \frac{y_m}{\mathrm{Im}\Lambda_{k_1}}\right), \tag{7.37}$$

$$y_m = \frac{(W+1)^2}{W-1}, \tag{7.38}$$

where we assumed that $\eta_{k_1k_1}$ is real and positive (see below for explanation). The solution (7.37) exists ($I_{k_1} > 0$) provided that $\mathrm{Im}\Lambda_{k_1}$ exceeds y_m and $W > 1$. Intensity I_k is greater when the mode is delocalized (large $\eta_{k_1k_1}$), or when $\mathrm{Im}\Lambda_{k_1}$ is far beyond the threshold

y_m (large $\mathrm{Im}\Lambda_{k_1} - y_m$). As we shall now discuss, this simple picture is strongly modified in the multimode situation, where several modes compete for gain.

In the large N limit, we numerically checked that coefficients η_{nk} are self-averaging quantities with negligibly small fluctuations around their means $\langle \eta_{nk} \rangle$. In addition, at low atomic density $\rho\lambda_0^3 \lesssim 10$, R_k^i behave almost as independent Gaussian random variables (see Fig. 6.20) and thus

$$\langle \eta_{nk} \rangle \simeq \frac{1}{N}\left(1 + 2\delta_{nk}\right). \tag{7.39}$$

Replacing η_{nk} in Eq. (7.33) by (7.39), we can express the stationary solutions for mode intensities in terms of the inverse of the $N_L \times N_L$ matrix η (with matrix elements η_{nk}):

$$\left(\eta^{-1}\right)_{nk} = \frac{N}{2}\frac{N_L+1}{N_L+2}\delta_{nk} - \frac{N}{2}\frac{1}{N_L+2}(1-\delta_{nk}). \tag{7.40}$$

This yields:

$$I_k = N\frac{(W+1)^2}{4}\left[\frac{1}{N_L+2} - \frac{y_m}{2}\left(\frac{1}{\mathrm{Im}\Lambda_k} - \frac{1}{N_L+2}\sum_{n=1}^{N_L}\frac{1}{\mathrm{Im}\Lambda_n}\right)\right], \tag{7.41}$$

where the number N_L of lasing modes is still unknown.

Adapting standard analysis of mode competition [23, 36, 39], we introduce

$$y_0 = \min_{\{k=1,\ldots,N_L\}}\left(\mathrm{Im}\Lambda_k\right), \tag{7.42}$$

that corresponds to the less favorable lasing mode, *i.e.* the one that has zero intensity. According to Eq. (7.41), y_0 is given by

$$\frac{1}{y_0} = \frac{1}{N_L+2}\left(\frac{2}{y_m} + \sum_{n=1}^{N_L}\frac{1}{\mathrm{Im}\Lambda_n}\right). \tag{7.43}$$

Besides, the number N_L of lasing modes can formally be written as

$$N_L = \sum_{k=1}^{N}\int_{y_0}^{\infty} \mathrm{d}y\, \delta(y - \mathrm{Im}\Lambda_k). \tag{7.44}$$

Our goal is to compute the intensity of the smoothed field,

$$\begin{aligned} I &= \sum_{i=1}^{N}|\Omega_i|^2 = \sum_{i=1}^{N}\sum_{k=1}^{N_L}\sum_{n=1}^{N_L} a_k^* a_n e^{-\mathrm{i}(\omega_n-\omega_k)t} R_k^{i*} R_n^i \\ &\simeq \sum_{i=1}^{N}\sum_{k=1}^{N_L}|a_k|^2 R_k^{i*}R_k^i = \sum_{k=1}^{N_L}|a_k|^2\langle \mathbf{R}_k|\mathbf{R}_k\rangle \\ &\simeq \sum_{k=1}^{N_L} I_k. \end{aligned} \tag{7.45}$$

For this purpose, we use Eq. (7.43) to reduce Eq. (7.41) to

$$I_k = N\frac{(W+1)^2}{8}y_m\left(\frac{1}{y_0} - \frac{1}{\mathrm{Im}\Lambda_k}\right). \tag{7.46}$$

Combining Eqs. (7.43), (7.45) and (7.46), we finally obtain a simple expression for the intensity:

$$I = N\frac{(W+1)^2}{4}\left(1-\frac{y_m}{y_0}\right). \tag{7.47}$$

The fact that I is proportional to $y_0 - y_m$ is somewhat surprising inasmuch as modes with $\mathrm{Im}\Lambda_k < y_0$ do not participate in the lasing process. In this sense, we could have expected $I \propto \max(\mathrm{Im}\Lambda_k) - y_0$. Note also that y_0 is not equal to y_m even for $N_L = 1$. Indeed, it is possible to recover Eq. (7.37) from Eqs. (7.43) and (7.47), with $\eta_{k_1k_1} = 3/N$.

Equations (7.43), (7.44) and (7.47) apply for any realization of the Green's matrix, *i.e.* for any spatial configuration of the N atoms. Coupled equations (7.43) and (7.44) can be solved iteratively to find y_0 and therefore the intensity (7.47). In the next section, we calculate the average intensity $\langle I\rangle$ and the average number $\langle N_L\rangle$ of lasing modes with the help of our analytic theory for the eigenvalue density $p(\Lambda)$ of the Green's matrix (chapter 6).

7.2.4 Statistical treatment

We average Eqs. (7.43), (7.44) and (7.47) over all possible configurations of N atoms in space and approximate $\langle 1/y_0\rangle$ by $1/\langle y_0\rangle$ (this is reasonable since y_0 has small fluctuations around its mean):

$$\frac{1}{\langle y_0\rangle} \simeq \frac{1}{\langle N_L\rangle + 2}\left(\frac{2}{y_m} + N\int_{\langle y_0\rangle}^{\infty} \mathrm{dIm}\Lambda\,\frac{p(\mathrm{Im}\Lambda)}{\mathrm{Im}\Lambda}\right), \tag{7.48}$$

$$\langle N_L\rangle \simeq N\int_{\langle y_0\rangle}^{\infty} \mathrm{dIm}\Lambda\, p(\mathrm{Im}\Lambda), \tag{7.49}$$

$$\langle I\rangle \simeq N\frac{(W+1)^2}{4}\left(1-\frac{y_m}{\langle y_0\rangle}\right). \tag{7.50}$$

To solve these equations, we need a model for $p(\mathrm{Im}\Lambda)$, the marginal distribution of the imaginary part of the eigenvalues of the Green's matrix. From here on, we assume that the N atoms are randomly distributed in a sphere of radius R, at a moderate density $\rho\lambda_0^3 \lesssim 10$. From the analysis of section 6.5, we know that $p(\mathrm{Im}\Lambda)$ vanishes for $\mathrm{Im}\Lambda = y_M$, with y_M solution of [see Eq. (6.117)]

$$y_M^2 = \frac{3}{8}b_0 h\left(-\frac{b_0}{2y_M}\right), \tag{7.51}$$

where $h(x)$ is given by Eq. (6.115). In addition, $p(\mathrm{Im}\Lambda) \propto 1/(\mathrm{Im}\Lambda + 1)$ for $\mathrm{Im}\Lambda < y_M$ [see Figs. 6.18 and 6.19]; and, by definition of $G(\omega_0)$ [Eq. (6.101)], $\langle \mathrm{Im}\Lambda\rangle = 0$. The latter properties combined with the normalization condition of $p(\mathrm{Im}\Lambda)$ yield

$$p(\mathrm{Im}\Lambda) \simeq \frac{1}{(y_M+1)(\mathrm{Im}\Lambda+1)} \quad \text{for} \quad -1 + (y_M+1)e^{-(y_M+1)} < \mathrm{Im}\Lambda < y_M, \tag{7.52}$$

and $p(\mathrm{Im}\Lambda) = 0$ elsewhere. Here we assumed that $y_M \gg 1$, which is satisfied because lasing occurs for $y_M > \langle y_0\rangle > y_m \geq 8$ [see Eq. (7.38)]. Inserting (7.52) into Eqs. (7.48) and (7.49), we find that $\langle y_0\rangle$ is solution of

$$\frac{1}{\langle y_0\rangle} = \frac{1}{N\ln\left(\frac{y_M+1}{\langle y_0\rangle+1}\right) + 2(1+y_M)}\left[\frac{2(1+y_M)}{y_m} + N\ln\left(\frac{y_M}{\langle y_0\rangle}\right) - N\ln\left(\frac{y_M+1}{\langle y_0\rangle+1}\right)\right]. \tag{7.53}$$

Solving this equation allows to find the number of lasing modes

$$\langle N_L \rangle = \frac{N}{1+y_M} \ln\left(\frac{y_M+1}{\langle y_0 \rangle + 1}\right), \tag{7.54}$$

as well as the average intensity (7.50). A good approximation of Eq. (7.53) is found in the limit $N \to \infty$, where we have $y_M - \langle y_0 \rangle \ll 1$. Expanding the logarithms in series in Eq. (7.53), we obtain[2]

$$\frac{\langle y_0 \rangle^2}{y_M} - 2\left[\frac{(y_M+1)^2}{N y_m} + 1\right]\langle y_0 \rangle + \frac{2}{N}(y_M+1)^2 = 0. \tag{7.55}$$

In the limit $N \to \infty$, the solution of Eq. (7.55) reads:

$$\langle y_0 \rangle = y_M \left[1 - \sqrt{\frac{2(y_M+1)^2}{N}\left(\frac{1}{y_m} - \frac{1}{y_M}\right)}\right] + \mathcal{O}\left(\frac{1}{N}\right), \tag{7.56}$$

Hence, for a given optical thickness $b_0 \gg 1$, $y_M - \langle y_0 \rangle$ scales as $1/\sqrt{N}$, meaning that the fraction of lasing modes, $\langle N_L \rangle / N$, vanishes in the limit $N \to \infty$. The intensity and the number of modes are

$$\langle I \rangle = N \frac{(W+1)^2}{4}\left(1 - \frac{y_m}{y_M}\right) + \mathcal{O}\left(\sqrt{N}\right), \tag{7.57}$$

$$\langle N_L \rangle = \sqrt{2N}\frac{y_M}{y_M+1}\sqrt{\frac{1}{y_m} - \frac{1}{y_M}} + \mathcal{O}(1), \tag{7.58}$$

where y_m and y_M are given by Eqs. (7.38) and (7.51), respectively. These results can be compared with the intensity $\langle I^0 \rangle$ and the number of lasing modes $\langle N_L^0 \rangle$ that we would have found in the absence of mode competition, when all modes with $\mathrm{Im}\Lambda_k > y_0 = y_m$ participate in the lasing process. Repeating the reasoning of the previous section with $\eta_{nk} = c\delta_{nk}/N$ instead of (7.39) yields

$$\langle I^0 \rangle = \frac{N^2}{c}\frac{(W+1)^2}{4}\frac{y_M - y_m}{y_M+1}\left(1 - \frac{y_m}{y_M}\right), \tag{7.59}$$

$$\langle N_L^0 \rangle = N\frac{y_M - y_m}{(y_M+1)^2}. \tag{7.60}$$

The scaling of $\langle I \rangle$ and $\langle I^0 \rangle$ with N can be qualitatively understood by expressing the total intensity as a product of the number of lasing modes and the intensity of a typical mode $(y_M - y_0)/\eta$ ($\eta \sim 1/N$):

$$\langle I \rangle \sim \langle N_L \rangle \frac{y_M - y_0}{\eta} \quad \text{with} \quad \frac{\langle N_L \rangle}{N} \sim y_M - y_0, \tag{7.61}$$

$$\langle I^0 \rangle \sim \langle N_L^0 \rangle \frac{y_M - y_0}{\eta} \quad \text{with} \quad \frac{\langle N_L^0 \rangle}{N} \sim y_M - y_0. \tag{7.62}$$

While $y_M - y_0 \sim 1$ in the absence of mode competition ($y_0 = y_m$), $y_M - y_0 \sim 1/\sqrt{N}$ when the modes couple between them.

[2] Eq. (7.55) can also be derived from Eq. (7.49) with $p(\mathrm{Im}\Lambda) \simeq 1/(y_M+1)^2$ for $\langle y_0 \rangle < \mathrm{Im}\Lambda < y_M$.

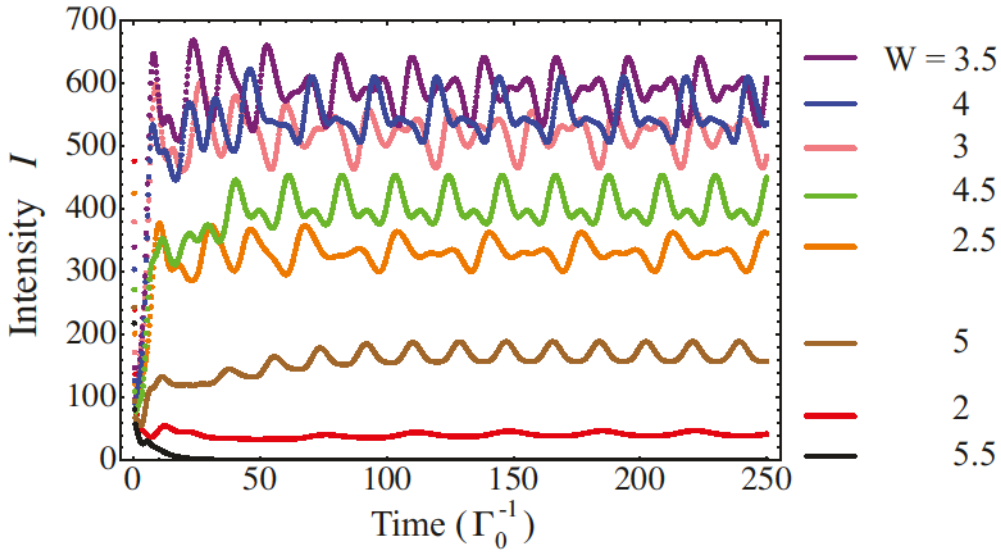

Figure 7.5: Numerical calculation of the intensity $I(t) = \sum_{i=1}^{N} |\Omega_i(t)|^2$ following from Eqs. (7.5), (7.6) and (7.21), for a typical random configuration of $N = 10^3$ atoms distributed in a sphere of radius R; $b_0 = 6N/(k_0R)^2 = 40$. The pumping rate W is varied from 2 to 5.5.

In order to test the validity of the result (7.57), we solved numerically the $2N$ equations (7.5) and (7.6) with $N = 10^3$ and $b_0 = 40$, for different values of the pump W, and 10 random configurations of the N atoms. The result for the intensity $I(t) = \sum_{i=1}^{N} |\Omega_i(t)|^2$ [$\Omega_i(t)$ is defined by Eq. (7.21)] of a typical configuration is shown in Fig. 7.5. For $W \gtrsim 2$, the number of lasing modes increases with the pumping rate. As a result, the mean intensity in the stationary regime increases, and the profile of $I(t)$ eventually becomes chaotic if the number of lasing modes is large enough. Fig. 7.6(a) shows that our analytic solution (7.57) is in good agreement with the numerical solution of Eqs. (7.5) and (7.6) averaged over 10 random configurations of atoms. We also illustrate in Fig. 7.6(b) how the number of lasing modes (7.58) evolves with W and b_0. Note that $\langle N_L \rangle$ is always bounded from above by $\sqrt{N}/2$, a value that is reached for $W = 3$ in the limit $b_0 \to \infty$.

An interesting feature of lasing in a cloud of cold atoms illustrated by Figs. 7.5 and 7.6 is the halt of lasing at too strong pumps. This can be easily understood by noting that random lasing requires both amplification and scattering to be sufficiently strong, and that both of these important ingredients are provided by the same atoms. At low pump [$W \lesssim 2$ in Figs. 7.5 and 7.6(b)], the scattering is strong, but the amplification is not enough to lase. In contrast, when the pump is strong ($W \gtrsim 5$), the scattering strength decreases because the atomic transition starts to be saturated, and lasing stops.

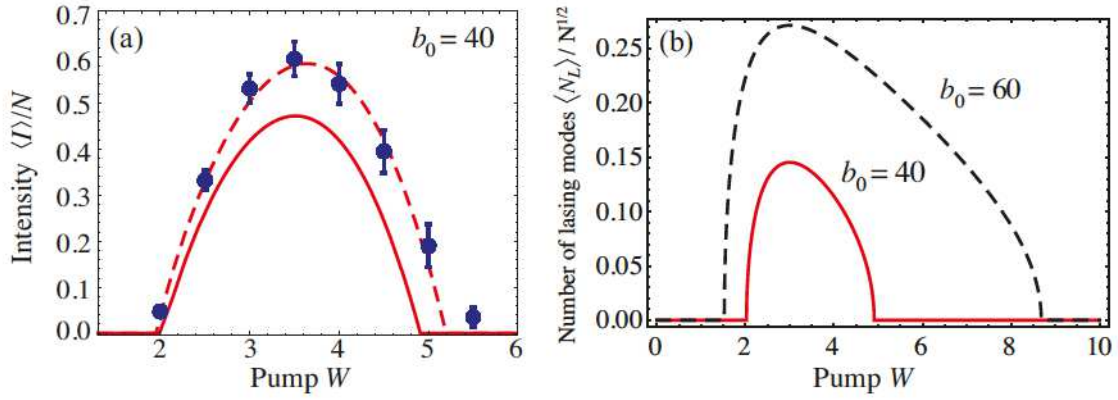

Figure 7.6: (a) The average stationary intensity $\langle I \rangle$ at $b_0 = 40$ obtained from the numerical solution of Eqs. (7.5) and (7.6) for $N = 10^3$ ($\rho\lambda_0^3 = 32.23$) after averaging over 10 random configurations of atoms (symbols). For each configuration and each W, we averaged the numerical solution $I(t)$ over $t = (200\text{–}250)\Gamma_0^{-1}$ (see Fig. 7.5). The analytic solution (7.57) is shown by the solid line. The dashed line corresponds to $y_M = 9.15$ instead of 8.93 [this value follows from Eq. (7.51)] for the solid line. (b) Average number of lasing modes (7.58), *i.e.* of eigenvectors $\mathbf{R}_k$ of $G(\omega_0)$ that have non-vanishing amplitudes $a_k(t)$ in the expansion (7.30) of the field $\mathbf{\Omega}$, in the long-time limit.

7.3 Threshold for passive scatterers embedded in an amplifying medium

7.3.1 Threshold condition

Let us now consider lasing in an ensemble of N passive (*i.e.* not pumped) scatterers embedded in an amplifying medium. Amplification is described by a polarization P_a in the propagation equation for the electric field:

$$\left[\Delta_{\mathbf{r}} + \frac{\omega_L^2}{c^2}\right] E(\mathbf{r}, \omega_L) = -\frac{\omega_L^2}{\epsilon_0 c^2} \left[P(\mathbf{r}, \omega_L) + P_a(\mathbf{r}, \omega_L)\right], \tag{7.63}$$

where $P(\mathbf{r}, \omega_L) = \sum_i^N D_i(\omega_L)\delta(\mathbf{r} - \mathbf{r}_i)$ is the polarization due to the N passive scatterers [Eq. (2.5)]. For simplicity, we use the scalar description of the field. As discussed in section 4.1, when population inversion in the amplifying medium is stationary, Eq. (7.63) can be rewritten as

$$\left[\Delta_{\mathbf{r}} + \frac{\omega_L^2}{c^2} n_a(\mathbf{r}, \omega_L)^2\right] E(\mathbf{r}, \omega_L) = -\frac{\omega_L^2}{\epsilon_0 c^2} P(\mathbf{r}, \omega_L), \tag{7.64}$$

where $n_a(\mathbf{r}, \omega_L)$ is the refractive index of the amplifying medium. If the latter is made of atoms of polarizability α_a, the linear polarization is $P_a(\mathbf{r}, \omega_L) \simeq \epsilon_0 \rho \alpha_a(\mathbf{r}, \omega_L) E(\mathbf{r}, \omega_L)$, yielding

$$n_a(\mathbf{r}, \omega_L) = \sqrt{1 + \rho\alpha_a(\mathbf{r}, \omega_L)}. \tag{7.65}$$

Eq. (7.65) is valid if the size of the medium is smaller than the scattering mean free path associated with the amplifying medium, and for $|\rho\alpha_a| \ll 1$. Corrections to the expression (7.65) can be obtained using the Lorentz-Lorentz formula [49]. From here on, we assume

that the pump is uniform, so that amplification is entirely characterized by the refractive index

$$n_a \simeq 1 + \mathrm{i}\,\mathrm{Im}n_a \quad \text{with} \quad \mathrm{Im}n_a < 0. \tag{7.66}$$

Eq. (7.64) shows that the $N \times N$ Green's matrix that controls the lasing threshold condition (4.33) is now given by

$$G_a(\omega_0)_{ij} = (1-\delta_{ij})\frac{\exp(\mathrm{i}k_0 n_a|\mathbf{r}_i - \mathbf{r}_j|)}{k_0|\mathbf{r}_i - \mathbf{r}_j|}. \tag{7.67}$$

In addition, since the passive atoms are not pump their dimensionless polarizability $\tilde{\alpha}$ satisfies the optical theorem (4.29). In terms of the eigenvalues $\Lambda_k(\omega_0, n_a)$ of $G_a(\omega_0)$, the lasing threshold (4.33) becomes ($\omega_L \simeq \omega_0$):

$$\mathrm{Im}\Lambda_k(\omega_0, n_a) = -1, \tag{7.68}$$

meaning that lasing starts when at least one of the eigenvalue of $G_a(\omega_0)$ has its imaginary part smaller than -1. On average, this occurs when the two-dimensional domain $\mathcal{D}_\Lambda$ occupied by the eigenvalues of $G_a(\omega_0)$ crosses the line $\mathrm{Im}\Lambda = -1$ on the complex plane. The next section is devoted to the determination of the domain $\mathcal{D}_\Lambda$.

7.3.2 Eigenvalue distribution of an amplifying Green's matrix

The eigenvalue distribution and the eigenvector correlator of the non-Hermitian ERM (7.67) can be found by solving Eqs. (6.34), (6.35), (6.40), and (6.41), with $A = G_a(\omega_0)$. Let us concentrate on the low density regime $\rho\lambda_0^3 \lesssim 10$, for which the reasoning of section 6.5.1.a can be easily adapted. Traces appearing in Eqs. (6.40) and (6.41) are expressed in the $|\mathbf{r}\rangle$-representation according to Eqs. (6.106) and (6.107), where $T(\mathbf{r},\mathbf{r}') = \rho\langle\mathbf{r}|\hat{A}|\mathbf{r}'\rangle = \rho\exp(\mathrm{i}k_0 n_a|\mathbf{r}-\mathbf{r}'|)/k_0|\mathbf{r}-\mathbf{r}'|$ obeys

$$\left(\Delta_{\mathbf{r}} + k_0^2 n_a^2\right) T(\mathbf{r},\mathbf{r}') = -\frac{4\pi\rho}{k_0}\delta^{(3)}(\mathbf{r}-\mathbf{r}'). \tag{7.69}$$

On the other hand, the unknown quantity $S_0(\mathbf{r},\mathbf{r}')$ is the solution of the integral equation (6.108). Applying the operator $\Delta_{\mathbf{r}} + k_0^2 n_a^2$ to Eq. (6.108) and making use of Eq. (7.69), we obtain

$$\Delta_{\mathbf{r}} S_0(\mathbf{r},\mathbf{r}') + k_0^2\left[n_a^2 + g\frac{\rho\lambda_0^3}{2\pi^2}\Pi_V(\mathbf{r})\right] S_0(\mathbf{r},\mathbf{r}') = -\frac{4\pi\rho}{k_0}\delta^{(3)}(\mathbf{r}-\mathbf{r}'), \tag{7.70}$$

where $\Pi_V(\mathbf{r}) = 1$ for $\mathbf{r} \in V$ and 0 elsewhere. At low densities, an approximate solution of this equation is

$$S_0(\mathbf{r},\mathbf{r}') \simeq \rho\frac{\exp\left[\mathrm{i}\kappa_a(g)|\mathbf{r}-\mathbf{r}'|\right]}{k_0|\mathbf{r}-\mathbf{r}'|}, \tag{7.71}$$

$$\kappa_a(g) = k_0\sqrt{n_a^2 + \frac{g\rho\lambda_0^3}{2\pi^2}}. \tag{7.72}$$

Then, we insert the explicit expressions for $T(\mathbf{r},\mathbf{r}')$ and $S_0(\mathbf{r},\mathbf{r}')$ into Eqs. (6.106) and (6.107) and assume that the volume V is a sphere of radius R, so that Eqs. (6.40) and

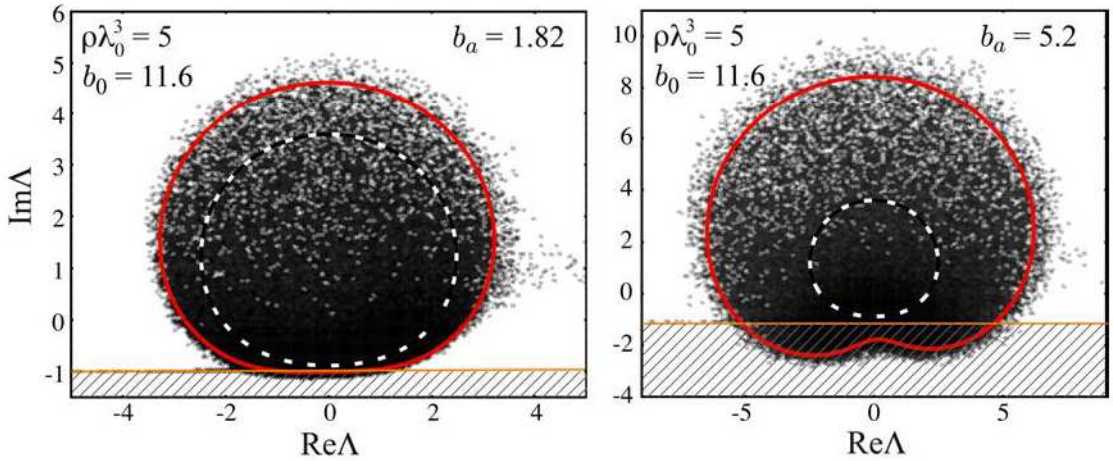

Figure 7.7: Density plots of the logarithm of eigenvalue density of the $N \times N$ random Green's matrix (7.67) obtained by numerical diagonalization of 100 realizations of the matrix for $N = 10^3$, $\rho\lambda_0^3 = 5$ ($k_0R = 22.79$), $\mathrm{Im}n_a = -0.02$ (left panel) and $\mathrm{Im}n_a = -0.057$ (right panel). Points $\mathbf{r}_i$ are randomly chosen inside a sphere of radius R. The solid red line represents the borderline of the support of eigenvalue density following from Eq. (7.78) [or equivalently, from Eq. (7.80)]; $b_0 = 6N/(k_0R)^2$ and $b_a = -4k_0R\mathrm{Im}n_a$. The dashed white line represents the borderline in the absence of amplification ($\mathrm{Im}n_a = 0$). The horizontal line $\mathrm{Im} = -1$ corresponds to the laser threshold, and the hatched domain indicates the part of the complex plane where eigenvalues Λ participate in the lasing process.

(6.41) for the borderline $z \in \delta\mathcal{D}$ of the support of eigenvalues become

$$z = \frac{1}{g} + 2\gamma g h[-\mathrm{i}\kappa_a(g)R - \mathrm{i}k_0 n_a R], \tag{7.73}$$

$$\frac{1}{|g|^2} = 2\gamma h[2\mathrm{Im}\kappa_a(g)R], \tag{7.74}$$

where γ and $h(x)$ are given by Eqs. (6.105) and (6.115), respectively; $z \in \delta\mathcal{D}$ is found upon elimination of g. In addition, an explicit equation for the resolvent $g(z)$ with $z \in \mathcal{D}$ follows from Eq. (6.170):

$$g(z) = \frac{z^* - 2\gamma g h[\mathrm{i}\kappa_a(g)^* R + \mathrm{i}k_0 n_a^* R]}{2\gamma h[2\mathrm{Im}\kappa_a(g)R]}, \tag{7.75}$$

allowing to solve for the eigenvalue distribution $p(\Lambda)$ with the help of Eq. (6.3). Finally, the second moment of $|\Lambda|$ evaluated from Eq. (6.50) reads

$$\langle|\Lambda|^2\rangle \simeq \frac{\mathrm{Tr}(\hat{T}\hat{T}^\dagger)}{2N} = \gamma h\left(2k_0R\,\mathrm{Im}n_a\right). \tag{7.76}$$

Note that $h(x)$ is a monotonically decaying function that obeys $h(0) = 1$, and exponentially diverges for $x < 0$, meaning that the second moment $\langle|\Lambda|^2\rangle$ grows rapidly when increasing the amplification parameter $\mathrm{Im}n_a < 0$.

At low densities, an accurate approximation of Eqs. (7.73) and (7.74) is obtained by replacing g by $1/z$. This leads to a borderline equation

$$|\Lambda|^2 = 2\gamma h[2\mathrm{Im}\kappa_a(1/\Lambda)R], \tag{7.77}$$

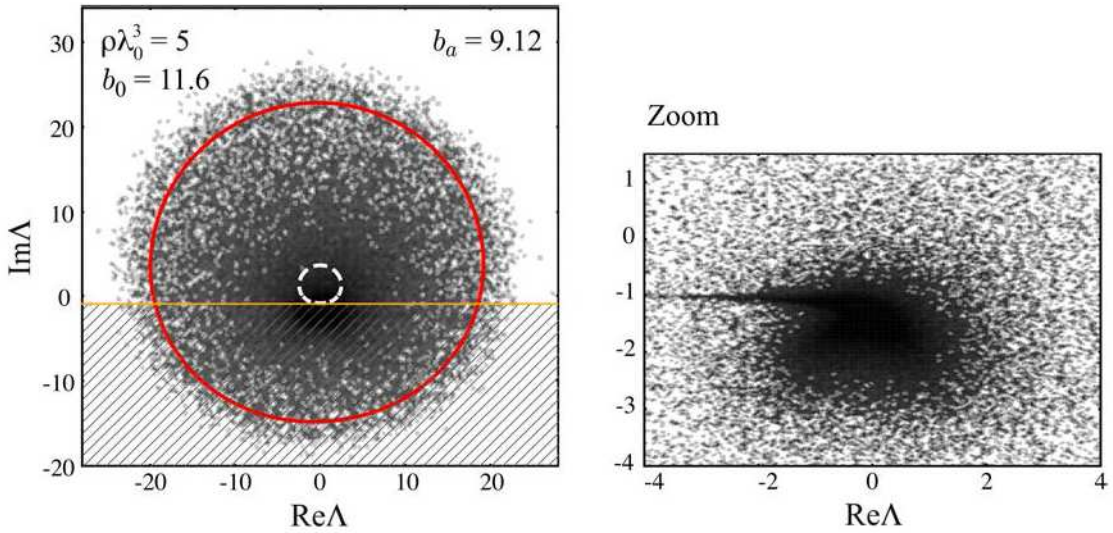

Figure 7.8: Same as Fig. 7.8 but for $\mathrm{Im}n_a = -0.1$. The right panel presents a zoom of the density plot of the left panel. It shows that most of the eigenvalues are concentrated near $\Lambda = 0$ and in the vicinity of the 'subradiant branch'.

that can be further simplified into

$$|\Lambda|^2 = 2\gamma h \left(2k_0 R\, \mathrm{Im}n_a - 8\gamma \frac{\mathrm{Im}\Lambda}{3|\Lambda|^2} \right), \tag{7.78}$$

where we assumed $\rho\lambda_0^3 \ll 1$ and $\mathrm{Im}n_a \ll 1$. Despite these assumptions, the borderline following from Eq. (7.78) is almost undistinguishable from the one inferred from Eqs. (7.73) and (7.74) in the regime $\rho\lambda_0^3 \lesssim 10$ where these analytical predictions are also in agreement with numerical simulations. As expected, Eq. (7.78) reduces to the borderline equation (6.117) of the Green's matrix $G(\omega_0)$ for $\mathrm{Im}n_a = 0$.

In Figs. 7.7 and 7.8, we compare the solution of Eq. (7.78) with results of numerical diagonalization of the $N \times N$ matrix (7.67) for $N = 10^3$, $\rho\lambda_0^3 = 5$ ($k_0R = 22.79$), and n_a given by Eq. (7.66) with $\mathrm{Im}n_a = -0.02$, -0.057, and -0.1. When the amplification $|\mathrm{Im}n_a|$ is increased, the eigenvalue domain grows in size. It deforms near $\Lambda = 0$ for small values of $k_0R|\mathrm{Im}n_a|$ (Fig. 7.7), and becomes a circle $|\Lambda|^2 = 2\gamma h(2k_0R\,\mathrm{Im}n_a)$ ($= 2\langle|\Lambda|^2\rangle$) in the limit $k_0R|\mathrm{Im}n_a| \gg 1$ (Fig. 7.8). Note that the subradiant branch $\Lambda = -G_a(\omega_0)_{12}$, that played the role of an 'escape channel' for the 'gas' of eigenvalues in the case $\mathrm{Im}n_a = 0$ (see sections 6.5.2 and 7.1.3), still preferentially attracts the eigenvalues in the case $\mathrm{Im}n_a < 0$, despite the fact that the borderline $\delta\mathcal{D}$ of the bulk goes beyond $-\langle\min[G_a(\omega_0)_{12}]\rangle$ (see the right panel of Fig. 7.8).

Physical implications relative to the lasing threshold are briefly investigated in the next section.

7.3.3 Prediction for the lasing threshold

In order to discuss the random lasing threshold following from Eq. (7.78), it is convenient to introduce the linear gain length l_g. The latter is defined as the path length over which light intensity is amplified by a factor e (provided that purely geometrical attenuation

of the intensity is disregarded):

$$l_g = \frac{-1}{2k_0 \mathrm{Im} n_a}. \tag{7.79}$$

By analogy with the on-resonance optical thickness $b_0 = 2R/l_0$, we also define a 'gain thickness' $b_a = 2R/l_g$. In terms of b_0 and b_a, the borderline equation (7.78) reads:

$$|\Lambda|^2 = \frac{3}{8} b_0 h \left(-\frac{b_a}{2} - \frac{b_0}{2} \frac{\mathrm{Im}\Lambda}{|\Lambda|^2} \right). \tag{7.80}$$

As we did in section 6.5.1.b for the free-space Green's matrix, we can compare the borderline equation (7.80) with the one obtained in the diffusion approximation. When scatterers are embedded in a continuous amplifying medium, the diffusion equation for the average intensity is still of the generic form (4.131), with $D = v l_0/3|\tilde{\alpha}(\omega_L)|^2$, and $Q = v[|\tilde{\alpha}(\omega_L)|^2/l_0 - \mathrm{Im}\tilde{\alpha}(\omega_L)/l_0 + 1/l_g]$ [see Eq. (4.121)]. The dimensionless polarizability $\tilde{\alpha}(\omega_L)$ of the scatterers can be arbitrary; in particular, we do not assume at this stage that the scatterers are not pumped. The threshold condition (4.135) becomes

$$\frac{\sqrt{3}}{2\pi} b_0 |\tilde{\alpha}(\omega_L)| \sqrt{|\tilde{\alpha}(\omega_L)|^2 - \mathrm{Im}\tilde{\alpha}(\omega_L) + \frac{b_a}{b_0}} \left(1 + \frac{1}{1 + 3b_0 |\tilde{\alpha}(\omega_L)|^2/4} \right) = 1, \tag{7.81}$$

where $b_a/b_0 = -4\pi^2 \mathrm{Im} n_a/\rho\lambda_0^3$. As we explained in section 6.5.1.b, the diffusive prediction for the borderline $\delta\mathcal{D}$ of the eigenvalue domain follows by replacing $\tilde{\alpha}(\omega_L)$ by $1/\Lambda$ in Eq. (7.81):

$$|\Lambda|^2 = \frac{\sqrt{3}}{2\pi} \sqrt{1 + \mathrm{Im}\Lambda + \frac{b_a}{b_0}|\Lambda|^2} \left(1 + \frac{|\Lambda|^2}{|\Lambda|^2 + 3b_0/4} \right). \tag{7.82}$$

For passive scatters, lasing starts when the condition (7.68) is obeyed. Since in the absence of pump, all eigenvalues of $G_a(\omega_0)$ satisfy $\mathrm{Im}\Lambda_k > -1$, lasing is triggered by the eigenvalue of $G_a(\omega_0)$ that has the smallest imaginary part. On average, lasing starts when the borderline $\delta\mathcal{D}$ crosses the line $\mathrm{Im}\Lambda = -1$. Furthermore, the inverse of the polarizability of passive scatterers is $1/\tilde{\alpha} = 2\delta_L - \mathrm{i}$, where $\delta_L = (\omega_0 - \omega_L)/\Gamma_0$ [see, *e.g.*, Eq. (4.9) for $W_i = 0$ and $s_i = 0$], so that the lasing frequency $\omega_L = \omega_0 - \Gamma_0\delta_L$ can be deduced from the abscissa $2\delta_L$ of the intersection point of $\delta\mathcal{D}$ with the line $\mathrm{Im}\Lambda = -1$. In Fig. 7.9, we compare the borderline inferred from Eq. (7.80) (solid line) with the diffusive prediction (7.82) (dashed line) in the regime of relatively large optical thickness $b_0 \gg 1$. If Eq. (7.80) gives a better global estimate of the domain occupied by the eigenvalues of $G_a(\omega_0)$ on the complex plane (left pannel), Eq. (7.82) is undoubtedly more accurate than Eq. (7.80) as far as far as the 'bottom' of the distribution is concerned (right pannel). This demonstrates that Eq. (7.82) should yield a fairly good prediction for the lasing threshold, as long as $b_0 \gg 1$ and $\rho\lambda_0^3 \lesssim 10$. At the time of writing this thesis, we are trying to obtain a better approximation of Eqs. (6.40) and (6.41) than (7.80) that could be as good as (7.82) to describe the bottom of the eigenvalue distribution of $G_a(\omega_0)$. Further work is also needed to investigate the eigenvalue distribution of $G_a(\omega_0)$ in the regime of high density $\rho\lambda_0^3 > 10$.

Preliminary results presented above demonstrate that our Euclidean matrix approach is well adapted to calculate the random lasing threshold, not only for models where scattering and gain are due to the same atoms (section 7.1), but also for systems where gain and scattering are independent. Interestingly, the nature of the lasing modes in the latter case is radically different from those in the former one. While lasing was

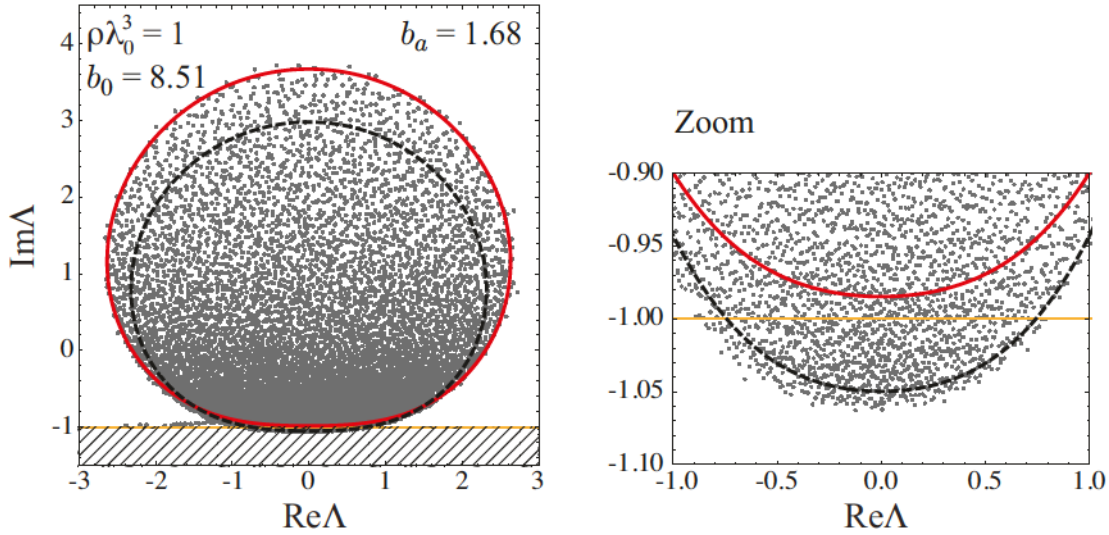

Figure 7.9: Eigenvalues of the $N \times N$ random Green's matrix (7.67) obtained by numerical diagonalization of the matrix for $N = 10^4$, $\rho\lambda_0^3 = 1$ ($k_0 R = 83.98$) and $\mathrm{Im} n_a = -0.005$. Points $\mathbf{r}_i$ are randomly chosen inside a sphere of radius R. The solid red line represents the borderline of the support of eigenvalue density following from Eq. (7.80). The dashed line shows the borderline following from the diffusion equation in an amplifying medium [Eq. (7.82)].

triggered by the eigenvalues of the Green's matrix $G(\omega_0)$ with the largest imaginary part $\mathrm{Im}\Lambda$ for both the incoherent gain and the coherent Mollow gain (section 7.1), it is now controlled by the eigenvalues of $G_a(\omega_0)$ that have the smallest $\mathrm{Im}\Lambda$. In this sense, the situation where gain and scattering are independent is much more intuitive because the first lasing modes are those that have the smallest decay rates in the absence of pump. Lasing modes may also differ by their degree of spatial localization. Indeed, contrary to the modes with large $\mathrm{Im}\Lambda$, eigenvectors of $G(\omega_0)$ or $G_a(\omega_0)$ with small $\mathrm{Im}\Lambda$ may be localized over a small fraction of the N points $\mathbf{r}_i$ (see Fig. 6.20). As we saw in section 7.2, this can have important consequences for the behavior of the random laser above threshold.

7.4 Conclusion and perspectives

In this chapter, we applied our non-Hermitian Euclidean random matrix theory to the problem of random lasing. It allowed us to find the lasing threshold without relying on the diffusion approximation or transport theory. We predicted, for example, the possibility of random lasing in a cloud of cold atoms for on-resonance optical thickness exceeding 35 for three- and 110 for two-level atoms ('Mollow laser'). In addition, microscopic quantum equations (7.1) and (7.2) for the dynamics of atomic operators in free space allowed us to express the spectrum of light below threshold, as well as the intensity of laser emission beyond threshold, in terms of the properties of the Green's matrix. In particular, we obtained the rate equations for the lasing modes without invoking a phenomenological 'bath' as in the standard laser theory [23], and without using the Feshbach projection technique promoted by Hackenbroich and coworkers [24–27, 36]. Our equations have

the advantage of being applicable for any geometry or dimensionality of the problem. Performing a statistical analysis, we provided analytical expressions for the spectrum below threshold that is reminiscent of the probability distribution of the 'collective Lamb shift', as well as for the average intensity and the average number of lasing modes. We showed that mode competition plays an important role in the random laser and leads to the scaling of the number of lasing modes with $\sqrt{N}$ (instead of N in the absence of mode competition), where N is the number of atoms. At the same time, the laser intensity scales with N (instead of N^2).

Regarding random lasers where scattering and gain are due to the same atoms, various extensions of the previous results may be considered. We showed that lasing is controlled, in the case of uniform pump, by the modes of the Green's matrix that have the largest imaginary part. It would be interesting to characterize the nature of these modes, that are delocalized over the whole system, in terms of transport or dynamic properties, and thus to compare them to other types of peculiar modes that may occur in disordered or chaotic systems (such as, *e.g.*, necklace states or whispering gallery modes). Another extension would be to study the full probability distributions of the intensity and of the number of lasing modes, that seem to be accessible using the results of section 7.2.3 together with the marginal distribution $p(\mathrm{Im}\Lambda)$. Finally, a more challenging problem is the characterization of first- and second-order coherence of the random laser beyond threshold, taking into account the quantum nature of the light-matter interaction. Second-order coherence may be studied by considering the intensity-intensity correlation $\langle I(t,\mathbf{r})I(t,\mathbf{r}')\rangle$ or by considering the mode-spacing statistics of the Green's matrix.

Last but not least, we also have seen that lasing in an ensemble of passive scatterers embedded in an amplifying matrix is triggered by the modes of the 'amplifying' Green's matrix $G_a(\omega_0)$ that have the smallest imaginary part. At small amplification, these modes do not differ much from those of $G(\omega_0)$, meaning that they appear in a part of the eigenvalue distribution where can coexist very different types of states: delocalized states, states localized on small clusters of scatterers (they are states that belong to the 'subradiant branch'), and Anderson-localized states. All of them may have an impact on the lasing process. We hope that our Euclidean random matrix approach will help, in the future, to clarify the respective role of these different states in the physics of random lasers.

Bibliography

[1] A. E. Siegman. *Lasers.* University Science Books, 1986.

[2] O. Svelto. *Principles of Lasers.* Plenum-Press, New York, fourth edition, 1998.

[3] D. S. Wiersma, *The physics and applications of random lasers*, Nature Phys. **4**, 359 (2008).

[4] H. Cao, *Review on latest developments in random lasers with coherent feedback*, J. Phys. A: Math. Gen. **38**, 10497 (2005).

[5] C. W. J. Beenakker, *Diffusive waves in Complex Media*, NATO Advancesd Studies Institute, Series C. **531**, 137 (1999).

[6] V. S. Letokhov, *Generation of light by a scattering medium with negative resonance absorption*, Sov. Phys. JETP **26**, 835 (1968).

[7] V. S. Letokhov, *Stimulated emission of an ensemble of scattering particles with negative absorption*, JETP Lett. **5**, 212 (1967).

[8] R. V. Ambartsumyan, P. G. Kryukov, V. S. Letokhov, and Yu. A. Matveets, *Emission Statistics of a Laser with Nonresonant feedback*, JETP Lett. **5**, 312 (1967).

[9] P. W. Anderson, *Absence of diffusion in certain random lattices*, Phys. Rev. **109**, 1492 (1958).

[10] D. S. Wiersma, M. P. van Alba, and A. Lagendijk, *Random laser?*, Nature **373**, 203 (1995).

[11] H. Cao, Y. G. Zhao, S. T. Ho, E. W. Seelig, Q. H. Wang, and R. P. H. Chang, *Random Lasing action in Semiconductor Powder*, Phys. Rev. Lett. **82**, 2278 (1999).

[12] R. C. Polson, A. Chipouline, and Z.V. Vardeny, *Random Lasing in π-Conjugated Films and Infiltrated Opals*, Adv. Mater. **13**, 760 (2001).

[13] H. Cao, J. Y. Xu, E. W. Seelig, and R. P. H. Chang, *Microlaser made of disordered media*, Appl. Phys. Lett. **76**, 2997 (2000).

[14] M. Bahoura and M. A. Noginov, *Determination of the transport mean free path in a solid-state random laser*, J. Opt. Soc. Am. B **20**, 2389 (2003).

[15] K. L. van der Mollen, R. W. Tjerkstra, A. P. Mosk, and A. Lagendijk, *Spatial Extent of Random Laser Modes*, Phys. Rev. Lett. **98**, 143901 (2007).

[16] D. S. Wiersma and S. Cavalieri, *Light emission: A temperature-tunable random laser*, Nature **414**, 708 (2001).

[17] X. wu, W. Fang, A. Yamilov, A. A. Chabanov, A. A. Asatryan, L. C. Botten, and H. Cao, *Random lasing in weakly scattering systems*, Phys. Rev. A **74**, 053812 (2006).

[18] V. M. Apalkov, M. E. Raikh, and B. Shapiro, *Random Resonators and Prelocalized Modes in Disordered Dielectric films*, Phys. Rev. Lett. **89**, 016802 (2002).

[19] A. A. Chabanov, Z. Q. Zhang, and A. Z. Genack, *Breakdown of Diffusion in Dynamics of Extended Waves in Mesoscopic Media*, Phys. Rev. Lett. **90**, 203903 (2003).

[20] S. Mujumdar, M. Ricci, R. Torre, and D. S. Wiersma, *Amplified Extended Modes in Random Lasers*, Phys. Rev. Lett. **93**, 053903 (2004).

[21] O. Zaitsev and L. Deych, *Recent developments in the theory of multimode random lasers*, J. Opt. **12**, 1 (2010).

[22] J. Andreasen, A. A. Asatyran, L. C. Botten, M. A. Byrne, H. Cao, L. Ge, L. Labonté, P. Sebbah, A. D. Stone, H. E. Türeci, and C. Vanneste, *Modes of random lasers*, Advances in Optics and Photonics **3**, 88 (2011).

[23] H. Haken. *Light, vol. 2: Laser light dynamics.* North-Holland physics publishing, 1985.

[24] G. Hackenbroich, C. Viviescas, and F. Haake, *Field Quantization for Chaotic Resonators with Overlapping Modes*, Phys. Rev. Lett. **89**, 083902 (2002).

[25] C. Viviescas and G. Hackenbroich, *Field Quantization for open optical cavities*, Phys. Rev. A **67**, 013805 (2003).

[26] G. Hackenbroich, C. Viviescas, and F. Haake, *Quantum statistics of overlapping modes in open resonators*, Phys. Rev. A **68**, 063805 (2003).

[27] C. Viviescas and G. Hackenbroich, *Quantum theory of multimode fields: applications to optical resonators*, J. Opt. B: Quantum Semiclass. Opt. **6**, 211 (2004).

[28] C. Vanneste, P. Sebbah, and H. Cao, *Lasing with Resonant Feedback in Weakly Scattering Random Systems*, Phys. Rev. Lett. **98**, 143902 (2007).

[29] C. Vanneste and P. Sebbah, *Selective Excitation of Localized Modes in Active Random Media*, Phys. Rev. Lett. **87**, 183903 (2001).

[30] X. Jiang and C. M. Soukoulis, *Time Dependent Theory for Random lasers*, Phys. Rev. Lett. **85**, 70 (2000).

[31] C. Conti and A. Fratalocci, *Dynamic light diffusion, three-dimensional Anderson localization and lasing in inverted opals*, Nature Phys. **4**, 794 (2008).

[32] H. E. Türeci, A. D. Stone, L. Ge, S. Rotter, and R. J. Tandy, *Ab initio self-consistent laser theory and random lasers*, Nonlinearity **22**, C1 (2009).

[33] L. Ge, Y. D. Chong, and A. D. Stone, *Steady-state ab initio laser theory: Generalizations and analytic results*, Phys. Rev. A **82**, 063824 (2010).

[34] H. E. Türeci, L. Ge, S. Rotter, and A. D. Stone, *Strong Interactions in Multimode Random Lasers*, Science **320**, 643 (2008).

[35] H. E. Türeci, A. D. Stone, and B. Collier, *Self-consistent multimode lasing theory for complex or random lasing media*, Phys. Rev. A **74**, 043822 (2006).

[36] G. Hackenbroich, *Statistical theory of multimode random lasers*, J. Phys. A: Math. Gen. **38**, 10537 (2005).

[37] O. Zaitsev, *Mode statistics in random lasers*, Phys. Rev. A **74**, 063803 (2006).

[38] O. Zaitsev, *Spacing statistics in two-mode random lasing*, Phys. Rev. A **76**, 043842 (2007).

[39] T. Sh. Misirpashaev and C. W. J. Beenakker, *Lasing threhold and mode competition in chaotic cavities*, Phys. Rev. A **57**, 2041 (1998).

[40] O. Zaitsev, L. Deych, and V. Shuvayev, *Statistical Properties of One-Dimensional Random Lasers*, Phys. Rev. Lett. **102**, 043906 (2009).

[41] C. Cohen-Tannoudji, J. Dupont-Roc, and G. Grynberg. *Photons and Atoms-Introduction to Quantum Electrodynamics.* Wiley Science Papers Series, New York, 1992.

[42] J. D. Jackson. *Classical electrodynamics.* John Wiley and Sons, New York, 1973.

[43] G. S. Agarwal, *Quantum Statistics of Spontaneous Emission and their Relation to Other Approaches*, Quantum Optics **70** (1974).

[44] K. Hammerer, A. S. Sørensen, and E. S. Polzik, *Quantum interface between light and atomic ensembles*, Rev. Mod. Phys. **82**, 10041 (2010).

[45] O. Morice. *Atomes refroidis par laser: du refroidissement sub-recul à la recherche d'effets quantiques collectifs.* (PhD Thesis), 1995.

[46] O. Morice, Y. Castin, and J. Dalibard, *Refractive index of a dilute Bose gas*, Phys. Rev. A **51**, 3896 (1995).

[47] R. H. Dicke, *Coherence in Spontaneous Radiation Processes*, Phys. Rev. **93**, 99 (1954).

[48] J. P. Gordon, J. Zeiger, and C. H. Townes, *The Maser–New Type of Microwave Amplifier, Frequency Standard, and Spectrometer*, Phys. Rev. **99**, 1264 (1955).

[49] A. Lagendijk and B. A. van Tiggelen, *Resonant Multiple Scattering of Light*, Phys. Rep. **270**, 143 (1996).

[50] C. W. Gardiner and P. Zoller. *Quantum Noise. A Handbook of Markovian and Non-Markovian Quantum Stochastic Methods with Applications to Quantum Optics.* Springer-Verlag, Berlin, second edition, 2000.

[51] H. Carmichael. *An Open Systems Approach to Quantum Optics.* Springer-Verlag, Berlin, 1993.

[52] C. Cohen-Tannoudji, J. Dupont-Roc, and G. Grynberg. *Atom-Photon interactions.* Wiley Science Papers Series, New York, 1998.

[53] M. O. Scully and M. S. Zubairy. *Quantum optics.* Cambridge University press, sixth edition, 2008.

[54] G. S. Agarwal, *Master-Equation Approach to Spontaneous Emission*, Phys. Rev. A **2**, 2038 (1970).

[55] R. H. Lehmberg, *Radiation from an N-atom system*, Phys. Rev. A **2**, 883 (1970).

[56] M. Gross and S. Haroche, *Superradiance : An Essay on the Theory of Collective Spontaneous Emission*, Phys. Rep. **93**, 301 (1982).

[57] D. F. V. James, *Frequency shifts in spontaneous emission from two interacting atoms*, Phys. Rev. A **47**, 1336 (1993).

[58] J. Guo and J. Cooper, *Cooling and resonance fluorescence of two atoms in a one-dimensional optical molasses*, Phys. Rev. A **51**, 3128 (1995).

[59] T. G. Rudolph, Z. Ficek, and B. J. Dalton, *Two-atom resonance fluorescence in running- and standing-wave laser fields*, Phys. Rev. A **52**, 636 (1995).

[60] S. Das, G. S. Agarwal, and M. O. Scully, *Quantum interferences in Cooperative Dicke Emission from Spatial Variation of the Laser-Phase*, Phys. Rev. Lett. **101**, 153601 (2008).

[61] T. Savels, A. P. Mosk, and A. Lagendijk, *Gain Narrowing in Few-Atom Systems*, Phys. Rev. Lett. **98**, 103601 (2007).

[62] H. Haken. *Light, vol. 1: Waves, photons, atoms.* North-Holland physics publishing, 1981.

[63] M. Lewenstein, Y. Zhu, and T. W. Mossberg, *Two-Photon Gain and Lasing in Strongly Driven Two-Level Atoms*, Phys. Rev. Lett. **71**, 3131 (1990).

[64] J. Zakrzewski, M. Lewenstein, and T. W. Mossberg, *Theory of dressed-state lasers. I. Effective Hamiltonians and stability properties*, Phys. Rev. A **44**, 7717 (1991).

[65] W. Guérin, N. Mercadier, F. Michaud, D. Brivio, L. S. Froufe-Pérez, R. Carminati, V. Eremeev, A. Goetschy, S.E. Skipetrov, and R. Kaiser, *Gain Narrowing in Few-Atom Systems*, J. Opt. **12**, 024002 (2010).

[66] B. Grémaud, T. Wellens, D. Delande, and C. Miniatura, *Coherent backscattering in nonlinear media: Quantum Langevin approach*, Phys. Rev. A **74**, 033808 (2006).

[67] F. Haake, H. King, G. Schröder, J. Haus, and R. Glauber, *Fluctuations in superfluorescence*, Phys. Rev. A **20**, 2047 (1979).

[68] Y. Castin and Klaus Mølmer, *Maxwell-Bloch equations: A unified view of nonlinear optics and nonlinear atom optics*, Phys. Rev. A **51**, R3426 (1995).

[69] M. Fleischhauer and M. D. Lukin, *Dark-State Polaritons in Electromagnetically Induced Transparency*, Phys. Rev. Lett. **84**, 5094 (2000).

[70] R. J. Glauber, *The Quantum Theory of Optical Coherence*, Phys. Rev. **130**, 2529 (1963).

[71] L. Mandel and E. Wolf. *Optical coherence and quantum optics.* Cambridge University press, 1995.

[72] C. Cohen-Tannoudji. *Lectures at the College de France.* 1978-1979.

[73] I. R. Senitzky, *Radiation-Reaction and Vacuum-Field Effects in Heisenberg-Picture Quantum Electrodynamics*, Phys. Rev. Lett. **31**, 955 (1973).

[74] L. You, J. Mostowski, and J. Cooper, *Cone emission from laser-pumped two-level atoms. I. Quantum theory of resonant light propagation*, Phys. Rev. A **46**, 2903 (1992).

[75] M. O. Scully and A. A. Svidzinsky, *The Lamb shift —Yesterday, Today, and Tomorrow*, Science **328**, 1239 (2010).

[76] M. Mézard, G. Parisi, and M.A. Virasoro. *Spin Glass Theory and Beyond.* World Scientific, Singapore, 1987.

[77] D. N. Aristov, *Indirect RKKY interaction in any dimensionality*, Phys. Rev. B **55**, 8064 (1997).

[78] C. A. Müller and C. Miniatura, *Multiple scattering of light by atoms with internal degeneracy*, J. Phys. A **35**, 10163 (2002).

[79] E. Akkermans, A. Gero, and R. Kaiser, *Photon Localization and Dicke Superradiance in Atomic Gases*, Phys. Rev. Lett. **101**, 103602 (2008).

[80] I. M. Sokolov, M. D. Kupriyanova, D. V. Kupriyanov, and M. D. Havey, *Light scattering from a dense and ultracold atomic gas*, Phys. Rev. A **79**, 053405 (2009).

[81] M. O. Scully, E. S. Fry, C. H. Raymond Ooi, and Krzysztof Wódkiewicz, *Directed Spontaneous Emission from an Extended Ensemble of N atoms: Timing is Everything*, Phys. Rev. Lett. **96**, 010501 (2006).

[82] A. A. Svidzinsky, Jun-Tao Chang, and M. O. Scully, *Dynamical Evolution of Correlated Spontaneous Emission of a Single Photon from a Uniformly Excited Cloud of N Atoms*, Phys. Rev. Lett. **100**, 160504 (2008).

[83] M. O. Scully, *Collective Lamb shift in Single Photon Dicke Superradiance*, Phys. Rev. Lett. **102**, 143601 (2009).

[84] F. M. Dittes, *The decay of quantum systems with a small number of open channels*, Phys. Rep. **339**, 215 (2000).

[85] M. Antezza and Y. Castin, *Spectrum of Light in a Quantum Fluctuating Periodic Structure*, Phys. Rev. Lett. **103**, 123903 (2009).

[86] V. Ernst, *Coherent Emission of Photon by many Atoms*, Z. Phys. **218**, 111 (1968).

[87] A. A. Svidzinsky and Jun-Tao Chang, *Cooperative spontaneous emission as a many-body eigenvalue problem*, Phys. Rev. A **77**, 043833 (2008).

[88] A. A. Svidzinsky and M. O. Scully, *Evolution of collective N atom states in single photon superradiance: Effect of virtual Lamb shift*, Opt. Commun. **282**, 2894 (2009).

[89] M. O. Scully and A. A. Svidzinsky, *The Super of Superradiance*, Science **325**, 1510 (2009).

[90] A. A. Svidzinsky, Jun-Tao Chang, and M. O. Scully, *Cooperative spontaneous emission of N atoms: Many-body eigenstates, the effect of virtual Lamb shift processes, and analogy with radiation of N classical oscillators*, Phys. Rev. A **81**, 053821 (2010).

[91] J. T. Manassah, *Superradiance from a cylindrically shaped cloud of N two-level atoms*, Phys. Rev. A **82**, 053816 (2010).

[92] R. Röhlsberger, K. Schlage, B. Sahoo, S. Couet, and R. Rüffer, *Collective Lamb shift in Single-Photon Superradiance*, Science **328**, 1248 (2010).

[93] D. F. Phillips, A. Fleischhauer, A. Mair, R. L. Walsworth, and M. D. Lukin, *Storage of light in atomic vapor*, Phys. Rev. Lett. **86**, 783 (2001).

[94] A. Kalachev, *Quantum storage on subradiant states in an extended atomic ensemble*, Phys. Rev. A **76**, 043812 (2007).

[95] P. Grangier, *Remember that photon*, Science **438**, 749 (2005).

[96] T. Chanelière, D. N. Matsukevitch, S. D. Jenkins, S. Y. Lan, T. A. B. Kennedy, and A. Kuzmich, *Storage and retrieval of single photons transmitted between remote quantum memories*, Science **438**, 833 (2005).

[97] G. Labeyrie, F. de Tomasi, J.-C. Bernard, C. A. Müller, C. Miniatura, and R. Kaiser, *Coherent Backscattering of Light by Cold Atoms*, Phys. Rev. Lett. **83**, 5266 (1999).

[98] G. Labeyrie, E. Vaujour, C. A. Müller, D. Delande, C. Miniatura, D. Wilkowski, and R. Kaiser, *Slow Diffusion of Light in a Cold Atomic Cloud*, Phys. Rev. Lett. **91**, 223904 (2003).

[99] R. Pierrat and R. Carminati, *Spontaneous decay rate of a dipole emitter in a strongly scattering disordered environment*, Phys. Rev. A **81**, 063802 (2010).

[100] A. Cazé, R. Pierrat, and R. Carminati, *Near-field interactions and nonuniversality in speckle patterns produced by a point source in a disordered medium*, Phys. Rev. A **82**, 043823 (2010).

[101] A. Lagendijk, B. A. van Tiggelen, and D. S. Wiersma, *Fifty years of Anderson localization*, Physics Today **62**, 24 (2009).

[102] *Special Issue: 50 years of Anderson localization*, Int. J. Mod. Phys. B **24**, 1501 (2010).

[103] T. Kottos, *Statistics of resonances and delay times in random media: beyond random matrix theory*, J. Phys. A: Math. Gen. **38**, 10761 (2005).

[104] F. A. Pinheiro, M. Rusek, A. Orlowski, and B. A. van Tiggelen, *Probing Anderson localization of light via decay rate statistics*, Phys. Rev. E **69**, 026605 (2004).

[105] M. Rusek, J. Mostowski, and A. Orlowski, *Random Green matrices: From proximity resonances to Anderson localization*, Phys. Rev. A **61**, 022704 (2000).

[106] P. Massignan and Y. Castin, *Three-dimensional strong localization of matter waves by scattering from atoms in a lattice with a confinement-induced resonance*, Phys. Rev. A **74**, 013616 (2006).

[107] M. Antezza, Y. Castin, and D. A. W. Hutchinson, *Quantitative study of two- and three-dimensional strong localization of matter waves by atomic scatterers*, Phys. Rev. A **82**, 043602 (2010).

[108] B. Grémaud and T. Wellens, *Speckle Instability: Coherent Effects in Nonlinear Disordered Media*, Phys. Rev. Lett. **104**, 133901 (2010).

[109] F. A. Pinheiro and L. C. Sampaio, *Lasing threshold of diffusive random lasers in three dimensions*, Phys. Rev. A **73**, 013826 (2006).

[110] M. Lax, *Formal Theory of Quantum Fluctuations from a Driven State*, Phys. Rev. **129**, 2342 (1963).

[111] M. Lax, *Quantum Noise. XI. Multitime Correspondence between Quantum and Classical Stochastic Processes*, Phys. Rev. **172**, 350 (1968).

[112] R. W. Boyd. *Nonlinear Optics.* Academic Press, London, 1992.

[113] T. Savels, A. P. Mosk, and A. Lagendijk, *Light scattering from three-level systems: The T matrix of a point dipole with gain*, Phys. Rev. A **71**, 043814 (2005).

[114] T. Savels. *An exploration of the smallest lasers possible.* Printpartners Ipskamp, Enschede, The Netherlands, 2007.

[115] B. R. Mollow, *Stimulated Emission and Absorption near Resonance for Driven Systems*, Phys. Rev. A **5**, 2217 (1972).

[116] F. Y. Wu, S. Ezkiel, M. Duclos, and B. R. Mollow, *Observation of Amplification in a Strongly Driven Two-Level Atomic System at Optical Frequencies*, Phys. Rev. A **5**, 2217 (1972).

[117] J. S. Hersch and E. J. Heller, *Observation of Proximity Resonances in a Parallel-Plate Waveguide*, Phys. Rev. Lett. **81**, 3059 (1998).

[118] E. J. Heller, *Quantum Proximity Resonances*, Phys. Rev. Lett. **77**, 4122 (1996).

[119] S. Li and E. J. Heller, *Quantum multiple scattering: Eigenmode expansion and its applications to proximity resonances*, Phys. Rev. A **67**, 032712 (2003).

[120] M. Rusek, J. Mostowski, and A. Orlowski, *Random Green matrices: From proximity resonances to Anderson localization*, Phys. Rev. A **61**, 022704 (2000).

[121] G. V. Varada and G. S. Agarwal, *Microscopic approach to correlation-induced frequency shifts*, Phys. Rev. A **44**, 7626 (1991).

[122] G. S. Agarwal, A. C. Brown, L. M. Narducci, and G. Vetri, *Collective atomic effects in resonance fluorescence*, Phys. Rev. A **15**, 1613 (1977).

[123] H. S. Freedhoff, *Collective atomic effects in resonance fluorescence: The scaling factor*, Phys. Rev. A **26**, 684 (1982).

[124] G. Lenz and P. Meystre, *Resonance fluorescence from two identical atoms in a standing-wave field*, Phys. Rev. A **48**, 3365 (1993).

[125] V. Shatokhin, T. Wellens, B. Grémaud, and A. Buchleitner, *Spectrum of coherently backscattered light from two atoms*, Phys. Rev. A **76**, 043832 (2007).

[126] H. Steudel, *Radiation rate and spectrum of a continuously pumped three-atom system*, J. Phys. B: Atom. Molec. Phys. **12**, 3309 (1979).

[127] P. Sheng. *Introduction to Wave Scattering, Localization and Mesoscopic Phenomena.* Springer-Verlag, Berlin, second edition, 2006.

[128] P. de Vries, D. V. van Coevorden, and A. Lagendijk, *Point scatterers for classical waves*, Rev. Mod. Phys. **70**, 447 (1998).

[129] M. C. van Rossum and Th. M. Nieuwenhuizen, *Multiple scattering of classical waves: microscopy, mesoscopy, and diffusion*, Rev. Mod. Phys. **71**, 313 (1999).

[130] T. Wellens, B. Grémaud, D. Delande, and C. Miniatura, *Coherent backscattering of light by two atoms in the saturated regime*, Phys. Rev. A **70**, 023817 (2004).

[131] E. Akkermans and G. Montambaux. *Mesoscopic Physics of Electrons and Photons.* Cambridge University Press, 2006.

[132] R. G. Newton. *Scattering Theory of Waves and Particles.* Springer-Verlag, Berlin, second edition, 1982.

[133] B. A. van Tiggelen, A. Lagendijk, and A. Tip, *Multiple scattering effects for the propagation of light in 3D slabs*, J. Phys. Condens. matter **2**, 7653 (1990).

[134] L. S. Froufe-Pérez, W. Guérin, R. Carminati, , and R. Kaiser, *Threshold of a Random Laser with Cold Atoms*, Phys. Rev. Lett. **102**, 173903 (2009).

[135] K. Drozdowicz, E. Krynicka, and J. Dabrowska, *Diffusion cooling of thermal neutrons in basic rock mineral by Monte Carlo simulation of the pulsed neutron experiments*, Appl. Radiat. Isot. **58**, 727 (2003).

[136] D. Vollhardt and P. Wölfe, *Diagrammatic, self-consistent treatment of the Anderson localisation problem in $d \leq 2$ dimensions*, Phys. Rev. B **22**, 4666 (1980).

[137] M. L. Mehta. *Random matrices.* Elsevier, Amsterdam, 2004.

[138] J. Wishart, *The generalized product moment distribution in samples from a normal multivariate population*, Biometrika A **20**, 32 (1928).

[139] E. P. Wigner, *Characteristic vectors of bordered matrices with infinite dimensions*, Ann. Math. **62**, 548 (1955).

[140] T. A. Brody, J. Flores, J. B. French, P. A. Mello, A. Pandey, and S. S. M. Wong, *Random-matrix physics: spectrum and strength fluctuations*, Rev. Mod. Phys. **53**, 385 (1981).

[141] C. W. J. Beenakker, *Random-matrix theory of quantum transport*, Rev. Mod. Phys. **69**, 731 (1997).

[142] T. Guhr, A. Müller-Groeling, and H. A. Weidenmüller, *Random-matrix theories in quantum physics: common concepts*, Phys. Rep. **299**, 189 (1998).

[143] A. M. Tulino and S. Verdú. *Random Matrix Theory and Wireless Communications.* Now Publishers, Delft, 2004.

[144] F. J. Dyson, *Statistical Theory of the Energy Levels of Complex Systems. I*, J. Math. Phys. **3**, 140 (1962).

[145] F. J. Dyson, *Statistical Theory of the Energy Levels of Complex Systems. II*, J. Math. Phys. **3**, 157 (1962).

[146] F. J. Dyson, *Statistical Theory of the Energy Levels of Complex Systems. III*, J. Math. Phys. **3**, 166 (1962).

[147] M. Mézard, G. Parisi, and A. Zee, *Spectra of euclidean random matrices*, Nucl. Phys. B **559**, 689 (1999).

[148] T. S. Grigera, V. Martin-Mayor, G. Parisi, and P. Verrocchio, *Vibrational Spectrum of Topologically Disordered Systems*, Phys. Rev. Lett. **87**, 085502 (2001).

[149] T. S. Grigera, M. Mézard, G. Parisi, and P. Verrocchio, *The dynamical structure factor in topologically disordered systems*, J. Chem. Phys. **114**, 8068 (2001).

[150] T. S. Grigera, V. Martin-Mayor, G. Parisi, and P. Verrocchio, *Vibrations in glasses and Euclidean random matrix theory*, J. Phys.: Condens. Matter **14**, 2167 (2002).

[151] T. S. Grigera, V. Martin-Mayor, G. Parisi, and P. Verrocchio, *Phonon interpretation of the 'boson peak' in supercooled liquids*, Nature **422**, 289 (2003).

[152] C. Ganter and W. Schirmacher, *Euclidean random matrix theory: low-frequency non-analyticities and Rayleigh scattering*, Phil. Mag. **91**, 1894 (2011).

[153] T. S. Grigera, V. Martin-Mayor, G. Parisi, P. Urbani, and P. Verrocchio, *On the high-density expansion for Euclidean random matrices*, J. Stat. Mech. **11**, P02015 (2011).

[154] C. Chamon and C. Mudry, *Density of states for dirty d-wave superconductors: A unified and dual approach for different types of disorder*, Phys. Rev. B **63**, 100503(R) (2001).

[155] A. Amir, Y. Oreg, and Y. Imry, *Localization, Anomalous diffusion, and Slow Relaxations: A Random Distance Matrix Approach*, Phys. Rev. Lett. **105**, 070601 (2010).

[156] E. Bogomolny, O. Bohigas, and C. Schmit, *Spectral properties of distance matrices*, J. Phys. A: Math. Gen. **36**, 3595 (2003).

[157] S. Ciliberti, T. S. Grigera, V. Martin-Mayor, G. Parisi, and P. Verrocchio, *Anderson localization in Euclidean random matrices*, Phys. Rev. B **71**, 153104 (2005).

[158] R. A. Janik and M. A. Nowak, *Wishart and anti-Wishart matrices*, J. Phys. A: Math Gen. **36**, 3629 (2003).

[159] V. A. Marchenko and L. A. Pastur, *Distribution of eigenvalues for some sets of random matrices*, Math. USSR-Sb **1**, 457 (1967).

[160] F. G. Tricomi. *Integral Equations.* Interscience, London, 1957.

[161] A. Zee, *Law of addition in random matrix theory*, Nucl. Phys. B **474**, 726 (1996).

[162] F. J. Dyson, *A Class of Matrix Ensembles*, J. Math. Phys. **13**, 90 (1972).

[163] M. Tierz, *The Stable Random Matrix Ensembles*, arXiv: cond-math/0106485v3 (2003).

[164] D. S. Dean and S. N. Majumdar, *Extreme value statistics of eigenvalues of Gaussian random matrices*, Phys. Rev. E **77**, 041108 (2008).

[165] S. N. Majumdar and M. Vergassola, *Large Deviations of the Maximum Eigenvalue for Wishart and Gaussian Random Matrices*, Phys. Rev. Lett. **102**, 060601 (2009).

[166] C. Nadal and S. N. Majumdar, *Nonintersecting Brownian interfaces and Wishart matrices*, Phys. Rev. E **79**, 061117 (2009).

[167] S. N. Majumdar, C. Nadal, A. Scardicchio, and P. Vivo, *Index Distribution of Gaussian Random Matrices*, Phys. Rev. Lett. **103**, 220603 (2009).

[168] K. B. Efetov. *Supersymmetry in Disorder and Chaos.* Cambridge University Press, Cambridge, 1997.

[169] F. Haake. *Quantum Signatures of Chaos.* Springer, Heidelberg, third edition, 2010.

[170] S. F. Edwards and R. C. Jones, *The eigenvalue spectrum of a large symmetric random matrix*, J. Phys. A: Math. Gen. **9**, 1595 (1976).

[171] A. M. Sengupta and P. P. Mitra, *Distributions of singular values for some random matrices*, Phys. Rev. E **60**, 3389 (1999).

[172] J. Jurkiewicz, G. Lukaszewski, and M. A. Nowak, *Diagrammatic approach to fluctuations in the Wishart ensemble*, Acta Phys. Pol. B **39**, 799 (2008).

[173] E. P. Wigner, *On the distribution of the roots of certain symmetric matrices*, Ann. Math. **67**, 325 (1958).

[174] Z. D. Bai, *Methodologies in spectral analysis of large dimensional random matrices, a review*, Stat. Sinica **9**, 611 (1999).

[175] D. V. Voiculescu, *Asymptotically commuting finite rank unitary operators without commuting approximants*, Acta. Sci. Math. **45**, 429 (1983).

[176] D. V. Voiculescu, K. J. Dykema, and A. Nica. *Free Random Variables.* American mathematical Society, 1992.

[177] A. Jarosz and M. A. Nowak, *Random Hermitian versus random non-Hermitian operators–unexpected links*, J. Phys. A: Math. Gen. **39**, 10107 (2006).

[178] R. A. Janik, M. A. Nowak, G. Papp, J. Wambach, and I. Zahed, *Non-Hermitian random matrix models: Free random variable approach*, Phys. Rev. E **55**, 4100 (1997).

[179] `http://www.netlib.org/lapack/`.

[180] I. S. Gradshteyn and I. M. Ryzhik. *Table of Integrals, Series and Products.* Academic Press, Inc., London, fourth edition, 1980.

[181] S. E. Skipetrov and A. Goetschy, *Euclidean random matrices for waves in random media*, J. Phys. A **44**, 065102 (2011).

[182] P. M. Morse and H. Feshbach. *Methods of Theoretical Physics.* McGraw-Hill, New York, 1953.

[183] E. Brézin and A. Zee, *Correlation functions in disordered systems*, Phys. Rev. E **49**, 2588 (1994).

[184] E. Brézin and A. Zee, *Universal relation between Green functions in random matrix theory*, Nucl. Phys. B **453**, 531 (1995).

[185] N. Hatano and D. R. Nelson, *Localization transitions in Non-Hermitian Quantum mechanics*, Phys. Rev. Lett. **77**, 570 (1996).

[186] R. A. Janik, M. A. Nowak, G. Papp, and I. Zahed, *Non-hermitian random matrix models*, Nucl. Phys. B **501**, 603 (1997).

[187] J. Feinberg and A. Zee, *Non-gaussian non-hermitian random matrix theory: Phase transition and addition formalism*, Nucl. Phys. B **501**, 643 (1997).

[188] J. Feinberg and A. Zee, *Non-hermitian random matrix theory: method of hermitian reduction*, Nucl. Phys. B **504**, 579 (1997).

[189] J. Feinberg and A. Zee, *Non-hermitian localization and delocalization*, Phys. Rev. E **59**, 6433 (1999).

[190] J. Feinberg and A. Zee, *Spectral curves of non-hermitian hamiltonians*, Nucl. Phys. B **552**, 599 (1999).

[191] J. Feinberg, *Non-Hermitian random matrix theory: summation of planar diagrams, the 'single-ring' theorem and the disc-annulus phase transition*, J. Phys. A: Math. gen. **39**, 10029 (2006).

[192] F. Haake, F. Izrailev, N. Lehmann, D. Saher, and H. J. Sommers, *Statistics of complex levels of random matrices for decaying systems*, Z. Phys. B **88**, 359 (1992).

[193] Y. V. Fyodorov and H. J. Sommers, *Statistical of resonance poles, phase shifts and time delays in quantum chaotic scattering*, J. Math. Phys. **38**, 1918 (1997).

[194] Y. V. Fyodorov and H. J. Sommers, *Random matrices close to Hermitian or unitarity: overview of methods and results*, J. Phys. A: Math. Gen. **36**, 3303 (2003).

[195] Y. V. Fyodorov, D. V. Savin, and H. J. Sommers, *Scattering, reflection and impedance of waves in chaotic and disordered systems with absorption*, J. Phys. A: Math. Gen. **38**, 10731 (2005).

[196] H. J. Sommers, A. Crisanti, H. Sompolinsky, and Y. Stein, *Spectrum of Large Random Asymmetric Matrices*, Phys. Rev. Lett. **60**, 1895 (1988).

[197] K. Rajan and L. F. Abbott, *Eigenvalue Spectra of Random Matrices for Neural Networks*, Phys. Rev. Lett. **97**, 188104 (2006).

[198] J. T. Chalker and Z. J. Wang, *Diffusion in a Random Velocity Field: Spectral Properties of a Non-Hermitian Fokker-Planck Operator*, Phys. Rev. Lett. **79**, 1797 (1997).

[199] M. A. Stephanov, *Random Matrix Model of QCD at finite Density and the Nature of the Quenched Limit*, Phys. Rev. Lett. **76**, 4472 (1996).

[200] J. J. M. Verbaarschot and T. Wettig, *Random matrix theory and chiral symmetry in QCD*, Annu. Rev. Nucl. Sci. **50**, 343 (2000).

[201] J. Ginibre, *Statistical Ensembles of Complex, Quaternion, and Real Matrices*, J. Math. Phys. **6**, 440 (1965).

[202] V. L. Girko, *Circular law*, Theory Probab. Appl. **29**, 694 (1985).

[203] R. A. Janik, M. A. Nowak, G. Papp, and I. Zahed, *Green's functions in non-hermitian random matrix models*, Physica E **9**, 456 (2001).

[204] J. T. Chalker and B. Mehlig, *Eigenvectors Statistics in non-Hermitian Random Matrix Ensembles*, Phys. Rev. Lett. **81**, 3367 (1998).

[205] R. A. Janik, W. Nörenberg, M. A. Nowak, G. Papp, and I. Zahed, *Correlations of eigenvectors for non-Hermitian random-matrix models*, Phys. Rev. E **60**, 2699 (1999).

[206] J. Feinberg, R. Scalettar, and A. Zee, *'Single ring theorem' and the disk-annulus phase transition*, J. Math. Phys. **42**, 5712 (2001).

[207] T. Rogers and I. P. Castillo, *Cavity approach to the spectral density of non-Hermitian sparse matrices*, Phys. Rev. E **79**, 012101 (2009).

[208] M. A. Stephanov, J. J. M. Verbaarschot, and T. Wettig. *Random Matrices.* Wiley Encyclopedia of Electrical and Electronics Engineering supplement I, New York, 2001.

[209] A. Jarosz and M. A. Nowak, *A novel approach to non-Hermitian random matrix models*, arXiv: math-ph/0402057 (2004).

[210] C. Mahaux and H. A. Weidenmüller. *Shell-model Approach to Nuclear Reactions.* North-Holland, Amsterdam, 1969.

[211] G. E. Mitchell, A. Richter, and H. A. Weidenmüller, *Random matrices and chaos in nuclear physics: Nuclear reactions*, Rev. Mod. Phys. **82**, 2845 (2010).

[212] N. Lehmann, D. Saher, V. V. Sokolov, and H. J. Sommers, *Chaotic scattering: the supersymmetry method for large number of channels*, Nucl. Phys. A **582**, 223 (1995).

[213] S. John, *Localization of light*, Physics Today **May 1991**, 32 (1991).

[214] D. J. Thouless, *Electrons in disordered systems and the theory of localization*, Phys. Rep. **13**, 93 (1997).

[215] E. Abrahams, P. W. Anderson, D. C. Licciardello, and T. V. Ramakrishnan, *Scaling theory of localization: absence of quantum diffusion in two dimensions*, Phys. Rev. Lett. **42**, 673 (1979).

[216] J. Wang and A. Z. Genack, *Transport through modes in random media*, Nature **471**, 345 (2011).

[217] C. A. Müller and D. Delande. *Disorder and Interferences: localization phenomena.* Les Houches School of Physics, Singapore, 2010.

[218] K. Slevin and T. Ohtsuki, *Corrections to Scaling at the Anderson Transition*, Phys. Rev. Lett. **82**, 382 (1999).

[219] G. Lemarié, B. Grémaud, and D. Delande, *Universality of the Anderson transition with the quasiperiodic kicked rotor*, Europhys. Lett. **87**, 37007 (2009).

[220] L. I. Deych, *Effects of Spatial Nonuniformity on Laser Dynamics*, Phys. Rev. Lett. **95**, 043902 (2005).

[221] D. S. Wiersma and A. Lagendijk, *Light diffusion with gain and random lasers*, Phys. Rev. E **54**, 4256 (1996).

[222] H. Cao, J. Y. Xu, and D. Z. Zhang, *Spatial Confinement of Laser Light in Active Random Media*, Phys. Rev. Lett. **84**, 5584 (2000).

[223] J. McKeever, A. Boca, A. D. Boozer, J. R. Buck, and H. J. Kimble, *Experimental realization of a one-atom laser in the regime of strong coupling*, Nature **425**, 268 (2003).

List of publications

A part of the work presented in this thesis is also published in:

- A. Goetschy and S. E. Skipetrov, *Euclidean matrix theory of random lasing in a cloud of cold atoms*, Europhys. Lett. **96**, 34005 (2011).

- A. Goetschy and S. E. Skipetrov, *Non-Hermitian Euclidean random matrix theory*, Phys. Rev. E **84**, 011150 (2011).

- S. E. Skipetrov and A. Goetschy, *Eigenvalue distributions of large Euclidean random matrices for waves in random media*, J. Phys. A: Math. Theor. **44**, 065102 (2011).

- W. Guérin, N. Mercadier, F. Michaud, D. Brivio, L. S. Froufe-Pérez, R. Carminati, V. Eremeev , A. Goetschy, S. E. Skipetrov, and R. Kaiser, *Towards a random laser with cold atoms*, J. Opt. **12**, 024002 (2010).

This thesis is devoted to the study of the properties of light emitted by a collection of atomic scatterers distributed at random positions in Euclidean space. In this respect, an *ab initio* theory of random lasing is formulated in terms of the statistical properties of the so-called 'Green's matrix'. This matrix belongs to the family of Euclidean random matrices (ERMs), for which we develop an analytic theory giving access to their eigenvalue distribution.

First, we derive quantum microscopic equations for the electric field and atomic operators, and show how the non-Hermitian Green's matrix (a matrix with elements equal to the Green's function of the Hemholtz equation between pairs of atoms in the system) emerges in the quantum formalism. We provide expressions for the intensity and the spectrum of light in terms of the Green's matrix, characterize quantum Langevin forces, and reveal how the semiclassical random laser threshold is washed out by quantum fluctuations (chapters 2 and 3).

A mesoscopic and semiclassical description of light scattered by pumped atoms is the subject of chapter 4. We provide a microscopic derivation of the transport equation in the presence of gain, reveal a mapping to ERMs, and analyze the lasing threshold inferred from the transport equation.

In chapters 5 and 6, we develop an analytic theory for Hermitian and non-Hermitian ERMs in the limit of large matrix size. We obtain self-consistent equations for the resolvent and the eigenvector correlator of an arbitrary ERM and apply our results to three different ERMs relevant to wave propagation in random media: the random Green's matrix, its imaginary part, and its real part. We are able to describe analytically with reasonable precision the full probability distribution of decay rates of light emitted by a large number of atoms, as well as of the collective frequency shift induced by the light-matter interaction. The signatures of Anderson localization in the properties of the Green's matrix are also discussed.

Finally, we combine microscopic equations of motion of light-matter interaction with our results for non-Hermitian ERMs to tackle the problem of random lasing. The lasing threshold and the intensity of laser emission are calculated analytically in the semiclassical approximation, and the spectrum of light below threshold is computed by taking into account quantum effects. Our theory applies from low to high density of atoms.

Cette thèse présente une étude des propriétés de la lumière émise par des diffuseurs atomiques distribués aléatoirement dans l'espace euclidien. Dans ce cadre, une théorie *ab initio* des lasers aléatoires est formulée en terme des propriétés statistiques de la 'matrice de Green'. Cette dernière appartient à la famille des matrices aléatoires euclidiennes (MAE) pour lesquelles nous développons une théorie analytique donnant notamment accès à la distribution de probabilité de leurs valeurs propres.

Dans un premier temps, nous établissons les équations quantiques microscopiques régissant la dynamique du champ électrique ainsi que celle des opérateurs atomiques, et explicitons comment la matrice de Green (dont les éléments sont égaux à la fonction de Green de l'équation de Helmholtz évaluée entre les différentes paires d'atomes constituant le milieu) émerge du formalisme quantique. Nous exprimons à la fois l'intensité et le spectre de la lumière en termes de la matrice de Green, caractérisons les forces de Langevin quantiques, et montrons de quelle manière le seuil semi-classique d'un laser aléatoire est affecté par la prise en considération des fluctuations quantiques (chapitres 2 et 3).

Une description mésoscopique et semi-classique de la lumière diffusée par des atomes soumis à une pompe externe est présentée dans le quatrième chapitre. Nous dérivons une équation de transport obéie par l'intensité moyenne en présence de gain, établissons un 'mapping' avec les MAE, et analysons la condition de seuil laser déduite de l'équation de transport.

Dans les chapitres 5 et 6, nous développons une théorie générale des MAE, hermitiennes et non hermitiennes, valide dans la limite de grande taille matricielle. Nous obtenons des équations couplées pour la résolvante et le corrélateur des vecteur propres d'une MAE arbitraire, puis testons la validité de nos résultats sur trois matrices jouant un rôle important dans l'étude de la propagation des ondes en milieux désordonnés: la matrice de Green, sa partie imaginaire, et sa partie réelle. Nous sommes ainsi capables de décrire analytiquement avec une bonne précision la distribution de probabilité des taux d'émission lumineux dus à un grand nombre d'atomes, ainsi que celle du déplacement lumineux collectif dû à l'interaction lumière-matière. Les signatures de la localisation d'Anderson dans les propriétés de la matrice de Green sont également discutées.

Finalement, nous combinons les équations microscopiques de l'interaction lumière-matière avec nos résultats relatifs aux MAE non-hermitiennes afin de caractériser dans le détail le comportement des lasers aléatoires. Le seuil laser ainsi que l'intensité au delà du seuil sont calculés analytiquement dans l'approximation semi-classique, et le spectre de la lumière sous le seuil est évalué en prenant en compte les effets quantiques. Notre théorie s'applique aussi bien à basse densité qu'à haute densité de diffuseurs atomiques.